

ipcc

INTERGOVERNMENTAL PANEL ON climate change

CLIMATE CHANGE 2013

The Physical Science Basis

WG I

WORKING GROUP I CONTRIBUTION TO THE
FIFTH ASSESSMENT REPORT OF THE
INTERGOVERNMENTAL PANEL ON CLIMATE CHANGE



Climate Change 2013

The Physical Science Basis

Working Group I Contribution to the Fifth Assessment Report of the Intergovernmental Panel on Climate Change

Edited by

Thomas F. Stocker

Working Group I Co-Chair
University of Bern

Dahe Qin

Working Group I Co-Chair
China Meteorological Administration

Gian-Kasper Plattner

Director of Science

Melinda M.B. Tignor

Director of Operations

Simon K. Allen

Senior Science Officer

Judith Boschung

Administrative Assistant

Alexander Nauels

Science Assistant

Yu Xia

Science Officer

Vincent Bex

IT Officer

Pauline M. Midgley

Head

Working Group I Technical Support Unit



CAMBRIDGE
UNIVERSITY PRESS

www.cambridge.org

CAMBRIDGE UNIVERSITY PRESS

Cambridge, New York, Melbourne, Madrid, Cape Town, Singapore, São Paulo, Delhi, Mexico City

Cambridge University Press

32 Avenue of the Americas, New York, NY 10013-2473, USA

www.cambridge.org

Information on this title: www.cambridge.org/9781107661820

© Intergovernmental Panel on Climate Change 2013

This publication is in copyright. Subject to statutory exception and to the provisions of relevant collective licensing agreements, no reproduction of any part may take place without the written permission of Cambridge University Press.

First published 2013

Printed in the United States of America

A catalog record for this publication is available from the British Library.

ISBN 978-1-107-05799-1 hardback

ISBN 978-1-107-66182-0 paperback

Cambridge University Press has no responsibility for the persistence or accuracy of URLs for external or third-party Internet Web sites referred to in this publication and does not guarantee that any content on such Web sites is, or will remain, accurate or appropriate.

Please use the following reference to the whole report:

IPCC, 2013: *Climate Change 2013: The Physical Science Basis. Contribution of Working Group I to the Fifth Assessment Report of the Intergovernmental Panel on Climate Change* [Stocker, T.F., D. Qin, G.-K. Plattner, M. Tignor, S.K. Allen, J. Boschung, A. Nauels, Y. Xia, V. Bex and P.M. Midgley (eds.)]. Cambridge University Press, Cambridge, United Kingdom and New York, NY, USA, 1535 pp.

Cover photo:

Folgefonna glacier on the high plateaus of Sørkjorden, Norway (60°03' N - 6°20' E) © Yann Arthus-Bertrand / Altitude.

Foreword, Preface and Dedication

Foreword

“Climate Change 2013: The Physical Science Basis” presents clear and robust conclusions in a global assessment of climate change science—not the least of which is that the science now shows with 95 percent certainty that human activity is the dominant cause of observed warming since the mid-20th century. The report confirms that warming in the climate system is unequivocal, with many of the observed changes unprecedented over decades to millennia: warming of the atmosphere and the ocean, diminishing snow and ice, rising sea levels and increasing concentrations of greenhouse gases. Each of the last three decades has been successively warmer at the Earth’s surface than any preceding decade since 1850.

These and other findings confirm and enhance our scientific understanding of the climate system and the role of greenhouse gas emissions; as such, the report demands the urgent attention of both policymakers and the general public.

As an intergovernmental body jointly established in 1988 by the World Meteorological Organization (WMO) and the United Nations Environment Programme (UNEP), the Intergovernmental Panel on Climate Change (IPCC) has provided policymakers with the most authoritative and objective scientific and technical assessments. Beginning in 1990, this series of IPCC Assessment Reports, Special Reports, Technical Papers, Methodology Reports and other products have become standard works of reference.

This Working Group I contribution to the IPCC’s Fifth Assessment Report contains important new scientific knowledge that can be used to produce climate information and services for assisting society to act to address the challenges of climate change. The timing is particularly significant, as this information provides a new impetus, through clear and indisputable physical science, to those negotiators responsible for concluding a new agreement under the United Nations Framework Convention on Climate Change in 2015.

Climate change is a long-term challenge, but one that requires urgent action given the pace and the scale by which greenhouse gases are accumulating in the atmosphere and the risks of a more than 2 degree Celsius temperature rise. Today we need to focus on the fundamentals and on the actions otherwise the risks we run will get higher with every year.

This Working Group I assessment was made possible thanks to the commitment and dedication of many hundreds of experts worldwide, representing a wide range of disciplines. WMO and UNEP are proud that so many of the experts belong to their communities and networks. We express our deep gratitude to all authors, review editors and expert reviewers for devoting their knowledge, expertise and time. We would like to thank the staff of the Working Group I Technical Support Unit and the IPCC Secretariat for their dedication.

We are also grateful to the governments that supported their scientists’ participation in developing this report and that contributed to the IPCC Trust Fund to provide for the essential participation of experts from developing countries and countries with economies in transition. We would like to express our appreciation to the government of Italy for hosting the scoping meeting for the IPCC’s Fifth Assessment Report, to the governments of China, France, Morocco and Australia for hosting drafting sessions of the Working Group I contribution and to the government of Sweden for hosting the Twelfth Session of Working Group I in Stockholm for approval of the Working Group I Report. The generous financial support by the government of Switzerland, and the logistical support by the University of Bern (Switzerland), enabled the smooth operation of the Working Group I Technical Support Unit. This is gratefully acknowledged.

We would particularly like to thank Dr. Rajendra Pachauri, Chairman of the IPCC, for his direction and guidance of the IPCC and we express our deep gratitude to Professor Qin Dahe and Professor Thomas Stocker, the Co-Chairs of Working Group I for their tireless leadership throughout the development and production of this report.

M. Jarraud
Secretary-General
World Meteorological Organization

A. Steiner
Executive Director
United Nations Environment Programme

Preface

The Working Group I contribution to the Fifth Assessment Report of the Intergovernmental Panel on Climate Change (IPCC) provides a comprehensive assessment of the physical science basis of climate change. It builds upon the Working Group I contribution to the IPCC's Fourth Assessment Report in 2007 and incorporates subsequent new findings from the Special Report on Managing the Risks of Extreme Events and Disasters to Advance Climate Change Adaptation, as well as from research published in the extensive scientific and technical literature. The assessment considers new evidence of past, present and projected future climate change based on many independent scientific analyses from observations of the climate system, paleoclimate archives, theoretical studies of climate processes and simulations using climate models.

Scope of the Report

During the process of scoping and approving the outline of its Fifth Assessment Report, the IPCC focussed on those aspects of the current understanding of the science of climate change that were judged to be most relevant to policymakers.

In this report, Working Group I has extended coverage of future climate change compared to earlier reports by assessing near-term projections and predictability as well as long-term projections and irreversibility in two separate chapters. Following the decisions made by the Panel during the scoping and outline approval, a set of new scenarios, the Representative Concentration Pathways, are used across all three Working Groups for projections of climate change over the 21st century. The coverage of regional information in the Working Group I report is expanded by specifically assessing climate phenomena such as monsoon systems and their relevance to future climate change in the regions.

The Working Group I Report is an assessment, not a review or a text book of climate science, and is based on the published scientific and technical literature available up to 15 March 2013. Underlying all aspects of the report is a strong commitment to assessing the science comprehensively, without bias and in a way that is relevant to policy but not policy prescriptive.

Structure of the Report

This report consists of a short Summary for Policymakers, a longer Technical Summary and fourteen thematic chapters plus annexes. An innovation in this Working Group I assessment is the Atlas of Global and Regional Climate Projections (Annex I) containing time series and maps of temperature and precipitation projections for 35 regions of the world, which enhances accessibility for stakeholders and users.

The Summary for Policymakers and Technical Summary of this report follow a parallel structure and each includes cross-references to the chapter and section where the material being summarised can be found in the underlying report. In this way, these summary components of the report provide a road-map to the contents of the entire report and a traceable account of every major finding.

In order to facilitate the accessibility of the findings of the Working Group I assessment for a wide readership and to enhance their usability for stakeholders, each section of the Summary for Policymakers has a highlighted headline statement. Taken together, these 19 headline statements provide an overarching summary in simple and quotable language that is supported by the scientists and approved by the member governments of the IPCC. Another innovative feature of this report is the presentation of Thematic Focus Elements in the Technical Summary that provide end to end assessments of important cross-cutting issues in the physical science basis of climate change.

Introduction (Chapter 1): This chapter provides information on the progress in climate change science since the First Assessment Report of the IPCC in 1990 and gives an overview of key concepts, indicators of climate change, the treatment of uncertainties and advances in measurement and modelling capabilities. This includes a description of the future scenarios and in particular the Representative Concentration Pathway scenarios used across all Working Groups for the IPCC's Fifth Assessment Report.

Observations and Paleoclimate Information (Chapters 2, 3, 4, 5): These chapters assess information from all climate system components on climate variability and change as obtained from instrumental records and climate archives. They cover all relevant aspects of the atmosphere including the stratosphere, the land surface, the oceans and the cryosphere. Timescales from days to decades (Chapters 2, 3 and 4) and from centuries to many millennia (Chapter 5) are considered.

Process Understanding (Chapters 6 and 7): These chapters cover all relevant aspects from observations and process understanding to projections from global to regional scales for two key topics. Chapter 6 covers the carbon cycle and its interactions with other biogeochemical cycles, in particular the nitrogen cycle, as well as feedbacks on the climate system. For the first time, there is a chapter dedicated to the assessment of the physical science basis of clouds and aerosols, their interactions and chemistry, and the role of water vapour, as well as their role in feedbacks on the climate system (Chapter 7).

From Forcing to Attribution of Climate Change (Chapters 8, 9, 10): All the information on the different drivers (natural and anthropogenic) of climate change is collected, expressed in terms of Radiative Forcing and assessed in Chapter 8. In Chapter 9, the hierarchy of climate models used in simulating past and present climate change is assessed and evaluated against observations and paleoclimate reconstructions.

Information regarding detection of changes on global to regional scales and their attribution to the increase in anthropogenic greenhouse gases is assessed in Chapter 10.

Future Climate Change, Predictability and Irreversibility (Chapters 11 and 12): These chapters assess projections of future climate change derived from climate models on time scales from decades to centuries at both global and regional scales, including mean changes, variability and extremes. Fundamental questions related to the predictability of climate as well as long term climate change, climate change commitments and inertia in the climate system are addressed. Knowledge on irreversible changes and surprises in the climate system is also assessed.

Integration (Chapters 13 and 14): These chapters synthesise all relevant information for two key topics of this assessment: sea level change (Chapter 13) and climate phenomena across the regions (Chapter 14). Chapter 13 presents an end to end assessment of information on sea level change based on paleoclimate reconstructions, observations and process understanding, and provides projections from global to regional scales. Chapter 14 assesses the most important modes of variability in the climate system, such as El Niño-Southern Oscillation, monsoon and many others, as well as extreme events. Furthermore, this chapter deals with interconnections between the climate phenomena, their regional expressions and their relevance for future regional climate change.

Maps assessed in Chapter 14, together with Chapters 11 and 12, form the basis of the Atlas of Global and Regional Climate Projections in Annex I, which is also available in digital format. Radiative forcings and estimates of future atmospheric concentrations from Chapters 7, 8, 11 and 12 form the basis of the Climate System Scenario Tables presented in Annex II. All material including high-resolution versions of the figures, underlying data and Supplementary Material to the chapters is also available online: www.climatechange2013.org.

The scientific community and the climate modelling centres around the world brought together their activities in the Coordinated Modelling Intercomparison Project Phase 5 (CMIP5), providing the basis for most of the assessment of future climate change in this report. Their efforts enable Working Group I to deliver comprehensive scientific information for the policymakers and the users of this report, as well as for the specific assessments of impacts carried out by IPCC Working Group II, and of costs and mitigation strategies, carried out by IPCC Working Group III.

Following the successful introduction in the previous Working Group I assessment in 2007, all chapters contain Frequently Asked Questions. In these the authors provide scientific answers to a range of general questions in a form that will be accessible to a broad readership and serves as a resource for teaching purposes. Finally, the report is accompanied by extensive Supplementary Material which is made available

in the online versions of the report to provide an additional level of detail, such as description of datasets, models, or methodologies used in chapter analyses, as well as material supporting the figures in the Summary for Policymakers.

The Process

This Working Group I Assessment Report represents the combined efforts of hundreds of leading experts in the field of climate science and has been prepared in accordance with rules and procedures established by the IPCC. A scoping meeting for the Fifth Assessment Report was held in July 2009 and the outlines for the contributions of the three Working Groups were approved at the 31st Session of the Panel in November 2009. Governments and IPCC observer organisations nominated experts for the author team. The team of 209 Coordinating Lead Authors and Lead Authors plus 50 Review Editors selected by the Working Group I Bureau was accepted at the 41st Session of the IPCC Bureau in May 2010. In addition, more than 600 Contributing Authors provided draft text and information to the author teams at their request. Drafts prepared by the authors were subject to two rounds of formal review and revision followed by a final round of government comments on the Summary for Policymakers. A total of 54,677 written review comments were submitted by 1089 individual expert reviewers and 38 governments. The Review Editors for each chapter monitored the review process to ensure that all substantive review comments received appropriate consideration. The Summary for Policymakers was approved line-by-line and the underlying chapters were then accepted at the 12th Session of IPCC Working Group I from 23–27 September 2007.

Acknowledgements

We are very grateful for the expertise, hard work, commitment to excellence and integrity shown throughout by the Coordinating Lead Authors and Lead Authors with important help by the many Contributing Authors. The Review Editors have played a critical role in assisting the author teams and ensuring the integrity of the review process. We express our sincere appreciation to all the expert and government reviewers. We would also like to thank the members of the Bureau of Working Group I: Jean Jouzel, Abdalah Mokssit, Fatemeh Rahimizadeh, Fredolin Tangang, David Wratt and Francis Zwiers, for their thoughtful advice and support throughout the preparation of the report.

We gratefully acknowledge the long-term efforts of the scientific community, organized and facilitated through the World Climate Research Programme, in particular CMIP5. In this effort by climate modelling centres around the world, more than 2 million gigabytes of numerical data have been produced, which were archived and distributed under the stewardship of the Program for Climate Model Diagnosis and Intercomparison. This represents an unprecedented concerted effort by the scientific community and their funding institutions.

Our sincere thanks go to the hosts and organizers of the four Working Group I Lead Author Meetings and the 12th Session of Working Group I. We gratefully acknowledge the support from the host countries: China, France, Morocco, Australia and Sweden. The support for their scientists provided by many governments as well as through the IPCC Trust Fund is much appreciated. The efficient operation of the Working Group I Technical Support Unit was made possible by the generous financial support provided by the government of Switzerland and logistical support from the University of Bern (Switzerland).

We would also like to thank Renate Christ, Secretary of the IPCC, and the staff of the IPCC Secretariat: Gaetano Leone, Jonathan Lynn, Mary Jean Burer, Sophie Schlingemann, Judith Ewa, Jesbin Baidya, Werani Zabula, Joelle Fernandez, Annie Courtin, Laura Biagioni and Amy Smith. Thanks are due to Francis Hayes who served as the conference officer for the Working Group I Approval Session.


Finally our particular appreciation goes to the Working Group I Technical Support Unit: Gian-Kasper Plattner, Melinda Tignor, Simon Allen, Judith Boschung, Alexander Nauels, Yu Xia, Vincent Bex and Pauline Midgley for their professionalism, creativity and dedication. Their tireless efforts to coordinate the Working Group I Report ensured a final product of high quality. They were assisted in this by Adrien Michel and Flavio Lehner with further support from Zhou Botao and Sun Ying. In addition, the following contributions are gratefully acknowledged: David Hansford (editorial assistance with the Frequently Asked Questions), UNEP/GRID-Geneva and University of Geneva (graphics assistance with the Frequently Asked Questions), Theresa Kornak (copyedit), Marilyn Anderson (index) and Michael Shibao (design and layout).



Rajendra K. Pachauri
IPCC Chair



Qin Dahe
IPCC WGI Co-Chair



Thomas F. Stocker
IPCC WGI Co-Chair

Dedication



Bert Bolin
(15 May 1925 – 30 December 2007)

The Working Group I contribution to the Fifth Assessment Report of the Intergovernmental Panel on Climate Change (IPCC) *Climate Change 2013: The Physical Science Basis* is dedicated to the memory of Bert Bolin, the first Chair of the IPCC.

As an accomplished scientist who published on both atmospheric dynamics and the carbon cycle, including processes in the atmosphere, oceans and biosphere, Bert Bolin realised the complexity of the climate system and its sensitivity to anthropogenic perturbation. He made a fundamental contribution to the organisation of international cooperation in climate research, being involved in the establishment of a number of global programmes.

Bert Bolin played a key role in the creation of the IPCC and its assessments, which are carried out in a unique and formalized process in order to provide a robust scientific basis for informed decisions regarding one of the greatest challenges of our time. His vision and leadership of the Panel as the founding Chair from 1988 to 1997 laid the basis for subsequent assessments including this one and are remembered with deep appreciation.

Contents

Front Matter

Foreword	v
Preface	vii
Dedication	xi

SPM

Summary for Policymakers	3
--------------------------------	---

TS

Technical Summary	33
-------------------------	----

Chapters

Chapter 1	Introduction	119
Chapter 2	Observations : Atmosphere and Surface	159
Chapter 3	Observations: Ocean	255
Chapter 4	Observations: Cryosphere	317
Chapter 5	Information from Paleoclimate Archives	383
Chapter 6	Carbon and Other Biogeochemical Cycles	465
Chapter 7	Clouds and Aerosols	571
Chapter 8	Anthropogenic and Natural Radiative Forcing	659
Chapter 9	Evaluation of Climate Models	741
Chapter 10	Detection and Attribution of Climate Change: from Global to Regional	867
Chapter 11	Near-term Climate Change: Projections and Predictability	953
Chapter 12	Long-term Climate Change: Projections, Commitments and Irreversibility	1029
Chapter 13	Sea Level Change	1137
Chapter 14	Climate Phenomena and their Relevance for Future Regional Climate Change	1217

Annexes

Annex I	Atlas of Global and Regional Climate Projections	1311
Annex II	Climate System Scenario Tables	1395
Annex III	Glossary	1447
Annex IV	Acronyms	1467
Annex V	Contributors to the IPCC WGI Fifth Assessment Report	1477
Annex VI	Expert Reviewers of the IPCC WGI Fifth Assessment Report	1497
Index		1523

Summary for Policymakers

Summary for Policymakers

Drafting Authors:

Lisa V. Alexander (Australia), Simon K. Allen (Switzerland/New Zealand), Nathaniel L. Bindoff (Australia), François-Marie Bréon (France), John A. Church (Australia), Ulrich Cubasch (Germany), Seita Emori (Japan), Piers Forster (UK), Pierre Friedlingstein (UK/Belgium), Nathan Gillett (Canada), Jonathan M. Gregory (UK), Dennis L. Hartmann (USA), Eystein Jansen (Norway), Ben Kirtman (USA), Reto Knutti (Switzerland), Krishna Kumar Kanikicharla (India), Peter Lemke (Germany), Jochem Marotzke (Germany), Valérie Masson-Delmotte (France), Gerald A. Meehl (USA), Igor I. Mokhov (Russian Federation), Shilong Piao (China), Gian-Kasper Plattner (Switzerland), Qin Dahe (China), Venkatachalam Ramaswamy (USA), David Randall (USA), Monika Rhein (Germany), Maisa Rojas (Chile), Christopher Sabine (USA), Drew Shindell (USA), Thomas F. Stocker (Switzerland), Lynne D. Talley (USA), David G. Vaughan (UK), Shang-Ping Xie (USA)

Draft Contributing Authors:

Myles R. Allen (UK), Olivier Boucher (France), Don Chambers (USA), Jens Hesselbjerg Christensen (Denmark), Philippe Ciais (France), Peter U. Clark (USA), Matthew Collins (UK), Josefino C. Comiso (USA), Viviane Vasconcellos de Menezes (Australia/Brazil), Richard A. Feely (USA), Thierry Fichfet (Belgium), Arlene M. Fiore (USA), Gregory Flato (Canada), Jan Fuglestvedt (Norway), Gabriele Hegerl (UK/Germany), Paul J. Hezel (Belgium/USA), Gregory C. Johnson (USA), Georg Kaser (Austria/Italy), Vladimir Kattsov (Russian Federation), John Kennedy (UK), Albert M. G. Klein Tank (Netherlands), Corinne Le Quéré (UK), Gunnar Myhre (Norway), Timothy Osborn (UK), Antony J. Payne (UK), Judith Perlwitz (USA), Scott Power (Australia), Michael Prather (USA), Stephen R. Rintoul (Australia), Joeri Rogelj (Switzerland/Belgium), Matilde Rusticucci (Argentina), Michael Schulz (Germany), Jan Sedláček (Switzerland), Peter A. Stott (UK), Rowan Sutton (UK), Peter W. Thorne (USA/Norway/UK), Donald Wuebbles (USA)

This Summary for Policymakers should be cited as:

IPCC, 2013: Summary for Policymakers. In: *Climate Change 2013: The Physical Science Basis. Contribution of Working Group I to the Fifth Assessment Report of the Intergovernmental Panel on Climate Change* [Stocker, T.F., D. Qin, G.-K. Plattner, M. Tignor, S.K. Allen, J. Boschung, A. Nauels, Y. Xia, V. Bex and P.M. Midgley (eds.)]. Cambridge University Press, Cambridge, United Kingdom and New York, NY, USA.

A. Introduction

The Working Group I contribution to the IPCC's Fifth Assessment Report (AR5) considers new evidence of climate change based on many independent scientific analyses from observations of the climate system, paleoclimate archives, theoretical studies of climate processes and simulations using climate models. It builds upon the Working Group I contribution to the IPCC's Fourth Assessment Report (AR4), and incorporates subsequent new findings of research. As a component of the fifth assessment cycle, the IPCC Special Report on Managing the Risks of Extreme Events and Disasters to Advance Climate Change Adaptation (SREX) is an important basis for information on changing weather and climate extremes.

This Summary for Policymakers (SPM) follows the structure of the Working Group I report. The narrative is supported by a series of overarching highlighted conclusions which, taken together, provide a concise summary. Main sections are introduced with a brief paragraph in italics which outlines the methodological basis of the assessment.

The degree of certainty in key findings in this assessment is based on the author teams' evaluations of underlying scientific understanding and is expressed as a qualitative level of confidence (from *very low* to *very high*) and, when possible, probabilistically with a quantified likelihood (from *exceptionally unlikely* to *virtually certain*). Confidence in the validity of a finding is based on the type, amount, quality, and consistency of evidence (e.g., data, mechanistic understanding, theory, models, expert judgment) and the degree of agreement¹. Probabilistic estimates of quantified measures of uncertainty in a finding are based on statistical analysis of observations or model results, or both, and expert judgment². Where appropriate, findings are also formulated as statements of fact without using uncertainty qualifiers. (See Chapter 1 and Box TS.1 for more details about the specific language the IPCC uses to communicate uncertainty).

The basis for substantive paragraphs in this Summary for Policymakers can be found in the chapter sections of the underlying report and in the Technical Summary. These references are given in curly brackets.

B. Observed Changes in the Climate System

Observations of the climate system are based on direct measurements and remote sensing from satellites and other platforms. Global-scale observations from the instrumental era began in the mid-19th century for temperature and other variables, with more comprehensive and diverse sets of observations available for the period 1950 onwards. Paleoclimate reconstructions extend some records back hundreds to millions of years. Together, they provide a comprehensive view of the variability and long-term changes in the atmosphere, the ocean, the cryosphere, and the land surface.

Warming of the climate system is unequivocal, and since the 1950s, many of the observed changes are unprecedented over decades to millennia. The atmosphere and ocean have warmed, the amounts of snow and ice have diminished, sea level has risen, and the concentrations of greenhouse gases have increased (see Figures SPM.1, SPM.2, SPM.3 and SPM.4). {2.2, 2.4, 3.2, 3.7, 4.2–4.7, 5.2, 5.3, 5.5–5.6, 6.2, 13.2}

¹ In this Summary for Policymakers, the following summary terms are used to describe the available evidence: limited, medium, or robust; and for the degree of agreement: low, medium, or high. A level of confidence is expressed using five qualifiers: very low, low, medium, high, and very high, and typeset in italics, e.g., *medium confidence*. For a given evidence and agreement statement, different confidence levels can be assigned, but increasing levels of evidence and degrees of agreement are correlated with increasing confidence (see Chapter 1 and Box TS.1 for more details).

² In this Summary for Policymakers, the following terms have been used to indicate the assessed likelihood of an outcome or a result: virtually certain 99–100% probability, very likely 90–100%, likely 66–100%, about as likely as not 33–66%, unlikely 0–33%, very unlikely 0–10%, exceptionally unlikely 0–1%. Additional terms (extremely likely: 95–100%, more likely than not >50–100%, and extremely unlikely 0–5%) may also be used when appropriate. Assessed likelihood is typeset in italics, e.g., *very likely* (see Chapter 1 and Box TS.1 for more details).

B.1 Atmosphere

Each of the last three decades has been successively warmer at the Earth's surface than any preceding decade since 1850 (see Figure SPM.1). In the Northern Hemisphere, 1983–2012 was *likely* the warmest 30-year period of the last 1400 years (*medium confidence*). {2.4, 5.3}

SPM

- The globally averaged combined land and ocean surface temperature data as calculated by a linear trend, show a warming of 0.85 [0.65 to 1.06] °C³, over the period 1880 to 2012, when multiple independently produced datasets exist. The total increase between the average of the 1850–1900 period and the 2003–2012 period is 0.78 [0.72 to 0.85] °C, based on the single longest dataset available⁴ (see Figure SPM.1). {2.4}
- For the longest period when calculation of regional trends is sufficiently complete (1901 to 2012), almost the entire globe has experienced surface warming (see Figure SPM.1). {2.4}
- In addition to robust multi-decadal warming, global mean surface temperature exhibits substantial decadal and interannual variability (see Figure SPM.1). Due to natural variability, trends based on short records are very sensitive to the beginning and end dates and do not in general reflect long-term climate trends. As one example, the rate of warming over the past 15 years (1998–2012; 0.05 [–0.05 to 0.15] °C per decade), which begins with a strong El Niño, is smaller than the rate calculated since 1951 (1951–2012; 0.12 [0.08 to 0.14] °C per decade)⁵. {2.4}
- Continental-scale surface temperature reconstructions show, with *high confidence*, multi-decadal periods during the Medieval Climate Anomaly (year 950 to 1250) that were in some regions as warm as in the late 20th century. These regional warm periods did not occur as coherently across regions as the warming in the late 20th century (*high confidence*). {5.5}
- It is *virtually certain* that globally the troposphere has warmed since the mid-20th century. More complete observations allow greater confidence in estimates of tropospheric temperature changes in the extratropical Northern Hemisphere than elsewhere. There is *medium confidence* in the rate of warming and its vertical structure in the Northern Hemisphere extra-tropical troposphere and *low confidence* elsewhere. {2.4}
- *Confidence* in precipitation change averaged over global land areas since 1901 is *low* prior to 1951 and *medium* afterwards. Averaged over the mid-latitude land areas of the Northern Hemisphere, precipitation has increased since 1901 (*medium confidence* before and *high confidence* after 1951). For other latitudes area-averaged long-term positive or negative trends have *low confidence* (see Figure SPM.2). {TS TFE.1, Figure 2; 2.5}
- Changes in many extreme weather and climate events have been observed since about 1950 (see Table SPM.1 for details). It is *very likely* that the number of cold days and nights has decreased and the number of warm days and nights has increased on the global scale⁶. It is *likely* that the frequency of heat waves has increased in large parts of Europe, Asia and Australia. There are *likely* more land regions where the number of heavy precipitation events has increased than where it has decreased. The frequency or intensity of heavy precipitation events has *likely* increased in North America and Europe. In other continents, *confidence* in changes in heavy precipitation events is at most *medium*. {2.6}

³ In the WGI contribution to the AR5, uncertainty is quantified using 90% uncertainty intervals unless otherwise stated. The 90% uncertainty interval, reported in square brackets, is expected to have a 90% likelihood of covering the value that is being estimated. Uncertainty intervals are not necessarily symmetric about the corresponding best estimate. A best estimate of that value is also given where available.

⁴ Both methods presented in this bullet were also used in AR4. The first calculates the difference using a best fit linear trend of all points between 1880 and 2012. The second calculates the difference between averages for the two periods 1850–1900 and 2003–2012. Therefore, the resulting values and their 90% uncertainty intervals are not directly comparable. {2.4}

⁵ Trends for 15-year periods starting in 1995, 1996, and 1997 are 0.13 [0.02 to 0.24] °C per decade, 0.14 [0.03 to 0.24] °C per decade, and, 0.07 [–0.02 to 0.18] °C per decade, respectively.

⁶ See the Glossary for the definition of these terms: cold days/cold nights, warm days/warm nights, heat waves.

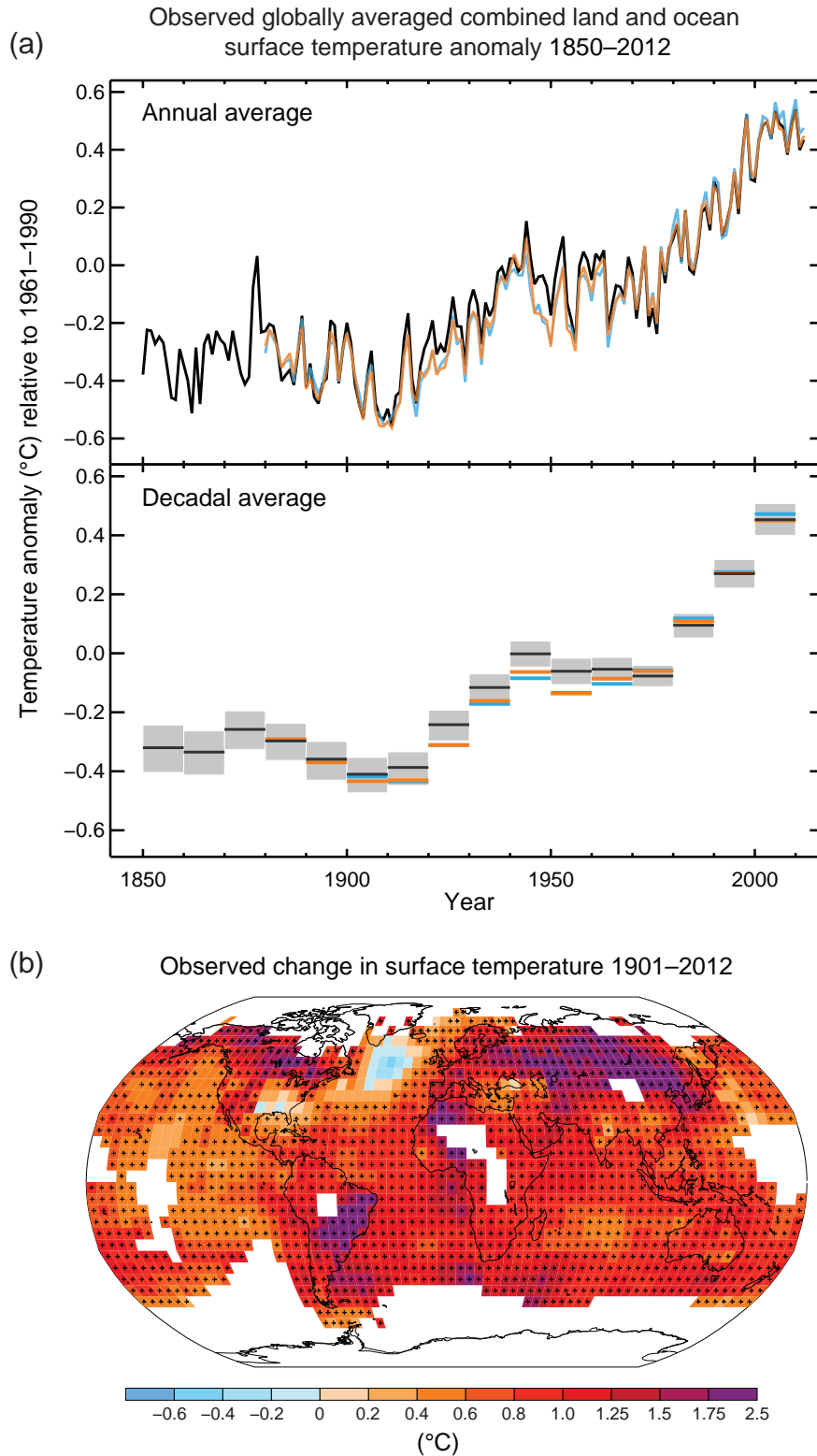


Figure SPM.1 | (a) Observed global mean combined land and ocean surface temperature anomalies, from 1850 to 2012 from three data sets. Top panel: annual mean values. Bottom panel: decadal mean values including the estimate of uncertainty for one dataset (black). Anomalies are relative to the mean of 1961–1990. (b) Map of the observed surface temperature change from 1901 to 2012 derived from temperature trends determined by linear regression from one dataset (orange line in panel a). Trends have been calculated where data availability permits a robust estimate (i.e., only for grid boxes with greater than 70% complete records and more than 20% data availability in the first and last 10% of the time period). Other areas are white. Grid boxes where the trend is significant at the 10% level are indicated by a + sign. For a listing of the datasets and further technical details see the Technical Summary Supplementary Material. [Figures 2.19–2.21; Figure TS.2]

Table SPM.1 | Extreme weather and climate events: Global-scale assessment of recent observed changes, human contribution to the changes, and projected further changes for the early (2016–2035) and late (2081–2100) 21st century. Bold indicates where the AR5 (black) provides a revised* global-scale assessment from the SREX (blue) or AR4 (red). Projections for early 21st century were not provided in previous assessment reports. Projections in the AR5 are relative to the reference period of 1986–2005, and use the new Representative Concentration Pathway (RCP) scenarios (see Box SPM.1) unless otherwise specified. See the Glossary for definitions of extreme weather and climate events.

Phenomenon and direction of trend	Assessment that changes occurred (typically since 1950 unless otherwise indicated)	Assessment of a human contribution to observed changes		Likelihood of further changes	
		Early 21st century	Late 21st century	Early 21st century	Late 21st century
Warmer and/or fewer cold days and nights over most land areas	Very likely (2.6) Very likely Very likely	Very likely (10.6) Likely Likely	Likely (11.3)	Virtually certain (12.4) Virtually certain Virtually certain	
Warmer and/or more frequent hot days and nights over most land areas	Very likely (2.6) Very likely Very likely	Very likely (10.6) Likely Likely (nights only)	Likely (11.3)	Virtually certain (12.4) Virtually certain Virtually certain	
Warm spells/heat waves. Frequency and/or duration increases over most land areas	Medium confidence on a global scale. Likely in large parts of Europe, Asia and Australia (2.6) Medium confidence in many (but not all) regions. Likely	Likely ^a (10.6)	Not formally assessed ^b (11.3)	Very likely (12.4) Very likely Very likely	
Heavy precipitation events. Increase in the frequency, intensity, and/or amount of heavy precipitation	Likely more land areas with increases than decreases ^c (2.6) Likely more land areas with increases than decreases. Likely over most land areas	Medium confidence (7.6, 10.6) Medium confidence More likely than not	Likely over many land areas (11.3)	Very likely over most of the mid-latitude land masses and over wet tropical regions (12.4) Likely over many areas Very likely over most land areas	
Increases in intensity and/or duration of drought	Low confidence on a global scale. Likely changes in some regions ^d (2.6) Medium confidence in some regions. Likely in many regions, since 1970 ^e	Low confidence (10.6) Medium confidence ^f More likely than not	Low confidence ^g (11.3)	Likely (medium confidence) on a regional to global scale ^h (12.4) Medium confidence in some regions. Likely ⁱ	
Increases in intense tropical cyclone activity	Low confidence in long term (centennial) changes. Virtually certain in North Atlantic since 1970 (2.6) Low confidence. Likely in some regions, since 1970	Low confidence (10.6) More likely than not	Low confidence (11.3)	More likely than not in the Western North Pacific and North Atlantic ^j (14.6) More likely than not in some basins. Likely	
Increased incidence and/or magnitude of extreme high sea level	Likely (since 1970) (3.7) Likely (late 20th century) (2.6)	Likely ^k (3.7) Likely ^k More likely than not ^k	Likely (13.7)	Very likely ^l (13.7) Very likely ^m Likely	

* The direct comparison of assessment findings between reports is difficult. For some climate variables, different aspects have been assessed, and the revised guidance note on uncertainties has been used for the SREX and AR5. The availability of new information, improved scientific understanding, continued analyses of data and models, and specific differences in methodologies applied in the assessed studies, all contribute to revised assessment findings.

Notes:

- a Attribution is based on available case studies. It is likely that human influence has more than doubled the probability of occurrence of some observed heat waves in some locations.
- b Models project near-term increases in the duration, intensity and spatial extent of heat waves and warm spells.
- c In most continents, confidence in trends is not higher than medium except in North America and Europe where there have been likely increases in either the frequency or intensity of heavy precipitation with some seasonal and/or regional variation. It is very likely that there have been increases in central North America.
- d The frequency and intensity of drought has likely increased in the Mediterranean and West Africa, and likely decreased in central North America and north-west Australia.
- e AR4 assessed the area affected by drought.
- f SREX assessed medium confidence that anthropogenic influence had contributed to some changes in the drought patterns observed in the second half of the 20th century, based on its attributed impact on precipitation and temperature changes. SREX assessed low confidence in the attribution of changes in droughts at the level of single regions.
- g There is low confidence in projected changes in soil moisture.
- h Regional to global-scale projected decreases in soil moisture and increased agricultural drought are likely (medium confidence) in presently dry regions by the end of this century under the RCP8.5 scenario. Soil moisture drying in the Mediterranean, Southwest US and southern African regions is consistent with projected changes in Hadley circulation and increased surface temperatures, so there is high confidence in likely surface drying in these regions by the end of this century under the RCP8.5 scenario.
- i There is medium confidence that a reduction in aerosol forcing over the North Atlantic has contributed at least in part to the observed increase in tropical cyclone activity since the 1970s in this region.
- j Based on expert judgment and assessment of projections which use an SRES A1B (or similar) scenario.
- k Attribution is based on the close relationship between observed changes in extreme and mean sea level.
- l There is high confidence that this increase in extreme high sea level will primarily be the result of an increase in mean sea level.
- m SREX assessed it to be very likely that mean sea level rise will contribute to future upward trends in extreme coastal high water levels.



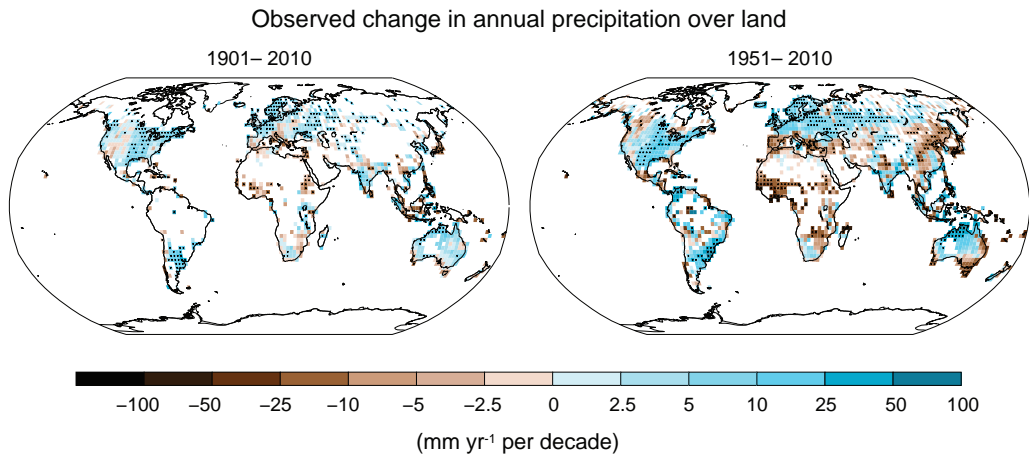


Figure SPM.2 | Maps of observed precipitation change from 1901 to 2010 and from 1951 to 2010 (trends in annual accumulation calculated using the same criteria as in Figure SPM.1) from one data set. For further technical details see the Technical Summary Supplementary Material. {TS TFE.1, Figure 2; Figure 2.29}

B.2 Ocean

Ocean warming dominates the increase in energy stored in the climate system, accounting for more than 90% of the energy accumulated between 1971 and 2010 (*high confidence*). It is *virtually certain* that the upper ocean (0–700 m) warmed from 1971 to 2010 (see Figure SPM.3), and it *likely* warmed between the 1870s and 1971. {3.2, Box 3.1}

- On a global scale, the ocean warming is largest near the surface, and the upper 75 m warmed by 0.11 [0.09 to 0.13] °C per decade over the period 1971 to 2010. Since AR4, instrumental biases in upper-ocean temperature records have been identified and reduced, enhancing confidence in the assessment of change. {3.2}
- It is *likely* that the ocean warmed between 700 and 2000 m from 1957 to 2009. Sufficient observations are available for the period 1992 to 2005 for a global assessment of temperature change below 2000 m. There were *likely* no significant observed temperature trends between 2000 and 3000 m for this period. It is *likely* that the ocean warmed from 3000 m to the bottom for this period, with the largest warming observed in the Southern Ocean. {3.2}
- More than 60% of the net energy increase in the climate system is stored in the upper ocean (0–700 m) during the relatively well-sampled 40-year period from 1971 to 2010, and about 30% is stored in the ocean below 700 m. The increase in upper ocean heat content during this time period estimated from a linear trend is *likely* 17 [15 to 19] × 10²² J⁷ (see Figure SPM.3). {3.2, Box 3.1}
- It is *about as likely as not* that ocean heat content from 0–700 m increased more slowly during 2003 to 2010 than during 1993 to 2002 (see Figure SPM.3). Ocean heat uptake from 700–2000 m, where interannual variability is smaller, *likely* continued unabated from 1993 to 2009. {3.2, Box 9.2}
- It is *very likely* that regions of high salinity where evaporation dominates have become more saline, while regions of low salinity where precipitation dominates have become fresher since the 1950s. These regional trends in ocean salinity provide indirect evidence that evaporation and precipitation over the oceans have changed (*medium confidence*). {2.5, 3.3, 3.5}
- There is no observational evidence of a trend in the Atlantic Meridional Overturning Circulation (AMOC), based on the decade-long record of the complete AMOC and longer records of individual AMOC components. {3.6}

⁷ A constant supply of heat through the ocean surface at the rate of 1 W m⁻² for 1 year would increase the ocean heat content by 1.1 × 10²² J.

B.3 Cryosphere

Over the last two decades, the Greenland and Antarctic ice sheets have been losing mass, glaciers have continued to shrink almost worldwide, and Arctic sea ice and Northern Hemisphere spring snow cover have continued to decrease in extent (*high confidence*) (see Figure SPM.3). {4.2–4.7}

- The average rate of ice loss⁸ from glaciers around the world, excluding glaciers on the periphery of the ice sheets⁹, was *very likely* 226 [91 to 361] Gt yr⁻¹ over the period 1971 to 2009, and *very likely* 275 [140 to 410] Gt yr⁻¹ over the period 1993 to 2009¹⁰. {4.3}
- The average rate of ice loss from the Greenland ice sheet has *very likely* substantially increased from 34 [–6 to 74] Gt yr⁻¹ over the period 1992 to 2001 to 215 [157 to 274] Gt yr⁻¹ over the period 2002 to 2011. {4.4}
- The average rate of ice loss from the Antarctic ice sheet has *likely* increased from 30 [–37 to 97] Gt yr⁻¹ over the period 1992–2001 to 147 [72 to 221] Gt yr⁻¹ over the period 2002 to 2011. There is *very high confidence* that these losses are mainly from the northern Antarctic Peninsula and the Amundsen Sea sector of West Antarctica. {4.4}
- The annual mean Arctic sea ice extent decreased over the period 1979 to 2012 with a rate that was *very likely* in the range 3.5 to 4.1% per decade (range of 0.45 to 0.51 million km² per decade), and *very likely* in the range 9.4 to 13.6% per decade (range of 0.73 to 1.07 million km² per decade) for the summer sea ice minimum (perennial sea ice). The average decrease in decadal mean extent of Arctic sea ice has been most rapid in summer (*high confidence*); the spatial extent has decreased in every season, and in every successive decade since 1979 (*high confidence*) (see Figure SPM.3). There is *medium confidence* from reconstructions that over the past three decades, Arctic summer sea ice retreat was unprecedented and sea surface temperatures were anomalously high in at least the last 1,450 years. {4.2, 5.5}
- It is *very likely* that the annual mean Antarctic sea ice extent increased at a rate in the range of 1.2 to 1.8% per decade (range of 0.13 to 0.20 million km² per decade) between 1979 and 2012. There is *high confidence* that there are strong regional differences in this annual rate, with extent increasing in some regions and decreasing in others. {4.2}
- There is *very high confidence* that the extent of Northern Hemisphere snow cover has decreased since the mid-20th century (see Figure SPM.3). Northern Hemisphere snow cover extent decreased 1.6 [0.8 to 2.4] % per decade for March and April, and 11.7 [8.8 to 14.6] % per decade for June, over the 1967 to 2012 period. During this period, snow cover extent in the Northern Hemisphere did not show a statistically significant increase in any month. {4.5}
- There is *high confidence* that permafrost temperatures have increased in most regions since the early 1980s. Observed warming was up to 3°C in parts of Northern Alaska (early 1980s to mid-2000s) and up to 2°C in parts of the Russian European North (1971 to 2010). In the latter region, a considerable reduction in permafrost thickness and areal extent has been observed over the period 1975 to 2005 (*medium confidence*). {4.7}
- Multiple lines of evidence support very substantial Arctic warming since the mid-20th century. {Box 5.1, 10.3}

⁸ All references to 'ice loss' or 'mass loss' refer to net ice loss, i.e., accumulation minus melt and iceberg calving.

⁹ For methodological reasons, this assessment of ice loss from the Antarctic and Greenland ice sheets includes change in the glaciers on the periphery. These peripheral glaciers are thus excluded from the values given for glaciers.

¹⁰ 100 Gt yr⁻¹ of ice loss is equivalent to about 0.28 mm yr⁻¹ of global mean sea level rise.

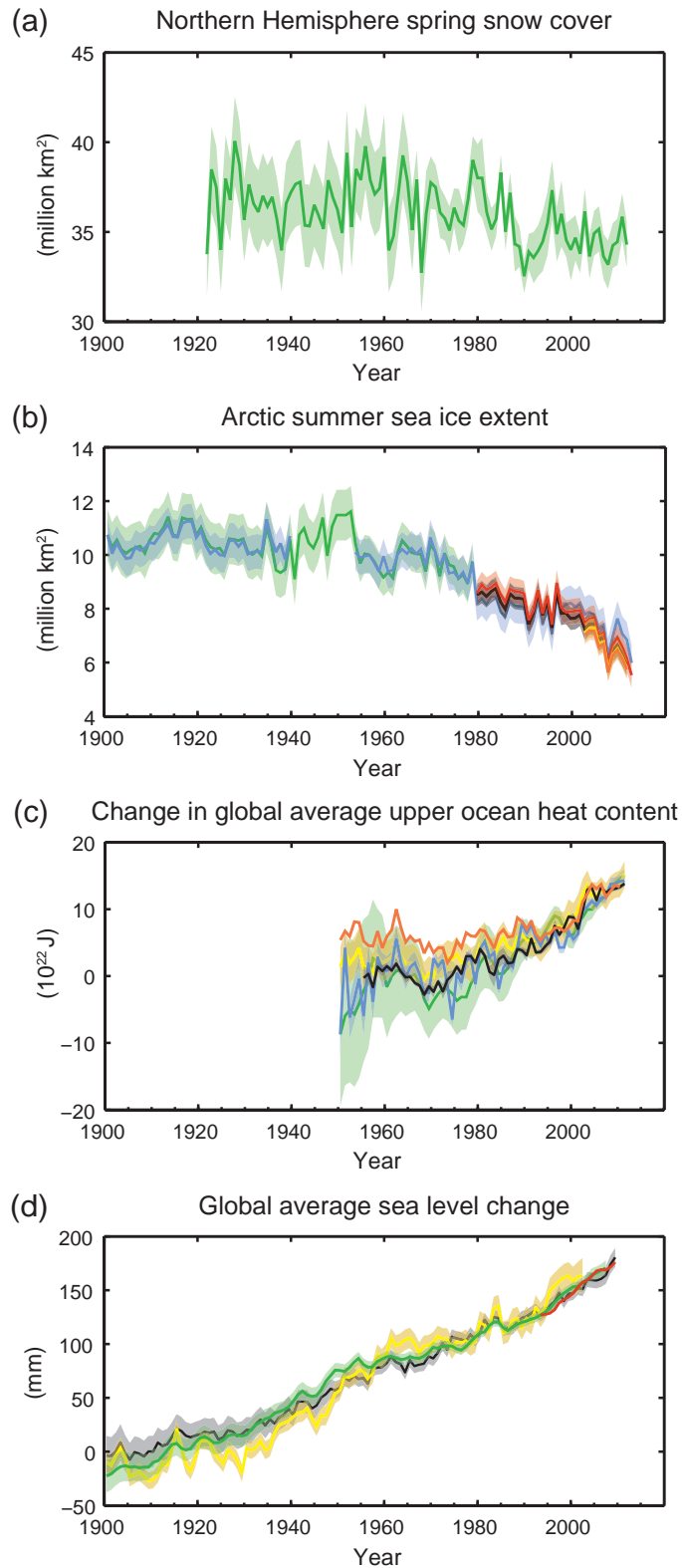


Figure SPM.3 | Multiple observed indicators of a changing global climate: (a) Extent of Northern Hemisphere March–April (spring) average snow cover; (b) extent of Arctic July–August–September (summer) average sea ice; (c) change in global mean upper ocean (0–700 m) heat content aligned to 2006–2010, and relative to the mean of all datasets for 1970; (d) global mean sea level relative to the 1900–1905 mean of the longest running dataset, and with all datasets aligned to have the same value in 1993, the first year of satellite altimetry data. All time-series (coloured lines indicating different data sets) show annual values, and where assessed, uncertainties are indicated by coloured shading. See Technical Summary Supplementary Material for a listing of the datasets. {Figures 3.2, 3.13, 4.19, and 4.3; FAQ 2.1, Figure 2; Figure TS.1}

B.4 Sea Level

The rate of sea level rise since the mid-19th century has been larger than the mean rate during the previous two millennia (*high confidence*). Over the period 1901 to 2010, global mean sea level rose by 0.19 [0.17 to 0.21] m (see Figure SPM.3). {3.7, 5.6, 13.2}

- Proxy and instrumental sea level data indicate a transition in the late 19th to the early 20th century from relatively low mean rates of rise over the previous two millennia to higher rates of rise (*high confidence*). It is *likely* that the rate of global mean sea level rise has continued to increase since the early 20th century. {3.7, 5.6, 13.2}
- It is *very likely* that the mean rate of global averaged sea level rise was 1.7 [1.5 to 1.9] mm yr⁻¹ between 1901 and 2010, 2.0 [1.7 to 2.3] mm yr⁻¹ between 1971 and 2010, and 3.2 [2.8 to 3.6] mm yr⁻¹ between 1993 and 2010. Tide-gauge and satellite altimeter data are consistent regarding the higher rate of the latter period. It is *likely* that similarly high rates occurred between 1920 and 1950. {3.7}
- Since the early 1970s, glacier mass loss and ocean thermal expansion from warming together explain about 75% of the observed global mean sea level rise (*high confidence*). Over the period 1993 to 2010, global mean sea level rise is, with *high confidence*, consistent with the sum of the observed contributions from ocean thermal expansion due to warming (1.1 [0.8 to 1.4] mm yr⁻¹), from changes in glaciers (0.76 [0.39 to 1.13] mm yr⁻¹), Greenland ice sheet (0.33 [0.25 to 0.41] mm yr⁻¹), Antarctic ice sheet (0.27 [0.16 to 0.38] mm yr⁻¹), and land water storage (0.38 [0.26 to 0.49] mm yr⁻¹). The sum of these contributions is 2.8 [2.3 to 3.4] mm yr⁻¹. {13.3}
- There is *very high confidence* that maximum global mean sea level during the last interglacial period (129,000 to 116,000 years ago) was, for several thousand years, at least 5 m higher than present, and *high confidence* that it did not exceed 10 m above present. During the last interglacial period, the Greenland ice sheet *very likely* contributed between 1.4 and 4.3 m to the higher global mean sea level, implying with *medium confidence* an additional contribution from the Antarctic ice sheet. This change in sea level occurred in the context of different orbital forcing and with high-latitude surface temperature, averaged over several thousand years, at least 2°C warmer than present (*high confidence*). {5.3, 5.6}

B.5 Carbon and Other Biogeochemical Cycles

The atmospheric concentrations of carbon dioxide, methane, and nitrous oxide have increased to levels unprecedented in at least the last 800,000 years. Carbon dioxide concentrations have increased by 40% since pre-industrial times, primarily from fossil fuel emissions and secondarily from net land use change emissions. The ocean has absorbed about 30% of the emitted anthropogenic carbon dioxide, causing ocean acidification (see Figure SPM.4). {2.2, 3.8, 5.2, 6.2, 6.3}

- The atmospheric concentrations of the greenhouse gases carbon dioxide (CO₂), methane (CH₄), and nitrous oxide (N₂O) have all increased since 1750 due to human activity. In 2011 the concentrations of these greenhouse gases were 391 ppm¹¹, 1803 ppb, and 324 ppb, and exceeded the pre-industrial levels by about 40%, 150%, and 20%, respectively. {2.2, 5.2, 6.1, 6.2}
- Concentrations of CO₂, CH₄, and N₂O now substantially exceed the highest concentrations recorded in ice cores during the past 800,000 years. The mean rates of increase in atmospheric concentrations over the past century are, with *very high confidence*, unprecedented in the last 22,000 years. {5.2, 6.1, 6.2}

¹¹ ppm (parts per million) or ppb (parts per billion, 1 billion = 1,000 million) is the ratio of the number of gas molecules to the total number of molecules of dry air. For example, 300 ppm means 300 molecules of a gas per million molecules of dry air.

- Annual CO₂ emissions from fossil fuel combustion and cement production were 8.3 [7.6 to 9.0] GtC¹² yr⁻¹ averaged over 2002–2011 (*high confidence*) and were 9.5 [8.7 to 10.3] GtC yr⁻¹ in 2011, 54% above the 1990 level. Annual net CO₂ emissions from anthropogenic land use change were 0.9 [0.1 to 1.7] GtC yr⁻¹ on average during 2002 to 2011 (*medium confidence*). {6.3}
- From 1750 to 2011, CO₂ emissions from fossil fuel combustion and cement production have released 375 [345 to 405] GtC to the atmosphere, while deforestation and other land use change are estimated to have released 180 [100 to 260] GtC. This results in cumulative anthropogenic emissions of 555 [470 to 640] GtC. {6.3}
- Of these cumulative anthropogenic CO₂ emissions, 240 [230 to 250] GtC have accumulated in the atmosphere, 155 [125 to 185] GtC have been taken up by the ocean and 160 [70 to 250] GtC have accumulated in natural terrestrial ecosystems (i.e., the cumulative residual land sink). {Figure TS.4, 3.8, 6.3}
- Ocean acidification is quantified by decreases in pH¹³. The pH of ocean surface water has decreased by 0.1 since the beginning of the industrial era (*high confidence*), corresponding to a 26% increase in hydrogen ion concentration (see Figure SPM.4). {3.8, Box 3.2}

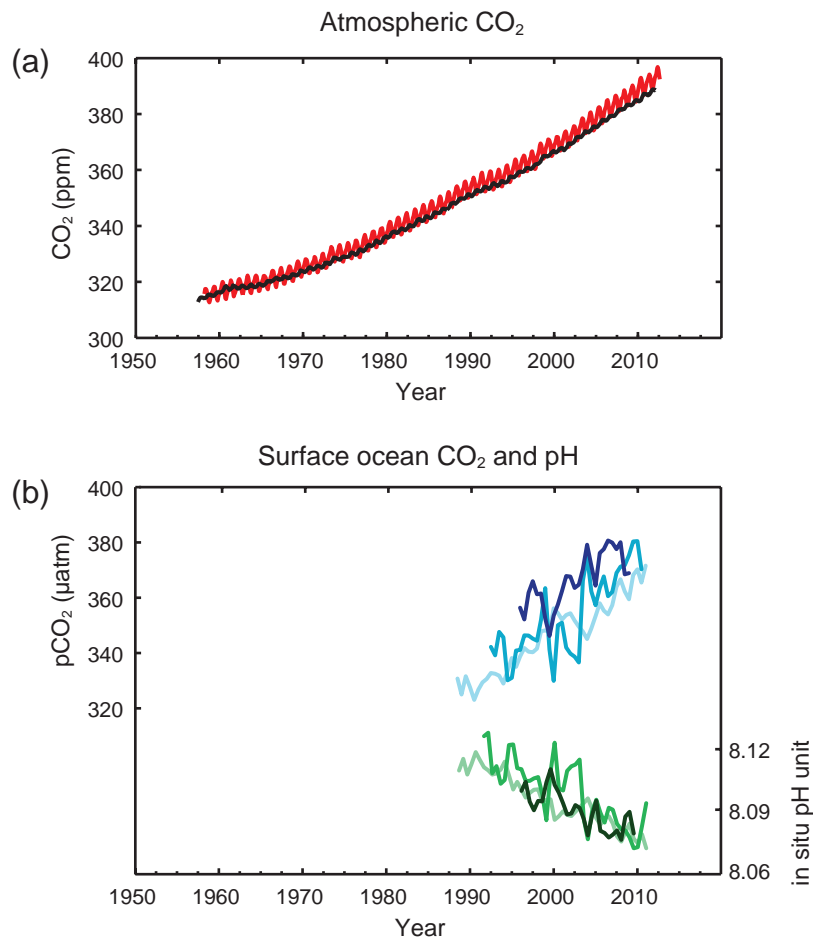


Figure SPM.4 | Multiple observed indicators of a changing global carbon cycle: (a) atmospheric concentrations of carbon dioxide (CO₂) from Mauna Loa (19°32'N, 155°34'W – red) and South Pole (89°59'S, 24°48'W – black) since 1958; (b) partial pressure of dissolved CO₂ at the ocean surface (blue curves) and in situ pH (green curves), a measure of the acidity of ocean water. Measurements are from three stations from the Atlantic (29°10'N, 15°30'W – dark blue/dark green; 31°40'N, 64°10'W – blue/green) and the Pacific Oceans (22°45'N, 158°00'W – light blue/light green). Full details of the datasets shown here are provided in the underlying report and the Technical Summary Supplementary Material. {Figures 2.1 and 3.18; Figure TS.5}

¹² 1 Gigatonne of carbon = 1 GtC = 10¹⁵ grams of carbon. This corresponds to 3.667 GtCO₂.

¹³ pH is a measure of acidity using a logarithmic scale: a pH decrease of 1 unit corresponds to a 10-fold increase in hydrogen ion concentration, or acidity.

C. Drivers of Climate Change

Natural and anthropogenic substances and processes that alter the Earth's energy budget are drivers of climate change. Radiative forcing¹⁴ (RF) quantifies the change in energy fluxes caused by changes in these drivers for 2011 relative to 1750, unless otherwise indicated. Positive RF leads to surface warming, negative RF leads to surface cooling. RF is estimated based on in-situ and remote observations, properties of greenhouse gases and aerosols, and calculations using numerical models representing observed processes. Some emitted compounds affect the atmospheric concentration of other substances. The RF can be reported based on the concentration changes of each substance¹⁵. Alternatively, the emission-based RF of a compound can be reported, which provides a more direct link to human activities. It includes contributions from all substances affected by that emission. The total anthropogenic RF of the two approaches are identical when considering all drivers. Though both approaches are used in this Summary for Policymakers, emission-based RFs are emphasized.

Total radiative forcing is positive, and has led to an uptake of energy by the climate system. The largest contribution to total radiative forcing is caused by the increase in the atmospheric concentration of CO₂ since 1750 (see Figure SPM.5). {3.2, Box 3.1, 8.3, 8.5}

- The total anthropogenic RF for 2011 relative to 1750 is 2.29 [1.13 to 3.33] W m⁻² (see Figure SPM.5), and it has increased more rapidly since 1970 than during prior decades. The total anthropogenic RF best estimate for 2011 is 43% higher than that reported in AR4 for the year 2005. This is caused by a combination of continued growth in most greenhouse gas concentrations and improved estimates of RF by aerosols indicating a weaker net cooling effect (negative RF). {8.5}
- The RF from emissions of well-mixed greenhouse gases (CO₂, CH₄, N₂O, and Halocarbons) for 2011 relative to 1750 is 3.00 [2.22 to 3.78] W m⁻² (see Figure SPM.5). The RF from changes in concentrations in these gases is 2.83 [2.26 to 3.40] W m⁻². {8.5}
- Emissions of CO₂ alone have caused an RF of 1.68 [1.33 to 2.03] W m⁻² (see Figure SPM.5). Including emissions of other carbon-containing gases, which also contributed to the increase in CO₂ concentrations, the RF of CO₂ is 1.82 [1.46 to 2.18] W m⁻². {8.3, 8.5}
- Emissions of CH₄ alone have caused an RF of 0.97 [0.74 to 1.20] W m⁻² (see Figure SPM.5). This is much larger than the concentration-based estimate of 0.48 [0.38 to 0.58] W m⁻² (unchanged from AR4). This difference in estimates is caused by concentration changes in ozone and stratospheric water vapour due to CH₄ emissions and other emissions indirectly affecting CH₄. {8.3, 8.5}
- Emissions of stratospheric ozone-depleting halocarbons have caused a net positive RF of 0.18 [0.01 to 0.35] W m⁻² (see Figure SPM.5). Their own positive RF has outweighed the negative RF from the ozone depletion that they have induced. The positive RF from all halocarbons is similar to the value in AR4, with a reduced RF from CFCs but increases from many of their substitutes. {8.3, 8.5}
- Emissions of short-lived gases contribute to the total anthropogenic RF. Emissions of carbon monoxide (CO) are *virtually certain* to have induced a positive RF, while emissions of nitrogen oxides (NO_x) are *likely* to have induced a net negative RF (see Figure SPM.5). {8.3, 8.5}
- The RF of the total aerosol effect in the atmosphere, which includes cloud adjustments due to aerosols, is -0.9 [-1.9 to -0.1] W m⁻² (*medium confidence*), and results from a negative forcing from most aerosols and a positive contribution

¹⁴ The strength of drivers is quantified as Radiative Forcing (RF) in units watts per square metre (W m⁻²) as in previous IPCC assessments. RF is the change in energy flux caused by a driver, and is calculated at the tropopause or at the top of the atmosphere. In the traditional RF concept employed in previous IPCC reports all surface and tropospheric conditions are kept fixed. In calculations of RF for well-mixed greenhouse gases and aerosols in this report, physical variables, except for the ocean and sea ice, are allowed to respond to perturbations with rapid adjustments. The resulting forcing is called Effective Radiative Forcing (ERF) in the underlying report. This change reflects the scientific progress from previous assessments and results in a better indication of the eventual temperature response for these drivers. For all drivers other than well-mixed greenhouse gases and aerosols, rapid adjustments are less well characterized and assumed to be small, and thus the traditional RF is used. {8.1}

¹⁵ This approach was used to report RF in the AR4 Summary for Policymakers.

from black carbon absorption of solar radiation. There is *high confidence* that aerosols and their interactions with clouds have offset a substantial portion of global mean forcing from well-mixed greenhouse gases. They continue to contribute the largest uncertainty to the total RF estimate. {7.5, 8.3, 8.5}

- The forcing from stratospheric volcanic aerosols can have a large impact on the climate for some years after volcanic eruptions. Several small eruptions have caused an RF of -0.11 [-0.15 to -0.08] W m^{-2} for the years 2008 to 2011, which is approximately twice as strong as during the years 1999 to 2002. {8.4}
- The RF due to changes in solar irradiance is estimated as 0.05 [0.00 to 0.10] W m^{-2} (see Figure SPM.5). Satellite observations of total solar irradiance changes from 1978 to 2011 indicate that the last solar minimum was lower than the previous two. This results in an RF of -0.04 [-0.08 to 0.00] W m^{-2} between the most recent minimum in 2008 and the 1986 minimum. {8.4}
- The total natural RF from solar irradiance changes and stratospheric volcanic aerosols made only a small contribution to the net radiative forcing throughout the last century, except for brief periods after large volcanic eruptions. {8.5}

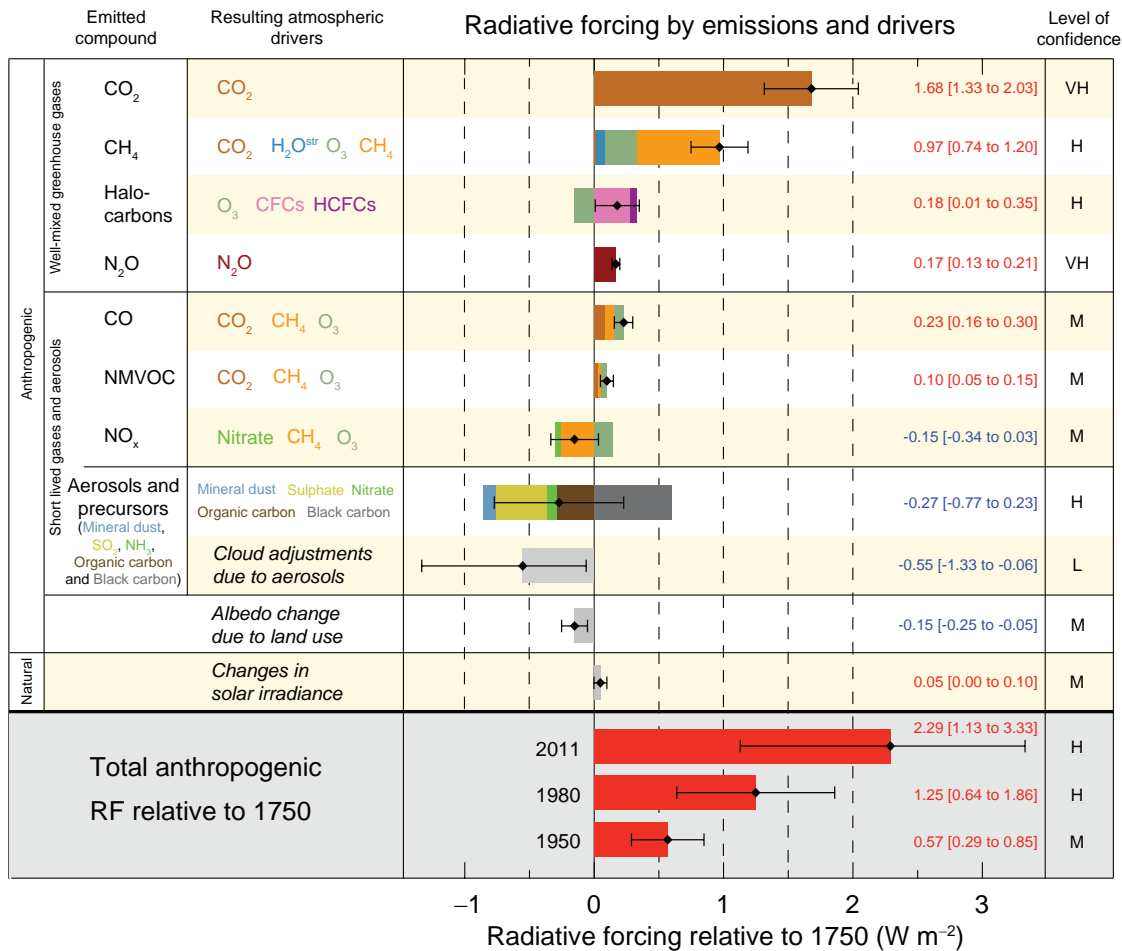


Figure SPM.5 | Radiative forcing estimates in 2011 relative to 1750 and aggregated uncertainties for the main drivers of climate change. Values are global average radiative forcing (RF¹⁴), partitioned according to the emitted compounds or processes that result in a combination of drivers. The best estimates of the net radiative forcing are shown as black diamonds with corresponding uncertainty intervals; the numerical values are provided on the right of the figure, together with the confidence level in the net forcing (VH – very high, H – high, M – medium, L – low, VL – very low). Albedo forcing due to black carbon on snow and ice is included in the black carbon aerosol bar. Small forcings due to contrails (0.05 W m^{-2} , including contrail induced cirrus), and HFCs, PFCs and SF₆ (total 0.03 W m^{-2}) are not shown. Concentration-based RFs for gases can be obtained by summing the like-coloured bars. Volcanic forcing is not included as its episodic nature makes it difficult to compare to other forcing mechanisms. Total anthropogenic radiative forcing is provided for three different years relative to 1750. For further technical details, including uncertainty ranges associated with individual components and processes, see the Technical Summary Supplementary Material. {8.5; Figures 8.14–8.18; Figures TS.6 and TS.7}

D. Understanding the Climate System and its Recent Changes

Understanding recent changes in the climate system results from combining observations, studies of feedback processes, and model simulations. Evaluation of the ability of climate models to simulate recent changes requires consideration of the state of all modelled climate system components at the start of the simulation and the natural and anthropogenic forcing used to drive the models. Compared to AR4, more detailed and longer observations and improved climate models now enable the attribution of a human contribution to detected changes in more climate system components.

Human influence on the climate system is clear. This is evident from the increasing greenhouse gas concentrations in the atmosphere, positive radiative forcing, observed warming, and understanding of the climate system. {2–14}

D.1 Evaluation of Climate Models

Climate models have improved since the AR4. Models reproduce observed continental-scale surface temperature patterns and trends over many decades, including the more rapid warming since the mid-20th century and the cooling immediately following large volcanic eruptions (*very high confidence*). {9.4, 9.6, 9.8}

- The long-term climate model simulations show a trend in global-mean surface temperature from 1951 to 2012 that agrees with the observed trend (*very high confidence*). There are, however, differences between simulated and observed trends over periods as short as 10 to 15 years (e.g., 1998 to 2012). {9.4, Box 9.2}
- The observed reduction in surface warming trend over the period 1998 to 2012 as compared to the period 1951 to 2012, is due in roughly equal measure to a reduced trend in radiative forcing and a cooling contribution from natural internal variability, which includes a possible redistribution of heat within the ocean (*medium confidence*). The reduced trend in radiative forcing is primarily due to volcanic eruptions and the timing of the downward phase of the 11-year solar cycle. However, there is *low confidence* in quantifying the role of changes in radiative forcing in causing the reduced warming trend. There is *medium confidence* that natural internal decadal variability causes to a substantial degree the difference between observations and the simulations; the latter are not expected to reproduce the timing of natural internal variability. There may also be a contribution from forcing inadequacies and, in some models, an overestimate of the response to increasing greenhouse gas and other anthropogenic forcing (dominated by the effects of aerosols). {9.4, Box 9.2, 10.3, Box 10.2, 11.3}
- On regional scales, the confidence in model capability to simulate surface temperature is less than for the larger scales. However, there is *high confidence* that regional-scale surface temperature is better simulated than at the time of the AR4. {9.4, 9.6}
- There has been substantial progress in the assessment of extreme weather and climate events since AR4. Simulated global-mean trends in the frequency of extreme warm and cold days and nights over the second half of the 20th century are generally consistent with observations. {9.5}
- There has been some improvement in the simulation of continental-scale patterns of precipitation since the AR4. At regional scales, precipitation is not simulated as well, and the assessment is hampered by observational uncertainties. {9.4, 9.6}
- Some important climate phenomena are now better reproduced by models. There is *high confidence* that the statistics of monsoon and El Niño-Southern Oscillation (ENSO) based on multi-model simulations have improved since AR4. {9.5}

- Climate models now include more cloud and aerosol processes, and their interactions, than at the time of the AR4, but there remains *low confidence* in the representation and quantification of these processes in models. {7.3, 7.6, 9.4, 9.7}
- There is robust evidence that the downward trend in Arctic summer sea ice extent since 1979 is now reproduced by more models than at the time of the AR4, with about one-quarter of the models showing a trend as large as, or larger than, the trend in the observations. Most models simulate a small downward trend in Antarctic sea ice extent, albeit with large inter-model spread, in contrast to the small upward trend in observations. {9.4}
- Many models reproduce the observed changes in upper-ocean heat content (0–700 m) from 1961 to 2005 (*high confidence*), with the multi-model mean time series falling within the range of the available observational estimates for most of the period. {9.4}
- Climate models that include the carbon cycle (Earth System Models) simulate the global pattern of ocean-atmosphere CO₂ fluxes, with outgassing in the tropics and uptake in the mid and high latitudes. In the majority of these models the sizes of the simulated global land and ocean carbon sinks over the latter part of the 20th century are within the range of observational estimates. {9.4}

D.2 Quantification of Climate System Responses

Observational and model studies of temperature change, climate feedbacks and changes in the Earth's energy budget together provide confidence in the magnitude of global warming in response to past and future forcing. {Box 12.2, Box 13.1}

- The net feedback from the combined effect of changes in water vapour, and differences between atmospheric and surface warming is *extremely likely* positive and therefore amplifies changes in climate. The net radiative feedback due to all cloud types combined is *likely* positive. Uncertainty in the sign and magnitude of the cloud feedback is due primarily to continuing uncertainty in the impact of warming on low clouds. {7.2}
- The equilibrium climate sensitivity quantifies the response of the climate system to constant radiative forcing on multi-century time scales. It is defined as the change in global mean surface temperature at equilibrium that is caused by a doubling of the atmospheric CO₂ concentration. Equilibrium climate sensitivity is *likely* in the range 1.5°C to 4.5°C (*high confidence*), *extremely unlikely* less than 1°C (*high confidence*), and *very unlikely* greater than 6°C (*medium confidence*)¹⁶. The lower temperature limit of the assessed *likely* range is thus less than the 2°C in the AR4, but the upper limit is the same. This assessment reflects improved understanding, the extended temperature record in the atmosphere and ocean, and new estimates of radiative forcing. {TS TFE.6, Figure 1; Box 12.2}
- The rate and magnitude of global climate change is determined by radiative forcing, climate feedbacks and the storage of energy by the climate system. Estimates of these quantities for recent decades are consistent with the assessed *likely* range of the equilibrium climate sensitivity to within assessed uncertainties, providing strong evidence for our understanding of anthropogenic climate change. {Box 12.2, Box 13.1}
- The transient climate response quantifies the response of the climate system to an increasing radiative forcing on a decadal to century timescale. It is defined as the change in global mean surface temperature at the time when the atmospheric CO₂ concentration has doubled in a scenario of concentration increasing at 1% per year. The transient climate response is *likely* in the range of 1.0°C to 2.5°C (*high confidence*) and *extremely unlikely* greater than 3°C. {Box 12.2}
- A related quantity is the transient climate response to cumulative carbon emissions (TCRE). It quantifies the transient response of the climate system to cumulative carbon emissions (see Section E.8). TCRE is defined as the global mean

¹⁶ No best estimate for equilibrium climate sensitivity can now be given because of a lack of agreement on values across assessed lines of evidence and studies.

surface temperature change per 1000 GtC emitted to the atmosphere. TCRE is *likely* in the range of 0.8°C to 2.5°C per 1000 GtC and applies for cumulative emissions up to about 2000 GtC until the time temperatures peak (see Figure SPM.10). {12.5, Box 12.2}

- Various metrics can be used to compare the contributions to climate change of emissions of different substances. The most appropriate metric and time horizon will depend on which aspects of climate change are considered most important to a particular application. No single metric can accurately compare all consequences of different emissions, and all have limitations and uncertainties. The Global Warming Potential is based on the cumulative radiative forcing over a particular time horizon, and the Global Temperature Change Potential is based on the change in global mean surface temperature at a chosen point in time. Updated values are provided in the underlying Report. {8.7}

D.3 Detection and Attribution of Climate Change

Human influence has been detected in warming of the atmosphere and the ocean, in changes in the global water cycle, in reductions in snow and ice, in global mean sea level rise, and in changes in some climate extremes (see Figure SPM.6 and Table SPM.1). This evidence for human influence has grown since AR4. It is *extremely likely* that human influence has been the dominant cause of the observed warming since the mid-20th century. {10.3–10.6, 10.9}

- It is *extremely likely* that more than half of the observed increase in global average surface temperature from 1951 to 2010 was caused by the anthropogenic increase in greenhouse gas concentrations and other anthropogenic forcings together. The best estimate of the human-induced contribution to warming is similar to the observed warming over this period. {10.3}
- Greenhouse gases contributed a global mean surface warming *likely* to be in the range of 0.5°C to 1.3°C over the period 1951 to 2010, with the contributions from other anthropogenic forcings, including the cooling effect of aerosols, *likely* to be in the range of –0.6°C to 0.1°C. The contribution from natural forcings is *likely* to be in the range of –0.1°C to 0.1°C, and from natural internal variability is *likely* to be in the range of –0.1°C to 0.1°C. Together these assessed contributions are consistent with the observed warming of approximately 0.6°C to 0.7°C over this period. {10.3}
- Over every continental region except Antarctica, anthropogenic forcings have *likely* made a substantial contribution to surface temperature increases since the mid-20th century (see Figure SPM.6). For Antarctica, large observational uncertainties result in *low confidence* that anthropogenic forcings have contributed to the observed warming averaged over available stations. It is *likely* that there has been an anthropogenic contribution to the very substantial Arctic warming since the mid-20th century. {2.4, 10.3}
- It is *very likely* that anthropogenic influence, particularly greenhouse gases and stratospheric ozone depletion, has led to a detectable observed pattern of tropospheric warming and a corresponding cooling in the lower stratosphere since 1961. {2.4, 9.4, 10.3}
- It is *very likely* that anthropogenic forcings have made a substantial contribution to increases in global upper ocean heat content (0–700 m) observed since the 1970s (see Figure SPM.6). There is evidence for human influence in some individual ocean basins. {3.2, 10.4}
- It is *likely* that anthropogenic influences have affected the global water cycle since 1960. Anthropogenic influences have contributed to observed increases in atmospheric moisture content in the atmosphere (*medium confidence*), to global-scale changes in precipitation patterns over land (*medium confidence*), to intensification of heavy precipitation over land regions where data are sufficient (*medium confidence*), and to changes in surface and sub-surface ocean salinity (*very likely*). {2.5, 2.6, 3.3, 7.6, 10.3, 10.4}

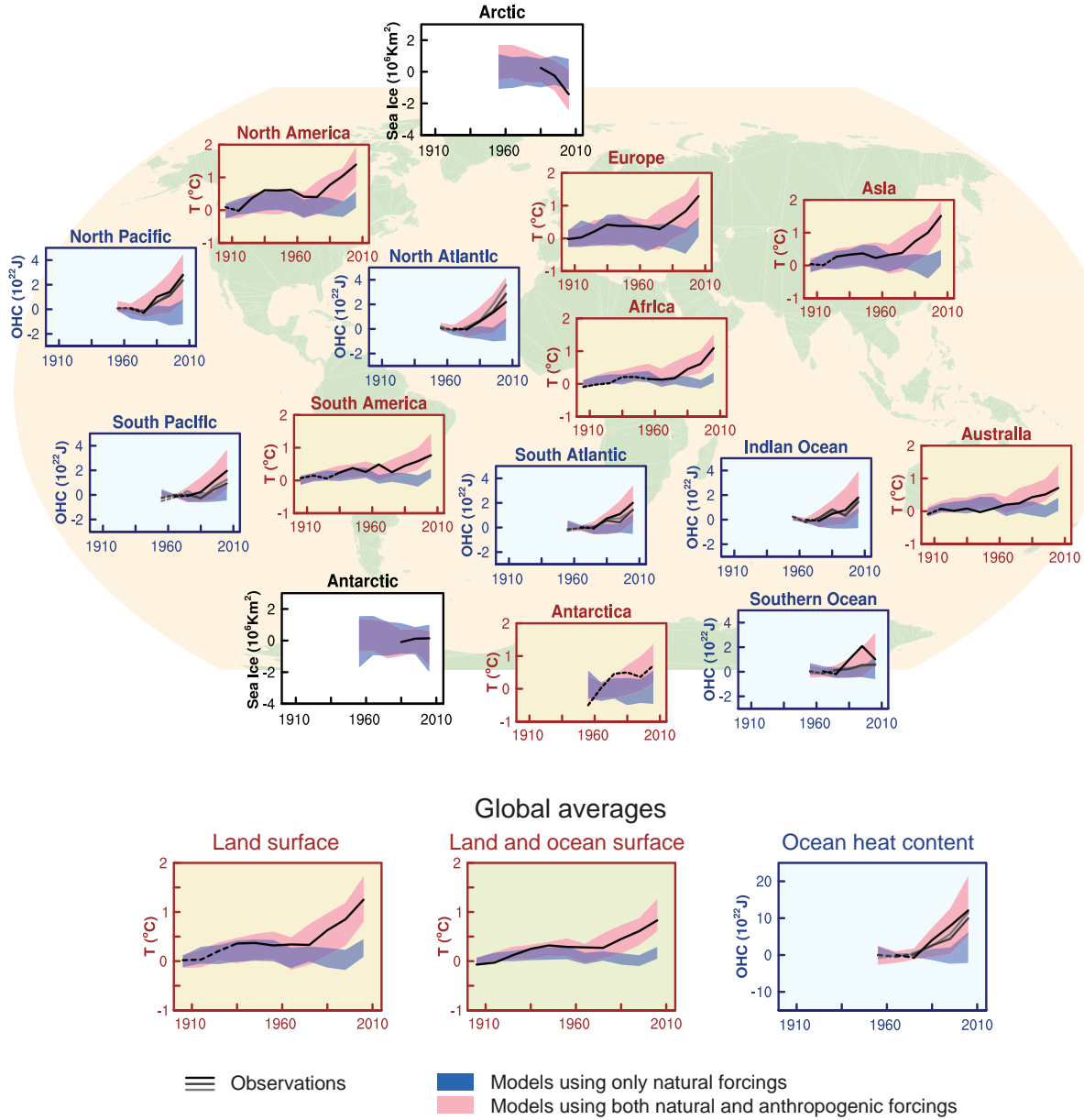


Figure SPM.6 | Comparison of observed and simulated climate change based on three large-scale indicators in the atmosphere, the cryosphere and the ocean: change in continental land surface air temperatures (yellow panels), Arctic and Antarctic September sea ice extent (white panels), and upper ocean heat content in the major ocean basins (blue panels). Global average changes are also given. Anomalies are given relative to 1880–1919 for surface temperatures, 1960–1980 for ocean heat content and 1979–1999 for sea ice. All time-series are decadal averages, plotted at the centre of the decade. For temperature panels, observations are dashed lines if the spatial coverage of areas being examined is below 50%. For ocean heat content and sea ice panels the solid line is where the coverage of data is good and higher in quality, and the dashed line is where the data coverage is only adequate, and thus, uncertainty is larger. Model results shown are Coupled Model Intercomparison Project Phase 5 (CMIP5) multi-model ensemble ranges, with shaded bands indicating the 5 to 95% confidence intervals. For further technical details, including region definitions see the Technical Summary Supplementary Material. {Figure 10.21; Figure TS.12}

- There has been further strengthening of the evidence for human influence on temperature extremes since the SREX. It is now *very likely* that human influence has contributed to observed global scale changes in the frequency and intensity of daily temperature extremes since the mid-20th century, and *likely* that human influence has more than doubled the probability of occurrence of heat waves in some locations (see Table SPM.1). {10.6}
- Anthropogenic influences have *very likely* contributed to Arctic sea ice loss since 1979. There is *low confidence* in the scientific understanding of the small observed increase in Antarctic sea ice extent due to the incomplete and competing scientific explanations for the causes of change and *low confidence* in estimates of natural internal variability in that region (see Figure SPM.6). {10.5}
- Anthropogenic influences *likely* contributed to the retreat of glaciers since the 1960s and to the increased surface mass loss of the Greenland ice sheet since 1993. Due to a low level of scientific understanding there is *low confidence* in attributing the causes of the observed loss of mass from the Antarctic ice sheet over the past two decades. {4.3, 10.5}
- It is *likely* that there has been an anthropogenic contribution to observed reductions in Northern Hemisphere spring snow cover since 1970. {10.5}
- It is *very likely* that there is a substantial anthropogenic contribution to the global mean sea level rise since the 1970s. This is based on the *high confidence* in an anthropogenic influence on the two largest contributions to sea level rise, that is thermal expansion and glacier mass loss. {10.4, 10.5, 13.3}
- There is *high confidence* that changes in total solar irradiance have not contributed to the increase in global mean surface temperature over the period 1986 to 2008, based on direct satellite measurements of total solar irradiance. There is *medium confidence* that the 11-year cycle of solar variability influences decadal climate fluctuations in some regions. No robust association between changes in cosmic rays and cloudiness has been identified. {7.4, 10.3, Box 10.2}

E. Future Global and Regional Climate Change

Projections of changes in the climate system are made using a hierarchy of climate models ranging from simple climate models, to models of intermediate complexity, to comprehensive climate models, and Earth System Models. These models simulate changes based on a set of scenarios of anthropogenic forcings. A new set of scenarios, the Representative Concentration Pathways (RCPs), was used for the new climate model simulations carried out under the framework of the Coupled Model Intercomparison Project Phase 5 (CMIP5) of the World Climate Research Programme. In all RCPs, atmospheric CO₂ concentrations are higher in 2100 relative to present day as a result of a further increase of cumulative emissions of CO₂ to the atmosphere during the 21st century (see Box SPM.1). Projections in this Summary for Policymakers are for the end of the 21st century (2081–2100) given relative to 1986–2005, unless otherwise stated. To place such projections in historical context, it is necessary to consider observed changes between different periods. Based on the longest global surface temperature dataset available, the observed change between the average of the period 1850–1900 and of the AR5 reference period is 0.61 [0.55 to 0.67] °C. However, warming has occurred beyond the average of the AR5 reference period. Hence this is not an estimate of historical warming to present (see Chapter 2).

Continued emissions of greenhouse gases will cause further warming and changes in all components of the climate system. Limiting climate change will require substantial and sustained reductions of greenhouse gas emissions. {6, 11–14}

- Projections for the next few decades show spatial patterns of climate change similar to those projected for the later 21st century but with smaller magnitude. Natural internal variability will continue to be a major influence on climate, particularly in the near-term and at the regional scale. By the mid-21st century the magnitudes of the projected changes are substantially affected by the choice of emissions scenario (Box SPM.1). {11.3, Box 11.1, Annex I}

- Projected climate change based on RCPs is similar to AR4 in both patterns and magnitude, after accounting for scenario differences. The overall spread of projections for the high RCPs is narrower than for comparable scenarios used in AR4 because in contrast to the SRES emission scenarios used in AR4, the RCPs used in AR5 are defined as concentration pathways and thus carbon cycle uncertainties affecting atmospheric CO₂ concentrations are not considered in the concentration-driven CMIP5 simulations. Projections of sea level rise are larger than in the AR4, primarily because of improved modelling of land-ice contributions. {11.3, 12.3, 12.4, 13.4, 13.5}

E.1 Atmosphere: Temperature

Global surface temperature change for the end of the 21st century is likely to exceed 1.5°C relative to 1850 to 1900 for all RCP scenarios except RCP2.6. It is likely to exceed 2°C for RCP6.0 and RCP8.5, and more likely than not to exceed 2°C for RCP4.5. Warming will continue beyond 2100 under all RCP scenarios except RCP2.6. Warming will continue to exhibit interannual-to-decadal variability and will not be regionally uniform (see Figures SPM.7 and SPM.8). {11.3, 12.3, 12.4, 14.8}

- The global mean surface temperature change for the period 2016–2035 relative to 1986–2005 will likely be in the range of 0.3°C to 0.7°C (*medium confidence*). This assessment is based on multiple lines of evidence and assumes there will be no major volcanic eruptions or secular changes in total solar irradiance. Relative to natural internal variability, near-term increases in seasonal mean and annual mean temperatures are expected to be larger in the tropics and subtropics than in mid-latitudes (*high confidence*). {11.3}
- Increase of global mean surface temperatures for 2081–2100 relative to 1986–2005 is projected to likely be in the ranges derived from the concentration-driven CMIP5 model simulations, that is, 0.3°C to 1.7°C (RCP2.6), 1.1°C to 2.6°C (RCP4.5), 1.4°C to 3.1°C (RCP6.0), 2.6°C to 4.8°C (RCP8.5). The Arctic region will warm more rapidly than the global mean, and mean warming over land will be larger than over the ocean (*very high confidence*) (see Figures SPM.7 and SPM.8, and Table SPM.2). {12.4, 14.8}
- Relative to the average from year 1850 to 1900, global surface temperature change by the end of the 21st century is projected to likely exceed 1.5°C for RCP4.5, RCP6.0 and RCP8.5 (*high confidence*). Warming is likely to exceed 2°C for RCP6.0 and RCP8.5 (*high confidence*), more likely than not to exceed 2°C for RCP4.5 (*high confidence*), but unlikely to exceed 2°C for RCP2.6 (*medium confidence*). Warming is unlikely to exceed 4°C for RCP2.6, RCP4.5 and RCP6.0 (*high confidence*) and is about as likely as not to exceed 4°C for RCP8.5 (*medium confidence*). {12.4}
- It is *virtually certain* that there will be more frequent hot and fewer cold temperature extremes over most land areas on daily and seasonal timescales as global mean temperatures increase. It is *very likely* that heat waves will occur with a higher frequency and duration. Occasional cold winter extremes will continue to occur (see Table SPM.1). {12.4}

E.2 Atmosphere: Water Cycle

Changes in the global water cycle in response to the warming over the 21st century will not be uniform. The contrast in precipitation between wet and dry regions and between wet and dry seasons will increase, although there may be regional exceptions (see Figure SPM.8). {12.4, 14.3}

- Projected changes in the water cycle over the next few decades show similar large-scale patterns to those towards the end of the century, but with smaller magnitude. Changes in the near-term, and at the regional scale will be strongly influenced by natural internal variability and may be affected by anthropogenic aerosol emissions. {11.3}

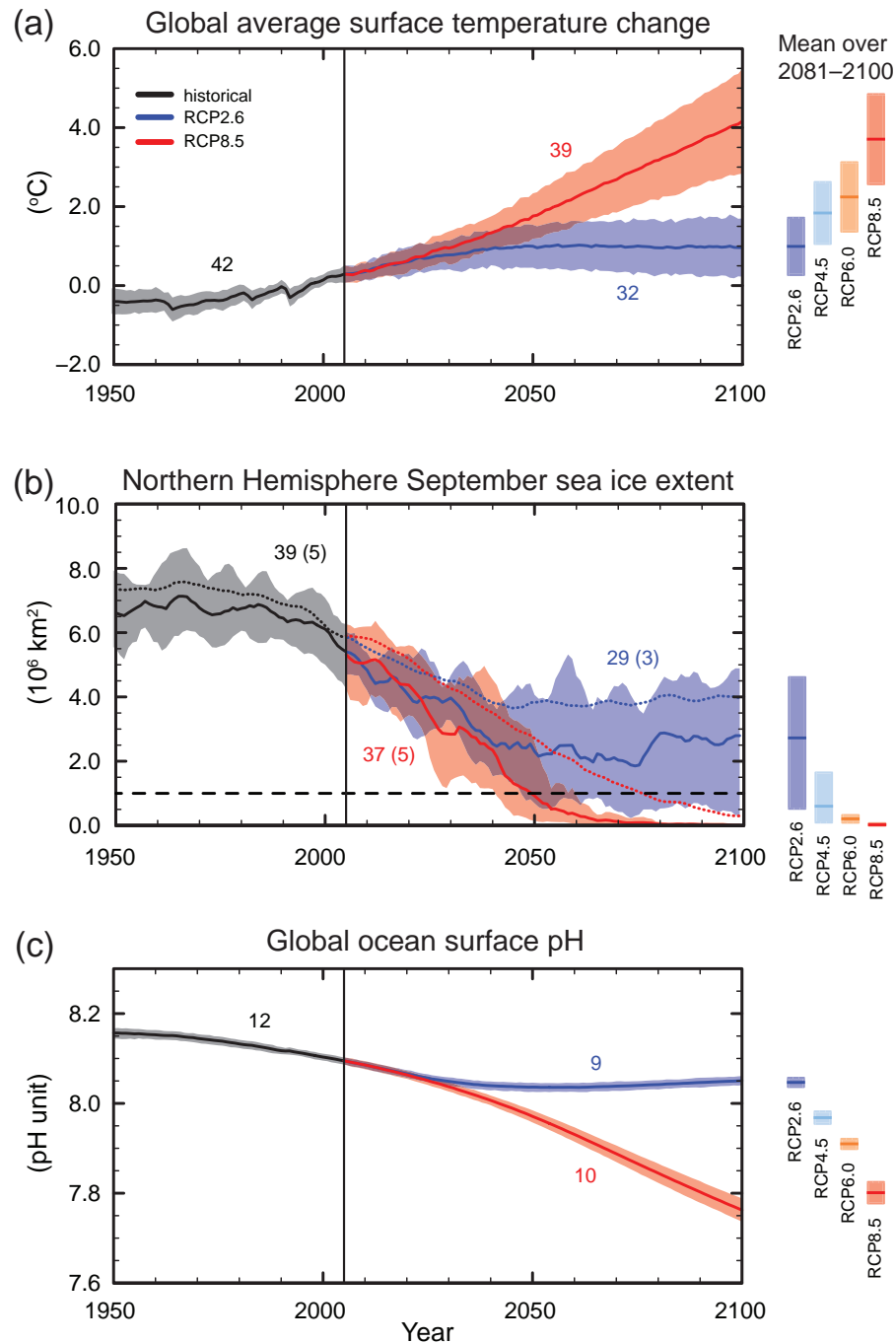


Figure SPM.7 | CMIP5 multi-model simulated time series from 1950 to 2100 for (a) change in global annual mean surface temperature relative to 1986–2005, (b) Northern Hemisphere September sea ice extent (5-year running mean), and (c) global mean ocean surface pH. Time series of projections and a measure of uncertainty (shading) are shown for scenarios RCP2.6 (blue) and RCP8.5 (red). Black (grey shading) is the modelled historical evolution using historical reconstructed forcings. The mean and associated uncertainties averaged over 2081–2100 are given for all RCP scenarios as colored vertical bars. The numbers of CMIP5 models used to calculate the multi-model mean is indicated. For sea ice extent (b), the projected mean and uncertainty (minimum-maximum range) of the subset of models that most closely reproduce the climatological mean state and 1979 to 2012 trend of the Arctic sea ice is given (number of models given in brackets). For completeness, the CMIP5 multi-model mean is also indicated with dotted lines. The dashed line represents nearly ice-free conditions (i.e., when sea ice extent is less than 10^6 km^2 for at least five consecutive years). For further technical details see the Technical Summary Supplementary Material [Figures 6.28, 12.5, and 12.28–12.31; Figures TS.15, TS.17, and TS.20]

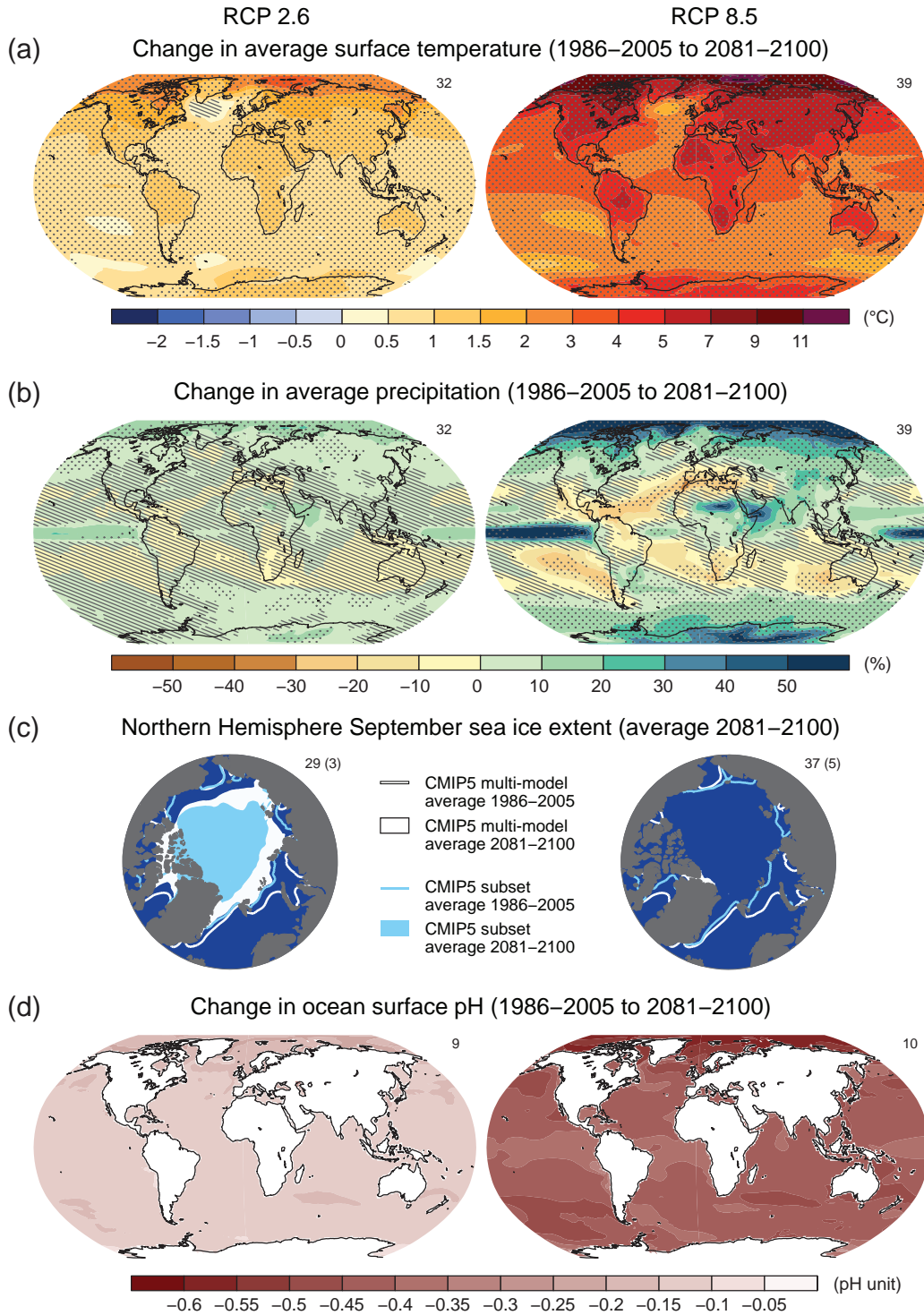


Figure SPM.8 | Maps of CMIP5 multi-model mean results for the scenarios RCP2.6 and RCP8.5 in 2081–2100 of (a) annual mean surface temperature change, (b) average percent change in annual mean precipitation, (c) Northern Hemisphere September sea ice extent, and (d) change in ocean surface pH. Changes in panels (a), (b) and (d) are shown relative to 1986–2005. The number of CMIP5 models used to calculate the multi-model mean is indicated in the upper right corner of each panel. For panels (a) and (b), hatching indicates regions where the multi-model mean is small compared to natural internal variability (i.e., less than one standard deviation of natural internal variability in 20-year means). Stippling indicates regions where the multi-model mean is large compared to natural internal variability (i.e., greater than two standard deviations of natural internal variability in 20-year means) and where at least 90% of models agree on the sign of change (see Box 12.1). In panel (c), the lines are the modelled means for 1986–2005; the filled areas are for the end of the century. The CMIP5 multi-model mean is given in white colour, the projected mean sea ice extent of a subset of models (number of models given in brackets) that most closely reproduce the climatological mean state and 1979 to 2012 trend of the Arctic sea ice extent is given in light blue colour. For further technical details see the Technical Summary Supplementary Material. {Figures 6.28, 12.11, 12.22, and 12.29; Figures TS.15, TS.16, TS.17, and TS.20}

- The high latitudes and the equatorial Pacific Ocean are *likely* to experience an increase in annual mean precipitation by the end of this century under the RCP8.5 scenario. In many mid-latitude and subtropical dry regions, mean precipitation will *likely* decrease, while in many mid-latitude wet regions, mean precipitation will *likely* increase by the end of this century under the RCP8.5 scenario (see Figure SPM.8). {7.6, 12.4, 14.3}
- Extreme precipitation events over most of the mid-latitude land masses and over wet tropical regions will *very likely* become more intense and more frequent by the end of this century, as global mean surface temperature increases (see Table SPM.1). {7.6, 12.4}
- Globally, it is *likely* that the area encompassed by monsoon systems will increase over the 21st century. While monsoon winds are *likely* to weaken, monsoon precipitation is *likely* to intensify due to the increase in atmospheric moisture. Monsoon onset dates are *likely* to become earlier or not to change much. Monsoon retreat dates will *likely* be delayed, resulting in lengthening of the monsoon season in many regions. {14.2}
- There is *high confidence* that the El Niño-Southern Oscillation (ENSO) will remain the dominant mode of interannual variability in the tropical Pacific, with global effects in the 21st century. Due to the increase in moisture availability, ENSO-related precipitation variability on regional scales will *likely* intensify. Natural variations of the amplitude and spatial pattern of ENSO are large and thus *confidence* in any specific projected change in ENSO and related regional phenomena for the 21st century remains *low*. {5.4, 14.4}

Table SPM.2 | Projected change in global mean surface air temperature and global mean sea level rise for the mid- and late 21st century relative to the reference period of 1986–2005. {12.4; Table 12.2, Table 13.5}

		2046–2065		2081–2100	
	Scenario	Mean	Likely range ^c	Mean	Likely range ^c
Global Mean Surface Temperature Change (°C)^a	RCP2.6	1.0	0.4 to 1.6	1.0	0.3 to 1.7
	RCP4.5	1.4	0.9 to 2.0	1.8	1.1 to 2.6
	RCP6.0	1.3	0.8 to 1.8	2.2	1.4 to 3.1
	RCP8.5	2.0	1.4 to 2.6	3.7	2.6 to 4.8
	Scenario	Mean	Likely range ^d	Mean	Likely range ^d
Global Mean Sea Level Rise (m)^b	RCP2.6	0.24	0.17 to 0.32	0.40	0.26 to 0.55
	RCP4.5	0.26	0.19 to 0.33	0.47	0.32 to 0.63
	RCP6.0	0.25	0.18 to 0.32	0.48	0.33 to 0.63
	RCP8.5	0.30	0.22 to 0.38	0.63	0.45 to 0.82

Notes:

^a Based on the CMIP5 ensemble; anomalies calculated with respect to 1986–2005. Using HadCRUT4 and its uncertainty estimate (5–95% confidence interval), the observed warming to the reference period 1986–2005 is 0.61 [0.55 to 0.67] °C from 1850–1900, and 0.11 [0.09 to 0.13] °C from 1980–1999, the reference period for projections used in AR4. *Likely* ranges have not been assessed here with respect to earlier reference periods because methods are not generally available in the literature for combining the uncertainties in models and observations. Adding projected and observed changes does not account for potential effects of model biases compared to observations, and for natural internal variability during the observational reference period {2.4; 11.2; Tables 12.2 and 12.3}

^b Based on 21 CMIP5 models; anomalies calculated with respect to 1986–2005. Where CMIP5 results were not available for a particular AOGCM and scenario, they were estimated as explained in Chapter 13, Table 13.5. The contributions from ice sheet rapid dynamical change and anthropogenic land water storage are treated as having uniform probability distributions, and as largely independent of scenario. This treatment does not imply that the contributions concerned will not depend on the scenario followed, only that the current state of knowledge does not permit a quantitative assessment of the dependence. Based on current understanding, only the collapse of marine-based sectors of the Antarctic ice sheet, if initiated, could cause global mean sea level to rise substantially above the *likely* range during the 21st century. There is *medium confidence* that this additional contribution would not exceed several tenths of a meter of sea level rise during the 21st century.

^c Calculated from projections as 5–95% model ranges. These ranges are then assessed to be *likely* ranges after accounting for additional uncertainties or different levels of confidence in models. For projections of global mean surface temperature change in 2046–2065 *confidence* is *medium*, because the relative importance of natural internal variability, and uncertainty in non-greenhouse gas forcing and response, are larger than for 2081–2100. The *likely* ranges for 2046–2065 do not take into account the possible influence of factors that lead to the assessed range for near-term (2016–2035) global mean surface temperature change that is lower than the 5–95% model range, because the influence of these factors on longer term projections has not been quantified due to insufficient scientific understanding. {11.3}

^d Calculated from projections as 5–95% model ranges. These ranges are then assessed to be *likely* ranges after accounting for additional uncertainties or different levels of confidence in models. For projections of global mean sea level rise *confidence* is *medium* for both time horizons.

E.3 Atmosphere: Air Quality

- The range in projections of air quality (ozone and PM_{2.5}¹⁷ in near-surface air) is driven primarily by emissions (including CH₄), rather than by physical climate change (*medium confidence*). There is *high confidence* that globally, warming decreases background surface ozone. High CH₄ levels (as in RCP8.5) can offset this decrease, raising background surface ozone by year 2100 on average by about 8 ppb (25% of current levels) relative to scenarios with small CH₄ changes (as in RCP4.5 and RCP6.0) (*high confidence*). {11.3}
- Observational and modelling evidence indicates that, all else being equal, locally higher surface temperatures in polluted regions will trigger regional feedbacks in chemistry and local emissions that will increase peak levels of ozone and PM_{2.5} (*medium confidence*). For PM_{2.5}, climate change may alter natural aerosol sources as well as removal by precipitation, but no confidence level is attached to the overall impact of climate change on PM_{2.5} distributions. {11.3}

E.4 Ocean

The global ocean will continue to warm during the 21st century. Heat will penetrate from the surface to the deep ocean and affect ocean circulation. {11.3, 12.4}

- The strongest ocean warming is projected for the surface in tropical and Northern Hemisphere subtropical regions. At greater depth the warming will be most pronounced in the Southern Ocean (*high confidence*). Best estimates of ocean warming in the top one hundred meters are about 0.6°C (RCP2.6) to 2.0°C (RCP8.5), and about 0.3°C (RCP2.6) to 0.6°C (RCP8.5) at a depth of about 1000 m by the end of the 21st century. {12.4, 14.3}
- It is *very likely* that the Atlantic Meridional Overturning Circulation (AMOC) will weaken over the 21st century. Best estimates and ranges¹⁸ for the reduction are 11% (1 to 24%) in RCP2.6 and 34% (12 to 54%) in RCP8.5. It is *likely* that there will be some decline in the AMOC by about 2050, but there may be some decades when the AMOC increases due to large natural internal variability. {11.3, 12.4}
- It is *very unlikely* that the AMOC will undergo an abrupt transition or collapse in the 21st century for the scenarios considered. There is *low confidence* in assessing the evolution of the AMOC beyond the 21st century because of the limited number of analyses and equivocal results. However, a collapse beyond the 21st century for large sustained warming cannot be excluded. {12.5}

E.5 Cryosphere

It is *very likely* that the Arctic sea ice cover will continue to shrink and thin and that Northern Hemisphere spring snow cover will decrease during the 21st century as global mean surface temperature rises. Global glacier volume will further decrease. {12.4, 13.4}

- Year-round reductions in Arctic sea ice extent are projected by the end of the 21st century from multi-model averages. These reductions range from 43% for RCP2.6 to 94% for RCP8.5 in September and from 8% for RCP2.6 to 34% for RCP8.5 in February (*medium confidence*) (see Figures SPM.7 and SPM.8). {12.4}

¹⁷ PM_{2.5} refers to particulate matter with a diameter of less than 2.5 micrometres, a measure of atmospheric aerosol concentration.

¹⁸ The ranges in this paragraph indicate a CMIP5 model spread.

- Based on an assessment of the subset of models that most closely reproduce the climatological mean state and 1979 to 2012 trend of the Arctic sea ice extent, a nearly ice-free Arctic Ocean¹⁹ in September before mid-century is *likely* for RCP8.5 (*medium confidence*) (see Figures SPM.7 and SPM.8). A projection of when the Arctic might become nearly ice-free in September in the 21st century cannot be made with confidence for the other scenarios. {11.3, 12.4, 12.5}
- In the Antarctic, a decrease in sea ice extent and volume is projected with *low confidence* for the end of the 21st century as global mean surface temperature rises. {12.4}
- By the end of the 21st century, the global glacier volume, excluding glaciers on the periphery of Antarctica, is projected to decrease by 15 to 55% for RCP2.6, and by 35 to 85% for RCP8.5 (*medium confidence*). {13.4, 13.5}
- The area of Northern Hemisphere spring snow cover is projected to decrease by 7% for RCP2.6 and by 25% in RCP8.5 by the end of the 21st century for the model average (*medium confidence*). {12.4}
- It is *virtually certain* that near-surface permafrost extent at high northern latitudes will be reduced as global mean surface temperature increases. By the end of the 21st century, the area of permafrost near the surface (upper 3.5 m) is projected to decrease by between 37% (RCP2.6) to 81% (RCP8.5) for the model average (*medium confidence*). {12.4}

E.6 Sea Level

Global mean sea level will continue to rise during the 21st century (see Figure SPM.9). Under all RCP scenarios, the rate of sea level rise will very likely exceed that observed during 1971 to 2010 due to increased ocean warming and increased loss of mass from glaciers and ice sheets. {13.3–13.5}

- Confidence in projections of global mean sea level rise has increased since the AR4 because of the improved physical understanding of the components of sea level, the improved agreement of process-based models with observations, and the inclusion of ice-sheet dynamical changes. {13.3–13.5}
- Global mean sea level rise for 2081–2100 relative to 1986–2005 will *likely* be in the ranges of 0.26 to 0.55 m for RCP2.6, 0.32 to 0.63 m for RCP4.5, 0.33 to 0.63 m for RCP6.0, and 0.45 to 0.82 m for RCP8.5 (*medium confidence*). For RCP8.5, the rise by the year 2100 is 0.52 to 0.98 m, with a rate during 2081 to 2100 of 8 to 16 mm yr⁻¹ (*medium confidence*). These ranges are derived from CMIP5 climate projections in combination with process-based models and literature assessment of glacier and ice sheet contributions (see Figure SPM.9, Table SPM.2). {13.5}
- In the RCP projections, thermal expansion accounts for 30 to 55% of 21st century global mean sea level rise, and glaciers for 15 to 35%. The increase in surface melting of the Greenland ice sheet will exceed the increase in snowfall, leading to a positive contribution from changes in surface mass balance to future sea level (*high confidence*). While surface melting will remain small, an increase in snowfall on the Antarctic ice sheet is expected (*medium confidence*), resulting in a negative contribution to future sea level from changes in surface mass balance. Changes in outflow from both ice sheets combined will *likely* make a contribution in the range of 0.03 to 0.20 m by 2081–2100 (*medium confidence*). {13.3–13.5}
- Based on current understanding, only the collapse of marine-based sectors of the Antarctic ice sheet, if initiated, could cause global mean sea level to rise substantially above the *likely* range during the 21st century. However, there is *medium confidence* that this additional contribution would not exceed several tenths of a meter of sea level rise during the 21st century. {13.4, 13.5}

¹⁹ Conditions in the Arctic Ocean are referred to as nearly ice-free when the sea ice extent is less than 10⁶ km² for at least five consecutive years.

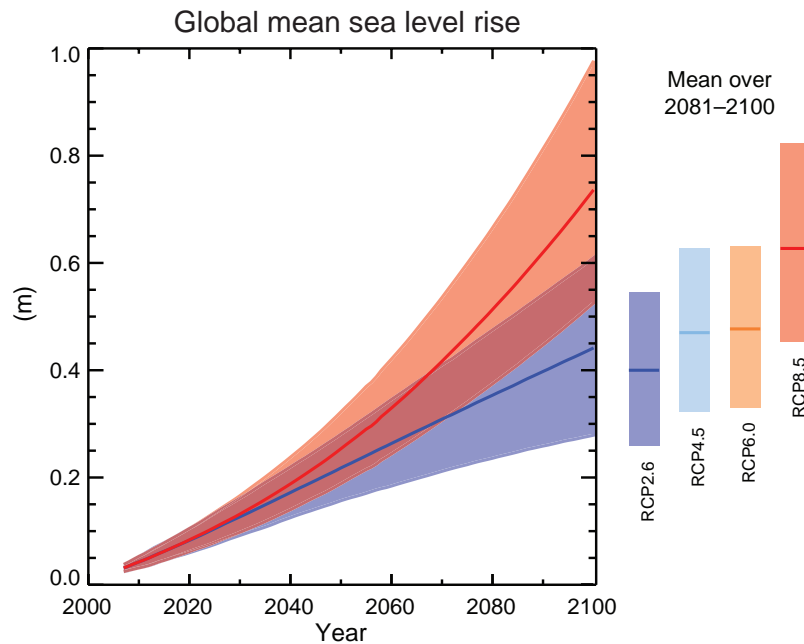


Figure SPM.9 | Projections of global mean sea level rise over the 21st century relative to 1986–2005 from the combination of the CMIP5 ensemble with process-based models, for RCP2.6 and RCP8.5. The assessed *likely* range is shown as a shaded band. The assessed *likely* ranges for the mean over the period 2081–2100 for all RCP scenarios are given as coloured vertical bars, with the corresponding median value given as a horizontal line. For further technical details see the Technical Summary Supplementary Material {Table 13.5, Figures 13.10 and 13.11; Figures TS.21 and TS.22}

- The basis for higher projections of global mean sea level rise in the 21st century has been considered and it has been concluded that there is currently insufficient evidence to evaluate the probability of specific levels above the assessed *likely* range. Many semi-empirical model projections of global mean sea level rise are higher than process-based model projections (up to about twice as large), but there is no consensus in the scientific community about their reliability and there is thus *low confidence* in their projections. {13.5}
- Sea level rise will not be uniform. By the end of the 21st century, it is *very likely* that sea level will rise in more than about 95% of the ocean area. About 70% of the coastlines worldwide are projected to experience sea level change within 20% of the global mean sea level change. {13.1, 13.6}

E.7 Carbon and Other Biogeochemical Cycles

Climate change will affect carbon cycle processes in a way that will exacerbate the increase of CO₂ in the atmosphere (*high confidence*). Further uptake of carbon by the ocean will increase ocean acidification. {6.4}

- Ocean uptake of anthropogenic CO₂ will continue under all four RCPs through to 2100, with higher uptake for higher concentration pathways (*very high confidence*). The future evolution of the land carbon uptake is less certain. A majority of models projects a continued land carbon uptake under all RCPs, but some models simulate a land carbon loss due to the combined effect of climate change and land use change. {6.4}
- Based on Earth System Models, there is *high confidence* that the feedback between climate and the carbon cycle is positive in the 21st century; that is, climate change will partially offset increases in land and ocean carbon sinks caused by rising atmospheric CO₂. As a result more of the emitted anthropogenic CO₂ will remain in the atmosphere. A positive feedback between climate and the carbon cycle on century to millennial time scales is supported by paleoclimate observations and modelling. {6.2, 6.4}

Table SPM.3 | Cumulative CO₂ emissions for the 2012 to 2100 period compatible with the RCP atmospheric concentrations simulated by the CMIP5 Earth System Models. {6.4, Table 6.12, Figure TS.19}

Scenario	Cumulative CO ₂ Emissions 2012 to 2100 ^a			
	GtC		GtCO ₂	
	Mean	Range	Mean	Range
RCP2.6	270	140 to 410	990	510 to 1505
RCP4.5	780	595 to 1005	2860	2180 to 3690
RCP6.0	1060	840 to 1250	3885	3080 to 4585
RCP8.5	1685	1415 to 1910	6180	5185 to 7005

Notes:

^a 1 Gigatonne of carbon = 1 GtC = 10¹⁵ grams of carbon. This corresponds to 3.667 GtCO₂.

- Earth System Models project a global increase in ocean acidification for all RCP scenarios. The corresponding decrease in surface ocean pH by the end of 21st century is in the range¹⁸ of 0.06 to 0.07 for RCP2.6, 0.14 to 0.15 for RCP4.5, 0.20 to 0.21 for RCP6.0, and 0.30 to 0.32 for RCP8.5 (see Figures SPM.7 and SPM.8). {6.4}
- Cumulative CO₂ emissions²⁰ for the 2012 to 2100 period compatible with the RCP atmospheric CO₂ concentrations, as derived from 15 Earth System Models, range¹⁸ from 140 to 410 GtC for RCP2.6, 595 to 1005 GtC for RCP4.5, 840 to 1250 GtC for RCP6.0, and 1415 to 1910 GtC for RCP8.5 (see Table SPM.3). {6.4}
- By 2050, annual CO₂ emissions derived from Earth System Models following RCP2.6 are smaller than 1990 emissions (by 14 to 96%). By the end of the 21st century, about half of the models infer emissions slightly above zero, while the other half infer a net removal of CO₂ from the atmosphere. {6.4, Figure TS.19}
- The release of CO₂ or CH₄ to the atmosphere from thawing permafrost carbon stocks over the 21st century is assessed to be in the range of 50 to 250 GtC for RCP8.5 (*low confidence*). {6.4}

E.8 Climate Stabilization, Climate Change Commitment and Irreversibility

Cumulative emissions of CO₂ largely determine global mean surface warming by the late 21st century and beyond (see Figure SPM.10). Most aspects of climate change will persist for many centuries even if emissions of CO₂ are stopped. This represents a substantial multi-century climate change commitment created by past, present and future emissions of CO₂. {12.5}

- Cumulative total emissions of CO₂ and global mean surface temperature response are approximately linearly related (see Figure SPM.10). Any given level of warming is associated with a range of cumulative CO₂ emissions²¹, and therefore, e.g., higher emissions in earlier decades imply lower emissions later. {12.5}
- Limiting the warming caused by anthropogenic CO₂ emissions alone with a probability of >33%, >50%, and >66% to less than 2°C since the period 1861–1880²², will require cumulative CO₂ emissions from all anthropogenic sources to stay between 0 and about 1570 GtC (5760 GtCO₂), 0 and about 1210 GtC (4440 GtCO₂), and 0 and about 1000 GtC (3670 GtCO₂) since that period, respectively²³. These upper amounts are reduced to about 900 GtC (3300 GtCO₂), 820 GtC (3010 GtCO₂), and 790 GtC (2900 GtCO₂), respectively, when accounting for non-CO₂ forcings as in RCP2.6. An amount of 515 [445 to 585] GtC (1890 [1630 to 2150] GtCO₂), was already emitted by 2011. {12.5}

²⁰ From fossil fuel, cement, industry, and waste sectors.

²¹ Quantification of this range of CO₂ emissions requires taking into account non-CO₂ drivers.

²² The first 20-year period available from the models.

²³ This is based on the assessment of the transient climate response to cumulative carbon emissions (TCRE, see Section D.2).

- A lower warming target, or a higher likelihood of remaining below a specific warming target, will require lower cumulative CO₂ emissions. Accounting for warming effects of increases in non-CO₂ greenhouse gases, reductions in aerosols, or the release of greenhouse gases from permafrost will also lower the cumulative CO₂ emissions for a specific warming target (see Figure SPM.10). {12.5}
- A large fraction of anthropogenic climate change resulting from CO₂ emissions is irreversible on a multi-century to millennial time scale, except in the case of a large net removal of CO₂ from the atmosphere over a sustained period. Surface temperatures will remain approximately constant at elevated levels for many centuries after a complete cessation of net anthropogenic CO₂ emissions. Due to the long time scales of heat transfer from the ocean surface to depth, ocean warming will continue for centuries. Depending on the scenario, about 15 to 40% of emitted CO₂ will remain in the atmosphere longer than 1,000 years. {Box 6.1, 12.4, 12.5}
- It is *virtually certain* that global mean sea level rise will continue beyond 2100, with sea level rise due to thermal expansion to continue for many centuries. The few available model results that go beyond 2100 indicate global mean sea level rise above the pre-industrial level by 2300 to be less than 1 m for a radiative forcing that corresponds to CO₂ concentrations that peak and decline and remain below 500 ppm, as in the scenario RCP2.6. For a radiative forcing that corresponds to a CO₂ concentration that is above 700 ppm but below 1500 ppm, as in the scenario RCP8.5, the projected rise is 1 m to more than 3 m (*medium confidence*). {13.5}

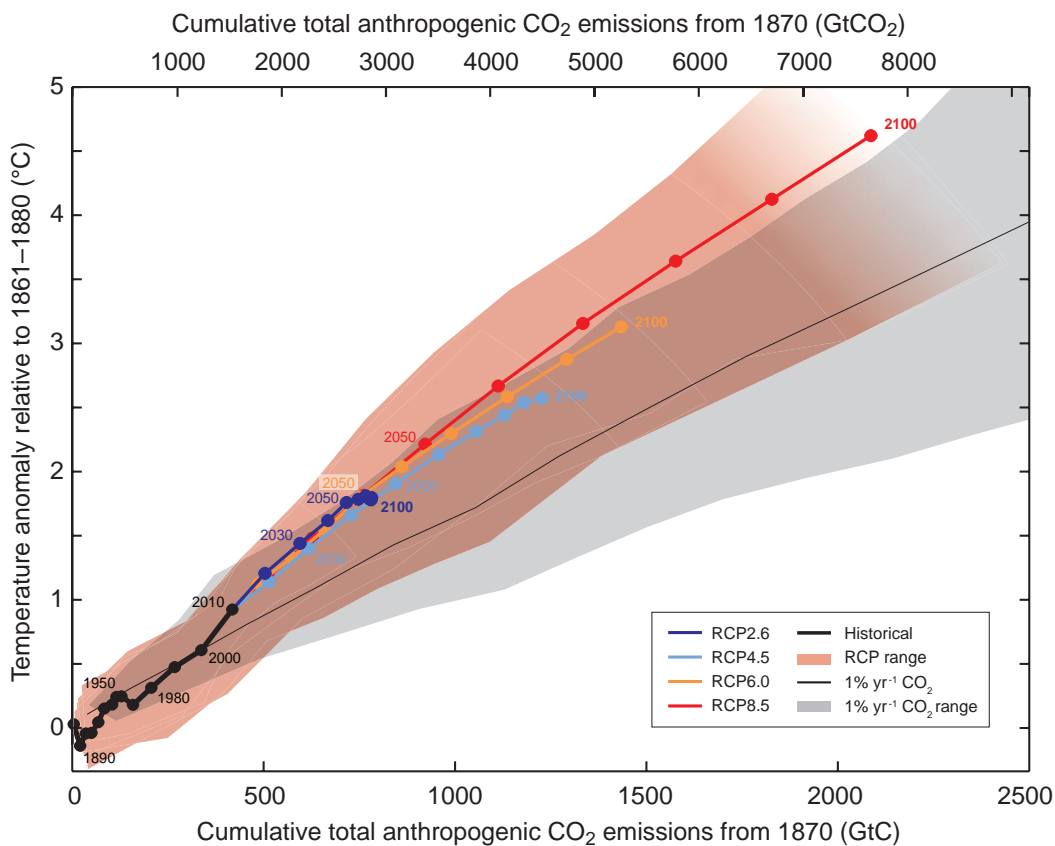


Figure SPM.10 | Global mean surface temperature increase as a function of cumulative total global CO₂ emissions from various lines of evidence. Multi-model results from a hierarchy of climate-carbon cycle models for each RCP until 2100 are shown with coloured lines and decadal means (dots). Some decadal means are labeled for clarity (e.g., 2050 indicating the decade 2040–2049). Model results over the historical period (1860 to 2010) are indicated in black. The coloured plume illustrates the multi-model spread over the four RCP scenarios and fades with the decreasing number of available models in RCP8.5. The multi-model mean and range simulated by CMIP5 models, forced by a CO₂ increase of 1% per year (1% yr⁻¹ CO₂ simulations), is given by the thin black line and grey area. For a specific amount of cumulative CO₂ emissions, the 1% per year CO₂ simulations exhibit lower warming than those driven by RCPs, which include additional non-CO₂ forcings. Temperature values are given relative to the 1861–1880 base period, emissions relative to 1870. Decadal averages are connected by straight lines. For further technical details see the Technical Summary Supplementary Material. {Figure 12.45; TS TFE.8, Figure 1}

- Sustained mass loss by ice sheets would cause larger sea level rise, and some part of the mass loss might be irreversible. There is *high confidence* that sustained warming greater than some threshold would lead to the near-complete loss of the Greenland ice sheet over a millennium or more, causing a global mean sea level rise of up to 7 m. Current estimates indicate that the threshold is greater than about 1°C (*low confidence*) but less than about 4°C (*medium confidence*) global mean warming with respect to pre-industrial. Abrupt and irreversible ice loss from a potential instability of marine-based sectors of the Antarctic ice sheet in response to climate forcing is possible, but current evidence and understanding is insufficient to make a quantitative assessment. {5.8, 13.4, 13.5}
- Methods that aim to deliberately alter the climate system to counter climate change, termed geoengineering, have been proposed. Limited evidence precludes a comprehensive quantitative assessment of both Solar Radiation Management (SRM) and Carbon Dioxide Removal (CDR) and their impact on the climate system. CDR methods have biogeochemical and technological limitations to their potential on a global scale. There is insufficient knowledge to quantify how much CO₂ emissions could be partially offset by CDR on a century timescale. Modelling indicates that SRM methods, if realizable, have the potential to substantially offset a global temperature rise, but they would also modify the global water cycle, and would not reduce ocean acidification. If SRM were terminated for any reason, there is *high confidence* that global surface temperatures would rise very rapidly to values consistent with the greenhouse gas forcing. CDR and SRM methods carry side effects and long-term consequences on a global scale. {6.5, 7.7}

Box SPM.1: Representative Concentration Pathways (RCPs)

Climate change projections in IPCC Working Group I require information about future emissions or concentrations of greenhouse gases, aerosols and other climate drivers. This information is often expressed as a scenario of human activities, which are not assessed in this report. Scenarios used in Working Group I have focused on anthropogenic emissions and do not include changes in natural drivers such as solar or volcanic forcing or natural emissions, for example, of CH₄ and N₂O.

For the Fifth Assessment Report of IPCC, the scientific community has defined a set of four new scenarios, denoted Representative Concentration Pathways (RCPs, see Glossary). They are identified by their approximate total radiative forcing in year 2100 relative to 1750: 2.6 W m⁻² for RCP2.6, 4.5 W m⁻² for RCP4.5, 6.0 W m⁻² for RCP6.0, and 8.5 W m⁻² for RCP8.5. For the Coupled Model Intercomparison Project Phase 5 (CMIP5) results, these values should be understood as indicative only, as the climate forcing resulting from all drivers varies between models due to specific model characteristics and treatment of short-lived climate forcers. These four RCPs include one mitigation scenario leading to a very low forcing level (RCP2.6), two stabilization scenarios (RCP4.5 and RCP6.0), and one scenario with very high greenhouse gas emissions (RCP8.5). The RCPs can thus represent a range of 21st century climate policies, as compared with the no-climate policy of the Special Report on Emissions Scenarios (SRES) used in the Third Assessment Report and the Fourth Assessment Report. For RCP6.0 and RCP8.5, radiative forcing does not peak by year 2100; for RCP2.6 it peaks and declines; and for RCP4.5 it stabilizes by 2100. Each RCP provides spatially resolved data sets of land use change and sector-based emissions of air pollutants, and it specifies annual greenhouse gas concentrations and anthropogenic emissions up to 2100. RCPs are based on a combination of integrated assessment models, simple climate models, atmospheric chemistry and global carbon cycle models. While the RCPs span a wide range of total forcing values, they do not cover the full range of emissions in the literature, particularly for aerosols.

Most of the CMIP5 and Earth System Model simulations were performed with prescribed CO₂ concentrations reaching 421 ppm (RCP2.6), 538 ppm (RCP4.5), 670 ppm (RCP6.0), and 936 ppm (RCP 8.5) by the year 2100. Including also the prescribed concentrations of CH₄ and N₂O, the combined CO₂-equivalent concentrations are 475 ppm (RCP2.6), 630 ppm (RCP4.5), 800 ppm (RCP6.0), and 1313 ppm (RCP8.5). For RCP8.5, additional CMIP5 Earth System Model simulations are performed with prescribed CO₂ emissions as provided by the integrated assessment models. For all RCPs, additional calculations were made with updated atmospheric chemistry data and models (including the Atmospheric Chemistry and Climate component of CMIP5) using the RCP prescribed emissions of the chemically reactive gases (CH₄, N₂O, HFCs, NO_x, CO, NMVOC). These simulations enable investigation of uncertainties related to carbon cycle feedbacks and atmospheric chemistry.

Technical Summary

TS

Technical Summary

Coordinating Lead Authors:

Thomas F. Stocker (Switzerland), Qin Dahe (China), Gian-Kasper Plattner (Switzerland)

Lead Authors:

Lisa V. Alexander (Australia), Simon K. Allen (Switzerland/New Zealand), Nathaniel L. Bindoff (Australia), François-Marie Bréon (France), John A. Church (Australia), Ulrich Cubasch (Germany), Seita Emori (Japan), Piers Forster (UK), Pierre Friedlingstein (UK/Belgium), Nathan Gillett (Canada), Jonathan M. Gregory (UK), Dennis L. Hartmann (USA), Eystein Jansen (Norway), Ben Kirtman (USA), Reto Knutti (Switzerland), Krishna Kumar Kanikicharla (India), Peter Lemke (Germany), Jochem Marotzke (Germany), Valérie Masson-Delmotte (France), Gerald A. Meehl (USA), Igor I. Mokhov (Russian Federation), Shilong Piao (China), Venkatachalam Ramaswamy (USA), David Randall (USA), Monika Rhein (Germany), Maisa Rojas (Chile), Christopher Sabine (USA), Drew Shindell (USA), Lynne D. Talley (USA), David G. Vaughan (UK), Shang-Ping Xie (USA)

Contributing Authors:

Myles R. Allen (UK), Olivier Boucher (France), Don Chambers (USA), Jens Hesselbjerg Christensen (Denmark), Philippe Ciais (France), Peter U. Clark (USA), Matthew Collins (UK), Josefino C. Comiso (USA), Viviane Vasconcellos de Menezes (Australia/Brazil), Richard A. Feely (USA), Thierry Fichefet (Belgium), Gregory Flato (Canada), Jesús Fidel González Rouco (Spain), Ed Hawkins (UK), Paul J. Hezel (Belgium/USA), Gregory C. Johnson (USA), Simon A. Josey (UK), Georg Kaser (Austria/Italy), Albert M.G. Klein Tank (Netherlands), Janina Körper (Germany), Gunnar Myhre (Norway), Timothy Osborn (UK), Scott B. Power (Australia), Stephen R. Rintoul (Australia), Joeri Rogelj (Switzerland/Belgium), Matilde Rusticucci (Argentina), Michael Schulz (Germany), Jan Sedláček (Switzerland), Peter A. Stott (UK), Rowan Sutton (UK), Peter W. Thorne (USA/Norway/UK), Donald Wuebbles (USA)

Review Editors:

Sylvie Joussaume (France), Joyce Penner (USA), Fredolin Tangang (Malaysia)

This Technical Summary should be cited as:

Stocker, T.F., D. Qin, G.-K. Plattner, L.V. Alexander, S.K. Allen, N.L. Bindoff, F.-M. Bréon, J.A. Church, U. Cubasch, S. Emori, P. Forster, P. Friedlingstein, N. Gillett, J.M. Gregory, D.L. Hartmann, E. Jansen, B. Kirtman, R. Knutti, K. Krishna Kumar, P. Lemke, J. Marotzke, V. Masson-Delmotte, G.A. Meehl, I.I. Mokhov, S. Piao, V. Ramaswamy, D. Randall, M. Rhein, M. Rojas, C. Sabine, D. Shindell, L.D. Talley, D.G. Vaughan and S.-P. Xie, 2013: Technical Summary. In: *Climate Change 2013: The Physical Science Basis. Contribution of Working Group I to the Fifth Assessment Report of the Intergovernmental Panel on Climate Change* [Stocker, T.F., D. Qin, G.-K. Plattner, M. Tignor, S.K. Allen, J. Boschung, A. Nauels, Y. Xia, V. Bex and P.M. Midgley (eds.)]. Cambridge University Press, Cambridge, United Kingdom and New York, NY, USA.

Table of Contents

TS.1 Introduction	35	TS.5 Projections of Global and Regional Climate Change	79
Box TS.1: Treatment of Uncertainty	36	TS.5.1 Introduction	79
TS.2 Observation of Changes in the Climate System	37	TS.5.2 Future Forcing and Scenarios	79
TS.2.1 Introduction	37	Box TS.6: The New Representative Concentration Pathway Scenarios and Coupled Model Intercomparison Project Phase 5 Models	79
TS.2.2 Changes in Temperature.....	37	TS.5.3 Quantification of Climate System Response.....	81
TS.2.3 Changes in Energy Budget and Heat Content	39	TS.5.4 Near-term Climate Change	85
TS.2.4 Changes in Circulation and Modes of Variability.....	39	TS.5.5 Long-term Climate Change	89
TS.2.5 Changes in the Water Cycle and Cryosphere.....	40	TS.5.6 Long-term Projections of Carbon and Other Biogeochemical Cycles.....	93
TS.2.6 Changes in Sea Level	46	Box TS.7: Climate Geoengineering Methods	98
TS.2.7 Changes in Extremes.....	46	TS.5.7 Long-term Projections of Sea Level Change	98
TS.2.8 Changes in Carbon and Other Biogeochemical Cycles.....	50	TS.5.8 Climate Phenomena and Regional Climate Change	105
TS.3 Drivers of Climate Change	53	TS.6 Key Uncertainties	114
TS.3.1 Introduction	53	TS.6.1 Key Uncertainties in Observation of Changes in the Climate System	114
TS.3.2 Radiative Forcing from Greenhouse Gases.....	53	TS.6.2 Key Uncertainties in Drivers of Climate Change	114
Box TS.2: Radiative Forcing and Effective Radiative Forcing	53	TS.6.3 Key Uncertainties in Understanding the Climate System and Its Recent Changes	114
TS.3.3 Radiative Forcing from Anthropogenic Aerosols.....	55	TS.6.4 Key Uncertainties in Projections of Global and Regional Climate Change.....	115
TS.3.4 Radiative Forcing from Land Surface Changes and Contrails.....	55	Thematic Focus Elements	
TS.3.5 Radiative Forcing from Natural Drivers of Climate Change	55	TFE.1 Water Cycle Change	42
TS.3.6 Synthesis of Forcings; Spatial and Temporal Evolution	56	TFE.2 Sea Level Change: Scientific Understanding and Uncertainties	47
TS.3.7 Climate Feedbacks	57	TFE.3 Comparing Projections from Previous IPCC Assessments with Observations	64
TS.3.8 Emission Metrics	58	TFE.4 The Changing Energy Budget of the Global Climate System	67
TS.4 Understanding the Climate System and Its Recent Changes	60	TFE.5 Irreversibility and Abrupt Change	70
TS.4.1 Introduction	60	TFE.6 Climate Sensitivity and Feedbacks	82
TS.4.2 Surface Temperature	60	TFE.7 Carbon Cycle Perturbation and Uncertainties	96
Box TS.3: Climate Models and the Hiatus in Global Mean Surface Warming of the Past 15 Years	61	TFE.8 Climate Targets and Stabilization	102
TS.4.3 Atmospheric Temperature	66	TFE.9 Climate Extremes	109
TS.4.4 Oceans	68	Supplementary Material	
TS.4.5 Cryosphere.....	69	<i>Supplementary Material is available in online versions of the report.</i>	
TS.4.6 Water Cycle.....	72		
TS.4.7 Climate Extremes	72		
TS.4.8 From Global to Regional	73		
Box TS.4: Model Evaluation	75		
Box TS.5: Paleoclimate	77		

TS.1 Introduction

Climate Change 2013: The Physical Science Basis is the contribution of Working Group I (WGI) to the Fifth Assessment Report (AR5) of the Intergovernmental Panel on Climate Change (IPCC). This comprehensive assessment of the physical aspects of climate change puts a focus on those elements that are relevant to understand past, document current and project future climate change. The assessment builds on the IPCC Fourth Assessment Report (AR4)¹ and the recent Special Report on Managing the Risk of Extreme Events and Disasters to Advance Climate Change Adaptation (SREX)² and is presented in 14 chapters and 3 annexes. The chapters cover direct and proxy observations of changes in all components of the climate system; assess the current knowledge of various processes within, and interactions among, climate system components, which determine the sensitivity and response of the system to changes in forcing; and quantify the link between the changes in atmospheric constituents, and hence radiative forcing (RF)³, and the consequent detection and attribution of climate change. Projections of changes in all climate system components are based on model simulations forced by a new set of scenarios. The Report also provides a comprehensive assessment of past and future sea level change in a dedicated chapter. Regional climate change information is presented in the form of an Atlas of Global and Regional Climate Projections (Annex I). This is complemented by Annex II: Climate System Scenario Tables and Annex III: Glossary.

The primary purpose of this Technical Summary (TS) is to provide the link between the complete assessment of the multiple lines of independent evidence presented in the 14 chapters of the main report and the highly condensed summary prepared as the WGI Summary for Policymakers (SPM). The Technical Summary thus serves as a starting point for those readers who seek the full information on more specific topics covered by this assessment. This purpose is facilitated by including pointers to the chapters and sections where the full assessment can be found. Policy-relevant topics, which cut across many chapters and involve many interlinked processes in the climate system, are presented here as Thematic Focus Elements (TFEs), allowing rapid access to this information.

An integral element of this report is the use of uncertainty language that permits a traceable account of the assessment (Box TS.1). The degree of certainty in key findings in this assessment is based on the author teams' evaluations of underlying scientific understanding and is expressed as a level of confidence that results from the type, amount, quality and consistency of evidence and the degree of agreement in

the scientific studies considered⁴. Confidence is expressed qualitatively. Quantified measures of uncertainty in a finding are expressed probabilistically and are based on a combination of statistical analyses of observations or model results, or both, and expert judgement. Where appropriate, findings are also formulated as statements of fact without using uncertainty qualifiers (see Chapter 1 and Box TS.1 for more details).

The Technical Summary is structured into four main sections presenting the assessment results following the storyline of the WGI contribution to AR5: Section TS.2 covers the assessment of observations of changes in the climate system; Section TS.3 summarizes the information on the different drivers, natural and anthropogenic, expressed in terms of RF; Section TS.4 presents the assessment of the quantitative understanding of observed climate change; and Section TS.5 summarizes the assessment results for projections of future climate change over the 21st century and beyond from regional to global scale. Section TS.6 combines and lists key uncertainties from the WGI assessment from Sections TS.2 to TS.5. The overall nine TFEs, cutting across the various components of the WGI AR5, are dispersed throughout the four main TS sections, are visually distinct from the main text and should allow stand-alone reading.

The basis for substantive paragraphs in this Technical Summary can be found in the chapter sections of the underlying report. These references are given in curly brackets.

¹ IPCC, 2007: *Climate Change 2007: The Physical Science Basis*. Contribution of Working Group I to the Fourth Assessment Report of the Intergovernmental Panel on Climate Change [Solomon, S., D. Qin, M. Manning, Z. Chen, M. Marquis, K.B. Averyt, M. Tignor and H.L. Miller (eds.)]. Cambridge University Press, Cambridge, United Kingdom and New York, NY, USA, 996 pp.

² IPCC, 2012: *Managing the Risks of Extreme Events and Disasters to Advance Climate Change Adaptation*. A Special Report of Working Groups I and II of the Intergovernmental Panel on Climate Change [Field, C.B., V. Barros, T.F. Stocker, D. Qin, D.J. Dokken, K.L. Ebi, M.D. Mastrandrea, K.J. Mach, G.-K. Plattner, S.K. Allen, M. Tignor and P. M. Midgley (eds.)]. Cambridge University Press, Cambridge, UK, and New York, NY, USA, 582 pp.

³ Radiative forcing (RF) is a measure of the net change in the energy balance of the Earth system in response to some external perturbation. It is expressed in watts per square metre ($W\ m^{-2}$); see Box TS.2.

⁴ Mastrandrea, M.D., C.B. Field, T.F. Stocker, O. Edenhofer, K.L. Ebi, D.J. Frame, H. Held, E. Kriegler, K.J. Mach, P.R. Matschoss, G.-K. Plattner, G.W. Yohe, and F.W. Zwiers, 2010: *Guidance Note for Lead Authors of the IPCC Fifth Assessment Report on Consistent Treatment of Uncertainties*. Intergovernmental Panel on Climate Change (IPCC).

Box TS.1 | Treatment of Uncertainty

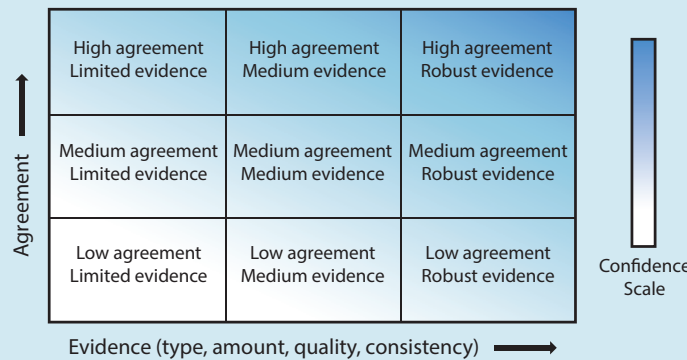
Based on the Guidance Note for Lead Authors of the IPCC Fifth Assessment Report on Consistent Treatment of Uncertainties, this WGI Technical Summary and the WGI Summary for Policymakers rely on two metrics for communicating the degree of certainty in key findings, which is based on author teams’ evaluations of underlying scientific understanding:

- Confidence in the validity of a finding, based on the type, amount, quality and consistency of evidence (e.g., mechanistic understanding, theory, data, models, expert judgement) and the degree of agreement. Confidence is expressed qualitatively.
- Quantified measures of uncertainty in a finding expressed probabilistically (based on statistical analysis of observations or model results, or expert judgement).

The AR5 Guidance Note refines the guidance provided to support the IPCC Third and Fourth Assessment Reports. Direct comparisons between assessment of uncertainties in findings in this Report and those in the AR4 and the SREX are difficult, because of the application of the revised guidance note on uncertainties, as well as the availability of new information, improved scientific understanding, continued analyses of data and models and specific differences in methodologies applied in the assessed studies. For some climate variables, different aspects have been assessed and therefore a direct comparison would be inappropriate.

Each key finding is based on an author team’s evaluation of associated evidence and agreement. The confidence metric provides a qualitative synthesis of an author team’s judgement about the validity of a finding, as determined through evaluation of evidence and agreement. If uncertainties can be quantified probabilistically, an author team can characterize a finding using the calibrated likelihood language or a more precise presentation of probability. Unless otherwise indicated, high or very high confidence is associated with findings for which an author team has assigned a likelihood term.

The following summary terms are used to describe the available evidence: limited, medium, or robust; and for the degree of agreement: low, medium, or high. A level of confidence is expressed using five qualifiers very low, low, medium, high, and very high, and typeset in italics, e.g., *medium confidence*. Box TS.1, Figure 1 depicts summary statements for evidence and agreement and their relationship to confidence. There is flexibility in this relationship; for a given evidence and agreement statement, different confidence levels can be assigned, but increasing levels of evidence and degrees of agreement correlate with increasing confidence.



Box TS.1, Figure 1 | A depiction of evidence and agreement statements and their relationship to confidence. Confidence increases toward the top right corner as suggested by the increasing strength of shading. Generally, evidence is most robust when there are multiple, consistent independent lines of high quality. {Figure 1.11}

The following terms have been used to indicate the assessed likelihood, and typeset in italics:

Term*	Likelihood of the outcome
<i>Virtually certain</i>	99–100% probability
<i>Very likely</i>	90–100% probability
<i>Likely</i>	66–100% probability
<i>About as likely as not</i>	33–66% probability
<i>Unlikely</i>	0–33% probability
<i>Very unlikely</i>	0–10% probability
<i>Exceptionally unlikely</i>	0–1% probability

* Additional terms (*extremely likely*: 95–100% probability, *more likely than not*: >50–100% probability, and *extremely unlikely*: 0–5% probability) may also be used when appropriate.

TS.2 Observation of Changes in the Climate System

TS.2.1 Introduction

Observations of the climate system are based on direct physical and biogeochemical measurements, and remote sensing from ground stations and satellites; information derived from paleoclimate archives provides a long-term context. Global-scale observations from the instrumental era began in the mid-19th century, and paleoclimate reconstructions extend the record of some quantities back hundreds to millions of years. Together, they provide a comprehensive view of the variability and long-term changes in the atmosphere, the ocean, the cryosphere and at the land surface.

The assessment of observational evidence for climate change is summarized in this section. Substantial advancements in the availability, acquisition, quality and analysis of observational data sets for the atmosphere, land surface, ocean and cryosphere have occurred since the AR4. Many aspects of the climate system are showing evidence of a changing climate. {2, 3, 4, 5, 6, 13}

TS.2.2 Changes in Temperature

TS.2.2.1 Surface

It is certain that global mean surface temperature (GMST) has increased since the late 19th century (Figures TS.1 and TS.2). Each of the past three decades has been successively warmer at the Earth's surface than any the previous decades in the instrumental record, and the decade of the 2000's has been the warmest. The globally averaged combined land and ocean temperature data as calculated by a linear trend⁵, show a warming of 0.85 [0.65 to 1.06] °C⁶, over the period 1880–2012, when multiple independently produced datasets exist, about 0.89 [0.69 to 1.08] °C over the period 1901–2012, and about 0.72 [0.49 to 0.89] °C over the period 1951–2012 when based on three independently-produced data sets. The total increase between the average of the 1850–1900 period and the 2003–2012 period is 0.78 [0.72 to 0.85] °C, based on the Hadley Centre/Climatic Research Unit gridded surface temperature data set 4 (HadCRUT4), the global mean surface temperature dataset with the longest record of the three independently-produced data sets. The warming from 1850–1900 to 1986–2005 (reference period for the modelling chapters and the Atlas in Annex I) is 0.61 [0.55 to 0.67] °C, when calculated using HadCRUT4 and its uncertainty estimates. It is also *virtually certain* that maximum and minimum temperatures over

land have increased on a global scale since 1950.⁷ {2.4.1, 2.4.3; Chapter 2 Supplementary Material Section 2.SM.3}

Despite the robust multi-decadal warming, there exists substantial interannual to decadal variability in the rate of warming, with several periods exhibiting weaker trends (including the warming hiatus since 1998) (Figure TS.1). The rate of warming over the past 15 years (1998–2012; 0.05 [–0.05 to +0.15] °C per decade) is smaller than the trend since 1951 (1951–2012; 0.12[0.08 to 0.14] °C per decade). Trends for short periods are uncertain and very sensitive to the start and end years. For example, trends for 15-year periods starting in 1995, 1996, and 1997 are 0.13 [0.02 to 0.24] °C per decade, 0.14 [0.03 to 0.24] °C per decade and 0.07 [–0.02 to 0.18] °C per decade, respectively. Several independently analysed data records of global and regional land surface air temperature obtained from station observations are in broad agreement that land surface air temperatures have increased. Sea surface temperatures (SSTs) have also increased. Intercomparisons of new SST data records obtained by different measurement methods, including satellite data, have resulted in better understanding of errors and biases in the records. {2.4.1–2.4.3; Box 9.2}

It is *unlikely* that any uncorrected urban heat island effects and land use change effects have raised the estimated centennial globally averaged land surface air temperature trends by more than 10% of the reported trend. This is an average value; in some regions that have rapidly developed urban heat island and land use change impacts on regional trends may be substantially larger. {2.4.1}

There is *high confidence* that annual mean surface warming since the 20th century has reversed long-term cooling trends of the past 5000 years in mid-to-high latitudes of the Northern Hemisphere (NH). For average annual NH temperatures, the period 1983–2012 was *very likely* the warmest 30-year period of the last 800 years (*high confidence*) and *likely* the warmest 30-year period of the last 1400 years (*medium confidence*). This is supported by comparison of instrumental temperatures with multiple reconstructions from a variety of proxy data and statistical methods, and is consistent with AR4. Continental-scale surface temperature reconstructions show, with *high confidence*, multi-decadal periods during the Medieval Climate Anomaly (950–1250) that were in some regions as warm as in the mid-20th century and in others as warm as in the late 20th century. With *high confidence*, these regional warm periods were not as synchronous across regions as the warming since the mid-20th century. Based on the comparison between reconstructions and simulations, there is *high confidence* that not only external orbital, solar and volcanic forcing, but also internal

⁵ The warming is reported as an unweighted average based on linear trend estimates calculated from Hadley Centre/Climatic Research Unit gridded surface temperature data set 4 (HadCRUT4), Merged Land–Ocean Surface Temperature Analysis (MLOST) and Goddard Institute for Space Studies Surface Temperature Analysis (GISTEMP) data sets (see Figure TS.2; Section 2.4.3).

⁶ In the WGI contribution to the AR5, uncertainty is quantified using 90% uncertainty intervals unless otherwise stated. The 90% uncertainty interval, reported in square brackets, is expected to have a 90% likelihood of covering the value that is being estimated. The upper endpoint of the uncertainty interval has a 95% likelihood of exceeding the value that is being estimated and the lower endpoint has a 95% likelihood of being less than that value. A best estimate of that value is also given where available. Uncertainty intervals are not necessarily symmetric about the corresponding best estimate.

⁷ Both methods presented in this paragraph to calculate temperature change were also used in AR4. The first calculates the difference using a best fit linear trend of all points between two years, e.g., 1880 and 2012. The second calculates the difference between averages for the two periods, e.g., 1850 to 1900 and 2003 to 2012. Therefore, the resulting values and their 90% uncertainty intervals are not directly comparable.

variability, contributed substantially to the spatial pattern and timing of surface temperature changes between the Medieval Climate Anomaly and the Little Ice Age (1450–1850). {5.3.5, 5.5.1}

TS.2.2.2 Troposphere and Stratosphere

Based on multiple independent analyses of measurements from radiosondes and satellite sensors, it is *virtually certain* that globally the troposphere has warmed and the stratosphere has cooled since the mid-20th century (Figure TS.1). Despite unanimous agreement on the sign of the trends, substantial disagreement exists between available estimates as to the rate of temperature changes, particularly outside the NH extratropical troposphere, which has been well sampled by

radiosondes. Hence there is only *medium confidence* in the rate of change and its vertical structure in the NH extratropical troposphere and *low confidence* elsewhere. {2.4.4}

TS.2.2.3 Ocean

It is *virtually certain* that the upper ocean (above 700 m) has warmed from 1971 to 2010, and *likely* that it has warmed from the 1870s to 1971 (Figure TS.1). There is less certainty in changes prior to 1971 because of relatively sparse sampling in earlier time periods. Instrumental biases in historical upper ocean temperature measurements have been identified and reduced since AR4, diminishing artificial decadal variation in temperature and upper ocean heat content, most prominent during the 1970s and 1980s. {3.2.1–3.2.3, 3.5.3}

TS

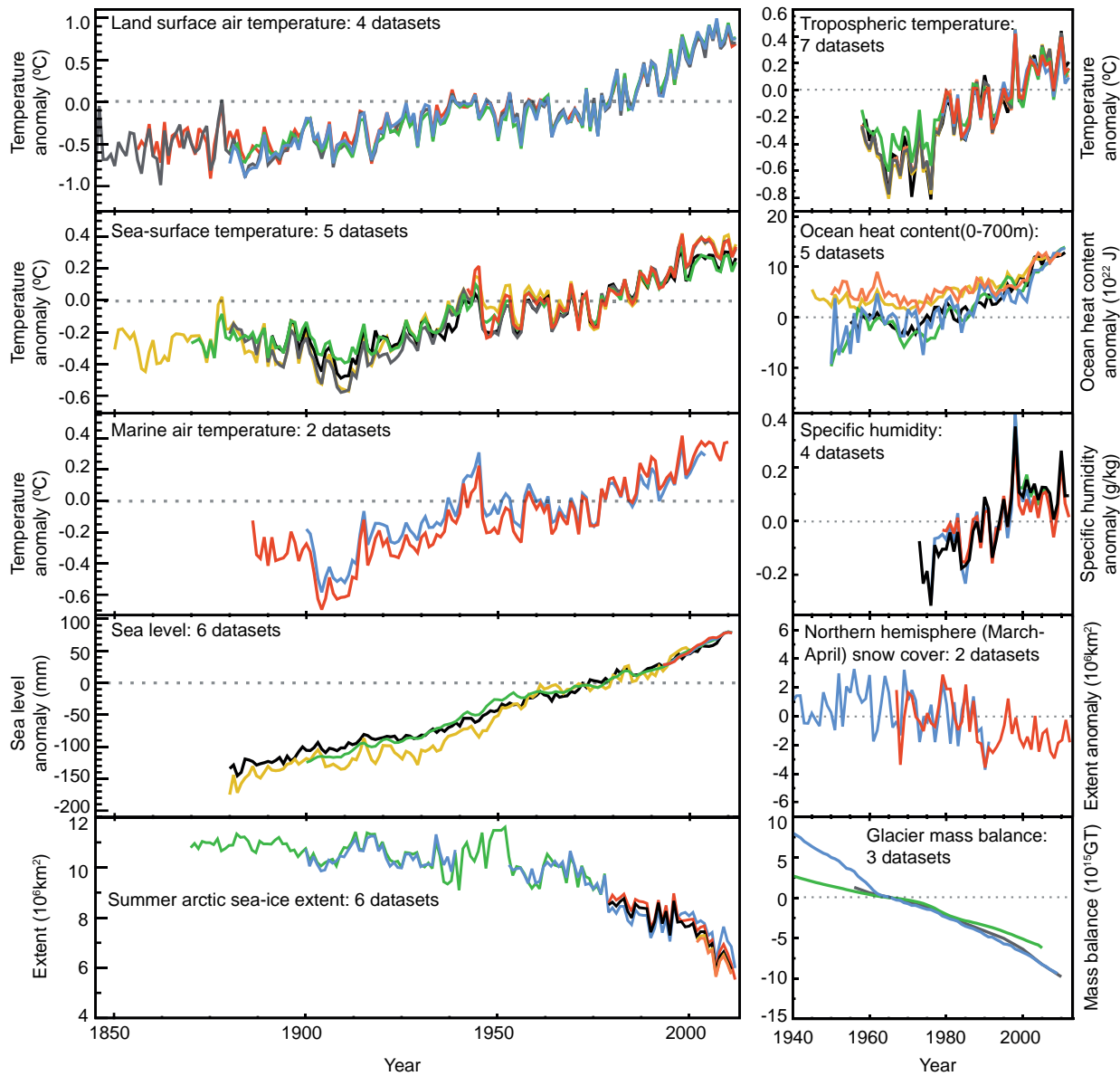


Figure TS.1 | Multiple complementary indicators of a changing global climate. Each line represents an independently derived estimate of change in the climate element. The time series presented are assessed in Chapters 2, 3 and 4. In each panel all data sets have been normalized to a common period of record. A full detailing of which source data sets go into which panel is given in Chapter 2 Supplementary Material Section 2.SM.5 and in the respective chapters. Further detail regarding the related Figure SPM.3 is given in the TS Supplementary Material. {FAQ 2.1, Figure 1; 2.4, 2.5, 3.2, 3.7, 4.5.2, 4.5.3}

It is *likely* that the ocean warmed between 700–2000 m from 1957 to 2009, based on 5-year averages. It is *likely* that the ocean warmed from 3000 m to the bottom from 1992 to 2005, while no significant trends in global average temperature were observed between 2000 and 3000 m depth from circa 1992 to 2005. Below 3000 m depth, the largest warming is observed in the Southern Ocean. {3.2.4, 3.5.1; Figures 3.2b, 3.3; FAQ 3.1}

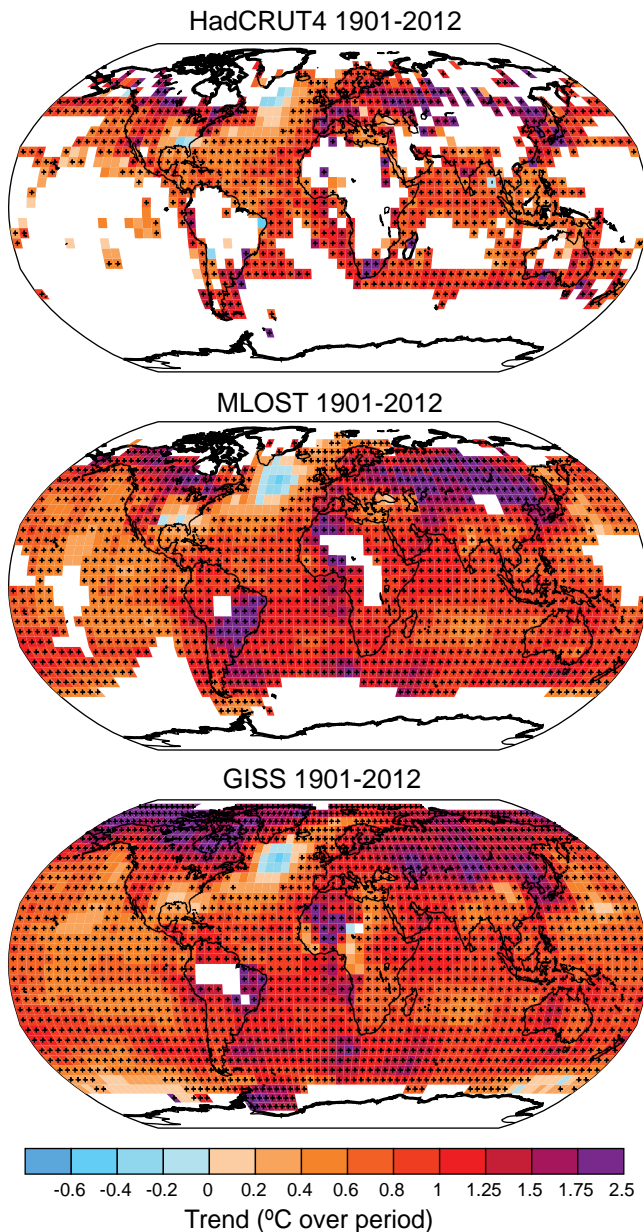


Figure TS.2 | Change in surface temperature over 1901–2012 as determined by linear trend for three data sets. White areas indicate incomplete or missing data. Trends have been calculated only for those grid boxes with greater than 70% complete records and more than 20% data availability in the first and last 10% of the time period. Black plus signs (+) indicate grid boxes where trends are significant (i.e., a trend of zero lies outside the 90% confidence interval). Differences in coverage primarily reflect the degree of interpolation to account for data void regions undertaken by the data set providers ranging from none beyond grid box averaging (Hadley Centre/Climatic Research Unit gridded surface temperature data set 4 (HadCRUT4)) to substantial (Goddard Institute for Space Studies Surface Temperature Analysis (GISTEMP)). Further detail regarding the related Figure SPM.1 is given in the TS Supplementary Material. {Figure 2.21}

TS.2.3 Changes in Energy Budget and Heat Content

The Earth has been in radiative imbalance, with more energy from the Sun entering than exiting the top of the atmosphere, since at least about 1970. It is *virtually certain* that the Earth has gained substantial energy from 1971 to 2010. The estimated increase in energy inventory between 1971 and 2010 is $274 [196 \text{ to } 351] \times 10^{21} \text{ J}$ (*high confidence*), with a heating rate of $213 \times 10^{12} \text{ W}$ from a linear fit to the annual values over that time period (see also TFE.4). {Boxes 3.1, 13.1}

Ocean warming dominates that total heating rate, with full ocean depth warming accounting for about 93% (*high confidence*), and warming of the upper (0 to 700 m) ocean accounting for about 64%. Melting ice (including Arctic sea ice, ice sheets and glaciers) and warming of the continents each account for 3% of the total. Warming of the atmosphere makes up the remaining 1%. The 1971–2010 estimated rate of ocean energy gain is $199 \times 10^{12} \text{ W}$ from a linear fit to data over that time period, equivalent to 0.42 W m^{-2} heating applied continuously over the Earth's entire surface, and 0.55 W m^{-2} for the portion owing to ocean warming applied over the ocean's entire surface area. The Earth's estimated energy increase from 1993 to 2010 is $163 [127 \text{ to } 201] \times 10^{21} \text{ J}$ with a trend estimate of $275 \times 10^{15} \text{ W}$. The ocean portion of the trend for 1993–2010 is $257 \times 10^{12} \text{ W}$, equivalent to a mean heat flux into the ocean of 0.71 W m^{-2} . {3.2.3, 3.2.4; Box 3.1}

It is *about as likely as not* that ocean heat content from 0–700 m increased more slowly during 2003 to 2010 than during 1993 to 2002 (Figure TS.1). Ocean heat uptake from 700–2000 m, where interannual variability is smaller, *likely* continued unabated from 1993 to 2009. {3.2.3, 3.2.4; Box 9.2}

TS.2.4 Changes in Circulation and Modes of Variability

Large variability on interannual to decadal time scales hampers robust conclusions on long-term changes in atmospheric circulation in many instances. *Confidence* is *high* that the increase of the northern mid-latitude westerly winds and the North Atlantic Oscillation (NAO) index from the 1950s to the 1990s, and the weakening of the Pacific Walker Circulation from the late 19th century to the 1990s, have been largely offset by recent changes. With *high confidence*, decadal and multi-decadal changes in the winter NAO index observed since the 20th century are not unprecedented in the context of the past 500 years. {2.7.2, 2.7.5, 2.7.8, 5.4.2; Box 2.5; Table 2.14}

It is *likely* that circulation features have moved poleward since the 1970s, involving a widening of the tropical belt, a poleward shift of storm tracks and jet streams and a contraction of the northern polar vortex. Evidence is more robust for the NH. It is *likely* that the Southern Annular Mode (SAM) has become more positive since the 1950s. The increase in the strength of the observed summer SAM since 1950 has been anomalous, with *medium confidence*, in the context of the past 400 years. {2.7.5, 2.7.6, 2.7.8, 5.4.2; Box 2.5; Table 2.14}

New results from high-resolution coral records document with *high confidence* that the El Niño-Southern Oscillation (ENSO) system has remained highly variable throughout the past 7000 years, showing no discernible evidence for an orbital modulation of ENSO. {5.4.1}

Recent observations have strengthened evidence for variability in major ocean circulation systems on time scales from years to decades. It is *very likely* that the subtropical gyres in the North Pacific and South Pacific have expanded and strengthened since 1993. Based on measurements of the full Atlantic Meridional Overturning Circulation (AMOC) and its individual components at various latitudes and different time periods, there is no evidence of a long-term trend. There is also no evidence for trends in the transports of the Indonesian Throughflow, the Antarctic Circumpolar Current (ACC) or in the transports between the Atlantic Ocean and Nordic Seas. However, a southward shift of the ACC by about 1° of latitude is observed in data spanning the time period 1950–2010 with *medium confidence*. {3.6}

TS.2.5 Changes in the Water Cycle and Cryosphere

TS.2.5.1 Atmosphere

Confidence in precipitation change averaged over global land areas is *low* prior to 1951 and *medium* afterwards because of insufficient data, particularly in the earlier part of the record (for an overview of observed and projected changes in the global water cycle see TFE.1). Further, when virtually all the land area is filled in using a reconstruction method, the resulting time series shows little change in land-based precipitation since 1901. NH mid-latitude land areas do show a *likely* overall increase in precipitation (*medium confidence* prior to 1951, but *high confidence* afterwards). For other latitudes area-averaged long-term positive or negative trends have *low confidence* (TFE.1, Figure 1). {2.5.1}

It is *very likely* that global near surface and tropospheric air specific humidity have increased since the 1970s. However, during recent years the near-surface moistening trend over land has abated (*medium confidence*) (Figure TS.1). As a result, fairly widespread decreases in relative humidity near the surface are observed over the land in recent years. {2.4.4, 2.5.5, 2.5.6}

Although trends of cloud cover are consistent between independent data sets in certain regions, substantial ambiguity and therefore *low confidence* remains in the observations of global-scale cloud variability and trends. {2.5.7}

TS.2.5.2 Ocean and Surface Fluxes

It is *very likely* that regional trends have enhanced the mean geographical contrasts in sea surface salinity since the 1950s: saline surface waters in the evaporation-dominated mid-latitudes have become more saline, while relatively fresh surface waters in rainfall-dominated tropical and polar regions have become fresher. The mean contrast between high- and low-salinity regions increased by 0.13 [0.08 to 0.17] from 1950 to 2008. It is *very likely* that the inter-basin contrast in freshwater content has increased: the Atlantic has become saltier and the Pacific and Southern Oceans have freshened. Although similar conclusions were reached in AR4, recent studies based on expanded data sets and new analysis approaches provide *high confidence* in this assessment. {3.3.2, 3.3.3, 3.9; FAQ 3.2}

The spatial patterns of the salinity trends, mean salinity and the mean distribution of evaporation minus precipitation are all similar (TFE.1, Figure 1). These similarities provide indirect evidence that the pattern of evaporation minus precipitation over the oceans has been enhanced since the 1950s (*medium confidence*). Uncertainties in currently available surface fluxes prevent the flux products from being reliably used to identify trends in the regional or global distribution of evaporation or precipitation over the oceans on the time scale of the observed salinity changes since the 1950s. {3.3.2–3.3.4, 3.4.2, 3.4.3, 3.9; FAQ 3.2}

TS.2.5.3 Sea Ice

Continuing the trends reported in AR4, there is *very high confidence* that the Arctic sea ice extent (annual, multi-year and perennial) decreased over the period 1979–2012 (Figure TS.1). The rate of the annual decrease was *very likely* between 3.5 and 4.1% per decade (range of 0.45 to 0.51 million km² per decade). The average decrease in decadal extent of annual Arctic sea ice has been most rapid in summer and autumn (*high confidence*), but the extent has decreased in every season, and in every successive decade since 1979 (*high confidence*). The extent of Arctic perennial and multi-year ice decreased between 1979 and 2012 (*very high confidence*). The rates are *very likely* 11.5 [9.4 to 13.6]% per decade (0.73 to 1.07 million km² per decade) for the sea ice extent at summer minimum (perennial ice) and *very likely* 13.5 [11 to 16] % per decade for multi-year ice. There is *medium confidence* from reconstructions that the current (1980–2012) Arctic summer sea ice retreat was unprecedented and SSTs were anomalously high in the perspective of at least the last 1,450 years. {4.2.2, 5.5.2}

It is *likely* that the annual period of surface melt on Arctic perennial sea ice lengthened by 5.7 [4.8 to 6.6] days per decade over the period 1979–2012. Over this period, in the region between the East Siberian Sea and the western Beaufort Sea, the duration of ice-free conditions increased by nearly 3 months. {4.2.2}

There is *high confidence* that the average winter sea ice thickness within the Arctic Basin decreased between 1980 and 2008. The average decrease was *likely* between 1.3 m and 2.3 m. *High confidence* in this assessment is based on observations from multiple sources: submarine, electromagnetic probes and satellite altimetry; and is consistent with the decline in multi-year and perennial ice extent. Satellite measurements made in the period 2010–2012 show a decrease in sea ice volume compared to those made over the period 2003–2008 (*medium confidence*). There is *high confidence* that in the Arctic, where the sea ice thickness has decreased, the sea ice drift speed has increased. {4.2.2}

It is *very likely* that the annual Antarctic sea ice extent increased at a rate of between 1.2 and 1.8% per decade (0.13 to 0.20 million km² per decade) between 1979 and 2012 (*very high confidence*). There was a greater increase in sea ice area, due to a decrease in the percentage of open water within the ice pack. There is *high confidence* that there are strong regional differences in this annual rate, with some regions increasing in extent/area and some decreasing. There are also contrasting regions around the Antarctic where the ice-free season has lengthened, and others where it has decreased over the satellite period (*high confidence*). {4.2.3}

TS.2.5.4 Glaciers and Ice Sheets

There is *very high confidence* that glaciers world-wide are persistently shrinking as revealed by the time series of measured changes in glacier length, area, volume and mass (Figures TS.1 and TS.3). The few exceptions are regionally and temporally limited. Measurements of glacier change have increased substantially in number since AR4. Most of the new data sets, along with a globally complete glacier inventory, have been derived from satellite remote sensing {4.3.1, 4.3.3}

There is *very high confidence* that, during the last decade, the largest contributions to global glacier ice loss were from glaciers in Alaska, the Canadian Arctic, the periphery of the Greenland ice sheet, the Southern Andes and the Asian mountains. Together these areas account for more than 80% of the total ice loss. Total mass loss from all glaciers in the world, excluding those on the periphery of the ice sheets, was *very likely* 226 [91 to 361] Gt yr⁻¹ (sea level equivalent, 0.62 [0.25 to 0.99] mm yr⁻¹) in the period 1971–2009, 275 [140 to 410] Gt yr⁻¹ (0.76 [0.39 to 1.13] mm yr⁻¹) in the period 1993–2009 and 301 [166 to 436] Gt yr⁻¹ (0.83 [0.46 to 1.20] mm yr⁻¹) between 2005 and 2009⁸. {4.3.3; Tables 4.4, 4.5}

There is *high confidence* that current glacier extents are out of balance with current climatic conditions, indicating that glaciers will continue to shrink in the future even without further temperature increase. {4.3.3}

There is *very high confidence* that the Greenland ice sheet has lost ice during the last two decades. Combinations of satellite and airborne remote sensing together with field data indicate with *high confidence* that the ice loss has occurred in several sectors and that large rates of mass loss have spread to wider regions than reported in AR4 (Figure TS.3). There is *high confidence* that the mass loss of the Greenland ice sheet has accelerated since 1992: the average rate has *very likely* increased from 34 [–6 to 74] Gt yr⁻¹ over the period 1992–2001 (sea level equivalent, 0.09 [–0.02 to 0.20] mm yr⁻¹), to 215 [157 to 274] Gt yr⁻¹ over the period 2002–2011 (0.59 [0.43 to 0.76] mm yr⁻¹). There is *high confidence* that ice loss from Greenland resulted from increased surface melt and runoff and increased outlet glacier discharge, and these occurred in similar amounts. There is *high confidence* that the area subject to summer melt has increased over the last two decades. {4.4.2, 4.4.3}

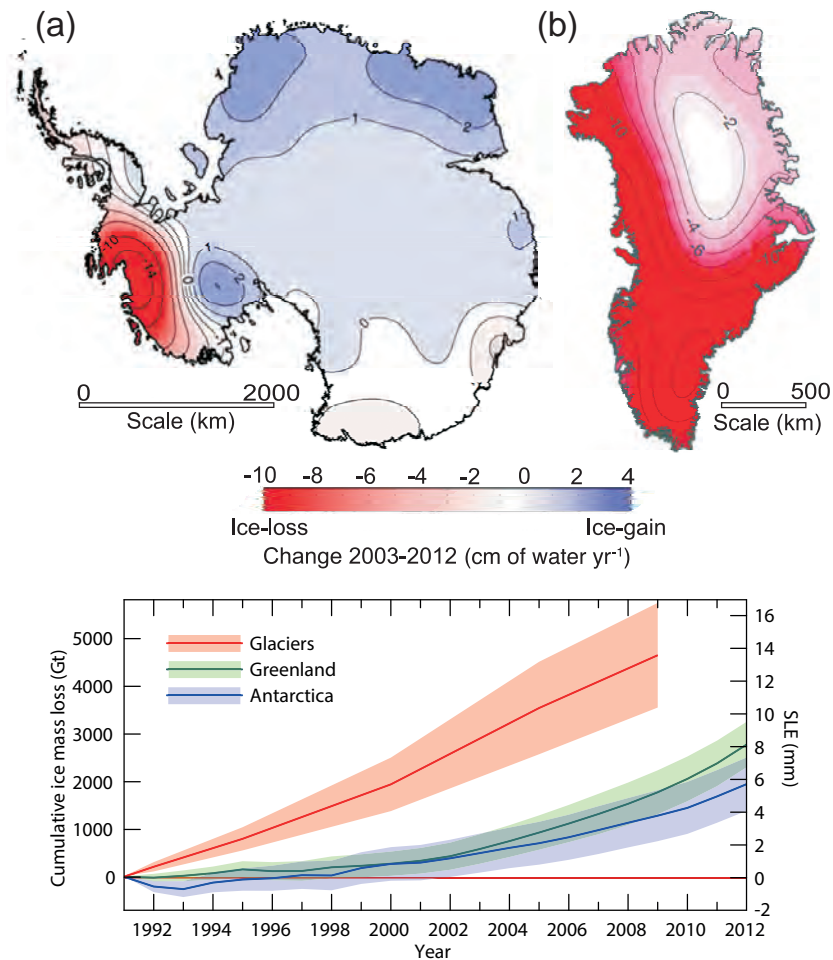


Figure TS.3 | (Upper) Distribution of ice loss determined from Gravity Recovery and Climate Experiment (GRACE) time-variable gravity for (a) Antarctica and (b) Greenland, shown in centimetres of water per year (cm of water yr⁻¹) for the period 2003–2012. (Lower) The assessment of the total loss of ice from glaciers and ice sheets in terms of mass (Gt) and sea level equivalent (mm). The contribution from glaciers excludes those on the periphery of the ice sheets. {4.3.4; Figures 4.12–4.14, 4.16, 4.17, 4.25}

⁸ 100 Gt yr⁻¹ of ice loss corresponds to about 0.28 mm yr⁻¹ of sea level equivalent.



Thematic Focus Elements

TFE.1 | Water Cycle Change

The water cycle describes the continuous movement of water through the climate system in its liquid, solid and vapour forms, and storage in the reservoirs of ocean, cryosphere, land surface and atmosphere. In the atmosphere, water occurs primarily as a gas, water vapour, but it also occurs as ice and liquid water in clouds. The ocean is primarily liquid water, but the ocean is partly covered by ice in polar regions. Terrestrial water in liquid form appears as surface water (lakes, rivers), soil moisture and groundwater. Solid terrestrial water occurs in ice sheets, glaciers, snow and ice on the surface and permafrost. The movement of water in the climate system is essential to life on land, as much of the water that falls on land as precipitation and supplies the soil moisture and river flow has been evaporated from the ocean and transported to land by the atmosphere. Water that falls as snow in winter can provide soil moisture in springtime and river flow in summer and is essential to both natural and human systems. The movement of fresh water between the atmosphere and the ocean can also influence oceanic salinity, which is an important driver of the density and circulation of the ocean. The latent heat contained in water vapour in the atmosphere is critical to driving the circulation of the atmosphere on scales ranging from individual thunderstorms to the global circulation of the atmosphere. {12.4.5; FAQ 3.2, FAQ 12.2}

Observations of Water Cycle Change

Because the saturation vapour pressure of air increases with temperature, it is expected that the amount of water vapour in air will increase with a warming climate. Observations from surface stations, radiosondes, global positioning systems and satellite measurements indicate increases in tropospheric water vapour at large spatial scales (TFE.1, Figure 1). It is *very likely* that tropospheric specific humidity has increased since the 1970s. The magnitude of the observed global change in tropospheric water vapour of about 3.5% in the past 40 years is consistent with the observed temperature change of about 0.5°C during the same period, and the relative humidity has stayed approximately constant. The water vapour change can be attributed to human influence with *medium confidence*. {2.5.4, 10.3.2}

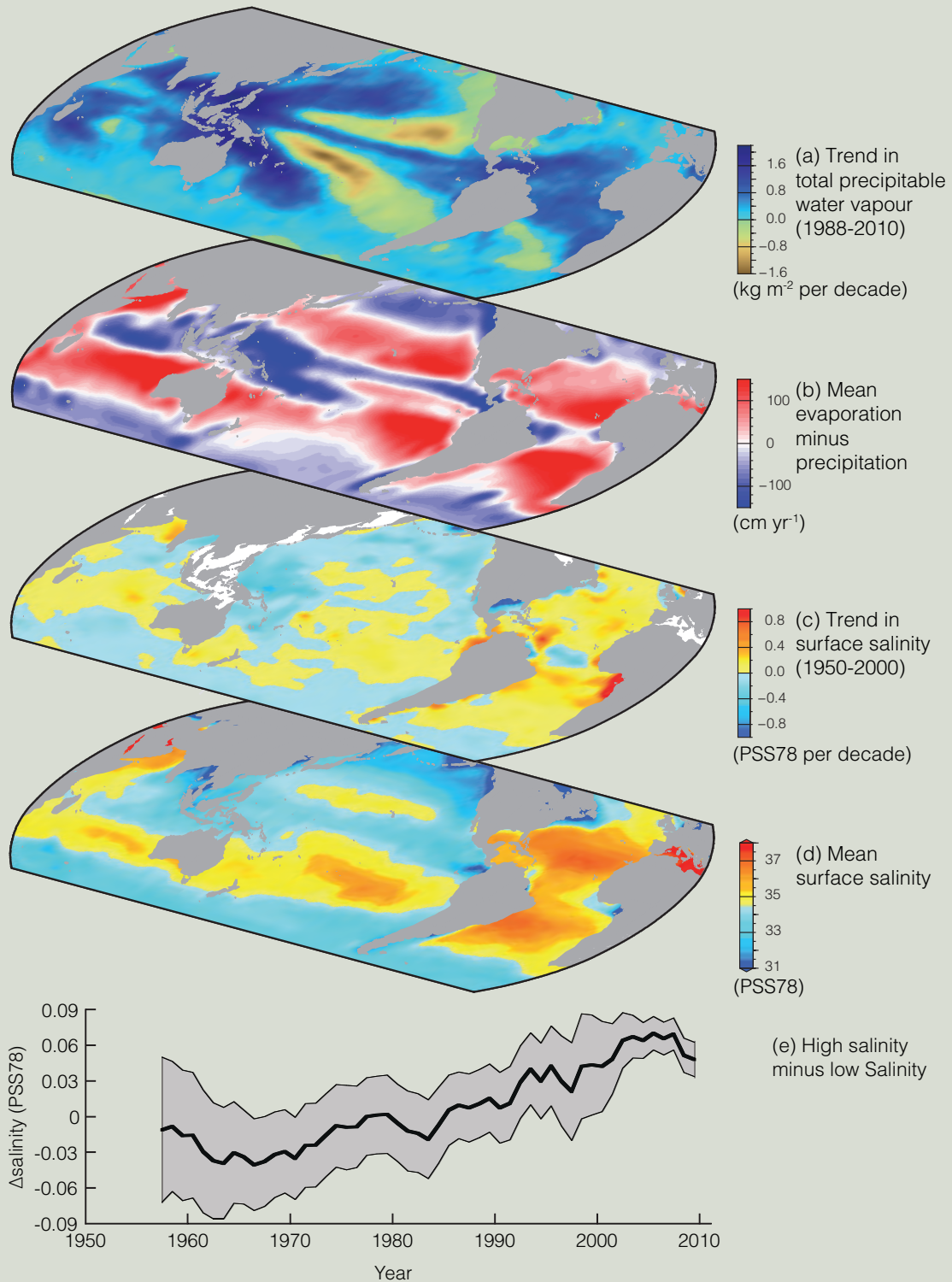
Changes in precipitation are harder to measure with the existing records, both because of the greater difficulty in sampling precipitation and also because it is expected that precipitation will have a smaller fractional change than the water vapour content of air as the climate warms. Some regional precipitation trends appear to be robust (TFE.1, Figure 2), but when virtually all the land area is filled in using a reconstruction method, the resulting time series of global mean land precipitation shows little change since 1900. At present there is *medium confidence* that there has been a significant human influence on global scale changes in precipitation patterns, including increases in Northern Hemisphere (NH) mid-to-high latitudes. Changes in the extremes of precipitation, and other climate extremes related to the water cycle are comprehensively discussed in TFE.9. {2.5.1, 10.3.2}

Although direct trends in precipitation and evaporation are difficult to measure with the available records, the observed oceanic surface salinity, which is strongly dependent on the difference between evaporation and precipitation, shows significant trends (TFE.1, Figure 1). The spatial patterns of the salinity trends since 1950 are very similar to the mean salinity and the mean distribution of evaporation minus precipitation: regions of high salinity where evaporation dominates have become more saline, while regions of low salinity where rainfall dominates have become fresher (TFE.1, Figure 1). This provides indirect evidence that the pattern of evaporation minus precipitation over the oceans has been enhanced since the 1950s (*medium confidence*). The inferred changes in evaporation minus precipitation are consistent with the observed increased water vapour content of the warmer air. It is *very likely* that observed changes in surface and subsurface salinity are due in part to anthropogenic climate forcings. {2.5, 3.3.2–3.3.4, 3.4, 3.9, 10.4.2; FAQ 3.2}

In most regions analysed, it is *likely* that decreasing numbers of snowfall events are occurring where increased winter temperatures have been observed. Both satellite and *in situ* observations show significant reductions in the NH snow cover extent over the past 90 years, with most of the reduction occurring in the 1980s. Snow cover decreased most in June when the average extent decreased *very likely* by 53% (40 to 66%) over the period 1967 to 2012. From 1922 to 2012 only data from March and April are available and show *very likely* a 7% (4.5 to 9.5%) decline. Because of earlier spring snowmelt, the duration of the NH snow season has declined by 5.3 days per decade since the 1972/1973 winter. It is *likely* that there has been an anthropogenic component to these observed reductions in snow cover since the 1970s. {4.5.2, 10.5.1, 10.5.3}

(continued on next page)

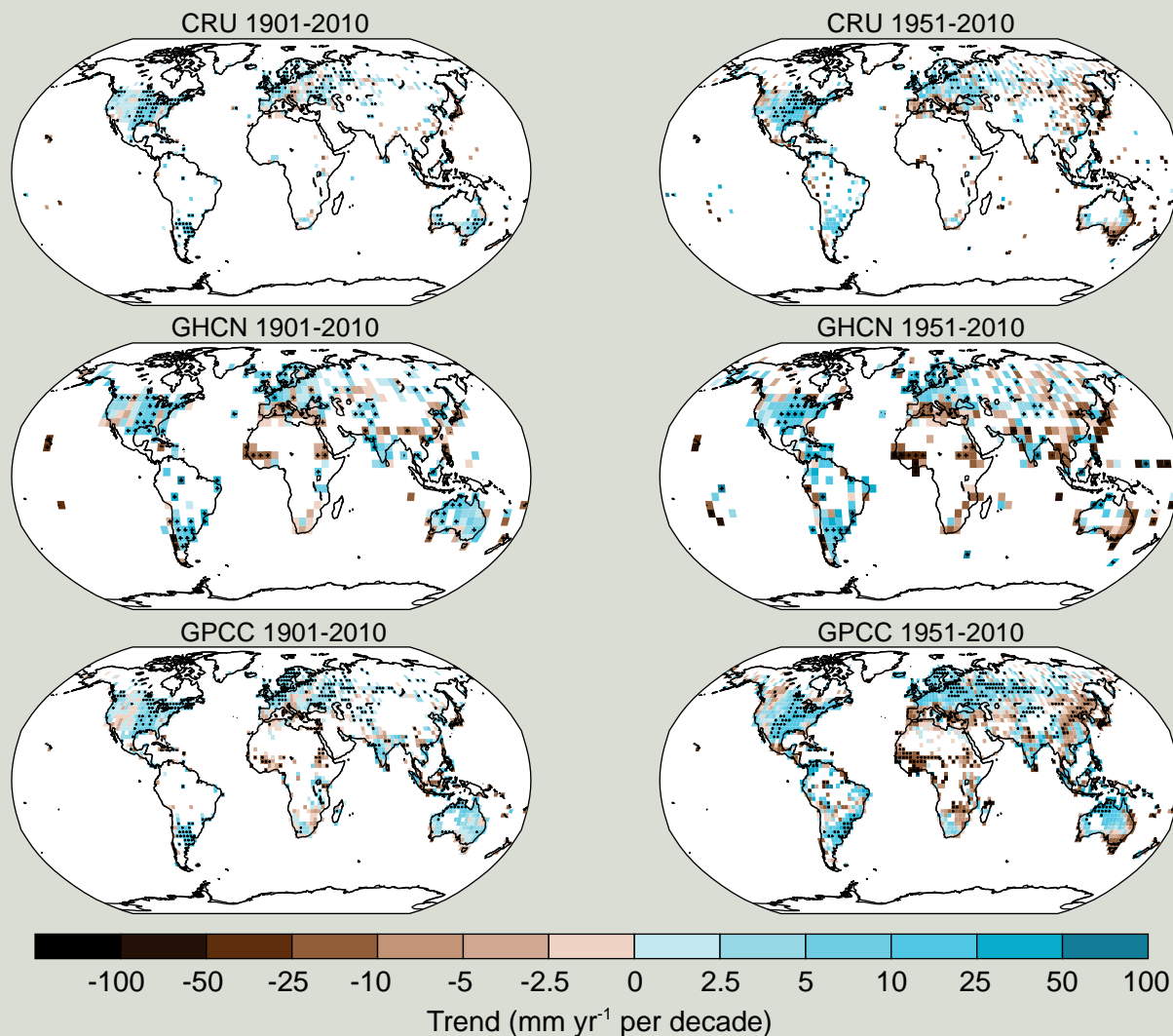
TFE.1 (continued)



TFE.1, Figure 1 | Changes in sea surface salinity are related to the atmospheric patterns of evaporation minus precipitation ($E - P$) and trends in total precipitable water: (a) Linear trend (1988 to 2010) in total precipitable water (water vapour integrated from the Earth's surface up through the entire atmosphere) (kg m^{-2} per decade) from satellite observations. (b) The 1979–2005 climatological mean net evaporation minus precipitation (cm yr^{-1}) from meteorological reanalysis data. (c) Trend (1950–2000) in surface salinity (Practical Salinity Scale 78 (PSS78) per 50 years). (d) The climatological mean surface salinity (PSS78) (blues <35 ; yellows-reds >35). (e) Global difference between salinity averaged over regions where the sea surface salinity is greater than the global mean sea surface salinity ("High Salinity") and salinity averaged over regions with values below the global mean ('Low Salinity'). For details of data sources see Figure 3.21 and FAQ 3.2, Figure 1. [3.9]

TS

TFE.1 (continued)



TFE.1, Figure 2 | Maps of observed precipitation change over land from 1901 to 2010 (left-hand panels) and 1951 to 2010 (right-hand panels) from the Climatic Research Unit (CRU), Global Historical Climatology Network (GHCN) and Global Precipitation Climatology Centre (GPCC) data sets. Trends in annual accumulation have been calculated only for those grid boxes with greater than 70% complete records and more than 20% data availability in first and last decile of the period. White areas indicate incomplete or missing data. Black plus signs (+) indicate grid boxes where trends are significant (i.e., a trend of zero lies outside the 90% confidence interval). Further detail regarding the related Figure SPM.2 is given in the TS Supplementary Material. {Figure 2.29; 2.5.1}

The most recent and most comprehensive analyses of river runoff do not support the IPCC Fourth Assessment Report (AR4) conclusion that global runoff has increased during the 20th century. New results also indicate that the AR4 conclusions regarding global increasing trends in droughts since the 1970s are no longer supported. {2.5.2, 2.6.2}

Projections of Future Changes

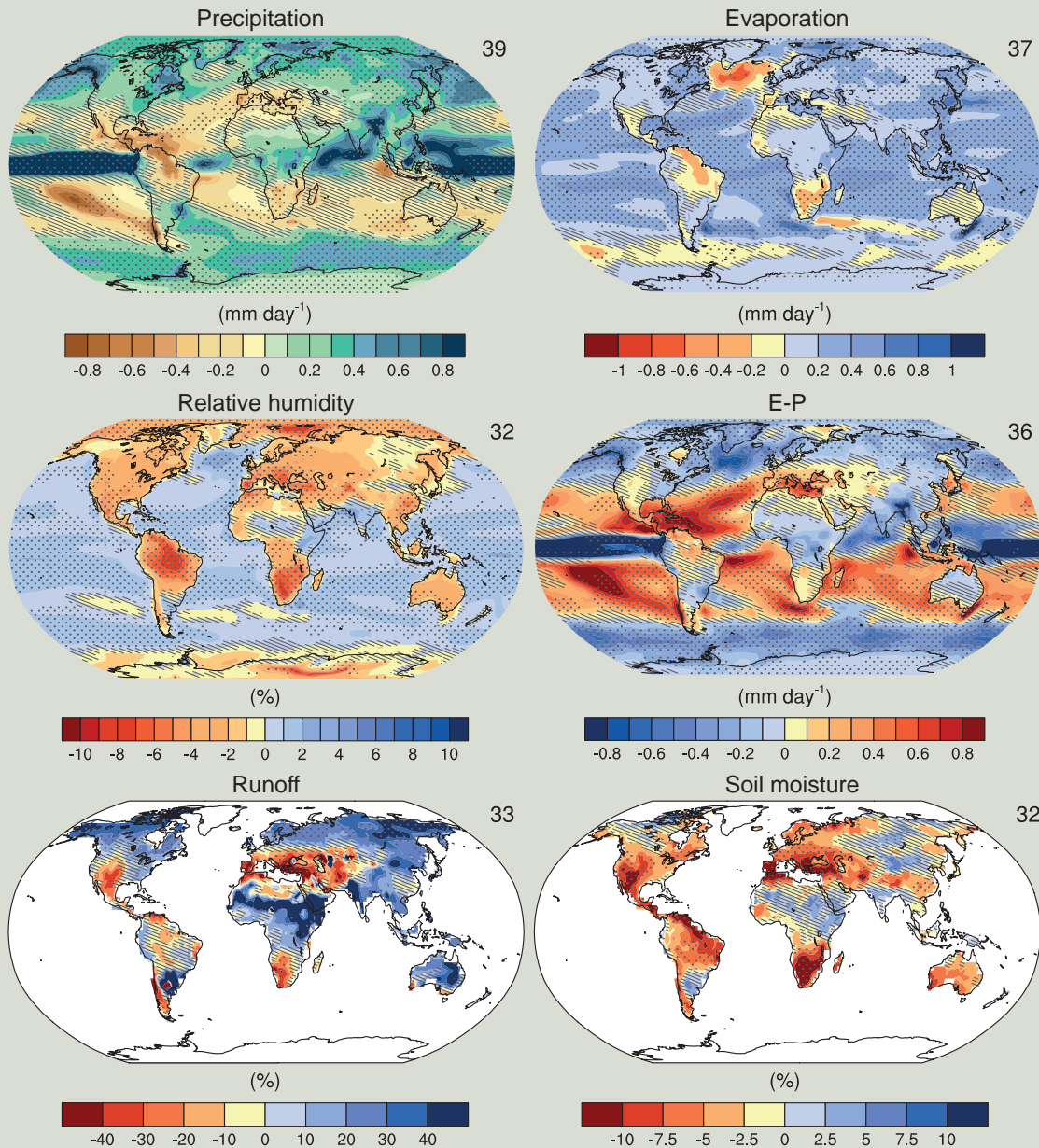
Changes in the water cycle are projected to occur in a warming climate (TFE.1, Figure 3, see also TS 4.6, TS 5.6, Annex I). Global-scale precipitation is projected to gradually increase in the 21st century. The precipitation increase is projected to be much smaller (about 2% K⁻¹) than the rate of lower tropospheric water vapour increase (about 7% K⁻¹), due to global energetic constraints. Changes of average precipitation in a much warmer world will not be uniform, with some regions experiencing increases, and others with decreases or not much change at all. The high latitude land masses are *likely* to experience greater amounts of precipitation due to the additional water carrying capacity of the warmer troposphere. Many mid-latitude and subtropical arid and semi-arid regions will *likely* experience less precipitation. The largest precipitation changes over northern Eurasia and North America are projected to occur during the winter. {12.4.5, Annex I}

(continued on next page)

TFE.1 (continued)

Regional to global-scale projections of soil moisture and drought remain relatively uncertain compared to other aspects of the water cycle. Nonetheless, drying in the Mediterranean, southwestern USA and southern African regions are consistent with projected changes in the Hadley Circulation, so drying in these regions as global temperatures increase is *likely* for several degrees of warming under the Representative Concentration Pathway RCP8.5. Decreases in runoff are *likely* in southern Europe and the Middle East. Increased runoff is *likely* in high northern latitudes, and consistent with the projected precipitation increases there. {12.4.5}

Annual mean hydrological cycle change (RCP8.5: 2081-2100)



TFE.1, Figure 3 | Annual mean changes in precipitation (P), evaporation (E), relative humidity, $E - P$, runoff and soil moisture for 2081–2100 relative to 1986–2005 under the Representative Concentration Pathway RCP8.5 (see Box TS.6). The number of Coupled Model Intercomparison Project Phase 5 (CMIP5) models to calculate the multi-model mean is indicated in the upper right corner of each panel. Hatching indicates regions where the multi-model mean change is less than one standard deviation of internal variability. Stippling indicates regions where the multi-model mean change is greater than two standard deviations of internal variability and where 90% of models agree on the sign of change (see Box 12.1). {Figures 12.25–12.27}

TS

There is *high confidence* that the Antarctic ice sheet has been losing ice during the last two decades (Figure TS.3). There is *very high confidence* that these losses are mainly from the northern Antarctic Peninsula and the Amundsen Sea sector of West Antarctica and *high confidence* that they result from the acceleration of outlet glaciers. The average rate of ice loss from Antarctica *likely* increased from 30 [−37 to 97] Gt yr^{−1} (sea level equivalent, 0.08 [−0.10 to 0.27] mm yr^{−1}) over the period 1992–2001, to 147 [72 to 221] Gt yr^{−1} over the period 2002–2011 (0.40 [0.20 to 0.61] mm yr^{−1}). {4.4.2, 4.4.3}

There is *high confidence* that in parts of Antarctica floating ice shelves are undergoing substantial changes. There is *medium confidence* that ice shelves are thinning in the Amundsen Sea region of West Antarctica, and *low confidence* that this is due to high ocean heat flux. There is *high confidence* that ice shelves around the Antarctic Peninsula continue a long-term trend of retreat and partial collapse that began decades ago. {4.4.2, 4.4.5}

TS.2.5.5 Snow Cover, Freshwater Ice and Frozen Ground

There is *very high confidence* that snow cover extent has decreased in the NH, especially in spring (Figure TS.1). Satellite records indicate that over the period 1967–2012, snow cover extent *very likely* decreased; the largest change, −53% [−40 to −66%], occurred in June. No month had statistically significant increases. Over the longer period, 1922–2012, data are available only for March and April, but these show *very likely* a 7% [4.5 to 9.5%] decline and a negative correlation (−0.76) with March to April 40°N to 60°N land temperature. In the Southern Hemisphere (SH), evidence is too limited to conclude whether changes have occurred. {4.5.2, 4.5.3}

Permafrost temperatures have increased in most regions around the world since the early 1980s (*high confidence*). These increases were in response to increased air temperature and to changes in the timing and thickness of snow cover (*high confidence*). The temperature increase for colder permafrost was generally greater than for warmer permafrost (*high confidence*). {4.7.2; Table 4.8}

TS.2.6 Changes in Sea Level

The primary contributions to changes in the volume of water in the ocean are the expansion of the ocean water as it warms and the transfer to the ocean of water currently stored on land, particularly from glaciers and ice sheets. Water impoundment in reservoirs and ground water depletion (and its subsequent runoff to the ocean) also affect sea level. Change in sea level relative to the land (relative sea level) can be significantly different from the global mean sea level (GMSL) change because of changes in the distribution of water in the ocean, vertical movement of the land and changes in the Earth's gravitational field. For an overview on the scientific understanding and uncertainties associated with recent (and projected) sea level change see TFE.2. {3.7.3, 13.1}

During warm intervals of the mid Pliocene (3.3 to 3.0 Ma), when there is *medium confidence* that GMSTs were 1.9°C to 3.6°C warmer than for pre-industrial climate and carbon dioxide (CO₂) levels were between 350 and 450 ppm, there is *high confidence* that GMSL was

above present, implying reduced volume of polar ice sheets. The best estimates from various methods imply with *high confidence* that sea level has not exceeded +20 m during the warmest periods of the Pliocene, due to deglaciation of the Greenland and West Antarctic ice sheets and areas of the East Antarctic ice sheet. {5.6.1, 13.2}

There is *very high confidence* that maximum GMSL during the last interglacial period (129 to 116 ka) was, for several thousand years, at least 5 m higher than present and *high confidence* that it did not exceed 10 m above present, implying substantial contributions from the Greenland and Antarctic ice sheets. This change in sea level occurred in the context of different orbital forcing and with high-latitude surface temperature, averaged over several thousand years, at least 2°C warmer than present (*high confidence*). Based on ice sheet model simulations consistent with elevation changes derived from a new Greenland ice core, the Greenland ice sheet *very likely* contributed between 1.4 m and 4.3 m sea level equivalent, implying with *medium confidence* a contribution from the Antarctic ice sheet to the GMSL during the Last Interglacial Period. {5.3.4, 5.6.2, 13.2.1}

Proxy and instrumental sea level data indicate a transition in the late 19th to the early 20th century from relatively low mean rates of rise over the previous two millennia to higher rates of rise (*high confidence*) {3.7, 3.7.4, 5.6.3, 13.2}

GMSL has risen by 0.19 [0.17 to 0.21] m, estimated from a linear trend over the period 1901–2010, based on tide gauge records and additionally on satellite data since 1993. It is *very likely* that the mean rate of sea level rise was 1.7 [1.5 to 1.9] mm yr^{−1} between 1901 and 2010. Between 1993 and 2010, the rate was *very likely* higher at 3.2 [2.8 to 3.6] mm yr^{−1}; similarly high rates *likely* occurred between 1920 and 1950. The rate of GMSL rise has *likely* increased since the early 1900s, with estimates ranging from 0.000 [−0.002 to 0.002] to 0.013 [−0.007 to 0.019] mm yr^{−2}. {3.7, 5.6.3, 13.2}

TS.2.7 Changes in Extremes

TS.2.7.1 Atmosphere

Recent analyses of extreme events generally support the AR4 and SREX conclusions (see TFE.9 and in particular TFE.9, Table 1, for a synthesis). It is *very likely* that the number of cold days and nights has decreased and the number of warm days and nights has increased on the global scale between 1951 and 2010. Globally, there is *medium confidence* that the length and frequency of warm spells, including heat waves, has increased since the middle of the 20th century, mostly owing to lack of data or studies in Africa and South America. However, it is *likely* that heat wave frequency has increased over this period in large parts of Europe, Asia and Australia. {2.6.1; Tables 2.12, 2.13}

It is *likely* that since about 1950 the number of heavy precipitation events over land has increased in more regions than it has decreased. Confidence is highest for North America and Europe where there have been *likely* increases in either the frequency or intensity of heavy precipitation with some seasonal and regional variations. It is *very likely* that there have been trends towards heavier precipitation events in central North America. {2.6.2; Table 2.13}

Thematic Focus Elements

TFE.2 | Sea Level Change: Scientific Understanding and Uncertainties

After the Last Glacial Maximum, global mean sea levels (GMSLs) reached close to present-day values several thousand years ago. Since then, it is *virtually certain* that the rate of sea level rise has increased from low rates of sea level change during the late Holocene (order tenths of mm yr^{-1}) to 20th century rates (order mm yr^{-1} , Figure TS1). {3.7, 5.6, 13.2}

Ocean thermal expansion and glacier mass loss are the dominant contributors to GMSL rise during the 20th century (*high confidence*). It is *very likely* that warming of the ocean has contributed 0.8 [0.5 to 1.1] mm yr^{-1} of sea level change during 1971–2010, with the majority of the contribution coming from the upper 700 m. The model mean rate of ocean thermal expansion for 1971–2010 is close to observations. {3.7, 13.3}

Observations, combined with improved methods of analysis, indicate that the global glacier contribution (excluding the peripheral glaciers around Greenland and Antarctica) to sea level was 0.25 to 0.99 mm yr^{-1} sea level equivalent during 1971–2010. *Medium confidence* in global glacier mass balance models used for projections of glacier changes arises from the process-based understanding of glacier surface mass balance, the consistency of observations and models of glacier changes, and the evidence that Atmosphere–Ocean General Circulation Model (AOGCM) climate simulations can provide realistic climate input. A simulation using observed climate data shows a larger rate of glacier mass loss during the 1930s than the simulations using AOGCM input, possibly a result of an episode of warming in Greenland associated with unforced regional climate variability. {4.3, 13.3}

Observations indicate that the Greenland ice sheet has *very likely* experienced a net loss of mass due to both increased surface melting and runoff, and increased ice discharge over the last two decades (Figure TS.3). Regional climate models indicate that Greenland ice sheet surface mass balance showed no significant trend from the 1960s to the 1980s, but melting and consequent runoff has increased since the early 1990s. This tendency is related to pronounced regional warming, which may be attributed to a combination of anomalous regional variability in recent years and anthropogenic climate change. *High confidence* in projections of future warming in Greenland and increased surface melting is based on the qualitative agreements of models in projecting amplified warming at high northern latitudes for well-understood physical reasons. {4.4, 13.3}

There is *high confidence* that the Antarctic ice sheet is in a state of net mass loss and its contribution to sea level is also *likely* to have increased over the last two decades. Acceleration in ice outflow has been observed since the 1990s, especially in the Amundsen Sea sector of West Antarctica. Interannual variability in accumulation is large and as a result no significant trend is present in accumulation since 1979 in either models or observations. Surface melting is currently negligible in Antarctica. {4.4, 13.3}

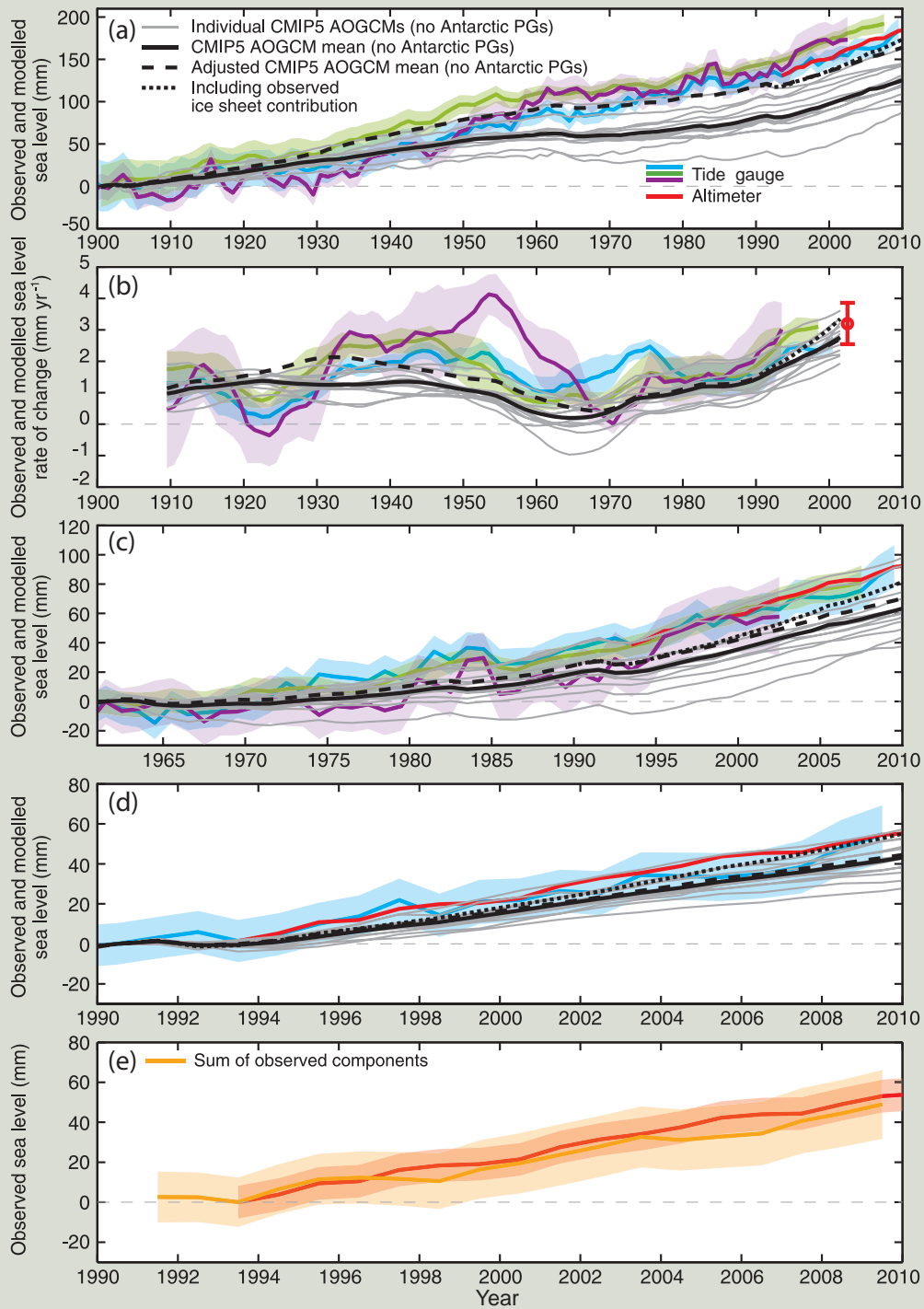
Model-based estimates of climate-related changes in water storage on land (as snow cover, surface water, soil moisture and ground water) do not show significant long-term contributions to sea level change for recent decades. However, human-induced changes (reservoir impoundment and groundwater depletion) have each contributed at least several tenths of mm yr^{-1} to sea level change. Reservoir impoundment exceeded groundwater depletion for the majority of the 20th century but the rate of groundwater depletion has increased and now exceeds the rate of impoundment. Their combined net contribution for the 20th century is estimated to be small. {13.3}

The observed GMSL rise for 1993–2010 is consistent with the sum of the observationally estimated contributions (TFE.2, Figure 1e). The closure of the observational budget for recent periods within uncertainties represents a significant advance since the IPCC Fourth Assessment Report in physical understanding of the causes of past GMSL change, and provides an improved basis for critical evaluation of models of these contributions in order to assess their reliability for making projections. {13.3}

The sum of modelled ocean thermal expansion and glacier contributions and the estimated change in land water storage (which is relatively small) accounts for about 65% of the observed GMSL rise for 1901–1990, and 90% for 1971–2010 and 1993–2010 (TFE.2, Figure 1). After inclusion of small long-term contributions from ice sheets and the possible greater mass loss from glaciers during the 1930s due to unforced climate variability, the sum of the modelled contribution is close to the observed rise. The addition of the observed ice sheet contribution since 1993 improves the agreement further between the observed and modelled sea level rise (TFE.2, Figure 1). The evidence now available gives a clearer account than in previous IPCC assessments of 20th century sea level change. {13.3}

(continued on next page)

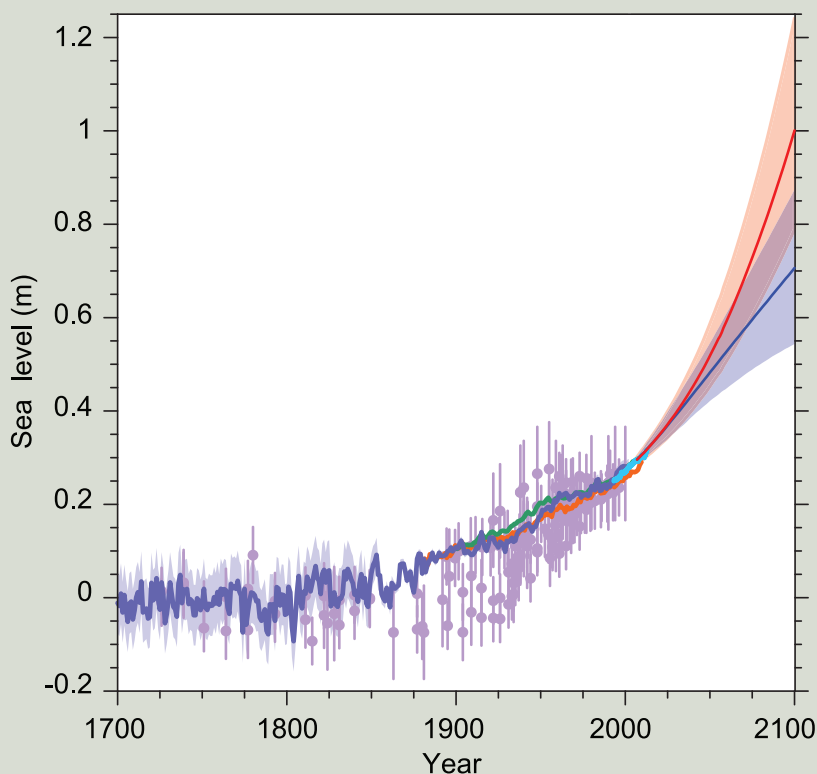
TFE.2 (continued)



TFE.2, Figure 1 | (a) The observed and modelled sea level for 1900 to 2010. (b) The rates of sea level change for the same period, with the satellite altimeter data shown as a red dot for the rate. (c) The observed and modelled sea level for 1961 to 2010. (d) The observed and modelled sea level for 1990 to 2010. Panel (e) compares the sum of the observed contributions (orange) and the observed sea level from the satellite altimeter data (red). Estimates of GMSL from different sources are given, with the shading indicating the uncertainty estimates (two standard deviations). The satellite altimeter data since 1993 are shown in red. The grey lines in panels (a)-(d) are the sums of the contributions from modelled ocean thermal expansion and glaciers (excluding glaciers peripheral to the Antarctic ice sheet), plus changes in land-water storage (see Figure 13.4). The black line is the mean of the grey lines plus a correction of thermal expansion for the omission of volcanic forcing in the Atmosphere–Ocean General Circulation Model (AOGCM) control experiments (see Section 13.3.1). The dashed black line (adjusted model mean) is the sum of the corrected model mean thermal expansion, the change in land water storage, the glacier estimate using observed (rather than modelled) climate (see Figure 13.4), and an illustrative long-term ice-sheet contribution (of 0.1 mm yr⁻¹). The dotted black line is the adjusted model mean but now including the observed ice-sheet contributions, which begin in 1993. Because the observational ice-sheet estimates include the glaciers peripheral to the Greenland and Antarctic ice sheets (from Section 4.4), the contribution from glaciers to the adjusted model mean excludes the peripheral glaciers (PGs) to avoid double counting. [13.3; Figure 13.7]

TFE.2 (continued)

When calibrated appropriately, recently improved dynamical ice sheet models can reproduce the observed rapid changes in ice sheet outflow for individual glacier systems (e.g., Pine Island Glacier in Antarctica; *medium confidence*). However, models of ice sheet response to global warming and particularly ice sheet–ocean interactions are incomplete and the omission of ice sheet models, especially of dynamics, from the model budget of the past means that they have not been as critically evaluated as other contributions. {13.3, 13.4}



TFE.2, Figure 2 | Compilation of paleo sealevel data (purple), tide gauge data (blue, red and green), altimeter data (light blue) and central estimates and *likely* ranges for projections of global mean sea level rise from the combination of CMIP5 and process-based models for RCP2.6 (blue) and RCP8.5 (red) scenarios, all relative to pre-industrial values. {Figures 13.3, 13.11, 13.27}

GMSL rise for 2081–2100 (relative to 1986–2005) for the Representative Concentration Pathways (RCPs) will *likely* be in the 5 to 95% ranges derived from Coupled Model Intercomparison Project Phase 5 (CMIP5) climate projections in combination with process-based models of other contributions (*medium confidence*), that is, 0.26 to 0.55 m (RCP2.6), 0.32 to 0.63 m (RCP4.5), 0.33 to 0.63 m (RCP6.0), 0.45 to 0.82 (RCP8.5) m (see Table TS.1 and Figure TS.15 for RCP forcing). For RCP8.5 the range at 2100 is 0.52 to 0.98 m. Confidence in the projected *likely* ranges comes from the consistency of process-based models with observations and physical understanding. It is assessed that there is currently insufficient evidence to evaluate the probability of specific levels above the *likely* range. Based on current understanding, only the collapse of marine-based sectors of the Antarctic ice sheet, if initiated, could cause GMSL to rise substantially above the *likely* range during the 21st century. There is a lack of consensus on the probability for such a collapse, and the potential additional contribution to GMSL rise cannot be precisely quantified, but there is *medium confidence* that it would not exceed several tenths of a metre of sea level rise during the 21st century. It is *virtually certain* that GMSL rise will continue beyond 2100. {13.5.1, 13.5.3}

Many semi-empirical models projections of GMSL rise are higher than process-based model projections, but there is no consensus in the scientific community about their reliability and there is thus *low confidence* in their projections. {13.5.2, 13.5.3}

TFE.2, Figure 2 combines the paleo, tide gauge and altimeter observations of sea level rise from 1700 with the projected GMSL change to 2100. {13.5, 13.7, 13.8}

There is *low confidence* in a global-scale observed trend in drought or dryness (lack of rainfall), owing to lack of direct observations, dependencies of inferred trends on the index choice and geographical inconsistencies in the trends. However, this masks important regional changes and, for example, the frequency and intensity of drought have *likely* increased in the Mediterranean and West Africa and *likely* decreased in central North America and northwest Australia since 1950. {2.6.2; Table 2.13}

There is *high confidence* for droughts during the last millennium of greater magnitude and longer duration than those observed since the beginning of the 20th century in many regions. There is *medium confidence* that more megadroughts occurred in monsoon Asia and wetter conditions prevailed in arid Central Asia and the South American monsoon region during the Little Ice Age (1450–1850) compared to the Medieval Climate Anomaly (950–1250). {5.5.4, 5.5.5}

Confidence remains *low* for long-term (centennial) changes in tropical cyclone activity, after accounting for past changes in observing capabilities. However, for the years since the 1970s, it is *virtually certain* that the frequency and intensity of storms in the North Atlantic have increased although the reasons for this increase are debated (see TFE.9). There is *low confidence* of large-scale trends in storminess over the last century and there is still insufficient evidence to determine whether robust trends exist in small-scale severe weather events such as hail or thunderstorms. {2.6.2–2.6.4}

With *high confidence*, floods larger than recorded since the 20th century occurred during the past five centuries in northern and central Europe, the western Mediterranean region and eastern Asia. There is *medium confidence* that in the Near East, India and central North America, modern large floods are comparable or surpass historical floods in magnitude and/or frequency. {5.5.5}

TS.2.7.2 Oceans

It is *likely* that the magnitude of extreme high sea level events has increased since 1970 (see TFE.9, Table 1). Most of the increase in extreme sea level can be explained by the mean sea level rise: changes in extreme high sea levels are reduced to less than 5 mm yr⁻¹ at 94% of tide gauges once the rise in mean sea level is accounted for. There is *medium confidence* based on reanalysis forced model hindcasts and ship observations that mean significant wave height has increased since the 1950s over much of the North Atlantic north of 45°N, with typical winter season trends of up to 20 cm per decade. {3.4.5, 3.7.5}

TS.2.8 Changes in Carbon and Other Biogeochemical Cycles

Concentrations of the atmospheric greenhouse gases (GHGs) carbon dioxide (CO₂), methane (CH₄) and nitrous oxide (N₂O) in 2011 exceed the range of concentrations recorded in ice cores during the past 800 kyr. Past changes in atmospheric GHG concentrations are determined

with *very high confidence* from polar ice cores. Since AR4 these records have been extended from 650 ka to 800 ka. {5.2.2}

With *very high confidence*, the current rates of CO₂, CH₄ and N₂O rise in atmospheric concentrations and the associated increases in RF are unprecedented with respect to the ‘highest resolution’ ice core records of the last 22 kyr. There is *medium confidence* that the rate of change of the observed GHG rise is also unprecedented compared with the lower resolution records of the past 800 kyr. {2.2.1, 5.2.2}

In several periods characterized by high atmospheric CO₂ concentrations, there is *medium confidence* that global mean temperature was significantly above pre-industrial level. During the mid-Pliocene (3.3 to 3.0 Ma), atmospheric CO₂ concentration between 350 ppm and 450 ppm (*medium confidence*) occurred when GMST was 1.9°C to 3.6°C warmer (*medium confidence*) than for pre-industrial climate. During the Early Eocene (52 to 48 Ma), atmospheric CO₂ concentration exceeded about 1000 ppm when GMST was 9°C to 14°C higher (*medium confidence*) than for pre-industrial conditions. {5.3.1}

TS.2.8.1 Carbon Dioxide

Between 1750 and 2011, CO₂ emissions from fossil fuel combustion and cement production are estimated from energy and fuel use statistics to have released 375 [345 to 405] PgC⁹. In 2002–2011, average fossil fuel and cement manufacturing emissions were 8.3 [7.6 to 9.0] PgC yr⁻¹ (*high confidence*), with an average growth rate of 3.2% yr⁻¹ (Figure TS.4). This rate of increase of fossil fuel emissions is higher than during the 1990s (1.0% yr⁻¹). In 2011, fossil fuel emissions were 9.5 [8.7 to 10.3] PgC. {2.2.1, 6.3.1; Table 6.1}

Between 1750 and 2011, land use change (mainly deforestation), derived from land cover data and modelling, is estimated to have released 180 [100 to 260] PgC. Land use change emissions between 2002 and 2011 are dominated by tropical deforestation, and are estimated at 0.9 [0.1 to 1.7] PgC yr⁻¹ (*medium confidence*), with possibly a small decrease from the 1990s due to lower reported forest loss during this decade. This estimate includes gross deforestation emissions of around 3 PgC yr⁻¹ compensated by around 2 PgC yr⁻¹ of forest regrowth in some regions, mainly abandoned agricultural land. {6.3.2; Table 6.2}

Of the 555 [470 to 640] PgC released to the atmosphere from fossil fuel and land use emissions from 1750 to 2011, 240 [230 to 250] PgC accumulated in the atmosphere, as estimated with very high accuracy from the observed increase of atmospheric CO₂ concentration from 278 [273 to 283] ppm¹⁰ in 1750 to 390.5 [390.4 to 390.6] ppm in 2011. The amount of CO₂ in the atmosphere grew by 4.0 [3.8 to 4.2] PgC yr⁻¹ in the first decade of the 21st century. The distribution of observed atmospheric CO₂ increases with latitude clearly shows that the increases are driven by anthropogenic emissions that occur primarily in the industrialized countries north of the equator. Based on annual average concentrations, stations in the NH show slightly higher concentrations than stations in the SH. An independent line of evidence

⁹ 1 Petagram of carbon = 1 PgC = 10¹⁵ grams of carbon = 1 Gigatonne of carbon = 1 GtC. This corresponds to 3.667 GtCO₂.

¹⁰ ppm (parts per million) or ppb (parts per billion, 1 billion = 1000 million) is the ratio of the number of greenhouse gas molecules to the total number of molecules of dry air. For example, 300 ppm means 300 molecules of a greenhouse gas per million molecules of dry air.

for the anthropogenic origin of the observed atmospheric CO₂ increase comes from the observed consistent decrease in atmospheric oxygen (O₂) content and a decrease in the stable isotopic ratio of CO₂ (¹³C/¹²C) in the atmosphere (Figure TS.5). {2.2.1, 6.1.3}

The remaining amount of carbon released by fossil fuel and land use emissions has been re-absorbed by the ocean and terrestrial ecosystems. Based on high agreement between independent estimates using different methods and data sets (e.g., oceanic carbon, oxygen and transient tracer data), it is *very likely* that the global ocean

inventory of anthropogenic carbon increased from 1994 to 2010. In 2011, it is estimated to be 155 [125 to 185] PgC. The annual global oceanic uptake rates calculated from independent data sets (from changes in the oceanic inventory of anthropogenic carbon, from measurements of the atmospheric oxygen to nitrogen ratio (O₂/N₂) or from CO₂ partial pressure (pCO₂) data) and for different time periods agree with each other within their uncertainties, and *very likely* are in the range of 1.0 to 3.2 PgC yr⁻¹. Regional observations of the storage rate of anthropogenic carbon in the ocean are in broad agreement with the expected rate resulting from the increase in atmospheric CO₂

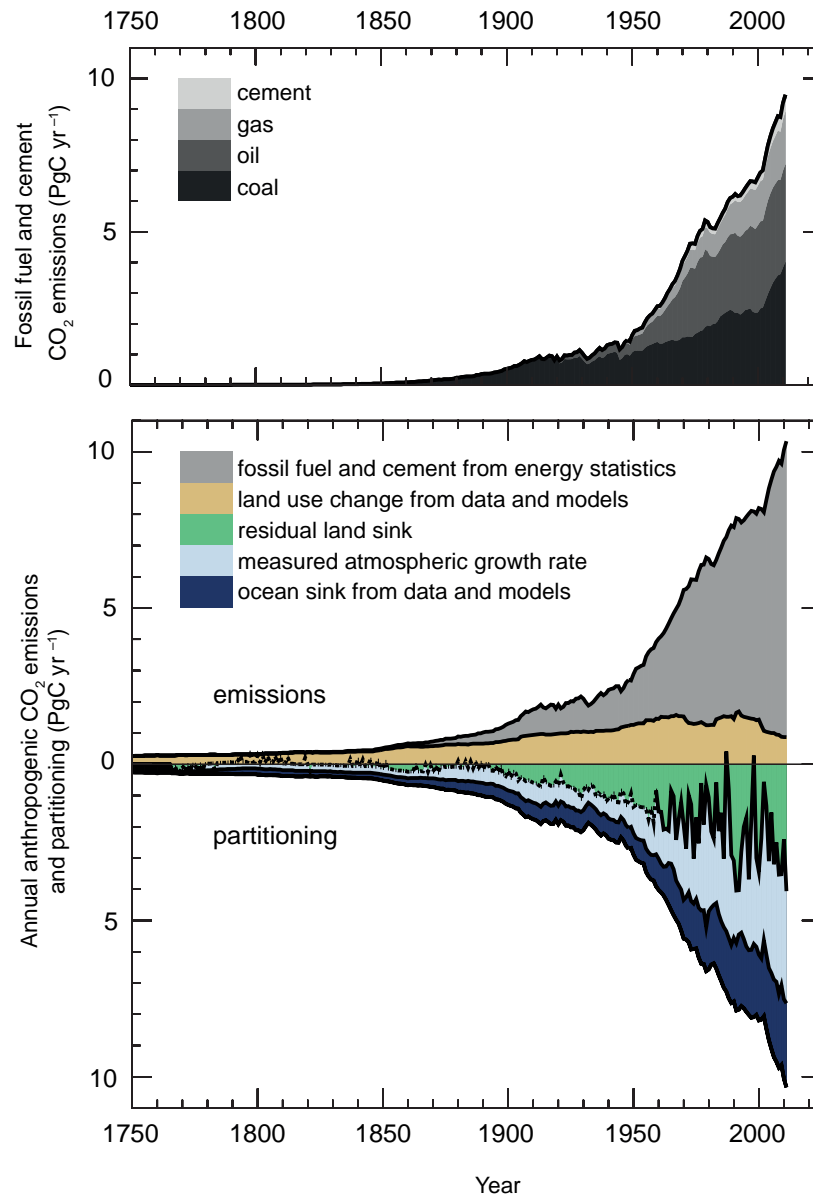


Figure TS.4 | Annual anthropogenic CO₂ emissions and their partitioning among the atmosphere, land and ocean (PgC yr⁻¹) from 1750 to 2011. (Top) Fossil fuel and cement CO₂ emissions by category, estimated by the Carbon Dioxide Information Analysis Center (CDIAC). (Bottom) Fossil fuel and cement CO₂ emissions as above. CO₂ emissions from net land use change, mainly deforestation, are based on land cover change data (see Table 6.2). The atmospheric CO₂ growth rate prior to 1959 is based on a spline fit to ice core observations and a synthesis of atmospheric measurements from 1959. The fit to ice core observations does not capture the large interannual variability in atmospheric CO₂ and is represented with a dashed line. The ocean CO₂ sink is from a combination of models and observations. The residual land sink (term in green in the figure) is computed from the residual of the other terms. The emissions and their partitioning include only the fluxes that have changed since 1750, and not the natural CO₂ fluxes (e.g., atmospheric CO₂ uptake from weathering, outgassing of CO₂ from lakes and rivers and outgassing of CO₂ by the ocean from carbon delivered by rivers; see Figure 6.1) between the atmosphere, land and ocean reservoirs that existed before that time and still exist today. The uncertainties in the various terms are discussed in Chapter 6 and reported in Table 6.1 for decadal mean values. {Figure 6.8}

TS

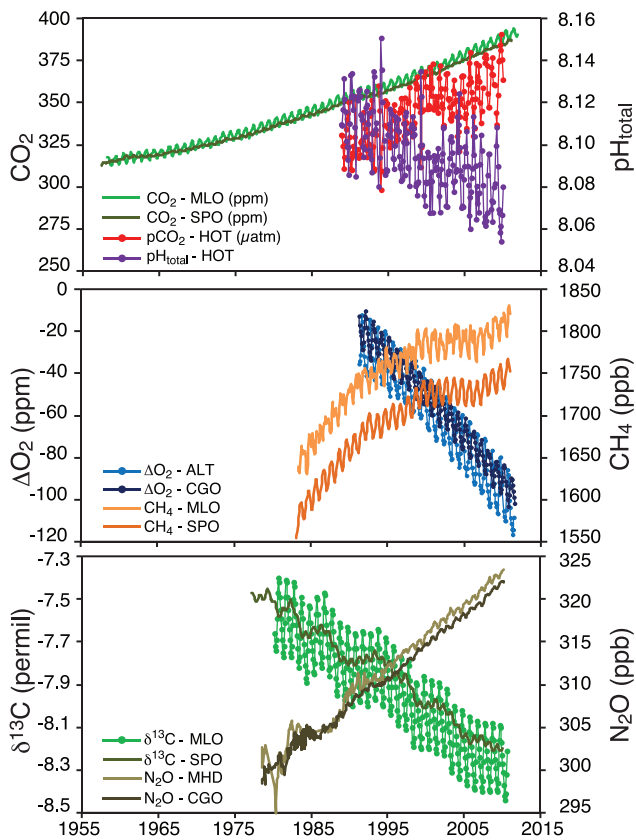


Figure TS.5 | Atmospheric concentration of CO₂, oxygen, ¹³C/¹²C stable isotope ratio in CO₂, as well as CH₄ and N₂O atmospheric concentrations and oceanic surface observations of CO₂ partial pressure (pCO₂) and pH, recorded at representative time series stations in the Northern and the Southern Hemispheres. MLO: Mauna Loa Observatory, Hawaii; SPO: South Pole; HOT: Hawaii Ocean Time-Series station; MHD: Mace Head, Ireland; CGO: Cape Grim, Tasmania; ALT: Alert, Northwest Territories, Canada. Further detail regarding the related Figure SPM.4 is given in the TS Supplementary Material. {Figures 3.18, 6.3; FAQ 3.3, Figure 1}

concentrations, but with significant spatial and temporal variations. {3.8.1, 6.3}

Natural terrestrial ecosystems (those not affected by land use change) are estimated by difference from changes in other reservoirs to have accumulated 160 [70 to 250] PgC between 1750 and 2011. The gain of carbon by natural terrestrial ecosystems is estimated to take place mainly through the uptake of CO₂ by enhanced photosynthesis at higher CO₂ levels and nitrogen deposition and longer growing seasons in mid and high latitudes. Natural carbon sinks vary regionally owing to physical, biological and chemical processes acting on different time scales. An excess of atmospheric CO₂ absorbed by land ecosystems gets stored as organic matter in diverse carbon pools, from short-lived (leaves, fine roots) to long-lived (stems, soil carbon). {6.3; Table 6.1}

TS.2.8.2 Carbon and Ocean Acidification

Oceanic uptake of anthropogenic CO₂ results in gradual acidification of the ocean. The pH¹¹ of ocean surface water has decreased by 0.1 since

the beginning of the industrial era (*high confidence*), corresponding to a 26% increase in hydrogen ion concentration. The observed pH trends range between −0.0014 and −0.0024 per year in surface waters. In the ocean interior, natural physical and biological processes, as well as uptake of anthropogenic CO₂, can cause changes in pH over decadal and longer time scales. {3.8.2; Box 3.2; Table 3.2; FAQ 3.3}

TS.2.8.3 Methane

The concentration of CH₄ has increased by a factor of 2.5 since pre-industrial times, from 722 [697 to 747] ppb in 1750 to 1803 [1799 to 1807] ppb in 2011 (Figure TS.5). There is *very high confidence* that the atmospheric CH₄ increase during the Industrial Era is caused by anthropogenic activities. The massive increase in the number of ruminants, the emissions from fossil fuel extraction and use, the expansion of rice paddy agriculture and the emissions from landfills and waste are the dominant anthropogenic CH₄ sources. Anthropogenic emissions account for 50 to 65% of total emissions. By including natural geological CH₄ emissions that were not accounted for in previous budgets, the fossil component of the total CH₄ emissions (i.e., anthropogenic emissions related to leaks in the fossil fuel industry and natural geological leaks) is now estimated to amount to about 30% of the total CH₄ emissions (*medium confidence*). {2.2.1, 6.1, 6.3.3}

In recent decades, CH₄ growth in the atmosphere has been variable. CH₄ concentrations were relatively stable for about a decade in the 1990s, but then started growing again starting in 2007. The exact drivers of this renewed growth are still debated. Climate-driven fluctuations of CH₄ emissions from natural wetlands (177 to 284 × 10¹² g (CH₄) yr⁻¹ for 2000–2009 based on bottom-up estimates) are the main drivers of the global interannual variability of CH₄ emissions (*high confidence*), with a smaller contribution from biomass burning emissions during high fire years {2.2.1, 6.3.3; Table 6.8}.

TS.2.8.4 Nitrous Oxide

Since pre-industrial times, the concentration of N₂O in the atmosphere has increased by a factor of 1.2 (Figure TS.5). Changes in the nitrogen cycle, in addition to interactions with CO₂ sources and sinks, affect emissions of N₂O both on land and from the ocean. {2.2.1, 6.4.6}

TS.2.8.5 Oceanic Oxygen

High agreement among analyses provides *medium confidence* that oxygen concentrations have decreased in the open ocean thermocline in many ocean regions since the 1960s. The general decline is consistent with the expectation that warming-induced stratification leads to a decrease in the supply of oxygen to the thermocline from near surface waters, that warmer waters can hold less oxygen and that changes in wind-driven circulation affect oxygen concentrations. It is *likely* that the tropical oxygen minimum zones have expanded in recent decades. {3.8.3}

¹¹ pH is a measure of acidity: a decrease in pH value means an increase in acidity, that is, acidification.

TS.3 Drivers of Climate Change

TS.3.1 Introduction

Human activities have changed and continue to change the Earth's surface and atmospheric composition. Some of these changes have a direct or indirect impact on the energy balance of the Earth and are thus drivers of climate change. Radiative forcing (RF) is a measure of the net change in the energy balance of the Earth system in response to some external perturbation (see Box TS.2), with positive RF leading to a warming and negative RF to a cooling. The RF concept is valuable for comparing the influence on GMST of most individual agents affecting the Earth's radiation balance. The quantitative values provided in AR5 are consistent with those in previous IPCC reports, though there have been some important revisions (Figure TS.6). Effective radiative forcing (ERF) is now used to quantify the impact of some forcing agents that involve rapid adjustments of components of the atmosphere and surface that are assumed constant in the RF concept (see Box TS.2). RF and ERF are estimated from the change between 1750 and 2011, referred to as 'Industrial Era', if other time periods are not explicitly stated. Uncertainties are given associated with the best estimates of RF and ERF, with values representing the 5 to 95% (90%) confidence range. {8.1, 7.1}

In addition to the global mean RF or ERF, the spatial distribution and temporal evolution of forcing, as well as climate feedbacks, play a role in determining the eventual impact of various drivers on climate. Land surface changes may also impact the local and regional climate through processes that are not radiative in nature. {8.1, 8.3.5, 8.6}

TS.3.2 Radiative Forcing from Greenhouse Gases

Human activity leads to change in the atmospheric composition either directly (via emissions of gases or particles) or indirectly (via atmospheric chemistry). Anthropogenic emissions have driven the changes

in well-mixed greenhouse gas (WMGHG) concentrations during the Industrial Era (see Section TS.2.8 and TFE.7). As historical WMGHG concentrations since the pre-industrial are well known based on direct measurements and ice core records, and WMGHG radiative properties are also well known, the computation of RF due to concentration changes provides tightly constrained values (Figure TS.6). There has not been significant change in our understanding of WMGHG radiative impact, so that the changes in RF estimates relative to AR4 are due essentially to concentration increases. The best estimate for WMGHG ERF is the same as RF, but the uncertainty range is twice as large due to the poorly constrained cloud responses. Owing to high-quality observations, it is certain that increasing atmospheric burdens of most WMGHGs, especially CO₂, resulted in a further increase in their RF from 2005 to 2011. Based on concentration changes, the RF of all WMGHGs in 2011 is 2.83 [2.54 to 3.12] W m⁻² (*very high confidence*). This is an increase since AR4 of 0.20 [0.18 to 0.22] W m⁻², with nearly all of the increase due to the increase in the abundance of CO₂ since 2005. The Industrial Era RF for CO₂ alone is 1.82 [1.63 to 2.01] W m⁻². Over the last 15 years, CO₂ has been the dominant contributor to the increase in RF from the WMGHGs, with RF of CO₂ having an average growth rate slightly less than 0.3 W m⁻² per decade. The uncertainty in the WMGHG RF is due in part to its radiative properties but mostly to the full accounting of atmospheric radiative transfer including clouds. {2.2.1, 5.2, 6.3, 8.3, 8.3.2; Table 6.1}

After a decade of near stability, the recent increase of CH₄ concentration led to an enhanced RF compared to AR4 by 2% to 0.48 [0.43 to 0.53] W m⁻². It is *very likely* that the RF from CH₄ is now larger than that of all halocarbons combined. {2.2.1, 8.3.2}

Atmospheric N₂O has increased by 6% since AR4, causing an RF of 0.17 [0.14 to 0.20] W m⁻². N₂O concentrations continue to rise while those of dichlorodifluoromethane (CF₂Cl₂, CFC-12), the third largest WMGHG contributor to RF for several decades, are decreasing due to phase-out of emissions of this chemical under the Montreal Protocol. Since

Box TS.2 | Radiative Forcing and Effective Radiative Forcing

RF and ERF are used to quantify the change in the Earth's energy balance that occurs as a result of an externally imposed change. They are expressed in watts per square metre (W m⁻²). RF is defined in AR5, as in previous IPCC assessments, as the change in net downward flux (shortwave + longwave) at the tropopause after allowing for stratospheric temperatures to readjust to radiative equilibrium, while holding other state variables such as tropospheric temperatures, water vapour and cloud cover fixed at the unperturbed values (see Glossary). {8.1.1}

Although the RF concept has proved very valuable, improved understanding has shown that including rapid adjustments of the Earth's surface and troposphere can provide a better metric for quantifying the climate response. These rapid adjustments occur over a variety of time scales, but are relatively distinct from responses to GMST change. Aerosols in particular impact the atmosphere temperature profile and cloud properties on a time scale much shorter than adjustments of the ocean (even the upper layer) to forcings. The ERF concept defined in AR5 allows rapid adjustments to perturbations, for all variables except for GMST or ocean temperature and sea ice cover. The ERF and RF values are significantly different for the anthropogenic aerosols, owing to their influence on clouds and on snow or ice cover. For other components that drive the Earth's energy balance, such as GHGs, ERF and RF are fairly similar, and RF may have comparable utility given that it requires fewer computational resources to calculate and is not affected by meteorological variability and hence can better isolate small forcings. In cases where RF and ERF differ substantially, ERF has been shown to be a better indicator of the GMST response and is therefore emphasized in AR5. {7.1, 8.1; Box 8.1}

AR4, N₂O has overtaken CFC-12 to become the third largest WMGHG contributor to RF. The RF from halocarbons is very similar to the value in AR4, with a reduced RF from CFCs but increases in many of their replacements. Four of the halocarbons (trichlorofluoromethane (CFCl₃, CFC-11), CFC-12, trichlorotrifluoroethane (CF₂ClCFCl₂, CFC-113) and chlorodifluoromethane (CHF₂Cl, HCFC-22) account for 85% of the total halocarbon RF. The former three compounds have declining RF over the last 5 years but are more than compensated for by the increased

RF from HCFC-22. There is *high confidence* that the growth rate in RF from all WMGHG is weaker over the last decade than in the 1970s and 1980s owing to a slower increase in the non-CO₂ RF. {2.2.1, 8.3.2}

The short-lived GHGs ozone (O₃) and stratospheric water vapour also contribute to anthropogenic forcing. Observations indicate that O₃ *likely* increased at many undisturbed (background) locations through the 1990s. These increases have continued mainly over Asia (though

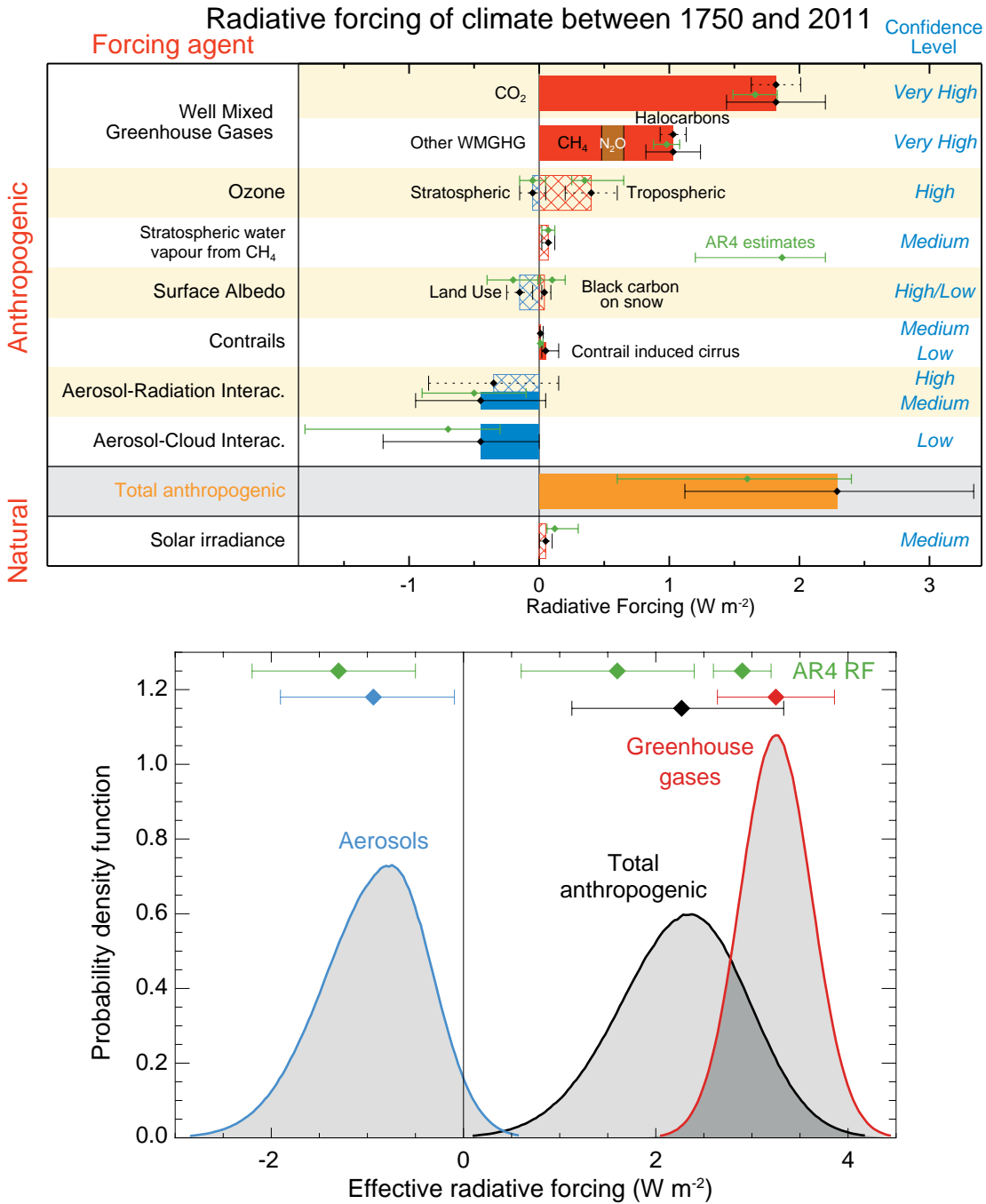


Figure TS.6 | Radiative forcing (RF) and Effective radiative forcing (ERF) of climate change during the Industrial Era. (Top) Forcing by concentration change between 1750 and 2011 with associated uncertainty range (solid bars are ERF, hatched bars are RF, green diamonds and associated uncertainties are for RF assessed in AR4). (Bottom) Probability density functions (PDFs) for the ERF for the aerosol, greenhouse gas (GHG) and total. The green lines show the AR4 RF 90% confidence intervals and can be compared with the red, blue and black lines which show the AR5 ERF 90% confidence intervals (although RF and ERF differ, especially for aerosols). The ERF from surface albedo changes and combined contrails and contrail-induced cirrus is included in the total anthropogenic forcing, but not shown as a separate PDF. For some forcing mechanisms (ozone, land use, solar) the RF is assumed to be representative of the ERF but an additional uncertainty of 17% is added in quadrature to the RF uncertainty. {Figures 8.15, 8.16}

observations cover a limited area) and flattened over Europe during the last decade. The total RF due to changes in O_3 is 0.35 [0.15 to 0.55] $W m^{-2}$ (*high confidence*), with RF due to tropospheric O_3 of 0.40 [0.20 to 0.60] $W m^{-2}$ (*high confidence*) and due to stratospheric O_3 of -0.05 [-0.15 to $+0.05$] $W m^{-2}$ (*high confidence*). O_3 is not emitted directly into the atmosphere; instead it is formed by photochemical reactions. In the troposphere these reactions involve precursor compounds that are emitted into the atmosphere from a variety of natural and anthropogenic sources. Tropospheric O_3 RF is largely attributed to increases in emissions of CH_4 , carbon monoxide, volatile organics and nitrogen oxides, while stratospheric RF results primarily from O_3 depletion by anthropogenic halocarbons. However, there is now strong evidence for substantial links between the changes in tropospheric and stratospheric O_3 and a total O_3 RF of 0.50 [0.30 to 0.70] $W m^{-2}$ is attributed to tropospheric O_3 precursor emissions and -0.15 [-0.30 to 0.00] $W m^{-2}$ to O_3 depletion by halocarbons. There is strong evidence that tropospheric O_3 also has a detrimental impact on vegetation physiology, and therefore on its CO_2 uptake. This reduced uptake leads to an indirect increase in the atmospheric CO_2 concentration. Thus a fraction of the CO_2 RF should be attributed to ozone or its precursors rather than direct emission of CO_2 , but there is a *low confidence* on the quantitative estimates. RF for stratospheric water vapour produced from CH_4 oxidation is 0.07 [0.02 to 0.12] $W m^{-2}$. Other changes in stratospheric water vapour, and all changes in water vapour in the troposphere, are regarded as a feedback rather than a forcing. {2.2.2, 8.1–8.3; FAQ 8.1}

TS.3.3 Radiative Forcing from Anthropogenic Aerosols

Anthropogenic aerosols are responsible for an RF of climate through multiple processes which can be grouped into two types: aerosol–radiation interactions (ari) and aerosol–cloud interactions (aci). There has been progress since AR4 on observing and modelling climate-relevant aerosol properties (including their size distribution, hygroscopicity, chemical composition, mixing state, optical and cloud nucleation properties) and their atmospheric distribution. Nevertheless, substantial uncertainties remain in assessments of long-term trends of global aerosol optical depth and other global properties of aerosols due to difficulties in measurement and lack of observations of some relevant parameters, high spatial and temporal variability and the relatively short observational records that exist. The anthropogenic RFari is given a best estimate of -0.35 [-0.85 to $+0.15$] $W m^{-2}$ (*high confidence*) using evidence from aerosol models and some constraints from observations. The RFari is caused by multiple aerosol types (see Section TS3.6). The rapid adjustment to RFari leads to further negative forcing, in particular through cloud adjustments, and is attributable primarily to black carbon. As a consequence, the ERFari is more negative than the RFari (*low confidence*) and given a best estimate of -0.45 [-0.95 to $+0.05$] $W m^{-2}$. The assessment for RFari is less negative than reported in AR4 because of a re-evaluation of aerosol absorption. The uncertainty estimate is wider but more robust. {2.2.3, 7.3, 7.5.2}

Improved understanding of aerosol–cloud interactions has led to a reduction in the magnitude of many global aerosol–cloud forcings estimates. The total ERF due to aerosols (ERFari+aci, excluding the effect of absorbing aerosol on snow and ice) is assessed to be -0.9 [-1.9 to -0.1] $W m^{-2}$ (*medium confidence*). This estimate encompasses all rapid adjustments, including changes to the cloud lifetime and aerosol

microphysical effects on mixed-phase, ice and convective clouds. This range was obtained by giving equal weight to satellite-based studies and estimates from climate models. It is consistent with multiple lines of evidence suggesting less negative estimates for aerosol–cloud interactions than those discussed in AR4. {7.4, 7.5, 8.5}

The RF from black carbon (BC) on snow and ice is assessed to be 0.04 [0.02 to 0.09] $W m^{-2}$ (*low confidence*). Unlike in the previous IPCC assessment, this estimate includes the effects on sea ice, accounts for more physical processes and incorporates evidence from both models and observations. This RF causes a two to four times larger GMST change per unit forcing than CO_2 primarily because all of the forcing energy is deposited directly into the cryosphere, whose evolution drives a positive albedo feedback on climate. This effect thus can represent a significant forcing mechanism in the Arctic and other snow- or ice-covered regions. {7.3, 7.5.2, 8.3.4, 8.5}

Despite the large uncertainty ranges on aerosol forcing, there is a *high confidence* that aerosols have offset a substantial portion of GHG forcing. Aerosol–cloud interactions can influence the character of individual storms, but evidence for a systematic aerosol effect on storm or precipitation intensity is more limited and ambiguous. {7.4, 7.6, 8.5}

TS.3.4 Radiative Forcing from Land Surface Changes and Contrails

There is robust evidence that anthropogenic land use changes such as deforestation have increased the land surface albedo, which leads to an RF of -0.15 [-0.25 to -0.05] $W m^{-2}$. There is still a large spread of quantitative estimates owing to different assumptions for the albedo of natural and managed surfaces (e.g., croplands, pastures). In addition, the time evolution of the land use change, and in particular how much was already completed in the reference year 1750, are still debated. Furthermore, land use change causes other modifications that are not radiative but impact the surface temperature, including modifications in the surface roughness, latent heat flux, river runoff and irrigation. These are more uncertain and they are difficult to quantify, but they tend to offset the impact of albedo changes at the global scale. As a consequence, there is low agreement on the sign of the net change in global mean temperature as a result of land use change. Land use change, and in particular deforestation, also has significant impacts on WMGHG concentrations. It contributes to the corresponding RF associated with CO_2 emissions or concentration changes. {8.3.5}

Persistent contrails from aviation contribute a positive RF of 0.01 [0.005 to 0.03] $W m^{-2}$ (*medium confidence*) for year 2011, and the combined contrail and contrail-cirrus ERF from aviation is assessed to be 0.05 [0.02 to 0.15] $W m^{-2}$ (*low confidence*). This forcing can be much larger regionally but there is now *medium confidence* that it does not produce observable regional effects on either the mean or diurnal range of surface temperature. {7.2.7}

TS.3.5 Radiative Forcing from Natural Drivers of Climate Change

Solar and volcanic forcings are the two dominant natural contributors to global climate change during the Industrial Era. Satellite observations

of total solar irradiance (TSI) changes since 1978 show quasi-periodic cyclical variation with a period of roughly 11 years. Longer term forcing is typically estimated by comparison of solar minima (during which variability is least). This gives an RF change of -0.04 [-0.08 to 0.00] W m^{-2} between the most recent (2008) minimum and the 1986 minimum. There is some diversity in the estimated trends of the composites of various satellite data, however. Secular trends of TSI before the start of satellite observations rely on a number of indirect proxies. The best estimate of RF from TSI changes over the industrial era is 0.05 [0.00 to 0.10] W m^{-2} (*medium confidence*), which includes greater RF up to around 1980 and then a small downward trend. This RF estimate is substantially smaller than the AR4 estimate due to the addition of the latest solar cycle and inconsistencies in how solar RF was estimated in earlier IPCC assessments. The recent solar minimum appears to have been unusually low and long-lasting and several projections indicate lower TSI for the forthcoming decades. However, current abilities to project solar irradiance are extremely limited so that there is *very low confidence* concerning future solar forcing. Nonetheless, there is a *high confidence* that 21st century solar forcing will be much smaller than the projected increased forcing due to WMGHGs. {5.2.1, 8.4.1; FAQ 5.1}

Changes in solar activity affect the cosmic ray flux impinging upon the Earth's atmosphere, which has been hypothesized to affect climate through changes in cloudiness. Cosmic rays enhance aerosol nucleation and thus may affect cloud condensation nuclei production in the free troposphere, but the effect is too weak to have any climatic influence during a solar cycle or over the last century (medium evidence, high agreement). No robust association between changes in cosmic rays and cloudiness has been identified. In the event that such an association existed, a mechanism other than cosmic ray-induced nucleation of new aerosol particles would be needed to explain it. {7.3, 7.4.6}

The RF of stratospheric volcanic aerosols is now well understood and there is a large RF for a few years after major volcanic eruptions (Box TS.5, Figure 1). Although volcanic eruptions inject both mineral particles and sulphate aerosol precursors into the atmosphere, it is the latter, because of their small size and long lifetimes, that are responsible for RF important for climate. The emissions of CO_2 from volcanic eruptions are at least 100 times smaller than anthropogenic emissions, and inconsequential for climate on century time scales. Large tropical volcanic eruptions have played an important role in driving annual to decadal scale climate change during the Industrial Era owing to their sometimes very large negative RF. There has not been any major volcanic eruption since Mt Pinatubo in 1991, which caused a 1-year RF of about -3.0 W m^{-2} , but several smaller eruptions have caused an RF averaged over the years 2008–2011 of -0.11 [-0.15 to -0.08] W m^{-2} (*high confidence*), twice as strong in magnitude compared to the 1999–2002 average. The smaller eruptions have led to better understanding of the dependence of RF on the amount of material from high-latitude injections as well as the time of the year when they take place. {5.2.1, 5.3.5, 8.4.2; Annex II}

TS.3.6 Synthesis of Forcings; Spatial and Temporal Evolution

A synthesis of the Industrial Era forcing finds that among the forcing agents, there is a *very high confidence* only for the WMGHG RF. Relative

to AR4, the confidence level has been elevated for seven forcing agents owing to improved evidence and understanding. {8.5; Figure 8.14}

The time evolution of the total anthropogenic RF shows a nearly continuous increase from 1750, primarily since about 1860. The total anthropogenic RF increase rate since 1960 has been much greater than during earlier Industrial Era periods, driven primarily by the continuous increase in most WMGHG concentrations. There is still low agreement on the time evolution of the total aerosol ERF, which is the primary factor for the uncertainty in the total anthropogenic forcing. The fractional uncertainty in the total anthropogenic forcing decreases gradually after 1950 owing to the smaller offset of positive WMGHG forcing by negative aerosol forcing. There is robust evidence and high agreement that natural forcing is a small fraction of the WMGHG forcing. Natural forcing changes over the last 15 years have *likely* offset a substantial fraction (at least 30%) of the anthropogenic forcing increase during this period (Box TS.3). Forcing by CO_2 is the largest single contributor to the total forcing during the Industrial Era and from 1980–2011. Compared to the entire Industrial Era, the dominance of CO_2 forcing is larger for the 1980–2011 change with respect to other WMGHGs, and there is *high confidence* that the offset from aerosol forcing to WMGHG forcing during this period was much smaller than over the 1950–1980 period. {8.5.2}

Forcing can also be attributed to emissions rather than to the resulting concentration changes (Figure TS.7). Carbon dioxide is the largest single contributor to historical RF from either the perspective of changes in the atmospheric concentration of CO_2 or the impact of changes in net emissions of CO_2 . The relative importance of other forcing agents can vary markedly with the perspective chosen, however. In particular, CH_4 emissions have a much larger forcing (about 1.0 W m^{-2} over the Industrial Era) than CH_4 concentration increases (about 0.5 W m^{-2}) due to several indirect effects through atmospheric chemistry. In addition, carbon monoxide emissions are *virtually certain* to cause a positive forcing, while emissions of reactive nitrogen oxides *likely* cause a net negative forcing but uncertainties are large. Emissions of ozone-depleting halocarbons *very likely* cause a net positive forcing as their direct radiative effect is larger than the impact of the stratospheric ozone depletion that they induce. Emissions of SO_2 , organic carbon and ammonia cause a negative forcing, while emissions of black carbon lead to positive forcing via aerosol–radiation interactions. Note that mineral dust forcing may include a natural component or a climate feedback effect. {7.3, 7.5.2, 8.5.1}

Although the WMGHGs show a spatially fairly homogeneous forcing, other agents such as aerosols, ozone and land use changes are highly heterogeneous spatially. RFari showed maximum negative values over eastern North America and Europe during the early 20th century, with large negative values extending to East and Southeast Asia, South America and central Africa by 1980. Since then, however, the magnitude has decreased over eastern North America and Europe due to pollution control, and the peak negative forcing has shifted to South and East Asia primarily as a result of economic growth and the resulting increase in emissions in those areas. Total aerosol ERF shows similar behaviour for locations with maximum negative forcing, but also shows substantial positive forcing over some deserts and the Arctic. In contrast, the global mean whole atmosphere ozone forcing increased throughout

the 20th century, and has peak positive amplitudes around 15°N to 30°N but negative values over Antarctica. Negative land use forcing by albedo changes has been strongest in industrialized and biomass burning regions. The inhomogeneous nature of these forcings can cause them to have a substantially larger influence on the hydrologic cycle than an equivalent global mean homogeneous forcing. {8.3.5, 8.6}

Over the 21st century, anthropogenic RF is projected to increase under the Representative Concentration Pathways (RCPs; see Box TS.6). Simple model estimates of the RF resulting from the RCPs, which include WMGHG emissions spanning a broad range of possible futures, show anthropogenic RF relative to 1750 increasing to 3.0 to 4.8 W m⁻² in 2050, and 2.7 to 8.4 W m⁻² at 2100. In the near term, the RCPs are quite similar to one another (and emissions of near-term climate forcers do not span the literature range of possible futures), with RF at 2030 ranging only from 2.9 to 3.3 W m⁻² (additional 2010 to 2030 RF of 0.7 to 1.1 W m⁻²), but they show highly diverging values for the second half of the 21st century driven largely by CO₂. Results based on

the RCP scenarios suggest only small changes in aerosol ERF between 2000 and 2030, followed by a strong reduction in the aerosols and a substantial weakening of the negative total aerosol ERF. Nitrate aerosols are an exception to this reduction, with a substantially increased negative forcing which is a robust feature among the few available models. The divergence across the RCPs indicates that, although a certain amount of future climate change is already 'in the system' due to the current radiative imbalance caused by historical emissions and the long lifetime of some atmospheric forcing agents, societal choices can still have a very large effect on future RF, and hence on climate change. {8.2, 8.5.3, 12.3; Figures 8.22, 12.4}

TS.3.7 Climate Feedbacks

Feedbacks will also play an important role in determining future climate change. Indeed, climate change may induce modification in the water, carbon and other biogeochemical cycles which may reinforce (positive feedback) or dampen (negative feedback) the expected

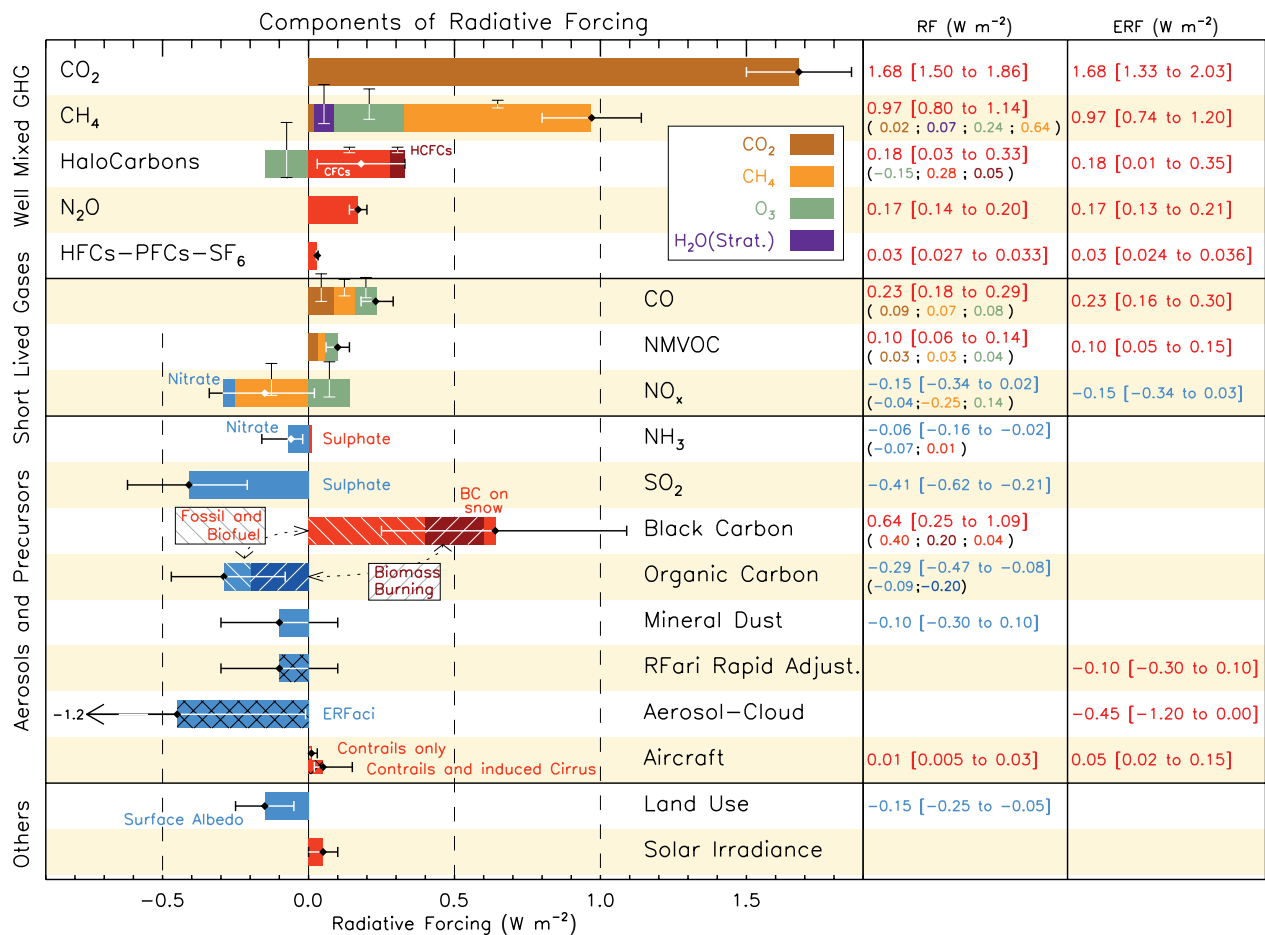


Figure TS.7 | Radiative forcing (RF) of climate change during the Industrial Era shown by emitted components from 1750 to 2011. The horizontal bars indicate the overall uncertainty, while the vertical bars are for the individual components (vertical bar lengths proportional to the relative uncertainty, with a total length equal to the bar width for a ±50% uncertainty). Best estimates for the totals and individual components (from left to right) of the response are given in the right column. Values are RF except for the effective radiative forcing (ERF) due to aerosol–cloud interactions (ERFaci) and rapid adjustment associated with the RF due to aerosol–radiation interaction (RFari Rapid Adjust.). Note that the total RF due to aerosol–radiation interaction (–0.35 Wm⁻²) is slightly different from the sum of the RF of the individual components (–0.33 Wm⁻²). The total RF due to aerosol–radiation interaction is the basis for Figure SPM.5. Secondary organic aerosol has not been included since the formation depends on a variety of factors not currently sufficiently quantified. The ERF of contrails includes contrail induced cirrus. Combining ERFaci –0.45 [–1.2 to 0.0] Wm⁻² and rapid adjustment of ari –0.1 [–0.3 to +0.1] Wm⁻² results in an integrated component of adjustment due to aerosols of –0.55 [–1.33 to –0.06] Wm⁻². CFCs = chlorofluorocarbons, HCFCs = hydrochlorofluorocarbons, HFCs = hydrofluorocarbons, PFCs = perfluorocarbons, NMVOC = Non-Methane Volatile Organic Compounds, BC = black carbon. Further detail regarding the related Figure SPM.5 is given in the TS Supplementary Material. {Figure 8.17}

TS

temperature increase. Snow and ice albedo feedbacks are known to be positive. The combined water vapour and lapse rate feedback is *extremely likely* to be positive and now fairly well quantified, while cloud feedbacks continue to have larger uncertainties (see TFE.6). In addition, the new Coupled Model Intercomparison Project Phase 5 (CMIP5) models consistently estimate a positive carbon-cycle feedback, that is, reduced natural CO₂ sinks in response to future climate change. In particular, carbon-cycle feedbacks in the oceans are positive in the models. Carbon sinks in tropical land ecosystems are less consistent, and may be susceptible to climate change via processes such as drought and fire that are sometimes not yet fully represented. A key update since AR4 is the introduction of nutrient dynamics in some of the CMIP5 land carbon models, in particular the limitations on plant growth imposed by nitrogen availability. The net effect of accounting for the nitrogen cycle is a smaller projected land sink for a given trajectory of anthropogenic CO₂ emissions (see TFE.7). {6.4, Box 6.1, 7.2}

Models and ecosystem warming experiments show high agreement that wetland CH₄ emissions will increase per unit area in a warmer climate, but wetland areal extent may increase or decrease depending on regional changes in temperature and precipitation affecting wetland hydrology, so that there is *low confidence* in quantitative projections of wetland CH₄ emissions. Reservoirs of carbon in hydrates and permafrost are very large, and thus could potentially act as very powerful feedbacks. Although poorly constrained, the 21st century global release of CH₄ from hydrates to the atmosphere is *likely* to be low due to the under-saturated state of the ocean, long ventilation time of the ocean and slow propagation of warming through the seafloor. There is *high confidence* that release of carbon from thawing permafrost provides a positive feedback, but there is *low confidence* in quantitative projections of its strength. {6.4.7}

Aerosol-climate feedbacks occur mainly through changes in the source strength of natural aerosols or changes in the sink efficiency of natural and anthropogenic aerosols; a limited number of modelling studies have assessed the magnitude of this feedback to be small with a *low confidence*. There is *medium confidence* for a weak feedback (of uncertain sign) involving dimethylsulphide, cloud condensation nuclei and cloud albedo due to a weak sensitivity of cloud condensation nuclei population to changes in dimethylsulphide emissions. {7.3.5}

TS.3.8 Emission Metrics

Different metrics can be used to quantify and communicate the relative and absolute contributions to climate change of emissions of different substances, and of emissions from regions/countries or sources/sectors. Up to AR4, the most common metric has been the Global Warming Potential (GWP) that integrates RF out to a particular time horizon. This metric thus accounts for the radiative efficiencies of the various substances, and their lifetimes in the atmosphere, and gives values relative to those for the reference gas CO₂. There is now increasing focus on the Global Temperature change Potential (GTP), which is based on the change in GMST at a chosen point in time, again relative to that caused by the reference gas CO₂, and thus accounts for climate response along with radiative efficiencies and atmospheric lifetimes. Both the GWP and the GTP use a time horizon (Figure TS.8 top), the choice of which is subjective and context dependent. In general, GWPs for near-term

climate forcers are higher than GTPs due to the equal time weighting in the integrated forcing used in the GWP. Hence the choice of metric can greatly affect the relative importance of near-term climate forcers and WMGHGs, as can the choice of time horizon. Analysis of the impact of current emissions (1-year pulse of emissions) shows that near-term climate forcers, such as black carbon, sulphur dioxide or CH₄, can have contributions comparable to that of CO₂ for short time horizons (of either the same or opposite sign), but their impacts become progressively less for longer time horizons over which emissions of CO₂ dominate (Figure TS.8 top). {8.7}

A large number of other metrics may be defined down the driver–response–impact chain. No single metric can accurately compare all consequences (i.e., responses in climate parameters over time) of different emissions, and a metric that establishes equivalence with regard to one effect will not give equivalence with regard to other effects. The choice of metric therefore depends strongly on the particular consequence one wants to evaluate. It is important to note that the metrics do not define policies or goals, but facilitate analysis and implementation of multi-component policies to meet particular goals. All choices of metric contain implicit value-related judgements such as type of effect considered and weighting of effects over time. Whereas GWP integrates the effects up to a chosen time horizon (i.e., giving equal weight to all times up to the horizon and zero weight thereafter), the GTP gives the temperature just for one chosen year with no weight on years before or after. {8.7}

The GWP and GTP have limitations and suffer from inconsistencies related to the treatment of indirect effects and feedbacks, for instance, if climate–carbon feedbacks are included for the reference gas CO₂ but not for the non-CO₂ gases. The uncertainty in the GWP increases with time horizon, and for the 100-year GWP of WMGHGs the uncertainty can be as large as ±40%. Several studies also point out that this metric is not well suited for policies with a maximum temperature target. Uncertainties in GTP also increase with time as they arise from the same factors contributing to GWP uncertainties along with additional contributions from it being further down the driver–response–impact chain and including climate response. The GTP metric is better suited to target-based policies, but is again not appropriate for every goal. Updated metric values accounting for changes in knowledge of lifetimes and radiative efficiencies and for climate–carbon feedbacks are now available. {8.7, Table 8.7, Table 8.A.1, Chapter 8 Supplementary Material Table 8.SM.16}

With these emission metrics, the climate impact of past or current emissions attributable to various activities can be assessed. Such activity-based accounting can provide additional policy-relevant information, as these activities are more directly affected by particular societal choices than overall emissions. A single year’s worth of emissions (a pulse) is often used to quantify the impact on future climate. From this perspective and with the absolute GTP metric used to illustrate the results, energy and industry have the largest contributions to warming over the next 50 to 100 years (Figure TS.8, bottom). Household fossil and biofuel, biomass burning and on-road transportation are also relatively large contributors to warming over these time scales, while current emissions from sectors that emit large amounts of CH₄ (animal husbandry, waste/landfills and agriculture) are also important over

shorter time horizons (up to about 20 years). Another useful perspective is to examine the effect of sustained current emissions. Because emitted substances are removed according to their residence time, short-lived species remain at nearly constant values while long-lived gases accumulate in this analysis. In both cases, the sectors that have the greatest long-term warming impacts (energy and industry) lead to cooling in the near term (primarily due to SO₂ emissions), and thus

emissions from those sectors can lead to opposite global mean temperature responses at short and long time scales. The relative importance of the other ERF sectors depends on the time and perspective chosen. As with RF or ERF, uncertainties in aerosol impacts are large, and in particular attribution of aerosol–cloud interactions to individual components is poorly constrained. {8.7; Chapter 8 Supplementary Material Figures 8.SM.9, 8.SM.10}

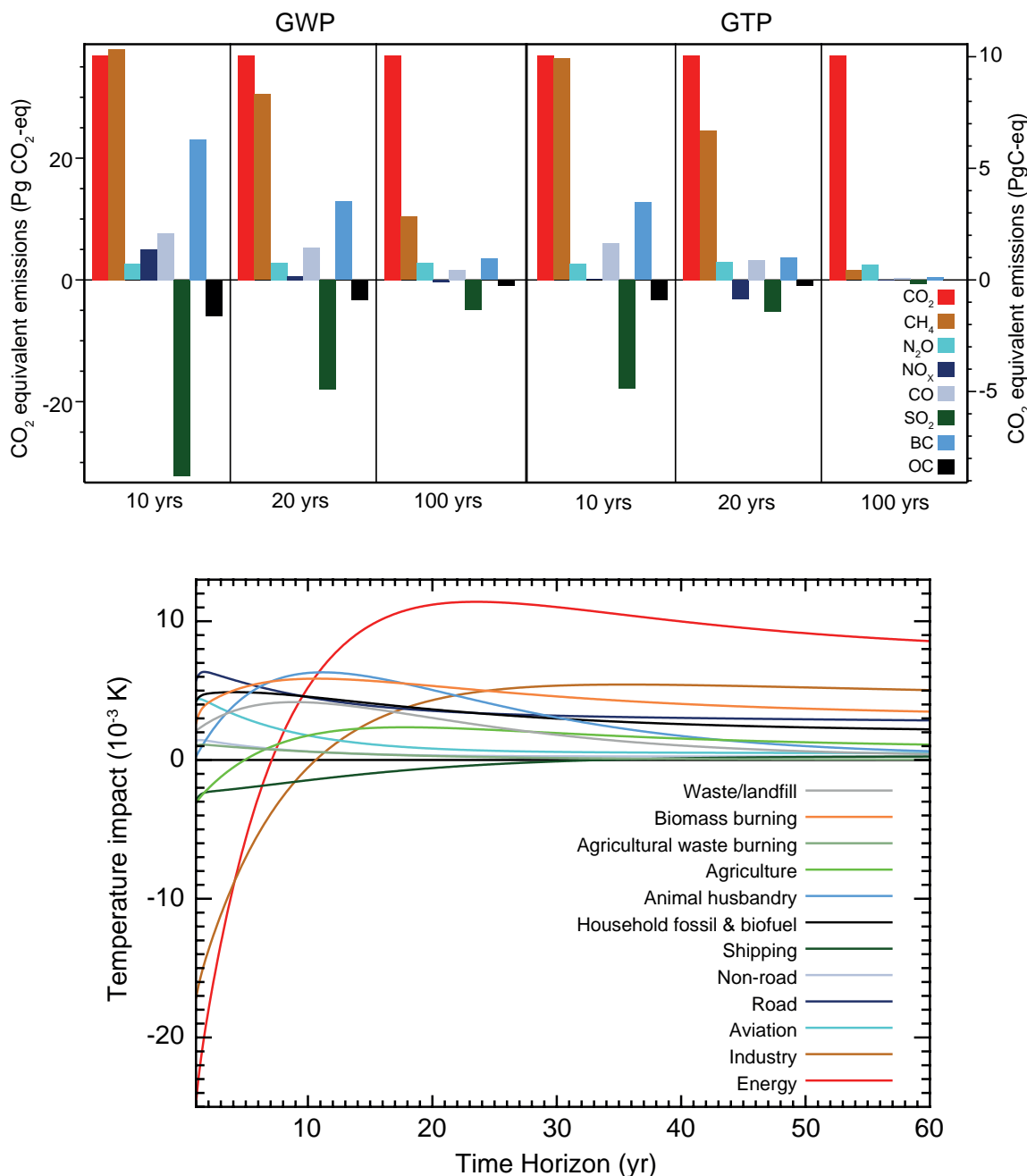


Figure TS.8 | (Upper) Global anthropogenic present-day emissions weighted by the Global Warming Potential (GWP) and the Global Temperature change Potential (GTP) for the chosen time horizons. Year 2008 (single-year pulse) emissions weighted by GWP, which is the global mean radiative forcing (RF) per unit mass emitted integrated over the indicated number of years relative to the forcing from CO₂ emissions, and GTP which estimates the impact on global mean temperature based on the temporal evolution of both RF and climate response per unit mass emitted relative to the impact of CO₂ emissions. The units are ‘CO₂ equivalents’, which reflects equivalence only in the impact parameter of the chosen metric (integrated RF over the chosen time horizon for GWP; temperature change at the chosen point in time for GTP), given as Pg(CO₂)eq (left axis) and PgCeq (right axis). (Bottom) The Absolute GTP (AGTP) as a function of time multiplied by the present-day emissions of all compounds from the indicated sectors is used to estimate global mean temperature response (AGTP is the same as GTP, except is not normalized by the impact of CO₂ emissions). There is little change in the relative values for the sectors over the 60 to 100-year time horizon. The effects of aerosol–cloud interactions and contrail-induced cirrus are not included in the upper panel. {Figures 8.32, 8.33}

TS

TS.4 Understanding the Climate System and Its Recent Changes

TS.4.1 Introduction

Understanding of the climate system results from combining observations, theoretical studies of feedback processes and model simulations. Compared to AR4, more detailed observations and improved climate models (see Box TS.4) now enable the attribution of detected changes to human influences in more climate system components. The consistency of observed and modelled changes across the climate system, including in regional temperatures, the water cycle, global energy budget, cryosphere and oceans (including ocean acidification), points to global climate change resulting primarily from anthropogenic increases in WMGHG concentrations. {10}

TS.4.2 Surface Temperature

Several advances since the AR4 have allowed a more robust quantification of human influence on surface temperature changes. Observational uncertainty has been explored much more thoroughly than previously and the assessment now considers observations from the first decade of the 21st century and simulations from a new generation of climate models whose ability to simulate historical climate has improved in many respects relative to the previous generation of models considered in AR4. Observed GMST anomalies relative to 1880–1919 in recent years lie well outside the range of GMST anomalies in CMIP5 simulations with natural forcing only, but are consistent with the ensemble of CMIP5 simulations including both anthropogenic and natural forcing (Figure TS.9) even though some individual models overestimate the warming trend, while others underestimate it. Simulations with WMGHG changes only, and no aerosol changes, generally exhibit stronger warming than has been observed (Figure TS.9). Observed temperature trends over the period 1951–2010, which are characterized by warming over most of the globe with the most intense warming over the NH continents, are, at most observed locations, consistent with the temperature trends in CMIP5 simulations including anthropogenic and natural forcings and inconsistent with the temperature trends in CMIP5 simulations including natural forcings only. A number of studies have investigated the effects of the Atlantic Multi-decadal Oscillation (AMO) on GMST. Although some studies find a significant role for the AMO in driving multi-decadal variability in GMST, the AMO exhibited little trend over the period 1951–2010 on which the current assessments are based, and the AMO is assessed with *high confidence* to have made little contribution to the GMST trend between 1951 and 2010 (considerably less than 0.1°C). {2.4, 9.8.1, 10.3; FAQ 9.1}

It is *extremely likely* that human activities caused more than half of the observed increase in global average surface temperature from 1951 to 2010. This assessment is supported by robust evidence from multiple studies using different methods. In particular, the temperature trend attributable to all anthropogenic forcings combined can be more closely constrained in multi-signal detection and attribution analyses. Uncertainties in forcings and in climate models' responses to those forcings, together with difficulty in distinguishing the patterns of temperature response due to WMGHGs and other anthropogenic forcings, prevent as precise a quantification of the temperature changes attributable to

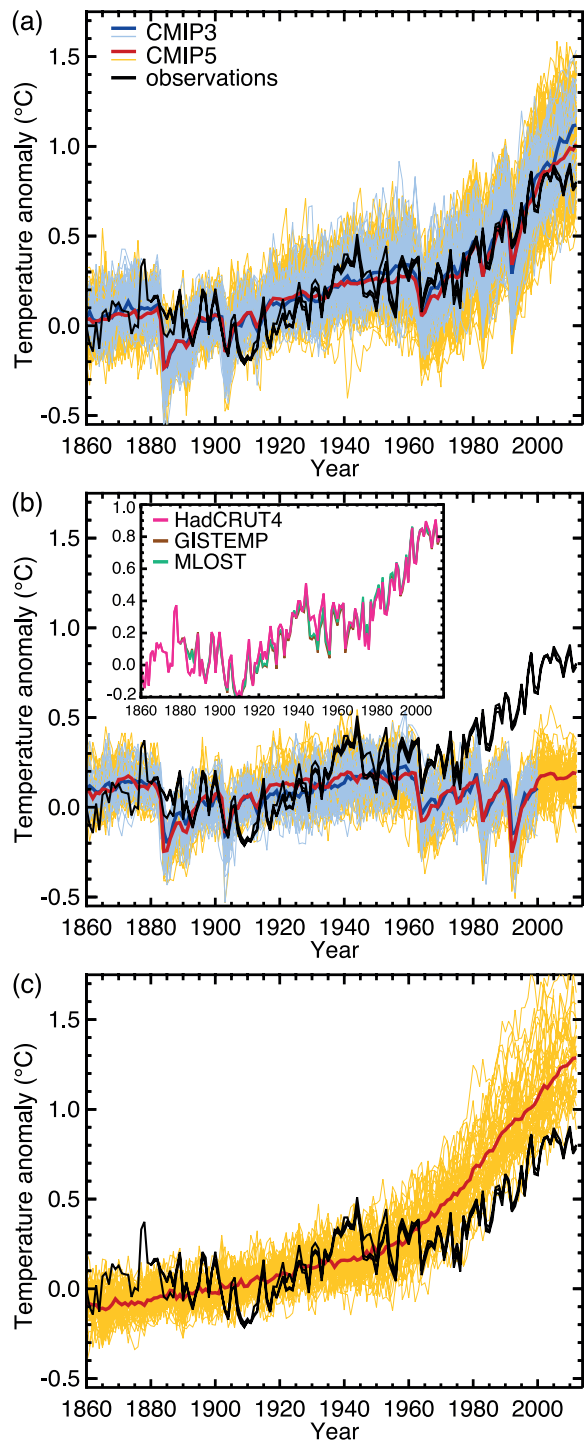


Figure TS.9 | Three observational estimates of global mean surface temperature (black lines) from the Hadley Centre/Climatic Research Unit gridded surface temperature data set 4 (HadCRUT4), Goddard Institute for Space Studies Surface Temperature Analysis (GISTEMP), and Merged Land–Ocean Surface Temperature Analysis (MLOST), compared to model simulations (CMIP3 models—thin blue lines and CMIP5 models—thin yellow lines) with anthropogenic and natural forcings (a), natural forcings only (b) and greenhouse gas forcing only (c). Thick red and blue lines are averages across all available CMIP5 and CMIP3 simulations respectively. All simulated and observed data were masked using the HadCRUT4 coverage (as this data set has the most restricted spatial coverage), and global average anomalies are shown with respect to 1880–1919, where all data are first calculated as anomalies relative to 1961–1990 in each grid box. Inset to (b) shows the three observational data sets distinguished by different colours. {Figure 10.1}

Box TS.3 | Climate Models and the Hiatus in Global Mean Surface Warming of the Past 15 Years

The observed GMST has shown a much smaller increasing linear trend over the past 15 years than over the past 30 to 60 years (Box TS.3, Figure 1a, c). Depending on the observational data set, the GMST trend over 1998–2012 is estimated to be around one third to one half of the trend over 1951–2012. For example, in HadCRUT4 the trend is 0.04°C per decade over 1998–2012, compared to 0.11°C per decade over 1951–2012. The reduction in observed GMST trend is most marked in NH winter. Even with this ‘hiatus’ in GMST trend, the decade of the 2000s has been the warmest in the instrumental record of GMST. Nevertheless, the occurrence of the hiatus in GMST trend during the past 15 years raises the two related questions of what has caused it and whether climate models are able to reproduce it. {2.4.3, 9.4.1; Box 9.2; Table 2.7}

Fifteen-year-long hiatus periods are common in both the observed and CMIP5 historical GMST time series. However, an analysis of the full suite of CMIP5 historical simulations (augmented for the period 2006–2012 by RCP4.5 simulations) reveals that 111 out of 114 realizations show a GMST trend over 1998–2012 that is higher than the entire HadCRUT4 trend ensemble (Box TS.3, Figure 1a; CMIP5 ensemble mean trend is 0.21°C per decade). This difference between simulated and observed trends could be caused by some combination of (a) internal climate variability, (b) missing or incorrect RF, and (c) model response error. These potential sources of the difference, which are not mutually exclusive, are assessed below, as is the cause of the observed GMST trend hiatus. {2.4.3, 9.3.2, 9.4.1; Box 9.2}

Internal Climate Variability

Hiatus periods of 10 to 15 years can arise as a manifestation of internal decadal climate variability, which sometimes enhances and sometimes counteracts the long-term externally forced trend. Internal variability thus diminishes the relevance of trends over periods as short as 10 to 15 years for long-term climate change. Furthermore, the timing of internal decadal climate variability is not expected to be matched by the CMIP5 historical simulations, owing to the predictability horizon of at most 10 to 20 years (CMIP5 historical simulations are typically started around nominally 1850 from a control run). However, climate models exhibit individual decades of GMST trend hiatus even during a prolonged phase of energy uptake of the climate system, in which case the energy budget would be balanced by increasing subsurface–ocean heat uptake. {2.4.3, 9.3.2, 11.2.2; Boxes 2.2, 9.2}

Owing to sampling limitations, it is uncertain whether an increase in the rate of subsurface–ocean heat uptake occurred during the past 15 years. However, it is *very likely* that the climate system, including the ocean below 700 m depth, has continued to accumulate energy over the period 1998–2010. Consistent with this energy accumulation, GMSL has continued to rise during 1998–2012, at a rate only slightly and insignificantly lower than during 1993–2012. The consistency between observed heat content and sea level changes yields *high confidence* in the assessment of continued ocean energy accumulation, which is in turn consistent with the positive radiative imbalance of the climate system. By contrast, there is limited evidence that the hiatus in GMST trend has been accompanied by a slower rate of increase in ocean heat content over the depth range 0 to 700 m, when comparing the period 2003–2010 against 1971–2010. There is low agreement on this slowdown, as three of five analyses show a slowdown in the rate of increase while the other two show the increase continuing unabated. {3.2.3, 3.2.4, 3.7, 8.5.1, 13.3; Boxes 3.1, 13.1}

During the 15-year period beginning in 1998, the ensemble of HadCRUT4 GMST trends lies below almost all model-simulated trends (Box TS.3, Figure 1a), whereas during the 15-year period ending in 1998, it lies above 93 out of 114 modelled trends (Box TS.3, Figure 1b; HadCRUT4 ensemble mean trend 0.26°C per decade, CMIP5 ensemble mean trend 0.16°C per decade). Over the 62-year period 1951–2012, observed and CMIP5 ensemble mean trend agree to within 0.02°C per decade (Box TS.3, Figure 1c; CMIP5 ensemble mean trend 0.13°C per decade). There is hence *very high confidence* that the CMIP5 models show long-term GMST trends consistent with observations, despite the disagreement over the most recent 15-year period. Due to internal climate variability, in any given 15-year period the observed GMST trend sometimes lies near one end of a model ensemble, an effect that is pronounced in Box TS.3, Figure 1a, b as GMST was influenced by a very strong El Niño event in 1998. {Box 9.2}

Unlike the CMIP5 historical simulations referred to above, some CMIP5 predictions were initialized from the observed climate state during the late 1990s and the early 21st century. There is medium evidence that these initialized predictions show a GMST lower by about 0.05°C to 0.1°C compared to the historical (uninitialized) simulations and maintain this lower GMST during the first few years of the simulation. In some initialized models this lower GMST occurs in part because they correctly simulate a shift, around 2000, from a positive to a negative phase of the Inter-decadal Pacific Oscillation (IPO). However, the improvement of this phasing of the IPO through initialization is not universal across the CMIP5 predictions. Moreover, although part of the GMST reduction through initialization indeed results from initializing at the correct phase of internal variability, another part may result from correcting a model bias that was caused by incorrect past forcing or incorrect model response to past forcing, especially in the ocean. The relative magnitudes of these effects are at present unknown; moreover, the quality of a forecasting system cannot be evaluated from a single prediction (here, a 10-year prediction within

(continued on next page)

Box TS.3 (continued)

the period 1998–2012). Overall, there is *medium confidence* that initialization leads to simulations of GMST during 1998–2012 that are more consistent with the observed trend hiatus than are the uninitialized CMIP5 historical simulations, and that the hiatus is in part a consequence of internal variability that is predictable on the multi-year time scale. {11.1, 11.2.3; Boxes 2.5, 9.2, 11.1, 11.2}

Radiative Forcing

On decadal to interdecadal time scales and under continually increasing ERF, the forced component of the GMST trend responds to the ERF trend relatively rapidly and almost linearly (*medium confidence*). The expected forced-response GMST trend is related to the ERF trend by a factor that has been estimated for the 1% per year CO₂ increases in the CMIP5 ensemble as 2.0 [1.3 to 2.7] W m⁻² °C⁻¹ (90% uncertainty range). Hence, an ERF trend can be approximately converted to a forced-response GMST trend, permitting an assessment of how much of the change in the GMST trends shown in Box TS.3, Figure 1 is due to a change in ERF trend. {Box 9.2}

The AR5 best-estimate ERF trend over 1998–2011 is 0.22 [0.10 to 0.34] W m⁻² per decade (90% uncertainty range), which is substantially lower than the trend over 1984–1998 (0.32 [0.22 to 0.42] W m⁻² per decade; note that there was a strong volcanic eruption in 1982) and the trend over 1951–2011 (0.31 [0.19 to 0.40] W m⁻² per decade; Box TS.3, Figure 1d–f; the end year 2011 is chosen because data availability is more limited than for GMST). The resulting forced-response GMST trend would approximately be 0.12 [0.05 to 0.29] °C per decade, 0.19 [0.09 to 0.39] °C per decade, and 0.18 [0.08 to 0.37] °C per decade for the periods 1998–2011, 1984–1998, and 1951–2011, respectively (the uncertainty ranges assume that the range of the conversion factor to GMST trend and the range of ERF trend itself are independent). The AR5 best-estimate ERF forcing trend difference between 1998–2011 and 1951–2011 thus might explain about one-half (0.05 °C per decade) of the observed GMST trend difference between these periods (0.06 to 0.08 °C per decade, depending on observational data set). {8.5.2}

The reduction in AR5 best-estimate ERF trend over 1998–2011 compared to both 1984–1998 and 1951–2011 is mostly due to decreasing trends in the natural forcings, -0.16 [-0.27 to -0.06] W m⁻² per decade over 1998–2011 compared to 0.01 [-0.00 to $+0.01$] W m⁻² per decade over 1951–2011. Solar forcing went from a relative maximum in 2000 to a relative minimum in 2009, with a peak-to-peak difference of around 0.15 W m⁻² and a linear trend over 1998–2011 of around -0.10 W m⁻² per decade. Furthermore, a series of small volcanic eruptions has increased the observed stratospheric aerosol loading after 2000, leading to an additional negative ERF linear-trend contribution of around -0.06 W m⁻² per decade over 1998–2011 (Box TS.3, Figure 1d, f). By contrast, satellite-derived estimates of tropospheric aerosol optical depth suggests little overall trend in global mean aerosol optical depth over the last 10 years, implying little change in ERF due to aerosol–radiative interaction (*low confidence* because of *low confidence* in aerosol optical depth trend itself). Moreover, because there is only *low confidence* in estimates of ERF due to aerosol–cloud interaction, there is likewise *low confidence* in its trend over the last 15 years. {2.2.3, 8.4.2, 8.5.1, 8.5.2, 10.3.1; Box 10.2; Table 8.5}

For the periods 1984–1998 and 1951–2011, the CMIP5 ensemble mean ERF trend deviates from the AR5 best-estimate ERF trend by only 0.01 W m⁻² per decade (Box TS.3, Figure 1e, f). After 1998, however, some contributions to a decreasing ERF trend are missing in the CMIP5 models, such as the increasing stratospheric aerosol loading after 2000 and the unusually low solar minimum in 2009. Nonetheless, over 1998–2011 the CMIP5 ensemble mean ERF trend is lower than the AR5 best-estimate ERF trend by 0.03 W m⁻² per decade (Box TS.3, Figure 1d). Furthermore, global mean aerosol optical depth in the CMIP5 models shows little trend over 1998–2012, similar to the observations. Although the forcing uncertainties are substantial, there are no apparent incorrect or missing global mean forcings in the CMIP5 models over the last 15 years that could explain the model–observations difference during the warming hiatus. {9.4.6}

Model Response Error

The discrepancy between simulated and observed GMST trends during 1998–2012 could be explained in part by a tendency for some CMIP5 models to simulate stronger warming in response to increases in greenhouse-gas concentration than is consistent with observations. Averaged over the ensembles of models assessed in Section 10.3.1, the best-estimate GHG and other anthropogenic scaling factors are less than one (though not significantly so, Figure 10.4), indicating that the model-mean GHG and other anthropogenic responses should be scaled down to best match observations. This finding provides evidence that some CMIP5 models show a larger response to GHGs and other anthropogenic factors (dominated by the effects of aerosols) than the real world (*medium confidence*). As a consequence, it is argued in Chapter 11 that near-term model projections of GMST increase should be scaled down by about 10%. This downward scaling is, however, not sufficient to explain the model mean overestimate of GMST trend over the hiatus period. {10.3.1, 11.3.6}

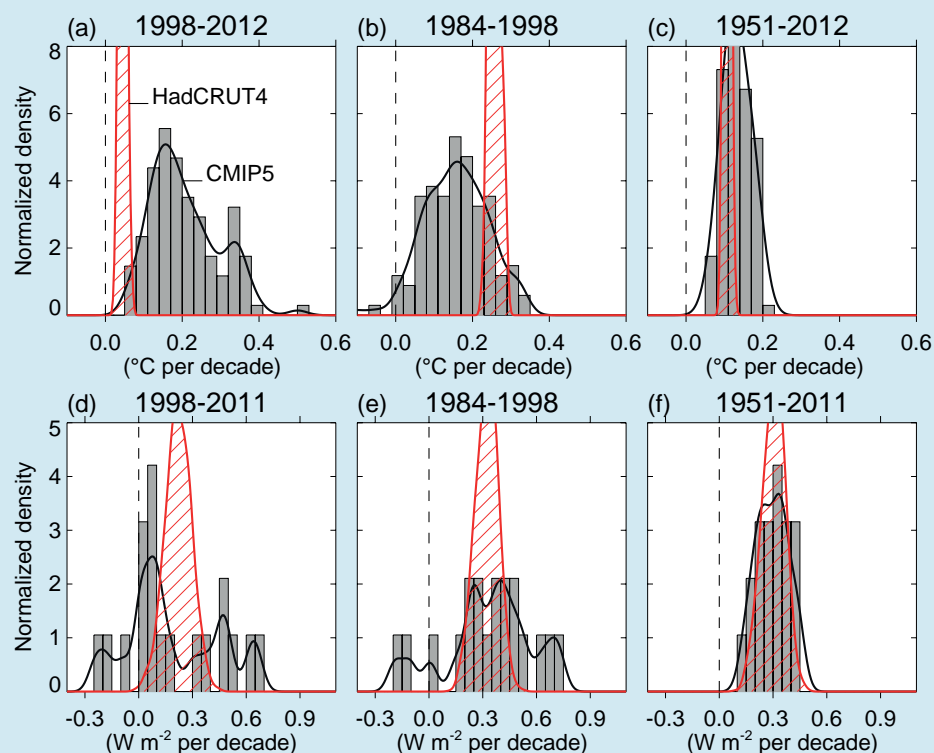
Another possible source of model error is the poor representation of water vapour in the upper atmosphere. It has been suggested that a reduction in stratospheric water vapour after 2000 caused a reduction in downward longwave radiation and hence a surface-cooling contribution, possibly missed by the models. However, this effect is assessed here to be small, because there was a recovery in stratospheric water vapour after 2005. {2.2.2, 9.4.1; Box 9.2} (continued on next page)

Box TS.3 (continued)

In summary, the observed recent warming hiatus, defined as the reduction in GMST trend during 1998–2012 as compared to the trend during 1951–2012, is attributable in roughly equal measure to a cooling contribution from internal variability and a reduced trend in external forcing (expert judgement, *medium confidence*). The forcing trend reduction is due primarily to a negative forcing trend from both volcanic eruptions and the downward phase of the solar cycle. However, there is *low confidence* in quantifying the role of forcing trend in causing the hiatus, because of uncertainty in the magnitude of the volcanic forcing trend and *low confidence* in the aerosol forcing trend. {Box 9.2}

Almost all CMIP5 historical simulations do not reproduce the observed recent warming hiatus. There is *medium confidence* that the GMST trend difference between models and observations during 1998–2012 is to a substantial degree caused by internal variability, with possible contributions from forcing error and some CMIP5 models overestimating the response to increasing GHG forcing. The CMIP5 model trend in ERF shows no apparent bias against the AR5 best estimate over 1998–2012. However, *confidence* in this assessment of CMIP5 ERF trend is *low*, primarily because of the uncertainties in model aerosol forcing and processes, which through spatial heterogeneity might well cause an undetected global mean ERF trend error even in the absence of a trend in the global mean aerosol loading. {Box 9.2}

The causes of both the observed GMST trend hiatus and of the model–observation GMST trend difference during 1998–2012 imply that, barring a major volcanic eruption, most 15-year GMST trends in the near-term future will be larger than during 1998–2012 (*high confidence*; see Section 11.3.6 for a full assessment of near-term projections of GMST). The reasons for this implication are fourfold: first, anthropogenic GHG concentrations are expected to rise further in all RCP scenarios; second, anthropogenic aerosol concentration is expected to decline in all RCP scenarios, and so is the resulting cooling effect; third, the trend in solar forcing is expected to be larger over most near-term 15-year periods than over 1998–2012 (*medium confidence*), because 1998–2012 contained the full downward phase of the solar cycle; and fourth, it is *more likely than not* that internal climate variability in the near term will enhance and not counteract the surface warming expected to arise from the increasing anthropogenic forcing. {Box 9.2}

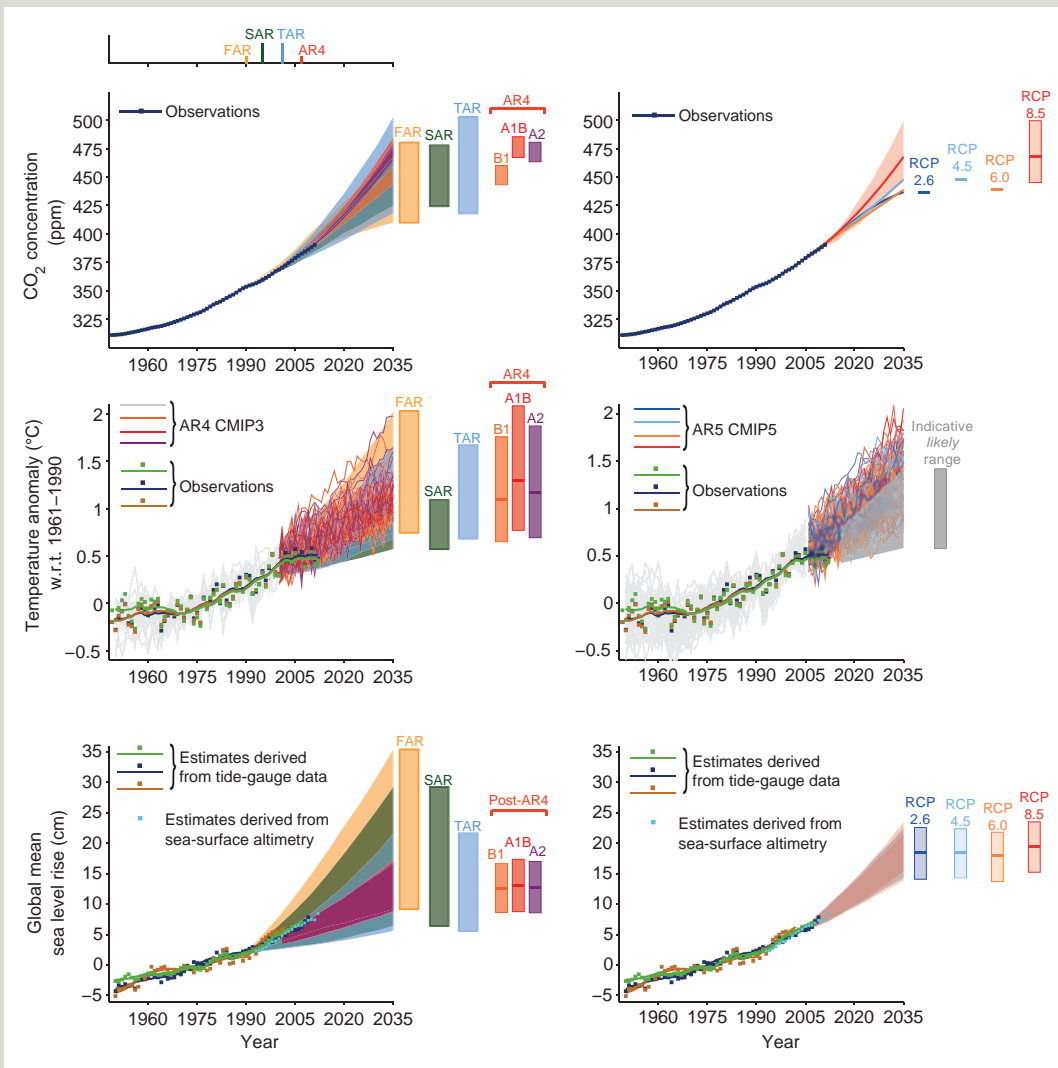


Box TS.3, Figure 1 | (Top) Observed and simulated GMST trends in °C per decade, over the periods 1998–2012 (a), 1984–1998 (b), and 1951–2012 (c). For the observations, 100 realizations of the Hadley Centre/Climatic Research Unit gridded surface temperature data set 4 (HadCRUT4) ensemble are shown (red, hatched). The uncertainty displayed by the ensemble width is that of the statistical construction of the global average only, in contrast to the trend uncertainties quoted in Section 2.4.3, which include an estimate of internal climate variability. Here, by contrast, internal variability is characterized through the width of the model ensemble. For the models, all 114 available CMIP5 historical realizations are shown, extended after 2005 with the RCP4.5 scenario and through 2012 (grey, shaded). (Bottom) Trends in effective radiative forcing (ERF, in W m⁻² per decade) over the periods 1998–2011 (d), 1984–1998 (e), and 1951–2011 (f). The figure shows AR5 best-estimate ERF trends (red, hatched) and CMIP5 ERF (grey, shaded). Black lines are smoothed versions of the histograms. Each histogram is normalized so that its area sums up to one. {2.4.3, 8.5.2; Box 9.2; Figure 8.18; Box 9.2, Figure 1}

Thematic Focus Elements

TFE.3 | Comparing Projections from Previous IPCC Assessments with Observations

Verification of projections is arguably the most convincing way of establishing the credibility of climate change science. Results of projected changes in carbon dioxide (CO₂), global mean surface temperature (GMST) and global mean sea level (GMSL) from previous IPCC assessment reports are quantitatively compared with the best available observational estimates. The comparison between the four previous reports highlights the evolution in our understanding of how the climate system responds to changes in both natural and anthropogenic forcing and provides an assessment of how the projections compare with observational estimates. TFE.3, Figure 1, for example, shows the projected and observed estimates of: (1) CO₂ changes (top row), (2) GMST anomaly relative to 1961–1990 (middle row) and (3) GMSL relative to 1961–1990 (bottom row). Results from previous assessment reports are in the left-hand column, and for completeness results from current assessment are given in the right-hand column. {2.4, 3.7, 6.3, 11.3, 13.3} (continued on next page)



TFE.3, Figure 1 | (Top left) Observed globally and annually averaged CO₂ concentrations in parts per million (ppm) since 1950 compared with projections from the previous IPCC assessments. Observed global annual CO₂ concentrations are shown in dark blue. The shading shows the largest model projected range of global annual CO₂ concentrations from 1950 to 2035 from FAR (First Assessment Report; Figure A.3 in the Summary for Policymakers (SPM) of IPCC 1990), SAR (Second Assessment Report; Figure 5b in the TS of IPCC 1996), TAR (Third Assessment Report; Appendix II of IPCC 2001), and for the IPCC Special Report on Emission Scenarios (SRES) A2, A1B and B1 scenarios presented in the AR4 (Fourth Assessment Report; Figure 10.26). The publication years of the assessment reports are shown. (Top right) Same observed globally averaged CO₂ concentrations and the projections from this report. Only RCP8.5 has a range of values because the emission-driven scenarios were carried out only for this RCP. For the other RCPs the best estimate is given. (Middle left) Estimated changes in the observed globally and annually averaged surface temperature anomaly relative to 1961–1990 (in °C) since 1950 compared with the range of projections from the previous IPCC assessments. Values are harmonized

TFE.3 (continued)

to start from the same value at 1990. Observed global annual temperature anomaly, relative to 1961–1990, from three data sets is shown as squares and smoothed time series as solid lines from the Hadley Centre/Climatic Research Unit gridded surface temperature data set 4 (HadCRUT4; bright green), Merged Land–Ocean Surface Temperature Analysis (MLOST; warm mustard) and Goddard Institute for Space Studies Surface Temperature Analysis (GISTEMP; dark blue) data sets. The coloured shading shows the projected range of global annual mean near surface temperature change from 1990 to 2035 for models used in FAR (Figure 6.11), SAR (Figure 19 in the TS of IPCC 1996), TAR (full range of TAR, Figure 9.13(b)). TAR results are based on the simple climate model analyses presented in this assessment and not on the individual full three-dimensional climate model simulations. For the AR4 results are presented as single model runs of the CMIP3 ensemble for the historical period from 1950 to 2000 (light grey lines) and for three SRES scenarios (A2, A1B and B1) from 2001 to 2035. For the three SRES scenarios the bars show the CMIP3 ensemble mean and the *likely* range given by -40% to $+60\%$ of the mean as assessed in Chapter 10 of AR4. (Middle right) Projections of annual mean global mean surface air temperature (GMST) for 1950–2035 (anomalies relative to 1961–1990) under different RCPs from CMIP5 models (light grey and coloured lines, one ensemble member per model), and observational estimates the same as the middle left panel. The grey shaded region shows the indicative *likely* range for annual mean GMST during the period 2016–2035 for all RCPs (see Figure TS.14 for more details). The grey bar shows this same indicative *likely* range for the year 2035. (Bottom left) Estimated changes in the observed global annual mean sea level (GMSL) since 1950. Different estimates of changes in global annual sea level anomalies from tide gauge data (dark blue, warm mustard, dark green) and based on annual averages of altimeter data (light blue) starting in 1993 (the values have been aligned to fit the 1993 value of the tide gauge data). Squares indicate annual mean values, solid lines smoothed values. The shading shows the largest model projected range of global annual sea level rise from 1950 to 2035 for FAR (Figures 9.6 and 9.7), SAR (Figure 21 in TS of IPCC, 1996), TAR (Appendix II of IPCC, 2001) and based on the CMIP3 model results available at the time of AR4 using the SRES A1B scenario. Note that in the AR4 no full range was given for the sea level projections for this period. Therefore, the figure shows results that have been published subsequent to the AR4. The bars at the right hand side of each graph show the full range given for 2035 for each assessment report. (Bottom right) Same observational estimate as bottom left. The bars are the *likely* ranges (*medium confidence*) for global mean sea level rise at 2035 with respect to 1961–1990 following the four RCPs. Appendix 1.A provides details on the data and calculations used to create these figures. See Chapters 1, 11 and 13 for more details. {Figures 1.4, 1.5, 1.10, 11.9, 11.19, 11.25, 13.11}

Carbon Dioxide Changes

From 1950 to 2011 the observed concentrations of atmospheric CO₂ have steadily increased. Considering the period 1990–2011, the observed CO₂ concentration changes lie within the envelope of the scenarios used in the four assessment reports. As the most recent assessment prior to the current, the IPCC Fourth Assessment Report (AR4) (TFE.3.Figure 1; top left) has the narrowest scenario range and the observed concentration follows this range. The results from the IPCC Fifth Assessment Report (AR5) (TFE.3, Figure 1; top right) are consistent with AR4, and during 2002–2011, atmospheric CO₂ concentrations increased at a rate of 1.9 to 2.1 ppm yr⁻¹. {2.2.1, 6.3; Table 6.1}

Global Mean Temperature Anomaly

Relative to the 1961–1990 mean, the GMST anomaly has been positive and larger than 0.25°C since 2001. Observations are generally well within the range of the extent of the earlier IPCC projections (TFE.3, Figure 1, middle left) This is also true for the Coupled Model Intercomparison Project Phase 5 (CMIP5) results (TFE.3, Figure 1; middle right) in the sense that the observed record lies within the range of the model projections, but on the lower end of the plume. Mt Pinatubo erupted in 1991 (see FAQ 11.2 for discussion of how volcanoes impact the climate system), leading to a brief period of relative global mean cooling during the early 1990s. The IPCC First, Second and Third Assessment Reports (FAR, SAR and TAR) did not include the effects of volcanic eruptions and thus failed to include the cooling associated with the Pinatubo eruption. AR4 and AR5, however, did include the effects from volcanoes and did simulate successfully the associated cooling. During 1995–2000 the global mean temperature anomaly was quite variable—a significant fraction of this variability was due to the large El Niño in 1997–1998 and the strong back-to-back La Niñas in 1999–2001. The projections associated with these assessment reports do not attempt to capture the actual evolution of these El Niño and La Niña events, but include them as a source of uncertainty due to natural variability as encompassed by, for example, the range given by the individual CMIP3 and CMIP5 simulations and projection (TFE.3, Figure 1). The grey wedge in TFE.3, Figure 1 (middle right) corresponds to the indicative *likely* range for annual temperatures, which is determined from the Representative Concentration Pathways (RCPs) assessed value for the 20-year mean 2016–2035 (see discussion of Figure TS.14 and Section 11.3.6 for details). From 1998 to 2012 the observational estimates have largely been on the low end of the range given by the scenarios alone in previous assessment reports and CMIP3 and CMIP5 projections. {2.4; Box 9.2}

Global Mean Sea Level

Based on both tide gauge and satellite altimetry data, relative to 1961–1990, the GMSL has continued to rise. While the increase is fairly steady, both observational records show short periods of either no change or a slight decrease. The observed estimates lie within the envelope of all the projections except perhaps in the very early 1990s. The sea level rise uncertainty due to scenario-related uncertainty is smallest for the most recent assessments (AR4 and AR5) and observed estimates lie well within this scenario-related uncertainty. It is *virtually certain* that over the 20th century sea level rose. The mean rate of sea level increase was 1.7 mm yr⁻¹ with a *very likely* range between 1.5 to 1.9 between 1901 and 2010 and this rate increased to 3.2 with a *likely* range of 2.8 to 3.6 mm yr⁻¹ between 1993 and 2010 (see TFE.2). {3.7.2, 3.7.4}

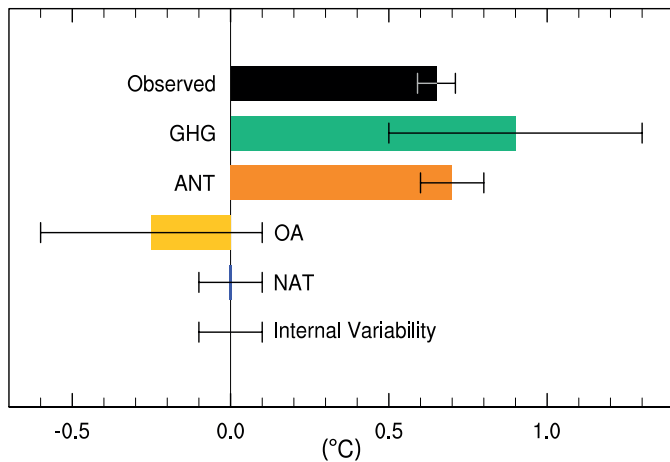


Figure TS.10 | Assessed *likely* ranges (whiskers) and their midpoints (bars) for warming trends over the 1951–2010 period due to well-mixed greenhouse gases (GHG), anthropogenic forcings (ANT) anthropogenic forcings other than well-mixed greenhouse gases (OA), natural forcings (NAT) and internal variability. The trend in the Hadley Centre/Climatic Research Unit gridded surface temperature data set 4 (HadCRUT4) observations is shown in black with its 5 to 95% uncertainty range due only to observational uncertainty in this record. {Figure 10.5}

WMGHGs and other anthropogenic forcings individually. Consistent with AR4, it is assessed that more than half of the observed increase in global average surface temperature from 1951 to 2010 is *very likely* due to the observed anthropogenic increase in WMGHG concentrations. WMGHGs contributed a global mean surface warming *likely* to be between 0.5°C and 1.3°C over the period between 1951 and 2010, with the contributions from other anthropogenic forcings *likely* to be between –0.6°C and 0.1°C and from natural forcings *likely* to be between –0.1°C and 0.1°C. Together these assessed contributions are consistent with the observed warming of approximately 0.6°C over this period (Figure TS.10). {10.3}

Solar forcing is the only known natural forcing acting to warm the climate over the 1951–2010 period but it has increased much less than WMGHG forcing, and the observed pattern of long-term tropospheric warming and stratospheric cooling is not consistent with the expected response to solar irradiance variations. Considering this evidence together with the assessed contribution of natural forcings to observed trends over this period, it is assessed that the contribution from solar forcing to the observed global warming since 1951 is *extremely unlikely* to be larger than that from WMGHGs. Because solar forcing has *very likely* decreased over a period with direct satellite measurements of solar output from 1986 to 2008, there is *high confidence* that changes in total solar irradiance have not contributed to global warming during that period. However, there is *medium confidence* that the 11-year cycle of solar variability influences decadal climate fluctuations in some regions through amplifying mechanisms. {8.4, 10.3; Box 10.2}

Observed warming over the past 60 years is far outside the range of internal climate variability estimated from pre-instrumental data, and it is also far outside the range of internal variability simulated in climate models. Model-based simulations of internal variability are assessed to be adequate to make this assessment. Further, the spatial pattern of

observed warming differs from those associated with internal variability. Based on this evidence, the contribution of internal variability to the 1951–2010 GMST trend was assessed to be *likely* between –0.1°C and 0.1°C, and it is *virtually certain* that warming since 1951 cannot be explained by internal variability alone. {9.5, 10.3, 10.7}

The instrumental record shows a pronounced warming during the first half of the 20th century. Consistent with AR4, it is assessed that the early 20th century warming is *very unlikely* to be due to internal variability alone. It remains difficult to quantify the contributions to this early century warming from internal variability, natural forcing and anthropogenic forcing, due to forcing and response uncertainties and incomplete observational coverage. {10.3}

TS.4.3 Atmospheric Temperature

A number of studies since the AR4 have investigated the consistency of simulated and observed trends in free tropospheric temperatures (see section TS.2). Most, though not all, CMIP3 and CMIP5 models overestimate the observed warming trend in the tropical troposphere during the satellite period 1979–2012. Roughly one half to two thirds of this difference from the observed trend is due to an overestimate of the SST trend, which is propagated upward because models attempt to maintain static stability. There is *low confidence* in these assessments, however, owing to the *low confidence* in observed tropical tropospheric trend rates and vertical structure. Outside the tropics, and over the period of the radiosonde record beginning in 1961, the discrepancy between simulated and observed trends is smaller. {2.4.4, 9.4, 10.3}

Analysis of both radiosonde and satellite data sets, combined with CMIP5 and CMIP3 simulations, continues to find that observed tropospheric warming is inconsistent with internal variability and simulations of the response to natural forcings alone. Over the period 1961–2010 CMIP5 models simulate tropospheric warming driven by WMGHG changes, with only a small offsetting cooling due to the combined effects of changes in reflecting and absorbing aerosols and tropospheric ozone. Taking this evidence together with the results of multi-signal detection and attribution analyses, it is *likely* that anthropogenic forcings, dominated by WMGHGs, have contributed to the warming of the troposphere since 1961. Uncertainties in radiosonde and satellite records makes assessment of causes of observed trends in the upper troposphere less confident than an assessment of the overall atmospheric temperature changes. {2.4.4, 9.4, 10.3}

CMIP5 simulations including WMGHGs, ozone and natural forcing changes broadly reproduce the observed evolution of lower stratospheric temperature, with some tendency to underestimate the observed cooling trend over the satellite era (see Section TS.2). New studies of stratospheric temperature, considering the responses to natural forcings, WMGHGs and ozone-depleting substances, demonstrate that it is *very likely* that anthropogenic forcings, dominated by the depletion of the ozone layer due to ozone depleting substances have contributed to the cooling of the lower stratosphere since 1979. CMIP5 models simulate only a very weak cooling of the lower stratosphere in response to historical WMGHG changes, and the influence of WMGHGs on lower stratospheric temperature has not been formally detected. Considering both regions together, it is *very likely* that anthropogenic

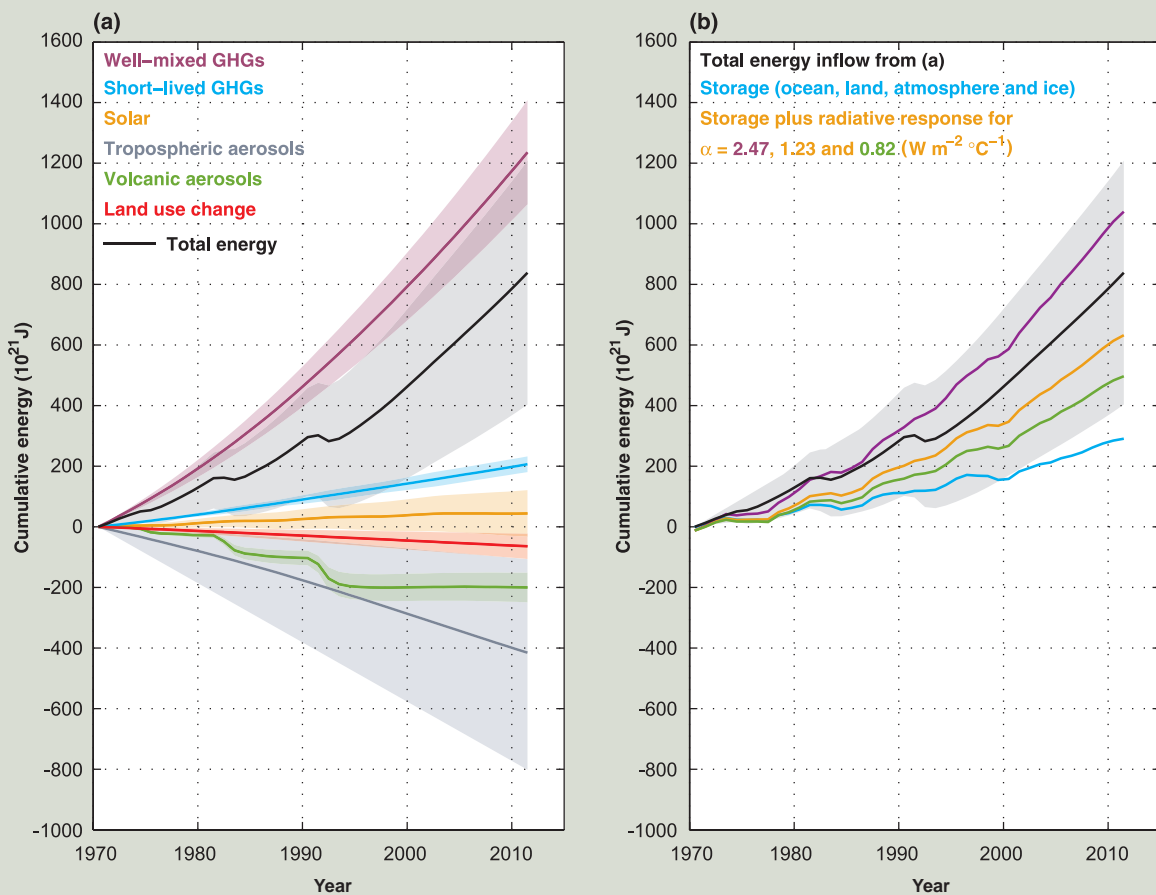
Thematic Focus Elements

TFE.4 | The Changing Energy Budget of the Global Climate System

The global energy budget is a fundamental aspect of the Earth’s climate system and depends on many phenomena within it. The ocean has stored about 93% of the increase in energy in the climate system over recent decades, resulting in ocean thermal expansion and hence sea level rise. The rate of storage of energy in the Earth system must be equal to the net downward radiative flux at the top of the atmosphere, which is the difference between effective radiative forcing (ERF) due to changes imposed on the system and the radiative response of the system. There are also significant transfers of energy between components of the climate system and from one location to another. The focus here is on the Earth’s global energy budget since 1970, when better global observational data coverage is available. {3.7, 9.4, 13.4; Box 3.1}

The ERF of the climate system has been positive as a result of increases in well-mixed (long-lived) greenhouse gas (GHG) concentrations, changes in short-lived GHGs (tropospheric and stratospheric ozone and stratospheric water vapour), and an increase in solar irradiance (TFE.4, Figure 1a). This has been partly compensated by a negative contribution to the ERF of the climate system as a result of changes in tropospheric aerosol, which predominantly reflect sunlight and furthermore enhance the brightness of clouds, although black carbon produces positive forcing. Explosive volcanic eruptions (such as El Chichón in Mexico in 1982 and Mt Pinatubo in the Philippines in 1991)

(continued on next page)



TFE.4, Figure 1 | The Earth’s energy budget from 1970 through 2011. (a) The cumulative energy inflow into the Earth system from changes in well-mixed and short-lived greenhouse gases, solar forcing, tropospheric aerosol forcing, volcanic forcing and changes in surface albedo due to land use change (all relative to 1860–1879) are shown by the coloured lines; these contributions are added to give the total energy inflow (black; contributions from black carbon on snow and contrails as well as contrail-induced cirrus are included but not shown separately). (b) The cumulative total energy inflow from (a, black) is balanced by the sum of the energy uptake of the Earth system (blue; energy absorbed in warming the ocean, the atmosphere and the land, as well as in the melting of ice) and an increase in outgoing radiation inferred from changes in the global mean surface temperature. The sum of these two terms is given for a climate feedback parameter α of 2.47, 1.23 and 0.82 $\text{W m}^{-2} \text{ } ^\circ\text{C}^{-1}$, corresponding to an equilibrium climate sensitivity of 1.5°C, 3.0°C and 4.5°C, respectively; 1.5°C to 4.5°C is assessed to be the *likely* range of equilibrium climate sensitivity. The energy budget would be closed for a particular value of α if the corresponding line coincided with the total energy inflow. For clarity, all uncertainties (shading) shown are *likely* ranges. {Box 12.2; Box 13.1, Figure 1}

TS

TFE.4 (continued)

can inject sulphur dioxide into the stratosphere, giving rise to stratospheric aerosol, which persists for several years. Stratospheric aerosol reflects some of the incoming solar radiation and thus gives a negative forcing. Changes in surface albedo from land use change have also led to a greater reflection of shortwave radiation back to space and hence a negative forcing. Since 1970, the net ERF of the climate system has increased, and the integrated impact of these forcings is an energy inflow over this period (TFE.4, Figure 1a). {2.3, 8.5; Box 13.1}

As the climate system warms, energy is lost to space through increased outgoing radiation. This radiative response by the system is due predominantly to increased thermal radiation, but it is modified by climate feedbacks such as changes in water vapour, clouds and surface albedo, which affect both outgoing longwave and reflected shortwave radiation. The top of the atmosphere fluxes have been measured by the Earth Radiation Budget Experiment (ERBE) satellites from 1985 to 1999 and the Cloud and the Earth's Radiant Energy System (CERES) satellites from March 2000 to the present. The top of the atmosphere radiative flux measurements are highly precise, allowing identification of changes in the Earth's net energy budget from year to year within the ERBE and CERES missions, but the absolute calibration of the instruments is not sufficiently accurate to allow determination of the absolute top of the atmosphere energy flux or to provide continuity across missions. TFE.4, Figure 1b relates the cumulative total energy change of the Earth system to the change in energy storage and the cumulative outgoing radiation. Calculation of the latter is based on the observed global mean surface temperature multiplied by the climate feedback parameter α , which in turn is related to the equilibrium climate sensitivity. The mid-range value for α , $1.23 \text{ W m}^{-2} \text{ }^{\circ}\text{C}^{-1}$, corresponds to an ERF for a doubled carbon dioxide (CO_2) concentration of $3.7 [2.96 \text{ to } 4.44] \text{ W m}^{-2}$ combined with an equilibrium climate sensitivity of 3.0°C . The climate feedback parameter α is *likely* to be in the range from $0.82 \text{ to } 2.47 \text{ W m}^{-2} \text{ }^{\circ}\text{C}^{-1}$ (corresponding to the *likely* range in equilibrium climate sensitivity of 1.5°C to 4.5°C). {9.7.1; Box 12.2}

If ERF were fixed, the climate system would eventually warm sufficiently that the radiative response would balance the ERF, and there would be no further change in energy storage in the climate system. However, the forcing is increasing, and the ocean's large heat capacity means that the climate system is not in radiative equilibrium and its energy content is increasing (TFE.4, Figure 1b). This storage provides strong evidence of a changing climate. The majority of this additional heat is in the upper 700 m of the ocean, but there is also warming in the deep and abyssal ocean. The associated thermal expansion of the ocean has contributed about 40% of the observed sea level rise since 1970. A small amount of additional heat has been used to warm the continents, warm and melt glacial and sea ice and warm the atmosphere. {13.4.2; Boxes 3.1, 13.1}

In addition to these forced variations in the Earth's energy budget, there is also internal variability on decadal time scales. Observations and models indicate that, because of the comparatively small heat capacity of the atmosphere, a decade of steady or even decreasing surface temperature can occur in a warming world. Climate model simulations suggest that these periods are associated with a transfer of heat from the upper to the deeper ocean, of the order 0.1 W m^{-2} , with a near-steady or an increased radiation to space, again of the order 0.1 W m^{-2} . Although these natural fluctuations represent a large amount of heat, they are significantly smaller than the anthropogenic forcing of the Earth's energy budget, particularly on time scales of several decades or longer. {9.4; Boxes 9.2, 13.1}

The available independent estimates of ERF, of observed heat storage, and of surface warming combine to give an energy budget for the Earth that is consistent with the assessed *likely* range of equilibrium climate sensitivity to within estimated uncertainties (*high confidence*). Quantification of the terms in the Earth's energy budget and verification that these terms balance over recent decades provides strong evidence for our understanding of anthropogenic climate change. {Box 13.1}

forcing, particularly WMGHGs and stratospheric ozone depletion, has led to a detectable observed pattern of tropospheric warming and lower stratospheric cooling since 1961. {2.4, 9.4, 10.3}

TS.4.4 Oceans

The observed upper-ocean warming during the late 20th and early 21st centuries and its causes have been assessed more completely since

AR4 using updated observations and more simulations (see Section TS.2.2). The long term trends and variability in the observations are most consistent with simulations of the response to both anthropogenic forcing and volcanic forcing. The anthropogenic fingerprint in observed upper-ocean warming, consisting of global mean and basin-scale pattern changes, has also been detected. This result is robust to a number of observational, model and methodological or structural uncertainties. It is *very likely* that anthropogenic forcings have made

a substantial contribution to upper ocean warming (above 700 m) observed since the 1970s. This anthropogenic ocean warming has contributed to global sea level rise over this period through thermal expansion. {3.2.2, 3.2.3, 3.7.2, 10.4.1, 10.4.3; Box 3.1}

Observed surface salinity changes also suggest a change in the global water cycle has occurred (see TFE.1). The long-term trends show that there is a strong positive correlation between the mean climate of the surface salinity and the temporal changes of surface salinity from 1950 to 2000. This correlation shows an enhancement of the climatological salinity pattern—so fresh areas have become fresher and salty areas saltier. The strongest anthropogenic signals are in the tropics (30°S to 30°N) and the Western Pacific. The salinity contrast between the Pacific and Atlantic Oceans has also increased with significant contributions from anthropogenic forcing. {3.3, 10.3.2, 10.4.2; FAQ 3.2}

On a global scale, surface and subsurface salinity changes (1955–2004) over the upper 250 m of the water column do not match changes expected from natural variability but do match the modelled distribution of forced changes (WMOGHGs and tropospheric aerosols). Natural external variability taken from the simulations with just the variations in solar and volcanic forcing does not match the observations at all, thus excluding the hypothesis that observed trends can be explained by just solar or volcanic variations. These lines of evidence and our understanding of the physical processes leads to the conclusion that it is *very likely* that anthropogenic forcings have made a discernible contribution to surface and subsurface oceanic salinity changes since the 1960s. {10.4.2; Table 10.1}

Oxygen is an important physical and biological tracer in the ocean. Global analyses of oxygen data from the 1960s to 1990s extend the spatial coverage from local to global scales and have been used in attribution studies with output from a limited range of Earth System Models (ESMs). It is concluded that there is *medium confidence* that the observed global pattern of decrease in dissolved oxygen in the oceans can be attributed in part to human influences. {3.8.3, 10.4.4; Table 10.1}

The observations show distinct trends for ocean acidification (which is observed to be between -0.0014 and -0.0024 pH units per year). There is *high confidence* that the pH of ocean surface seawater decreased by about 0.1 since the beginning of the industrial era as a consequence of the oceanic uptake of anthropogenic CO₂. {3.8.2, 10.4.4; Box 3.2; Table 10.1}

TS.4.5 Cryosphere

The reductions in Arctic sea ice extent and NH snow cover extent and widespread glacier retreat and increased surface melt of Greenland are all evidence of systematic changes in the cryosphere. All of these changes in the cryosphere have been linked to anthropogenic forcings. {4.2.2, 4.4–4.6, 10.5.1, 10.5.3; Table 10.1}

Attribution studies, comparing the seasonal evolution of Arctic sea ice extent from observations from the 1950s with that simulated by coupled model simulations, demonstrate that human influence on the sea ice extent changes can be robustly detected since the early 1990s.

The anthropogenic signal is also detectable for individual months from May to December, suggesting that human influence, strongest in late summer, now also extends into colder seasons. From these simulations of sea ice and observed sea ice extent from the instrumental record with high agreement between studies, it is concluded that anthropogenic forcings are *very likely* to have contributed to Arctic sea ice loss since 1979 (Figure TS.12). {10.5.1}

For Antarctic sea ice extent, the shortness of the observed record and differences in simulated and observed variability preclude an assessment of whether or not the observed increase since 1979 is inconsistent with internal variability. Untangling the processes involved with trends and variability in Antarctica and surrounding waters remains complex and several studies are contradictory. In conclusion, there is *low confidence* in the scientific understanding of the observed increase in Antarctic sea ice extent since 1979, due to the large differences between sea ice simulations from CMIP5 models and to the incomplete and competing scientific explanations for the causes of change and *low confidence* in estimates of internal variability (Figure TS.12). {9.4.3, 10.5.1; Table 10.1}

The Greenland ice sheet shows recent major melting episodes in response to record temperatures relative to the 20th century associated with persistent shifts in early summer atmospheric circulation, and these shifts have become more pronounced since 2007. Although many Greenland instrumental records are relatively short (two decades), regional modelling and observations tell a consistent story of the response of Greenland temperatures and ice sheet runoff to shifts in regional atmospheric circulation associated with larger scale flow patterns and global temperature increases. Mass loss and melt is also occurring in Greenland through the intrusion of warm water into the major fjords containing glaciers such as Jacobshaven Glacier. It is *likely* that anthropogenic forcing has contributed to surface melting of the Greenland ice sheet since 1993. {10.5.2; Table 10.1}

Estimates of ice mass in Antarctica since 2000 show that the greatest losses are at the edges. An analysis of observations underneath a floating ice shelf off West Antarctica leads to the conclusion that ocean warming in this region and increased transport of heat by ocean circulation are largely responsible for accelerating melt rates. The observational record of Antarctic mass loss is short and the internal variability of the ice sheet is poorly understood. Due to a low level of scientific understanding there is *low confidence* in attributing the causes of the observed loss of mass from the Antarctic ice sheet since 1993. {3.2, 4.2, 4.4.3, 10.5.2}

The evidence for the retreat of glaciers due to warming and moisture change is now more complete than at the time of AR4. There is *high confidence* in the estimates of observed mass loss and the estimates of natural variations and internal variability from long-term glacier records. Based on these factors and our understanding of glacier response to climatic drivers there is *high confidence* that a substantial part of the mass loss of glaciers is *likely* due to human influence. It is *likely* that there has been an anthropogenic component to observed reductions in NH snow cover since 1970. {4.3.3, 10.5.2, 10.5.3; Table 10.1}

Thematic Focus Elements

TFE.5 | Irreversibility and Abrupt Change

A number of components or phenomena within the climate system have been proposed as potentially exhibiting threshold behaviour. Crossing such thresholds can lead to an abrupt or irreversible transition into a different state of the climate system or some of its components.

Abrupt climate change is defined in this IPCC Fifth Assessment Report (AR5) as a large-scale change in the climate system that takes place over a few decades or less, persists (or is anticipated to persist) for at least a few decades and causes substantial disruptions in human and natural systems. There is information on potential consequences of some abrupt changes, but in general there is *low confidence* and little consensus on the likelihood of such events over the 21st century. Examples of components susceptible to such abrupt change are the strength of the Atlantic Meridional Overturning Circulation (AMOC), clathrate methane release, tropical and boreal forest dieback, disappearance of summer sea ice in the Arctic Ocean, long-term drought and monsoonal circulation. {5.7, 6.4.7, 12.5.5; Table 12.4}

A change is said to be *irreversible* if the recovery time scale from this state due to natural processes is significantly longer than the time it takes for the system to reach this perturbed state. Such behaviour may arise because the time scales for perturbations and recovery processes are different, or because climate change may persist due to the long residence time of a carbon dioxide (CO₂) perturbation in the atmosphere (see TFE.8). Whereas changes in Arctic Ocean summer sea ice extent, long-term droughts and monsoonal circulation are assessed to be reversible within years to decades, tropical or boreal forest dieback may be reversible only within centuries. Changes in clathrate methane and permafrost carbon release, Greenland and Antarctic ice sheet collapse may be irreversible during millennia after the causal perturbation. {5.8, 6.4.7, 12.5.5, 13.4.3, 13.4.4; Table 12.4}

Abrupt Climate Change Linked with AMOC

New transient climate model simulations have confirmed with *high confidence* that strong changes in the strength of the AMOC produce abrupt climate changes at global scale with magnitude and pattern resembling past glacial Dansgaard–Oeschger events and Heinrich stadials. Confidence in the link between changes in North Atlantic climate and low-latitude precipitation has increased since the IPCC Fourth Assessment Report (AR4). From new paleoclimate reconstructions and modelling studies, there is *very high confidence* that a reduced strength of the AMOC and the associated surface cooling in the North Atlantic region caused southward shifts of the Atlantic Intertropical Convergence Zone and affected the American (north and south), African and Asian monsoons. {5.7}

The interglacial mode of the AMOC can recover (*high confidence*) from a short-lived freshwater input into the sub-polar North Atlantic. Approximately 8.2 ka, a sudden freshwater release occurred during the final stages of North America ice sheet melting. Paleoclimate observations and model results indicate, with *high confidence*, a marked reduction in the strength of the AMOC followed by a rapid recovery, within approximately 200 years after the perturbation. {5.8.2}

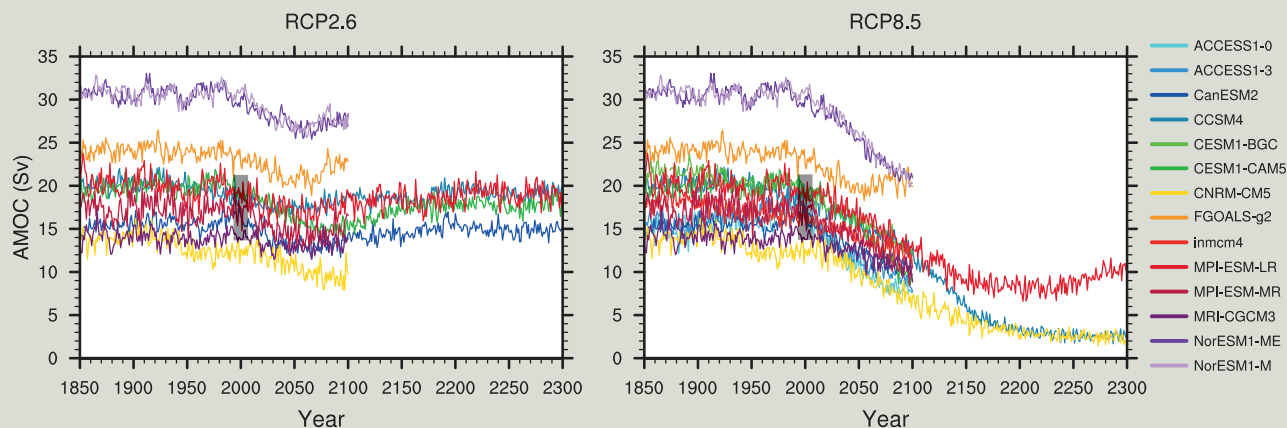
Although many more model simulations have been conducted since AR4 under a wide range of future forcing scenarios, projections of the AMOC behaviour have not changed. It remains *very likely* that the AMOC will weaken over the 21st century relative to 1850-1900 values. Best estimates and ranges for the reduction from the Coupled Model Intercomparison Project Phase 5 (CMIP5) are 11% (1 to 24%) for the Representative Concentration Pathway RCP2.6 and 34% (12 to 54%) for RCP8.5, but there is *low confidence* on the magnitude of weakening. It also remains *very unlikely* that the AMOC will undergo an abrupt transition or collapse in the 21st century for the scenarios considered (*high confidence*) (TFE.5, Figure 1). For an abrupt transition of the AMOC to occur, the sensitivity of the AMOC to forcing would have to be far greater than seen in current models, or would require meltwater flux from the Greenland ice sheet greatly exceeding even the highest of current projections. Although neither possibility can be excluded entirely, it is *unlikely* that the AMOC will collapse beyond the end of the 21st century for the scenarios considered, but a collapse beyond the 21st century for large sustained warming cannot be excluded. There is *low confidence* in assessing the evolution of AMOC beyond the 21st century because of limited number of analyses and equivocal results. {12.4.7, 12.5.5}

Potential Irreversibility of Changes in Permafrost, Methane Clathrates and Forests

In a warming climate, permafrost thawing may induce decomposition of carbon accumulated in frozen soils which could persist for hundreds to thousands of years, leading to an increase of atmospheric CO₂ and/or methane (CH₄)

(continued on next page)

TFE.5 (continued)



TFE.5, Figure 1 | Atlantic Meridional Overturning Circulation (AMOC) strength at 30°N (Sv) as a function of year, from 1850 to 2300 as simulated by different Atmosphere–Ocean General Circulation Models in response to scenario RCP2.6 (left) and RCP8.5 (right). The vertical black bar shows the range of AMOC strength measured at 26°N, from 2004 to 2011 [Figures 3.11, 12.35]

concentrations. The existing modelling studies of permafrost carbon balance under future warming that take into account at least some of the essential permafrost-related processes do not yield consistent results, beyond the fact that present-day permafrost will become a net emitter of carbon during the 21st century under plausible future warming scenarios (*low confidence*). This also reflects an insufficient understanding of the relevant soil processes during and after permafrost thaw, including processes leading to stabilization of unfrozen soil carbon, and precludes any quantitative assessment of the amplitude of irreversible changes in the climate system potentially related to permafrost degassing and associated feedbacks. {6.4.7, 12.5.5}

Anthropogenic warming will *very likely* lead to enhanced CH₄ emissions from both terrestrial and oceanic clathrates. Deposits of CH₄ clathrates below the sea floor are susceptible to destabilization via ocean warming. However, sea level rise due to changes in ocean mass enhances clathrate stability in the ocean. While difficult to formally assess, initial estimates of the 21st century feedback from CH₄ clathrate destabilization are small but not insignificant. It is *very unlikely* that CH₄ from clathrates will undergo catastrophic release during the 21st century (*high confidence*). On multi-millennial time scales, such CH₄ emissions may provide a positive feedback to anthropogenic warming and may be irreversible, due to the difference between release and accumulation time scales. {6.4.7, 12.5.5}

The existence of critical climate change driven dieback thresholds in the Amazonian and other tropical rainforests purely driven by climate change remains highly uncertain. The possibility of a critical threshold being crossed in precipitation volume and duration of dry seasons cannot be ruled out. The response of boreal forest to projected climate change is also highly uncertain, and the existence of critical thresholds cannot at present be ruled out. There is *low confidence* in projections of the collapse of large areas of tropical and/or boreal forests. {12.5.5}

Potential Irreversibility of Changes in the Cryosphere

The reversibility of sea ice loss has been directly assessed in sensitivity studies to CO₂ increase and decrease with Atmosphere–Ocean General Circulation Models (AOGCMs) or Earth System Models (ESMs). None of them show evidence of an irreversible change in Arctic sea ice at any point. By contrast, as a result of the strong coupling between surface and deep waters in the Southern Ocean, the Antarctic sea ice in some models integrated with ramp-up and ramp-down atmospheric CO₂ concentration exhibits some hysteresis behaviour. {12.5.5}

At present, both the Greenland and Antarctic ice sheets have a positive surface mass balance (snowfall exceeds melting), although both are losing mass because ice outflow into the sea exceeds the net surface mass balance. A positive feedback operates to reduce ice sheet volume and extent when a decrease of the surface elevation of the ice sheet induces a decreased surface mass balance. This arises generally through increased surface melting, and therefore applies in the 21st century to Greenland, but not to Antarctica, where surface melting is currently very small. Surface melting in Antarctica is projected to become important after several centuries under high well-mixed greenhouse gas radiative forcing scenarios. {4.4, 13.4.4; Boxes 5.2, 13.2}

Abrupt change in ice sheet outflow to the sea may be caused by unstable retreat of the grounding line in regions where the bedrock is below sea level and slopes downwards towards the interior of the ice sheet. This mainly

(continued on next page)

TS

TFE.5 (continued)

applies to West Antarctica, but also to parts of East Antarctica and Greenland. Grounding line retreat can be triggered by ice shelf decay, due to warmer ocean water under ice shelves enhancing submarine ice shelf melt, or melt water ponds on the surface of the ice shelf promoting ice shelf fracture. Because ice sheet growth is a slow process, such changes would be irreversible in the definition adopted here. {4.4.5; Box 13.2}

There is *high confidence* that the volumes of the Greenland and West Antarctic ice sheets were reduced during periods of the past few million years that were globally warmer than present. Ice sheet model simulations and geological data suggest that the West Antarctic ice sheet is very sensitive to subsurface ocean warming and imply with *medium confidence* a West Antarctic ice sheet retreat if atmospheric CO₂ concentration stays within, or above, the range of 350–450 ppm for several millennia. {5.8.1, 13.4.4; Box 13.2}

The available evidence indicates that global warming beyond a threshold would lead to the near-complete loss of the Greenland ice sheet over a millennium or longer, causing a global mean sea level rise of approximately 7 m. Studies with fixed present-day ice sheet topography indicate that the threshold is greater than 2°C but less than 4°C (*medium confidence*) of global mean surface temperature rise above pre-industrial. The one study with a dynamical ice sheet suggests the threshold is greater than about 1°C (*low confidence*) global mean warming with respect to pre-industrial. Considering the present state of scientific uncertainty, a *likely* range cannot be quantified. The complete loss of the Greenland ice sheet is not inevitable because this would take a millennium or more; if temperatures decline before the ice sheet has completely vanished, the ice sheet might regrow. However, some part of the mass loss might be irreversible, depending on the duration and degree of exceedance of the threshold, because the ice sheet may have multiple steady states, due to its interaction with regional climate. {13.4.3, 13.4.4}

TS

TS.4.6 Water Cycle

Since the AR4, new evidence has emerged of a detectable human influence on several aspects of the water cycle. There is *medium confidence* that observed changes in near-surface specific humidity since 1973 contain a detectable anthropogenic component. The anthropogenic water vapour fingerprint simulated by an ensemble of climate models has been detected in lower tropospheric moisture content estimates derived from Special Sensor Microwave/Imager (SSM/I) data covering the period 1988–2006. An anthropogenic contribution to increases in tropospheric specific humidity is found with *medium confidence*. {2.5, 10.3}

Attribution studies of global zonal mean terrestrial precipitation and Arctic precipitation both find a detectable anthropogenic influence. Overall there is *medium confidence* in a significant human influence on global scale changes in precipitation patterns, including increases in NH mid-to-high latitudes. Remaining observational and modelling uncertainties and the large effect of internal variability on observed precipitation preclude a more confident assessment. {2.5, 7.6, 10.3}

Based on the collected evidence for attributable changes (with varying levels of confidence and likelihood) in specific humidity, terrestrial precipitation and ocean surface salinity through its connection to precipitation and evaporation, and from physical understanding of the water cycle, it is *likely* that human influence has affected the global water cycle since 1960. This is a major advance since AR4. {2.4, 2.5, 3.3, 9.4.1, 10.3, 10.4.2; Table 10.1; FAQ 3.2}

TS.4.7 Climate Extremes

Several new attribution studies have found a detectable anthropogenic influence in the observed increased frequency of warm days and nights and decreased frequency of cold days and nights. Since the AR4 and SREX, there is new evidence for detection of human influence on extremely warm daytime temperature and there is new evidence that the influence of anthropogenic forcing may be detected separately from the influence of natural forcing at global scales and in some continental and sub-continental regions. This strengthens the conclusions from both AR4 and SREX, and it is now *very likely* that anthropogenic forcing has contributed to the observed changes in the frequency and intensity of daily temperature extremes on the global scale since the mid-20th century. It is *likely* that human influence has significantly increased the probability of occurrence of heat waves in some locations. See TFE.9 and TFE.9, Table 1 for a summary of the assessment of extreme weather and climate events. {10.6}

Since the AR4, there is some new limited direct evidence for an anthropogenic influence on extreme precipitation, including a formal detection and attribution study and indirect evidence that extreme precipitation would be expected to have increased given the evidence of anthropogenic influence on various aspects of the global hydrological cycle and *high confidence* that the intensity of extreme precipitation events will increase with warming, at a rate well exceeding that of the mean precipitation. In land regions where observational coverage is sufficient for assessment, there is *medium confidence* that anthropogenic forcing has contributed to a global-scale intensification of heavy precipitation over the second half of the 20th century. {7.6, 10.6}

Globally, there is *low confidence* in attribution of changes in tropical cyclone activity to human influence. This is due to insufficient observational evidence, lack of physical understanding of the links between anthropogenic drivers of climate and tropical cyclone activity, and the low level of agreement between studies as to the relative importance of internal variability, and anthropogenic and natural forcings. In the North Atlantic region there is *medium confidence* that a reduction in aerosol forcing over the North Atlantic has contributed at least in part to the observed increase in tropical cyclone activity there since the 1970s. There remains substantial disagreement on the relative importance of internal variability, WMGHG forcing and aerosols for this observed trend. {2.6, 10.6, 14.6}

Although the AR4 concluded that it is *more likely than not* that anthropogenic influence has contributed to an increased risk of drought in the second half of the 20th century, an updated assessment of the observational evidence indicates that the AR4 conclusions regarding global increasing trends in hydrological droughts since the 1970s are no longer supported. Owing to the *low confidence* in observed large-scale trends in dryness combined with difficulties in distinguishing decadal-scale variability in drought from long-term climate change, there is now *low confidence* in the attribution of changes in drought over global land since the mid-20th century to human influence. {2.6, 10.6}

TS.4.8 From Global to Regional

Taking a longer term perspective shows the substantial role played by external forcings in driving climate variability on hemispheric scales in pre-industrial times (Box TS.5). It is *very unlikely* that NH temperature variations from 1400 to 1850 can be explained by internal variability alone. There is *medium confidence* that external forcing contributed to NH temperature variability from 850 to 1400 and that external forcing contributed to European temperature variations over the last 5 centuries. {5.3.3, 5.5.1, 10.7.2, 10.7.5; Table 10.1}

Changes in atmospheric circulation are important for local climate change because they could lead to greater or smaller changes in climate in a particular region than elsewhere. It is *likely* that human influence has altered sea level pressure patterns globally. There is *medium confidence* that stratospheric ozone depletion has contributed to the observed poleward shift of the southern Hadley Cell border during austral summer. It is *likely* that stratospheric ozone depletion has contributed to the positive trend in the SAM seen in austral summer since the mid-20th century which corresponds to sea level pressure reductions over the high latitudes and increase in the subtropics (Figure TS.11). {10.3}

The evidence is stronger that observed changes in the climate system can now be attributed to human activities on global and regional scales in many components (Figure TS.12). Observational uncertainty has been explored much more thoroughly than previously, and fingerprints of human influence have been deduced from a new generation of climate models. There is improved understanding of ocean changes, including salinity changes, that are consistent with large scale intensification of the water cycle predicted by climate models. The changes in near surface temperatures, free atmosphere temperatures, ocean temperatures and NH snow cover and sea ice extent, when taken together, show not

just global mean changes, but also distinctive regional patterns consistent with the expected fingerprints of change from anthropogenic forcings and the expected responses from volcanic eruptions (Figure TS.12). {10.3–10.6, 10.9}

Human influence has been detected in nearly all of the major assessed components of the climate system (Figure TS.12). Taken together, the combined evidence increases the overall level of confidence in the attribution of observed climate change, and reduces the uncertainties associated with assessment based on a single climate variable. From this combined evidence it is *virtually certain* that human influence has warmed the global climate system. Anthropogenic influence has been identified in changes in temperature near the surface of the Earth, in the atmosphere and in the oceans, as well as in changes in the cryosphere, the water cycle and some extremes. There is strong evidence that excludes solar forcing, volcanoes and internal variability as the strongest drivers of warming since 1950. {10.9; Table 10.1; FAQ 5.1}

Over every continent except Antarctica, anthropogenic influence has *likely* made a substantial contribution to surface temperature increases since the mid-20th century (Figure TS.12). It is *likely* that there has been a significant anthropogenic contribution to the very substantial warming in Arctic land surface temperatures over the past 50 years. For Antarctica large observational uncertainties result in *low confidence* that anthropogenic influence has contributed to observed warming averaged over available stations. Detection and attribution at regional

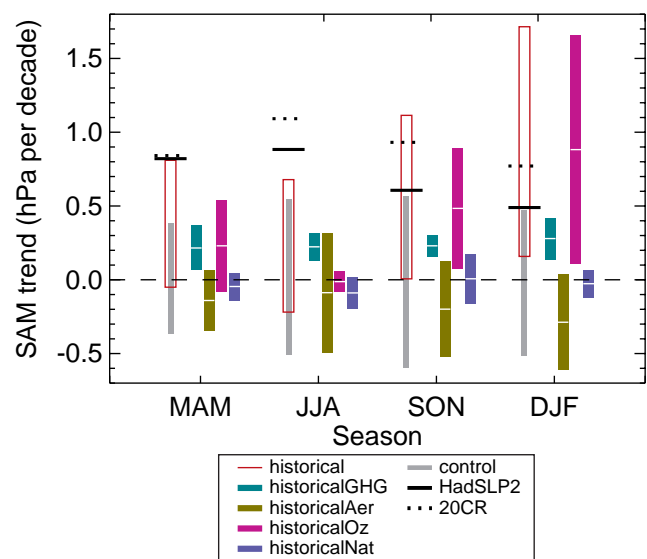


Figure TS.11 | Simulated and observed 1951–2011 trends in the Southern Annular Mode (SAM) index by season. The SAM index is a difference between zonal mean sea level pressure (SLP) at 40°S and 65°S. The SAM index is defined without normalization, so that the magnitudes of simulated and observed trends can be compared. Black lines show observed trends from the Hadley Centre Sea Level Pressure 2r (HadSLP2r) data set (solid), and the 20th Century Reanalysis (dotted). Grey bars show 5th to 95th percentile ranges of control trends, and red boxes show the 5th to 95th percentile range of trends in historical simulations including anthropogenic and natural forcings. Coloured bars show ensemble mean trends and their associated 5 to 95% confidence ranges simulated in response to well-mixed greenhouse gas (light green), aerosol (dark green), ozone (magenta) and natural forcing changes (blue) in CMIP5 individual-forcing simulations. (Figure 10.13b)

TS

scales is complicated by the greater role played by dynamical factors (circulation changes), a greater range of forcings that may be regionally important, and the greater difficulty of modelling relevant processes at regional scales. Nevertheless, human influence has *likely* contributed to temperature increases in many sub-continental regions. {10.3; Box 5.1}

The coherence of observed changes with simulations of anthropogenic and natural forcing in the physical system is remarkable (Figure TS.12), particularly for temperature-related variables. Surface temperature and

ocean heat content show emerging anthropogenic and natural signals in both records, and a clear separation from the alternative hypothesis of just natural variations. These signals do not appear just in the global means, but also appear at regional scales on continents and in ocean basins in each of these variables. Sea ice extent emerges clearly from the range of internal variability for the Arctic. At sub-continental scales human influence is *likely* to have substantially increased the probability of occurrence of heat waves in some locations. {Table 10.1}

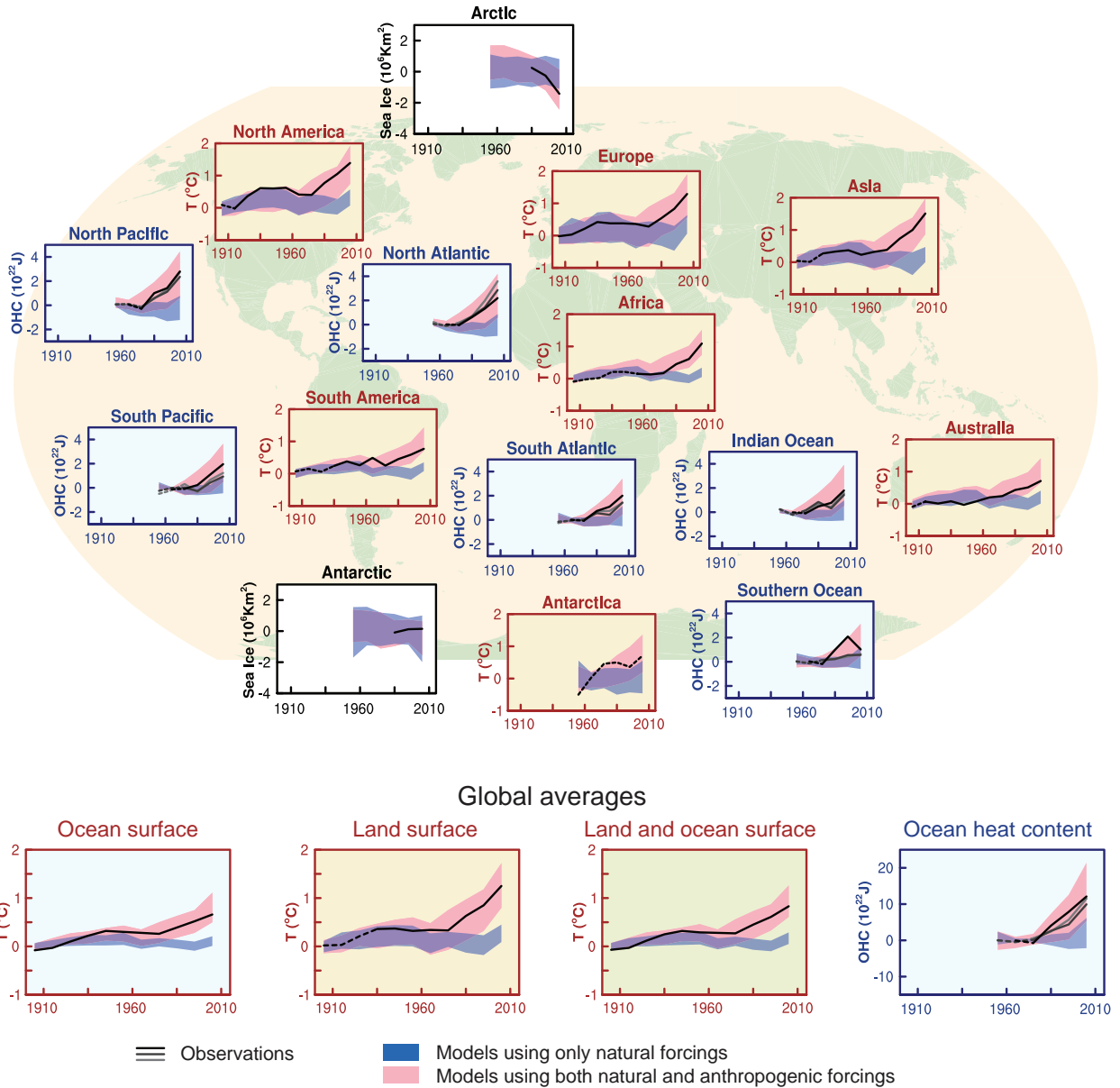


Figure TS.12 | Comparison of observed and simulated change in the climate system, at regional scales (top panels) and global scales (bottom four panels). Brown panels are land surface temperature time series, blue panels are ocean heat content time series and white panels are sea ice time series (decadal averages). Each panel shows observations (black or black and shades of grey), and the 5 to 95% range of the simulated response to natural forcings (blue shading) and natural and anthropogenic forcings (pink shading), together with the corresponding ensemble means (dark blue and dark red respectively). The observed surface temperature is from the Hadley Centre/Climatic Research Unit gridded surface temperature data set 4 (HadCRUT4). Three observed records of ocean heat content (OHC) are shown. Sea ice anomalies (rather than absolute values) are plotted and based on models in Figure 10.16. The observations lines are either solid or dashed and indicate the quality of the observations and estimates. For land and ocean surface temperatures panels and precipitation panels, solid observation lines indicate where spatial coverage of areas being examined is above 50% coverage and dashed observation lines where coverage is below 50%. For example, data coverage of Antarctica never goes above 50% of the land area of the continent. For ocean heat content and sea ice panels the solid observations line is where the coverage of data is good and higher in quality, and the dashed line is where the data coverage is only adequate. This figure is based on Figure 10.21 except presented as decadal averages rather than yearly averages. Further detail regarding the related Figure SPM.6 is given in the TS Supplementary Material. {Figure 10.21}

Box TS.4 | Model Evaluation

Climate models have continued to be improved since the AR4, and many models have been extended into Earth System Models (ESMs) by including the representation of biogeochemical cycles important to climate change. Box TS.4, Figure 1 provides a partial overview of model capabilities as assessed in this report, including improvements or lack thereof relative to models that were assessed in the AR4 or that were available at the time of the AR4. {9.1, 9.8.1; Box 9.1}

The ability of climate models to simulate surface temperature has improved in many, though not all, important aspects relative to the generation of models assessed in the AR4. There continues to be *very high confidence* that models reproduce the observed large-scale time-mean surface temperature patterns (pattern correlation of about 0.99), although systematic errors of several degrees Celsius are found in some regions. There is *high confidence* that on the regional scale (sub-continental and smaller), time-mean surface temperature is better simulated than at the time of the AR4; however, confidence in model capability is lower than for the large scale. Models are able to reproduce the magnitude of the observed global mean or northern-hemisphere-mean temperature variability on interannual to centennial time scales. Models are also able to reproduce the large-scale patterns of temperature during the Last Glacial Maximum indicating an ability to simulate a climate state much different from the present (see also Box TS.5). {9.4.1, 9.6.1}

There is *very high confidence* that models reproduce the general features of the global and annual mean surface temperature changes over the historical period, including the warming in the second half of the 20th century and the cooling immediately following large volcanic eruptions. Most simulations of the historical period do not reproduce the observed reduction in global mean surface warming trend over the last 10 to 15 years (see Box TS.3). There is *medium confidence* that the trend difference between models and observations during 1998–2012 is to a substantial degree caused by internal variability, with possible contributions from forcing inadequacies in models and some models overestimating the response to increasing greenhouse gas forcing. Most, though not all, models overestimate the observed warming trend in the tropical troposphere over the last 30 years, and tend to underestimate the long-term lower-stratospheric cooling trend. {9.4.1; Box 9.2}

The simulation of large-scale patterns of precipitation has improved somewhat since the AR4, although models continue to perform less well for precipitation than for surface temperature. The spatial pattern correlation between modelled and observed annual mean precipitation has increased from 0.77 for models available at the time of the AR4 to 0.82 for current models. At regional scales, precipitation is not simulated as well, and the assessment remains difficult owing to observational uncertainties. {9.4.1, 9.6.1}

Many models are able to reproduce the observed changes in upper-ocean heat content from 1961 to 2005. The time series of the multi-model mean falls within the range of the available observational estimates for most of the period. {9.4.2}

There is robust evidence that the downward trend in Arctic summer sea ice extent is better simulated than at the time of the AR4. About one quarter of the models show a trend as strong as, or stronger, than the trend in observations over the satellite era 1979–2012. Most models simulate a small decreasing trend in Antarctic sea ice extent, albeit with large inter-model spread, in contrast to the small increasing trend in observations. {9.4.3}

There has been substantial progress since the AR4 in the assessment of model simulations of extreme events. Changes in the frequency of extreme warm and cold days and nights over the second half of the 20th century are consistent between models and observations, with the ensemble mean global mean time series generally falling within the range of observational estimates. The majority of models underestimate the sensitivity of extreme precipitation to temperature variability or trends, especially in the tropics. {9.5.4}

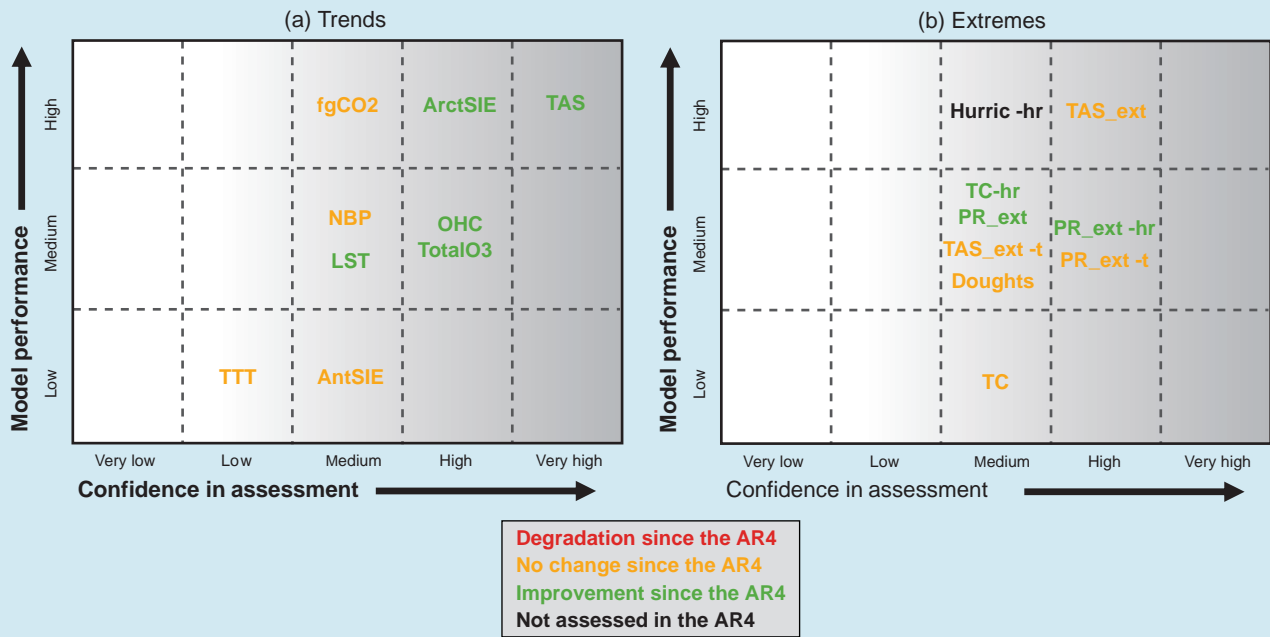
In the majority of the models that include an interactive carbon cycle, the simulated global land and ocean carbon sinks over the latter part of the 20th century fall within the range of observational estimates. However, models systematically underestimate the NH land sink implied by atmospheric inversion techniques. {9.4.5}

Regional downscaling methods provide climate information at the smaller scales needed for many climate impact studies. There is *high confidence* that downscaling adds value both in regions with highly variable topography and for various small-scale phenomena. {9.6.4}

The model spread in equilibrium climate sensitivity ranges from 2.1°C to 4.7°C and is very similar to the assessment in the AR4. There is *very high confidence* that the primary factor contributing to the spread in equilibrium climate sensitivity continues to be the cloud feedback. This applies to both the modern climate and the last glacial maximum. There is likewise *very high confidence* that, consistent with observations, models show a strong positive correlation between tropospheric temperature and water vapour on regional to global scales, implying a positive water vapour feedback in both models and observations. {5.3.3, 9.4.1, 9.7} (continued on next page)

Box TS.4 (continued)

Climate models are based on physical principles, and they reproduce many important elements of observed climate. Both aspects contribute to our confidence in the models' suitability for their application in detection and attribution studies (see Chapter 10) and for quantitative future predictions and projections (see Chapters 11 to 14). There is increasing evidence that some elements of observed variability or trends are well correlated with inter-model differences in model projections for quantities such as Arctic summer sea ice trends, the snow–albedo feedback, and the carbon loss from tropical land. However, there is still no universal strategy for transferring a model's past performance to a relative weight of this model in a multi-model-ensemble mean of climate projections. {9.8.3}



Box TS.4, Figure 1 | Summary of how well the current-generation climate models simulate important features of the climate of the 20th century. Confidence in the assessment increases towards the right as suggested by the increasing strength of shading. Model quality increases from bottom to top. The colour coding indicates improvements from the models available at the time of the AR4 to the current assessment. There have been a number of improvements since the AR4, and some some modelled quantities are not better simulated. The major climate quantities are listed in this summary and none shows degradation. The assessment is based mostly on the multi-model mean, not excluding that deviations for individual models could exist. Assessed model quality is simplified for representation in this figure; details of each assessment are found in Chapter 9. {9.8.1; Figure 9.44}

The figure highlights the following key features, with the sections that back up the assessment added in brackets:

(a) Trends in:

- AntSIE Antarctic sea ice extent {9.4.3}
- ArctSIE Arctic sea ice extent {9.4.3}
- fgCO2 Global ocean carbon sink {9.4.5}
- LST Lower-stratospheric temperature {9.4.1.}
- NBP Global land carbon sink {9.4.5}
- OHC Global ocean heat content {9.4.2}
- TotalO3 Total-column ozone {9.4.1}
- TAS Surface air temperature {9.4.1}
- TTT Tropical tropospheric temperature {9.4.1}

(b) Extremes:

- Droughts Droughts {9.5.4}
- Hurric-hr Year-to-year count of Atlantic hurricanes in high-resolution AGCMs {9.5.4}
- PR_ext Global distribution of precipitation extremes {9.5.4}
- PR_ext-hr Global distribution of precipitation extremes in high-resolution AGCMs {9.5.4}
- PR_ext-t Global trends in precipitation extremes {9.5.4}
- TAS_ext Global distributions of surface air temperature extremes {9.5.4}
- TAS_ext-t Global trends in surface air temperature extremes {9.5.4}
- TC Tropical cyclone tracks and intensity {9.5.4}
- TC-hr Tropical cyclone tracks and intensity in high-resolution AGCMs {9.5.4}

Box TS.5 | Paleoclimate

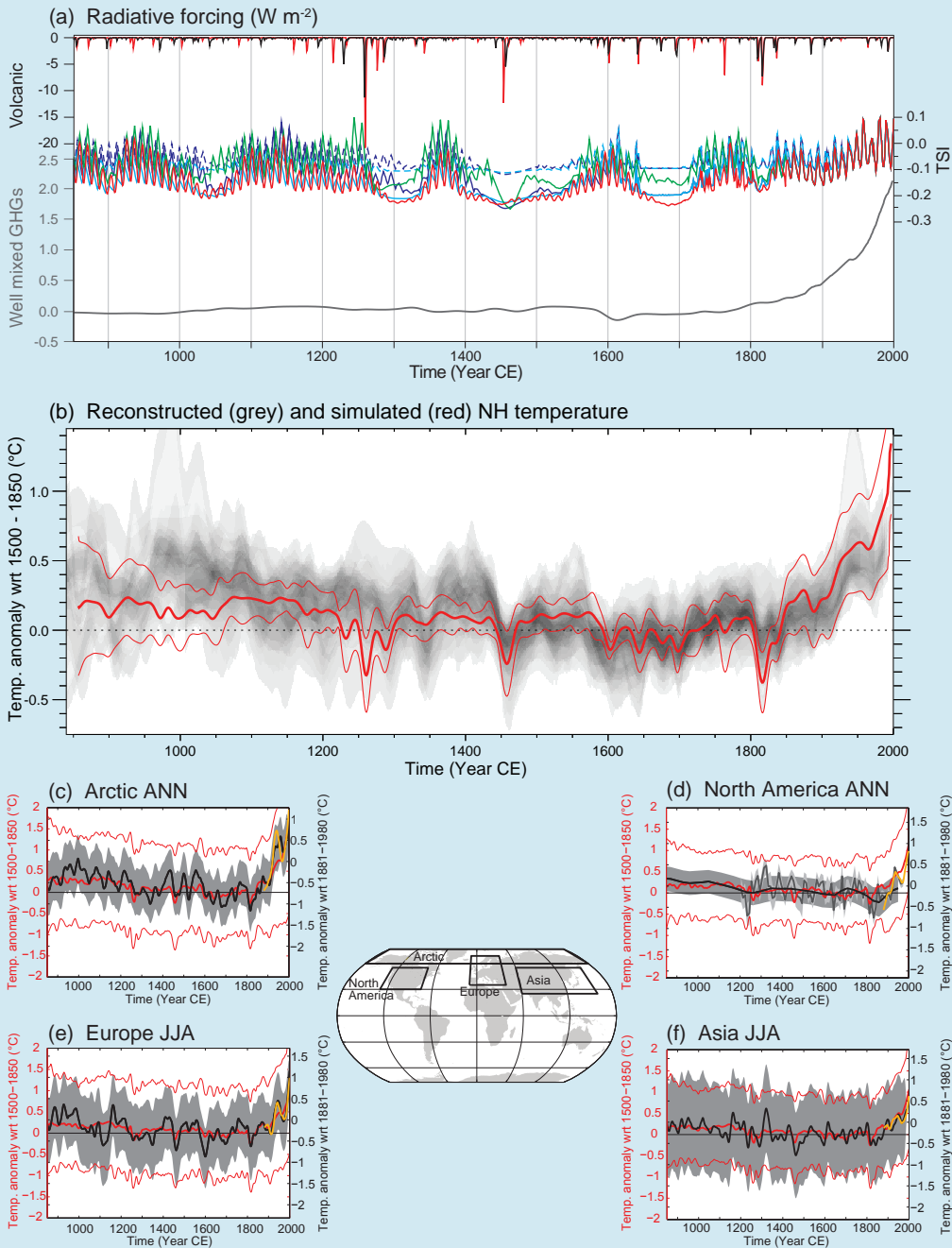
Reconstructions from paleoclimate archives allow current changes in atmospheric composition, sea level and climate (including extreme events such as droughts and floods), as well as future projections, to be placed in a broader perspective of past climate variability (see Section TS.2). {5.2–5.6, 6.2, 10.7}

Past climate information also documents the behaviour of slow components of the climate system including the carbon cycle, ice sheets and the deep ocean for which instrumental records are short compared to their characteristic time scales of responses to perturbations, thus informing on mechanisms of abrupt and irreversible changes. Together with the knowledge of past external climate forcings, syntheses of paleoclimate data have documented polar amplification, characterized by enhanced temperature changes in the Arctic compared to the global mean, in response to high or low CO₂ concentrations. {5.2.1, 5.2.2, 5.6, 5.7, 5.8, 6.2, 8.4.2, 13.2.1, 13.4; Boxes 5.1, 5.2}

Since AR4, the inclusion of paleoclimate simulations in the PMIP3 (Paleoclimate Modelling Intercomparison Project)/CMIP5 framework has enabled paleoclimate information to be more closely linked with future climate projections. Paleoclimate information for the mid-Holocene (6 ka), the Last Glacial Maximum (approximately 21 ka), and last millennium has been used to test the ability of models to simulate realistically the magnitude and large-scale patterns of past changes. Combining information from paleoclimate simulations and reconstructions enables to quantify the response of the climate system to radiative perturbations, constraints to be placed on the range of equilibrium climate sensitivity, and past patterns of internal climate variability to be documented on inter-annual to multi-centennial scales. {5.3.1–5.3.5, 5.4, 5.5.1, 9.4.1, 9.4.2, 9.5.3, 9.7.2, 10.7.2, 14.1.2}

Box TS.5, Figure 1 illustrates the comparison between the last millennium Paleoclimate Modelling Intercomparison Project Phase 3 (PMIP3)/CMIP5 simulations and reconstructions, together with the associated solar, volcanic and WGMHG RFs. For average annual NH temperatures, the period 1983–2012 was *very likely* the warmest 30-year period of the last 800 years (*high confidence*) and *likely* the warmest 30-year period of the last 1400 years (*medium confidence*). This is supported by comparison of instrumental temperatures with multiple reconstructions from a variety of proxy data and statistical methods, and is consistent with AR4. In response to solar, volcanic and anthropogenic radiative changes, climate models simulate multi-decadal temperature changes in the last 1200 years in the NH that are generally consistent in magnitude and timing with reconstructions, within their uncertainty ranges. Continental-scale temperature reconstructions show, with *high confidence*, multi-decadal periods during the Medieval Climate Anomaly (about 950 to 1250) that were in some regions as warm as the mid-20th century and in others as warm as in the late 20th century. With *high confidence*, these regional warm periods were not as synchronous across regions as the warming since the mid-20th century. Based on the comparison between reconstructions and simulations, there is *high confidence* that not only external orbital, solar and volcanic forcing but also internal variability contributed substantially to the spatial pattern and timing of surface temperature changes between the Medieval Climate Anomaly and the Little Ice Age (about 1450 to 1850). However, there is only *very low confidence* in quantitative estimates of their relative contributions. It is *very unlikely* that NH temperature variations from 1400 to 1850 can be explained by internal variability alone. There is *medium confidence* that external forcing contributed to Northern Hemispheric temperature variability from 850 to 1400 and that external forcing contributed to European temperature variations over the last 5 centuries. {5.3.5, 5.5.1, 10.7.2, 10.7.5; Table 10.1} (*continued on next page*)

Box TS.5 (continued)



Box TS.5, Figure 1 | Last-millennium simulations and reconstructions. (a) 850–2000 PMIP3/CMIP5 radiative forcing due to volcanic, solar and well-mixed greenhouse gases. Different colours illustrate the two existing data sets for volcanic forcing and four estimates of solar forcing. For solar forcing, solid (dashed) lines stand for reconstruction variants in which background changes in irradiance are (not) considered; (b) 850–2000 PMIP3/CMIP5 simulated (red) and reconstructed (shading) Northern Hemisphere (NH) temperature changes. The thick red line depicts the multi-model mean while the thin red lines show the multi-model 90% range. The overlap of reconstructed temperatures is shown by grey shading; all data are expressed as anomalies from their 1500–1850 mean and smoothed with a 30-year filter. Note that some reconstructions represent a smaller spatial domain than the full NH or a specific season, while annual temperatures for the full NH mean are shown for the simulations. (c), (d), (e) and (f) Arctic and North America annual mean temperature, and Europe and Asia June, July and August (JJA) temperature, from 950 to 2000 from reconstructions (black line), and PMIP3/CMIP5 simulations (thick red, multi-model mean; thin red, 90% multi-model range). All red curves are expressed as anomalies from their 1500–1850 mean and smoothed with a 30-year filter. The shaded envelope depicts the uncertainties from each reconstruction (Arctic: 90% confidence bands, North American: ± 2 standard deviation. Asia: ± 2 root mean square error. Europe: 95% confidence bands). For comparison with instrumental record, the Climatic Research Unit land station Temperature (CRUTEM4) data set is shown (yellow line). These instrumental data are not necessarily those used in calibration of the reconstructions, and thus may show greater or lesser correspondence with the reconstructions than the instrumental data actually used for calibration; cutoff timing may also lead to end effects for smoothed data shown. All lines are smoothed by applying a 30-year moving average. Map shows the individual regions for each reconstruction. {5.3.5; Table 5.A.1; Figures 5.1, 5.8, 5.12}

TS.5 Projections of Global and Regional Climate Change

TS.5.1 Introduction

Projections of changes in the climate system are made using a hierarchy of climate models ranging from simple climate models, to models of intermediate complexity, to comprehensive climate models, and Earth System Models (ESMs). These models simulate changes based on a set of scenarios of anthropogenic forcings. A new set of scenarios, the Representative Concentration Pathways (RCPs), was used for the new climate model simulations carried out under the framework of the Coupled Model Intercomparison Project Phase 5 (CMIP5) of the World Climate Research Programme. A large number of comprehensive climate models and ESMs have participated in CMIP5, whose results form the core of the climate system projections.

This section summarizes the assessment of these climate change projections. First, future forcing and scenarios are presented. The following subsections then address various aspects of projections of global and regional climate change, including near-term (up to about mid-century) and long-term (end of the 21st century) projections in the atmosphere, ocean and cryosphere; projections of carbon and other biogeochemical

cycles; projections in sea level change; and finally changes to climate phenomena and other aspects of regional climate over the 21st century. Projected changes are given relative to the 1986–2005 average unless indicated otherwise. Projections of climate change on longer term and information on climate stabilization and targets are provided in TFE.8. Methods to counter climate change, termed geoengineering, have been proposed and an overview is provided in Box TS.7. {11.3, 12.3–12.5, 13.5–13.7, 14.1–14.6, Annex I}

TS.5.2 Future Forcing and Scenarios

In this assessment report a series of new RCPs are used that largely replace the IPCC Special Report on Emission Scenarios (SRES) scenarios (see Box TS.6 and Annex II for Climate System Scenario Tables). They produce a range of responses from ongoing warming, to approximately stabilized forcing, to a stringent mitigation scenario (RCP2.6) that stabilizes and then slowly reduces the RF after mid-21st century. In contrast to the AR4, the climate change from the RCP scenarios in the AR5 is framed as a combination of adaptation and mitigation. Mitigation actions starting now in the various RCP scenarios do not produce discernibly different climate change outcomes for the next 30 years or so, whereas long-term climate change after mid-century is appreciably different across the RCPs. {Box 1.1}

Box TS.6 | The New Representative Concentration Pathway Scenarios and Coupled Model Intercomparison Project Phase 5 Models

Future anthropogenic emissions of GHGs, aerosol particles and other forcing agents such as land use change are dependent on socio-economic factors, and may be affected by global geopolitical agreements to control those emissions to achieve mitigation. AR4 made extensive use of the SRES scenarios that do not include additional climate initiatives, which means that no scenarios were available that explicitly assume implementation of the United Nations Framework Convention on Climate Change (UNFCCC) or the emissions targets of the Kyoto Protocol. However, GHG emissions are directly affected by non-climate change policies designed for a wide range of other purposes. The SRES scenarios were developed using a sequential approach, that is, socioeconomic factors fed into emissions scenarios, which were then used in simple climate models to determine concentrations of GHGs, and other agents required to drive the more complex AOGCMs. In this report, outcomes of climate simulations that use new scenarios (some of which include implied policy actions to achieve mitigation) referred to as RCPs are assessed. These RCPs represent a larger set of mitigation scenarios and were selected to have different targets in terms of radiative forcing at 2100 (about 2.6, 4.5, 6.0 and 8.5 W m⁻²; Figure TS.15). The scenarios should be considered plausible and illustrative, and do not have probabilities attached to them. {12.3.1; Box 1.1}

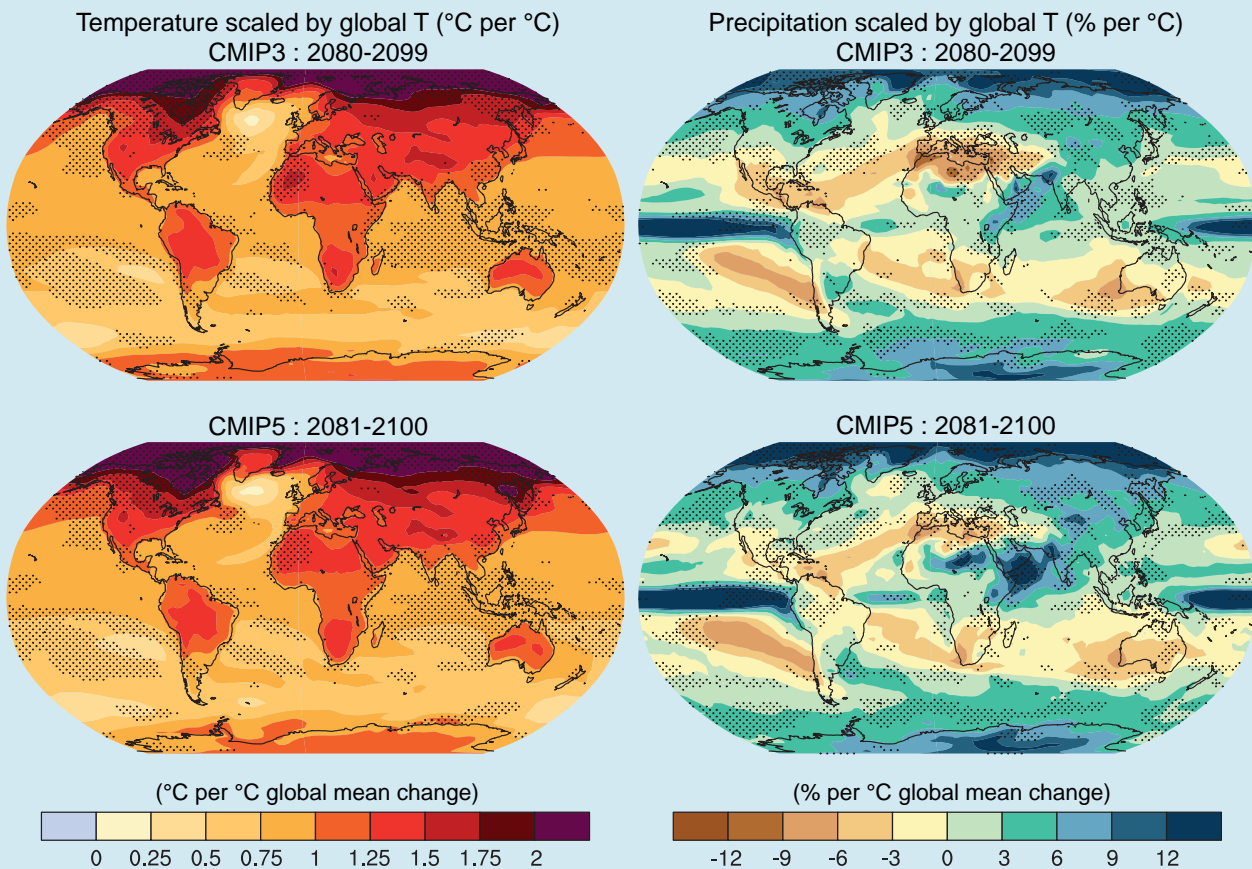
The RCPs were developed using Integrated Assessment Models (IAMs) that typically include economic, demographic, energy, and simple climate components. The emission scenarios they produce are then run through a simple model to produce time series of GHG concentrations that can be run in AOGCMs. The emission time series from the RCPs can then be used directly in ESMs that include interactive biogeochemistry (at least a land and ocean carbon cycle). {12.3.1; Box 1.1}

The CMIP5 multi-model experiment (coordinated through the World Climate Research Programme) presents an unprecedented level of information on which to base assessments of climate variability and change. CMIP5 includes new ESMs in addition to AOGCMs, new model experiments and more diagnostic output. CMIP5 is much more comprehensive than the preceding CMIP3 multi-model experiment that was available at the time of the IPCC AR4. CMIP5 has more than twice as many models, many more experiments (that also include experiments to address understanding of the responses in the future climate change scenario runs), and nearly 2 × 10¹⁵ bytes of data (as compared to over 30 × 10¹² bytes of data in CMIP3). A larger number of forcing agents are treated more completely in the CMIP5 models, with respect to aerosols and land use particularly. Black carbon aerosol is now a commonly included forcing agent. Considering CO₂, both ‘concentrations-driven’ projections and ‘emissions-driven’ projections are assessed from CMIP5. These allow quantification of the physical response uncertainties as well as climate–carbon cycle interactions. {1.5.2}

(continued on next page)

Box TS.6 (continued)

The assessment of the mean values and ranges of global mean temperature changes in AR4 would not have been substantially different if the CMIP5 models had been used in that report. The differences in global temperature projections can largely be attributed to the different scenarios. The global mean temperature response simulated by CMIP3 and CMIP5 models is very similar, both in the mean and the model range, transiently and in equilibrium. The range of temperature change across all scenarios is wider because the RCPs include a strong mitigation scenario (RCP2.6) that had no equivalent among the SRES scenarios used in CMIP3. For each scenario, the 5 to 95% range of the CMIP5 projections is obtained by approximating the CMIP5 distributions by a normal distribution with same mean and standard deviation and assessed as being *likely* for projections of global temperature change for the end of the 21st century. Probabilistic projections with simpler models calibrated to span the range of equilibrium climate sensitivity assessed by the AR4 provide uncertainty ranges that are consistent with those from CMIP5. In AR4 the uncertainties in global temperature projections were found to be approximately constant when expressed as a fraction of the model mean warming (constant fractional uncertainty). For the higher RCPs, the uncertainty is now estimated to be smaller than with the AR4 method for long-term climate change, because the carbon cycle–climate feedbacks are not relevant for the concentration-driven RCP projections (in contrast, the assessed projection uncertainties of global temperature in AR4 did account of carbon cycle–climate feedbacks, even though these were not part of the CMIP3 models). When forced with RCP8.5, CO₂ emissions, as opposed to the RCP8.5 CO₂ concentrations, CMIP5 ESMs with interactive carbon cycle simulate, on average, a 50 (–140 to +210) ppm (CMIP5 model spread) larger atmospheric CO₂ concentration and 0.2°C larger global surface temperature increase by 2100. For the low RCPs the fractional uncertainty is larger because internal variability and non-CO₂ forcings make a larger relative contribution to the total uncertainty. {12.4.1, 12.4.8, 12.4.9} (continued on next page)



Box TS.6, Figure 1 | Patterns of temperature (left column) and percent precipitation change (right column) for the CMIP3 models average (first row) and CMIP5 models average (second row), scaled by the corresponding global average temperature changes. The patterns are computed in both cases by taking the difference between the averages over the last 20 years of the 21st century experiments (2080–2099 for CMIP3 and 2081–2100 for CMIP5) and the last 20 years of the historic experiments (1980–1999 for CMIP3, 1986–2005 for CMIP5) and rescaling each difference by the corresponding change in global average temperature. This is done first for each individual model, then the results are averaged across models. Stippling indicates a measure of significance of the difference between the two corresponding patterns obtained by a bootstrap exercise. Two subsets of the pooled set of CMIP3 and CMIP5 ensemble members of the same size as the original ensembles, but without distinguishing CMIP3 from CMIP5 members, were randomly sampled 500 times. For each random sample the corresponding patterns and their difference are computed, then the true difference is compared, grid-point by grid-point, to the distribution of the bootstrapped differences, and only grid-points at which the value of the difference falls in the tails of the bootstrapped distribution (less than the 2.5th percentiles or the 97.5th percentiles) are stippled. {Figure 12.4.1}

Box TS.6 (continued)

There is overall consistency between the projections of temperature and precipitation based on CMIP3 and CMIP5, both for large-scale patterns and magnitudes of change (Box TS.6, Figure 1). Model agreement and confidence in projections depends on the variable and on spatial and temporal averaging, with better agreement for larger scales. Confidence is higher for temperature than for those quantities related to the water cycle or atmospheric circulation. Improved methods to quantify and display model robustness have been developed to indicate where lack of agreement across models on local trends is a result of internal variability, rather than models actually disagreeing on their forced response. Understanding of the sources and means of characterizing uncertainties in long-term large scale projections of climate change has not changed significantly since AR4, but new experiments and studies have continued to work towards a more complete and rigorous characterization. {9.7.3, 12.2, 12.4.1, 12.4.4, 12.4.5, 12.4.9; Box 12.1}

The well-established stability of geographical patterns of temperature and precipitation change during a transient experiment remains valid in the CMIP5 models (Box TS.6, Figure 1). Patterns are similar over time and across scenarios and to first order can be scaled by the global mean temperature change. There remain limitations to the validity of this technique when it is applied to strong mitigation scenarios, to scenarios where localized forcings (e.g., aerosols) are significant and vary in time and for variables other than average seasonal mean temperature and precipitation. {12.4.2}

The range in anthropogenic aerosol emissions across all scenarios has a larger impact on near-term climate projections than the corresponding range in long-lived GHGs, particularly on regional scales and for hydrological cycle variables. The RCP scenarios do not span the range of future aerosol emissions found in the SRES and alternative scenarios (Box TS.6). {11.3.1, 11.3.6}

If rapid reductions in sulphate aerosol are undertaken for improving air quality or as part of decreasing fossil-fuel CO₂ emissions, then there is *medium confidence* that this could lead to rapid near-term warming. There is evidence that accompanying controls on CH₄ emissions would offset some of this sulphate-induced warming, although the cooling from CH₄ mitigation will emerge more slowly than the warming from sulphate mitigation due to the different time scales over which atmospheric concentrations of these substances decrease in response to decreases in emissions. Although removal of black carbon aerosol could also counter warming associated with sulphate removal, uncertainties are too large to constrain the net sign of the global temperature response to black carbon emission reductions, which depends on reduction of co-emitted (reflective) aerosols and on aerosol indirect effects. {11.3.6}

Including uncertainties in projecting the chemically reactive GHGs CH₄ and N₂O from RCP emissions gives a range in abundance pathways that is *likely* 30% larger than the range in RCP concentrations used to force the CMIP5 climate models. Including uncertainties in emission estimates from agricultural, forest and land use sources, in atmospheric lifetimes, and in chemical feedbacks, results in a much wider range of abundances for N₂O, CH₄ and HFCs and their RF. In the case of CH₄, by year 2100 the *likely* range of RCP8.5 CH₄ abundance extends 520 ppb above the single-valued RCP8.5 CH₄ abundance, and RCP2.6 CH₄ extends 230 ppb below RCP2.6 CH₄. {11.3.5}

There is *very low confidence* in projections of natural forcing. Major volcanic eruptions cause a negative RF up to several watts per square metre, with a typical lifetime of one year, but the possible occurrence

and timing of future eruptions is unknown. Except for the 11-year solar cycle, changes in the total solar irradiance are uncertain. Except where explicitly indicated, future volcanic eruptions and changes in total solar irradiance additional to a repeating 11-year solar cycle are not included in the projections of near- and long-term climate assessed. {8, 11.3.6}

TS.5.3 Quantification of Climate System Response

Estimates of the equilibrium climate sensitivity (ECS) based on observed climate change, climate models and feedback analysis, as well as paleoclimate evidence indicate that ECS is positive, *likely* in the range 1.5°C to 4.5°C with *high confidence*, *extremely unlikely* less than 1°C (*high confidence*) and *very unlikely* greater than 6°C (*medium confidence*). Earth system sensitivity over millennia time scales including long-term feedbacks not typically included in models could be significantly higher than ECS (see TFE.6 for further details). {5.3.1, 10.8; Box 12.2}

With *high confidence* the transient climate response (TCR) is positive, *likely* in the range 1°C to 2.5°C and *extremely unlikely* greater than 3°C, based on observed climate change and climate models (see TFE.6 for further details). {10.8; Box 12.2}

The ratio of GMST change to total cumulative anthropogenic carbon emissions is relatively constant and independent of the scenario, but is model dependent, as it is a function of the model cumulative airborne fraction of carbon and the transient climate response. For any given temperature target, higher emissions in earlier decades therefore imply lower emissions by about the same amount later on. The transient climate response to cumulative carbon emission (TCRE) is *likely* between 0.8°C to 2.5°C per 1000 PgC (*high confidence*), for cumulative carbon emissions less than about 2000 PgC until the time at which temperatures peak (see TFE.8 for further details). {10.8, 12.5.4; Box 12.2}

Thematic Focus Elements

TFE.6 | Climate Sensitivity and Feedbacks

The description of climate change as a response to a forcing that is amplified by feedbacks goes back many decades. The concepts of radiative forcing (RF) and climate feedbacks continue to be refined, and limitations are now better understood; for instance, feedbacks may be much faster than the surface warming, feedbacks depend on the type of forcing agent (e.g., greenhouse gas (GHG) vs. solar forcing), or may have intrinsic time scales (associated mainly with vegetation change and ice sheets) of several centuries to millennia. The analysis of physical feedbacks in models and from observations remains a powerful framework that provides constraints on transient future warming for different scenarios, on climate sensitivity and, combined with estimates of carbon cycle feedbacks (see TFE.5), determines the GHG emissions that are compatible with climate stabilization or targets (see TFE.8). {7.1, 9.7.2, 12.5.3; Box 12.2}

The water vapour/lapse rate, albedo and cloud feedbacks are the principal determinants of equilibrium climate sensitivity. All of these feedbacks are assessed to be positive, but with different levels of likelihood assigned ranging from *likely* to *extremely likely*. Therefore, there is *high confidence* that the net feedback is positive and the black body response of the climate to a forcing will therefore be amplified. Cloud feedbacks continue to be the largest uncertainty. The net feedback from water vapour and lapse rate changes together is *extremely likely* positive and approximately doubles the black body response. The mean value and spread of these two processes in climate models are essentially unchanged from the IPCC Fourth Assessment Report (AR4), but are now supported by stronger observational evidence and better process understanding of what determines relative humidity distributions. Clouds respond to climate forcing mechanisms in multiple ways and individual cloud feedbacks can be positive or negative. Key issues include the representation of both deep and shallow cumulus convection, micro-physical processes in ice clouds and partial cloudiness that results from small-scale variations of cloud-producing and cloud-dissipating processes. New approaches to diagnosing cloud feedback in General Circulation Models (GCMs) have clarified robust cloud responses, while continuing to implicate low cloud cover as the most important source of intermodel spread in simulated cloud feedbacks. The net radiative feedback due to all cloud types is *likely* positive. This conclusion is reached by considering a plausible range for unknown contributions by processes yet to be accounted for, in addition to those occurring in current climate models. Observations alone do not currently provide a robust, direct constraint, but multiple lines of evidence now indicate positive feedback contributions from changes in both the height of high clouds and the horizontal distribution of clouds. The additional feedback from low cloud amount is also positive in most climate models, but that result is not well understood, nor effectively constrained by observations, so *confidence* in it is *low*. {7.2.4–7.2.6, 9.7.2}

The representation of aerosol–cloud processes in climate models continues to be a challenge. Aerosol and cloud variability at scales significantly smaller than those resolved in climate models, and the subtle responses of clouds to aerosol at those scales, mean that, for the foreseeable future, climate models will continue to rely on parameterizations of aerosol–cloud interactions or other methods that represent subgrid variability. This implies large uncertainties for estimates of the forcings associated with aerosol–cloud interactions. {7.4, 7.5.3, 7.5.4}

Equilibrium climate sensitivity (ECS) and transient climate response (TCR) are useful metrics summarising the global climate system's temperature response to an externally imposed RF. ECS is defined as the equilibrium change in annual mean global mean surface temperature (GMST) following a doubling of the atmospheric carbon dioxide (CO₂) concentration, while TCR is defined as the annual mean GMST change at the time of CO₂ doubling following a linear increase in CO₂ forcing over a period of 70 years (see Glossary). Both metrics have a broader application than these definitions imply: ECS determines the eventual warming in response to stabilisation of atmospheric composition on multi-century time scales, while TCR determines the warming expected at a given time following any steady increase in forcing over a 50- to 100-year time scale. {Box 12.2; 12.5.3}

ECS and TCR can be estimated from various lines of evidence (TFE.6, Figures 1 and 2). The estimates can be based on the values of ECS and TCR diagnosed from climate models, or they can be constrained by analysis of feedbacks in climate models, patterns of mean climate and variability in models compared to observations, temperature fluctuations as reconstructed from paleoclimate archives, observed and modelled short term perturbations of the energy balance like those caused by volcanic eruptions, and the observed surface and ocean temperature trends since pre-industrial. For many applications, the limitations of the forcing-feedback analysis framework and the dependence of feedbacks on time scales and the climate state must be kept in mind. {5.3.1, 5.3.3, 9.7.1–9.7.3, 10.8.1, 10.8.2, 12.5.3; Box 5.2; Table 9.5} *(continued on next page)*

TFE.6 (continued)

Newer studies of constraints on ECS are based on the observed warming since pre-industrial, analysed using simple and intermediate complexity models, improved statistical methods and several different and newer data sets. Together with paleoclimate constraints but without considering the CMIP based evidence these studies show ECS is *likely* between 1.5°C to 4.5°C (*medium confidence*) and *extremely unlikely* less than 1.0°C. {5.3.1, 5.3.3, 10.8.2; Boxes 5.2, 12.2}

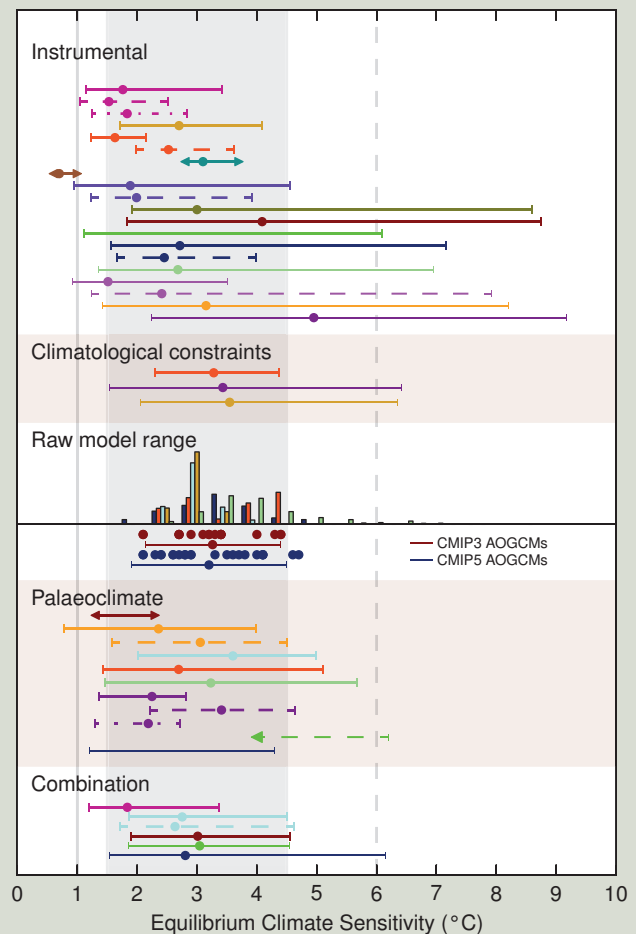
Estimates based on Atmosphere–Ocean General Circulation Models (AOGCMs) and feedback analysis indicate a range of 2°C to 4.5°C, with the Coupled Model Intercomparison Project Phase 5 (CMIP5) model mean at 3.2°C, similar to CMIP3. High climate sensitivities are found in some perturbed parameter ensembles models, but recent comparisons of perturbed-physics ensembles against the observed climate find that models with ECS values in the range 3°C to 4°C show the smallest errors for many fields. Relationships between climatological quantities and climate sensitivity are often found within a specific perturbed parameter ensemble model but in many cases the relationship is not robust across perturbed parameter ensembles models from different models or in CMIP3 and CMIP5. The assessed literature suggests that the range of climate sensitivities and transient responses covered by CMIP3 and CMIP5 cannot be narrowed significantly by constraining the models with observations of the mean climate and variability. Studies based on perturbed parameter ensembles models and CMIP3 support the conclusion that a credible representation of the mean climate and variability is very difficult to achieve with ECSs below 2°C. {9.2.2, 9.7.3; Box 12.2}

New estimates of ECS based on reconstructions and simulations of the Last Glacial Maximum (21 ka to 19 ka) show that values below 1°C as well as above 6°C are *very unlikely*. In some models climate sensitivity differs between warm and cold climates because of differences in the representation of cloud feedbacks. Estimates of an Earth system sensitivity including slow feedbacks (e.g., ice sheets or vegetation) are even more difficult to relate to climate sensitivity of the current climate state. The main limitations of ECS estimates from paleoclimate states are uncertainties in proxy data, spatial coverage of the data, uncertainties in some forcings, and structural limitations in models used in model–data comparisons. {5.3, 10.8.2, 12.5.3}

Bayesian methods to constrain ECS or TCR are sensitive to the assumed prior distributions. They can in principle yield narrower estimates by combining constraints from the observed warming trend, volcanic eruptions, model climatology and paleoclimate, and that has been done in some studies, but there is no consensus on how this should be done robustly. This approach is sensitive to the assumptions regarding the independence of the various lines of evidence, the possibility of shared biases in models or feedback estimates and the assumption that each individual line of evidence is unbiased. The combination of different estimates in this assessment is based on expert judgement. {10.8.2; Box 12.2}

Based on the combined evidence from observed climate change including the observed 20th century warming, climate models, feedback analysis and paleoclimate, as discussed above, ECS is *likely* in the range 1.5°C to 4.5°C with *high confidence*. ECS is positive, *extremely unlikely*

(continued on next page)



TFE.6, Figure 1 | Probability density functions, distributions and ranges for equilibrium climate sensitivity, based on Figure 10.20b plus climatological constraints shown in IPCC AR4 (Box AR4 10.2 Figure 1), and results from CMIP5 (Table 9.5). The grey shaded range marks the *likely* 1.5°C to 4.5°C range, grey solid line the *extremely unlikely* less than 1°C, the grey dashed line the *very unlikely* greater than 6°C. See Figure 10.20b and Chapter 10 Supplementary Material for full caption and details. {Box 12.2, Figure 1}

TS

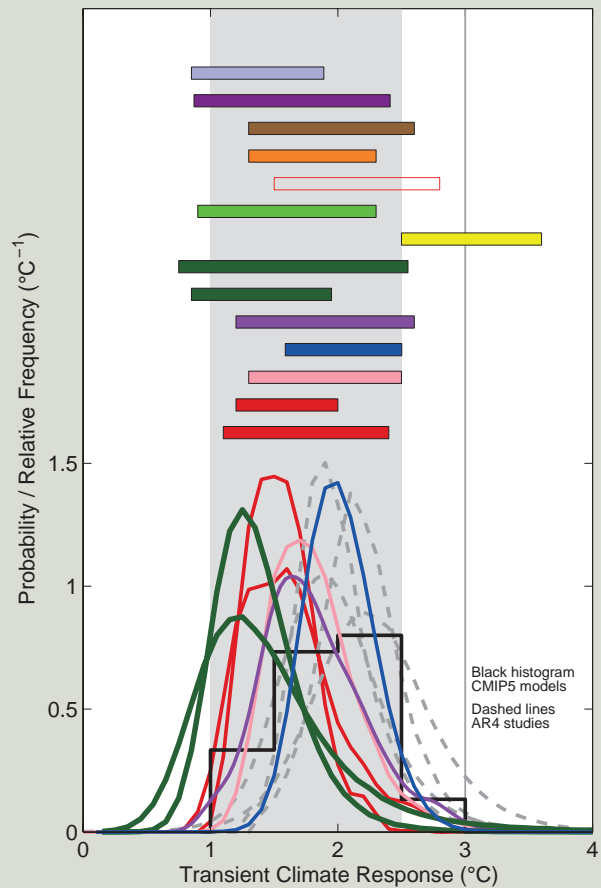
TFE.6 (continued)

less than 1°C (*high confidence*), and *very unlikely* greater than 6°C (*medium confidence*). The tails of the ECS distribution are now better understood. Multiple lines of evidence provide *high confidence* that an ECS value less than 1°C is *extremely unlikely*. The upper limit of the *likely* range is unchanged compared to AR4. The lower limit of the *likely* range of 1.5°C is less than the lower limit of 2°C in AR4. This change reflects the evidence from new studies of observed temperature change, using the extended records in atmosphere and ocean. These studies suggest a best fit to the observed surface and ocean warming for ECS values in the lower part of the *likely* range. Note that these studies are not purely observational, because they require an estimate of the response to RF from models. In addition, the uncertainty in ocean heat uptake remains substantial. Accounting for short-term variability in simple models remains challenging, and it is important not to give undue weight to any short time period which might be strongly affected by internal variability. On the other hand, AOGCMs with observed climatology with ECS values in the upper part of the 1.5 to 4.5°C range show very good agreement with observed climatology, but the simulation of key feedbacks like clouds remains challenging in those models. The estimates from the observed warming, paleoclimate, and from climate models are consistent within their uncertainties, each is supported by many studies and multiple data sets, and in combination they provide *high confidence* for the assessed *likely* range. Even though this assessed range is similar to previous reports, confidence today is much higher as a result of high quality and longer observational records with a clearer anthropogenic signal, better process understanding, more and better understood evidence from paleoclimate reconstructions, and better climate models with higher resolution that capture many more processes more realistically. All these lines of evidence individually support the assessed *likely* range of 1.5°C to 4.5°C. {3.2, 9.7.3, 10.8; Boxes 9.2, 13.1}

On time scales of many centuries and longer, additional feedbacks with their own intrinsic time scales (e.g., vegetation, ice sheets) may become important but are not usually modelled in AOGCMs. The resulting equilibrium temperature response to a doubling of CO₂ on millennial time scales or Earth system sensitivity is less well constrained but *likely* to be larger than ECS, implying that lower atmospheric CO₂ concentrations are compatible with limiting warming to below a given temperature level. These slow feedbacks are less likely to be proportional to global mean temperature change, implying that Earth system sensitivity changes over time. Estimates of Earth system sensitivity are also difficult to relate to climate sensitivity of the current climate state. {5.3.3, 10.8.2, 12.5.3}

For scenarios of increasing RF, TCR is a more informative indicator of future climate change than ECS. This assessment concludes with *high confidence* that the TCR is *likely* in the range 1°C to 2.5°C, close to the estimated 5 to 95% range of CMIP5 (1.2°C to 2.4°C), is positive and *extremely unlikely* greater than 3°C. As with the ECS, this is an expert-assessed range, supported by several different and partly independent lines of evidence, each based on multiple studies, models and data sets. TCR is estimated from the observed global changes in surface temperature, ocean heat uptake and RF including detection/attribution studies identifying the response patterns to increasing GHG concentrations, and the results of CMIP3 and CMIP5. Estimating TCR suffers from fewer difficulties in terms of state- or time-dependent feedbacks, and is less affected by uncertainty as to how much energy is taken up by the

(continued on next page)



TFE.6, Figure 2 | Probability density functions, distributions and ranges (5 to 95%) for the transient climate response from different studies, based on Figure 10.20a, and results from CMIP5 (black histogram, Table 9.5). The grey shaded range marks the *likely* 1°C to 2.5°C range, the grey solid line marks the *extremely unlikely* greater than 3°C. See Figure 10.20a and Chapter 10 Supplementary Material for full caption and details. {Box 12.2, Figure 2}

TFE.6 (continued)

ocean. Unlike ECS, the ranges of TCR estimated from the observed warming and from AOGCMs agree well, increasing our confidence in the assessment of uncertainties in projections over the 21st century.

The assessed ranges of ECS and TCR are largely consistent with the observed warming, the estimated forcing and the projected future warming. In contrast to AR4, no best estimate for ECS is given because of a lack of agreement on the best estimate across lines of evidence and studies and an improved understanding of the uncertainties in estimates based on the observed warming. Climate models with ECS values in the upper part of the *likely* range show very good agreement with observed climatology, whereas estimates derived from observed climate change tend to best fit the observed surface and ocean warming for ECS values in the lower part of the *likely* range. In estimates based on the observed warming the most likely value is sensitive to observational and model uncertainties, internal climate variability and to assumptions about the prior distribution of ECS. In addition, “best estimate” and “most likely value” are defined in various ways in different studies. {9.7.1, 10.8.1, 12.5.3; Table 9.5}

TS

TS.5.4 Near-term Climate Change

Near-term decadal climate prediction provides information not available from existing seasonal to interannual (months to a year or two) predictions or from long-term (mid 21st century and beyond) climate change projections. Prediction efforts on seasonal to interannual time scales require accurate estimates of the initial climate state with less focus extended to changes in external forcing¹², whereas long-term climate projections rely more heavily on estimations of external forcing with little reliance on the initial state of internal variability. Estimates of near-term climate depend on the committed warming (caused by the inertia of the oceans as they respond to historical external forcing) the time evolution of internally generated climate variability, and the future path of external forcing. Near-term predictions out to about a decade (Figure TS.13) depend more heavily on an accurate depiction of the internally generated climate variability. {11.1, 12, 14}

Further near-term warming from past emissions is unavoidable owing to thermal inertia of the oceans. This warming will be increased by ongoing emissions of GHGs over the near term, and the climate observed in the near term will also be strongly influenced by the internally generated variability of the climate system. Previous IPCC Assessments only described climate-change projections wherein the externally forced component of future climate was included but no attempt was made to initialize the internally generated climate variability. Decadal climate predictions, on the other hand, are intended to predict both the externally forced component of future climate change, and the internally generated component. Near-term predictions do not provide detailed information of the evolution of weather. Instead they can provide estimated changes in the time evolution of the statistics of near-term climate. {11.1, 11.2.2; Box 11.1; FAQ 11.1}

Retrospective prediction experiments have been used to assess forecast quality. There is *high confidence* that the retrospective prediction experiments for forecast periods of up to 10 years exhibit positive skill

when verified against observations over large regions of the planet and of the global mean. Observation-based initialization of the forecasts contributes to the skill of predictions of annual mean temperature for the first couple of years and to the skill of predictions of the GMST and the temperature over the North Atlantic, regions of the South Pacific and the tropical Indian Ocean up to 10 years (*high confidence*) partly due to a correction of the forced response. Probabilistic temperature predictions are statistically reliable (see Section 11.2.3 for definition of reliability) owing to the correct representation of global trends, but still unreliable at the regional scale when probabilities are computed from the multi-model ensemble. Predictions initialized over 2000–2005 improve estimates of the recent global mean temperature hiatus. Predictions of precipitation over continental areas with large forced trends also exhibit positive skill. {11.2.2, 11.2.3; Box 9.2}

TS.5.4.1 Projected Near-term Changes in Climate

Projections of near-term climate show small sensitivity to GHG scenarios compared to model spread, but substantial sensitivity to uncertainties in aerosol emissions, especially on regional scales and for hydrological cycle variables. In some regions, the local and regional responses in precipitation and in mean and extreme temperature to land use change will be larger than those due to large-scale GHGs and aerosol forcing. These scenarios presume that there are no major volcanic eruptions and that anthropogenic aerosol emissions are rapidly reduced during the near term. {11.3.1, 11.3.2, 11.3.6}

TS.5.4.2 Projected Near-term Changes in Temperature

In the absence of major volcanic eruptions—which would cause significant but temporary cooling—and, assuming no significant future long-term changes in solar irradiance, it is *likely* that the GMST anomaly for the period 2016–2035, relative to the reference period of 1986–2005 will be in the range 0.3°C to 0.7°C (*medium confidence*). This is based on multiple lines of evidence. This range is consistent

¹² Seasonal-to-interannual predictions typically include the impact of external forcing.

with the range obtained by using CMIP5 5 to 95% model trends for 2012–2035. It is also consistent with the CMIP5 5 to 95% range for all four RCP scenarios of 0.36°C to 0.79°C, using the 2006–2012 reference period, after the upper and lower bounds are reduced by 10% to take into account the evidence that some models may be too sensitive to anthropogenic forcing (see Table TS.1 and Figure TS.14). {11.3.6}

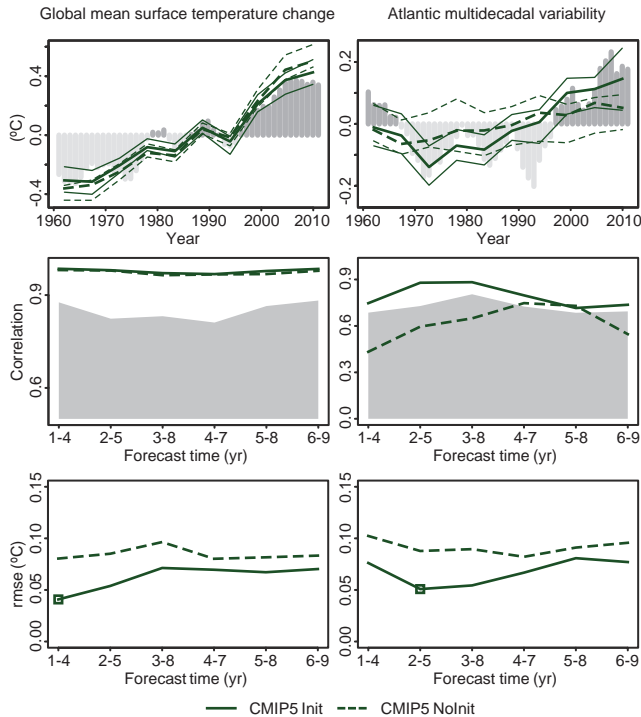


Figure TS.13 | Decadal prediction forecast quality of several climate indices. (Top row) Time series of the 2- to 5-year average ensemble mean initialized hindcast anomalies and the corresponding non-initialized experiments for three climate indices: global mean surface temperature (GMST, left) and the Atlantic Multi-decadal Variability (AMV, right). The observational time series, Goddard Institute of Space Studies Goddard Institute for Space Studies Surface Temperature Analysis (GISTEMP) global mean temperature and Extended Reconstructed Sea Surface Temperature (ERSST) for the AMV, are represented with dark grey (positive anomalies) and light grey (negative anomalies) vertical bars, where a 4-year running mean has been applied for consistency with the time averaging of the predictions. Predicted time series are shown for the CMIP5 Init (solid) and NoInit (dotted) simulations with hindcasts started every 5 years over the period 1960–2005. The lower and upper quartile of the multi-model ensemble are plotted using thin lines. The AMV index was computed as the sea surface temperature (SST) anomalies averaged over the region Equator to 60°N and 80°W to 0°W minus the SST anomalies averaged over 60°S to 60°N. Note that the vertical axes are different for each time series. (Middle row) Correlation of the ensemble mean prediction with the observational reference along the forecast time for 4-year averages of the three sets of CMIP5 hindcasts for Init (solid) and NoInit (dashed). The one-sided 95% confidence level with a *t* distribution is represented in grey. The effective sample size has been computed taking into account the autocorrelation of the observational time series. A two-sided *t* test (where the effective sample size has been computed taking into account the autocorrelation of the observational time series) has been used to test the differences between the correlation of the initialized and non-initialized experiments, but no differences were found statistically significant with a confidence equal or higher than 90%. (Bottom row) Root mean square error (RMSE) of the ensemble mean prediction along the forecast time for 4-year averages of the CMIP5 hindcasts for Init (solid) and NoInit (dashed). A two-sided *F* test (where the effective sample size has been computed taking into account the autocorrelation of the observational time series) has been used to test the ratio between the RMSE of the Init and NoInit, and those forecast times with differences statistically significant with a confidence equal or higher than 90% are indicated with an open square. {Figure 11.3}

Higher concentrations of GHGs and lower amounts of sulphate aerosol lead to greater warming. In the near-term, differences in global mean surface air temperature across RCP scenarios for a single climate model are typically smaller than across climate models for a single RCP scenario. In 2030, the CMIP5 ensemble median values for global mean temperature differ by at most 0.2°C between the RCP scenarios, whereas the model spread (defined as the 17 to 83% range) for each RCP is around 0.4°C. The inter-scenario spread increases in time and by 2050 is comparable to the model spread. Regionally, the largest differences in surface air temperature between RCP scenarios are found in the Arctic. {11.3.2. 11.3.6}

The projected warming of global mean temperatures implies *high confidence* that new levels of warming relative to 1850–1900 mean climate will be crossed, particularly under higher GHG emissions scenarios. Relative to a reference period of 1850–1900, under RCP4.5 or RCP6.0, it is *more likely than not* that the mean GMST for the period 2016–2035 will be more than 1°C above the mean for 1850–1900, and *very unlikely* that it will be more than 1.5°C above the 1850–1900 mean (*medium confidence*). {11.3.6}

A future volcanic eruption similar in size to the 1991 eruption of Mt Pinatubo would cause a rapid drop in global mean surface air temperature of about 0.5°C in the following year, with recovery over the next few years. Larger eruptions, or several eruptions occurring close together in time, would lead to larger and more persistent effects. {11.3.6}

Possible future changes in solar irradiance could influence the rate at which GMST increases, but there is *high confidence* that this influence will be small in comparison to the influence of increasing concentrations of GHGs in the atmosphere. {11.3.6}

The spatial patterns of near-term warming projected by the CMIP5 models following the RCP scenarios (Figure TS.15) are broadly consistent with the AR4. It is *very likely* that anthropogenic warming of surface air temperature over the next few decades will proceed more rapidly over land areas than over oceans, and it is *very likely* that the anthropogenic warming over the Arctic in winter will be greater than the global mean warming, consistent with the AR4. Relative to background levels of internally generated variability there is *high confidence* that the anthropogenic warming relative to the reference period is expected to be larger in the tropics and subtropics than in mid-latitudes. {11.3.2}

It is *likely* that in the next decades the frequency of warm days and warm nights will increase in most land regions, while the frequency of cold days and cold nights will decrease. Models also project increases in the duration, intensity and spatial extent of heat waves and warm spells for the near term. These changes may proceed at a different rate than the mean warming. For example, several studies project that European high-percentile summer temperatures are projected to warm faster than mean temperatures (see also TFE.9). {11.3.2}

Global mean temperature near-term projections relative to 1986–2005

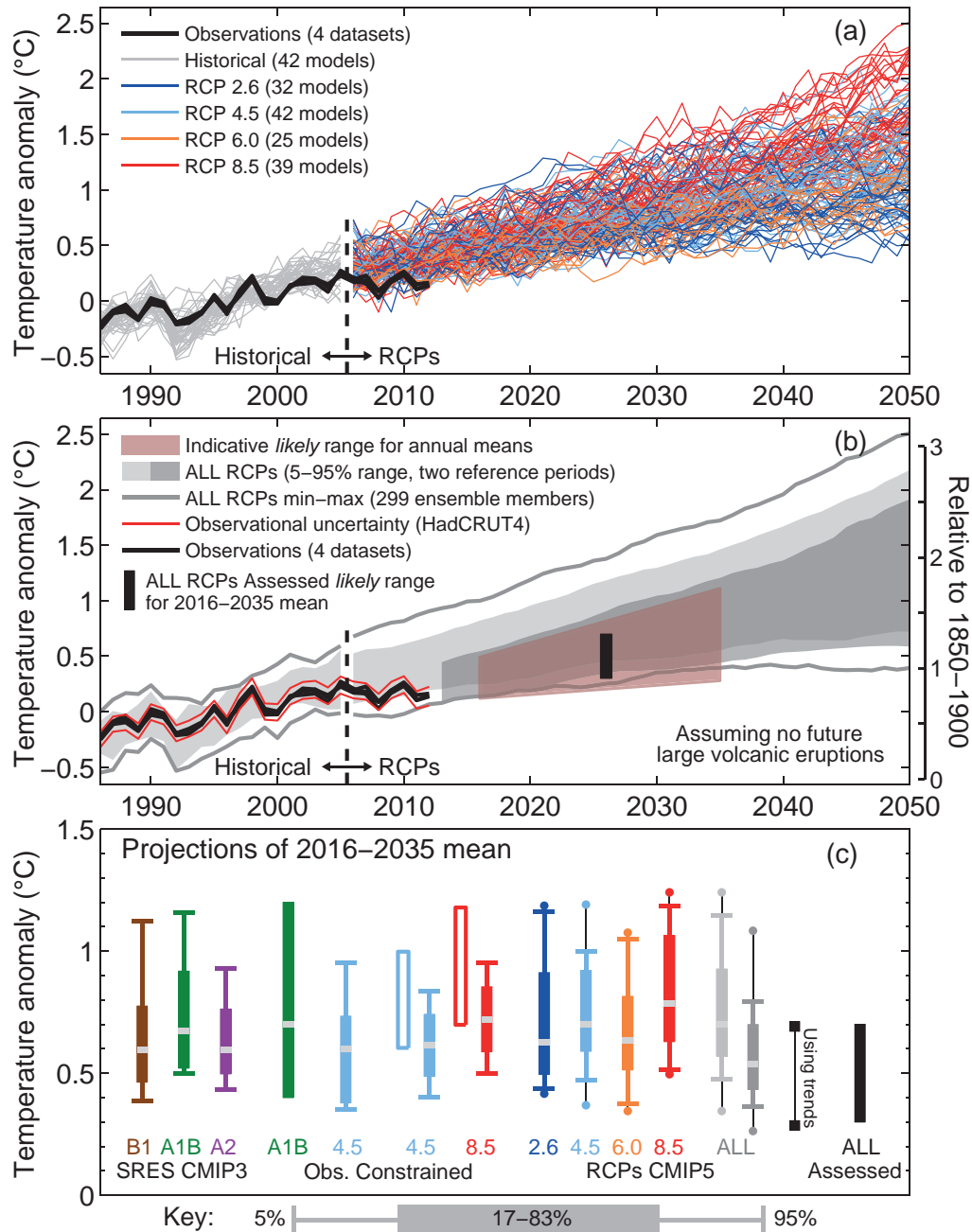


Figure TS.14 | Synthesis of near-term projections of global mean surface air temperature (GMST). (a) Projections of annual mean GMST 1986–2050 (anomalies relative to 1986–2005) under all RCPs from CMIP5 models (grey and coloured lines, one ensemble member per model), with four observational estimates (Hadley Centre/Climatic Research Unit gridded surface temperature data set 4 (HadCRUT4), European Centre for Medium Range Weather Forecasts (ECMWF) interim re-analysis of the global atmosphere and surface conditions (ERA-Interim), Goddard Institute for Space Studies Surface Temperature Analysis (GISTEMP), National Oceanic and Atmospheric Administration (NOAA)) for the period 1986–2012 (black lines). (b) As (a) but showing the 5 to 95% range of annual mean CMIP5 projections (using one ensemble member per model) for all RCPs using a reference period of 1986–2005 (light grey shade) and all RCPs using a reference period of 2006–2012, together with the observed anomaly for (2006–2012) minus (1986–2005) of 0.16°C (dark grey shade). The percentiles for 2006 onwards have been smoothed with a 5-year running mean for clarity. The maximum and minimum values from CMIP5 using all ensemble members and the 1986–2005 reference period are shown by the grey lines (also smoothed). Black lines show annual mean observational estimates. The red shaded region shows the indicative *likely* range for annual mean GMST during the period 2016–2035 based on the ‘ALL RCPs Assessed’ *likely* range for the 20-year mean GMST anomaly for 2016–2035, which is shown as a black bar in both (b) and (c) (see text for details). The temperature scale relative to 1850–1900 mean climate on the right-hand side assumes a warming of GMST prior to 1986–2005 of 0.61°C estimated from HadCRUT4. (c) A synthesis of projections for the mean GMST anomaly for 2016–2035 relative to 1986–2005. The box and whiskers represent the 66% and 90% ranges. Shown are: unconstrained SRES CMIP3 and RCP CMIP5 projections; observationally constrained projections for the SRES A1B and, the RCP4.5 and 8.5 scenarios; unconstrained projections for all four RCP scenarios using two reference periods as in (b) (light grey and dark grey shades), consistent with (b); 90% range estimated using CMIP5 trends for the period 2012–2035 and the observed GMST anomaly for 2012; an overall *likely* (>66%) assessed range for all RCP scenarios. The dots for the CMIP5 estimates show the maximum and minimum values using all ensemble members. The medians (or maximum likelihood estimate; green filled bar) are indicated by a grey band. (Adapted from Figure 11.25.) See Section 11.3.6 for details. [Figure 11.25]



TS.5.4.3 Projected Near-term Changes in the Water Cycle

Zonal mean precipitation will *very likely* increase in high and some of the mid latitudes, and will *more likely than not* decrease in the subtropics. At more regional scales precipitation changes may be dominated by a combination of natural internal variability, volcanic forcing and anthropogenic aerosol effects. {11.3.2}

Over the next few decades increases in near-surface specific humidity are *very likely*. It is *likely* that there will be increases in evaporation in many regions. There is *low confidence* in projected changes in soil moisture and surface runoff. {11.3.2}

In the near term, it is *likely* that the frequency and intensity of heavy precipitation events will increase over land. These changes are primarily driven by increases in atmospheric water vapour content, but also affected by changes in atmospheric circulation. The impact of anthropogenic forcing at regional scales is less obvious, as regional-scale changes are strongly affected by natural variability and also depend on the course of future aerosol emissions, volcanic forcing and land use changes (see also TFE.9). {11.3.2}

TS.5.4.4 Projected Near-term Changes in Atmospheric Circulation

Internally generated climate variability and multiple RF agents (e.g., volcanoes, GHGs, ozone and anthropogenic aerosols) will all contribute to near-term changes in the atmospheric circulation. For example, it is *likely* that the annual mean Hadley Circulation and the SH mid-latitude westerlies will shift poleward, while it is *likely* that the projected recovery of stratospheric ozone and increases in GHG concentrations will have counteracting impacts on the width of the Hadley Circulation and the meridional position of the SH storm track. Therefore it is *unlikely* that they will continue to expand poleward as rapidly as in recent decades. {11.3.2}

There is *low confidence* in near-term projections of the position and strength of NH storm tracks. Natural variations are larger than the projected impact of GHGs in the near term. {11.3.2}

There is *low confidence* in basin-scale projections of changes in intensity and frequency of tropical cyclones in all basins to the mid-21st century. This *low confidence* reflects the small number of studies exploring near-term tropical cyclone activity, the differences across published projections of tropical cyclone activity, and the large role for natural variability. There is *low confidence* in near-term projections for increased tropical cyclone intensity in the Atlantic; this projection is in part due to projected reductions in aerosol loading. {11.3.2}

TS.5.4.5 Projected Near-term Changes in the Ocean

It is *very likely* that globally averaged surface and vertically averaged ocean temperatures will increase in the near-term. In the absence of multiple major volcanic eruptions, it is *very likely* that globally averaged surface and depth-averaged temperatures averaged for 2016–2035 will be warmer than those averaged over 1986–2005. {11.3.3}

It is *likely* that salinity will increase in the tropical and (especially) subtropical Atlantic, and decrease in the western tropical Pacific over the next few decades. Overall, it is *likely* that there will be some decline in the Atlantic Meridional Overturning Circulation by 2050 (*medium confidence*). However, the rate and magnitude of weakening is very uncertain and decades when this circulation increases are also to be expected. {11.3.3}

TS.5.4.6 Projected Near-term Changes in the Cryosphere

A nearly ice-free Arctic Ocean (sea ice extent less than 10⁶ km² for at least five consecutive years) in September is *likely* before mid-century under RCP8.5 (*medium confidence*). This assessment is based on a subset of models that most closely reproduce the climatological mean state and 1979 to 2012 trend of Arctic sea ice cover. It is *very likely* that there will be further shrinking and thinning of Arctic sea ice cover, and decreases of northern high-latitude spring time snow cover and near surface permafrost as GMST rises (Figures TS.17 and TS.18). There is *low confidence* in projected near-term decreases in the Antarctic sea ice extent and volume. {11.3.4}

TS.5.4.7 Possibility of Near-term Abrupt Changes in Climate

There are various mechanisms that could lead to changes in global or regional climate that are abrupt by comparison with rates experienced in recent decades. The likelihood of such changes is generally lower for the near term than for the long term. For this reason the relevant mechanisms are primarily assessed in the TS.5 sections on long-term changes and in TFE.5. {11.3.4}

TS.5.4.8 Projected Near-term Changes in Air Quality

The range in projections of air quality (O₃ and PM_{2.5} in surface air) is driven primarily by emissions (including CH₄), rather than by physical climate change (*medium confidence*). The response of air quality to climate-driven changes is more uncertain than the response to emission-driven changes (*high confidence*). Globally, warming decreases background surface O₃ (*high confidence*). High CH₄ levels (such as RCP8.5 and SRES A2) can offset this decrease, raising 2100 background surface O₃ on average by about 8 ppb (25% of current levels) relative to scenarios with small CH₄ changes (such as RCP4.5 and RCP6.0) (*high confidence*). On a continental scale, projected air pollution levels are lower under the new RCP scenarios than under the SRES scenarios because the SRES did not incorporate air quality legislation (*high confidence*). {11.3.5, 11.3.5.2; Figures 11.22 and 11.23ab, All.4.2, All.7.1–All.7.4}

Observational and modelling evidence indicates that, all else being equal, locally higher surface temperatures in polluted regions will trigger regional feedbacks in chemistry and local emissions that will increase peak levels of O₃ and PM_{2.5} (*medium confidence*). Local emissions combined with background levels and with meteorological conditions conducive to the formation and accumulation of pollution are known to produce extreme pollution episodes on local and regional scales. There is *low confidence* in projecting changes in meteorological blocking associated with these extreme episodes. For PM_{2.5}, climate change may alter natural aerosol sources (wildfires, wind-lofted

dust, biogenic precursors) as well as precipitation scavenging, but no confidence level is attached to the overall impact of climate change on PM_{2.5} distributions. {11.3.5, 11.3.5.2; Box 14.2}

TS.5.5 Long-term Climate Change

TS.5.5.1 Projected Long-term Changes in Global Temperature

Global mean temperatures will continue to rise over the 21st century under all of the RCPs. From around the mid-21st century, the rate of global warming begins to be more strongly dependent on the scenario (Figure TS.15). {12.4.1}

Under the assumptions of the concentration-driven RCPs, GMSTs for 2081–2100, relative to 1986–2005 will *likely* be in the 5 to 95% range of the CMIP5 models; 0.3°C to 1.7°C (RCP2.6), 1.1 to 2.6°C (RCP4.5), 1.4°C to 3.1°C (RCP6.0), 2.6°C to 4.8°C (RCP8.5) (see Table TS.1). With *high confidence*, the 5 to 95% range of CMIP5 is assessed as *likely* rather than *very likely* based on the assessment of TCR (see TFE.6).

The 5 to 95% range of CMIP5 for global mean temperature change is also assessed as *likely* for mid-21st century, but only with *medium confidence*. With respect to 1850–1900 mean conditions, global temperatures averaged in the period 2081–2100 are projected to *likely* exceed 1.5°C above 1850–1900 values for RCP4.5, RCP6.0 and RCP8.5 (*high confidence*) and are *likely* to exceed 2°C above 1850–1900 values for RCP6.0 and RCP8.5 (*high confidence*). Temperature change above 2°C relative to 1850–1900 under RCP2.6 is *unlikely* (*medium confidence*). Warming above 4°C by 2081–2100 is *unlikely* in all RCPs (*high confidence*) except for RCP8.5, where it is *about as likely as not* (*medium confidence*). {12.4.1; Tables 12.2, 12.3}

TS.5.5.2 Projected Long-term Changes in Regional Temperature

There is *very high confidence* that globally averaged changes over land will exceed changes over the ocean at the end of the 21st century by a factor that is *likely* in the range 1.4 to 1.7. In the absence of a strong reduction in the Atlantic Meridional Overturning, the Arctic region is projected to warm most (*very high confidence*) (Figure TS.15). As

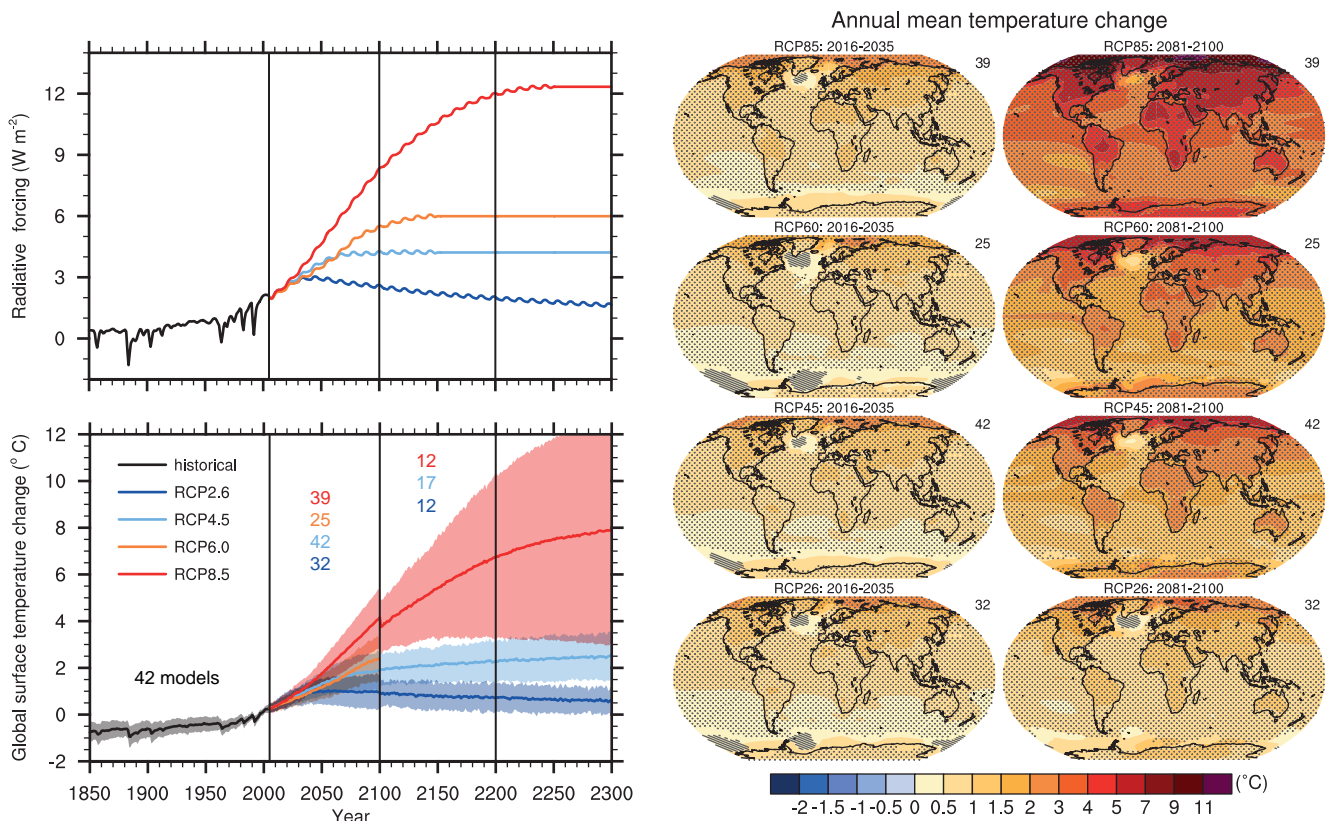


Figure TS.15 | (Top left) Total global mean radiative forcing for the four RCP scenarios based on the Model for the Assessment of Greenhouse-gas Induced Climate Change (MAGICC) energy balance model. Note that the actual forcing simulated by the CMIP5 models differs slightly between models. (Bottom left) Time series of global annual mean surface air temperature anomalies (relative to 1986–2005) from CMIP5 concentration-driven experiments. Projections are shown for each RCP for the multi-model mean (solid lines) and ± 1.64 standard deviation (5 to 95%) across the distribution of individual models (shading), based on annual means. The 1.64 standard deviation range based on the 20 yr averages 2081–2100, relative to 1986–2005, are interpreted as *likely* changes for the end of the 21st century. Discontinuities at 2100 are due to different numbers of models performing the extension runs beyond the 21st century and have no physical meaning. Numbers in the same colours as the lines indicate the number of different models contributing to the different time periods. Maps: Multi-model ensemble average of annual mean surface air temperature change (compared to 1986–2005 base period) for 2016–2035 and 2081–2100, for RCP2.6, 4.5, 6.0 and 8.5. Hatching indicates regions where the multi-model mean signal is less than one standard deviation of internal variability. Stippling indicates regions where the multi-model mean signal is greater than two standard deviations of internal variability and where 90% of the models agree on the sign of change. The number of CMIP5 models used is indicated in the upper right corner of each panel. Further detail regarding the related Figures SPM.7a and SPM.8.a is given in the TS Supplementary Material. {Box 12.1; Figures 12.4, 12.5, 12.11; Annex I}

Table TS.1 | Projected change in global mean surface air temperature and global mean sea level rise for the mid- and late 21st century relative to the reference period of 1986–2005. {12.4.1; Tables 12.2,13.5}

		2046–2065		2081–2100	
	Scenario	Mean	Likely range ^c	Mean	Likely range ^c
Global Mean Surface Temperature Change (°C) ^a	RCP2.6	1.0	0.4 to 1.6	1.0	0.3 to 1.7
	RCP4.5	1.4	0.9 to 2.0	1.8	1.1 to 2.6
	RCP6.0	1.3	0.8 to 1.8	2.2	1.4 to 3.1
	RCP8.5	2.0	1.4 to 2.6	3.7	2.6 to 4.8
	Scenario	Mean	Likely range ^d	Mean	Likely range ^d
Global Mean Sea Level Rise (m) ^b	RCP2.6	0.24	0.17 to 0.32	0.40	0.26 to 0.55
	RCP4.5	0.26	0.19 to 0.33	0.47	0.32 to 0.63
	RCP6.0	0.25	0.18 to 0.32	0.48	0.33 to 0.63
	RCP8.5	0.30	0.22 to 0.38	0.63	0.45 to 0.82

- Notes:
- ^a Based on the CMIP5 ensemble; anomalies calculated with respect to 1986–2005. Using HadCRUT4 and its uncertainty estimate (5–95% confidence interval), the observed warming to the reference period 1986–2005 is 0.61 [0.55 to 0.67] °C from 1850–1900, and 0.11 [0.09 to 0.13] °C from 1980–1999, the reference period for projections used in AR4. *Likely* ranges have not been assessed here with respect to earlier reference periods because methods are not generally available in the literature for combining the uncertainties in models and observations. Adding projected and observed changes does not account for potential effects of model biases compared to observations, and for natural internal variability during the observational reference period. {2.4; 11.2; Tables 12.2 and 12.3}
 - ^b Based on 21 CMIP5 models; anomalies calculated with respect to 1986–2005. Where CMIP5 results were not available for a particular AOGCM and scenario, they were estimated as explained in Chapter 13, Table 13.5. The contributions from ice sheet rapid dynamical change and anthropogenic land water storage are treated as having uniform probability distributions, and as largely independent of scenario. This treatment does not imply that the contributions concerned will not depend on the scenario followed, only that the current state of knowledge does not permit a quantitative assessment of the dependence. Based on current understanding, only the collapse of marine-based sectors of the Antarctic ice sheet, if initiated, could cause global mean sea level to rise substantially above the *likely* range during the 21st century. There is *medium confidence* that this additional contribution would not exceed several tenths of a metre of sea level rise during the 21st century.
 - ^c Calculated from projections as 5–95% model ranges. These ranges are then assessed to be *likely* ranges after accounting for additional uncertainties or different levels of confidence in models. For projections of global mean surface temperature change in 2046–2065 *confidence* is *medium*, because the relative importance of natural internal variability, and uncertainty in non-greenhouse gas forcing and response, are larger than for 2081–2100. The *likely* ranges for 2046–2065 do not take into account the possible influence of factors that lead to the assessed range for near-term (2016–2035) global mean surface temperature change that is lower than the 5–95% model range, because the influence of these factors on longer term projections has not been quantified due to insufficient scientific understanding. {11.3}
 - ^d Calculated from projections as 5–95% model ranges. These ranges are then assessed to be *likely* ranges after accounting for additional uncertainties or different levels of confidence in models. For projections of global mean sea level rise *confidence* is *medium* for both time horizons.

GMST rises, the pattern of atmospheric zonal mean temperatures show warming throughout the troposphere and cooling in the stratosphere, consistent with previous assessments. The consistency is especially clear in the tropical upper troposphere and the northern high latitudes. {12.4.3; Box 5.1}

It is *virtually certain* that, in most places, there will be more hot and fewer cold temperature extremes as global mean temperatures increase. These changes are expected for events defined as extremes on both daily and seasonal time scales. Increases in the frequency, duration and magnitude of hot extremes along with heat stress are expected; however, occasional cold winter extremes will continue to occur. Twenty-year return values of low-temperature events are projected to increase at a rate greater than winter mean temperatures in most regions, with the largest changes in the return values of low temperatures at high latitudes. Twenty-year return values for high-temperature events are projected to increase at a rate similar to or greater than the rate of increase of summer mean temperatures in most regions. Under RCP8.5 it is *likely* that, in most land regions, a current 20-year high-temperature event will occur more frequently by the end of the 21st century (at least doubling its frequency, but in many regions becoming an annual or 2-year event) and a current 20-year low-temperature event will become exceedingly rare (See also TFE.9). {12.4.3}

Models simulate a decrease in cloud amount in the future over most of the tropics and mid-latitudes, due mostly to reductions in low clouds. Changes in marine boundary layer clouds are most uncertain. Increases in cloud fraction and cloud optical depth and therefore cloud reflection are simulated in high latitudes, poleward of 50°. {12.4.3}

TS.5.5.3 Projected Long-term Changes in Atmospheric Circulation

Mean sea level pressure is projected to decrease in high latitudes and increase in the mid-latitudes as global temperatures rise. In the tropics, the Hadley and Walker Circulations are *likely* to slow down. Poleward shifts in the mid-latitude jets of about 1 to 2 degrees latitude are *likely* at the end of the 21st century under RCP8.5 in both hemispheres (*medium confidence*), with weaker shifts in the NH. In austral summer, the additional influence of stratospheric ozone recovery in the SH opposes changes due to GHGs there, though the net response varies strongly across models and scenarios. Substantial uncertainty and thus *low confidence* remains in projecting changes in NH storm tracks, especially for the North Atlantic basin. The Hadley Cell is *likely* to widen, which translates to broader tropical regions and a poleward encroachment of subtropical dry zones. In the stratosphere, the Brewer–Dobson circulation is *likely* to strengthen. {12.4.4}

TS.5.5.4 Projected Long-term Changes in the Water Cycle

On the planetary scale, relative humidity is projected to remain roughly constant, but specific humidity to increase in a warming climate. The projected differential warming of land and ocean promotes changes in atmospheric moistening that lead to small decreases in near-surface relative humidity over most land areas with the notable exception of parts of tropical Africa (*medium confidence*) (see TFE.1, Figure 1). {12.4.5}

It is *virtually certain* that, in the long term, global precipitation will increase with increased GMST. Global mean precipitation will increase at a rate per °C smaller than that of atmospheric water vapour. It will *likely* increase by 1 to 3% °C⁻¹ for scenarios other than RCP2.6. For RCP2.6 the range of sensitivities in the CMIP5 models is 0.5 to 4% °C⁻¹ at the end of the 21st century. {7.6.2, 7.6.3, 12.4.1}

Changes in average precipitation in a warmer world will exhibit substantial spatial variation under RCP8.5. Some regions will experience increases, other regions will experience decreases and yet others will not experience significant changes at all (see Figure TS.16). There is *high confidence* that the contrast of annual mean precipitation between dry and wet regions and that the contrast between wet and dry seasons will increase over most of the globe as temperatures increase. The general pattern of change indicates that high latitudes are *very likely* to experience greater amounts of precipitation due to the increased specific humidity of the warmer troposphere as well as increased transport of water vapour from the tropics by the end of this

century under the RCP8.5 scenario. Many mid-latitude and subtropical arid and semi-arid regions will *likely* experience less precipitation and many moist mid-latitude regions will *likely* experience more precipitation by the end of this century under the RCP8.5 scenario. Maps of precipitation change for the four RCP scenarios are shown in Figure TS.16. {12.4.2, 12.4.5}

Globally, for short-duration precipitation events, a shift to more intense individual storms and fewer weak storms is *likely* as temperatures increase. Over most of the mid-latitude land masses and over wet tropical regions, extreme precipitation events will *very likely* be more intense and more frequent in a warmer world. The global average sensitivity of the 20-year return value of the annual maximum daily precipitation ranges from 4% °C⁻¹ of local temperature increase (average of CMIP3 models) to 5.3% °C⁻¹ of local temperature increase (average of CMIP5 models), but regionally there are wide variations. {12.4.2, 12.4.5}

Annual surface evaporation is projected to increase as global temperatures rise over most of the ocean and is projected to change over land following a similar pattern as precipitation. Decreases in annual runoff are *likely* in parts of southern Europe, the Middle East and southern Africa by the end of this century under the RCP8.5 scenario. Increases in annual runoff are *likely* in the high northern latitudes corresponding to large increases in winter and spring precipitation by the end of the 21st century under the RCP8.5 scenario. Regional to global-scale projected decreases in soil moisture and increased risk of agricultural drought are *likely* in presently dry regions and are projected with *medium confidence* by the end of this century under the RCP8.5 scenario. Prominent

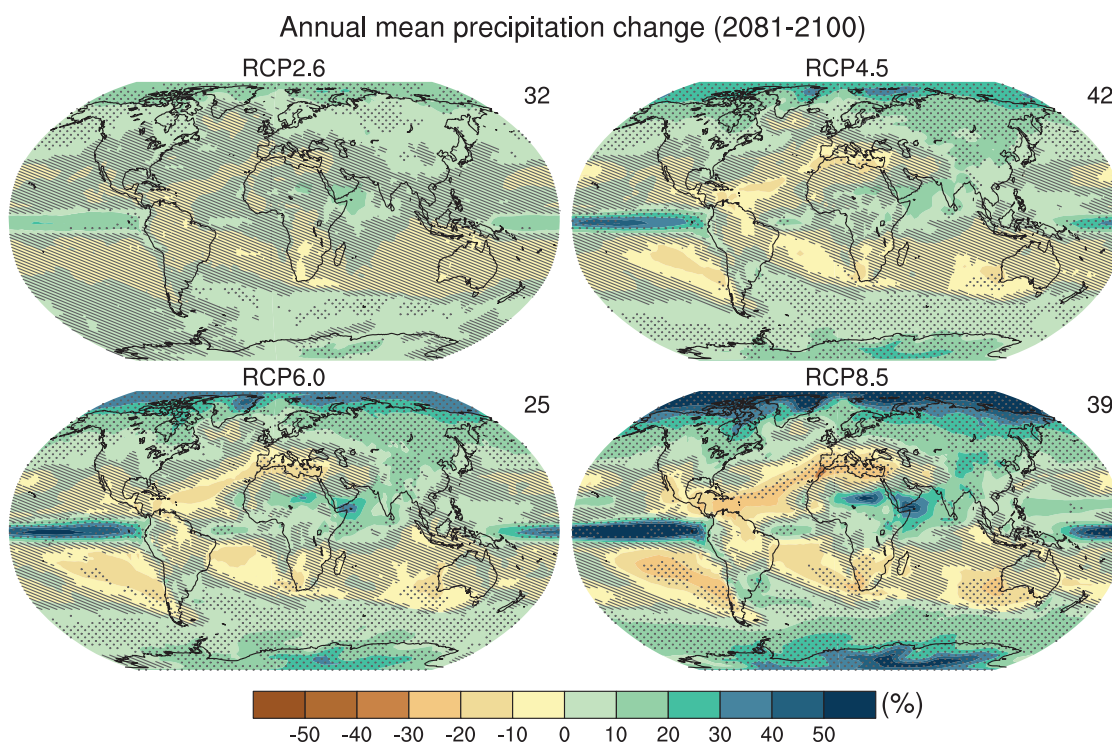


Figure TS.16 | Maps of multi-model results for the scenarios RCP2.6, RCP4.5, RCP6.0 and RCP8.5 in 2081–2100 of average percent change in mean precipitation. Changes are shown relative to 1986–2005. The number of CMIP5 models to calculate the multi-model mean is indicated in the upper right corner of each panel. Hatching indicates regions where the multi-model mean signal is less than 1 standard deviation of internal variability. Stippling indicates regions where the multi-model mean signal is greater than 2 standard deviations of internal variability and where 90% of models agree on the sign of change (see Box 12.1). Further detail regarding the related Figure SPM.8b is given in the TS Supplementary Material. {Figure 12.22; Annex I}

areas of projected decreases in evaporation include southern Africa and northwestern Africa along the Mediterranean. Soil moisture drying in the Mediterranean and southern African regions is consistent with projected changes in Hadley Circulation and increased surface temperatures, so surface drying in these regions as global temperatures increase is *likely* with *high confidence* by the end of this century under the RCP8.5 scenario. In regions where surface moistening is projected, changes are generally smaller than natural variability on the 20-year time scale. A summary of the projected changes in the water cycle from the CMIP5 models is shown in TFE.1, Figure 1. {12.4.5; Box 12.1}

TS.5.5.5 Projected Long-term Changes in the Cryosphere

It is *very likely* that the Arctic sea ice cover will continue shrinking and thinning year-round in the course of the 21st century as GMST rises. At the same time, in the Antarctic, a decrease in sea ice extent and volume is expected, but with *low confidence*. The CMIP5 multi-model projections give average reductions in Arctic sea ice extent for 2081–2100 compared to 1986–2005 ranging from 8% for RCP2.6 to 34% for RCP8.5 in February and from 43% for RCP2.6 to 94% for RCP8.5 in September (*medium confidence*) (Figure TS.17). A nearly ice-free Arctic Ocean (sea ice extent less than 10^6 km² for at least five consecutive years) in September before mid-century is *likely* under RCP8.5 (*medium confidence*), based on an assessment of a subset of models that most closely reproduce the climatological mean state and 1979–2012 trend of the Arctic sea ice cover. Some climate projections exhibit 5- to 10-year periods of sharp summer Arctic sea ice decline—even steeper

than observed over the last decade—and it is *likely* that such instances of rapid ice loss will occur in the future. There is little evidence in global climate models of a tipping point (or critical threshold) in the transition from a perennially ice-covered to a seasonally ice-free Arctic Ocean beyond which further sea ice loss is unstoppable and irreversible. In the Antarctic, the CMIP5 multi-model mean projects a decrease in sea ice extent that ranges from 16% for RCP2.6 to 67% for RCP8.5 in February and from 8% for RCP2.6 to 30% for RCP8.5 in September for 2081–2100 compared to 1986–2005. There is, however, *low confidence* in those projections because of the wide inter-model spread and the inability of almost all of the available models to reproduce the overall increase of the Antarctic sea ice areal coverage observed during the satellite era. {12.4.6, 12.5.5}

It is *very likely* that NH snow cover will reduce as global temperatures rise over the coming century. A retreat of permafrost extent with rising global temperatures is *virtually certain*. Snow cover changes result from precipitation and ablation changes, which are sometimes opposite. Projections of the NH spring snow covered area by the end of the 21st century vary between a decrease of 7 [3 to 10] % (RCP2.6) and 25 [18 to 32] % (RCP8.5) (Figure TS.18), but *confidence* is those numbers is only *medium* because snow processes in global climate models are strongly simplified. The projected changes in permafrost are a response not only to warming, but also to changes in snow cover, which exerts a control on the underlying soil. By the end of the 21st century, diagnosed near-surface permafrost area is projected to decrease by between 37% (RCP2.6) to 81% (RCP8.5) (*medium confidence*). {12.4.6}

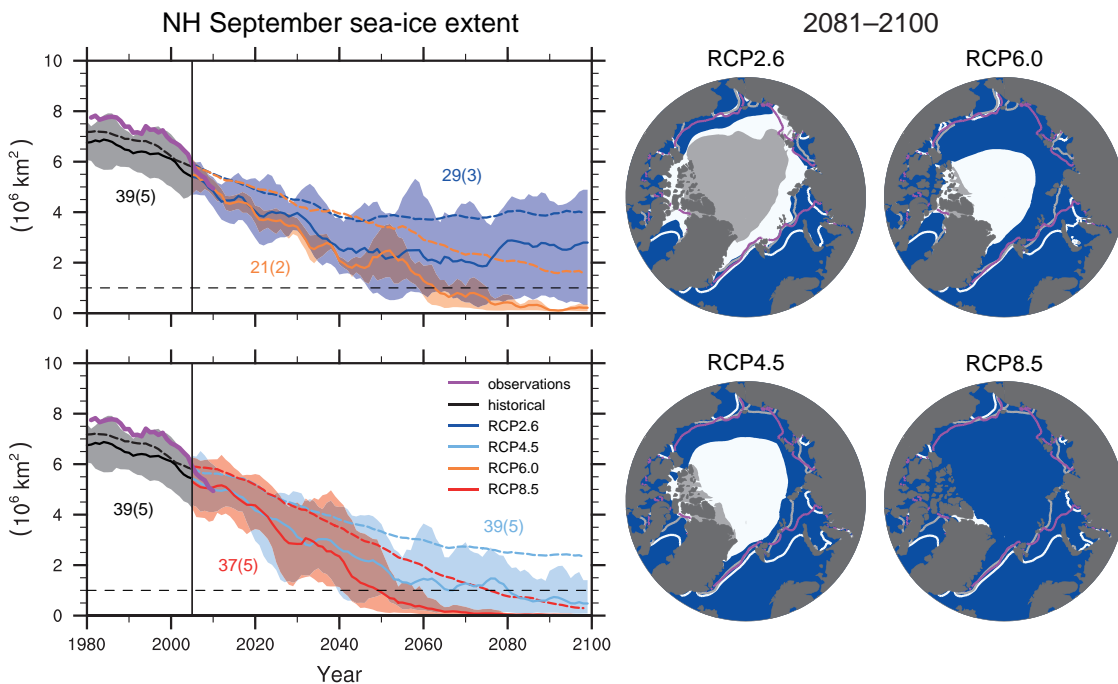


Figure TS.17 | Northern Hemisphere (NH) sea ice extent in September over the late 20th century and the whole 21st century for the scenarios RCP2.6, RCP4.5, RCP6.0 and RCP8.5 in the CMIP5 models, and corresponding maps of multi-model results in 2081–2100 of NH September sea ice extent. In the time series, the number of CMIP5 models to calculate the multi-model mean is indicated (subset in brackets). Time series are given as 5-year running means. The projected mean sea ice extent of a subset of models that most closely reproduce the climatological mean state and 1979–2012 trend of the Arctic sea ice is given (solid lines), with the minimum to maximum range of the subset indicated with shading. Black (grey shading) is the modelled historical evolution using historical reconstructed forcings. The CMIP5 multi-model mean is indicated with dashed lines. In the maps, the CMIP5 multi-model mean is given in white and the results for the subset in grey. Filled areas mark the averages over the 2081–2100 period, lines mark the sea ice extent averaged over the 1986–2005 period. The observed sea ice extent is given in pink as a time series and averaged over 1986–2005 as a pink line in the map. Further detail regarding the related Figures SPM.7b and SPM.8c is given in the TS Supplementary Material. {Figures 12.18, 12.29, 12.31}

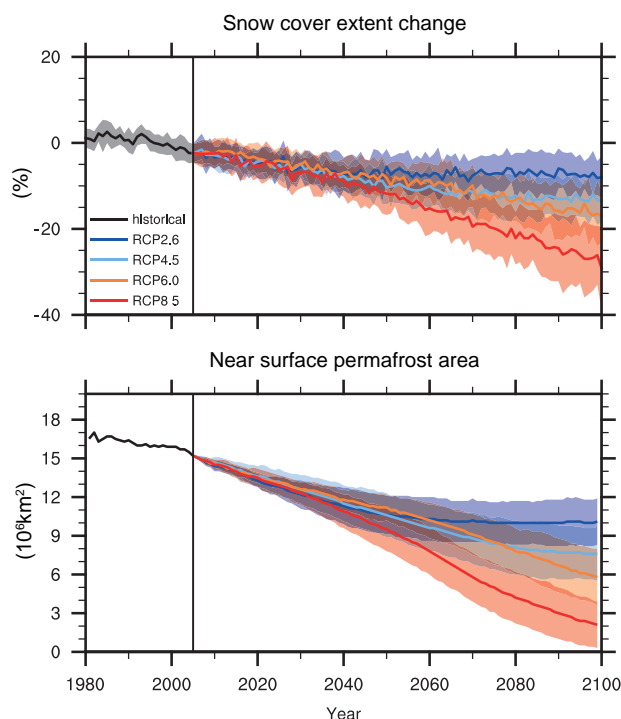


Figure TS.18 | (Top) Northern Hemisphere (NH) spring (March to April average) relative snow-covered area (RSCA) in CMIP5, obtained by dividing the simulated 5-year box smoothed spring snow-covered area (SCA) by the simulated average spring SCA of 1986–2005 reference period. (Bottom) NH diagnosed near-surface permafrost area in CMIP5, using 20-year average monthly surface air temperatures and snow depths. Lines indicate the multi model average, shading indicates the inter-model spread (one standard deviation). [Figures 12.32, 12.33]

TS.5.5.6 Projected Long-term Changes in the Ocean

Over the course of the 21st century, the global ocean will warm in all RCP scenarios. The strongest ocean warming is projected for the surface in subtropical and tropical regions. At greater depth the warming is projected to be most pronounced in the Southern Ocean. Best estimates of ocean warming in the top one hundred metres are about 0.6°C (RCP2.6) to 2.0°C (RCP8.5), and 0.3°C (RCP2.6) to 0.6°C (RCP8.5) at a depth of about 1 km by the end of the 21st century. For RCP4.5 by the end of the 21st century, half of the energy taken up by the ocean is in the uppermost 700 m, and 85% is in the uppermost 2000 m. Due to the long time scales of this heat transfer from the surface to depth, ocean warming will continue for centuries, even if GHG emissions are decreased or concentrations kept constant, and will result in a continued contribution to sea level rise (see Section TS5.7). [12.4.3, 12.4.7]

TS.5.6 Long-term Projections of Carbon and Other Biogeochemical Cycles

Projections of the global carbon cycle to 2100 using the CMIP5 ESMs represent a wider range of complex interactions between the carbon cycle and the physical climate system. [6]

With *very high confidence*, ocean carbon uptake of anthropogenic CO₂ will continue under all four RCPs through to 2100, with higher uptake

in higher concentration pathways. The future evolution of the land carbon uptake is much more uncertain. A majority of CMIP5 ESMs project a continued net carbon uptake by land ecosystems through 2100. Yet, a minority of models simulate a net CO₂ source to the atmosphere by 2100 due to the combined effect of climate change and land use change. In view of the large spread of model results and incomplete process representation, there is *low confidence* on the magnitude of modelled future land carbon changes. [6.4.3]

There is *high confidence* that climate change will partially offset increases in global land and ocean carbon sinks caused by rising atmospheric CO₂. Yet, there are regional differences among CMIP5 ESMs in the response of ocean and land CO₂ fluxes to climate. There is high agreement between models that tropical ecosystems will store less carbon in a warmer climate. There is medium agreement between the CMIP5 ESMs that at high latitudes warming will increase land carbon storage, although none of these models accounts for decomposition of carbon in permafrost which may offset increased land carbon storage. There is *high confidence* that reductions in permafrost extent due to warming will cause thawing of some currently frozen carbon. However, there is *low confidence* on the magnitude of carbon losses through CO₂ and CH₄ emissions to the atmosphere with a range from 50 to 250 PgC between 2000 and 2100 for RCP8.5. [6.4.2, 6.4.3]

The loss of carbon from frozen soils constitutes a positive radiative feedback that is missing in current coupled ESM projections. There is high agreement between CMIP5 ESMs that ocean warming and circulation changes will reduce the rate of ocean carbon uptake in the Southern Ocean and North Atlantic, but that carbon uptake will nevertheless persist in those regions. [6.4.2]

It is *very likely*, based on new experimental results and modelling, that nutrient shortage will limit the effect of rising atmospheric CO₂ on future land carbon sinks for the four RCP scenarios. There is *high confidence* that low nitrogen availability will limit carbon storage on land even when considering anthropogenic nitrogen deposition. The role of phosphorus limitation is more uncertain. [6.4.6]

For the ESMs simulations driven by CO₂ concentrations, representation of the land and ocean carbon cycle allows quantification of the fossil fuel emissions compatible with the RCP scenarios. Between 2012 and 2100, ESM results imply cumulative compatible fossil fuel emissions of 270 [140 to 410] PgC for RCP2.6, 780 [595 to 1005] PgC for RCP4.5, 1060 [840 to 1250] PgC for RCP6.0 and 1685 [1415 to 1910] PgC for RCP8.5 (values quoted to nearest 5 PgC, range ±1 standard deviation derived from CMIP5 model results) (Figure TS.19). For RCP2.6, the models project an average 50% (range 14 to 96%) emission reduction by 2050 relative to 1990 levels. By the end of the 21st century, about half of the models infer emissions slightly above zero, while the other half infer a net removal of CO₂ from the atmosphere (see also Box TS.7). [6.4.3; Table 6.12]

When forced with RCP8.5 CO₂ emissions, as opposed to the RCP8.5 CO₂ concentrations, CMIP5 ESMs with interactive carbon cycles simulate, on average, a 50 (–140 to +210) ppm larger atmospheric CO₂ concentration and a 0.2 (–0.4 to +0.9) °C larger global surface temperature increase by 2100 (CMIP5 model spread). [12.4.8]

It is *virtually certain* that the increased storage of carbon by the ocean will increase acidification in the future, continuing the observed trends of the past decades. Ocean acidification in the surface ocean will follow atmospheric CO₂ and it will also increase in the deep ocean as CO₂ continues to penetrate the abyss. The CMIP5 models consistently project worldwide increased ocean acidification to 2100 under all

RCPs. The corresponding decrease in surface ocean pH by the end of 21st century is 0.065 (0.06 to 0.07) for RCP2.6, 0.145 (0.14 to 0.15) for RCP4.5, 0.203 (0.20 to 0.21) for RCP6.0 and 0.31 (0.30 to 0.32) for RCP8.5 (CMIP5 model spread) (Figure TS.20). Surface waters are projected to become seasonally corrosive to aragonite in parts of the Arctic and in some coastal upwelling systems within a decade, and

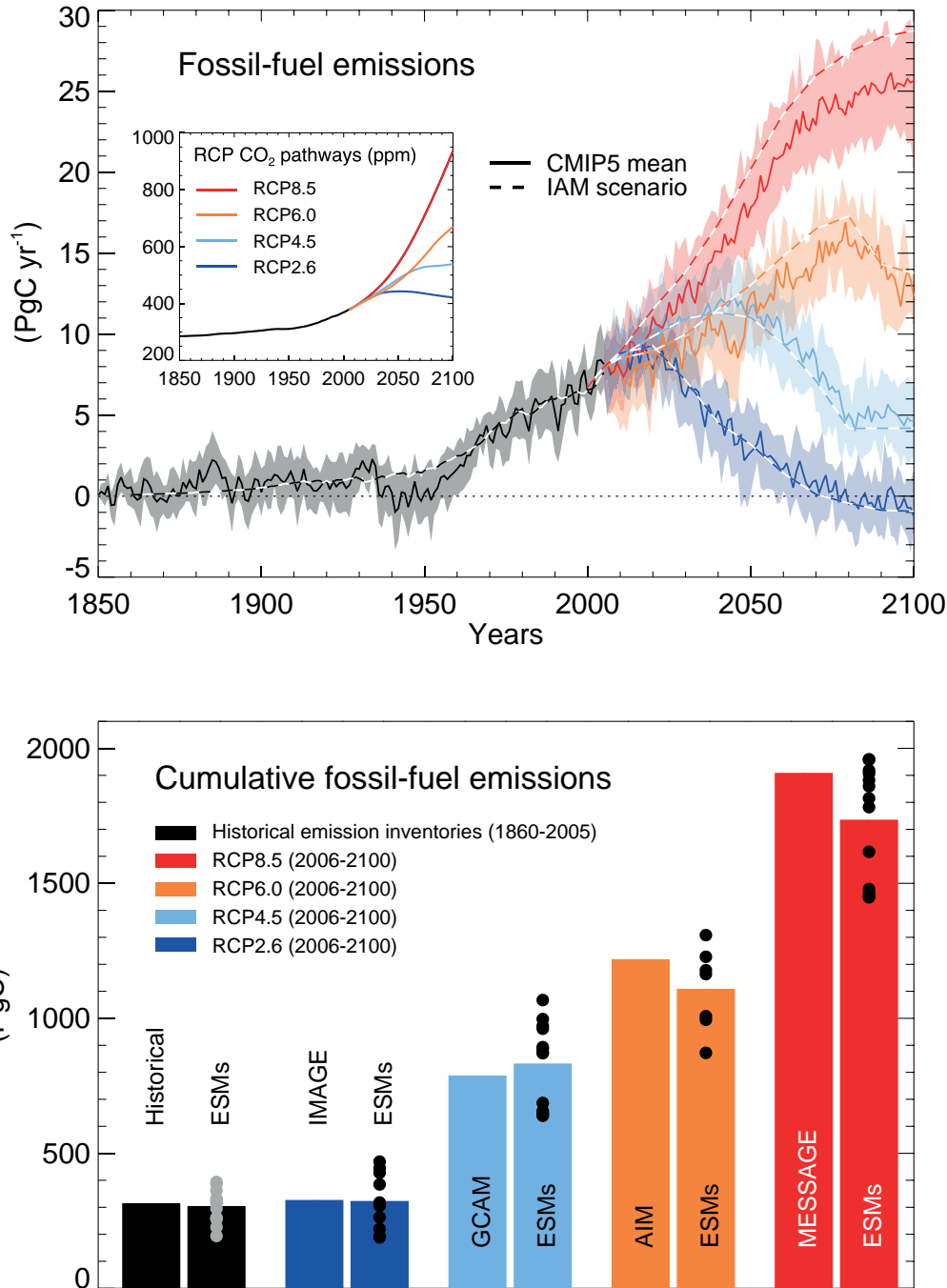


Figure TS.19 | Compatible fossil fuel emissions simulated by the CMIP5 models for the four RCP scenarios. (Top) Time series of annual emission (PgC yr⁻¹). Dashed lines represent the historical estimates and RCP emissions calculated by the Integrated Assessment Models (IAMs) used to define the RCP scenarios, solid lines and plumes show results from CMIP5 Earth System Models (ESMs, model mean, with one standard deviation shaded). (Bottom) Cumulative emissions for the historical period (1860–2005) and 21st century (defined in CMIP5 as 2006–2100) for historical estimates and RCP scenarios. Left bars are cumulative emissions from the IAMs, right bars are the CMIP5 ESMs multi-model mean estimate and dots denote individual ESM results. From the CMIP5 ESMs results, total carbon in the land-atmosphere–ocean system can be tracked and changes in this total must equal fossil fuel emissions to the system. Hence the compatible emissions are given by cumulative emissions = $\Delta C_A + \Delta C_L + \Delta C_O$, while emission rate = $d/dt [C_A + C_L + C_O]$, where C_A , C_L , C_O are carbon stored in atmosphere, land and ocean respectively. Other sources and sinks of CO₂ such as from volcanism, sedimentation or rock weathering, which are very small on centennial time scales are not considered here. [Box 6.4; Figure 6.25]

in parts of the Southern Ocean within one to three decades in most scenarios. Aragonite, a less stable form of calcium carbonate, undersaturation becomes widespread in these regions at atmospheric CO₂ levels of 500 to 600 ppm. {6.4.4}

It is *very likely* that the dissolved oxygen content of the ocean will decrease by a few percent during the 21st century in response to surface warming. CMIP5 models suggest that this decrease in dissolved oxygen will predominantly occur in the subsurface mid-latitude

oceans, caused by enhanced stratification, reduced ventilation and warming. However, there is no consensus on the future development of the volume of hypoxic and suboxic waters in the open ocean because of large uncertainties in potential biogeochemical effects and in the evolution of tropical ocean dynamics. {6.4.5}

With *very high confidence*, the carbon cycle in the ocean and on land will continue to respond to climate change and atmospheric CO₂ increases that arise during the 21st century (see TFE.7 and TFE 8). {6.4}

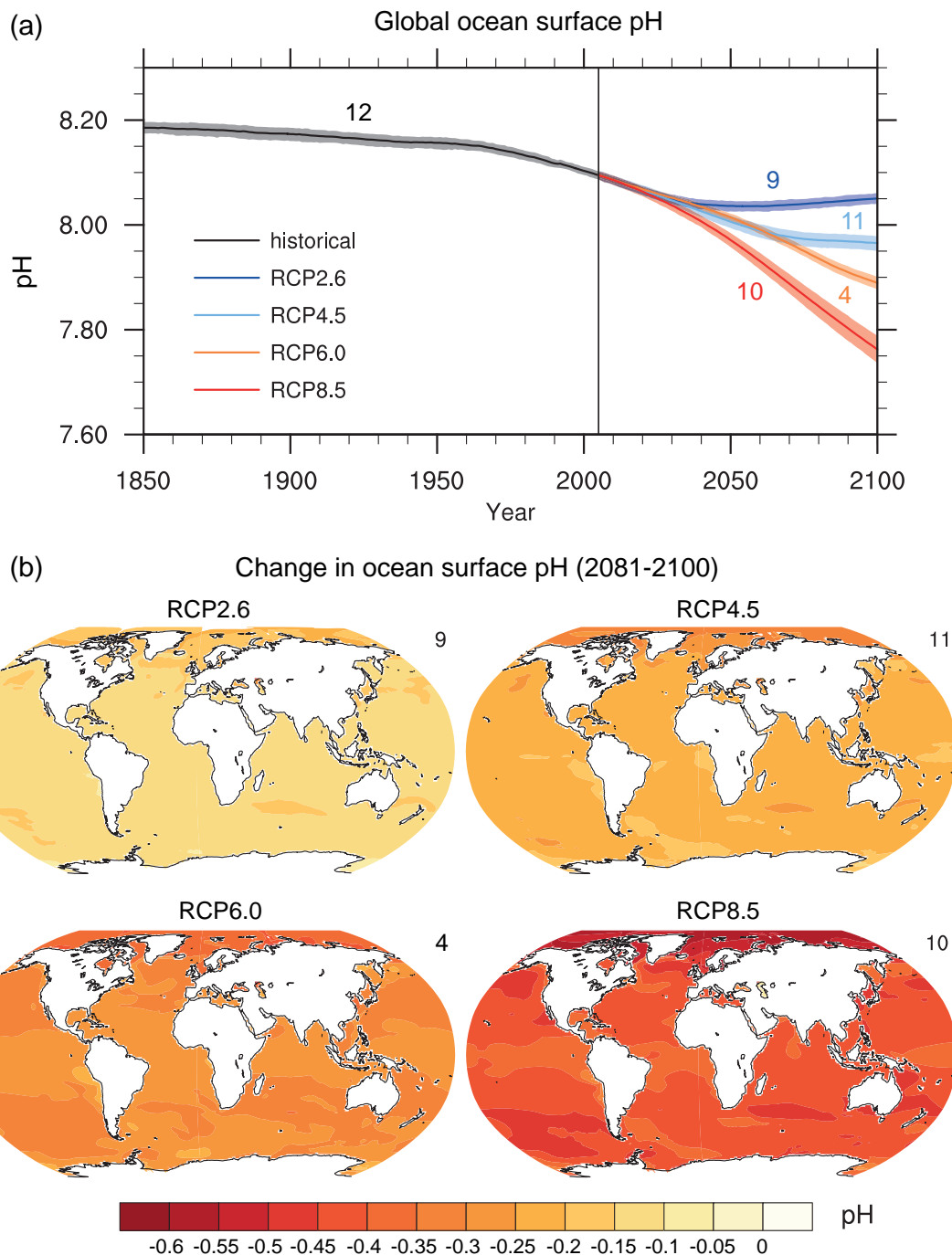


Figure TS.20 | (a) Time series (model averages and minimum to maximum ranges) and (b) maps of multi-model surface ocean pH for the scenarios RCP2.6, RCP4.5, RCP6.0 and RCP8.5 in 2081–2100. The maps in (b) show change in global ocean surface pH in 2081–2100 relative to 1986–2005. The number of CMIP5 models to calculate the multi-model mean is indicated in the upper right corner of each panel. Further detail regarding the related Figures SPM.7c and SPM.8.d is given in the TS Supplementary Material. [Figure 6.28]

TS

Thematic Focus Elements

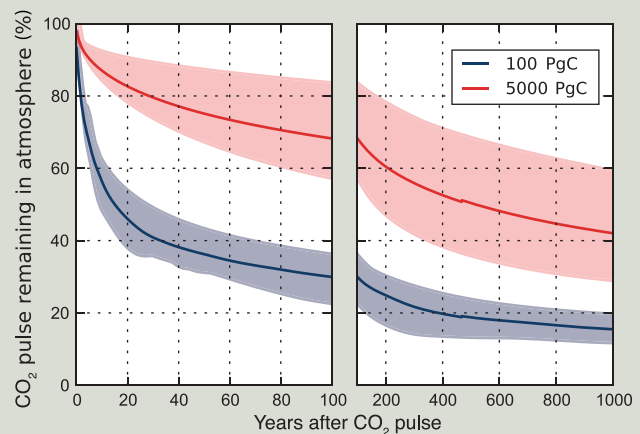
TFE.7 | Carbon Cycle Perturbation and Uncertainties

The natural carbon cycle has been perturbed since the beginning of the Industrial Revolution (about 1750) by the anthropogenic release of carbon dioxide (CO₂) to the atmosphere, virtually all from fossil fuel combustion and land use change, with a small contribution from cement production. Fossil fuel burning is a process related to energy production. Fossil fuel carbon comes from geological deposits of coal, oil and gas that were buried in the Earth crust for millions of years. Land use change CO₂ emissions are related to the conversion of natural ecosystems into managed ecosystems for food, feed and timber production with CO₂ being emitted from the burning of plant material or from the decomposition of dead plants and soil organic carbon. For instance when a forest is cleared, the plant material may be released to the atmosphere quickly through burning or over many years as the dead biomass and soil carbon decay on their own. {6.1, 6.3; Table 6.1}

The human caused excess of CO₂ in the atmosphere is partly removed from the atmosphere by carbon sinks in land ecosystems and in the ocean, currently leaving less than half of the CO₂ emissions in the atmosphere. Natural carbon sinks are due to physical, biological and chemical processes acting on different time scales. An excess of atmospheric CO₂ supports photosynthetic CO₂ fixation by plants that is stored as plant biomass or in the soil. The residence times of stored carbon on land depends on the compartments (plant/soil) and composition of the organic carbon, with time horizons varying from days to centuries. The increased storage in terrestrial ecosystems not affected by land use change is *likely* to be caused by enhanced photosynthesis at higher CO₂ levels and nitrogen deposition, and changes in climate favoring carbon sinks such as longer growing seasons in mid-to-high latitudes. {6.3, 6.3.1}

The uptake of anthropogenic CO₂ by the ocean is primarily a response to increasing CO₂ in the atmosphere. Excess atmospheric CO₂ absorbed by the surface ocean or transported to the ocean through aquatic systems (e.g., rivers, groundwaters) gets buried in coastal sediments or transported to deep waters where it is stored for decades to centuries. The deep ocean carbon can dissolve ocean carbonate sediments to store excess CO₂ on time scales of centuries to millennia. Within a 1 kyr, the remaining atmospheric fraction of the CO₂ emissions will be between 15 and 40%, depending on the amount of carbon released (TFE.7, Figure 1). On geological time scales of 10 kyr or longer, additional CO₂ is removed very slowly from the atmosphere by rock weathering, pulling the remaining atmospheric CO₂ fraction down to 10 to 25% after 10 kyr. {Box 6.1}

The carbon cycle response to future climate and CO₂ changes can be viewed as two strong and opposing feedbacks. The concentration–carbon feedback determines changes in storage due to elevated CO₂, and the climate–carbon feedback determines changes in carbon storage due to changes in climate. There is *high confidence* that increased atmospheric CO₂ will lead to increased land and ocean carbon uptake but by an uncertain amount. Models agree on the positive sign of land and ocean response to rising CO₂ but show only medium and low agreement for the magnitude of ocean and land carbon uptake respectively (TFE.7, Figure 2). Future climate change will decrease land and ocean carbon uptake compared to the case with constant climate (*medium confidence*). This is further supported by paleoclimate observations and modelling indicating that there is a positive feedback between climate and the carbon cycle on century to millennial time scales. Models agree on the sign, globally negative, of land and ocean response to climate change but show low agreement on the magnitude of this response, especially for the land (TFE.7, Figure 2). A key update since the IPCC Fourth Assessment Report (AR4) is the introduction of nutrient dynamics in some land carbon models, in particular the limitations on plant growth imposed by nitrogen availability. There is *high confidence* that, at the global scale, relative to the Coupled Model Intercomparison Project Phase 5 (CMIP5) carbon-only Earth System



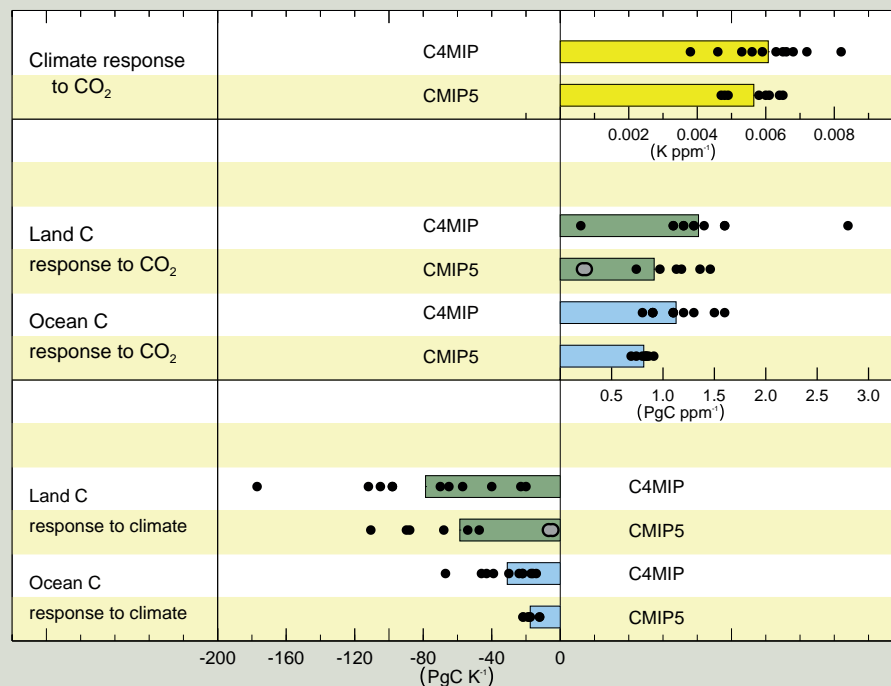
TFE.7, Figure 1 | Percentage of initial atmospheric CO₂ perturbation remaining in the atmosphere in response to an idealized instantaneous CO₂ emission pulse in year 0 as calculated by a range of coupled climate–carbon cycle models. Multi-model mean (line) and the uncertainty interval (maximum model range, shading) simulated during 100 years (left) and 1 kyr (right) following the instantaneous emission pulse of 100 PgC (blue) and 5,000 PgC (red). {Box 6.1, Figure 1}

(continued on next page)

TS

TFE.7 (continued)

Models (ESMs), CMIP5 ESMs including a land nitrogen cycle will reduce the strength of both the concentration–carbon feedback and the climate–carbon feedback of land ecosystems (TFE.7, Figure 2). Inclusion of nitrogen-cycle processes increases the spread across the CMIP5 ensemble. The CMIP5 spread in ocean sensitivity to CO₂ and climate appears reduced compared to AR4 (TFE.7, Figure 2). {6.2.3, 6.4.2}



TFE.7, Figure 2 | Comparison of carbon cycle feedback metrics between the ensemble of seven General Circulation Models (GCMs) and four Earth System Models of Intermediate Complexity (EMICs) at the time of AR4 (Coupled Carbon Cycle Climate Model Intercomparison Project (C⁴MIP)) under the SRES A2 scenario and the eight CMIP5 models under the 140-year 1% CO₂ increase per year scenario. Black dots represent a single model simulation and coloured bars the mean of the multi-model results, grey dots are used for models with a coupled terrestrial nitrogen cycle. The comparison with C⁴MIP models is for context, but these metrics are known to be variable across different scenarios and rates of change (see Section 6.4.2). The SRES A2 scenario is closer in rate of change to a 0.5% CO₂ increase per year scenario and as such it should be expected that the CMIP5 climate–carbon sensitivity terms are comparable, but the concentration–carbon sensitivity terms are *likely* to be around 20% smaller for CMIP5 than for C⁴MIP due to lags in the ability of the land and ocean to respond to higher rates of CO₂ increase. This dependence on scenario reduces confidence in any quantitative statements of how CMIP5 carbon cycle feedbacks differ from C⁴MIP. {Figure 6.21}

With *very high confidence*, ocean carbon uptake of anthropogenic CO₂ emissions will continue under all four Representative Concentration Pathways (RCPs) through to 2100, with higher uptake corresponding to higher concentration pathways. The future evolution of the land carbon uptake is much more uncertain, with a majority of models projecting a continued net carbon uptake under all RCPs, but with some models simulating a net loss of carbon by the land due to the combined effect of climate change and land use change. In view of the large spread of model results and incomplete process representation, there is *low confidence* on the magnitude of modelled future land carbon changes. {6.4.3; Figure 6.24}

Biogeochemical cycles and feedbacks other than the carbon cycle play an important role in the future of the climate system, although the carbon cycle represents the strongest of these. Changes in the nitrogen cycle, in addition to interactions with CO₂ sources and sinks, affect emissions of nitrous oxide (N₂O) both on land and from the ocean. The human-caused creation of reactive nitrogen has increased steadily over the last two decades and is dominated by the production of ammonia for fertilizer and industry, with important contributions from legume cultivation and combustion of fossil fuels. {6.3}

Many processes, however, are not yet represented in coupled climate-biogeochemistry models (e.g., other processes involving other biogenic elements such as phosphorus, silicon and iron) so their magnitudes have to be estimated in offline or simpler models, which make their quantitative assessment difficult. It is *likely* that there will be nonlinear interactions between many of these processes, but these are not yet well quantified. Therefore any assessment of the future feedbacks between climate and biogeochemical cycles still contains large uncertainty. {6.4}

TS

Box TS.7 | Climate Geoengineering Methods

Geoengineering is defined as the deliberate large-scale intervention in the Earth system to counter undesirable impacts of climate change on the planet. Carbon Dioxide Reduction (CDR) aims to slow or perhaps reverse projected increases in the future atmospheric CO₂ concentrations, accelerating the natural removal of atmospheric CO₂ and increasing the storage of carbon in land, ocean and geological reservoirs. Solar Radiation Management (SRM) aims to counter the warming associated with increasing GHG concentrations by reducing the amount of sunlight absorbed by the climate system. A related technique seeks to deliberately decrease the greenhouse effect in the climate system by altering high-level cloudiness. {6.5, 7.7; FAQ 7.3}

CDR methods could provide mitigation of climate change if CO₂ can be reduced, but there are uncertainties, side effects and risks, and implementation would depend on technological maturity along with economic, political and ethical considerations. CDR would *likely* need to be deployed at large-scale and over at least one century to be able to significantly reduce CO₂ concentrations. There are biogeochemical, and currently technical limitations that make it difficult to provide quantitative estimates of the potential for CDR. It is *virtually certain* that CO₂ removals from the atmosphere by CDR would be partially offset by outgassing of CO₂ previously stored in ocean and terrestrial carbon reservoirs. Some of the climatic and environmental side effects of CDR methods are associated with altered surface albedo from afforestation, ocean de-oxygenation from ocean fertilization, and enhanced N₂O emissions. Land-based CDR methods would probably face competing demands for land. The level of *confidence* on the effectiveness of CDR methods and their side effects on carbon and other biogeochemical cycles is *low*. {6.5; Box 6.2; FAQ 7.3}

SRM remains unimplemented and untested but, if realizable, could offset a global temperature rise and some of its effects. There is *medium confidence* that SRM through stratospheric aerosol injection is scalable to counter the RF and some of the climate effects expected from a twofold increase in CO₂ concentration. There is no consensus on whether a similarly large RF could be achieved from cloud brightening SRM due to insufficient understanding of aerosol–cloud interactions. It does not appear that land albedo change SRM could produce a large RF. Limited literature on other SRM methods precludes their assessment. {7.7.2, 7.7.3}

Numerous side effects, risks and shortcomings from SRM have been identified. SRM would produce an inexact compensation for the RF by GHGs. Several lines of evidence indicate that SRM would produce a small but significant decrease in global precipitation (with larger differences on regional scales) if the global surface temperature were maintained. Another side effect that is relatively well characterized is the likelihood of modest polar stratospheric ozone depletion associated with stratospheric aerosol SRM. There could also be other as yet unanticipated consequences. {7.6.3, 7.7.3, 7.7.4}

As long as GHG concentrations continued to increase, the SRM would require commensurate increase, exacerbating side effects. In addition, scaling SRM to substantial levels would carry the risk that if the SRM were terminated for any reason, there is *high confidence* that surface temperatures would increase rapidly (within a decade or two) to values consistent with the GHG forcing, which would stress systems sensitive to the rate of climate change. Finally, SRM would not compensate for ocean acidification from increasing CO₂. {7.7.3, 7.7.4}

TS.5.7 Long-term Projections of Sea Level Change

TS.5.7.1 Projections of Global Mean Sea Level Change for the 21st Century

GMSL rise for 2081–2100 (relative to 1986–2005) for the RCPs will *likely* be in the 5 to 95% ranges derived from CMIP5 climate projections in combination with process-based models of glacier and ice sheet surface mass balance, with possible ice sheet dynamical changes assessed from the published literature. These *likely* ranges are 0.26 to 0.55 m (RCP2.6), 0.32 to 0.63 m (RCP4.5), 0.33 to 0.63 m (RCP6.0) and 0.45 to 0.82 m (RCP8.5) (*medium confidence*) (Table TS.1, Figure TS.21). For RCP8.5 the range at 2100 is 0.52 to 0.98 m. The central projections for GMSL rise in all scenarios lie within a range of 0.05 m until the middle of the century, when they begin to diverge; by the late 21st century, they have a spread of 0.25 m. Although RCP4.5 and RCP6.0 are very

similar at the end of the century, RCP4.5 has a greater rate of rise earlier in the century than RCP6.0. GMSL rise depends on the pathway of CO₂ emissions, not only on the cumulative total; reducing emissions earlier rather than later, for the same cumulative total, leads to a larger mitigation of sea level rise. {12.4.1, 13.4.1, 13.5.1; Table 13.5}

Confidence in the projected *likely* ranges comes from the consistency of process-based models with observations and physical understanding. The basis for higher projections has been considered and it has been concluded that there is currently insufficient evidence to evaluate the probability of specific levels above the *likely* range. Based on current understanding, only the collapse of marine-based sectors of the Antarctic ice sheet, if initiated, could cause GMSL to rise substantially above the *likely* range during the 21st century. There is a lack of consensus on the probability for such a collapse, and the potential additional contribution to GMSL rise cannot be precisely quantified,

but there is *medium confidence* that it would not exceed several tenths of a metre of sea level rise during the 21st century. {13.5.1, 13.5.3}

Under all the RCP scenarios, the time-mean rate of GMSL rise during the 21st century is *very likely* to exceed the rate observed during 1971–2010. In the projections, the rate of rise initially increases. In RCP2.6 it becomes roughly constant (central projection about 4.5 mm yr⁻¹) before the middle of the century, and subsequently declines slightly. The rate of rise becomes roughly constant in RCP4.5 and RCP6.0 by the end of the 21st century, whereas acceleration continues throughout the century in RCP8.5 (reaching 11 [8 to 16] mm yr⁻¹ during 2081–2100). {13.5.1; Table 13.5}

In all RCP scenarios, thermal expansion is the largest contribution, accounting for about 30 to 55% of the total. Glaciers are the next largest, accounting for 15–35%. By 2100, 15 to 55% of the present glacier volume is projected to be eliminated under RCP2.6, and 35 to 85% under RCP8.5 (*medium confidence*). The increase in surface melting in Greenland is projected to exceed the increase in accumulation, and there is *high confidence* that the surface mass balance changes on the Greenland ice sheet will make a positive contribution to sea level rise over the 21st century. On the Antarctic ice sheet, surface melting is projected to remain small, while there is *medium confidence* that snowfall will increase (Figure TS.21). {13.3.3, 13.4.3, 13.4.4, 13.5.1; Table 13.5}

There is *medium confidence* in the ability to model future rapid changes in ice sheet dynamics on decadal time scales. At the time of the AR4, scientific understanding was not sufficient to allow an assessment of the possibility of such changes. Since the publication of the AR4, there has been substantial progress in understanding the relevant processes as well as in developing new ice sheet models that are capable of simulating them. However, the published literature as yet provides only a partially sufficient basis for making projections related to particular scenarios. In our projections of GMSL rise by 2081–2100, the *likely* range from rapid changes in ice outflow is 0.03 to 0.20 m from the two ice sheets combined, and its inclusion is the most important reason why the projections are greater than those given in the AR4. {13.1.5, 13.5.1, 13.5.3}

Semi-empirical models are designed to reproduce the observed sea level record over their period of calibration, but do not attribute sea level rise to its individual physical components. For RCPs, some semi-empirical models project a range that overlaps the process-based *likely* range while others project a median and 95-percentile that are about twice as large as the process-based models. In nearly every case, the semi-empirical model 95th percentile is higher than the process-based *likely* range. For 2081–2100 (relative to 1986–2005) under RCP4.5, semi-empirical models give median projections in the range 0.56 to 0.97 m, and their 95th percentiles extend to about 1.2 m. This difference implies either that there is some contribution which is presently

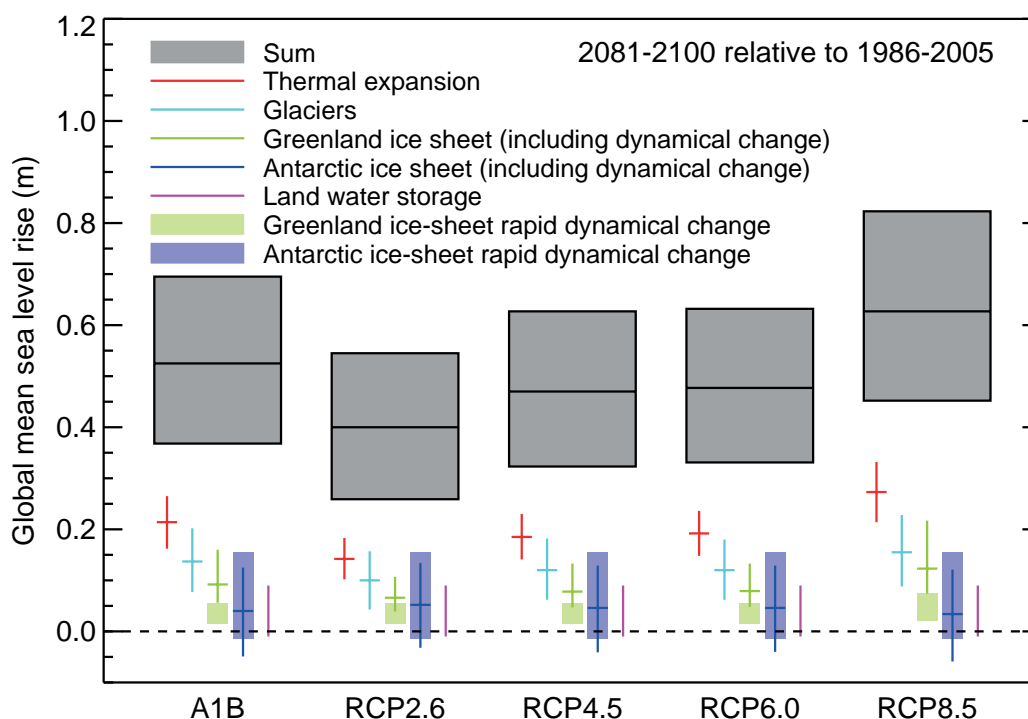


Figure TS.21 | Projections from process-based models with *likely* ranges and median values for global mean sea level (GMSL) rise and its contributions in 2081–2100 relative to 1986–2005 for the four RCP scenarios and scenario SRES A1B used in the AR4. The contributions from ice sheets include the contributions from ice sheet rapid dynamical change, which are also shown separately. The contributions from ice sheet rapid dynamics and anthropogenic land water storage are treated as having uniform probability distributions, and as independent of scenario (except that a higher rate of change is used for Greenland ice sheet outflow under RCP8.5). This treatment does not imply that the contributions concerned will not depend on the scenario followed, only that the current state of knowledge does not permit a quantitative assessment of the dependence. See discussion in Sections 13.5.1 and 13.5.3 and Supplementary Material for methods. Based on current understanding, only the collapse of the marine-based sectors of the Antarctic ice sheet, if initiated, could cause GMSL to rise substantially above the *likely* range during the 21st century. This potential additional contribution cannot be precisely quantified but there is *medium confidence* that it would not exceed several tenths of a metre during the 21st century. {Figure 13.10}

TS

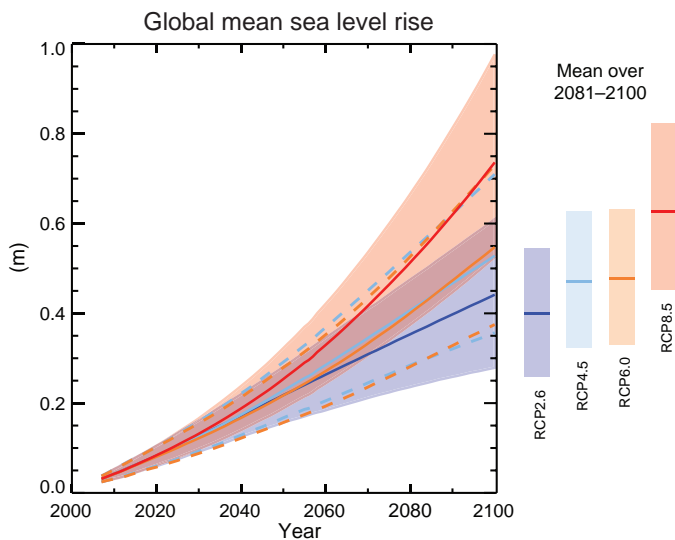


Figure TS.22 | Projections from process-based models of global mean sea level (GMSL) rise relative to 1986–2005 for the four RCP scenarios. The solid lines show the median projections, the dashed lines show the *likely* ranges for RCP4.5 and RCP6.0, and the shading the *likely* ranges for RCP2.6 and RCP8.5. The time means for 2081–2100 are shown as coloured vertical bars. See Sections 13.5.1 and 13.5.3 and Supplementary Material for methods. Based on current understanding, only the collapse of the marine-based sectors of the Antarctic ice sheet, if initiated, could cause GMSL to rise substantially above the *likely* range during the 21st century. This potential additional contribution cannot be precisely quantified but there is *medium confidence* that it would not exceed several tenths of a metre during the 21st century. Further detail regarding the related Figure SPM.9 is given in the TS Supplementary Material. {Table 13.5; Figures 13.10, 13.11}

unidentified or underestimated by process-based models, or that the projections of semi-empirical models are overestimates. Making projections with a semi-empirical model assumes that sea level change in the future will have the same relationship as it has had in the past to RF or global mean temperature change. This may not hold if potentially nonlinear physical processes do not scale in the future in ways which can be calibrated from the past. There is no consensus in the scientific community about the reliability of semi-empirical model projections, and *confidence* in them is assessed to be *low*. {13.5.2, 13.5.3}

TS.5.7.2 Projections of Global Mean Sea Level Change Beyond 2100

It is *virtually certain* that GMSL rise will continue beyond 2100. The few available model results that go beyond 2100 indicate global mean sea level rise above the pre-industrial level (defined here as an equilibrium 280 ppm atmospheric CO₂ concentration) by 2300 to be less than 1 m for a RF that corresponds to CO₂ concentrations that peak and decline and remain below 500 ppm, as in the scenario RCP2.6. For a RF that corresponds to a CO₂ concentration that is above 700 ppm but below 1500 ppm, as in the scenario RCP8.5, the projected rise is 1 m to more than 3 m (*medium confidence*). {13.5.4}

Sea level rise due to ocean thermal expansion will continue for centuries to millennia. The amount of ocean thermal expansion increases with global warming (models give a range of 0.2 to 0.6 m °C⁻¹). The glacier contribution decreases over time as their volume (currently

about 0.43 m sea level equivalent) decreases. In Antarctica, beyond 2100 and with higher GHG scenarios, the increase in surface melting could exceed the increase in accumulation. {13.5.2, 13.5.4}

The available evidence indicates that global warming greater than a certain threshold would lead to the near-complete loss of the Greenland ice sheet over a millennium or more, causing a GMSL rise of about 7 m. Studies with fixed present-day ice sheet topography indicate the threshold is greater than 2°C but less than 4°C of GMST rise with respect to pre-industrial (*medium confidence*). The one study with a dynamical ice sheet suggests the threshold is greater than about 1°C (*low confidence*) global mean warming with respect to pre-industrial. Considering the present state of scientific uncertainty, a *likely* range cannot be quantified. The complete loss of the ice sheet is not inevitable because this would take a millennium or more; if temperatures decline before the ice sheet is eliminated, the ice sheet might regrow. However, some part of the mass loss might be irreversible, depending on the duration and degree of exceedance of the threshold, because the ice sheet may have multiple steady states, due to its interaction with its regional climate. {13.4.3, 13.5.4}

Currently available information indicates that the dynamical contribution of the ice sheets will continue beyond 2100, but *confidence* in projections is *low*. In Greenland, ice outflow induced from interaction with the ocean is self-limiting as the ice sheet margin retreats inland from the coast. By contrast, the bedrock topography of Antarctica is such that there may be enhanced rates of mass loss as the ice retreats. About 3.3 m of equivalent global sea level of the West Antarctic ice sheet is grounded on areas with downward sloping bedrock, which may be subject to potential ice loss via the marine ice sheet instability. Abrupt and irreversible ice loss from a potential instability of marine-based sectors of the Antarctic Ice Sheet in response to climate forcing is possible, but current evidence and understanding is insufficient to make a quantitative assessment. Due to relatively weak snowfall on Antarctica and the slow ice motion in its interior, it can be expected that the West Antarctic ice sheet would take at least several thousand years to regrow if it was eliminated by dynamic ice discharge. Consequently any significant ice loss from West Antarctic that occurs within the next century will be irreversible on a multi-centennial to millennial time scale. {5.8, 13.4.3, 13.4.4, 13.5.4}

TS.5.7.3 Projections of Regional Sea Level Change

Regional sea level will change due to dynamical ocean circulation changes, changes in the heat content of the ocean, mass redistribution in the entire Earth system and changes in atmospheric pressure. Ocean dynamical change results from changes in wind and buoyancy forcing (heat and freshwater), associated changes in the circulation, and redistribution of heat and freshwater. Over time scales longer than a few days, regional sea level also adjusts nearly isostatically to regional changes in sea level atmospheric pressure relative to its mean over the ocean. Ice sheet mass loss (both contemporary and past), glacier mass loss and changes in terrestrial hydrology cause water mass redistribution among the cryosphere, the land and the oceans, giving rise to distinctive regional changes in the solid Earth, Earth rotation and the gravity field. In some coastal locations, changes in the hydrological cycle, ground subsidence associated with anthropogenic activity,

tectonic processes and coastal processes can dominate the relative sea level change, that is, the change in sea surface height relative to the land. {13.1.3, 13.6.2, 13.6.3, 13.6.4}

By the end of the 21st century, sea level change will have a strong regional pattern, which will dominate over variability, with many regions *likely* experiencing substantial deviations from the global mean change (Figure TS.23). It is *very likely* that over about 95% of the ocean will experience regional relative sea level rise, while most regions experiencing a sea level fall are located near current and former glaciers and ice sheets. Local sea level changes deviate more than 10% and 25% from the global mean projection for as much as 30% and 9% of the ocean area, respectively, indicating that spatial variations can be large. Regional changes in sea level reach values of up to 30% above the global mean value in the Southern Ocean and around North America, between 10% and 20% in equatorial regions, and up to 50% below the global mean in the Arctic region and some regions near Antarctica. About 70% of the coastlines worldwide are projected to experience a relative sea level change within 20% of the GMSL change. Over decadal periods, the rates of regional relative sea level change as a result of climate variability can differ from the global average rate by more than 100%. {13.6.5}

TS.5.7.4 Projections of Change in Sea Level Extremes and Waves During the 21st Century

It is *very likely* that there will be a significant increase in the occurrence of future sea level extremes by the end of the 21st century, with a *likely* increase in the early 21st century (see TFE.9, Table 1). This increase will primarily be the result of an increase in mean sea level (*high confidence*), with extreme return periods decreasing by at least an order of magnitude in some regions by the end of the 21st century. There is *low confidence* in region-specific projections of storminess and associated storm surges. {13.7.2}

It is *likely (medium confidence)* that annual mean significant wave heights will increase in the Southern Ocean as a result of enhanced wind speeds. Southern Ocean-generated swells are *likely* to affect heights, periods and directions of waves in adjacent basins. It is *very likely* that wave heights and the duration of the wave season will increase in the Arctic Ocean as a result of reduced sea ice extent. In general, there is *low confidence* in region-specific projections due to the *low confidence* in tropical and extratropical storm projections, and to the challenge of down-scaling future wind states from coarse resolution climate models. {13.7.3}

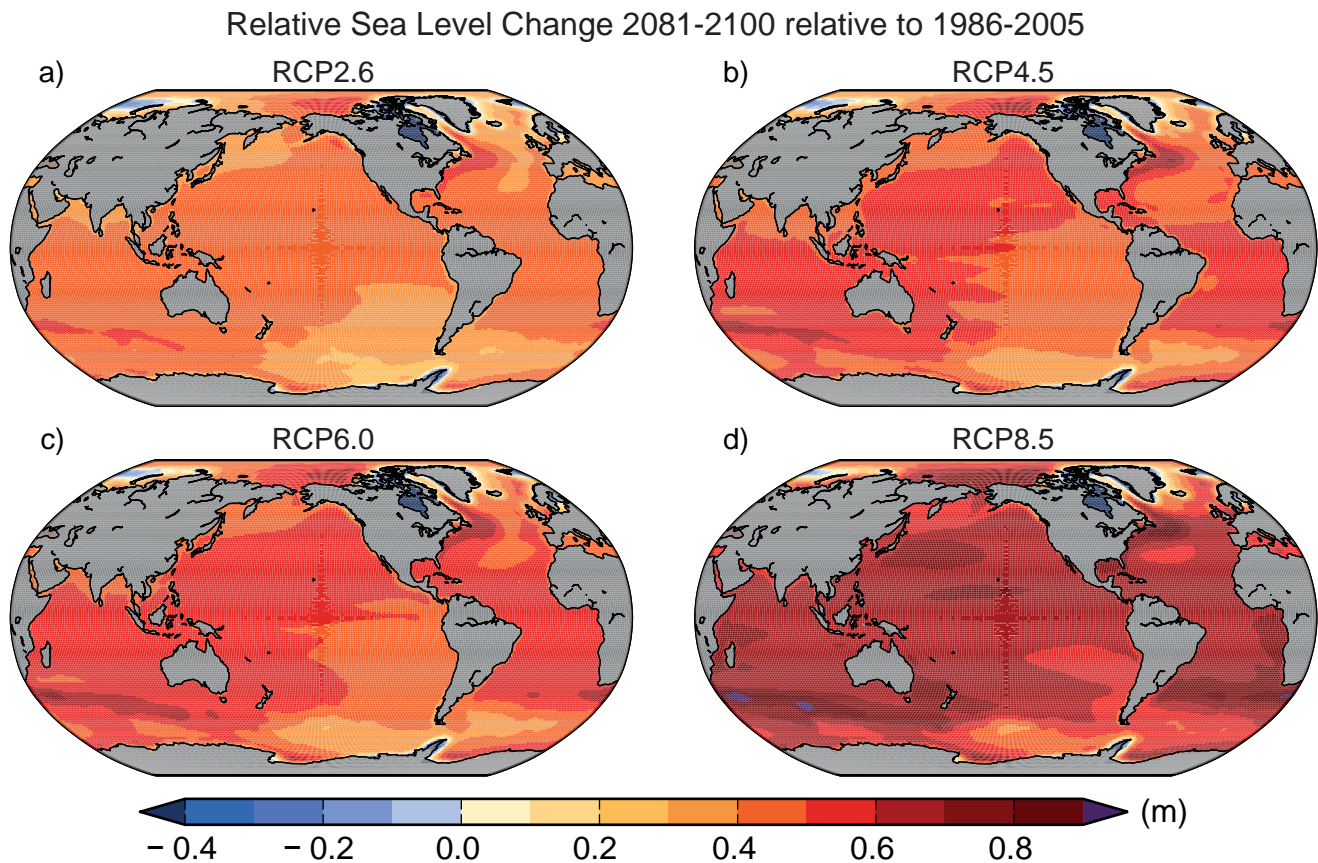


Figure TS.23 | Ensemble mean net regional relative sea level change (metres) evaluated from 21 CMIP5 models for the RCP scenarios (a) 2.6, (b) 4.5, (c) 6.0 and (d) 8.5 between 1986–2005 and 2081–2100. Each map includes effects of atmospheric loading, plus land-ice, glacial isostatic adjustment (GIA) and terrestrial water sources. {Figure 13.20}

Thematic Focus Elements

TFE.8 | Climate Targets and Stabilization

The concept of stabilization is strongly linked to the ultimate objective of the United Nations Framework Convention on Climate Change (UNFCCC), which is ‘to achieve [...] stabilization of greenhouse gas concentrations in the atmosphere at a level that would prevent dangerous anthropogenic interference with the climate system’. Recent policy discussions focused on limits to a global temperature increase, rather than to greenhouse gas (GHG) concentrations, as climate targets in the context of the UNFCCC objectives. The most widely discussed is that of 2°C, that is, to limit global temperature increase relative to pre-industrial times to below 2°C, but targets other than 2°C have been proposed (e.g., returning warming to well below 1.5°C global warming relative to pre-industrial, or returning below an atmospheric carbon dioxide (CO₂) concentration of 350 ppm). Climate targets generally mean avoiding a warming beyond a predefined threshold. Climate impacts, however, are geographically diverse and sector specific, and no objective threshold defines when dangerous interference is reached. Some changes may be delayed or irreversible, and some impacts could be beneficial. It is thus not possible to define a single critical objective threshold without value judgements and without assumptions on how to aggregate current and future costs and benefits. This TFE does not advocate or defend any threshold or objective, nor does it judge the economic or political feasibility of such goals, but assesses, based on the current understanding of climate and carbon cycle feedbacks, the climate projections following the Representative Concentration Pathways (RCPs) in the context of climate targets, and the implications of different long-term temperature stabilization objectives on allowed carbon emissions. Further below it is highlighted that temperature stabilization does not necessarily imply stabilization of the entire Earth system. {12.5.4}

Temperature targets imply an upper limit on the total radiative forcing (RF). Differences in RF between the four RCP scenarios are relatively small up to 2030, but become very large by the end of the 21st century and dominated by CO₂ forcing. Consequently, in the near term, global mean surface temperatures (GMSTs) are projected to continue to rise at a similar rate for the four RCP scenarios. Around the mid-21st century, the rate of global warming begins to be more strongly dependent on the scenario. By the end of the 21st century, global mean temperatures will be warmer than present day under all the RCPs, global temperature change being largest (>0.3°C per decade) in the highest RCP8.5 and significantly lower in RCP2.6, particularly after about 2050 when global surface temperature response stabilizes (and declines thereafter) (see Figure TS.15). {11.3.1, 12.3.3, 12.4.1}

In the near term (2016–2035), global mean surface warming is *more likely than not* to exceed 1°C and *very unlikely* to be more than 1.5°C relative to the average from year 1850 to 1900 (assuming 0.61°C warming from 1850–1900 to 1986–2005) (*medium confidence*). By the end of the 21st century (2081–2100), global mean surface warming, relative to 1850–1900, is *likely* to exceed 1.5°C for RCP4.5, RCP6.0 and RCP8.5 (*high confidence*) and is *likely* to exceed 2°C for RCP6.0 and RCP8.5 (*high confidence*). It is *more likely than not* to exceed 2°C for RCP4.5 (*medium confidence*). Global mean surface warming above 2°C under RCP2.6 is *unlikely* (*medium confidence*). Global mean surface warming above 4°C by 2081–2100 is *unlikely* in all RCPs (*high confidence*) except for RCP8.5 where it is *about as likely as not* (*medium confidence*). {11.3.6, 12.4.1; Table 12.3}

Continuing GHG emissions beyond 2100 as in the RCP8.5 extension induces a total RF above 12 W m⁻² by 2300, with global warming reaching 7.8 [3.0 to 12.6] °C for 2281–2300 relative to 1986–2005. Under the RCP4.5 extension, where radiative forcing is kept constant (around 4.5 W m⁻²) beyond 2100, global warming reaches 2.5 [1.5 to 3.5] °C. Global warming reaches 0.6 [0.0 to 1.2] °C under the RCP2.6 extension where sustained negative emissions lead to a further decrease in RF, reaching values below present-day RF by 2300. See also Box TS.7. {12.3.1, 12.4.1, 12.5.1}

The total amount of anthropogenic CO₂ released in the atmosphere since pre-industrial (often termed cumulative carbon emission, although it applies only to CO₂ emissions) is a good indicator of the atmospheric CO₂ concentration and hence of the global warming response. The ratio of GMST change to total cumulative anthropogenic CO₂ emissions is relatively constant over time and independent of the scenario. This near-linear relationship between total CO₂ emissions and global temperature change makes it possible to define a new quantity, the transient climate response to cumulative carbon emission (TCRE), as the transient GMST change for a given amount of cumulated anthropogenic CO₂ emissions, usually 1000 PgC (TFE.8, Figure 1). TCRE is model dependent, as it is a function of the cumulative CO₂ airborne fraction and the transient climate response, both quantities varying significantly across models. Taking into account the available information from multiple lines of evidence (observations, models and process understanding), the near linear relationship between cumulative CO₂ emissions and peak global mean temperature is

(continued on next page)

TFE.8 (continued)

well established in the literature and robust for cumulative total CO₂ emissions up to about 2000 PgC. It is consistent with the relationship inferred from past cumulative CO₂ emissions and observed warming, is supported by process understanding of the carbon cycle and global energy balance, and emerges as a robust result from the entire hierarchy of models. Expert judgment based on the available evidence suggests that TCRE is *likely* between 0.8°C and 2.5°C per 1000 PgC, for cumulative emissions less than about 2000 PgC until the time at which temperature peaks (TFE.8, Figure 1a). {6.4.3, 12.5.4; Box 12.2}

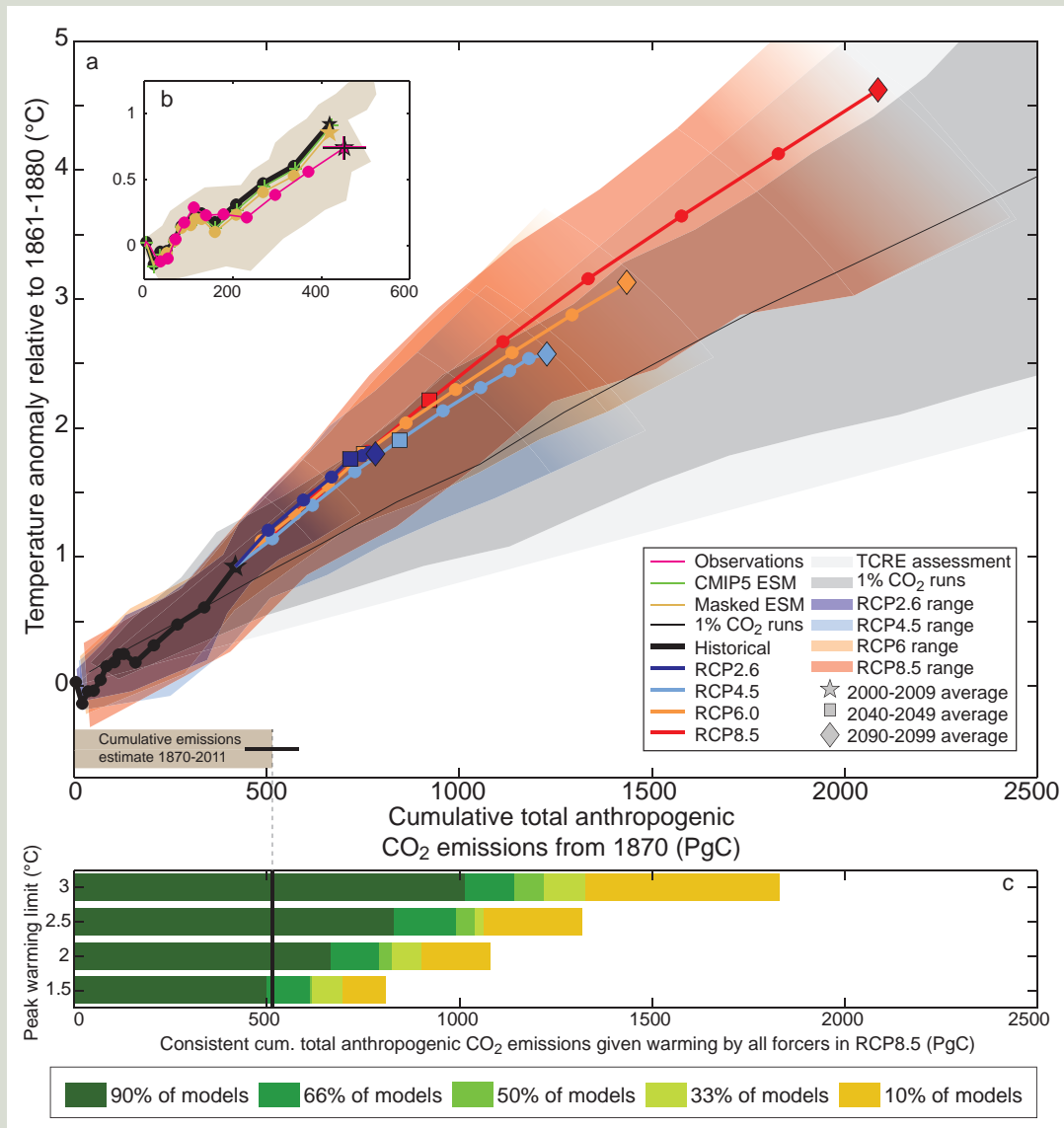
CO₂-induced warming is projected to remain approximately constant for many centuries following a complete cessation of emissions. A large fraction of climate change is thus irreversible on a human time scale, except if net anthropogenic CO₂ emissions were strongly negative over a sustained period. Based on the assessment of TCRE (assuming a normal distribution with a ± 1 standard deviation range of 0.8 to 2.5°C per 1000 PgC), limiting the warming caused by anthropogenic CO₂ emissions alone (i.e., ignoring other radiative forcings) to less than 2°C since the period 1861–1880 with a probability of >33%, >50% and >66%, total CO₂ emissions from all anthropogenic sources would need to be below a cumulative budget of about 1570 PgC, 1210 PgC and 1000 PgC since 1870, respectively. An amount of 515 [445 to 585] PgC was emitted between 1870 and 2011 (TFE.8, Figure 1a,b). Higher emissions in earlier decades therefore imply lower or even negative emissions later on. Accounting for non-CO₂ forcings contributing to peak warming implies lower cumulated CO₂ emissions. Non-CO₂ forcing constituents are important, requiring either assumptions on how CO₂ emission reductions are linked to changes in other forcings, or separate emission budgets and climate modelling for short-lived and long-lived gases. So far, not many studies have considered non-CO₂ forcings. Those that do consider them found significant effects, in particular warming of several tenths of a degree for abrupt reductions in emissions of short-lived species, like aerosols. Accounting for an unanticipated release of GHGs from permafrost or methane hydrates, not included in studies assessed here, would also reduce the anthropogenic CO₂ emissions compatible with a given temperature target. Requiring a higher likelihood of temperatures remaining below a given temperature target would further reduce the compatible emissions (TFE.8, Figure 1c). When accounting for the non-CO₂ forcings as in the RCP scenarios, compatible carbon emissions since 1870 are reduced to about 900 PgC, 820 PgC and 790 PgC to limit warming to less than 2°C since the period 1861–1880 with a probability of >33%, >50%, and >66%, respectively. These estimates were derived by computing the fraction of the Coupled Model Intercomparison Project Phase 5 (CMIP5) Earth System Models (ESMs) and Earth System Models of Intermediate Complexity (EMICs) that stay below 2°C for given cumulative emissions following RCP8.5, as shown in TFE.8 Fig. 1c. The non-CO₂ forcing in RCP8.5 is higher than in RCP2.6. Because all likelihood statements in calibrated IPCC language are open intervals, the estimates provided are thus both conservative and consistent choices valid for non-CO₂ forcings across all RCP scenarios. There is no RCP scenario which limits warming to 2°C with probabilities of >33% or >50%, and which could be used to directly infer compatible cumulative emissions. For a probability of >66% RCP2.6 can be used as a comparison. Combining the average back-calculated fossil fuel carbon emissions for RCP2.6 between 2012 and 2100 (270 PgC) with the average historical estimate of 515 PgC gives a total of 785 PgC, i.e., 790 PgC when rounded to 10 PgC. As the 785 PgC estimate excludes an explicit assessment of future land-use change emissions, the 790 PgC value also remains a conservative estimate consistent with the overall likelihood assessment. The ranges of emissions for these three likelihoods based on the RCP scenarios are rather narrow, as they are based on a single scenario and on the limited sample of models available (TFE.8 Fig. 1c). In contrast to TCRE they do not include observational constraints or account for sources of uncertainty not sampled by the models. The concept of a fixed cumulative CO₂ budget holds not just for 2°C, but for any temperature level explored with models so far (up to about 5°C, see Figures 12.44 to 12.46). Higher temperature targets would allow larger cumulative budgets, while lower temperature target would require lower cumulative budgets (TFE.8, Figure 1). {6.3.1, 12.5.2, 12.5.4}

The climate system has multiple time scales, ranging from annual to multi-millennial, associated with different thermal and carbon reservoirs. These long time scales induce a commitment warming ‘already in the pipe-line’. Stabilization of the forcing would not lead to an instantaneous stabilization of the warming. For the RCP scenarios and their extensions to 2300, the fraction of realized warming, at that time when RF stabilizes, would be about 75 to 85% of the equilibrium warming. For a 1% yr⁻¹ CO₂ increase to 2 × CO₂ or 4 × CO₂ and constant forcing thereafter, the fraction of realized warming would be much smaller, about 40 to 70% at the time when the forcing is kept constant. Owing to the long time scales in the deep ocean, full equilibrium is reached only after hundreds to thousands of years. {12.5.4}

(continued on next page)

TS

TFE.8 (continued)



TFE.8, Figure 1 | Global mean temperature increase since 1861–1880 as a function of cumulative total global CO₂ emissions from various lines of evidence. (a) Decadal average results are shown over all CMIP5 Earth System Model of Intermediate Complexity (EMICs) and Earth System Models (ESMs) for each RCP respectively, with coloured lines (multi-model average), decadal markers (dots) and with three decades (2000–2009, 2040–2049 and 2090–2099) highlighted with a star, square and diamond, respectively. The historical time period up to decade 2000–2009 is taken from the CMIP5 historical runs prolonged by RCP8.5 for 2006–2010 and is indicated with a black thick line and black symbols. Coloured ranges illustrate the model spread (90% range) over all CMIP5 ESMs and EMICs and do not represent a formal uncertainty assessment. Ranges are filled as long as data of all models is available and until peak temperature. They are faded out for illustrative purposes afterward. CMIP5 simulations with 1% yr⁻¹ CO₂ increase only are illustrated by the dark grey area (range definition similar to RCPs above) and the black thin line (multi-model average). The light grey cone represents this Report’s assessment of the transient climate response to emissions (TCRE) from CO₂ only. Estimated cumulative historical CO₂ emissions from 1870 to 2011 with associated uncertainties are illustrated by the grey bar at the bottom of (a). (b) Comparison of historical model results with observations. The magenta line and uncertainty ranges are based on observed emissions from Carbon Dioxide Information Analysis Center (CDIAC) extended by values of the Global Carbon project until 2010 and observed temperature estimates of the Hadley Centre/Climatic Research Unit gridded surface temperature data set 4 (HadCRUT4). The uncertainties in the last decade of observations are based on the assessment in this report. The black thick line is identical to the one in (a). The thin green line with crosses is as the black line but for ESMs only. The yellow-brown line and range show these ESM results until 2010, when corrected for HadCRUT4’s incomplete geographical coverage over time. All values are given relative to the 1861–1880 base period. All time-series are derived from decadal averages to illustrate the long-term trends. Note that observations are in addition subject to internal climate variability, adding an uncertainty of about 0.1°C. (c) Cumulative CO₂ emissions over the entire industrial era, consistent with four illustrative peak global temperature limits (1.5°C, 2°C, 2.5°C and 3°C, respectively) when taking into account warming by all forcers. Horizontal bars indicate consistent cumulative emission budgets as a function of the fraction of models (CMIP5 ESMs and EMICs) that at least hold warming below a given temperature limit. Note that the fraction of models cannot be interpreted as a probability. The budgets are derived from the RCP8.5 runs, with relative high non-CO₂ forcing over the 21st century. If non-CO₂ are significantly reduced, the CO₂ emissions compatible with a specific temperature limit might be slightly higher, but only to a very limited degree, as illustrated by the other coloured lines in (a), which assume significantly lower non-CO₂ forcing. Further detail regarding the related Figure SPM.10 is given in the TS Supplementary Material. {Figure 12.45}

TFE.8 (continued)

The commitment to past emissions is a persistent warming for hundreds of years, continuing at about the level of warming that has been realized when emissions were ceased. The persistence of this CO₂-induced warming after emission have ceased results from a compensation between the delayed commitment warming described above and the slow reduction in atmospheric CO₂ resulting from ocean and land carbon uptake. This persistence of warming also results from the nonlinear dependence of RF on atmospheric CO₂, that is, the relative decrease in forcing being smaller than the relative decrease in CO₂ concentration. For high climate sensitivities, and in particular if sulphate aerosol emissions are eliminated at the same time as GHG emissions, the commitment from past emission can be strongly positive, and is a superposition of a fast response to reduced aerosols emissions and a slow response to reduced CO₂. {12.5.4}

Stabilization of global temperature does not imply stabilization for all aspects of the climate system. Processes related to vegetation change, changes in the ice sheets, deep ocean warming and associated sea level rise and potential feedbacks linking, for example, ocean and the ice sheets have their own intrinsic long time scales. Ocean acidification will *very likely* continue in the future as long as the oceans will continue to take up atmospheric CO₂. Committed land ecosystem carbon cycle changes will manifest themselves further beyond the end of the 21st century. It is *virtually certain* that global mean sea level rise will continue beyond 2100, with sea level rise due to thermal expansion to continue for centuries to millennia. Global mean sea level rise depends on the pathway of CO₂ emissions, not only on the cumulative total; reducing emissions earlier rather than later, for the same cumulative total, leads to a larger mitigation of sea level rise. {6.4.4, 12.5.4, 13.5.4}

TS

TS.5.8 Climate Phenomena and Regional Climate Change

This section assesses projected changes over the 21st century in large-scale climate phenomena that affect regional climate (Table TS.2). Some of these phenomena are defined by climatology (e.g., monsoons), and some by interannual variability (e.g., El Niño), the latter affecting climate extremes such as floods, droughts and heat waves. Changes in statistics of weather phenomena such as tropical cyclones and extratropical storms are also summarized here. {14.8}

TS.5.8.1 Monsoon Systems

Global measures of monsoon by the area and summer precipitation are *likely* to increase in the 21st century, while the monsoon circulation weakens. Monsoon onset dates are *likely* to become earlier or not to change much while monsoon withdrawal dates are *likely* to delay, resulting in a lengthening of the monsoon season in many regions (Figure TS.24). The increase in seasonal mean precipitation is pronounced in the East and South Asian summer monsoons while the change in other monsoon regions is subject to larger uncertainties. {14.2.1}

There is *medium confidence* that monsoon-related interannual rainfall variability will increase in the future. Future increase in precipitation extremes related to the monsoon is *very likely* in South America, Africa, East Asia, South Asia, Southeast Asia and Australia. {14.2.1, 14.8.5, 14.8.7, 14.8.9, 14.8.11–14.8.13}

There is *medium confidence* that overall precipitation associated with the Asian-Australian monsoon will increase but with a north–south asymmetry: Indian monsoon rainfall is projected to increase, while projected changes in the Australian summer monsoon rainfall are

small. There is *medium confidence* in that the Indian summer monsoon circulation weakens, but this is compensated by increased atmospheric moisture content, leading to more rainfall. For the East Asian summer monsoon, both monsoon circulation and rainfall are projected to increase. {14.2.2, 14.8.9, 14.8.11, 14.8.13}

There is *low confidence* in projections of the North American and South American monsoon precipitation changes, but *medium confidence* that the North American monsoon will arrive and persist later in the annual cycle, and *high confidence* in expansion of South American Monsoon area. {14.2.3, 14.8.3–14.8.5}

There is *low confidence* in projections of a small delay in the West African rainy season, with an intensification of late-season rains. The limited skills of model simulations for the region suggest *low confidence* in the projections. {14.2.4, 14.8.7}

TS.5.8.2 Tropical Phenomena

Precipitation change varies in space, increasing in some regions and decreasing in some others. The spatial distribution of tropical rainfall changes is *likely* shaped by the current climatology and ocean warming pattern. The first effect is to increase rainfall near the currently rainy regions, and the second effect increases rainfall where the ocean warming exceeds the tropical mean. There is *medium confidence* that tropical rainfall projections are more reliable for the seasonal than annual mean changes. {7.6.2, 12.4.5, 14.3.1}

There is *medium confidence* in future increase in seasonal mean precipitation on the equatorial flank of the Intertropical Convergence Zone and a decrease in precipitation in the subtropics including parts

Table TS.2 | Overview of projected regional changes and their relation to major climate phenomena. A phenomenon is considered relevant when there is both sufficient confidence that it has an influence on the given region, and when there is sufficient confidence that the phenomenon will change, particularly under the RCP4.5 or higher end scenarios. See Section 14.8 and Tables 14.2 and 14.3 for full assessment of the confidence in these changes, and their relevance for regional climate. {14.8; Tables 14.2, 14.3}

Regions	Projected Major Changes in Relation to Phenomena
Arctic {14.8.2}	Wintertime changes in temperature and precipitation resulting from the small projected increase in North Atlantic Oscillation (NAO); enhanced warming and sea ice melting; significant increase in precipitation by mid-century due mostly to enhanced precipitation in extratropical cyclones.
North America {14.8.3}	Monsoon precipitation will shift later in the annual cycle; increased precipitation in extratropical cyclones will lead to large increases in wintertime precipitation over the northern third of the continent; extreme precipitation increases in tropical cyclones making landfall along the western coast of USA and Mexico, the Gulf Mexico, and the eastern coast of USA and Canada.
Central America and Caribbean {14.8.4}	Projected reduction in mean precipitation and increase in extreme precipitation; more extreme precipitation in tropical cyclones making landfall along the eastern and western coasts.
South America {14.8.5}	A southward displaced South Atlantic Convergence Zone increases precipitation in the southeast; positive trend in the Southern Annular Mode displaces the extratropical storm track southward, decreasing precipitation in central Chile and increasing it at the southern tip of South America.
Europe and Mediterranean {14.8.6}	Enhanced extremes of storm-related precipitation and decreased frequency of storm-related precipitation over the eastern Mediterranean.
Africa {14.8.7}	Enhanced summer monsoon precipitation in West Africa; increased short rain in East Africa due to the pattern of Indian Ocean warming; increased rainfall extremes of landfall cyclones on the east coast (including Madagascar).
Central and North Asia {14.8.8}	Enhanced summer precipitation; enhanced winter warming over North Asia.
East Asia {14.8.9}	Enhanced summer monsoon precipitation; increased rainfall extremes of landfall typhoons on the coast; reduction in the midwinter suppression of extratropical cyclones.
West Asia {14.8.10}	Increased rainfall extremes of landfall cyclones on the Arabian Peninsula; decreased precipitation in northwest Asia due to a northward shift of extratropical storm tracks.
South Asia {14.8.11}	Enhanced summer monsoon precipitation; increased rainfall extremes of landfall cyclones on the coasts of the Bay of Bengal and Arabian Sea.
Southeast Asia {14.8.12}	Reduced precipitation in Indonesia during July to October due to the pattern of Indian Ocean warming; increased rainfall extremes of landfall cyclones on the coasts of the South China Sea, Gulf of Thailand and Andaman Sea.
Australia and New Zealand {14.8.13}	Summer monsoon precipitation may increase over northern Australia; more frequent episodes of the zonal South Pacific Convergence Zone may reduce precipitation in northeastern Australia; increased warming and reduced precipitation in New Zealand and southern Australia due to projected positive trend in the Southern Annular Mode; increased extreme precipitation associated with tropical and extratropical storms
Pacific Islands {14.8.14}	Tropical convergence zone changes affect rainfall and its extremes; more extreme precipitation associated with tropical cyclones
Antarctica {14.8.15}	Increased warming over Antarctic Peninsula and West Antarctic related to the positive trend in the Southern Annular Mode; increased precipitation in coastal areas due to a poleward shift of storm track.

of North and Central Americas, the Caribbean, South America, Africa and West Asia. There is *medium confidence* that the interannual occurrence of zonally oriented South Pacific Convergence Zone events will increase, leading possibly to more frequent droughts in the southwest Pacific. There is *medium confidence* that the South Atlantic Convergence Zone will shift southwards, leading to a precipitation increase over southeastern South America and a reduction immediately north of the convergence zone. {14.3.1, 14.8.3–14.8.5, 14.8.7, 14.8.11, 14.8.14}

The tropical Indian Ocean is *likely* to feature a zonal pattern with reduced warming and decreased rainfall in the east (including Indonesia), and enhanced warming and increased rainfall in the west (including East Africa). The Indian Ocean dipole mode of interannual variability is *very likely* to remain active, affecting climate extremes in East Africa, Indonesia and Australia. {14.3.3, 14.8.7, 14.8.12}

There is *low confidence* in the projections for the tropical Atlantic—both for the mean and interannual modes, because of large errors in model simulations in the region. Future projections in Atlantic hurricanes and tropical South American and West African precipitation are therefore of *low confidence*. {14.3.4, 14.6.1, 14.8.5, 14.8.7}

It is currently not possible to assess how the Madden–Julian Oscillation will change owing to the poor skill in model simulations of this intraseasonal phenomenon and the sensitivity to ocean warming patterns. Future projections of regional climate extremes in West Asia, Southeast Asia and Australia are therefore of *low confidence*. {5.5.2, 14.3.4, 14.8.10, 14.8.12, 14.8.13}

TS.5.8.3 El Niño-Southern Oscillation

There is *high confidence* that the El Niño-Southern Oscillation (ENSO) will remain the dominant mode of natural climate variability in the 21st century with global influences in the 21st century, and that regional rainfall variability it induces *likely* intensifies. Natural variations of the amplitude and spatial pattern of ENSO are so large that *confidence* in any projected change for the 21st century remains *low*. The projected change in El Niño amplitude is small for both RCP4.5 and RCP8.5 compared to the spread of the change among models (Figure TS.25). Over the North Pacific and North America, patterns of temperature and precipitation anomalies related to El Niño and La Niña (teleconnections) are *likely* to move eastwards in the future (*medium confidence*), while *confidence* is *low* in changes in climate impacts on other regions including Central and South Americas, the Caribbean, Africa, most of Asia, Australia and most Pacific Islands. In a warmer climate, the increase in atmospheric moisture intensifies temporal variability

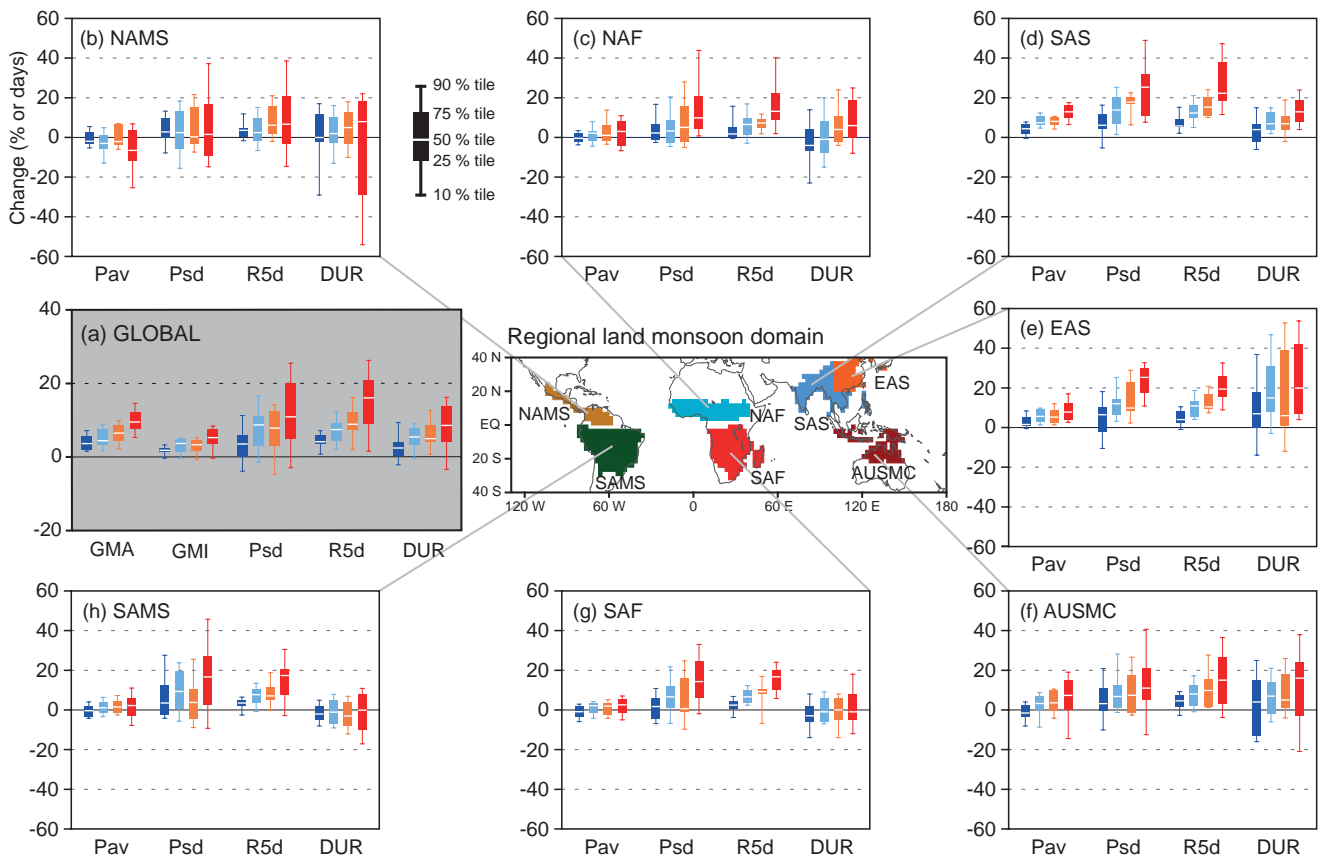


Figure TS.24 | Future change in monsoon statistics between the present-day (1986–2005) and the future (2080–2099) based on CMIP5 ensemble from RCP2.6 (dark blue; 18 models), RCP4.5 (blue; 24), RCP6.0 (yellow; 14), and RCP8.5 (red; 26) simulations. (a) GLOBAL: Global monsoon area (GMA), global monsoon intensity (GMI), standard deviation of inter-annual variability in seasonal precipitation (Psd), seasonal maximum 5-day precipitation total (R5d) and monsoon season duration (DUR). Regional land monsoon domains determined by 24 multi-model mean precipitation in the present-day. (b)–(h) Future change in regional land monsoon statistics: seasonal average precipitation (Pav), Psd, R5d, and DUR in (b) North America (NAMS), (c) North Africa (NAF), (d) South Asia (SAS), (e) East Asia (EAS), (f) Australia-Maritime continent (AUSMC), (g) South Africa (SAF) and (h) South America (SAMS). Units are % except for DUR (days). Box-and-whisker plots show the 10th, 25th, 50th, 75th and 90th percentiles. All the indices are calculated for the summer season (May to September for the Northern, and November to March for the Southern Hemisphere) over each model’s monsoon domains. [Figures 14.3, 14.4, 14.6, 14.7]

TS

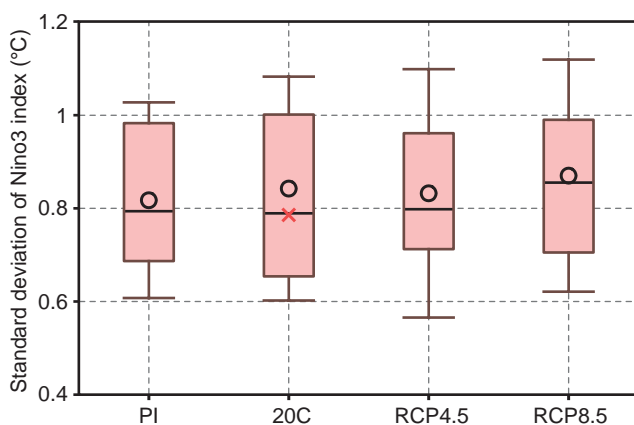


Figure TS.25 | Standard deviation in CMIP5 multi-model ensembles of sea surface temperature variability over the eastern equatorial Pacific Ocean (Nino3 region: 5°S to 5°N, 150°W to 90°W), a measure of El Niño amplitude, for the pre-industrial (PI) control and 20th century (20C) simulations, and 21st century projections using RCP4.5 and RCP8.5. Open circles indicate multi-model ensemble means, and the red cross symbol is the observed standard deviation for the 20th century. Box-and-whisker plots show the 16th, 25th, 50th, 75th and 84th percentiles. [Figure 14.14]

of precipitation even if atmospheric circulation variability remains the same. This applies to ENSO-induced precipitation variability but the possibility of changes in ENSO teleconnections complicates this general conclusion, making it somewhat regional-dependent. {12.4.5, 14.4, 14.8.3–14.8.5, 14.8.7, 14.8.9, 14.8.11–14.8.14}

TS.5.8.4 Cyclones

Projections for the 21st century indicate that it is *likely* that the global frequency of tropical cyclones will either decrease or remain essentially unchanged, concurrent with a *likely* increase in both global mean tropical cyclone maximum wind speed and rain rates (Figure TS.26). The influence of future climate change on tropical cyclones is *likely* to vary by region, but there is *low confidence* in region-specific projections. The frequency of the most intense storms will *more likely than not* increase in some basins. More extreme precipitation near the centers of tropical cyclones making landfall is projected in North and Central America, East Africa, West, East, South and Southeast Asia as well as in Australia and many Pacific islands (*medium confidence*). {14.6.1, 14.8.3, 14.8.4, 14.8.7, 14.8.9–14.8.14}

The global number of extratropical cyclones is *unlikely* to decrease by more than a few percent and future changes in storms are *likely* to be small compared to natural interannual variability and substantial variations between models. A small poleward shift is *likely* in the SH storm track but the magnitude of this change is model dependent. It is *unlikely* that the response of the North Atlantic storm track in climate projections is a simple poleward shift. There is *medium confidence* in a projected poleward shift in the North Pacific storm track. There is *low confidence* in the impact of storm track changes on regional climate at the surface. More precipitation in extratropical cyclones leads to a winter precipitation increase in Arctic, Northern Europe, North America and the mid-to-high-latitude SH. {11.3.2, 12.4.4, 14.6.2, 14.8.2, 14.8.3, 14.8.5, 14.8.6, 14.8.13, 14.8.15}

TS.5.8.5 Annular and Dipolar Modes of Variability

Future boreal wintertime North Atlantic Oscillation (NAO) is *very likely* to exhibit large natural variations as observed in the past. The NAO is *likely* to become slightly more positive (on average), with some, but not very well documented implications for winter conditions in the Arctic,

North America and Eurasia. The austral summer/autumn positive trend in Southern Annular Mode (SAM) is *likely* to weaken considerably as stratospheric ozone recovers through the mid-21st century with some, but not very well documented, implications for South America, Africa, Australia, New Zealand and Antarctica. {11.3.2, 14.5.2, 14.8.5, 14.8.7, 14.8.13, 14.8.15}

TS.5.8.6 Additional Phenomena

It is *unlikely* that the Atlantic Multi-decadal Oscillation (AMO) will change its behaviour as the mean climate changes. However, natural fluctuations in the AMO over the coming few decades are *likely* to influence regional climates at least as strongly as will human-induced changes with implications for Atlantic major hurricane frequency, the West African monsoon and North American and European summer conditions. {14.2.4, 14.5.1, 14.6.1, 14.7.6, 14.8.2, 14.8.3, 14.8.6, 14.8.8}

There is *medium confidence* that the frequency of NH and SH blocking will not increase, while the trends in blocking intensity and persistence remain uncertain. {Box 14.2}

TS

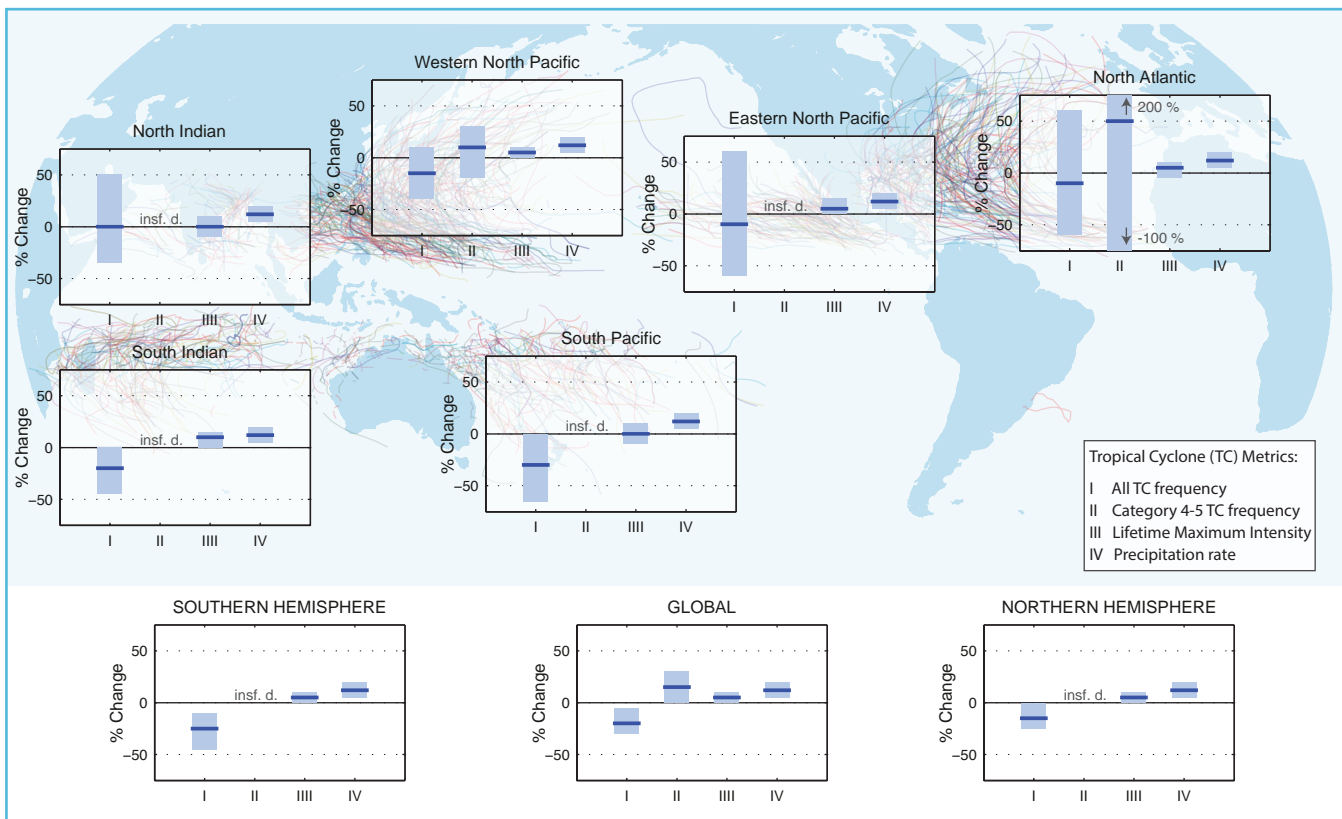


Figure TS.26 | Projected changes in tropical cyclone statistics. All values represent expected percent change in the average over period 2081–2100 relative to 2000–2019, under an A1B-like scenario, based on expert judgement after subjective normalization of the model projections. Four metrics were considered: the percent change in I) the total annual frequency of tropical storms, II) the annual frequency of Category 4 and 5 storms, III) the mean Lifetime Maximum Intensity (LMI; the maximum intensity achieved during a storm’s lifetime) and IV) the precipitation rate within 200 km of storm center at the time of LMI. For each metric plotted, the solid blue line is the best guess of the expected percent change, and the coloured bar provides the 67% (*likely*) confidence interval for this value (note that this interval ranges across –100% to +200% for the annual frequency of Category 4 and 5 storms in the North Atlantic). Where a metric is not plotted, there are insufficient data (denoted X) available to complete an assessment. A randomly drawn (and coloured) selection of historical storm tracks are underlaid to identify regions of tropical cyclone activity. See Section 14.6.1 for details. {14.6.1}

Thematic Focus Elements

TFE.9 | Climate Extremes

Assessing changes in climate extremes poses unique challenges, not just because of the intrinsically rare nature of these events, but because they invariably happen in conjunction with disruptive conditions. They are strongly influenced by both small- and large-scale weather patterns, modes of variability, thermodynamic processes, land-atmosphere feedbacks and antecedent conditions. Much progress has been made since the IPCC Fourth Assessment Report (AR4) including the comprehensive assessment of extremes undertaken by the IPCC Special Report on Managing the Risk of Extreme Events and Disasters to Advance Climate Change Adaptation (SREX) but also because of the amount of observational evidence available, improvements in our understanding and the ability of models to simulate extremes. {1.3.3, 2.6, 7.6, 9.5.4}

For some climate extremes such as droughts, floods and heat waves, several factors need to be combined to produce an extreme event. Analyses of rarer extremes such as 1-in-20- to 1-in-100-year events using Extreme Value Theory are making their way into a growing body of literature. Other recent advances concern the notion of 'fraction of attributable risk' that aims to link a particular extreme event to specific causal relationships. {1.3.3, 2.6.1, 2.6.2, 10.6.2, 12.4.3; Box 2.4}

TFE.9, Table 1 indicates the changes that have been observed in a range of weather and climate extremes over the last 50 years, the assessment of the human contribution to those changes, and how those extremes are expected to change in the future. The table also compares the current assessment with that of the AR4 and the SREX where applicable. {2.6, 3.7, 10.6, 11.3, 12.4, 14.6}

Temperature Extremes, Heat Waves and Warm Spells

It is *very likely* that both maximum and minimum temperature extremes have warmed over most land areas since the mid-20th century. These changes are well simulated by current climate models, and it is *very likely* that anthropogenic forcing has affected the frequency of these extremes and *virtually certain* that further changes will occur. This supports AR4 and SREX conclusions although with greater confidence in the anthropogenic forcing component. {2.6.1, 9.5.4, 10.6.1, 12.4.3}

For land areas with sufficient data there has been an overall increase in the number of warm days and nights. Similar decreases are seen in the number of cold days and nights. It is *very likely* that increases in unusually warm days and nights and/or reductions in unusually cold days and nights including frosts have occurred over this period across most continents. Warm spells or heat waves containing consecutive extremely hot days or nights are often associated with quasi-stationary anticyclonic circulation anomalies and are also affected by pre-existing soil conditions and the persistence of soil moisture anomalies that can amplify or dampen heat waves particularly in moisture-limited regions. Most global land areas, with a few exceptions, have experienced more heat waves since the middle of the 20th century. Several studies suggest that increases in mean temperature account for most of the changes in heat wave frequency, however, heat wave intensity/amplitude is highly sensitive to changes in temperature variability and the shape of the temperature distribution and heat wave definition also plays a role. Although in some regions instrumental periods prior to the 1950s had more heat waves (e.g., USA), for other regions such as Europe, an increase in heat wave frequency in the period since the 1950s stands out in long historical temperature series. {2.6, 2.6.1, 5.5.1; Box 2.4; Tables 2.12, 2.13; FAQ 2.2}

The observed features of temperature extremes and heat waves are well simulated by climate models and are similar to the spread among observationally based estimates in most regions. Regional downscaling now offers credible information on the spatial scales required for assessing extremes and improvements in the simulation of the El Niño-Southern Oscillation from Coupled Model Intercomparison Project Phase 3 (CMIP3) to Phase 5 (CMIP5) and other large-scale phenomena is crucial. However simulated changes in frequency and intensity of extreme events is limited by observed data availability and quality issues and by the ability of models to reliably simulate certain feedbacks and mean changes in key features of circulation such as blocking. {2.6, 2.7, 9.4, 9.5.3, 9.5.4, 9.6, 9.6.1, 10.3, 10.6, 14.4; Box 14.2}

Since AR4, the understanding of mechanisms and feedbacks leading to changes in extremes has improved. There continues to be strengthening evidence for a human influence on the observed frequency of extreme temperatures and heat waves in some regions. Near-term (decadal) projections suggest *likely* increases in temperature extremes but with little distinguishable separation between emissions scenarios (TFE.9, Figure 1). Changes may proceed at

(continued on next page)

TS

TFE.9, Table 1 | Extreme weather and climate events: Global-scale assessment of recent observed changes, human contribution to the changes and projected further changes for the early (2016–2035) and late (2081–2100) 21st century. Bold indicates where the AR5 (black) provides a revised* global-scale assessment from the Special Report on Managing the Risk of Extreme Events and Disasters to Advance Climate Change Adaptation (SREX, blue) or AR4 (red). Projections for early 21st century were not provided in previous assessment reports. Projections in the AR5 are relative to the reference period of 1986–2005, and use the new RCP scenarios unless otherwise specified. See the Glossary for definitions of extreme weather and climate events.

Phenomenon and direction of trend	Assessment that changes occurred (typically since 1950 unless otherwise indicated)	Assessment of a human contribution to observed changes	Likelihood of further changes	
			Early 21st century	Late 21st century
Warmer and/or fewer cold days and nights over most land areas	Very likely {2.6} Very likely Very likely	Very likely {10.6}	Likely {11.3}	Virtually certain {12.4}
Warmer and/or more frequent hot days and nights over most land areas	Very likely {2.6}	Very likely {10.6}	Likely {11.3}	Virtually certain {12.4}
Warm spells/heat waves. Frequency and/or duration increases over most land areas	Medium confidence on a global scale Likely in large parts of Europe, Asia and Australia {2.6}	Likely* {10.6}	Not formally assessed ^b {11.3}	Very likely {12.4}
Heavy precipitation events. Increase in the frequency, intensity, and/or amount of heavy precipitation	Medium confidence in many (but not all) regions Likely {2.6}	Not formally assessed More likely than not {10.6}	Likely over many land areas {11.3}	Very likely over most of the mid-latitude land masses and over wet tropical regions {12.4}
Increases in intensity and/or duration of drought	Likely more land areas with increases than decreases ^c {2.6}	Medium confidence More likely than not {10.6}	Likely over many areas Very likely over most land areas {11.3}	Likely (medium confidence) on a regional to global scale ^d {12.4}
Increases in intense tropical cyclone activity	Low confidence on a global scale Likely changes in some regions ^e {2.6}	Low confidence {10.6}	Low confidence ^e {11.3}	Medium confidence in some regions Likely ^f {12.4}
Increased incidence and/or magnitude of extreme high sea level	Low confidence in long term (centennial) changes Virtually certain in North Atlantic since 1970 {2.6}	Low confidence ^g {10.6}	Low confidence {11.3}	More likely than not in the Western North Pacific and North Atlantic ^h {14.6}
	Low confidence Likely in some regions, since 1970	Low confidence More likely than not	Likely ⁱ {13.7}	More likely than not in some basins Likely {13.7}
	Likely (since 1970)	Likely* {3.7}	Likely ^j {13.7}	Very likely ^k {13.7}
	Likely (late 20th century)	Likely* More likely than not ^l	Likely ^m More likely than not ⁿ	Very likely ^o Likely

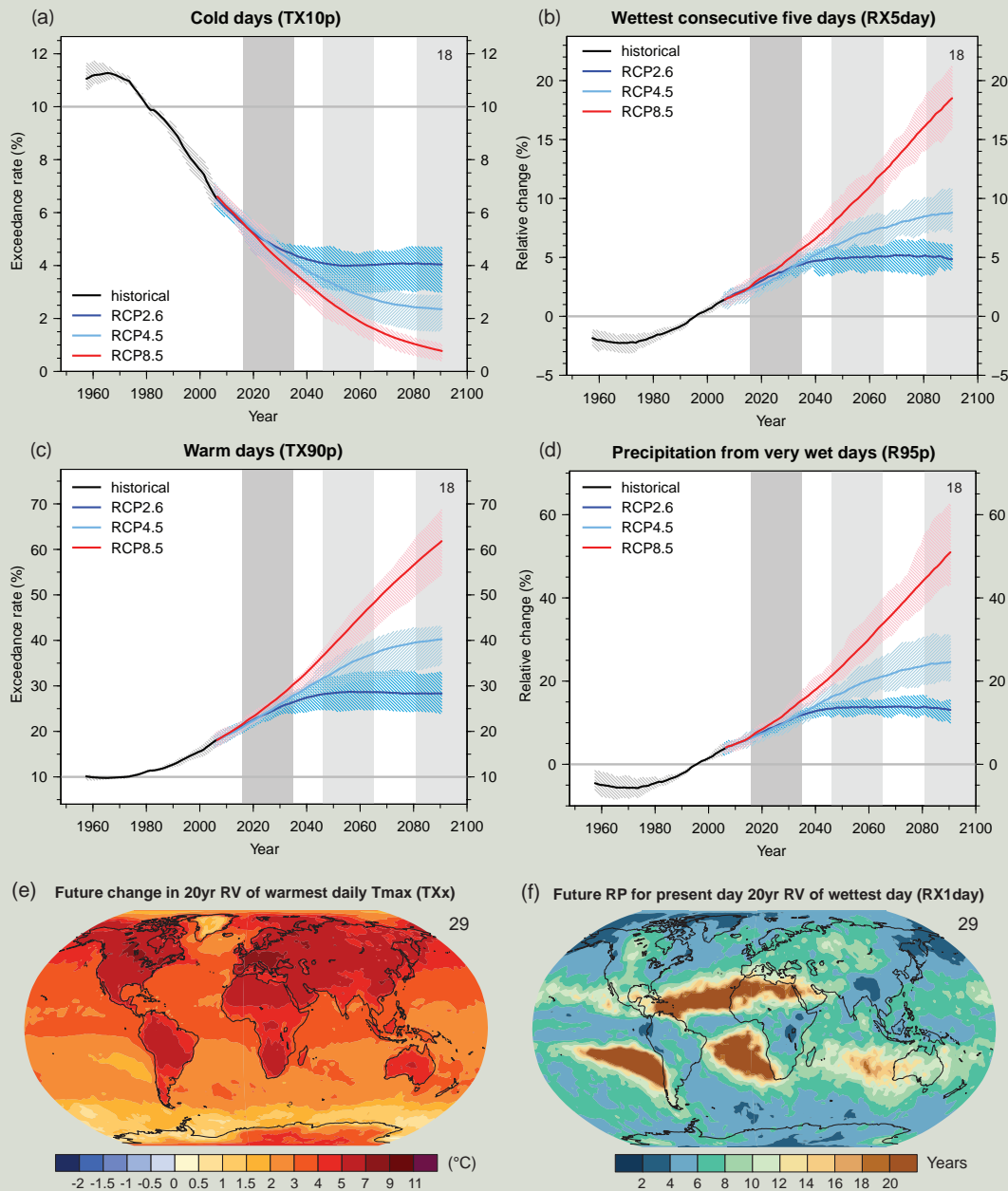
* The direct comparison of assessment findings between reports is difficult. For some climate variables, different aspects have been assessed, and the revised guidance note on uncertainties has been used for the SREX and AR5. The availability of new information, improved scientific understanding, continued analyses of data and models, and specific differences in methodologies applied in the assessed studies, all contribute to revised assessment findings.

Notes:
 a Attribution is based on available case studies. It is likely that human influence has more than doubled the probability of occurrence of some observed heat waves in some locations.
 b Models project near-term increases in the duration, intensity and spatial extent of heat waves and warm spells.
 c In most continents, confidence in trends is not higher than medium except in North America and Europe where there have been likely increases in either the frequency or intensity of heavy precipitation with some seasonal and/or regional variation. It is very likely that there have been increases in central North America.
 d The frequency and intensity of drought has likely increased in the Mediterranean and West Africa and likely decreased in central North America and north-west Australia.
 e AR4 assessed the area affected by drought.
 f SREX assessed medium confidence that anthropogenic influence had contributed to some changes in the drought patterns observed in the second half of the 20th century, based on its attributed impact on precipitation and temperature changes. SREX assessed low confidence in the attribution of changes in droughts at the level of single regions.
 g There is low confidence in projected changes in soil moisture.
 h Regional to global-scale projected decreases in soil moisture and increased agricultural drought are likely (medium confidence) in presently dry regions by the end of this century under the RCP8.5 scenario. Soil moisture drying in the Mediterranean, Southwest USA and southern African regions is consistent with projected changes in Hadley circulation and increased surface temperatures, so there is high confidence in likely surface drying in these regions by the end of this century under the RCP8.5 scenario.
 i Based on expert judgment and assessment of projections which use an SRES A1B (or similar) scenario.
 j Attribution is based on the close relationship between observed changes in extreme and mean sea level.
 k There is high confidence that this increase in extreme high sea level will primarily be the result of an increase in mean sea level. There is low confidence in region-specific projections of storminess and associated storm surges.
 l SREX assessed it to be very likely that mean sea level rise will contribute to future upward trends in extreme coastal high water levels.

TFE.9 (continued)

a different rate than the mean warming however, with several studies showing that projected European high-percentile summer temperatures will warm faster than mean temperatures. Future changes associated with the warming of temperature extremes in the long-term are *virtually certain* and scale with the strength of emissions scenario, that is, greater anthropogenic emissions correspond to greater warming of extremes (TFE.9, Figure 1). For high-emissions scenarios, it is *likely* that, in most land regions, a current 1-in-20-year maximum temperature event

(continued on next page)



TFE.9, Figure 1 | Global projections of the occurrence of (a) cold days (TX10p)—percentage of days annually with daily maximum surface air temperature (Tmax) below the 10th percentile of Tmax for 1961 to 1990, (b) wettest consecutive five days (RX5day)—percentage change relative to 1986–2005 in annual maximum consecutive 5-day precipitation totals, (c) warm days (TX90p)—percentage of days annually with daily maximum surface air temperature (Tmax) exceeding the 90th percentile of Tmax for 1961 to 1990 and (d) very wet day precipitation (R95p)—percentage change relative to 1986–2005 of annual precipitation from days >95th percentile. Results are shown from CMIP5 for the RCP2.6, RCP4.5 and RCP8.5 scenarios. Solid lines indicate the ensemble median and shading indicates the interquartile spread between individual projections (25th and 75th percentiles). Maps show (e) the change from 1986–2005 to 2081–2100 in 20-year return values (RV) of daily maximum temperatures, TXx, and (f) the 2081–2100 return period (RP) for rare daily precipitation values, RX1day, that have a 20-year return period during 1986–2005. Both maps are based on the CMIP5 RCP8.5 scenario. The number of models used to calculate the multi-model mean is indicated in each panel. See Box 2.4, Table 1 for index definitions. {Figures 11.17, 12.14, 12.26, 12.27}

TS

TFE.9 (continued)

will at least double in frequency but in many regions will become an annual or a 1-in-2-year event by the end of the 21st century. The magnitude of both high and low temperature extremes is expected to increase at least at the same rate as the mean, but with 20-year return values for low temperature events projected to increase at a rate greater than winter mean temperatures in most regions. {10.6.1, 11.3.2, 12.4.3}

Precipitation Extremes

It is *likely* that the number of heavy precipitation events over land has increased in more regions than it has decreased in since the mid-20th century, and there is *medium confidence* that anthropogenic forcing has contributed to this increase. {2.6.2, 10.6.1}

There has been substantial progress between CMIP3 and CMIP5 in the ability of models to simulate more realistic precipitation extremes. However, evidence suggests that the majority of models underestimate the sensitivity of extreme precipitation to temperature variability or trends especially in the tropics, which implies that models may underestimate the projected increase in extreme precipitation in the future. While progress has been made in understanding the processes that drive extreme precipitation, challenges remain in quantifying cloud and convective effects in models for example. The complexity of land surface and atmospheric processes limits confidence in regional projections of precipitation change, especially over land, although there is a component of a 'wet-get-wetter' and 'dry-get-drier' response over oceans at the large scale. Even so, there is *high confidence* that, as the climate warms, extreme precipitation rates (e.g., on daily time scales) will increase faster than the time average. Changes in local extremes on daily and sub-daily time scales are expected to increase by roughly 5 to 10% per °C of warming (*medium confidence*). {7.6, 9.5.4}

For the near and long term, CMIP5 projections confirm a clear tendency for increases in heavy precipitation events in the global mean seen in the AR4, but there are substantial variations across regions (TFE.9, Figure 1). Over most of the mid-latitude land masses and over wet tropical regions, extreme precipitation will *very likely* be more intense and more frequent in a warmer world. {11.3.2, 12.4.5}

Floods and Droughts

There continues to be a lack of evidence and thus *low confidence* regarding the sign of trend in the magnitude and/or frequency of floods on a global scale over the instrumental record. There is *high confidence* that past floods larger than those recorded since 1900 have occurred during the past five centuries in northern and central Europe, western Mediterranean region, and eastern Asia. There is *medium confidence* that modern large floods are comparable to or surpass historical floods in magnitude and/or frequency in the Near East, India and central North America. {2.6.2, 5.5.5}

Compelling arguments both for and against significant increases in the land area affected by drought and/or dryness since the mid-20th century have resulted in a *low confidence* assessment of observed and attributable large-scale trends. This is due primarily to a lack and quality of direct observations, dependencies of inferred trends on the index choice, geographical inconsistencies in the trends and difficulties in distinguishing decadal scale variability from long term trends. On millennial time scales, there is *high confidence* that proxy information provides evidence of droughts of greater magnitude and longer duration than observed during the 20th century in many regions. There is *medium confidence* that more megadroughts occurred in monsoon Asia and wetter conditions prevailed in arid Central Asia and the South American monsoon region during the Little Ice Age (1450 to 1850) compared to the Medieval Climate Anomaly (950 to 1250). {2.6.2, 5.5.4, 5.5.5, 10.6.1}

Under the Representative Concentration Pathway RCP8.5, projections by the end of the century indicate an increased risk of drought is *likely (medium confidence)* in presently dry regions linked to regional to global-scale projected decreases in soil moisture. Soil moisture drying is most prominent in the Mediterranean, Southwest USA, and southern Africa, consistent with projected changes in the Hadley Circulation and increased surface temperatures, and surface drying in these regions is *likely (high confidence)* by the end of the century under RCP8.5. {12.4.5}

Extreme Sea Level

It is *likely* that the magnitude of extreme high sea level events has increased since 1970 and that most of this rise can be explained by increases in mean sea level. When mean sea level changes is taken into account, changes in extreme high sea levels are reduced to less than 5 mm y^{-1} at 94% of tide gauges. In the future it is *very likely* that there will be a significant increase in the occurrence of sea level extremes and similarly to past observations, this increase will primarily be the result of an increase in mean sea level. {3.7.5, 13.7.2}

(continued on next page)

TFE.9 (continued)

Tropical and Extratropical Cyclones

There is *low confidence* in long-term (centennial) changes in tropical cyclone activity, after accounting for past changes in observing capabilities. However over the satellite era, increases in the frequency and intensity of the strongest storms in the North Atlantic are robust (*very high confidence*). However, the cause of this increase is debated and there is *low confidence* in attribution of changes in tropical cyclone activity to human influence owing to insufficient observational evidence, lack of physical understanding of the links between anthropogenic drivers of climate and tropical cyclone activity and the low level of agreement between studies as to the relative importance of internal variability, and anthropogenic and natural forcings. {2.6.3, 10.6.1, 14.6.1}

Some high-resolution atmospheric models have realistically simulated tracks and counts of tropical cyclones and models generally are able to capture the general characteristics of storm tracks and extratropical cyclones with evidence of improvement since the AR4. Storm track biases in the North Atlantic have improved slightly, but models still produce a storm track that is too zonal and underestimate cyclone intensity. {9.4.1, 9.5.4}

While projections indicate that it is *likely* that the global frequency of tropical cyclones will either decrease or remain essentially unchanged, concurrent with a *likely* increase in both global mean tropical cyclone maximum wind speed and rainfall rates, there is lower confidence in region-specific projections of frequency and intensity. However, due to improvements in model resolution and downscaling techniques, it is *more likely than not* that the frequency of the most intense storms will increase substantially in some basins under projected 21st century warming (see Figure TS.26). {11.3.2, 14.6.1}

Research subsequent to the AR4 and SREX continues to support a *likely* poleward shift of storm tracks since the 1950s. However over the last century there is *low confidence* of a clear trend in storminess due to inconsistencies between studies or lack of long-term data in some parts of the world (particularly in the Southern Hemisphere (SH)). {2.6.4, 2.7.6}

Despite systematic biases in simulating storm tracks, most models and studies are in agreement that the global number of extratropical cyclones is *unlikely* to decrease by more than a few per cent. A small poleward shift is *likely* in the SH storm track. It is *more likely than not (medium confidence)* for a projected poleward shift in the North Pacific storm track but it is *unlikely* that the response of the North Atlantic storm track is a simple poleward shift. There is *low confidence* in the magnitude of regional storm track changes, and the impact of such changes on regional surface climate. {14.6.2}

TS

TS.6 Key Uncertainties

This final section of the Technical Summary provides readers with a short overview of key uncertainties in the understanding of the climate system and the ability to project changes in response to anthropogenic influences. The overview is not comprehensive and does not describe in detail the basis for these findings. These are found in the main body of this Technical Summary and in the underlying chapters to which each bullet points in the curly brackets.

TS.6.1 Key Uncertainties in Observation of Changes in the Climate System

- There is only *medium to low confidence* in the rate of change of tropospheric warming and its vertical structure. Estimates of tropospheric warming rates encompass surface temperature warming rate estimates. There is *low confidence* in the rate and vertical structure of the stratospheric cooling. {2.4.4}
- *Confidence* in global precipitation change over land is *low* prior to 1951 and *medium* afterwards because of data incompleteness. {2.5.1}
- Substantial ambiguity and therefore *low confidence* remains in the observations of global-scale cloud variability and trends. {2.5.6}
- There is *low confidence* in an observed global-scale trend in drought or dryness (lack of rainfall), due to lack of direct observations, methodological uncertainties and choice and geographical inconsistencies in the trends. {2.6.2}
- There is *low confidence* that any reported long-term (centennial) changes in tropical cyclone characteristics are robust, after accounting for past changes in observing capabilities. {2.6.3}
- Robust conclusions on long-term changes in large-scale atmospheric circulation are presently not possible because of large variability on interannual to decadal time scales and remaining differences between data sets. {2.7}
- Different global estimates of sub-surface ocean temperatures have variations at different times and for different periods, suggesting that sub-decadal variability in the temperature and upper heat content (0 to 700 m) is still poorly characterized in the historical record. {3.2}
- Below ocean depths of 700 m the sampling in space and time is too sparse to produce annual global ocean temperature and heat content estimates prior to 2005. {3.2.4}
- Observational coverage of the ocean deeper than 2000 m is still limited and hampers more robust estimates of changes in global ocean heat content and carbon content. This also limits the quantification of the contribution of deep ocean warming to sea level rise. {3.2, 3.7, 3.8; Box 3.1}

- The number of continuous observational time series measuring the strength of climate relevant ocean circulation features (e.g., the meridional overturning circulation) is limited and the existing time series are still too short to assess decadal and longer trends. {3.6}
- In Antarctica, available data are inadequate to assess the status of change of many characteristics of sea ice (e.g., thickness and volume). {4.2.3}
- On a global scale the mass loss from melting at calving fronts and iceberg calving are not yet comprehensively assessed. The largest uncertainty in estimated mass loss from glaciers comes from the Antarctic, and the observational record of ice–ocean interactions around both ice sheets remains poor. {4.3.3, 4.4}

TS.6.2 Key Uncertainties in Drivers of Climate Change

- Uncertainties in aerosol–cloud interactions and the associated radiative forcing remain large. As a result, uncertainties in aerosol forcing remain the dominant contributor to the overall uncertainty in net anthropogenic forcing, despite a better understanding of some of the relevant atmospheric processes and the availability of global satellite monitoring. {2.2, 7.3–7.5, 8.5}
- The cloud feedback is *likely* positive but its quantification remains difficult. {7.2}
- Paleoclimate reconstructions and Earth System Models indicate that there is a positive feedback between climate and the carbon cycle, but *confidence* remains *low* in the strength of this feedback, particularly for the land. {6.4}

TS.6.3 Key Uncertainties in Understanding the Climate System and Its Recent Changes

- The simulation of clouds in AOGCMs has shown modest improvement since AR4; however, it remains challenging. {7.2, 9.2.1, 9.4.1, 9.7.2}
- Observational uncertainties for climate variables other than temperature, uncertainties in forcings such as aerosols, and limits in process understanding continue to hamper attribution of changes in many aspects of the climate system. {10.1, 10.3, 10.7}
- Changes in the water cycle remain less reliably modelled in both their changes and their internal variability, limiting confidence in attribution assessments. Observational uncertainties and the large effect of internal variability on observed precipitation also precludes a more confident assessment of the causes of precipitation changes. {2.5.1, 2.5.4, 10.3.2}
- Modelling uncertainties related to model resolution and incorporation of relevant processes become more important at regional scales, and the effects of internal variability become more significant. Therefore, challenges persist in attributing observed change to external forcing at regional scales. {2.4.1, 10.3.1}

- The ability to simulate changes in frequency and intensity of extreme events is limited by the ability of models to reliably simulate mean changes in key features. {10.6.1}
- In some aspects of the climate system, including changes in drought, changes in tropical cyclone activity, Antarctic warming, Antarctic sea ice extent, and Antarctic mass balance, *confidence* in attribution to human influence remains *low* due to modelling uncertainties and low agreement between scientific studies. {10.3.1, 10.5.2, 10.6.1}

TS.6.4 Key Uncertainties in Projections of Global and Regional Climate Change

- Based on model results there is limited confidence in the predictability of yearly to decadal averages of temperature both for the global average and for some geographical regions. Multi-model results for precipitation indicate a generally low predictability. Short-term climate projection is also limited by the uncertainty in projections of natural forcing. {11.1, 11.2, 11.3.1, 11.3.6; Box 11.1}
- There is *medium confidence* in near-term projections of a northward shift of NH storm track and westerlies. {11.3.2}
- There is generally *low confidence* in basin-scale projections of significant trends in tropical cyclone frequency and intensity in the 21st century. {11.3.2, 14.6.1}
- Projected changes in soil moisture and surface run off are not robust in many regions. {11.3.2, 12.4.5}
- Several components or phenomena in the climate system could potentially exhibit abrupt or nonlinear changes, but for many phenomena there is *low confidence* and little consensus on the likelihood of such events over the 21st century. {12.5.5}
- There is *low confidence* on magnitude of carbon losses through CO₂ or CH₄ emissions to the atmosphere from thawing permafrost. There is *low confidence* in projected future CH₄ emissions from natural sources due to changes in wetlands and gas hydrate release from the sea floor. {6.4.3, 6.4.7}
- There is *medium confidence* in the projected contributions to sea level rise by models of ice sheet dynamics for the 21st century, and *low confidence* in their projections beyond 2100. {13.3.3}
- There is *low confidence* in semi-empirical model projections of global mean sea level rise, and no consensus in the scientific community about their reliability. {13.5.2, 13.5.3}
- There is *low confidence* in projections of many aspects of climate phenomena that influence regional climate change, including changes in amplitude and spatial pattern of modes of climate variability. {9.5.3, 14.2–14.7}



Chapters

1

Introduction

Coordinating Lead Authors:

Ulrich Cubasch (Germany), Donald Wuebbles (USA)

Lead Authors:

Deliang Chen (Sweden), Maria Cristina Facchini (Italy), David Frame (UK/New Zealand), Natalie Mahowald (USA), Jan-Gunnar Winther (Norway)

Contributing Authors:

Achim Brauer (Germany), Lydia Gates (Germany), Emily Janssen (USA), Frank Kaspar (Germany), Janina Körper (Germany), Valérie Masson-Delmotte (France), Malte Meinshausen (Australia/Germany), Matthew Menne (USA), Carolin Richter (Switzerland), Michael Schulz (Germany), Uwe Schulzweida (Germany), Bjorn Stevens (Germany/USA), Rowan Sutton (UK), Kevin Trenberth (USA), Murat Türkeş (Turkey), Daniel S. Ward (USA)

Review Editors:

Yihui Ding (China), Linda Mearns (USA), Peter Wadhams (UK)

This chapter should be cited as:

Cubasch, U., D. Wuebbles, D. Chen, M.C. Facchini, D. Frame, N. Mahowald, and J.-G. Winther, 2013: Introduction. In: *Climate Change 2013: The Physical Science Basis. Contribution of Working Group I to the Fifth Assessment Report of the Intergovernmental Panel on Climate Change* [Stocker, T.F., D. Qin, G.-K. Plattner, M. Tignor, S.K. Allen, J. Boschung, A. Nauels, Y. Xia, V. Bex and P.M. Midgley (eds.)]. Cambridge University Press, Cambridge, United Kingdom and New York, NY, USA.

Table of Contents

1

Executive Summary.....	121
1.1 Chapter Preview.....	123
1.2 Rationale and Key Concepts of the WGI Contribution.....	123
1.2.1 Setting the Stage for the Assessment.....	123
1.2.2 Key Concepts in Climate Science.....	123
1.2.3 Multiple Lines of Evidence for Climate Change.....	129
1.3 Indicators of Climate Change.....	130
1.3.1 Global and Regional Surface Temperatures.....	131
1.3.2 Greenhouse Gas Concentrations.....	132
1.3.3 Extreme Events	134
1.3.4 Climate Change Indicators.....	136
1.4 Treatment of Uncertainties	138
1.4.1 Uncertainty in Environmental Science.....	138
1.4.2 Characterizing Uncertainty.....	138
1.4.3 Treatment of Uncertainty in IPCC.....	139
1.4.4 Uncertainty Treatment in This Assessment.....	139
1.5 Advances in Measurement and Modelling Capabilities.....	142
1.5.1 Capabilities of Observations	142
1.5.2 Capabilities in Global Climate Modelling.....	144
Box 1.1: Description of Future Scenarios	147
1.6 Overview and Road Map to the Rest of the Report	151
1.6.1 Topical Issues	151
References	152
Appendix 1.A: Notes and Technical Details on Figures Displayed in Chapter 1.....	155
Frequently Asked Questions	
FAQ 1.1 If Understanding of the Climate System Has Increased, Why Hasn't the Range of Temperature Projections Been Reduced?	140

Executive Summary

Human Effects on Climate

Human activities are continuing to affect the Earth's energy budget by changing the emissions and resulting atmospheric concentrations of radiatively important gases and aerosols and by changing land surface properties. Previous assessments have already shown through multiple lines of evidence that the climate is changing across our planet, largely as a result of human activities. The most compelling evidence of climate change derives from observations of the atmosphere, land, oceans and cryosphere. Unequivocal evidence from *in situ* observations and ice core records shows that the atmospheric concentrations of important greenhouse gases such as carbon dioxide (CO₂), methane (CH₄), and nitrous oxide (N₂O) have increased over the last few centuries. {1.2.2, 1.2.3}

The processes affecting climate can exhibit considerable natural variability. Even in the absence of external forcing, periodic and chaotic variations on a vast range of spatial and temporal scales are observed. Much of this variability can be represented by simple (e.g., unimodal or power law) distributions, but many components of the climate system also exhibit multiple states—for instance, the glacial–interglacial cycles and certain modes of internal variability such as El Niño–Southern Oscillation (ENSO). Movement between states can occur as a result of natural variability, or in response to external forcing. The relationship among variability, forcing and response reveals the complexity of the dynamics of the climate system: the relationship between forcing and response for some parts of the system seems reasonably linear; in other cases this relationship is much more complex. {1.2.2}

Multiple Lines of Evidence for Climate Change

Global mean surface air temperatures over land and oceans have increased over the last 100 years. Temperature measurements in the oceans show a continuing increase in the heat content of the oceans. Analyses based on measurements of the Earth's radiative budget suggest a small positive energy imbalance that serves to increase the global heat content of the Earth system. Observations from satellites and *in situ* measurements show a trend of significant reductions in the mass balance of most land ice masses and in Arctic sea ice. The oceans' uptake of CO₂ is having a significant effect on the chemistry of sea water. Paleoclimatic reconstructions have helped place ongoing climate change in the perspective of natural climate variability. {1.2.3; Figure 1.3}

Observations of CO₂ concentrations, globally averaged temperature and sea level rise are generally well within the range of the extent of the earlier IPCC projections. The recently observed increases in CH₄ and N₂O concentrations are smaller than those assumed in the scenarios in the previous assessments. Each IPCC assessment has used new projections of future climate change that have become more detailed as the models have become more advanced. Similarly, the scenarios used in the IPCC assessments have themselves changed over time to reflect the state of knowledge. The range of climate projections from model results provided and assessed in the first IPCC assessment in 1990 to those in the 2007 AR4 provides an opportunity to compare the projections with the actually observed changes, thereby examining the deviations of the projections from the observations over time. {1.3.1, 1.3.2, 1.3.4; Figures 1.4, 1.5, 1.6, 1.7, 1.10}

Climate change, whether driven by natural or human forcing, can lead to changes in the likelihood of the occurrence or strength of extreme weather and climate events or both. Since the AR4, the observational basis has increased substantially, so that some extremes are now examined over most land areas. Furthermore, more models with higher resolution and a greater number of regional models have been used in the simulations and projections of extremes. {1.3.3; Figure 1.9}

Treatment of Uncertainties

For AR5, the three IPCC Working Groups use two metrics to communicate the degree of certainty in key findings: (1) Confidence is a qualitative measure of the validity of a finding, based on the type, amount, quality and consistency of evidence (e.g., data, mechanistic understanding, theory, models, expert judgment) and the degree of agreement¹; and (2) Likelihood provides a quantified measure of uncertainty in a finding expressed probabilistically (e.g., based on statistical analysis of observations or model results, or both, and expert judgement)². {1.4; Figure 1.11}

Advances in Measurement and Modelling Capabilities

Over the last few decades, new observational systems, especially satellite-based systems, have increased the number of observations of the Earth's climate by orders of magnitude. Tools to analyse and process these data have been developed or enhanced to cope with this large increase in information, and more climate proxy data have been acquired to improve our knowledge of past changes in climate. Because the Earth's climate system is characterized on multiple spatial and temporal scales, new observations may reduce the uncertainties surrounding the understanding of short timescale

¹ In this Report, the following summary terms are used to describe the available evidence: limited, medium, or robust; and for the degree of agreement: low, medium, or high. A level of confidence is expressed using five qualifiers: very low, low, medium, high, and very high, and typeset in italics, e.g., *medium confidence*. For a given evidence and agreement statement, different confidence levels can be assigned, but increasing levels of evidence and degrees of agreement are correlated with increasing confidence (see Section 1.4 and Box TS.1 for more details).

² In this Report, the following terms have been used to indicate the assessed likelihood of an outcome or a result: Virtually certain 99–100% probability, Very likely 90–100%, Likely 66–100%, About as likely as not 33–66%, Unlikely 0–33%, Very unlikely 0–10%, Exceptionally unlikely 0–1%. Additional terms (Extremely likely: 95–100%, More likely than not >50–100%, and Extremely unlikely 0–5%) may also be used when appropriate. Assessed likelihood is typeset in italics, e.g., *very likely* (see Section 1.4 and Box TS.1 for more details).

processes quite rapidly. However, processes that occur over longer timescales may require very long observational baselines before much progress can be made. {1.5.1; Figure 1.12}

Increases in computing speed and memory have led to the development of more sophisticated models that describe physical, chemical and biological processes in greater detail. Modelling strategies have been extended to provide better estimates of the uncertainty in climate change projections. The model comparisons with observations have pushed the analysis and development of the models. The inclusion of 'long-term' simulations has allowed incorporation of information from paleoclimate data to inform projections. Within uncertainties associated with reconstructions of past climate variables from proxy record and forcings, paleoclimate information from the Mid Holocene, Last Glacial Maximum, and Last Millennium have been used to test the ability of models to simulate realistically the magnitude and large-scale patterns of past changes. {1.5.2; Figures 1.13, 1.14}

As part of the process of getting model analyses for a range of alternative images of how the future may unfold, four new scenarios for future emissions of important gases and aerosols have been developed for the AR5, referred to as Representative Concentration Pathways (RCPs). {Box 1.1}

1.1 Chapter Preview

This introductory chapter serves as a lead-in to the science presented in the Working Group I (WGI) contribution to the Intergovernmental Panel on Climate Change (IPCC) Fifth Assessment Report (AR5). Chapter 1 in the IPCC Fourth Assessment Report (AR4) (Le Treut et al., 2007) provided a historical perspective on the understanding of climate science and the evidence regarding human influence on the Earth's climate system. Since the last assessment, the scientific knowledge gained through observations, theoretical analyses, and modelling studies has continued to increase and to strengthen further the evidence linking human activities to the ongoing climate change. In AR5, Chapter 1 focuses on the concepts and definitions applied in the discussions of new findings in the other chapters. It also examines several of the key indicators for a changing climate and shows how the current knowledge of those indicators compares with the projections made in previous assessments. The new scenarios for projected human-related emissions used in this assessment are also introduced. Finally, the chapter discusses the directions and capabilities of current climate science, while the detailed discussion of new findings is covered in the remainder of the WGI contribution to the AR5.

1.2 Rationale and Key Concepts of the WGI Contribution

1.2.1 Setting the Stage for the Assessment

The IPCC was set up in 1988 by the World Meteorological Organization and the United Nations Environment Programme to provide governments with a clear view of the current state of knowledge about the science of climate change, potential impacts, and options for adaptation and mitigation through regular assessments of the most recent information published in the scientific, technical and socio-economic literature worldwide. The WGI contribution to the IPCC AR5 assesses the current state of the physical sciences with respect to climate change. This report presents an assessment of the current state of research results and is not a discussion of all relevant papers as would be included in a review. It thus seeks to make sure that the range of scientific views, as represented in the peer-reviewed literature, is considered and evaluated in the assessment, and that the state of the science is concisely and accurately presented. A transparent review process ensures that disparate views are included (IPCC, 2012a).

As an overview, Table 1.1 shows a selection of key findings from earlier IPCC assessments. This table provides a non-comprehensive selection of key assessment statements from previous assessment reports—IPCC First Assessment Report (FAR, IPCC, 1990), IPCC Second Assessment Report (SAR, IPCC, 1996), IPCC Third Assessment Report (TAR, IPCC, 2001) and IPCC Fourth Assessment Report (AR4, IPCC, 2007)—with a focus on policy-relevant quantities that have been evaluated in each of the IPCC assessments.

Scientific hypotheses are contingent and always open to revision in light of new evidence and theory. In this sense the distinguishing features of scientific enquiry are the search for truth and the willingness to subject itself to critical re-examination. Modern research science

conducts this critical revision through processes such as the peer review. At conferences and in the procedures that surround publication in peer-reviewed journals, scientific claims about environmental processes are analysed and held up to scrutiny. Even after publication, findings are further analysed and evaluated. That is the self-correcting nature of the scientific process (more details are given in AR4 Chapter 1 and Le Treut et al., 2007).

Science strives for objectivity but inevitably also involves choices and judgements. Scientists make choices regarding data and models, which processes to include and which to leave out. Usually these choices are uncontroversial and play only a minor role in the production of research. Sometimes, however, the choices scientists make are sources of disagreement and uncertainty. These are usually resolved by further scientific enquiry into the sources of disagreement. In some cases, experts cannot reach a consensus view. Examples in climate science include how best to evaluate climate models relative to observations, how best to evaluate potential sea level rise and how to evaluate probabilistic projections of climate change. In many cases there may be no definitive solution to these questions. The IPCC process is aimed at assessing the literature as it stands and attempts to reflect the level of reasonable scientific consensus as well as disagreement.

To assess areas of scientific controversy, the peer-reviewed literature is considered and evaluated. Not all papers on a controversial point can be discussed individually in an assessment, but every effort has been made here to ensure that all views represented in the peer-reviewed literature are considered in the assessment process. A list of topical issues is given in Table 1.3.

The Earth sciences study the multitude of processes that shape our environment. Some of these processes can be understood through idealized laboratory experiments, by altering a single element and then tracing through the effects of that controlled change. However, as in other natural and the social sciences, the openness of environmental systems, in terms of our lack of control of the boundaries of the system, their spatially and temporally multi-scale character and the complexity of interactions, often hamper scientists' ability to definitively isolate causal links. This in turn places important limits on the understanding of many of the inferences in the Earth sciences (e.g., Oreskes et al., 1994). There are many cases where scientists are able to make inferences using statistical tools with considerable evidential support and with high degrees of confidence, and conceptual and numerical modelling can assist in forming understanding and intuition about the interaction of dynamic processes.

1.2.2 Key Concepts in Climate Science

Here, some of the key concepts in climate science are briefly described; many of these were summarized more comprehensively in earlier IPCC assessments (Baede et al., 2001). We focus only on a certain number of them to facilitate discussions in this assessment.

First, it is important to distinguish the meaning of weather from climate. Weather describes the conditions of the atmosphere at a certain place and time with reference to temperature, pressure, humidity, wind, and other key parameters (meteorological elements); the

Table 1.1 | Historical overview of major conclusions of previous IPCC assessment reports. The table provides a non-comprehensive selection of key statements from previous assessment reports—IPCC First Assessment Report (FAR; IPCC, 1990), IPCC Second Assessment Report (SAR; IPCC, 1996), IPCC Third Assessment Report (TAR; IPCC, 2001) and IPCC Fourth Assessment Report (AR4; IPCC, 2007)—with a focus on global mean surface air temperature and sea level change as two policy relevant quantities that have been covered in IPCC since the first assessment report.

Topic	FAR SPM Statement	SAR SPM Statement	TAR SPM Statement	AR4 SPM Statement
Human and Natural Drivers of Climate Change	There is a natural greenhouse effect which already keeps the Earth warmer than it would otherwise be. Emissions resulting from human activities are substantially increasing the atmospheric concentrations of the greenhouse gases carbon dioxide, methane, chlorofluorocarbons and nitrous oxide. These increases will enhance the greenhouse effect, resulting on average in an additional warming of the Earth's surface. Continued emissions of these gases at present rates would commit us to increased concentrations for centuries ahead.	Greenhouse gas concentrations have continued to increase. These trends can be attributed largely to human activities, mostly fossil fuel use, land use change and agriculture. Anthropogenic aerosols are short-lived and tend to produce negative radiative forcing.	Emissions of greenhouse gases and aerosols due to human activities continue to alter the atmosphere in ways that are expected to affect the climate. The atmospheric concentration of CO ₂ has increased by 31% since 1750 and that of methane by 151%. Anthropogenic aerosols are short-lived and mostly produce negative radiative forcing by their direct effect. There is more evidence for their indirect effect, which is negative, although of very uncertain magnitude. Natural factors have made small contributions to radiative forcing over the past century.	Global atmospheric concentrations of carbon dioxide, methane and nitrous oxide have increased markedly as a result of human activities since 1750 and now far exceed pre-industrial values determined from ice cores spanning many thousands of years. The global increases in carbon dioxide concentration are due primarily to fossil fuel use and land use change, while those of methane and nitrous oxide are primarily due to agriculture. <i>Very high confidence</i> that the global average net effect of human activities since 1750 has been one of warming, with a radiative forcing of +1.6 [+0.6 to +2.4] W m ⁻² .
	Temperature	Global mean surface air temperature has increased by 0.3°C to 0.6°C over the last 100 years, with the five global-average warmest years being in the 1980s.	Climate has changed over the past century. Global mean surface temperature has increased by between about 0.3 and 0.6°C since the late 19th century. Recent years have been among the warmest since 1860, despite the cooling effect of the 1991 Mt. Pinatubo volcanic eruption.	An increasing body of observations gives a collective picture of a warming world and other changes in the climate system. The global average temperature has increased since 1861. Over the 20th century the increase has been 0.6°C. Some important aspects of climate appear not to have changed.
Sea Level	Over the same period global sea level has increased by 10 to 20 cm. These increases have not been smooth with time, nor uniform over the globe.	Global sea level has risen by between 10 and 25 cm over the past 100 years and much of the rise may be related to the increase in global mean temperature.	Tide gauge data show that global average sea level rose between 0.1 and 0.2 m during the 20th century.	Global average sea level rose at an average rate of 1.8 [1.3 to 2.3] mm per year over 1961 to 2003. The rate was faster over 1993 to 2003: about 3.1 [2.4 to 3.8] mm per year. The total 20th century rise is estimated to be 0.17 [0.12 to 0.22] m.
A Palaeoclimatic Perspective	Climate varies naturally on all timescales from hundreds of millions of years down to the year-to-year. Prominent in the Earth's history have been the 100,000 year glacial-interglacial cycles when climate was mostly cooler than at present. Global surface temperatures have typically varied by 5°C to 7°C through these cycles, with large changes in ice volume and sea level, and temperature changes as great as 10°C to 15°C in some middle and high latitude regions of the Northern Hemisphere. Since the end of the last ice age, about 10,000 years ago, global surface temperatures have probably fluctuated by little more than 1°C. Some fluctuations have lasted several centuries, including the Little Ice Age which ended in the nineteenth century and which appears to have been global in extent.	The limited available evidence from proxy climate indicators suggests that the 20th century global mean temperature is at least as warm as any other century since at least 1400 AD. Data prior to 1400 are too sparse to allow the reliable estimation of global mean temperature.	New analyses of proxy data for the Northern Hemisphere indicate that the increase in temperature in the 20th century is likely to have been the largest of any century during the past 1,000 years. It is also likely that, in the Northern Hemisphere, the 1990s was the warmest decade and 1998 the warmest year. Because less data are available, less is known about annual averages prior to 1,000 years before present and for conditions prevailing in most of the Southern Hemisphere prior to 1861.	Palaeoclimatic information supports the interpretation that the warmth of the last half century is unusual in at least the previous 1,300 years. The last time the polar regions were significantly warmer than present for an extended period (about 125,000 years ago), reductions in polar ice volume led to 4 to 6 m of sea level rise.

(continued on next page)

(Table 1.1 continued)

Topic	FAR SPM Statement	SAR SPM Statement	TAR SPM Statement	AR4 SPM Statement
Understanding and Attributing Climate Change	The size of this warming is broadly consistent with predictions of climate models, but it is also of the same magnitude as natural climate variability. Thus the observed increase could be largely due to this natural variability; alternatively this variability and other human factors could have offset a still larger human-induced greenhouse warming. The unequivocal detection of the enhanced greenhouse effect from observations is not likely for a decade or more.	The balance of evidence suggests a discernible human influence on global climate. Simulations with coupled atmosphere-ocean models have provided important information about decade to century timescale natural internal climate variability.	There is new and stronger evidence that most of the warming observed over the last 50 years is attributable to human activities. There is a longer and more scrutinized temperature record and new model estimates of variability. Reconstructions of climate data for the past 1,000 years indicate this warming was unusual and is unlikely to be entirely natural in origin.	Most of the observed increase in global average temperatures since the mid-20th century is very likely due to the increase in anthropogenic greenhouse gas concentrations. Discernible human influences now extend to other aspects of climate, including ocean warming, continental-average temperatures, temperature extremes and wind patterns.
	Projections of Future Changes in Climate	Climate is expected to continue to change in the future. For the mid-range IPCC emission scenario, IS92a, assuming the 'best estimate' value of climate sensitivity and including the effects of future increases in aerosols, models project an increase in global mean surface air temperature relative to 1990 of about 2°C by 2100.	Global average temperature and sea level are projected to rise under all IPCC SRES scenarios. The globally averaged surface temperature is projected to increase by 1.4°C to 5.8°C over the period 1990 to 2100. Confidence in the ability of models to project future climate has increased. Anthropogenic climate change will persist for many centuries.	For the next two decades, a warming of about 0.2°C per decade is projected for a range of SRES emission scenarios. Even if the concentrations of all greenhouse gases and aerosols had been kept constant at year 2000 levels, a further warming of about 0.1°C per decade would be expected. There is now higher confidence in projected patterns of warming and other regional-scale features, including changes in wind patterns, precipitation and some aspects of extremes and of ice. Anthropogenic warming and sea level rise would continue for centuries, even if greenhouse gas concentrations were to be stabilised.
Sea Level	An average rate of global mean sea level rise of about 6 cm per decade over the next century (with an uncertainty range of 3 to 10 cm per decade) is projected.	Models project a sea level rise of 50 cm from the present to 2100.	Global mean sea level is projected to rise by 0.09 to 0.88 m between 1990 and 2100.	Global sea level rise for the range of scenarios is projected as 0.18 to 0.59 m by the end of the 21st century.

presence of clouds, precipitation; and the occurrence of special phenomena, such as thunderstorms, dust storms, tornados and others. Climate in a narrow sense is usually defined as the average weather, or more rigorously, as the statistical description in terms of the mean and variability of relevant quantities over a period of time ranging from months to thousands or millions of years. The relevant quantities are most often surface variables such as temperature, precipitation and wind. Classically the period for averaging these variables is 30 years, as defined by the World Meteorological Organization. Climate in a wider sense also includes not just the mean conditions, but also the associated statistics (frequency, magnitude, persistence, trends, etc.), often combining parameters to describe phenomena such as droughts. Climate change refers to a change in the state of the climate that can be identified (e.g., by using statistical tests) by changes in the mean and/or the variability of its properties, and that persists for an extended period, typically decades or longer.

The Earth's climate system is powered by solar radiation (Figure 1.1). Approximately half of the energy from the Sun is supplied in the visible part of the electromagnetic spectrum. As the Earth's tempera-

ture has been relatively constant over many centuries, the incoming solar energy must be nearly in balance with outgoing radiation. Of the incoming solar shortwave radiation (SWR), about half is absorbed by the Earth's surface. The fraction of SWR reflected back to space by gases and aerosols, clouds and by the Earth's surface (albedo) is approximately 30%, and about 20% is absorbed in the atmosphere. Based on the temperature of the Earth's surface the majority of the outgoing energy flux from the Earth is in the infrared part of the spectrum. The longwave radiation (LWR, also referred to as infrared radiation) emitted from the Earth's surface is largely absorbed by certain atmospheric constituents—water vapour, carbon dioxide (CO₂), methane (CH₄), nitrous oxide (N₂O) and other greenhouse gases (GHGs); see Annex III for Glossary—and clouds, which themselves emit LWR into all directions. The downward directed component of this LWR adds heat to the lower layers of the atmosphere and to the Earth's surface (greenhouse effect). The dominant energy loss of the infrared radiation from the Earth is from higher layers of the troposphere. The Sun provides its energy to the Earth primarily in the tropics and the subtropics; this energy is then partially redistributed to middle and high latitudes by atmospheric and oceanic transport processes.

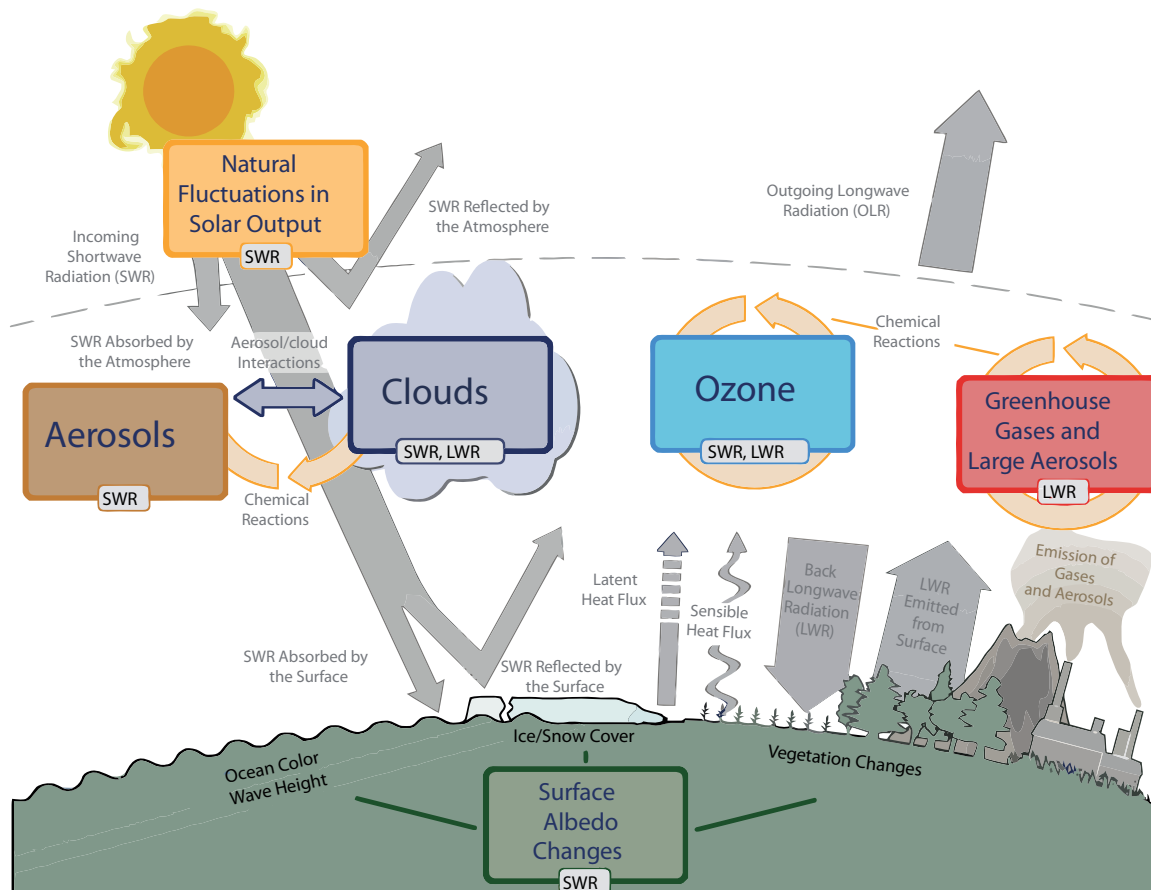


Figure 1.1 | Main drivers of climate change. The radiative balance between incoming solar shortwave radiation (SWR) and outgoing longwave radiation (OLR) is influenced by global climate 'drivers'. Natural fluctuations in solar output (solar cycles) can cause changes in the energy balance (through fluctuations in the amount of incoming SWR) (Section 2.3). Human activity changes the emissions of gases and aerosols, which are involved in atmospheric chemical reactions, resulting in modified O₃ and aerosol amounts (Section 2.2). O₃ and aerosol particles absorb, scatter and reflect SWR, changing the energy balance. Some aerosols act as cloud condensation nuclei modifying the properties of cloud droplets and possibly affecting precipitation (Section 7.4). Because cloud interactions with SWR and LWR are large, small changes in the properties of clouds have important implications for the radiative budget (Section 7.4). Anthropogenic changes in GHGs (e.g., CO₂, CH₄, N₂O, O₃, CFCs) and large aerosols (>2.5 μm in size) modify the amount of outgoing LWR by absorbing outgoing LWR and re-emitting less energy at a lower temperature (Section 2.2). Surface albedo is changed by changes in vegetation or land surface properties, snow or ice cover and ocean colour (Section 2.3). These changes are driven by natural seasonal and diurnal changes (e.g., snow cover), as well as human influence (e.g., changes in vegetation types) (Forster et al., 2007).

Changes in the global energy budget derive from either changes in the net incoming solar radiation or changes in the outgoing longwave radiation (OLR). Changes in the net incoming solar radiation derive from changes in the Sun's output of energy or changes in the Earth's albedo. Reliable measurements of total solar irradiance (TSI) can be made only from space, and the precise record extends back only to 1978. The generally accepted mean value of the TSI is about 1361 W m^{-2} (Kopp and Lean, 2011; see Chapter 8 for a detailed discussion on the TSI); this is lower than the previous value of 1365 W m^{-2} used in the earlier assessments. Short-term variations of a few tenths of a percent are common during the approximately 11-year sunspot solar cycle (see Sections 5.2 and 8.4 for further details). Changes in the outgoing LWR can result from changes in the temperature of the Earth's surface or atmosphere or changes in the emissivity (measure of emission efficiency) of LWR from either the atmosphere or the Earth's surface. For the atmosphere, these changes in emissivity are due predominantly to changes in cloud cover and cloud properties, in GHGs and in aerosol concentrations. The radiative energy budget of the Earth is almost in balance (Figure 1.1), but ocean heat content and satellite measurements indicate a small positive imbalance (Murphy et al., 2009; Trenberth et al., 2009; Hansen et al., 2011) that is consistent with the rapid changes in the atmospheric composition.

In addition, some aerosols increase atmospheric reflectivity, whereas others (e.g., particulate black carbon) are strong absorbers and also modify SWR (see Section 7.2 for a detailed assessment). Indirectly, aerosols also affect cloud albedo, because many aerosols serve as cloud condensation nuclei or ice nuclei. This means that changes in aerosol types and distribution can result in small but important changes in cloud albedo and lifetime (Section 7.4). Clouds play a critical role in climate because they not only can increase albedo, thereby cooling the planet, but also because of their warming effects through infrared radiative transfer. Whether the net radiative effect of a cloud is one of cooling or of warming depends on its physical properties (level of occurrence, vertical extent, water path and effective cloud particle size) as well as on the nature of the cloud condensation nuclei population (Section 7.3). Humans enhance the greenhouse effect directly by emitting GHGs such as CO_2 , CH_4 , N_2O and chlorofluorocarbons (CFCs) (Figure 1.1). In addition, pollutants such as carbon monoxide (CO), volatile organic compounds (VOC), nitrogen oxides (NO_x) and sulphur dioxide (SO_2), which by themselves are negligible GHGs, have an indirect effect on the greenhouse effect by altering, through atmospheric chemical reactions, the abundance of important gases to the amount of outgoing LWR such as CH_4 and ozone (O_3), and/or by acting as precursors of secondary aerosols. Because anthropogenic emission sources simultaneously can emit some chemicals that affect climate and others that affect air pollution, including some that affect both, atmospheric chemistry and climate science are intrinsically linked.

In addition to changing the atmospheric concentrations of gases and aerosols, humans are affecting both the energy and water budget of the planet by changing the land surface, including redistributing the balance between latent and sensible heat fluxes (Sections 2.5, 7.2, 7.6 and 8.2). Land use changes, such as the conversion of forests to cultivated land, change the characteristics of vegetation, including its colour, seasonal growth and carbon content (Houghton, 2003; Foley et al., 2005). For example, clearing and burning a forest to prepare agricultural

land reduces carbon storage in the vegetation, adds CO_2 to the atmosphere, and changes the reflectivity of the land (surface albedo), rates of evapotranspiration and longwave emissions (Figure 1.1).

Changes in the atmosphere, land, ocean, biosphere and cryosphere—both natural and anthropogenic—can perturb the Earth's radiation budget, producing a radiative forcing (RF) that affects climate. RF is a measure of the net change in the energy balance in response to an external perturbation. The drivers of changes in climate can include, for example, changes in the solar irradiance and changes in atmospheric trace gas and aerosol concentrations (Figure 1.1). The concept of RF cannot capture the interactions of anthropogenic aerosols and clouds, for example, and thus in addition to the RF as used in previous assessments, Sections 7.4 and 8.1 introduce a new concept, effective radiative forcing (ERF), that accounts for rapid response in the climate system. ERF is defined as the change in net downward flux at the top of the atmosphere after allowing for atmospheric temperatures, water vapour, clouds and land albedo to adjust, but with either sea surface temperatures (SSTs) and sea ice cover unchanged or with global mean surface temperature unchanged.

Once a forcing is applied, complex internal feedbacks determine the eventual response of the climate system, and will in general cause this response to differ from a simple linear one (IPCC, 2001, 2007). There are many feedback mechanisms in the climate system that can either amplify ('positive feedback') or diminish ('negative feedback') the effects of a change in climate forcing (Le Treut et al., 2007) (see Figure 1.2 for a representation of some of the key feedbacks). An example of a positive feedback is the water vapour feedback whereby an increase in surface temperature enhances the amount of water vapour present in the atmosphere. Water vapour is a powerful GHG: increasing its atmospheric concentration enhances the greenhouse effect and leads to further surface warming. Another example is the ice albedo feedback, in which the albedo decreases as highly reflective ice and snow surfaces melt, exposing the darker and more absorbing surfaces below. The dominant negative feedback is the increased emission of energy through LWR as surface temperature increases (sometimes also referred to as blackbody radiation feedback). Some feedbacks operate quickly (hours), while others develop over decades to centuries; in order to understand the full impact of a feedback mechanism, its timescale needs to be considered. Melting of land ice sheets can take days to millennia.

A spectrum of models is used to project quantitatively the climate response to forcings. The simplest energy balance models use one box to represent the Earth system and solve the global energy balance to deduce globally averaged surface air temperature. At the other extreme, full complexity three-dimensional climate models include the explicit solution of energy, momentum and mass conservation equations at millions of points on the Earth in the atmosphere, land, ocean and cryosphere. More recently, capabilities for the explicit simulation of the biosphere, the carbon cycle and atmospheric chemistry have been added to the full complexity models, and these models are called Earth System Models (ESMs). Earth System Models of Intermediate Complexity include the same processes as ESMs, but at reduced resolution, and thus can be simulated for longer periods (see Annex III for Glossary and Section 9.1).

1 An equilibrium climate experiment is an experiment in which a climate model is allowed to adjust fully to a specified change in RF. Such experiments provide information on the difference between the initial and final states of the model simulated climate, but not on the time-dependent response. The equilibrium response in global mean surface air temperature to a doubling of atmospheric concentration of CO₂ above pre-industrial levels (e.g., Arrhenius, 1896; see Le Treut et al., 2007 for a comprehensive list) has often been used as the basis for the concept of equilibrium climate sensitivity (e.g., Hansen et al., 1981; see Meehl et al., 2007 for a comprehensive list). For more realistic simulations of climate, changes in RF are applied gradually over time, for example, using historical reconstructions of the CO₂, and these simulations are called transient simulations. The temperature response in these transient simulations is different than in an equilibrium simulation. The transient climate response is defined as the change in global surface temperature at the time of atmospheric CO₂ doubling in a global coupled ocean–atmosphere climate model simulation where concentrations of CO₂ were increased by 1% yr⁻¹. The transient climate response

is a measure of the strength and rapidity of the surface temperature response to GHG forcing. It can be more meaningful for some problems as well as easier to derive from observations (see Figure 10.20; Section 10.8; Chapter 12; Knutti et al., 2005; Frame et al., 2006; Forest et al., 2008), but such experiments are not intended to replace the more realistic scenario evaluations.

Climate change commitment is defined as the future change to which the climate system is committed by virtue of past or current forcings. The components of the climate system respond on a large range of timescales, from the essentially rapid responses that characterise some radiative feedbacks to millennial scale responses such as those associated with the behaviour of the carbon cycle (Section 6.1) and ice sheets (see Figure 1.2 and Box 5.1). Even if anthropogenic emissions were immediately ceased (Matthews and Weaver, 2010) or if climate forcings were fixed at current values (Wigley, 2005), the climate system would continue to change until it came into equilibrium with those forcings (Section 12.5). Because of the slow response time of some components

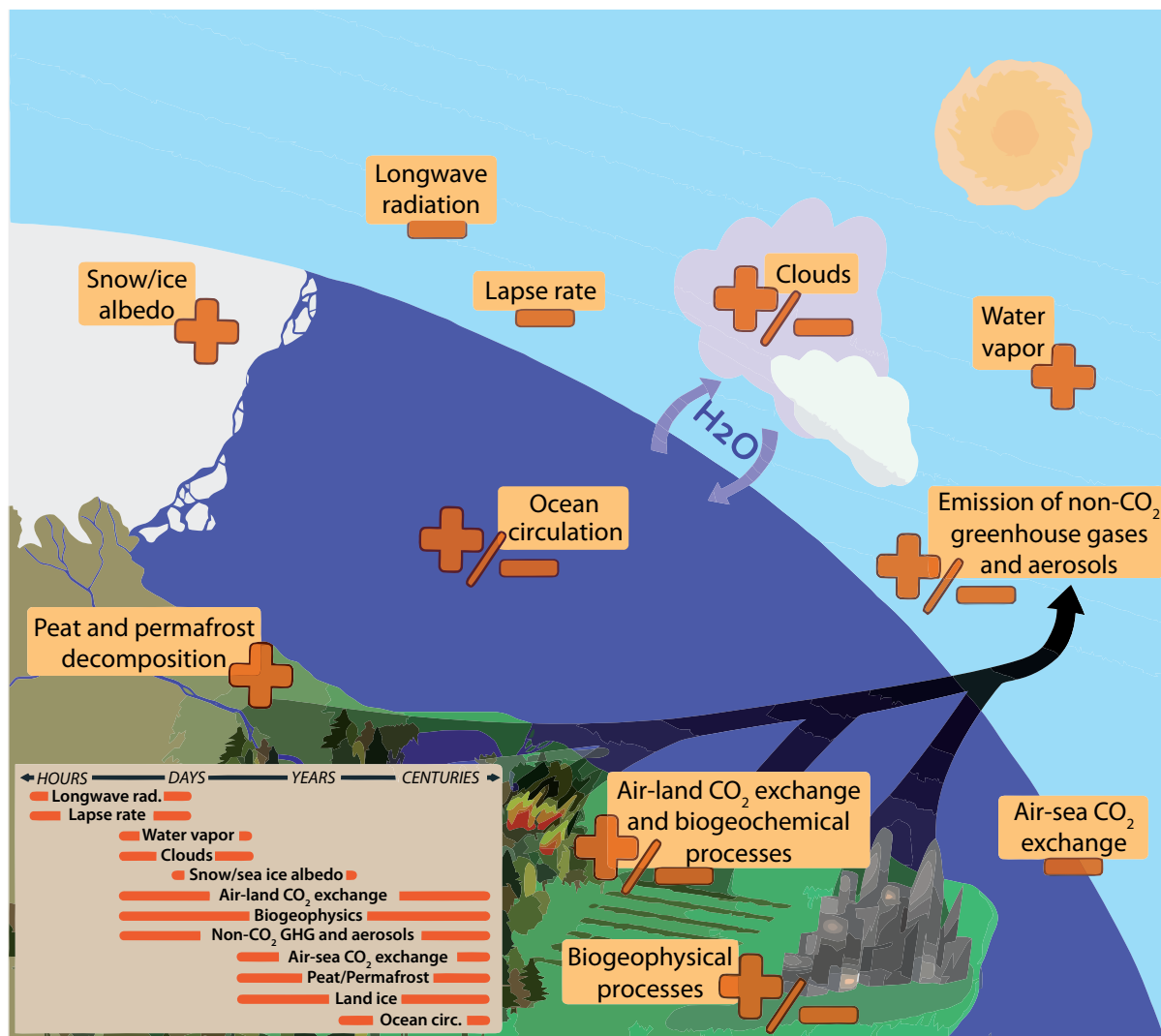


Figure 1.2 | Climate feedbacks and timescales. The climate feedbacks related to increasing CO₂ and rising temperature include negative feedbacks (–) such as LWR, lapse rate (see Glossary in Annex III), and air–sea carbon exchange and positive feedbacks (+) such as water vapour and snow/ice albedo feedbacks. Some feedbacks may be positive or negative (±): clouds, ocean circulation changes, air–land CO₂ exchange, and emissions of non-GHGs and aerosols from natural systems. In the smaller box, the large difference in timescales for the various feedbacks is highlighted.

of the climate system, equilibrium conditions will not be reached for many centuries. Slow processes can sometimes be constrained only by data collected over long periods, giving a particular salience to paleoclimate data for understanding equilibrium processes. Climate change commitment is indicative of aspects of inertia in the climate system because it captures the ongoing nature of some aspects of change.

A summary of perturbations to the forcing of the climate system from changes in solar radiation, GHGs, surface albedo and aerosols is presented in Box 13.1. The energy fluxes from these perturbations are balanced by increased radiation to space from a warming Earth, reflection of solar radiation and storage of energy in the Earth system, principally the oceans (Box 3.1, Box 13.1).

The processes affecting climate can exhibit considerable natural variability. Even in the absence of external forcing, periodic and chaotic variations on a vast range of spatial and temporal scales are observed. Much of this variability can be represented by simple (e.g., unimodal or power law) distributions, but many components of the climate system also exhibit multiple states—for instance, the glacial-interglacial cycles and certain modes of internal variability such as El Niño–Southern Oscillation (ENSO) (see Box 2.5 for details on patterns and indices of climate variability). Movement between states can occur as a result of natural variability, or in response to external forcing. The relationship between variability, forcing and response reveals the complexity of the dynamics of the climate system: the relationship between forcing and response for some parts of the system seems reasonably linear; in other cases this relationship is much more complex, characterised by hysteresis (the dependence on past states) and a non-additive combination of feedbacks.

Related to multiple climate states, and hysteresis, is the concept of irreversibility in the climate system. In some cases where multiple states and irreversibility combine, bifurcations or ‘tipping points’ can be reached (see Section 12.5). In these situations, it is difficult if not impossible for the climate system to revert to its previous state, and the change is termed irreversible over some timescale and forcing range. A small number of studies using simplified models find evidence for global-scale ‘tipping points’ (e.g., Lenton et al., 2008); however, there is no evidence for global-scale tipping points in any of the most comprehensive models evaluated to date in studies of climate evolution in the 21st century. There is evidence for threshold behaviour in certain aspects of the climate system, such as ocean circulation (see Section 12.5) and ice sheets (see Box 5.1), on multi-centennial-to-millennial timescales. There are also arguments for the existence of regional tipping points, most notably in the Arctic (e.g., Lenton et al., 2008; Duarte et al., 2012; Wadhams, 2012), although aspects of this are contested (Armour et al., 2011; Tietsche et al., 2011).

1.2.3 Multiple Lines of Evidence for Climate Change

While the first IPCC assessment depended primarily on observed changes in surface temperature and climate model analyses, more recent assessments include multiple lines of evidence for climate change. The first line of evidence in assessing climate change is based on careful analysis of observational records of the atmosphere, land, ocean and cryosphere systems (Figure 1.3). There is incontrovertible

evidence from *in situ* observations and ice core records that the atmospheric concentrations of GHGs such as CO₂, CH₄, and N₂O have increased substantially over the last 200 years (Sections 6.3 and 8.3). In addition, instrumental observations show that land and sea surface temperatures have increased over the last 100 years (Chapter 2). Satellites allow a much broader spatial distribution of measurements, especially over the last 30 years. For the upper ocean temperature the observations indicate that the temperature has increased since at least 1950 (Willis et al., 2010; Section 3.2). Observations from satellites and *in situ* measurements suggest reductions in glaciers, Arctic sea ice and ice sheets (Sections 4.2, 4.3 and 4.4). In addition, analyses based on measurements of the radiative budget and ocean heat content suggest a small imbalance (Section 2.3). These observations, all published in peer-reviewed journals, made by diverse measurement groups in multiple countries using different technologies, investigating various climate-relevant types of data, uncertainties and processes, offer a wide range of evidence on the broad extent of the changing climate throughout our planet.

Conceptual and numerical models of the Earth’s climate system offer another line of evidence on climate change (discussions in Chapters 5 and 9 provide relevant analyses of this evidence from paleoclimatic to recent periods). These use our basic understanding of the climate system to provide self-consistent methodologies for calculating impacts of processes and changes. Numerical models include the current knowledge about the laws of physics, chemistry and biology, as well as hypotheses about how complicated processes such as cloud formation can occur. Because these models can represent only the existing state of knowledge and technology, they are not perfect; they are, however, important tools for analysing uncertainties or unknowns, for testing different hypotheses for causation relative to observations, and for making projections of possible future changes.

One of the most powerful methods for assessing changes occurring in climate involves the use of statistical tools to test the analyses from models relative to observations. This methodology is generally called detection and attribution in the climate change community (Section 10.2). For example, climate models indicate that the temperature response to GHG increases is expected to be different than the effects from aerosols or from solar variability. Radiosonde measurements and satellite retrievals of atmospheric temperature show increases in tropospheric temperature and decreases in stratospheric temperatures, consistent with the increases in GHG effects found in climate model simulations (e.g., increases in CO₂, changes in O₃), but if the Sun was the main driver of current climate change, stratospheric and tropospheric temperatures would respond with the same sign (Hegerl et al., 2007).

Resources available prior to the instrumental period—historical sources, natural archives, and proxies for key climate variables (e.g., tree rings, marine sediment cores, ice cores)—can provide quantitative information on past regional to global climate and atmospheric composition variability and these data contribute another line of evidence. Reconstructions of key climate variables based on these data sets have provided important information on the responses of the Earth system to a variety of external forcings and its internal variability over a wide range of timescales (Hansen et al., 2006; Mann et al.,

2008). Paleoclimatic reconstructions thus offer a means for placing the current changes in climate in the perspective of natural climate variability (Section 5.1). AR5 includes new information on external RFs caused by variations in volcanic and solar activity (e.g., Steinhilber et al., 2009; see Section 8.4). Extended data sets on past changes in atmospheric concentrations and distributions of atmospheric GHG concentrations (e.g., Lüthi et al., 2008; Beerling and Royer, 2011) and mineral aerosols (Lambert et al., 2008) have also been used to attribute reconstructed paleoclimate temperatures to past variations in external forcings (Section 5.2).

1.3 Indicators of Climate Change

There are many indicators of climate change. These include physical responses such as changes in the following: surface temperature, atmospheric water vapour, precipitation, severe events, glaciers, ocean and land ice, and sea level. Some key examples of such changes in

important climate parameters are discussed in this section and all are assessed in much more detail in other chapters.

As was done to a more limited extent in AR4 (Le Treut et al., 2007), this section provides a test of the planetary-scale hypotheses of climate change against observations. In other words, how well do the projections used in the past assessments compare with observations to date? Seven additional years of observations are now available to evaluate earlier model projections. The projected range that was given in each assessment is compared to observations. The largest possible range of scenarios available for a specific variable for each of the previous assessment reports is shown in the figures.

Based on the assessment of AR4, a number of the key climate and associated environmental parameters are presented in Figure 1.3, which updates the similar figure in the Technical Summary (TS) of IPCC (2001). This section discusses the recent changes in several indicators, while more thorough assessments for each of these indicators are

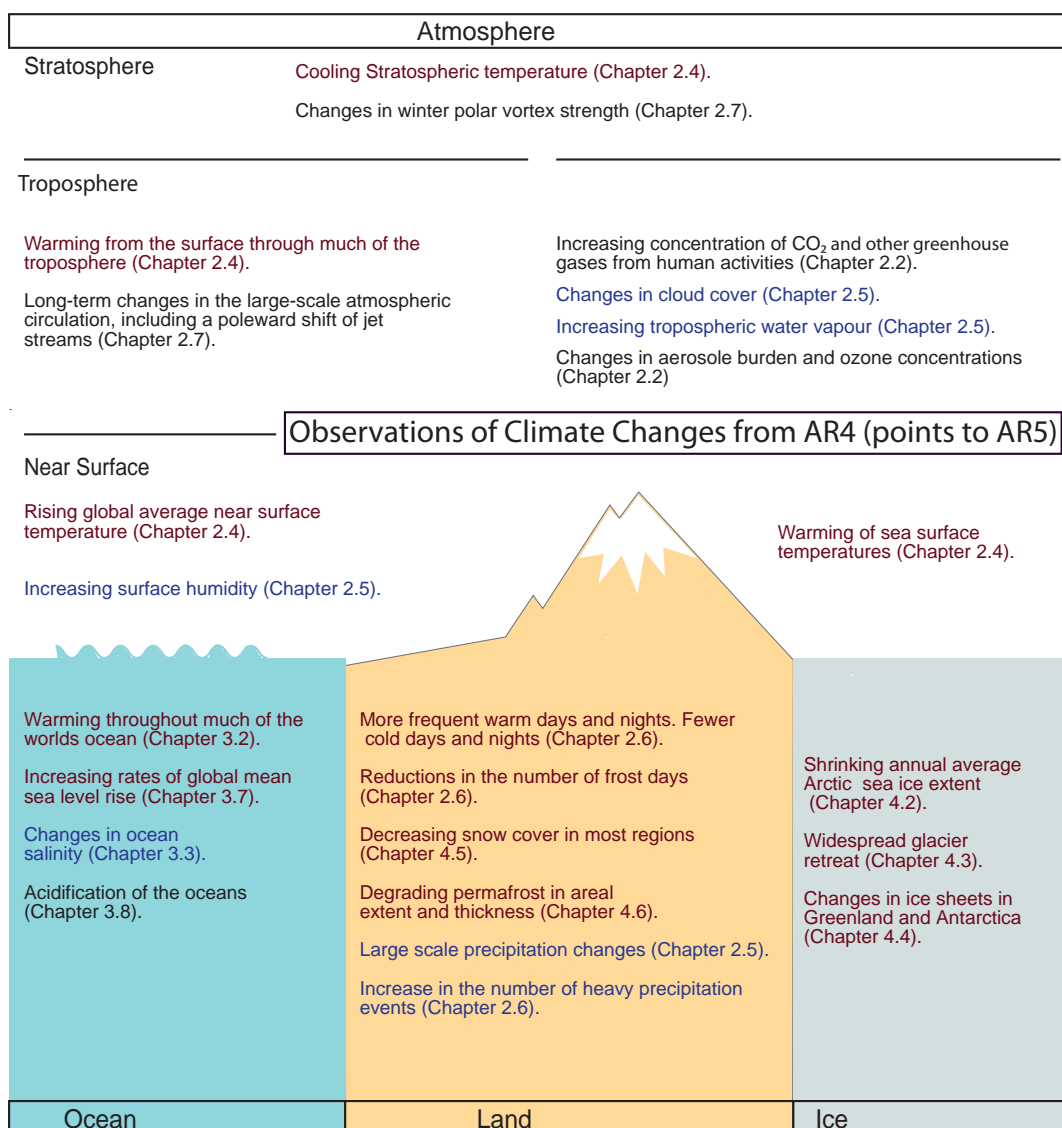


Figure 1.3 | Overview of observed climate change indicators as listed in AR4. Chapter numbers indicate where detailed discussions for these indicators are found in AR5 (temperature: red; hydrological: blue; others: black).

provided in other chapters. Also shown in parentheses in Figure 1.3 are the chapter and section where those indicators of change are assessed in AR5.

Note that projections presented in the IPCC assessments are not predictions (see the Glossary in Annex III); the analyses in the discussion below only examine the short-term plausibility of the projections up to AR4, including the scenarios for future emissions and the models used to simulate these scenarios in the earlier assessments. Model results from the Coupled Model Intercomparison Project Phase 5 (CMIP5) (Taylor et al., 2012) used in AR5 are therefore not included in this section; Chapters 11 and 12 describe the projections from the new modelling studies. Note that none of the scenarios examined in the IPCC assessments were ever intended to be short-term predictors of change.

1.3.1 Global and Regional Surface Temperatures

Observed changes in global mean surface air temperature since 1950 (from three major databases, as anomalies relative to 1961–1990) are shown in Figure 1.4. As in the prior assessments, global climate

models generally simulate global temperatures that compare well with observations over climate timescales (Section 9.4). Even though the projections from the models were never intended to be predictions over such a short timescale, the observations through 2012 generally fall within the projections made in all past assessments. The 1990–2012 data have been shown to be consistent with the FAR projections (IPCC, 1990), and not consistent with zero trend from 1990, even in the presence of substantial natural variability (Frame and Stone, 2013).

The scenarios were designed to span a broad range of plausible futures, but are not aimed at predicting the most likely outcome. The scenarios considered for the projections from the earlier reports (FAR, SAR) had a much simpler basis than those of the Special Report on Emission Scenarios (SRES) (IPCC, 2000) used in the later assessments. For example, the FAR scenarios did not specify future aerosol distributions. AR4 presented a multiple set of projections that were simulated using comprehensive ocean–atmosphere models provided by CMIP3 and these projections are continuations of transient simulations of the 20th century climate. These projections of temperature provide in addition a measure of the natural variability that could not be obtained

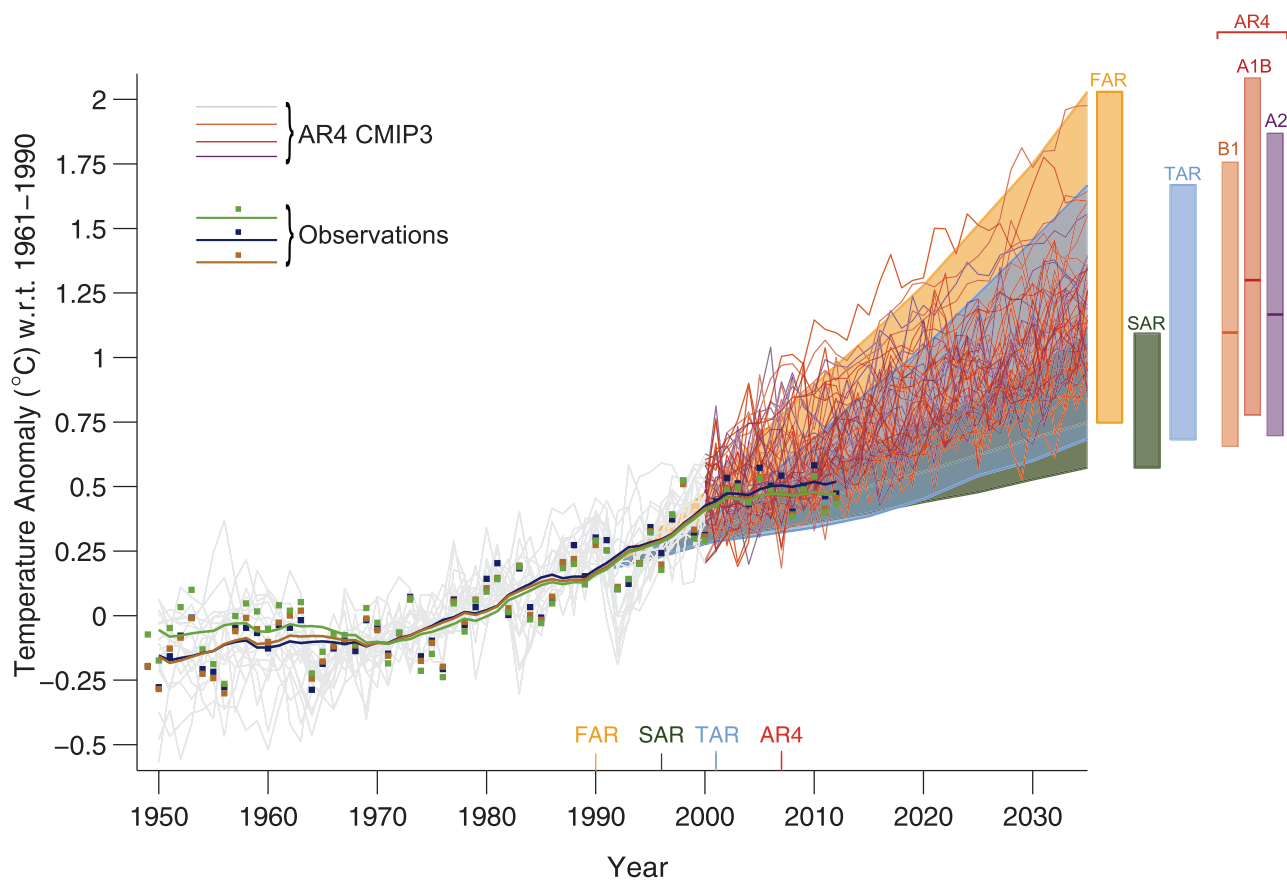


Figure 1.4 | Estimated changes in the observed globally and annually averaged surface temperature anomaly relative to 1961–1990 (in °C) since 1950 compared with the range of projections from the previous IPCC assessments. Values are harmonized to start from the same value in 1990. Observed global annual mean surface air temperature anomaly, relative to 1961–1990, is shown as squares and smoothed time series as solid lines (NASA (dark blue), NOAA (warm mustard), and the UK Hadley Centre (bright green) reanalyses). The coloured shading shows the projected range of global annual mean surface air temperature change from 1990 to 2035 for models used in FAR (Figure 6.11 in Bretherton et al., 1990), SAR (Figure 19 in the TS of IPCC, 1996), TAR (full range of TAR Figure 9.13(b) in Cubasch et al., 2001). TAR results are based on the simple climate model analyses presented and not on the individual full three-dimensional climate model simulations. For the AR4 results are presented as single model runs of the CMIP3 ensemble for the historical period from 1950 to 2000 (light grey lines) and for three scenarios (A2, A1B and B1) from 2001 to 2035. The bars at the right-hand side of the graph show the full range given for 2035 for each assessment report. For the three SRES scenarios the bars show the CMIP3 ensemble mean and the *likely* range given by –40% to +60% of the mean as assessed in Meehl et al. (2007). The publication years of the assessment reports are shown. See Appendix 1.A for details on the data and calculations used to create this figure.

from the earlier projections based on models of intermediate complexity (Cubasch et al., 2001).

Note that before TAR the climate models did not include natural forcing (such as volcanic activity and solar variability). Even in AR4 not all models included natural forcing and some also did not include aerosols. Those models that allowed for aerosol effects presented in the AR4 simulated, for example, the cooling effects of the 1991 Mt Pinatubo eruption and agree better with the observed temperatures than the previous assessments that did not include those effects.

The bars on the side for FAR, SAR and TAR represent the range of results for the scenarios at the end of the time period and are not error bars. In contrast to the previous reports, the AR4 gave an assessment of the individual scenarios with a mean estimate (cross bar; ensemble mean of the CMIP3 simulations) and a *likely* range (full bar; -40% to $+60\%$ of the mean estimate) (Meehl et al., 2007).

In summary, the trend in globally averaged surface temperatures falls within the range of the previous IPCC projections. During the last decade the trend in the observations is smaller than the mean of the projections of AR4 (see Section 9.4.1, Box 9.2 for a detailed assessment of the hiatus in global mean surface warming in the last 15 years). As shown by Hawkins and Sutton (2009), trends in the observations during short-timescale periods (decades) can be dominated by natural variability in the Earth's climate system. Similar episodes are also seen in climate model experiments (Easterling and Wehner, 2009). Due to

their experimental design these episodes cannot be duplicated with the same timing as the observed episodes in most of the model simulations; this affects the interpretation of recent trends in the scenario evaluations (Section 11.2). Notwithstanding these points, there is evidence that early forecasts that carried formal estimates of uncertainty have proved highly consistent with subsequent observations (Allen et al., 2013). If the contributions of solar variability, volcanic activity and ENSO are removed from the observations the remaining trend of surface air temperature agree better with the modelling studies (Rahmstorf et al., 2012).

1.3.2 Greenhouse Gas Concentrations

Key indicators of global climate change also include the changing concentrations of the radiatively important GHGs that are significant drivers for this change (e.g., Denman et al., 2007; Forster et al., 2007). Figures 1.5 through 1.7 show the recent globally and annually averaged observed concentrations for the gases of most concern, CO_2 , CH_4 , and N_2O (see Sections 2.2, 6.3 and 8.3 for more detailed discussion of these and other key gases). As discussed in the later chapters, accurate measurements of these long-lived gases come from a number of monitoring stations throughout the world. The observations in these figures are compared with the projections from the previous IPCC assessments.

The model simulations begin with historical emissions up to 1990. The further evolution of these gases was described by scenario projections. TAR and AR4 model concentrations after 1990 are based on the SRES

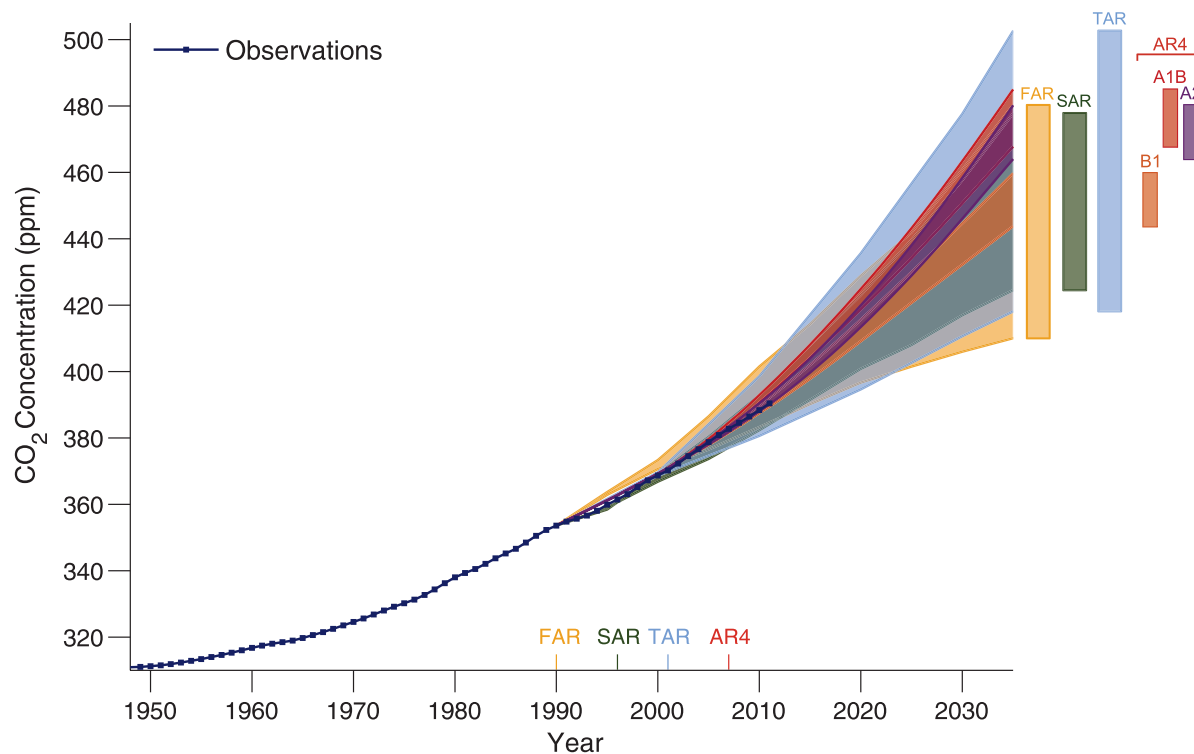


Figure 1.5 | Observed globally and annually averaged CO_2 concentrations in parts per million (ppm) since 1950 compared with projections from the previous IPCC assessments. Observed global annual CO_2 concentrations are shown in dark blue. The shading shows the largest model projected range of global annual CO_2 concentrations from 1950 to 2035 from FAR (Figure A.3 in the Summary for Policymakers of IPCC, 1990); SAR (Figure 5b in the Technical Summary of IPCC, 1996); TAR (Appendix II of IPCC, 2001); and from the A2, A1B and B1 scenarios presented in the AR4 (Figure 10.26 in Meehl et al., 2007). The bars at the right-hand side of the graph show the full range given for 2035 for each assessment report. The publication years of the assessment reports are shown. See Appendix 1.A for details on the data and calculations used to create this figure.

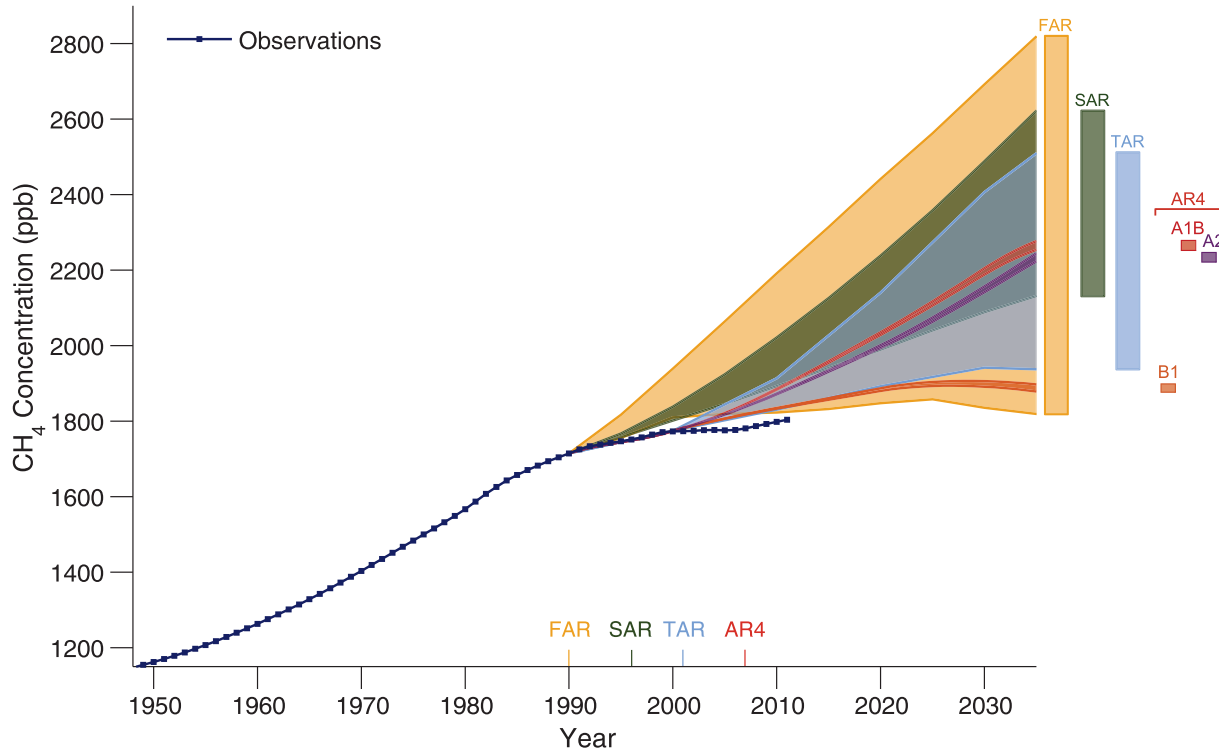


Figure 1.6 | Observed globally and annually averaged CH₄ concentrations in parts per billion (ppb) since 1950 compared with projections from the previous IPCC assessments. Estimated observed global annual CH₄ concentrations are shown in dark blue. The shading shows the largest model projected range of global annual CH₄ concentrations from 1950 to 2035 from FAR (Figure A.3 of the Annex of IPCC, 1990); SAR (Table 2.5a in Schimel et al., 1996); TAR (Appendix II of IPCC, 2001); and from the A2, A1B and B1 scenarios presented in the AR4 (Figure 10.26 in Meehl et al., 2007). The bars at the right-hand side of the graph show the full range given for 2035 for each assessment report. The publication years of the assessment reports are shown. See Appendix 1.A for details on the data and calculations used to create this figure.

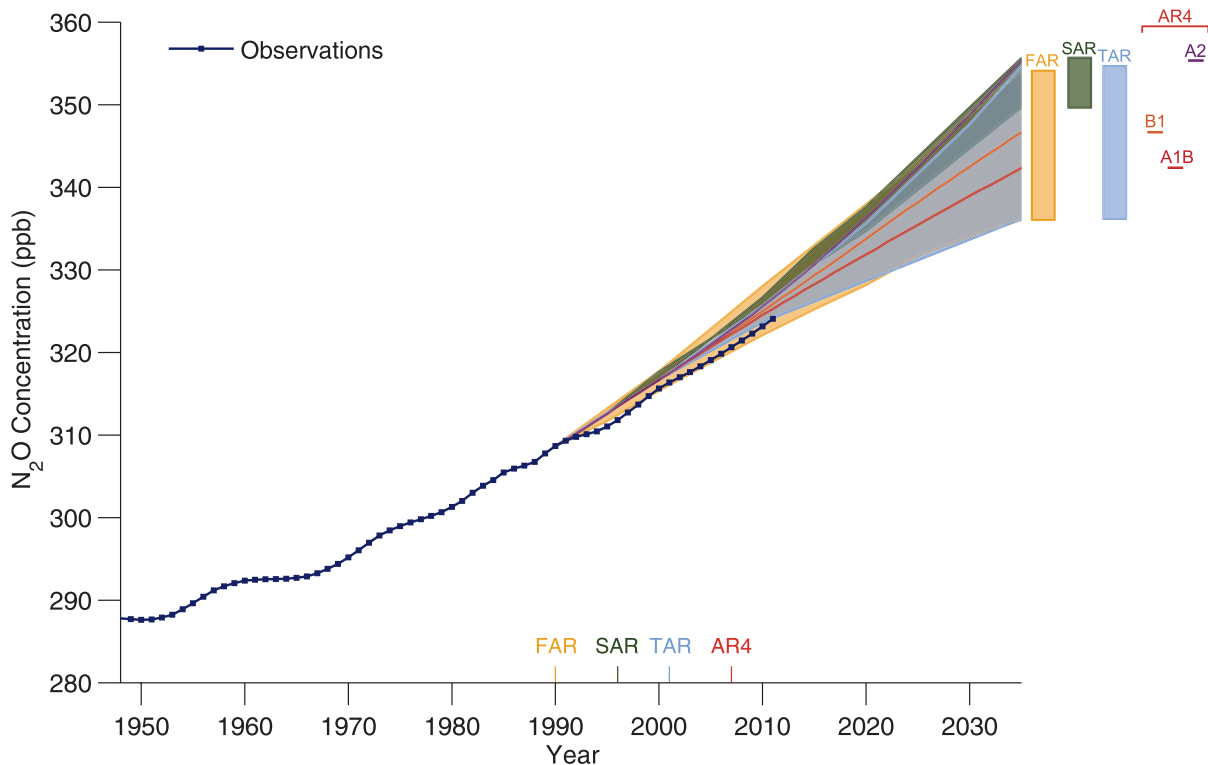


Figure 1.7 | Observed globally and annually averaged N₂O concentrations in parts per billion (ppb) since 1950 compared with projections from the previous IPCC assessments. Observed global annual N₂O concentrations are shown in dark blue. The shading shows the largest model projected range of global annual N₂O concentrations from 1950 to 2035 from FAR (Figure A3 in the Annex of IPCC, 1990), SAR (Table 2.5b in Schimel et al., 1996), TAR (Appendix II of IPCC, 2001), and from the A2, A1B and B1 scenarios presented in the AR4 (Figure 10.26 in Meehl et al., 2007). The bars at the right hand side of the graph show the full range given for 2035 for each assessment report. The publication years of the assessment reports are shown. See Appendix 1.A for details on the data and calculations used to create this figure.

scenarios but those model results may also account for historical emissions analyses. The recent observed trends in CO₂ concentrations tend to be in the middle of the scenarios used for the projections (Figure 1.5).

As discussed in Dlugokencky et al. (2009), trends in CH₄ showed a stabilization from 1999 to 2006, but CH₄ concentrations have been increasing again starting in 2007 (see Sections 2.2 and 6.3 for more discussion on the budget and changing concentration trends for CH₄). Because at the time the scenarios were developed (e.g., the SRES scenarios were developed in 2000), it was thought that past trends would continue, the scenarios used and the resulting model projections assumed in FAR through AR4 all show larger increases than those observed (Figure 1.6).

Concentrations of N₂O have continued to increase at a nearly constant rate (Elkins and Dutton, 2010) since about 1970 as shown in Figure 1.7. The observed trends tend to be in the lower part of the projections for the previous assessments.

1.3.3 Extreme Events

Climate change, whether driven by natural or human forcings, can lead to changes in the likelihood of the occurrence or strength of extreme weather and climate events such as extreme precipitation events or warm spells (see Chapter 3 of the IPCC Special Report on Managing the Risks of Extreme Events and Disasters to Advance Climate Change Adaptation (SREX); Seneviratne et al., 2012). An extreme weather event is one that is rare at a particular place and/or time of year. Definitions of 'rare' vary, but an extreme weather event would normally be as rare as or rarer than the 10th or 90th percentile of a probability density function estimated from observations (see also Glossary in Annex III and FAQ 2.2). By definition, the characteristics of what is called extreme weather may vary from place to place in an absolute sense. At present, single extreme events cannot generally be directly attributed to anthropogenic influence, although the change in likelihood for the event to occur has been determined for some events by accounting for observed changes in climate (see Section 10.6). When a pattern of extreme weather persists for some time, such as a season, it may be classified as an extreme climate event, especially if it yields an average or total that is itself extreme (e.g., drought or heavy rainfall over a season). For some climate extremes such as drought, floods and heat waves, several factors such as duration and intensity need to be combined to produce an extreme event (Seneviratne et al., 2012).

The probability of occurrence of values of a climate or weather variable can be described by a probability density function (PDF) that for some variables (e.g., temperature) is shaped similar to a Gaussian curve. A PDF is a function that indicates the relative chances of occurrence of different outcomes of a variable. Simple statistical reasoning indicates that substantial changes in the frequency of extreme events (e.g., the maximum possible 24-hour rainfall at a specific location) can result from a relatively small shift in the distribution of a weather or climate variable. Figure 1.8a shows a schematic of such a PDF and illustrates the effect of a small shift in the mean of a variable on the frequency of extremes at either end of the distribution. An increase in the frequency of one extreme (e.g., the number of hot days) can be accompanied by

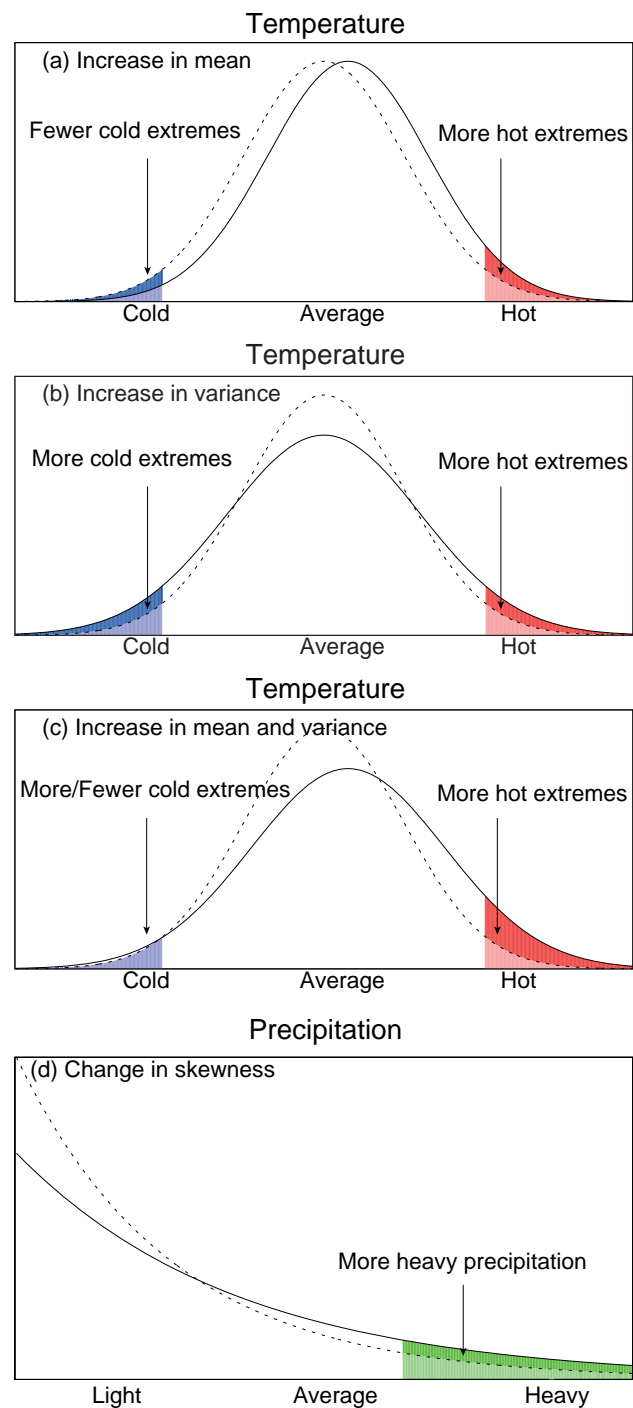


Figure 1.8 | Schematic representations of the probability density function of daily temperature, which tends to be approximately Gaussian, and daily precipitation, which has a skewed distribution. Dashed lines represent a previous distribution and solid lines a changed distribution. The probability of occurrence, or frequency, of extremes is denoted by the shaded areas. In the case of temperature, changes in the frequencies of extremes are affected by changes (a) in the mean, (b) in the variance or shape, and (c) in both the mean and the variance. (d) In a skewed distribution such as that of precipitation, a change in the mean of the distribution generally affects its variability or spread, and thus an increase in mean precipitation would also imply an increase in heavy precipitation extremes, and vice-versa. In addition, the shape of the right-hand tail could also change, affecting extremes. Furthermore, climate change may alter the frequency of precipitation and the duration of dry spells between precipitation events. (Parts a–c modified from Folland et al., 2001, and d modified from Peterson et al., 2008, as in Zhang and Zwiers, 2012.)

a decline in the opposite extreme (in this case the number of cold days such as frost days). Changes in the variability, skewness or the shape of the distribution can complicate this simple picture (Figure 1.8b, c and d).

While the SAR found that data and analyses of extremes related to climate change were sparse, improved monitoring and data for changes in extremes were available for the TAR, and climate models were being analysed to provide projections of extremes. In AR4, the observational basis of analyses of extremes had increased substantially, so that some extremes were now examined over most land areas (e.g., rainfall extremes). More models with higher resolution, and a larger number

of regional models have been used in the simulation and projection of extremes, and ensemble integrations now provide information about PDFs and extremes.

Since the TAR, climate change studies have especially focused on changes in the global statistics of extremes, and observed and projected changes in extremes have been compiled in the so-called 'Extremes'-Table (Figure 1.9). This table has been modified further to account for the SREX assessment. For some extremes ('higher maximum temperature', 'higher minimum temperature', 'precipitation extremes', 'droughts or dryness'), all of these assessments found an increasing trend in the observations and in the projections. In the observations for

Changes in Phenomenon	Uncertainty in observed changes (since about the mid-20th century)			Uncertainty in projected changes (up to 2100)		
	TAR	AR4	SREX	TAR	AR4	SREX
Higher maximum temperatures and more hot days	Likely over nearly all land areas	Very Likely over most land areas	Very Likely at a global scale	Very Likely over nearly all land areas	Virtually Certain over most land areas	Virtually Certain at a global scale
Higher minimum temperatures, fewer cold days	Very Likely over nearly all land areas	Very Likely over most land areas	Very Likely at a global scale	Very Likely over nearly all land areas	Virtually Certain over most land areas	Virtually Certain at a global scale
Warm spells/heat waves, frequency, length or intensity increases	-	Likely over most land areas	Medium Confidence in many regions	-	Very Likely over most land areas	Very Likely over most land areas
Precipitation extremes	Likely ¹ , over many Northern Hemisphere mid-to high latitude land areas	Likely ² over most areas	Likely ³	Very Likely ¹ over many areas	Very Likely ²	Likely ^{2,4} in many land areas of the globe
Droughts or dryness	Likely ⁵ , in a few areas	Likely ⁶ , in many regions since 1970s	Medium Confidence in more intense and longer droughts in some regions, but some opposite trend exists	Likely ⁵ , over most mid-latitude continental interiors (Lack of consistent projections in other areas)	Likely ⁶	Medium Confidence ⁷ that droughts will intensify in some seasons and areas; Overall low confidence elsewhere
Changes in tropical cyclone activity (i.e. intensity, frequency, duration)	Not Observed ⁸ , in the few analyses available	Likely ⁹ , in some regions since 1970	Low confidence ¹⁰	Likely ⁸ , over some areas	Likely ⁹	Likely ¹¹
Increase in extreme sea level (excludes tsunamis)	-	Likely	Likely ¹²	-	Likely	Very Likely ¹³

¹ More intense precipitation events

² Heavy precipitation events. Frequency (or proportion of total rainfall from heavy falls) increases

³ Statistically significant trends in the number of heavy precipitation events in some regions. It is *likely* that more of these regions have experienced increases than decreases.

⁴ See SREX Table 3-3 for details on precipitation extremes for the different regions.

⁵ Increased summer continental drying and associated risk of drought

⁶ Area affected by droughts increases

⁷ Some areas include southern Europe and the Mediterranean region, central Europe, central North America and Mexico, northeast Brazil and southern Africa

⁸ Increase in tropical cyclone peak wind intensities

⁹ Increase in intense tropical cyclone activity

¹⁰ In any observed long-term (i.e., 40 years or more) after accounting for past changes in observing capabilities (see SREX, section 3.4.4)

¹¹ Increase in average tropical cyclone maximum wind speed is, although not in all ocean basins; either decrease or no change in the global frequency of tropical cyclones

¹² Increase in extreme coastal high water worldwide related to increases in mean sea level in the late 20th century

¹³ Mean sea level rise will contribute to upward trends in extreme coastal high water levels

Figure 1.9 | Change in the confidence levels for extreme events based on prior IPCC assessments: TAR, AR4 and SREX. Types of extreme events discussed in all three reports are highlighted in green. Confidence levels are defined in Section 1.4. Similar analyses for AR5 are discussed in later chapters. Please note that the nomenclature for confidence level changed from AR4 to SREX and AR5.

the 'higher maximum temperature' the likelihood level was raised from *likely* in the TAR to *very likely* in SREX. While the diurnal temperature range was assessed in the Extremes-Table of the TAR, it was no longer included in the Extremes-Table of AR4, since it is not considered a climate extreme in a narrow sense. Diurnal temperature range was, however, reported to decrease for 21st century projections in AR4 (Meehl et al., 2007). In projections for precipitation extremes, the spatial relevance has been improved from *very likely* 'over many Northern Hemisphere mid-latitudes to high latitudes land areas' from the TAR to *very likely* for all regions in AR4 (these 'uncertainty labels' are discussed in Section 1.4). However, likelihood in trends in projected precipitation extremes was downscaled to *likely* in the SREX as a result of a perception of biases and a fairly large spread in the precipitation projections in some regions. SREX also had less confidence than TAR and AR4 in the trends for droughts and dryness, 'due to lack of direct observations, some geographical inconsistencies in the trends, and some dependencies of inferred trends on the index choice' (IPCC, 2012b).

For some extremes (e.g., 'changes in tropical cyclone activity') the definition changed between the TAR and the AR4. Whereas the TAR only made a statement about the peak wind speed of tropical cyclones, the AR4 also stressed the overall increase in intense tropical cyclone activity. The 'low confidence' for any long term trend (>40 years) in the observed changes of the tropical cyclone activities is due to uncertainties in past observational capabilities (IPCC, 2012b). The 'increase in extreme sea level' has been added in the AR4. Such an increase is *likely* according to the AR4 and the SREX for observed trends, and *very likely* for the climate projections reported in the SREX.

The assessed likelihood of anthropogenic contributions to trends is lower for variables where the assessment is based on indirect evidence. Especially for extremes that are the result of a combination of factors such as droughts, linking a particular extreme event to specific causal relationships is difficult to determine (e.g., difficult to establish the clear role of climate change in the event) (see Section 10.6 and Peterson et al., 2012). In some cases (e.g., precipitation extremes), however, it may be possible to estimate the human-related contribution to such changes in the probability of occurrence of extremes (Pall et al., 2011; Seneviratne et al., 2012).

1.3.4 Climate Change Indicators

Climate change can lead to other effects on the Earth's physical system that are also indicators of climate change. Such integrative indicators include changes in sea level (ocean warming + land ice melt), in ocean acidification (ocean uptake of CO₂) and in the amount of ice on ocean and land (temperature and hydrological changes). See Chapters 3, 4 and 13 for detailed assessment.

1.3.4.1 Sea Level

Global mean sea level is an important indicator of climate change (Section 3.7 and Chapter 13). The previous assessments have all shown that observations indicate that the globally averaged sea level is rising. Direct observations of sea level change have been made for more than 150 years with tide gauges, and for more than 20 years with satellite radar altimeters. Although there is regional variability from

non-uniform density change, circulation changes, and deformation of ocean basins, the evidence indicates that the global mean sea level is rising, and that this is *likely* (according to AR4 and SREX) resulting from global climate change (ocean warming plus land ice melt; see Chapter 13 for AR5 findings). The historical tide gauge record shows that the average rate of global mean sea level rise over the 20th century was $1.7 \pm 0.2 \text{ mm yr}^{-1}$ (e.g., Church and White, 2011). This rate increased to $3.2 \pm 0.4 \text{ mm yr}^{-1}$ since 1990, mostly because of increased thermal expansion and land ice contributions (Church and White, 2011; IPCC, 2012b). Although the long-term sea level record shows decadal and multi-decadal oscillations, there is evidence that the rate of global mean sea level rise during the 20th century was greater than during the 19th century.

All of the previous IPCC assessments have projected that global sea level will continue to rise throughout this century for the scenarios examined. Figure 1.10 compares the observed sea level rise since 1950 with the projections from the prior IPCC assessments. Earlier models had greater uncertainties in modelling the contributions, because of limited observational evidence and deficiencies in theoretical understanding of relevant processes. Also, projections for sea level change in the prior assessments are scenarios for the response to anthropogenic forcing only; they do not include unforced or natural interannual variability. Nonetheless, the results show that the actual change is in the middle of projected changes from the prior assessments, and towards the higher end of the studies from TAR and AR4.

1.3.4.2 Ocean Acidification

The observed decrease in ocean pH resulting from increasing concentrations of CO₂ is another indicator of global change. As discussed in AR4, the ocean's uptake of CO₂ is having a significant impact on the chemistry of sea water. The average pH of ocean surface waters has fallen by about 0.1 units, from about 8.2 to 8.1 (total scale) since 1765 (Section 3.8). Long time series from several ocean sites show ongoing declines in pH, consistent with results from repeated pH measurements on ship transects spanning much of the globe (Sections 3.8 and 6.4; Byrne et al., 2010; Midorikawa et al., 2010). Ocean time-series in the North Atlantic and North Pacific record a decrease in pH ranging between -0.0015 and -0.0024 per year (Section 3.8). Due to the increased storage of carbon by the ocean, ocean acidification will increase in the future (Chapter 6). In addition to other impacts of global climate change, ocean acidification poses potentially serious threats to the health of the world's oceans ecosystems (see AR5 WGII assessment).

1.3.4.3 Ice

Rapid sea ice loss is one of the most prominent indicators of Arctic climate change (Section 4.2). There has been a trend of decreasing Northern Hemisphere sea ice extent since 1978, with the summer of 2012 being the lowest in recorded history (see Section 4.2 for details). The 2012 minimum sea ice extent was 49% below the 1979 to 2000 average and 18% below the previous record from 2007. The amount of multi-year sea ice has been reduced, i.e., the sea ice has been thinning and thus the ice volume is reduced (Haas et al., 2008; Kwok et al., 2009). These changes make the sea ice less resistant to wind forcing.

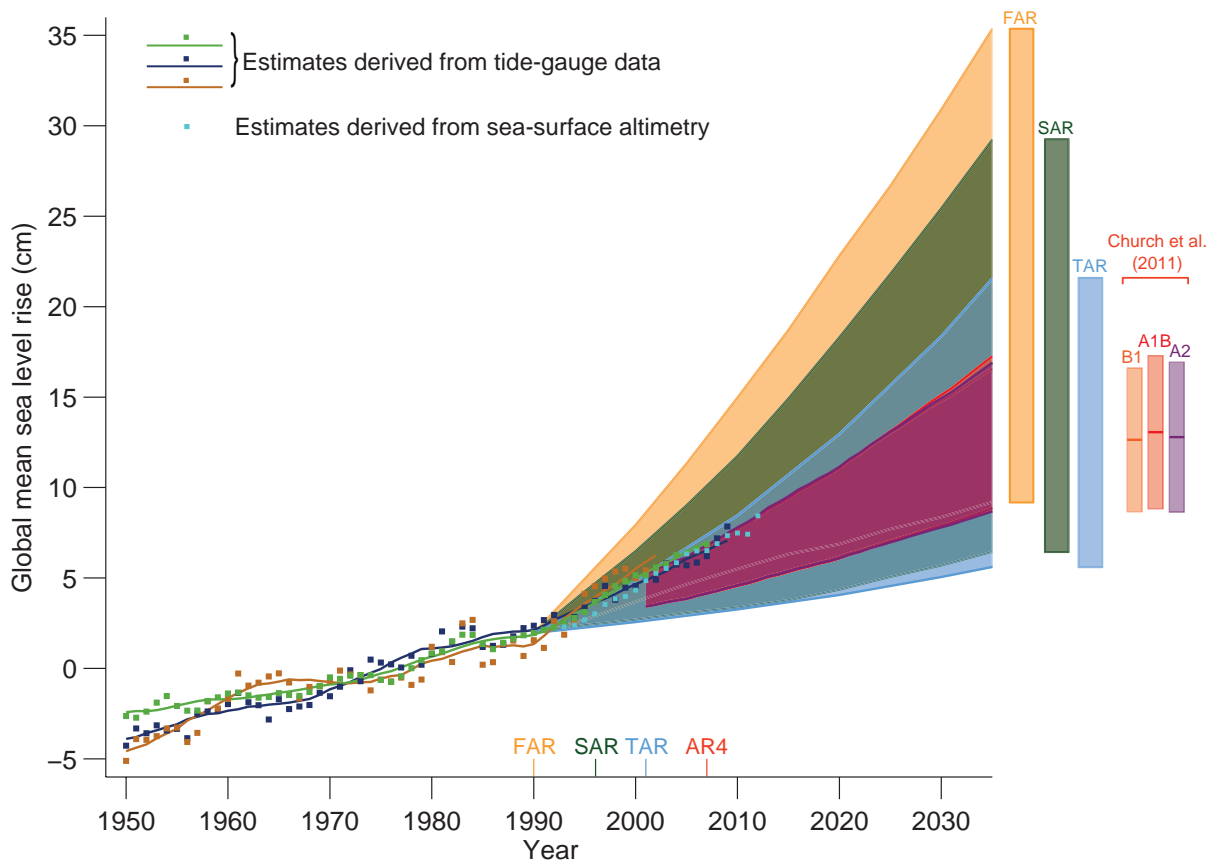


Figure 1.10 | Estimated changes in the observed global annual mean sea level (GMSL) since 1950 relative to 1961–1990. Estimated changes in global annual sea level anomalies are presented based on tide gauge data (warm mustard: Jevrejeva et al., 2008; dark blue: Church and White, 2011; dark green: Ray and Douglas, 2011) and based on sea surface altimetry (light blue). The altimetry data start in 1993 and are harmonized to start from the mean 1993 value of the tide gauge data. Squares indicate annual mean values and solid lines smoothed values. The shading shows the largest model projected range of global annual sea level rise from 1950 to 2035 for FAR (Figures 9.6 and 9.7 in Warrick and Oerlemans, 1990), SAR (Figure 21 in TS of IPCC, 1996), TAR (Appendix II of IPCC, 2001) and for Church et al. (2011) based on the Coupled Model Intercomparison Project Phase 3 (CMIP3) model results not assessed at the time of AR4 using the SRES B1, A1B and A2 scenarios. Note that in the AR4 no full range was given for the sea level projections for this period. Therefore, the figure shows results that have been published subsequent to the AR4. The bars at the right-hand side of the graph show the full range given for 2035 for each assessment report. For Church et al. (2011) the mean sea level rise is indicated in addition to the full range. See Appendix 1.A for details on the data and calculations used to create this figure.

Sea ice extent has been diminishing significantly faster than projected by most of the AR4 climate models (SWIPA, 2011). While AR4 found no consistent trends in Antarctica sea ice, more recent studies indicate a small increase (Section 4.2). Various studies since AR4 suggest that this has resulted in a deepening of the low-pressure systems in West Antarctica that in turn caused stronger winds and enhanced ice production in the Ross Sea (Goosse et al., 2009; Turner and Overland, 2009).

AR4 concluded that taken together, the ice sheets in Greenland and Antarctica have *very likely* been contributing to sea level rise. The Greenland Ice Sheet has lost mass since the early 1990s and the rate of loss has increased (see Section 4.4). The interior, high-altitude areas are thickening due to increased snow accumulation, but this is more than counterbalanced by the ice loss due to melt and ice discharge (AMAP, 2009; Ettema et al., 2009). Since 1979, the area experiencing surface melting has increased significantly (Tedesco, 2007; Mernild et al., 2009), with 2010 breaking the record for surface melt area, runoff, and mass loss, and the unprecedented areal extent of surface melt of the Greenland Ice Sheet in 2012 (Nghiem et al., 2012). Overall, the Antarctic continent now experiences a net loss of ice (Section 4.4). Significant mass loss has been occurring in the Amundsen Sea sector

of West Antarctica and the northern Antarctic Peninsula. The ice sheet on the rest of the continent is relatively stable or thickening slightly (Lemke et al., 2007; Scott et al., 2009; Turner et al., 2009). Since AR4, there have been improvements in techniques of measurement, such as gravity, altimetry and mass balance, and understanding of the change (Section 4.4).

As discussed in the earlier assessments, most glaciers around the globe have been shrinking since the end of the Little Ice Age, with increasing rates of ice loss since the early 1980s (Section 4.3). The vertical profiles of temperature measured through the entire thickness of mountain glaciers, or through ice sheets, provide clear evidence of a warming climate over recent decades (e.g., Lüthi and Funk, 2001; Hoelzle et al., 2011). As noted in AR4, the greatest mass losses per unit area in the last four decades have been observed in Patagonia, Alaska, northwest USA, southwest Canada, the European Alps, and the Arctic. Alaska and the Arctic are especially important regions as contributors to sea level rise (Zemp et al., 2008, 2009).

1.4 Treatment of Uncertainties

1.4.1 Uncertainty in Environmental Science

Science always involves uncertainties. These arise at each step of the scientific method: in the development of models or hypotheses, in measurements and in analyses and interpretation of scientific assumptions. Climate science is not different in this regard from other areas of science. The complexity of the climate system and the large range of processes involved bring particular challenges because, for example, gaps in direct measurements of the past can be filled only by reconstructions using proxy data.

Because the Earth's climate system is characterized by multiple spatial and temporal scales, uncertainties do not usually reduce at a single, predictable rate: for example, new observations may reduce the uncertainties surrounding short-timescale processes quite rapidly, while longer timescale processes may require very long observational baselines before much progress can be made. Characterization of the interaction between processes, as quantified by models, can be improved by model development, or can shed light on new areas in which uncertainty is greater than previously thought. The fact that there is only a single realization of the climate, rather than a range of different climates from which to draw, can matter significantly for certain lines of enquiry, most notably for the detection and attribution of causes of climate change and for the evaluation of projections of future states.

1.4.2 Characterizing Uncertainty

'Uncertainty' is a complex and multifaceted property, sometimes originating in a lack of information, and at other times from quite fundamental disagreements about what is known or even knowable (Moss and Schneider, 2000). Furthermore, scientists often disagree about the best or most appropriate way to characterize these uncertainties: some can be quantified easily while others cannot. Moreover, appropriate characterization is dependent on the intended use of the information and the particular needs of that user community.

Scientific uncertainty can be partitioned in various ways, in which the details of the partitioning usually depend on the context. For instance, the process and classifications used for evaluating observational uncertainty in climate science is not the same as that employed to evaluate projections of future change. Uncertainty in measured quantities can arise from a range of sources, such as statistical variation, variability, inherent randomness, inhomogeneity, approximation, subjective judgement, and linguistic imprecision (Morgan et al., 1990), or from calibration methodologies, instrumental bias or instrumental limitations (JCGM, 2008).

In the modelling studies that underpin projections of future climate change, it is common to partition uncertainty into four main categories: scenario uncertainty, due to uncertainty of future emissions of GHGs and other forcing agents; 'model uncertainty' associated with climate models; internal variability and initial condition uncertainty; and forcing and boundary condition uncertainty for the assessment of historical and paleoclimate simulations (e.g., Collins and Allen, 2002; Yip et al., 2011).

Model uncertainty is an important contributor to uncertainty in climate predictions and projections. It includes, but is not restricted to, the uncertainties introduced by errors in the model's representation of dynamical and physical and bio-geochemical aspects of the climate system as well as in the model's response to external forcing. The phrase 'model uncertainty' is a common term in the climate change literature, but different studies use the phrase in different senses: some use it to represent the range of behaviours observed in ensembles of climate model (model spread), while others use it in more comprehensive senses (see Sections 9.2, 11.2 and 12.2). Model spread is often used as a measure of climate response uncertainty, but such a measure is crude as it takes no account of factors such as model quality (Chapter 9) or model independence (e.g., Masson and Knutti, 2011; Pennell and Reichler, 2011), and not all variables of interest are adequately simulated by global climate models.

To maintain a degree of terminological clarity this report distinguishes between 'model spread' for this narrower representation of climate model responses and 'model uncertainty' which describes uncertainty about the extent to which any particular climate model provides an accurate representation of the real climate system. This uncertainty arises from approximations required in the development of models. Such approximations affect the representation of all aspects of the climate including the response to external forcings.

Model uncertainty is sometimes decomposed further into parametric and structural uncertainty, comprising, respectively, uncertainty in the values of model parameters and uncertainty in the underlying model structure (see Section 12.2). Some scientific research areas, such as detection and attribution and observationally-constrained model projections of future climate, incorporate significant elements of both observational and model-based science, and in these instances both sets of relevant uncertainties need to be incorporated.

Scenario uncertainty refers to the uncertainties that arise due to limitations in our understanding of future emissions, concentration or forcing trajectories. Scenarios help in the assessment of future developments in complex systems that are either inherently unpredictable, or that have high scientific uncertainties (IPCC, 2000). The societal choices defining future climate drivers are surrounded by considerable uncertainty, and these are explored by examining the climate response to a wide range of possible futures. In past reports, emissions scenarios from the SRES (IPCC, 2000) were used as the main way of exploring uncertainty in future anthropogenic climate drivers. Recent research has made use of Representative Concentration Pathways (RCP) (van Vuuren et al., 2011a, 2011b).

Internal or natural variability, the natural fluctuations in climate, occur in the absence of any RF of the Earth's climate (Hawkins and Sutton, 2009). Climate varies naturally on nearly all time and space scales, and quantifying precisely the nature of this variability is challenging, and is characterized by considerable uncertainty. The analysis of internal and forced contributions to recent climate is discussed in Chapter 10. The fractional contribution of internal variability compared with other forms of uncertainty varies in time and in space, but usually diminishes with time as other sources of uncertainty become more significant (Hawkins and Sutton, 2009; see also Chapter 11 and FAQ 1.1).

In the WGI contribution to the AR5, uncertainty is quantified using 90% uncertainty intervals unless otherwise stated. The 90% uncertainty interval, reported in square brackets, is expected to have a 90% likelihood of covering the value that is being estimated. The value that is being estimated has a 5% likelihood of exceeding the upper endpoint of the uncertainty interval, and the value has a 5% likelihood of being less than that the lower endpoint of the uncertainty interval. A best estimate of that value is also given where available. Uncertainty intervals are not necessarily symmetric about the corresponding best estimate.

In a subject as complex and diverse as climate change, the information available as well as the way it is expressed, and often the interpretation of that material, varies considerably with the scientific context. In some cases, two studies examining similar material may take different approaches even to the quantification of uncertainty. The interpretation of similar numerical ranges for similar variables can differ from study to study. Readers are advised to pay close attention to the caveats and conditions that surround the results presented in peer-reviewed studies, as well as those presented in this assessment. To help readers in this complex and subtle task, the IPCC draws on specific, calibrated language scales to express uncertainty (Mastrandrea et al., 2010), as well as specific procedures for the expression of uncertainty (see Table 1.2). The aim of these structures is to provide tools through which chapter teams might consistently express uncertainty in key results.

1.4.3 Treatment of Uncertainty in IPCC

In the course of the IPCC assessment procedure, chapter teams review the published research literature, document the findings (including uncertainties), assess the scientific merit of this information, identify the key findings, and attempt to express an appropriate measure of the uncertainty that accompanies these findings using a shared guidance procedure. This process has changed over time. The early Assessment Reports (FAR and SAR) were largely qualitative. As the field has grown and matured, uncertainty is being treated more explicitly, with a greater emphasis on the expression, where possible and appropriate, of quantified measures of uncertainty.

Although IPCC's treatment of uncertainty has become more sophisticated since the early reports, the rapid growth and considerable diversity of climate research literature presents ongoing challenges. In the wake of the TAR the IPCC formed a Cross-Working Group team charged with identifying the issues and compiling a set of Uncertainty Guidance Notes that could provide a structure for consistent treatment of uncertainty across the IPCC's remit (Manning et al., 2004). These expanded on the procedural elements of Moss and Schneider (2000) and introduced calibrated language scales designed to enable chapter teams to use the appropriate level of precision to describe findings. These notes were revised between the TAR and AR4 and again between AR4 and AR5 (Mastrandrea et al., 2010).

Recently, increased engagement of social scientists (e.g., Patt and Schrag, 2003; Kandlikar et al., 2005; Risbey and Kandlikar, 2007; Broomell and Budescu, 2009; Budescu et al., 2009; CCSP, 2009) and expert advisory panels (CCSP, 2009; InterAcademy Council, 2010) in the area of uncertainty and climate change has helped clarify issues

and procedures to improve presentation of uncertainty. Many of the recommendations of these groups are addressed in the revised Guidance Notes. One key revision relates to clarification of the relationship between the 'confidence' and 'likelihood' language, and pertains to demarcation between qualitative descriptions of 'confidence' and the numerical representations of uncertainty that are expressed by the likelihood scale. In addition, a finding that includes a probabilistic measure of uncertainty does not require explicit mention of the level of confidence associated with that finding if the level of *confidence* is *high* or *very high*. This is a concession to stylistic clarity and readability: if something is described as having a high likelihood, then in the absence of additional qualifiers it should be inferred that it also has *high* or *very high confidence*.

1.4.4 Uncertainty Treatment in This Assessment

All three IPCC Working Groups in the AR5 have agreed to use two metrics for communicating the degree of certainty in key findings (Mastrandrea et al., 2010):

- Confidence in the validity of a finding, based on the type, amount, quality, and consistency of evidence (e.g., data, mechanistic understanding, theory, models, expert judgment) and the degree of agreement. Confidence is expressed qualitatively.
- Quantified measures of uncertainty in a finding expressed probabilistically (based on statistical analysis of observations or model results, or expert judgement).

A level of confidence synthesizes the Chapter teams' judgements about the validity of findings as determined through evaluation of the available evidence and the degree of scientific agreement. The evidence and agreement scale underpins the assessment, as it is on the basis of evidence and agreement that statements can be made with scientific confidence (in this sense, the evidence and agreement scale replaces the 'level of scientific understanding' scale used in previous WGI assessments). There is flexibility in this relationship; for a given evidence and agreement statement, different confidence levels could be assigned, but increasing levels of evidence and degrees of agreement are correlated with increasing confidence. Confidence cannot necessarily be assigned for all combinations of evidence and agreement, but where key variables are highly uncertain, the available evidence and scientific agreement regarding that variable are presented and discussed. Confidence should not be interpreted probabilistically, and it is distinct from 'statistical confidence'.

The confidence level is based on the evidence (robust, medium and limited) and the agreement (high, medium and low). A combination of different methods, e.g., observations and modelling, is important for evaluating the confidence level. Figure 1.11 shows how the combined evidence and agreement results in five levels for the confidence level used in this assessment.

The qualifier 'likelihood' provides calibrated language for describing quantified uncertainty. It can be used to express a probabilistic estimate of the occurrence of a single event or of an outcome, for example, a climate parameter, observed trend, or projected change

Frequently Asked Questions

FAQ 1.1 | If Understanding of the Climate System Has Increased, Why Hasn't the Range of Temperature Projections Been Reduced?

1

The models used to calculate the IPCC's temperature projections agree on the direction of future global change, but the projected size of those changes cannot be precisely predicted. Future greenhouse gas (GHG) emission rates could take any one of many possible trajectories, and some underlying physical processes are not yet completely understood, making them difficult to model. Those uncertainties, combined with natural year-to-year climate variability, produce an 'uncertainty range' in temperature projections.

The uncertainty range around projected GHG and aerosol precursor emissions (which depend on projections of future social and economic conditions) cannot be materially reduced. Nevertheless, improved understanding and climate models—along with observational constraints—may reduce the uncertainty range around some factors that influence the climate's response to those emission changes. The complexity of the climate system, however, makes this a slow process. (FAQ1.1, Figure 1)

Climate science has made many important advances since the last IPCC assessment report, thanks to improvements in measurements and data analysis in the cryosphere, atmosphere, land, biosphere and ocean systems. Scientists also have better understanding and tools to model the role of clouds, sea ice, aerosols, small-scale ocean mixing, the carbon cycle and other processes. More observations mean that models can now be evaluated more thoroughly, and projections can be better constrained. For example, as models and observational analysis have improved, projections of sea level rise have become more accurate, balancing the current sea level rise budget.

Despite these advances, there is still a range in plausible projections for future global and regional climate—what scientists call an 'uncertainty range'. These uncertainty ranges are specific to the variable being considered (precipitation vs. temperature, for instance) and the spatial and temporal extent (such as regional vs. global averages). Uncertainties in climate projections arise from natural variability and uncertainty around the rate of future emissions and the climate's response to them. They can also occur because representations of some known processes are as yet unrefined, and because some processes are not included in the models.

There are fundamental limits to just how precisely annual temperatures can be projected, because of the chaotic nature of the climate system. Furthermore, decadal-scale projections are sensitive to prevailing conditions—such as the temperature of the deep ocean—that are less well known. Some natural variability over decades arises from interactions between the ocean, atmosphere, land, biosphere and cryosphere, and is also linked to phenomena such as the El Niño-Southern Oscillation (ENSO) and the North Atlantic Oscillation (see Box 2.5 for details on patterns and indices of climate variability).

Volcanic eruptions and variations in the sun's output also contribute to natural variability, although they are externally forced and explainable. This natural variability can be viewed as part of the 'noise' in the climate record, which provides the backdrop against which the 'signal' of anthropogenic climate change is detected.

Natural variability has a greater influence on uncertainty at regional and local scales than it does over continental or global scales. It is inherent in the Earth system, and more knowledge will not eliminate the uncertainties it brings. However, some progress is possible—particularly for projections up to a few years ahead—which exploit advances in knowledge of, for instance, the cryosphere or ocean state and processes. This is an area of active research. When climate variables are averaged over decadal timescales or longer, the relative importance of internal variability diminishes, making the long-term signals more evident (FAQ1.1, Figure 1). This long-term perspective is consistent with a common definition of climate as an average over 30 years.

A second source of uncertainty stems from the many possible trajectories that future emission rates of GHGs and aerosol precursors might take, and from future trends in land use. Nevertheless, climate projections rely on input from these variables. So to obtain these estimates, scientists consider a number of alternative scenarios for future human society, in terms of population, economic and technological change, and political choices. They then estimate the likely emissions under each scenario. The IPCC informs policymaking, therefore climate projections for different emissions scenarios can be useful as they show the possible climatic consequences of different policy choices. These scenarios are intended to be compatible with the full range of emissions scenarios described in the current scientific literature, with or without climate policy. As such, they are designed to sample uncertainty in future scenarios. *(continued on next page)*

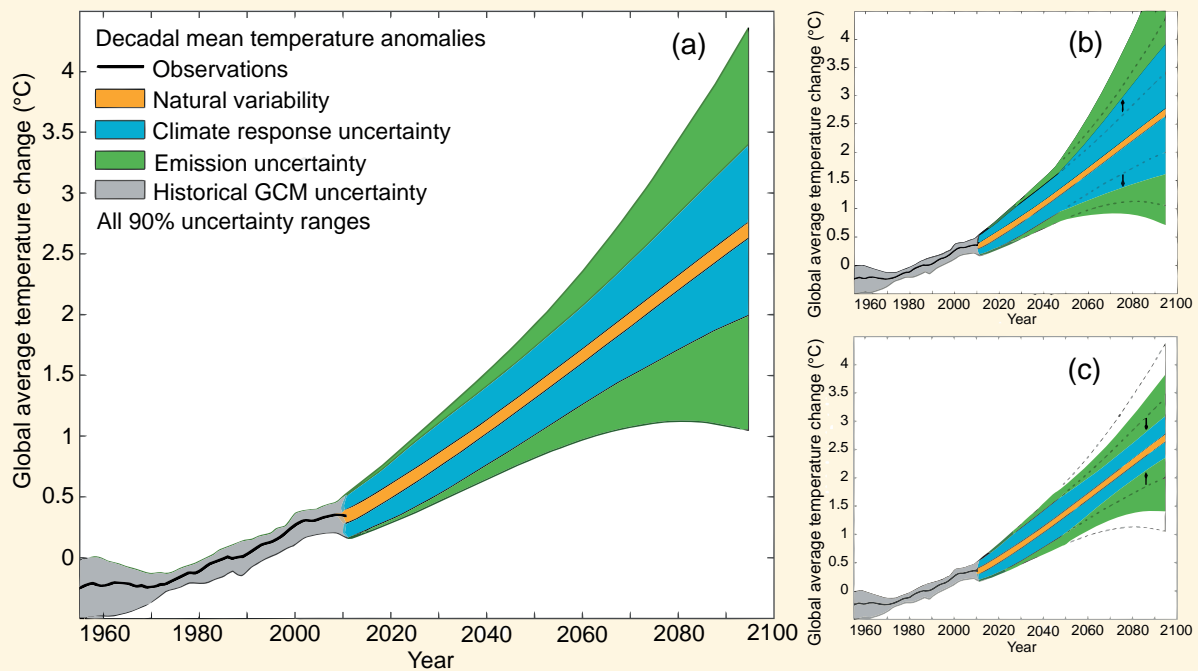
FAQ 1.1 (continued)

Projections for the next few years and decades are sensitive to emissions of short-lived compounds such as aerosols and methane. More distant projections, however, are more sensitive to alternative scenarios around long-lived GHG emissions. These scenario-dependent uncertainties will not be reduced by improvements in climate science, and will become the dominant uncertainty in projections over longer timescales (e.g., 2100) (FAQ 1.1, Figure 1).

The final contribution to the uncertainty range comes from our imperfect knowledge of how the climate will respond to future anthropogenic emissions and land use change. Scientists principally use computer-based global climate models to estimate this response. A few dozen global climate models have been developed by different groups of scientists around the world. All models are built on the same physical principles, but some approximations are needed because the climate system is so complex. Different groups choose slightly different approximations to represent specific processes in the atmosphere, such as clouds. These choices produce differences in climate projections from different models. This contribution to the uncertainty range is described as ‘response uncertainty’ or ‘model uncertainty’.

The complexity of the Earth system means that future climate could follow many different scenarios, yet still be consistent with current understanding and models. As observational records lengthen and models improve, researchers should be able, within the limitations of the range of natural variability, to narrow that range in probable temperature in the next few decades (FAQ 1.1, Figure 1). It is also possible to use information about the current state of the oceans and cryosphere to produce better projections up to a few years ahead.

As science improves, new geophysical processes can be added to climate models, and representations of those already included can be improved. These developments can appear to increase model-derived estimates of climate response uncertainty, but such increases merely reflect the quantification of previously unmeasured sources of uncertainty (FAQ 1.1, Figure 1). As more and more important processes are added, the influence of unquantified processes lessens, and there can be more confidence in the projections.



FAQ 1.1, Figure 1 | Schematic diagram showing the relative importance of different uncertainties, and their evolution in time. (a) Decadal mean surface temperature change (°C) from the historical record (black line), with climate model estimates of uncertainty for historical period (grey), along with future climate projections and uncertainty. Values are normalised by means from 1961 to 1980. Natural variability (orange) derives from model interannual variability, and is assumed constant with time. Emission uncertainty (green) is estimated as the model mean difference in projections from different scenarios. Climate response uncertainty (blue-solid) is based on climate model spread, along with added uncertainties from the carbon cycle, as well as rough estimates of additional uncertainty from poorly modelled processes. Based on Hawkins and Sutton (2011) and Huntingford et al. (2009). (b) Climate response uncertainty can appear to increase when a new process is discovered to be relevant, but such increases reflect a quantification of previously unmeasured uncertainty, or (c) can decrease with additional model improvements and observational constraints. The given uncertainty range of 90% means that the temperature is estimated to be in that range, with a probability of 90%.

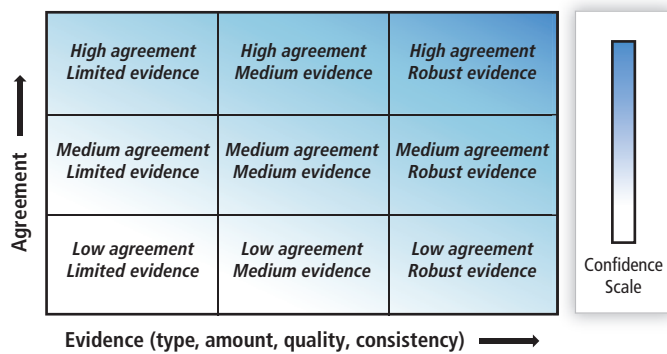


Figure 1.11 | The basis for the confidence level is given as a combination of evidence (limited, medium, robust) and agreement (low, medium and high) (Mastrandrea et al., 2010).

lying in a given range. Statements made using the likelihood scale may be based on statistical or modelling analyses, elicitation of expert views, or other quantitative analyses. Where sufficient information is available it is preferable to eschew the likelihood qualifier in favour of the full probability distribution or the appropriate probability range. See Table 1.2 for the list of ‘likelihood’ qualifiers to be used in AR5.

Many social sciences studies have found that the interpretation of uncertainty is contingent on the presentation of information, the context within which statements are placed and the interpreter’s own lexical preferences. Readers often adjust their interpretation of probabilistic language according to the magnitude of perceived potential consequences (Patt and Schrag, 2003; Patt and Dessai, 2005). Furthermore, the framing of a probabilistic statement impinges on how it is interpreted (Kahneman and Tversky, 1979): for example, a 10% chance of dying is interpreted more negatively than a 90% chance of surviving.

In addition, work examining expert judgement and decision making shows that people—including scientific experts—are prone to a range of heuristics and biases that affect their judgement (e.g., Kahneman et al., 1982). For example, in the case of expert judgements there is a tendency towards overconfidence both at the individual level (Morgan et al., 1990) and at the group level as people converge on a view and draw confidence in its reliability from each other. However, in an assessment of the state of scientific knowledge across a field

Table 1.2 | Likelihood terms associated with outcomes used in the AR5.

Term	Likelihood of the Outcome
<i>Virtually certain</i>	99–100% probability
<i>Very likely</i>	90–100% probability
<i>Likely</i>	66–100% probability
<i>About as likely as not</i>	33–66% probability
<i>Unlikely</i>	0–33% probability
<i>Very unlikely</i>	0–10% probability
<i>Exceptionally unlikely</i>	0–1% probability

Notes:

Additional terms that were used in limited circumstances in the AR4 (*extremely likely* = 95–100% probability, *more likely than not* = >50–100% probability, and *extremely unlikely* = 0–5% probability) may also be used in the AR5 when appropriate.

such as climate change—characterized by complexity of process and heterogeneity of data constraints—some degree of expert judgement is inevitable (Mastrandrea et al., 2010).

These issues were brought to the attention of chapter teams so that contributors to the AR5 might be sensitized to the ways presentation, framing, context and potential biases might affect their own assessments and might contribute to readers’ understanding of the information presented in this assessment. There will always be room for debate about how to summarize such a large and growing literature. The uncertainty guidance is aimed at providing a consistent, calibrated set of words through which to communicate the uncertainty, confidence and degree of consensus prevailing in the scientific literature. In this sense the guidance notes and practices adopted by IPCC for the presentation of uncertainties should be regarded as an interdisciplinary work in progress, rather than as a finalized, comprehensive approach. Moreover, one precaution that should be considered is that translation of this assessment from English to other languages may lead to a loss of precision.

1.5 Advances in Measurement and Modelling Capabilities

Since AR4, measurement capabilities have continued to advance. The models have been improved following the progress in the understanding of physical processes within the climate system. This section illustrates some of those developments.

1.5.1 Capabilities of Observations

Improved understanding and systematic monitoring of Earth’s climate requires observations of various atmospheric, oceanic and terrestrial parameters and therefore has to rely on various technologies (ranging from ground-based instruments to ships, buoys, ocean profilers, balloons, aircraft, satellite-borne sensors, etc.). The Global Climate Observing System (GCOS, 2009) defined a list of so-called Essential Climate Variables, that are technically and economically feasible to observe, but some of the associated observing systems are not yet operated in a systematic manner. However, during recent years, new observational systems have increased the number of observations by orders of magnitude and observations have been made at places where there have been no data before (see Chapters 2, 3 and 4 for an assessment of changes in observations). Parallel to this, tools to analyse and process the data have been developed and enhanced to cope with the increase of information and to provide a more comprehensive picture of the Earth’s climate. At the same time, it should be kept in mind that there has been some limited progress in developing countries in filling gaps in their *in situ* observing networks, but developed countries have made little progress in ensuring long-term continuity for several important observing systems (GCOS, 2009). In addition, more proxy (non-instrumental) data have been acquired to provide a more comprehensive picture of climate changes in the past (see Chapter 5). Efforts are also occurring to digitize historic observations, mainly of ground-station data from periods prior to the second half of the 20th century (Brunet and Jones, 2011).

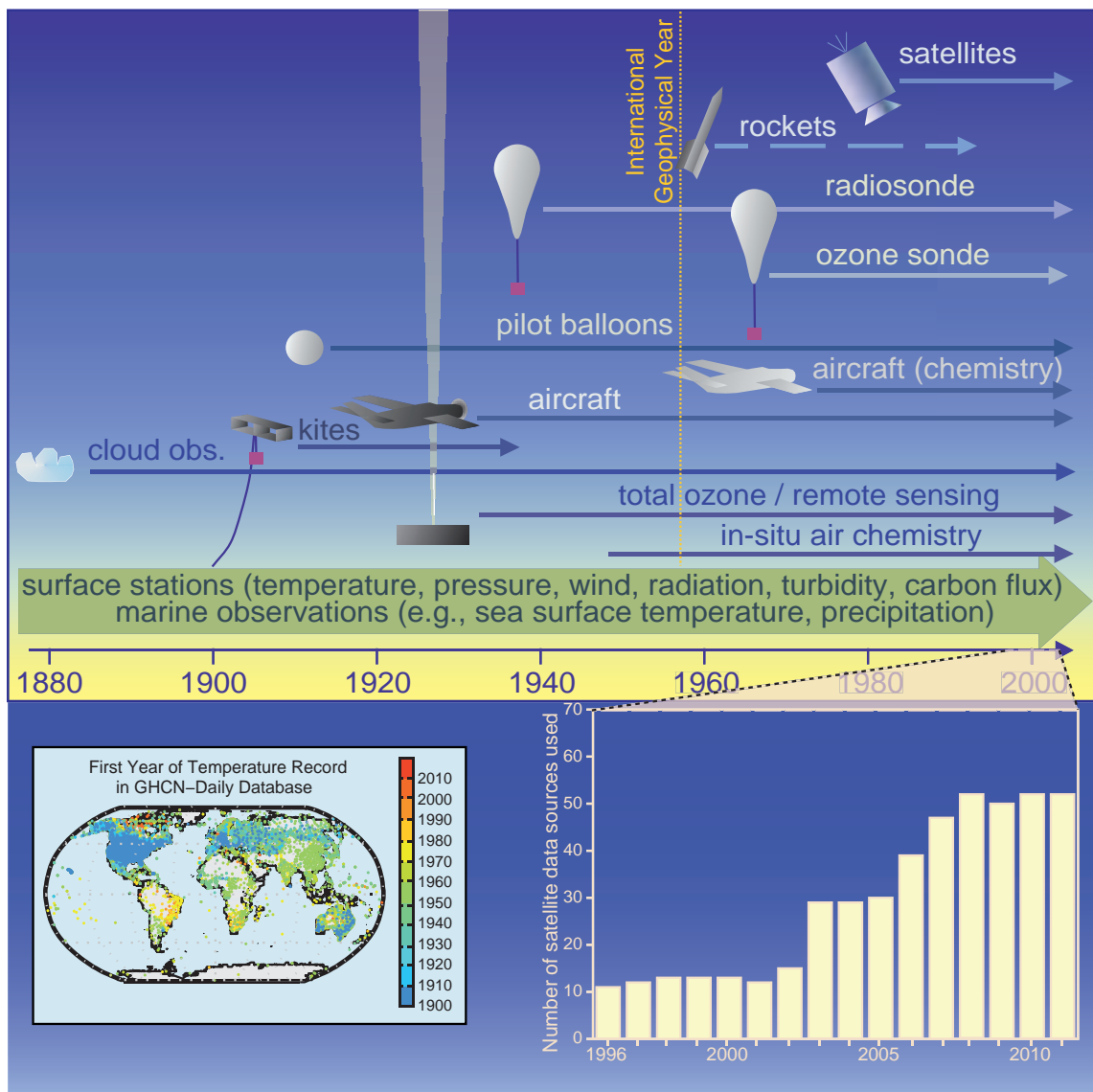


Figure 1.12 | Development of capabilities of observations. Top: Changes in the mix and increasing diversity of observations over time create challenges for a consistent climate record (adapted from Brönnimann et al., 2008). Bottom left: First year of temperature data in Global Historical Climatology Network (GHCN) daily database (available at <http://www.ncdc.noaa.gov/oa/climate/ghcn-daily/>; Menne et al., 2012). Bottom right: Number of satellite instruments from which data have been assimilated in the European Centre for Medium-Range Weather Forecasts production streams for each year from 1996 to 2010. This figure is used as an example to demonstrate the fivefold increase in the usage of satellite data over this time period.

Reanalysis is a systematic approach to produce gridded dynamically consistent data sets for climate monitoring and research by assimilating all available observations with help of a climate model (Box 2.3). Model-based reanalysis products play an important role in obtaining a consistent picture of the climate system. However, their usefulness in detecting long-term climate trends is currently limited by changes over time in observational coverage and biases, linked to the presence of biases in the assimilating model (see also Box 2.3 in Chapter 2). Because AR4 both the quantity and quality of the observations that are assimilated through reanalysis have increased (GCOS, 2009). As an example, there has been some overall increase in mostly atmospheric observations assimilated in European Centre for Medium-Range Weather Forecasts Interim Reanalysis since 2007 (Dee et al., 2011). The overwhelming majority of the data, and most of the increase over recent years, come from satellites (Figure 1.12) (GCOS, 2011). For

example, information from Global Positioning System radio occultation measurements has increased significantly since 2007. The increases in data from fixed stations are often associated with an increased frequency of reporting, rather than an increase in the number of stations. Increases in data quality come from improved instrument design or from more accurate correction in the ground-station processing that is applied before the data are transmitted to users and data centres. As an example for *in situ* data, temperature biases of radiosonde measurements from radiation effects have been reduced over recent years. The new generation of satellite sensors such as the high spectral resolution infrared sounders (such as the Atmospheric Infrared Sounder and the Infrared Atmospheric Sounding Interferometer) are instrumental to achieving a better temporal stability for recalibrating sensors such as the High-Resolution Infrared Radiation Sounder. Few instruments (e.g., the Advanced Very High Resolution Radiometer) have now been

in orbit for about three decades, but these were not originally designed for climate applications and therefore require careful re-calibration.

A major achievement in ocean observation is due to the implementation of the Argo global array of profiling floats system (GCOS, 2009). Deployment of Argo floats began in 2000, but it took until 2007 for numbers to reach the design target of 3000 floats. Since 2000 the ice-free upper 2000 m of the ocean have been observed systematically for temperature and salinity for the first time in history, because both the Argo profiling float and surface drifting buoy arrays have reached global coverage at their target numbers (in January 2009, there were 3291 floats operating). Biases in historical ocean data have been identified and reduced, and new analytical approaches have been applied (e.g., Willis et al., 2009). One major consequence has been the reduction of an artificial decadal variation in upper ocean temperature and heat content that was apparent in the observational assessment for AR4 (see Section 3.2). The spatial and temporal coverage of biogeochemical measurements in the ocean has also expanded. Satellite observations for sea level (Sections 3.7 and 13.2), sea surface salinity (Section 3.3), sea ice (Section 4.2) and ocean colour have also been further developed over the past few years.

Progress has also been made with regard to observation of terrestrial Essential Climate Variables. Major advances have been achieved in remote sensing of soil moisture due to the launch of the Soil Moisture and Oceanic Salinity mission in 2009 but also due to new retrieval techniques that have been applied to data from earlier and ongoing missions (see Seneviratne et al., 2010 for a detailed review). However, these measurements have limitations. For example, the methods fail under dense vegetation and they are restricted to the surface soil. Updated Advanced Very High Resolution Radiometer-based Normalized Differenced Vegetation Index data provide new information on the change in vegetation. During the International Polar Year 2007–2009 the number of borehole sites was significantly increased and therefore allows a better monitoring of the large-scale permafrost features (see Section 4.7).

1.5.2 Capabilities in Global Climate Modelling

Several developments have especially pushed the capabilities in modelling forward over recent years (see Figure 1.13 and a more detailed discussion in Chapters 6, 7 and 9).

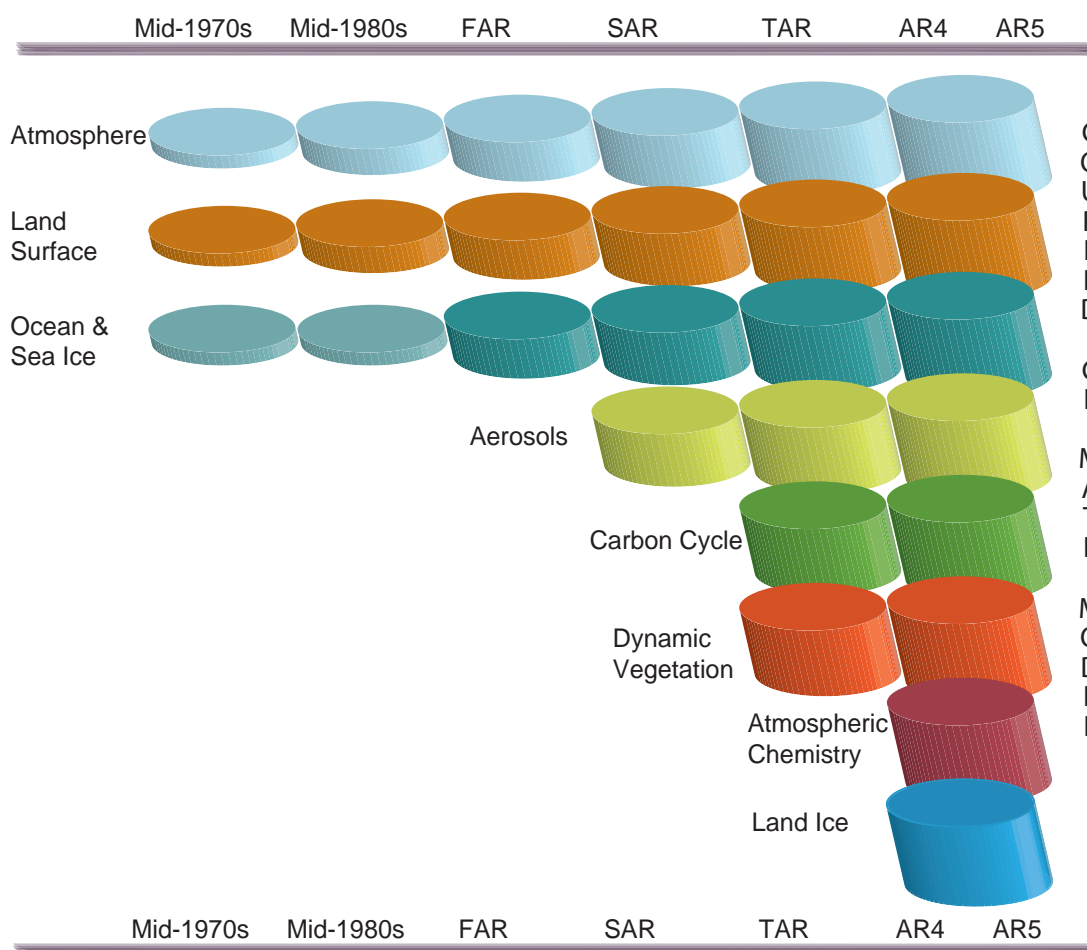


Figure 1.13 | The development of climate models over the last 35 years showing how the different components were coupled into comprehensive climate models over time. In each aspect (e.g., the atmosphere, which comprises a wide range of atmospheric processes) the complexity and range of processes has increased over time (illustrated by growing cylinders). Note that during the same time the horizontal and vertical resolution has increased considerably e.g., for spectral models from T21L9 (roughly 500 km horizontal resolution and 9 vertical levels) in the 1970s to T95L95 (roughly 100 km horizontal resolution and 95 vertical levels) at present, and that now ensembles with at least three independent experiments can be considered as standard.

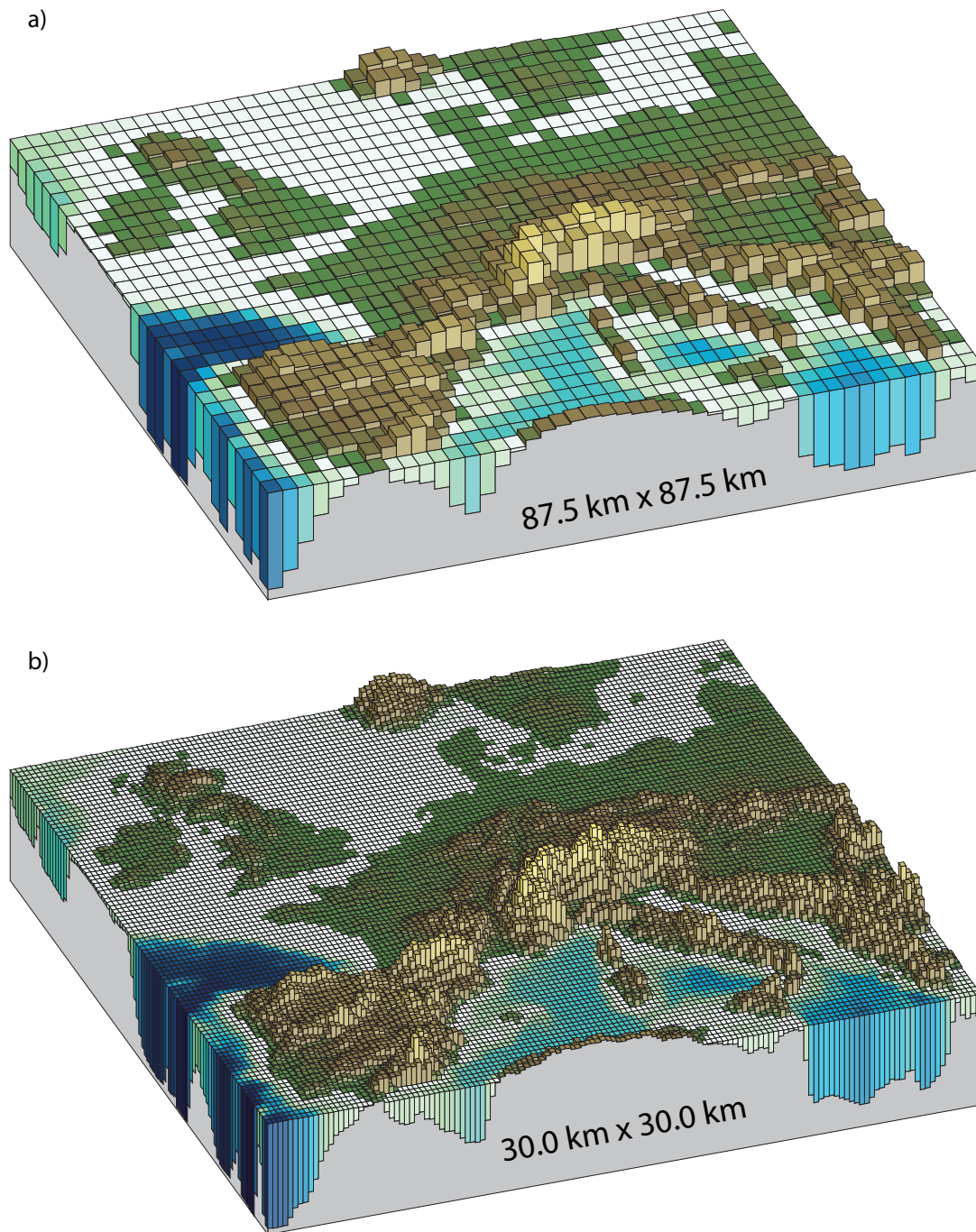


Figure 1.14 | Horizontal resolutions considered in today's higher resolution models and in the very high resolution models now being tested: (a) Illustration of the European topography at a resolution of 87.5×87.5 km; (b) same as (a) but for a resolution of 30.0×30.0 km.

There has been a continuing increase in horizontal and vertical resolution. This is especially seen in how the ocean grids have been refined, and sophisticated grids are now used in the ocean and atmosphere models making optimal use of parallel computer architectures. More models with higher resolution are available for more regions. Figure 1.14a and 1.14b show the large effect on surface representation from a horizontal grid spacing of 87.5 km (higher resolution than most current global models and similar to that used in today's highly resolved models) to a grid spacing of 30.0 km (similar to the current regional climate models).

Representations of Earth system processes are much more extensive and improved, particularly for the radiation and the aerosol cloud interactions and for the treatment of the cryosphere. The representation of the carbon cycle was added to a larger number of models and has been improved since AR4. A high-resolution stratosphere is now included in many models. Other ongoing process development in climate models includes the enhanced representation of nitrogen effects on the carbon cycle. As new processes or treatments are added to the models, they are also evaluated and tested relative to available observations (see Chapter 9 for more detailed discussion).

Ensemble techniques (multiple calculations to increase the statistical sample, to account for natural variability, and to account for uncertainty in model formulations) are being used more frequently, with larger samples and with different methods to generate the samples (different models, different physics, different initial conditions). Coordinated projects have been set up to generate and distribute large samples (ENSEMBLES, climateprediction.net, Program for Climate Model Diagnosis and Intercomparison).

The model comparisons with observations have pushed the analysis and development of the models. CMIP5, an important input to the AR5, has produced a multi-model data set that is designed to advance our understanding of climate variability and climate change. Building on previous CMIP efforts, such as the CMIP3 model analysis reported in AR4, CMIP5 includes 'long-term' simulations of 20th century climate and projections for the 21st century and beyond. See Chapters 9, 10, 11 and 12 for more details on the results derived from the CMIP5 archive.

Since AR4, the incorporation of 'long-term' paleoclimate simulations in the CMIP5 framework has allowed incorporation of information from paleoclimate data to inform projections. Within uncertainties associated with reconstructions of past climate variables from proxy records and forcings, paleoclimate information from the Mid Holocene, Last Glacial Maximum and Last Millennium have been used to test the ability of models to simulate realistically the magnitude and large-scale patterns of past changes (Section 5.3, Box 5.1 and 9.4).

The capabilities of ESMs continue to be enhanced. For example, there are currently extensive efforts towards developing advanced treatments for the processes affecting ice sheet dynamics. Other enhancements are being aimed at land surface hydrology, and the effects of agriculture and urban environments.

As part of the process of getting model analyses for a range of alternative assumptions about how the future may unfold, scenarios for future emissions of important gases and aerosols have been generated for the IPCC assessments (e.g., see the SRES scenarios used in TAR and AR4). The emissions scenarios represent various development pathways based on well-defined assumptions. The scenarios are used to calculate future changes in climate, and are then archived in the Climate Model Intercomparison Project (e.g., CMIP3 for AR4; CMIP5 for AR5). For CMIP5, four new scenarios, referred to as Representative Concentration Pathways (RCPs) were developed (Section 12.3; Moss et al., 2010). See Box 1.1 for a more thorough discussion of the RCP scenarios. Because results from both CMIP3 and CMIP5 will be presented in the later chapters (e.g., Chapters 8, 9, 11 and 12), it is worthwhile considering the differences and similarities between the SRES and the RCP scenarios. Figure 1.15, acting as a prelude to the discussion in Box 1.1, shows that the RF for several of the SRES and RCP scenarios are similar over time and thus should provide results that can be used to compare climate modelling studies.

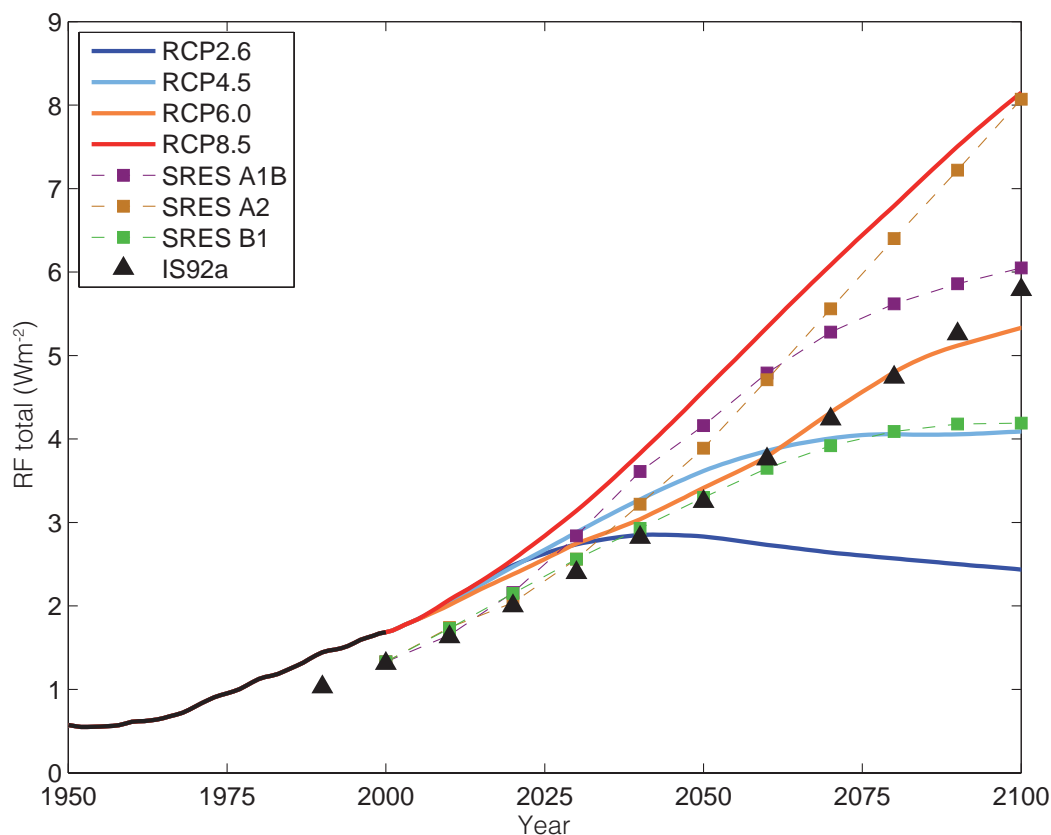


Figure 1.15 | Historical and projected total anthropogenic RF (W m^{-2}) relative to preindustrial (about 1765) between 1950 and 2100. Previous IPCC assessments (SAR IS92a, TAR/AR4 SRES A1B, A2 and B1) are compared with representative concentration pathway (RCP) scenarios (see Chapter 12 and Box 1.1 for their extensions until 2300 and Annex II for the values shown here). The total RF of the three families of scenarios, IS92, SRES and RCP, differ for example, for the year 2000, resulting from the knowledge about the emissions assumed having changed since the TAR and AR4.

Box 1.1 | Description of Future Scenarios

Long-term climate change projections require assumptions on human activities or natural effects that could alter the climate over decades and centuries. Defined scenarios are useful for a variety of reasons, e.g., assuming specific time series of emissions, land use, atmospheric concentrations or RF across multiple models allows for coherent climate model intercomparisons and synthesis. Scenarios can be formed in a range of ways, from simple, idealized structures to inform process understanding, through to comprehensive scenarios produced by Integrated Assessment Models (IAMs) as internally consistent sets of assumptions on emissions and socio-economic drivers (e.g., regarding population and socio-economic development).

Idealized Concentration Scenarios

As one example of an idealized concentration scenario, a 1% yr⁻¹ compound increase of atmospheric CO₂ concentration until a doubling or a quadrupling of its initial value has been widely used in the past (Covey et al., 2003). An exponential increase of CO₂ concentrations induces an essentially linear increase in RF (Myhre et al., 1998) due to a ‘saturation effect’ of the strong absorbing bands. Such a linear ramp function is highly useful for comparative diagnostics of models’ climate feedbacks and inertia. The CMIP5 intercomparison project again includes such a stylized pathway up to a quadrupling of CO₂ concentrations, in addition to an instantaneous quadrupling case.

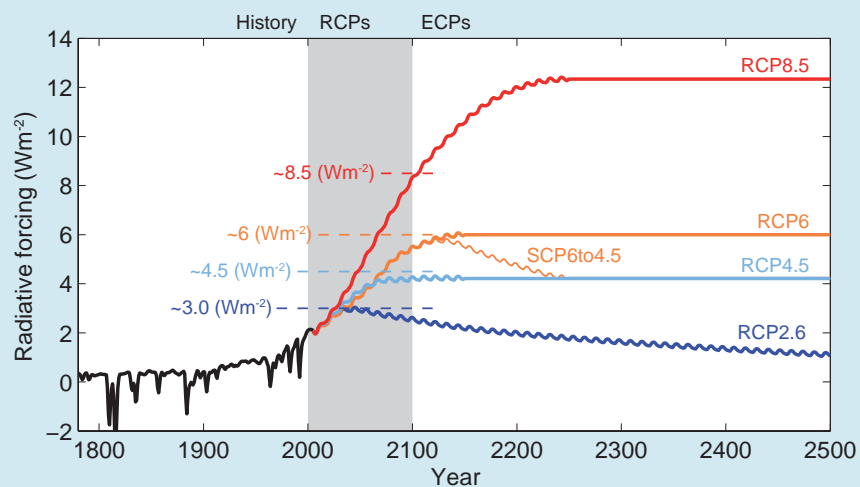
The Socio-Economic Driven SRES Scenarios

The SRES suite of scenarios were developed using IAMs and resulted from specific socio-economic scenarios from storylines about future demographic and economic development, regionalization, energy production and use, technology, agriculture, forestry and land use (IPCC, 2000). The climate change projections undertaken as part of CMIP3 and discussed in AR4 were based primarily on the SRES A2, A1B and B1 scenarios. However, given the diversity in models’ carbon cycle and chemistry schemes, this approach implied differences in models’ long lived GHG and aerosol concentrations for the same emissions scenario. As a result of this and other shortcomings, revised scenarios were developed for AR5 to allow atmosphere-ocean general circulation model (AOGCM) (using concentrations) simulations to be compared with those ESM simulations that use emissions to calculate concentrations.

Representative Concentration Pathway Scenarios and Their Extensions

Representative Concentration Pathway (RCP) scenarios (see Section 12.3 for a detailed description of the scenarios; Moss et al., 2008; Moss et al., 2010; van Vuuren et al., 2011b) are new scenarios that specify concentrations and corresponding emissions, but are not directly based on socio-economic storylines like the SRES scenarios. The RCP scenarios are based on a different approach and include more consistent short-lived gases and land use changes. They are not necessarily more capable of representing future developments than the SRES scenarios. Four RCP scenarios were selected from the published literature (Fujino et al., 2006; Smith and Wigley, 2006; Riahi et al., 2007; van Vuuren et al., 2007; Hijikata et al., 2008; Wise et al., 2009) and updated for use within CMIP5 (Masui et al., 2011; Riahi et al., 2011; Thomson et al., 2011; van Vuuren et al., 2011a). The four scenarios are identified by the 21st century peak or stabilization value of the RF derived by the reference model (in W m⁻²) (Box 1.1, Figure 1): the lowest RCP, RCP2.6 (also referred to as

(continued on next page)

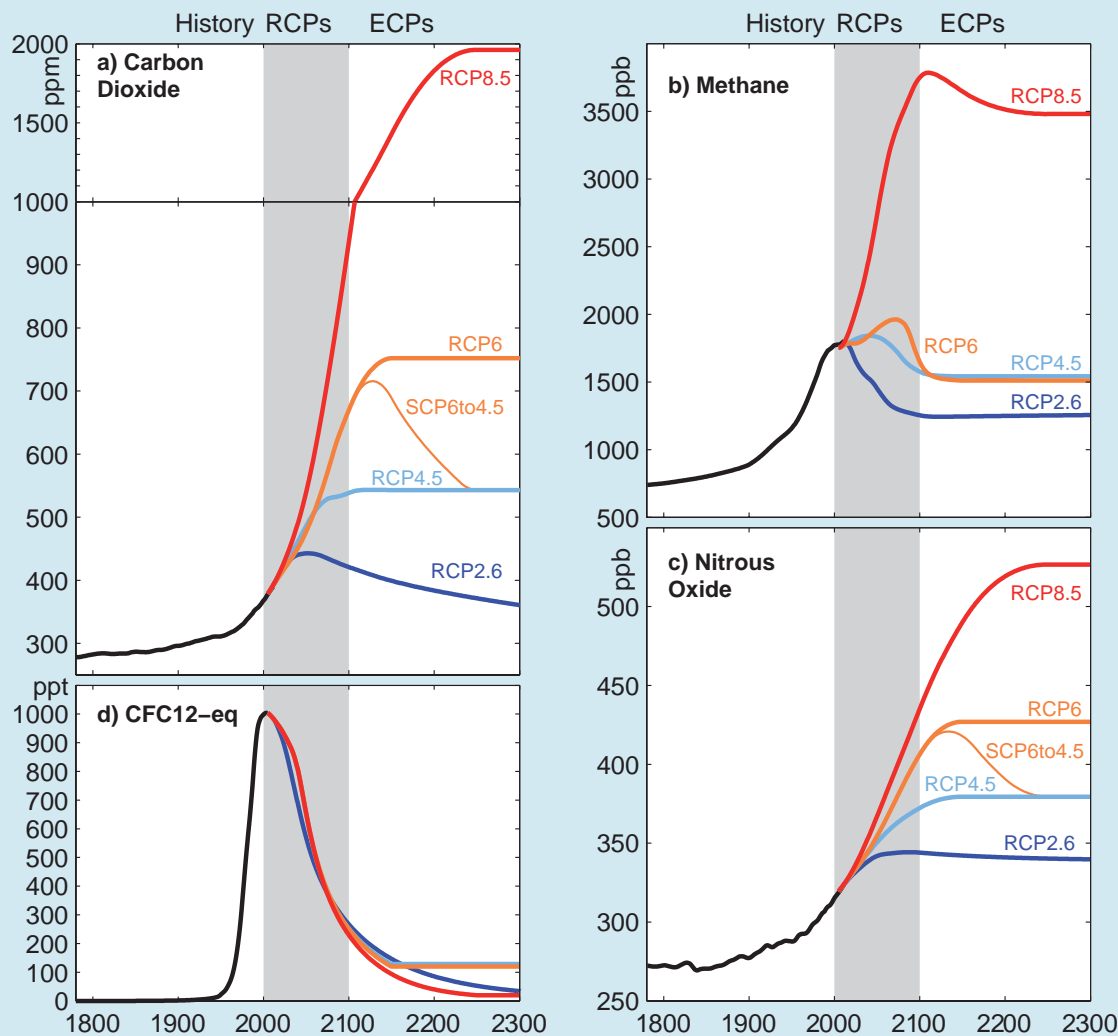


Box 1.1, Figure 1 | Total RF (anthropogenic plus natural) for RCPs and extended concentration pathways (ECP)—for RCP2.6, RCP4.5, and RCP6, RCP8.5, as well as a supplementary extension RCP6 to 4.5 with an adjustment of emissions after 2100 to reach RCP4.5 concentration levels in 2250 and thereafter. Note that the stated RF levels refer to the illustrative default median estimates only. There is substantial uncertainty in current and future RF levels for any given scenario. Short-term variations in RF are due to both volcanic forcings in the past (1800–2000) and cyclical solar forcing assuming a constant 11-year solar cycle (following the CMIP5 recommendation), except at times of stabilization. (Reproduced from Figure 4 in Meinshausen et al., 2011.)

Box 1.1 (continued)

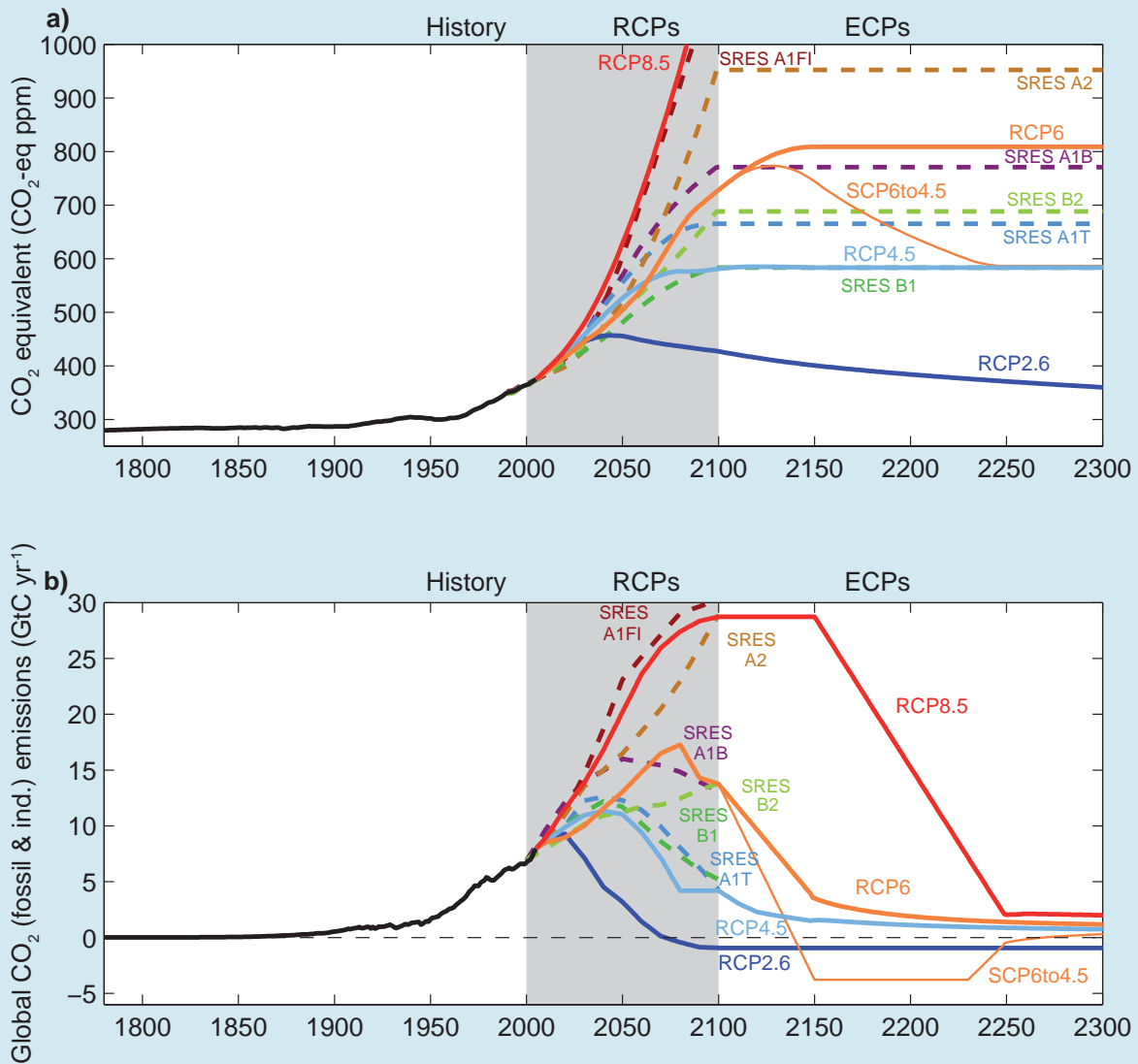
RCP3-PD) which peaks at 3 W m^{-2} and then declines to approximately 2.6 W m^{-2} by 2100; the medium-low RCP4.5 and the medium-high RCP6 aiming for stabilization at 4.5 and 6 W m^{-2} , respectively around 2100; and the highest one, RCP8.5, which implies a RF of 8.5 W m^{-2} by 2100, but implies rising RF beyond that date (Moss et al., 2010). In addition there is a supplementary extension SCP6to4.5 with an adjustment of emissions after 2100 to reach RCP 4.5 concentration levels in 2250 and thereafter. The RCPs span the full range of RF associated with emission scenarios published in the peer-reviewed literature at the time of the development of the RCPs, and the two middle scenarios were chosen to be roughly equally spaced between the two extremes (2.6 and 8.5 W m^{-2}). These forcing values should be understood as comparative labels representative of the forcing associated with each scenario, which will vary somewhat from model to model. This is because concentrations or emissions (rather than the RF) are prescribed in the CMIP5 climate model runs.

Various steps were necessary to turn the selected 'raw' RCPs into emission scenarios from IAMs and to turn these into data sets usable by the climate modelling community, including the extension with historical emissions (Granier et al., 2011; Meinshausen et al., 2011), the harmonization (smoothly connected historical reconstruction) and gridding of land use data sets (Hurtt et al., 2011), the provision of atmospheric chemistry modelling studies, particularly for tropospheric ozone (Lamarque et al., 2011), analyses of 2000–2005 GHG emission levels, and extension of GHG concentrations with historical GHG concentrations and harmonization with analyses of 2000–2005 GHG concentrations levels (Meinshausen et al., 2011). The final RCP data sets comprise land use data, harmonized GHG emissions and concentrations, gridded reactive gas and aerosol emissions, as well as ozone and aerosol abundance fields (Figures 2, 3, and 4 in Box 1.1). (continued on next page)



Box 1.1, Figure 2 | Concentrations of GHG following the 4 RCPs and their extensions (ECP) to 2300. (Reproduced from Figure 5 in Meinshausen et al., 2011.) Also see Annex II Table AII.4.1 for CO_2 , Table AII.4.2 for CH_4 , Table AII.4.3 for N_2O .

Box 1.1 (continued)



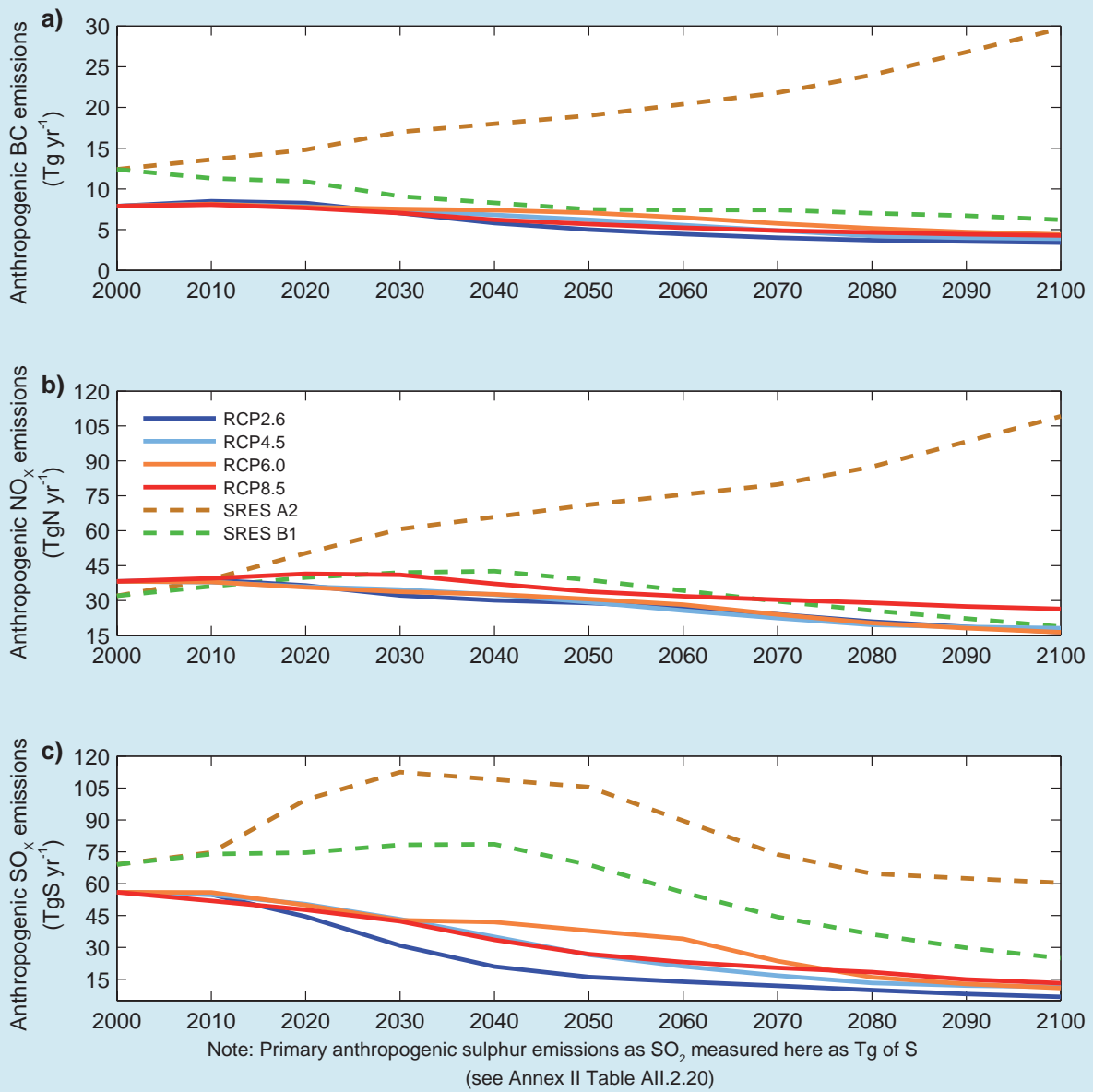
Box 1.1, Figure 3 | (a) Equivalent CO₂ concentration and (b) CO₂ emissions (except land use emissions) for the four RCPs and their ECPs as well as some SRES scenarios.

To aid model understanding of longer-term climate change implications, these RCPs were extended until 2300 (Meinshausen et al., 2011) under reasonably simple and somewhat arbitrary assumptions regarding post-2100 GHG emissions and concentrations. In order to continue to investigate a broad range of possible climate futures, the two outer RCPs, RCP2.6 and RCP8.5 assume constant emissions after 2100, while the two middle RCPs aim for a smooth stabilization of concentrations by 2150. RCP8.5 stabilizes concentrations only by 2250, with CO₂ concentrations of approximately 2000 ppm, nearly seven times the pre-industrial levels. As the RCP2.6 implies netnegative CO₂ emissions after around 2070 and throughout the extension, CO₂ concentrations are slowly reduced towards 360 ppm by 2300.

Comparison of SRES and RCP Scenarios

The four RCP scenarios used in CMIP5 lead to RF values that span a range larger than that of the three SRES scenarios used in CMIP3 (Figure 12.3). RCP4.5 is close to SRES B1, RCP6 is close to SRES A1B (more after 2100 than during the 21st century) and RCP8.5 is somewhat higher than A2 in 2100 and close to the SRES A1FI scenario (Figure 3 in Box 1.1). RCP2.6 is lower than any of the SRES scenarios (see also Figure 1.15). (continued on next page)

Box 1.1 (continued)



Box 1.1, Figure 4 | (a) Anthropogenic BC emissions (Annex II Table AII.2.22), (b) anthropogenic NO_x emissions (Annex II Table AII.2.18), and (c) anthropogenic SO_x emissions (Annex II Table AII.2.20).

1.6 Overview and Road Map to the Rest of the Report

As this chapter has shown, understanding of the climate system and the changes occurring in it continue to advance. The notable scientific advances and associated peer-reviewed publications since AR4 provide the basis for the assessment of the science as found in Chapters 2 to 14. Below a quick summary of these chapters and their objectives is provided.

Observations and Paleoclimate Information (Chapters 2, 3, 4 and 5): These chapters assess information from all climate system components on climate variability and change as obtained from instrumental records and climate archives. This group of chapters covers all relevant aspects of the atmosphere including the stratosphere, the land surface, the oceans and the cryosphere. Information on the water cycle, including evaporation, precipitation, runoff, soil moisture, floods, drought, etc. is assessed. Timescales from daily to decades (Chapters 2, 3 and 4) and from centuries to many millennia (Chapter 5) are considered.

Process Understanding (Chapters 6 and 7): These chapters cover all relevant aspects from observations and process understanding, to projections from global to regional scale. Chapter 6 covers the carbon cycle and its interactions with other biogeochemical cycles, in particular the nitrogen cycle, as well as feedbacks on the climate system. Chapter 7 treats in detail clouds and aerosols, their interactions and chemistry, the role of water vapour, as well as their role in feedbacks on the climate system.

From Forcing to Attribution of Climate Change (Chapters 8, 9 and 10): In these chapters, all the information on the different drivers (natural and anthropogenic) of climate change is collected, expressed in terms of RF, and assessed (Chapter 8). As part of this, the science of metrics commonly used in the literature to compare radiative effects from a range of agents (Global Warming Potential, Global Temperature Change Potential and others) is covered. In Chapter 9, the hierarchy of climate models used in simulating past and present climate change is assessed. Information regarding detection and attribution of changes on global to regional scales is assessed in Chapter 10.

Future Climate Change and Predictability (Chapters 11 and 12): These chapters assess projections of future climate change derived from climate models on timescales from decades to centuries at both global and regional scales, including mean changes, variability and extremes. Fundamental questions related to the predictability of climate as well as long-term climate change, climate change commitments and inertia in the climate system are addressed.

Integration (Chapters 13 and 14): These chapters integrate all relevant information for two key topics in WGI AR5: sea level change (Chapter 13) and climate phenomena across the regions (Chapter 14). Chapter 13 assesses information on sea level change ranging from observations and process understanding to projections from global to regional scales. Chapter 14 assesses the most important modes of variability in the climate system and extreme events. Furthermore, this chapter deals with interconnections between the climate phenomena, their regional expressions, and their relevance for future regional

climate change. Maps produced and assessed in Chapter 14, together with Chapters 11 and 12, form the basis of the Atlas of Global and Regional Climate Projections in Annex I. RFs and estimates of future atmospheric concentrations from Chapters 7, 8, 11 and 12 form the basis of the Climate System Scenario Tables in Annex II.

1.6.1 Topical Issues

A number of topical issues are discussed throughout the assessment. These issues include those of areas where there is contention in the peer-reviewed literature and where questions have been raised that are being addressed through ongoing research. Table 1.3 provides a non-comprehensive list of many of these and the chapters where they are discussed.

Table 1.3 | Key topical issues discussed in the assessment.

Topic	Section
Abrupt change and irreversibility	5.7, 12.5, 13.4
Aerosols	6.4, 7.3, 7.4, 7.5, 7.6, 8.3, 11.3, 14.1
Antarctic climate change	5.8, 9.4, 10.3, 13.3
Arctic sea ice change	4.2, 5.5, 9.4, 10.3, 11.3, 12.4
Hydrological cycle changes	2.5, 2.6, 3.3, 3.4, 3.5, 7.6, 10.3, 12.4
Carbon-climate feedbacks	6.4, 12.4
Climate sensitivity	5.3, 9.7, 10.8, 12.5
Climate stabilization	6.3, 6.4, 12.5
Cloud feedbacks	5.3, 7.2, 9.7, 11.3, 12.4
Cosmic ray effects on clouds	7.4
Decadal climate variability	5.3, 9.5, 10.3
Earth's Energy (trends, distribution and budget)	2.3, 3.2, 13.3
El Niño-Southern Oscillation	2.7, 5.4, 9.4, 9.5, 14.4
Geo-engineering	6.4, 7.7
Glacier change	4.3, 5.5, 10.5, 13.3
Ice sheet dynamics and mass balance assessment	4.4, 5.3, 5.6, 10.5, 13.3
Monsoons	2.7, 5.5, 9.5, 14.2
Ocean acidification	3.8, 6.4
Permafrost change	4.7, 6.3, 10.5
Solar effects on climate change	5.2, 8.4
Sea level change, including regional effects	3.7, 5.6, 13.1
Temperature trends since 1998	2.4, 3.2, 9.4
Tropical cyclones	2.6, 10.6, 14.6
Upper troposphere temperature trends	2.4, 9.4

References

- Allen, M. R., J. F. B. Mitchell, and P. A. Stott, 2013: Test of a decadal climate forecast. *Nature Geosci.*, **6**, 243–244.
- AMAP, 2009: Summary – The Greenland Ice Sheet in a Changing Climate: Snow, Water, Ice and Permafrost in the Arctic (SWIPA). Arctic Monitoring and Assessment Programme (AMAP), 22 pp.
- Armour, K. C., I. Eisenman, E. Blanchard-Wrigglesworth, K. E. McCusker, and C. M. Bitz, 2011: The reversibility of sea ice loss in a state-of-the-art climate model. *Geophys. Res. Lett.*, **38**.
- Arrhenius, S., 1896: On the influence of carbonic acid in the air upon the temperature of the ground. *Philos. Mag.*, **41**, 237–276.
- Baede, A. P. M., E. Ahlonsou, Y. Ding, and D. Schimel, 2001: The climate system: An overview. In: *Climate Change 2001: The Scientific Basis. Contribution of Working Group I to the Third Assessment Report of the Intergovernmental Panel on Climate Change* [J. T. Houghton, Y. Ding, D. J. Griggs, M. Noquer, P. J. van der Linden, X. Dai, K. Maskell and C. A. Johnson (eds.)]. Cambridge University Press, Cambridge, United Kingdom and New York, NY, USA.
- Beerling, D. J., and D. L. Royer, 2011: Convergent Cenozoic CO₂ history. *Nature Geosci.*, **4**, 418–420.
- Bretherton, F. P., K. Bryan, and J. D. Woodes, 1990: Time-dependent greenhouse-gas-induced climate change. In: *Climate Change: The IPCC Scientific Assessment* [J. T. Houghton, G. J. Jenkins and J. J. Ephraums (eds.)]. Cambridge University Press, Cambridge, United Kingdom and New York, NY, USA, 177–193.
- Brönnimann, S., T. Ewen, J. Luterbacher, H. F. Diaz, R. S. Stolarski, and U. Neu, 2008: A focus on climate during the past 100 years. In: *Climate Variability and Extremes during the Past 100 Years* [S. Brönnimann, J. Luterbacher, T. Ewen, H. F. Diaz, R. S. Stolarski and U. Neu (eds.)]. Springer Science+Business Media, Heidelberg, Germany and New York, NY, USA, pp. 1–25.
- Broomell, S., and D. Budescu, 2009: Why are experts correlated? Decomposing correlations between judges. *Psychometrika*, **74**, 531–553.
- Brunet, M., and P. Jones, 2011: Data rescue initiatives: Bringing historical climate data into the 21st century. *Clim. Res.*, **47**, 29–40.
- Budescu, D., S. Broomell, and H.-H. Por, 2009: Improving communication of uncertainty in the reports of the Intergovernmental Panel on Climate Change. *Psychol. Sci.*, **20**, 299–308.
- Byrne, R., S. Mecking, R. Feely, and X. Liu, 2010: Direct observations of basin-wide acidification of the North Pacific Ocean. *Geophys. Res. Lett.*, **37**.
- CCSP, 2009: *Best Practice Approaches for Characterizing, Communicating, and Incorporating Scientific Uncertainty in Climate Decision Making*. U.S. Climate Change Science Program, Washington, DC, USA, 96 pp.
- Church, J. A., and N. J. White, 2011: Sea-level rise from the late 19th to the early 21st century. *Surv. Geophys.*, **32**, 585–602.
- Church, J. A., J. M. Gregory, N. J. White, S. M. Platten, and J. X. Mitrovica, 2011: Understanding and projecting sea level change. *Oceanography*, **24**, 130–143.
- Cleveland, W. S., 1979: Robust locally weighted regression and smoothing scatterplots. *J. Am. Stat. Assoc.*, **74**, 829–836.
- Collins, M., and M. R. Allen, 2002: Assessing the relative roles of initial and boundary conditions in interannual to decadal climate predictability. *J. Clim.*, **15**, 3104–3109.
- Covey, C., et al., 2003: An overview of results from the Coupled Model Intercomparison Project. *Global Planet. Change*, **37**, 103–133.
- Cubasch, U., et al., 2001: Projections of future climate change. In: *Climate Change 2001: The Scientific Basis. Contribution of Working Group I to the Third Assessment Report of the Intergovernmental Panel on Climate Change* [J. T. Houghton, Y. Ding, D. J. Griggs, M. Noquer, P. J. van der Linden, X. Dai, K. Maskell and C. A. Johnson (eds.)]. Cambridge University Press, Cambridge, United Kingdom and New York, NY, USA, 527–582.
- Dee, D. P., et al., 2011: The ERA-Interim reanalysis: Configuration and performance of the data assimilation system. *Q. J. R. Meteorol. Soc.*, **137**, 553–597.
- Denman, K. L., et al., 2007: Couplings between changes in the climate system and biogeochemistry. In: *Climate Change 2007: The Physical Science Basis. Contribution of Working Group I to the Fourth Assessment Report of the Intergovernmental Panel on Climate Change* [Solomon, S., D. Qin, M. Manning, Z. Chen, M. Marquis, K. B. Averyt, M. Tignor and H. L. Miller (eds.)]. Cambridge University Press, Cambridge, United Kingdom and New York, NY, USA, 501–587.
- Drugokenky, E. J., et al., 2009: Observational constraints on recent increases in the atmospheric CH₄ burden. *Geophys. Res. Lett.*, **36**, L18803.
- Duarte, C. M., T. M. Lenton, P. Wadhams, and P. Wassmann, 2012: Commentary: Abrupt climate change in the Arctic. *Nature Clim. Change*, **2**, 60–62.
- Easterling, D. R., and M. F. Wehner, 2009: Is the climate warming or cooling? *Geophys. Res. Lett.*, **36**, L08706.
- Elkins, J., and G. Dutton, 2010: Nitrous oxide and sulfur hexafluoride. Section in State of the Climate in 2009. *Bull. Am. Meteorol. Soc.*, **91**, 44–45.
- Ettema, J., M. R. van den Broeke, E. van Meijgaard, W. J. van de Berg, J. L. Bamber, J. E. Box, and R. C. Bales, 2009: Higher surface mass balance of the Greenland ice sheet revealed by high-resolution climate modeling. *Geophys. Res. Lett.*, **36**, L12501.
- Foley, J., et al., 2005: Global consequences of land use. *Science*, **309**, 570–574.
- Folland, C. K., et al., 2001: Observed climate variability and change. In: *Climate Change 2001: The Scientific Basis. Contribution of Working Group I to the Third Assessment Report of the Intergovernmental Panel on Climate Change* [J. T. Houghton, Y. Ding, D. J. Griggs, M. Noquer, P. J. van der Linden, X. Dai, K. Maskell and C. A. Johnson (eds.)]. Cambridge University Press, Cambridge, United Kingdom and New York, NY, USA, 101–181.
- Forest, C. E., P. H. Stone, and A. P. Sokolov, 2008: Constraining climate model parameters from observed 20th century changes. *Tellus A*, **60**, 911–920.
- Forster, P., et al., 2007: Changes in atmospheric constituents and in radiative forcing. In: *Climate Change 2007: The Physical Science Basis. Contribution of Working Group I to the Fourth Assessment Report of the Intergovernmental Panel on Climate Change* [Solomon, S., D. Qin, M. Manning, Z. Chen, M. Marquis, K. B. Averyt, M. Tignor and H. L. Miller (eds.)]. Cambridge University Press, Cambridge, United Kingdom and New York, NY, USA, 131–234.
- Frame, D. J., and D. A. Stone, 2013: Assessment of the first consensus prediction on climate change. *Nature Clim. Change*, **3**, 357–359.
- Frame, D. J., D. A. Stone, P. A. Stott, and M. R. Allen, 2006: Alternatives to stabilization scenarios. *Geophys. Res. Lett.*, **33**.
- Fujino, J., R. Nair, M. Kainuma, T. Masui, and Y. Matsuoka, 2006: Multi-gas mitigation analysis on stabilization scenarios using aim global model. *Energy J.*, **0**, 343–353.
- GCOS, 2009: Progress Report on the Implementation of the Global Observing System for Climate in Support of the UNFCCC 2004–2008, GCOS-129 (WMO/TD-No. 1489; GOOS-173; GTOS-70), Geneva, Switzerland.
- GCOS, 2011: Systematic Observation Requirements for Satellite-based Products for Climate Supplemental details to the satellite-based component of the Implementation Plan for the Global Observing System for Climate in Support of the UNFCCC – 2011 Update, (GCOS-154) – December 2011, Geneva, Switzerland.
- Goosse, H., W. Lefebvre, A. de Montety, E. Crespin, and A. H. Orsi, 2009: Consistent past half-century trends in the atmosphere, the sea ice and the ocean at high southern latitudes. *Clim. Dyn.*, **33**, 999–1016.
- Granier, C., et al., 2011: Evolution of anthropogenic and biomass burning emissions of air pollutants at global and regional scales during the 1980–2010 period. *Clim. Change*, **109**, 163–190.
- Haas, C., A. Pfaffling, S. Hendricks, L. Rabenstein, J. L. Etienne, and I. Rigor, 2008: Reduced ice thickness in Arctic Transpolar Drift favors rapid ice retreat. *Geophys. Res. Lett.*, **35**, L17501.
- Hansen, J., D. Johnson, A. Lacis, S. Lebedeff, P. Lee, D. Rind, and G. Russell, 1981: Climate impact of increasing atmospheric carbon dioxide. *Science*, **213**, 957–966.
- Hansen, J., M. Sato, R. Ruedy, K. Lo, D. W. Lea, and M. Medina-Elizade, 2006: Global temperature change. *Proc. Natl. Acad. Sci. U.S.A.*, **103**, 14288–14293.
- Hansen, J., R. Ruedy, M. Sato, and K. Lo, 2010: Global surface temperature change. *Rev. Geophys.*, **48**, RG4004.
- Hansen, J., M. Sato, P. Kharecha, and K. von Schuckmann, 2011: Earth's energy imbalance and implications. *Atmos. Chem. Phys.*, **11**, 13421–13449.
- Hawkins, E., and R. Sutton, 2009: The potential to narrow uncertainty in regional climate predictions. *Bull. Am. Meteorol. Soc.*, **90**, 1095–1107.
- Hawkins, E., and R. Sutton, 2011: The potential to narrow uncertainty in projections of regional precipitation change. *Clim. Dyn.*, **37**, 407–418.

- Hegerl, G. C., et al., 2007: Understanding and attributing climate change. In: *Climate Change 2007: The Physical Science Basis. Contribution of Working Group I to the Fourth Assessment Report of the Intergovernmental Panel on Climate Change* [Solomon, S., D. Qin, M. Manning, Z. Chen, M. Marquis, K. B. Averyt, M. Tignor and H. L. Miller (eds.)]. Cambridge University Press, Cambridge, United Kingdom and New York, NY, USA, 665–745.
- Hijioka, Y., Y. Matsuoka, H. Nishimoto, M. Masui, and M. Kainuma, 2008: Global GHG emission scenarios under GHG concentration stabilization targets. *JGEE*, **13**, 97–108.
- Hoelzle, M., G. Darms, M. P. Lüthi, and S. Suter, 2011: Evidence of accelerated englacial warming in the Monte Rosa area, Switzerland/Italy. *Cryosphere*, **5**, 231–243.
- Houghton, R., 2003: Revised estimates of the annual net flux of carbon to the atmosphere from changes in land use and land management 1850–2000. *Tellus B*, **55**, 378–390.
- Huntingford, C., J. Lowe, B. Booth, C. Jones, G. Harris, L. Gohar, and P. Meir, 2009: Contributions of carbon cycle uncertainty to future climate projection spread. *Tellus B*, doi:10.1111/j.1600-0889.2009.00414.x, 355–360.
- Hurt, G. C., et al., 2011: Harmonization of land-use scenarios for the period 1500–2100: 600 years of global gridded annual land-use transitions, wood harvest, and resulting secondary lands. *Clim. Change*, **109**, 117–161.
- InterAcademy Council, 2010: Climate change assessments. In: *Review of the Processes and Procedures of the IPCC*, Amsterdam, The Netherlands.
- IPCC, 1990: *Climate Change: The IPCC Scientific Assessment* [J. T. Houghton, G. J. Jenkins and J. J. Ephraums (eds.)]. Cambridge University Press, Cambridge, United Kingdom and New York, NY, USA, 212 pp.
- IPCC, 1996: *Climate Change 1995: The Science of Climate Change. Contribution of Working Group I to the Second Assessment Report of the Intergovernmental Panel on Climate Change*. Cambridge University Press, Cambridge, United Kingdom and New York, NY, USA, 584 pp.
- IPCC, 2000: IPCC Special Report on Emissions Scenarios. Prepared by Working Group III of the Intergovernmental Panel on Climate Change, Cambridge University Press, Cambridge, United Kingdom, pp 570.
- IPCC, 2001: *Climate Change 2001: The Scientific Basis. Contribution of Working Group I to the Third Assessment Report of the Intergovernmental Panel on Climate Change* [J. T. Houghton, Y. Ding, D. J. Griggs, M. Noguer, P. J. van der Linden, X. Dai, K. Maskell and C. A. Johnson (eds.)]. Cambridge University Press, Cambridge, United Kingdom and New York, NY, USA, 881 pp.
- IPCC, 2007: *Climate Change 2007: The Physical Science Basis. Contribution of Working Group I to the Fourth Assessment Report of the Intergovernmental Panel on Climate Change (IPCC)* [Solomon, S., D. Qin, M. Manning, Z. Chen, M. Marquis, K. B. Averyt, M. Tignor and H. L. Miller (eds.)]. Cambridge University Press, 996 pp.
- IPCC, 2012a: Procedures for the preparation, review, acceptance, adoption, approval and publication of IPCC reports. Appendix A to the Principles Governing IPCC Work, Geneva, Switzerland, 6–9 June 2012, 29 pp.
- IPCC, 2012b: *Managing the Risks of Extreme Events and Disasters to Advance Climate Change Adaptation. Special Report of the Intergovernmental Panel on Climate Change*. [Field, C. B., V. Barros, T. F. Stocker, D. Qin, D. J. Dokken, K. L. Ebi, M. D. Mastrandrea, K. J. Mach, G.-K. Plattner, S. K. Allen, M. Tignor, and P. M. Midgley (Eds.)]. Cambridge University Press, Cambridge, United Kingdom, 582 pp.
- JCGM, 2008: JCGM 100: 2008. GUM 1995 with minor corrections. Evaluation of measurement data—Guide to the expression of uncertainty in measurement. Joint Committee for Guides in Metrology.
- Jevrejeva, S., J. C. Moore, A. Grinsted, and P. L. Woodworth, 2008: Recent global sea level acceleration started over 200 years ago? *Geophys. Res. Lett.*, **35**, L08715.
- Kahneman, D., and A. Tversky, 1979: Prospect theory: An analysis of decision under risk. *Econometrica*, **47**, 263–291.
- Kahneman, D., P. Slovic, and A. Tversky, Eds., 1982: *Judgment under Uncertainty: Heuristics and Biases*. Cambridge University Press, Cambridge, United Kingdom and New York, NY, USA, 544 pp.
- Kandlikar, M., J. Risbey, and S. Dessai, 2005: Representing and communicating deep uncertainty in climate-change assessments. *C. R. Geosci.*, **337**, 443–455.
- Knutti, R., F. Joos, S. A. Müller, G. K. Plattner, and T. F. Stocker, 2005: Probabilistic climate change projections for CO₂ stabilization profiles. *Geophys. Res. Lett.*, **32**, L20707.
- Knutti, R., et al., 2008: A review of uncertainties in global temperature projections over the twenty-first century. *J. Clim.*, **21**, 2651–2663.
- Kopp, G., and J. L. Lean, 2011: A new, lower value of total solar irradiance: Evidence and climate significance. *Geophys. Res. Lett.*, **38**, L01706.
- Kwok, R., G. F. Cunningham, M. Wensnahan, I. Rigor, H. J. Zwally, and D. Yi, 2009: Thinning and volume loss of the Arctic Ocean sea ice cover: 2003–2008. *J. Geophys. Res. Oceans*, **114**, C07005.
- Lamarque, J. F., et al., 2011: Global and regional evolution of short-lived radiatively-active gases and aerosols in the Representative Concentration Pathways. *Clim. Change*, **109**, 191–212.
- Lambert, F., et al., 2008: Dust-climate couplings over the past 800,000 years from the EPICA Dome C ice core. *Nature*, **452**, 616–619.
- Lemke, P., et al., 2007: Observations: Changes in snow, ice and frozen ground. In: *Climate Change 2007: The Physical Science Basis. Contribution of Working Group I to the Fourth Assessment Report of the Intergovernmental Panel on Climate Change* [Solomon, S., D. Qin, M. Manning, Z. Chen, M. Marquis, K. B. Averyt, M. Tignor and H. L. Miller (eds.)]. Cambridge University Press, Cambridge, United Kingdom and New York, NY, USA, 339–383.
- Lenton, T., H. Held, E. Kriegler, J. Hall, W. Lucht, S. Rahmstorf, and H. Schellnhuber, 2008: Tipping elements in the Earth's climate system. *Proc. Natl. Acad. Sci. U.S.A.*, **105**, 1786–1793.
- Le Treut, H., et al., 2007: Historical Overview of Climate Change. In: *Climate Change 2007: The Physical Science Basis. Contribution of Working Group I to the Fourth Assessment Report of the Intergovernmental Panel on Climate Change* [Solomon, S., D. Qin, M. Manning, Z. Chen, M. Marquis, K. B. Averyt, M. Tignor and H. L. Miller (eds.)]. Cambridge University Press, Cambridge, United Kingdom and New York, NY, USA, pp. 94–127.
- Lüthi, M., and M. Funk, 2001: Modelling heat flow in a cold, high-altitude glacier: Interpretation of measurements from Colle Gnifetti, Swiss Alps. *J. Glaciol.*, **47**, 314–324.
- Lüthi, D., et al., 2008: High-resolution carbon dioxide concentration record 650,000–800,000 years before present. *Nature*, **453**, 379–382.
- Mann, M., Z. Zhang, M. Hughes, R. Bradley, S. Miller, S. Rutherford, and F. Ni, 2008: Proxy-based reconstructions of hemispheric and global surface temperature variations over the past two millennia. *Proc. Natl. Acad. Sci. U.S.A.*, **105**, 13252–13257.
- Manning, M., et al., 2004: *IPCC workshop Report: Describing scientific uncertainties in climate change to support analysis of risk and of options* [IPCC IPCC Working Group I Technical Support Unit (ed.)]. Available at <http://www.ipcc.ch/> (accessed 07-10-2013), 138.
- Masson, D., and R. Knutti, 2011: Climate model genealogy. *Geophys. Res. Lett.*, **38**, L08703.
- Mastrandrea, M. D., et al., 2010: Guidance notes for lead authors of the IPCC Fifth Assessment Report on Consistent Treatment of Uncertainties. Available at <http://www.ipcc.ch> (accessed 07-10-2013).
- Masui, T., et al., 2011: An emission pathway for stabilization at 6 Wm⁻² radiative forcing. *Clim. Change*, **109**, 59–76.
- Matthews, H. D., and A. J. Weaver, 2010: Committed climate warming. *Nature Geosci.*, **3**, 142–143.
- Meehl, G. A., et al., 2007: Global climate projections. In: *Climate Change 2007: The Physical Science Basis. Contribution of Working Group I to the Fourth Assessment Report of the Intergovernmental Panel on Climate Change* [Solomon, S., D. Qin, M. Manning, Z. Chen, M. Marquis, K. B. Averyt, M. Tignor and H. L. Miller (eds.)]. Cambridge University Press, Cambridge, United Kingdom and New York, NY, USA, 749–845.
- Meinshausen, M., et al., 2011: The RCP greenhouse gas concentrations and their extensions from 1765 to 2300. *Clim. Change*, **109**, 213–241.
- Menne, M. J., I. Durre, R. S. Vose, B. E. Gleason, and T. G. Houston, 2012: An overview of the Global Historical Climatology Network-Daily Database. *J. Atmos. Ocean. Technol.*, **29**, 897–910.
- Mernild, S. H., G. E. Liston, C. A. Hiemstra, K. Steffen, E. Hanna, and J. H. Christensen, 2009: Greenland ice sheet surface mass-balance modelling and freshwater flux for 2007, and in a 1995–2007 perspective. *Hydrol. Proc.*, **23**, 2470–2484.
- Midorikawa, T., et al., 2010: Decreasing pH trend estimated from 25-yr time series of carbonate parameters in the western North Pacific. *Tellus B*, **62**, 649–659.
- Morgan, M. G., M. Henrion, and M. Small, 1990: *Uncertainty: A Guide to Dealing with Uncertainty in Quantitative Risk and Policy Analysis*. Cambridge University Press, Cambridge, United Kingdom and New York, NY, USA, 332 pp.
- Morice, C. P., J. J. Kennedy, N. A. Rayner, and P. D. Jones, 2012: Quantifying uncertainties in global and regional temperature change using an ensemble of observational estimates: The HadCRUT4 data set. *J. Geophys. Res. Atmos.*, **117**, D08101.

- Moss, R. H., and S. H. Schneider, 2000: Uncertainties in the IPCC TAR: Recommendations to lead authors for more consistent assessment and reporting. In: *Guidance Papers on the Cross Cutting Issues of the Third Assessment Report of the IPCC*. World Meteorological Organization, Geneva, pp. 33–51.
- Moss, R., et al., 2008: *Towards New Scenarios for Analysis of Emissions, Climate Change, Impacts, and Response Strategies*. Geneva, Intergovernmental Panel on Climate Change, 132 pp.
- Moss, R., et al., 2010: The next generation of scenarios for climate change research and assessment. *Nature*, **463**, 747–756.
- Murphy, D., S. Solomon, R. Portmann, K. Rosenlof, P. Forster, and T. Wong, 2009: An observationally based energy balance for the Earth since 1950. *J. Geophys. Res. Atmos.*, **114**, D17107.
- Myhre, G., E. Highwood, K. Shine, and F. Stordal, 1998: New estimates of radiative forcing due to well mixed greenhouse gases. *Geophys. Res. Lett.*, **25**, 2715–2718.
- Nghiem, S. V., et al., 2012: The extreme melt across the Greenland ice sheet in 2012. *Geophys. Res. Lett.*, **39**, L20502.
- Oreskes, N., K. Shrader-Frechette, and K. Belitz, 1994: Verification, validation, and confirmation of numerical models in the earth sciences. *Science*, **263**, 641–646.
- Pall, P., et al., 2011: Anthropogenic greenhouse gas contribution to flood risk in England and Wales in autumn 2000. *Nature*, **470**, 382–385.
- Patt, A. G., and D. P. Schrag, 2003: Using specific language to describe risk and probability. *Clim. Change*, **61**, 17–30.
- Patt, A. G., and S. Dessai, 2005: Communicating uncertainty: Lessons learned and suggestions for climate change assessment. *C. R. Geosci.*, **337**, 425–441.
- Pennell, C., and T. Reichler, 2011: On the effective number of climate models. *J. Clim.*, **24**, 2358–2367.
- Peterson, T. C., P. A. Stott, and S. Herring, 2012: Explaining extreme events of 2011 from a climate perspective. *Bull. Am. Meteorol. Soc.*, **93**, 1041–1067.
- Peterson, T. C., et al., 2008: Why weather and climate extremes matter. In: *Weather and Climate Extremes in a Changing Climate. Regions of Focus: North America, Hawaii, Caribbean, and U.S. Pacific Islands*, [Karl, T. R., G. A. Meehl, C. D. Miller, S. J. Hassol, A. M. Waple, and W. L. Murray (eds.)]. A Report by the U.S. Climate Change Science Program and the Subcommittee on Global Change Research, Washington, DC., USA, 11–33.
- Rahmstorf, S., G. Foster, and A. Cazenave, 2012: Comparing climate projections to observations up to 2011. *Environ. Res. Lett.*, **7**, 044035.
- Ray, R. D., and B. C. Douglas, 2011: Experiments in reconstructing twentieth-century sea levels. *Prog. Oceanogr.*, **91**, 496–515.
- Riahi, K., A. Grübler, and N. Nakicenovic, 2007: Scenarios of long-term socio-economic and environmental development under climate stabilization. *Technol. Forecast Soc Change*, **74**, 887–935.
- Riahi, K., et al., 2011: RCP 8.5–A scenario of comparatively high greenhouse gas emissions. *Clim. Change*, **109**, 33–57.
- Risbey, J. S., and M. Kandlikar, 2007: Expressions of likelihood and confidence in the IPCC uncertainty assessment process. *Clim. Change*, **85**, 19–31.
- Schimel, D., et al., 1996: Radiative forcing of climate change. In: *Climate Change 1995: The Science of Climate Change, Contribution of Working Group I to the Second Assessment Report of the Intergovernmental Panel on Climate Change* [J. T. Houghton, L. G. Meiro Filho, B. A. Callander, N. Harris, A. Kattenburg and K. Maskell (eds.)]. Cambridge University Press, Cambridge, United Kingdom and New York, NY, USA, 69–131.
- Scott, J. T. B., G. H. Gudmundsson, A. M. Smith, R. G. Bingham, H. D. Pritchard, and D. G. Vaughan, 2009: Increased rate of acceleration on Pine Island Glacier strongly coupled to changes in gravitational driving stress. *The Cryosphere*, **3**, 125–131.
- Seneviratne, S., et al., 2010: Investigating soil moisture-climate interactions in a changing climate: A review. *Earth-Sci. Rev.*, **99**, 125–161.
- Seneviratne, S. I., et al., 2012: Chapter 3: Changes in climate extremes and their Impacts on the Natural Physical Environment. In: *SREX: Special Report on Managing the Risks of Extreme Events and Disasters to Advance Climate Change Adaptation* [C. B. Field, et al. (eds.)]. Cambridge University Press, Cambridge, United Kingdom and New York, NY, USA, pp.109–230.
- Smith, S., and T. Wigley, 2006: Multi-gas forcing stabilization with Minicam. *Energy J.*, 373–391.
- Smith, T. M., R. W. Reynolds, T. C. Peterson, and J. Lawrimore, 2008: Improvements to NOAA's historical merged land-ocean surface temperature analysis (1880–2005). *J. Clim.*, **21**, 2283–2296.
- Steinhilber, F., J. Beer, and C. Fröhlich, 2009: Total solar irradiance during the Holocene. *Geophys. Res. Lett.*, **36**, L19704.
- SWIPA, 2011: Snow, water, ice and permafrost in the Arctic. SWIPA 2011 Executive Summary. AMAP, Oslo, Norway, 16 pp.
- Taylor, K. E., R. J. Stouffer, and G. A. Meehl, 2012: An overview of CMIP5 and the experiment design. *Bull. Am. Meteorol. Soc.*, **93**, 485–498.
- Tedesco, M., 2007: A new record in 2007 for melting in Greenland. *EOS, Trans. Am. Geophys. Union*, **88**, 383.
- Thomson, A. M., et al., 2011: RCP4.5: A pathway for stabilization of radiative forcing by 2100. *Clim. Change*, **109**, 77–94.
- Tietsche, S., D. Notz, J. H. Jungclauss, and J. Marotzke, 2011: Recovery mechanisms of Arctic summer sea ice. *Geophys. Res. Lett.*, **38**, L02707.
- Trenberth, K. E., J. T. Fasullo, and J. Kiehl, 2009: Earth's global energy budget. *Bull. Am. Meteorol. Soc.*, **90**, 311–323.
- Turner, J., and J. E. Overland, 2009: Contrasting climate change in the two polar regions. *Polar Res.*, **28**, 146–164.
- Turner, J., et al., 2009: Antarctic Climate Change and the environment. Scientific Committee on Antarctic Research, Cambridge, United Kingdom, 526 pp.
- van Vuuren, D., et al., 2007: Stabilizing greenhouse gas concentrations at low levels: An assessment of reduction strategies and costs. *Clim. Change*, **81**, 119–159.
- van Vuuren, D. P., et al., 2011a: RCP2.6: Exploring the possibility to keep global mean temperature increase below 2°C. *Clim. Change*, **109**, 95–116.
- van Vuuren, D. P., et al., 2011b: The representative concentration pathways: An overview. *Clim. Change*, **109**, 5–31.
- Wadhams, P., 2012: Arctic ice cover, ice thickness and tipping points. *Ambio*, **41**, 23–33.
- Warrick, R., and J. Oerlemans, 1990: Sea level rise. In: *Climate Change: The IPCC Scientific Assessment* [J. T. Houghton, G. J. Jenkins and J. J. Ephraums (eds.)]. Cambridge University Press, Cambridge, United Kingdom and New York, NY, USA, 261–281.
- Wigley, T. M. L., 2005: The climate change commitment. *Science*, **307**, 1766–1769.
- Willis, J. K., J. M. Lyman, G. C. Johnson, and J. Gilson, 2009: In situ data biases and recent ocean heat content variability. *J. Atmos. Ocean. Technol.*, **26**, 846–852.
- Willis, J., D. Chambers, C. Kuo, and C. Shum, 2010: Global sea level rise recent progress and challenges for the decade to come. *Oceanography*, **23**, 26–35.
- Wise, M., et al., 2009: Implications of limiting CO₂ concentrations for land use and energy. *Science*, **324**, 1183–1186.
- Yip, S., C. A. T. Ferro, D. B. Stephenson, and E. Hawkins, 2011: A simple, coherent framework for partitioning uncertainty in climate predictions. *J. Climate*, **24**, 4634–4643.
- Zemp, M., I. Roer, A. Käab, M. Hoelzle, F. Paul, and W. Haeberli, 2008: Global glacier changes: Facts and figures. United Nations Environment Programme and World Glacier Monitoring Service, 88 pp.
- Zemp, M., M. Hoelzle, and W. Haeberli, 2009: Six decades of glacier mass-balance observations: A review of the worldwide monitoring network. *Ann. Glaciol.*, **50**, 101–111.
- Zhang, X., and F. Zwiers, 2012: Statistical indices for the diagnosing and detecting changes in extremes. In: *Extremes in a Changing Climate: Detection, Analysis and Uncertainty* [A. AghaKouchak, D. Easterling, K. Hsu, S. Schubert, and S. Sorooshian (eds.)]. Springer Science+Business Media, Heidelberg, Germany and New York, NY, USA, 1–14.

Appendix 1.A: Notes and Technical Details on Figures Displayed in Chapter 1

Figure 1.4: Documentation of Data Sources

Observed Temperature

NASA GISS evaluation of the observations: Hansen et al. (2010) updated: The data were downloaded from http://data.giss.nasa.gov/gistemp/tabledata_v3/GLB.Ts+dSST.txt. Annual means are used (January to December) and anomalies are calculated relative to 1961–1990.

NOAA NCDC evaluation of the observations: Smith et al. (2008) updated: The data were downloaded from ftp://ftp.ncdc.noaa.gov/pub/data/anomalies/annual.land_ocean.90S.90N.df_1901-2000mean.dat. Annual mean anomalies are calculated relative to 1961–1990.

Hadley Centre evaluation of the observations: Morice et al. (2012): The data were downloaded from http://www.metoffice.gov.uk/hadobs/hadcrut4/data/current/download.html#regional_series. Annual mean anomalies are calculated relative to 1961–1990 based on the ensemble median.

IPCC Range of Projections

Table 1.A.1 | FAR: The data have been digitized using a graphics tool from FAR Chapter 6, Figure 6.11 (Bretherton et al., 1990) in 5-year increments as anomalies relative to 1990 (°C).

Year	Lower Bound (Scenario D)	Upper Bound (Business as Usual)
1990	0.00	0.00
1995	0.09	0.14
2000	0.15	0.30
2005	0.23	0.53
2010	0.28	0.72
2015	0.33	0.91
2020	0.39	1.11
2025	0.45	1.34
2030	0.52	1.58
2035	0.58	1.86

Table 1.A.2 | SAR: The data have been digitized using a graphics tool from Figure 19 of the TS (IPCC, 1996) in 5-year increments as anomalies relative to 1990. The scenarios include changes in aerosols beyond 1990 (°C).

Year	Lower Bound (IS92c/1.5)	Upper Bound (IS92e/4.5)
1990	0.00	0.00
1995	0.05	0.09
2000	0.11	0.17
2005	0.16	0.28
2010	0.19	0.38
2015	0.23	0.47
2020	0.27	0.57
2025	0.31	0.67
2030	0.36	0.79
2035	0.41	0.92

Table 1.A.3 | TAR: The data have been digitized using a graphics tool from Figure 9.13(b) (Cubasch et al., 2001) in 5-year increments based on the GFDL_R15_a and DOE PCM parameter settings (°C).

Year	Lower Bound	Upper Bound
1990	0.00	0.00
1995	0.05	0.09
2000	0.11	0.20
2005	0.14	0.34
2010	0.17	0.52
2015	0.22	0.70
2020	0.28	0.87
2025	0.37	1.08
2030	0.43	1.28
2035	0.52	1.50

AR4: The temperature projections of the AR4 are presented for three SRES scenarios: B1, A1B and A2. Annual mean anomalies relative to 1961–1990 of the individual CMIP3 ensemble simulations (as used in AR4 SPM Figure SPM5) are shown. One outlier has been eliminated based on the advice of the model developers because of the model drift that leads to an unrealistic temperature evolution. As assessed by Meehl et al. (2007), the *likely* range for the temperature change is given by the ensemble mean temperature change +60% and –40% of the ensemble mean temperature change. Note that in the AR4 the uncertainty range was explicitly estimated for the end of the 21st century results. Here, it is shown for 2035. The time dependence of this range has been assessed in Knutti et al. (2008). The relative uncertainty is approximately constant over time in all estimates from different sources, except for the very early decades when natural variability is being considered (see Figure 3 in Knutti et al., 2008).

Data Processing

Observations

The observations are shown from 1950 to 2012 as annual mean anomaly relative to 1961–1990 (squares). For smoothing, first, the trend of each of the observational data sets was calculated by locally weighted scatter plot smoothing (Cleveland, 1979; $f = 1/3$). Then, the 11-year running means of the residuals were determined with reflected ends for the last 5 years. Finally, the trend was added back to the 11-year running means of the residuals.

Projections

For FAR, SAR and TAR, the projections have been harmonized to match the average of the three smoothed observational data sets at 1990.

Figure 1.5: Documentation of Data Sources

Observed CO₂ Concentrations

Global annual mean CO₂ concentrations are presented as annual mean values from Annex II Table AII.1.1a.

IPCC Range of Projections

Table 1.A.4 | FAR: The data have been digitized using a graphics tool from Figure A.3 (Annex, IPCC, 1990) as anomalies compared to 1990 in 5-year increments (ppm) and the observed 1990 value (353.6) has been added.

Year	Lower Bound (Scenario D)	Upper Bound (Business as Usual)
1990	353.6	353.6
1995	362.8	363.7
2000	370.6	373.3
2005	376.5	386.5
2010	383.2	401.5
2015	390.2	414.3
2020	396.6	428.8
2025	401.5	442.0
2030	406.0	460.7
2035	410.0	480.3

Table 1.A.5 | SAR: The data have been digitized using a graphics tool from Figure 5b in the TS (IPCC, 1996) in 5-year increments (ppm) as anomalies compared to 1990 and the observed 1990 value (353.6) has been added.

Year	Lower Bound (IS92c)	Upper Bound (IS92e)
1990	353.6	353.6
1995	358.4	359.0
2000	366.8	369.2
2005	373.7	380.4
2010	382.3	392.9
2015	391.4	408.0
2020	400.7	423.0
2025	408.0	439.6
2030	416.9	457.7
2035	424.5	477.7

TAR: The data were taken in 10-year increments from table Appendix II (IPCC, 2001) SRES Data Tables Table II.2.1 (ISAM model high and low setting). The scenarios that give the upper bound or lower bound respectively vary over time.

AR4: The data used was obtained from Figure 10.26 in Chapter 10 of AR4 (Meehl et al., 2007, provided by Malte Meinshausen). Annual means are used.

Data Processing

The projections have been harmonized to start from the observed value in 1990.

Figure 1.6: Documentation of Data Sources

Observed CH₄ Concentrations

Global annual mean CH₄ concentrations are presented as annual mean values from Annex II Table AII.1.1a.

IPCC Range of Projections

Table 1.A.6 | FAR: The data have been digitized using a graphics tool from FAR SPM Figure 5 (IPCC, 1990) in 5-year increments (ppb) as anomalies compared to 1990 the observed 1990 value (1714.4) has been added.

Year	Lower Bound (Scenario D)	Upper Bound (Business as Usual)
1990	1714.4	1714.4
1995	1775.7	1816.7
2000	1809.7	1938.7
2005	1819.0	2063.8
2010	1823.1	2191.1
2015	1832.3	2314.1
2020	1847.7	2441.3
2025	1857.9	2562.3
2030	1835.3	2691.6
2035	1819.0	2818.8

SAR: The data were taken in 5-year increments from Table 2.5a (Schimel et al., 1996). The scenarios that give the upper bound or lower bound respectively vary over time.

TAR: The data were taken in 10-year increments from Appendix II SRES Data Tables Table II.2.2 (IPCC, 2001). The upper bound is given by the A1p scenario, the lower bound by the B1p scenario.

AR4: The data used was obtained from Figure 10.26 in Chapter 10 of AR4 (Meehl et al., 2007, provided by Malte Meinshausen). Annual means are used.

Data Processing

The observations are shown as annual means. The projections have been harmonized to start from the same value in 1990.

Figure 1.7: Documentation of Data Sources

Observed N₂O Concentrations

Global annual mean N₂O concentrations are presented as annual mean values from Annex II Table AII.1.1a.

IPCC Range of Projections

Table 1.A.7: FAR | The data have been digitized using a graphics tool from FAR A.3 (Annex, IPCC, 1990) in 5-year increments (ppb) as anomalies compared to 1990 and the observed 1990 value (308.7) has been added.

Year	Lower Bound (Scenario D)	Upper Bound (Business as Usual)
1990	308.7	308.7
1995	311.7	313.2
2000	315.4	317.7
2005	318.8	322.9
2010	322.1	328.0
2015	325.2	333.0
2020	328.2	337.9
2025	331.7	343.0
2030	334.0	348.9
2035	336.1	354.1

SAR: The data were taken in 5-year increments from Table 2.5b (Schimel et al., 1996). The upper bound is given by the IS92e and IS92f scenario, the lower bound by the IS92d scenario.

TAR: The data were taken in 10-year increments from Appendix II SRES Data Tables Table II.2.3 (IPCC, 2001). The upper bound is given by the A1FI scenario, the lower bound by the B2 and A1T scenario.

AR4: The data used was obtained from Figure 10.26 in Chapter 10 of AR4 (Meehl et al., 2007, provided by Malte Meinshausen). Annual means are used.

Data Processing

The observations are shown as annual means. No smoothing is applied. The projections have been harmonized to start from the same value in 1990.

Figure 1.10: Documentation of Data Sources

Observed Global Mean Sea Level Rise

Three data sets based on tide gauge measurements are presented: Church and White (2011), Jevrejeva et al. (2008), and Ray and Douglas (2011). Annual mean anomalies are calculated relative to 1961–1990.

Estimates based on sea surface altimetry are presented as the ensemble mean of five different data sets (Section 3.7, Figure 3.13, Section 13.2, Figure 13.3) from 1993 to 2012. Annual means have been calculated. The data are harmonized to start from the mean of the three tide gauge based estimates (see above) at 1993.

IPCC Range of Projections

Table 1.A.8 | FAR: The data have been digitized using a graphics tool from Chapter 9, Figure 9.6 for the upper bound and Figure 9.7 for the lower bound (Warrick and Oerlemans, 1990) in 5-year increments as anomalies relative to 1990 (cm) and the observed anomaly relative to 1961–1990 (2.0 cm) has been added.

Year	Lower Bound (Scenario D)	Upper Bound (Business as Usual)
1990	2.0	2.0
1995	2.7	5.0
2000	3.7	7.9
2005	4.6	11.3
2010	5.5	15.0
2015	6.3	18.7
2020	6.9	22.8
2025	7.7	26.7
2030	8.4	30.9
2035	9.2	35.4

Table 1.A.9 | SAR: The data have been digitized using a graphics tool from Figure 21 (TS, IPCC, 1996) in 5-year increments as anomalies relative to 1990 (cm) and the observed anomaly relative to 1961–1990 (2.0 cm) has been added.

Year	Lower Bound (IS92c/1.5)	Upper Bound (IS92e/4.5)
1990	2.0	2.0
1995	2.4	4.3
2000	2.7	6.5
2005	3.1	9.0
2010	3.4	11.7
2015	3.8	14.9
2020	4.4	18.3
2025	5.1	21.8
2030	5.7	25.4
2035	6.4	29.2

TAR: The data are given in Table II.5.1 in 10-year increments. They are harmonized to start from mean of the observed anomaly relative to 1961–1990 at 1990 (2.0 cm).

AR4: The AR4 did not give a time-dependent estimate of sea level rise. These analyses have been conducted post AR4 by Church et al. (2011) based on the CMIP3 model results that were available at the time of AR4. Here, the SRES B1, A1B and A2 scenarios are shown from Church et al. (2011). The data start in 2001 and are given as anomalies with respect to 1990. They are displayed from 2001 to 2035, but the anomalies are harmonized to start from mean of the observed anomaly relative to 1961–1990 at 1990 (2.0 cm).

Data Processing

The observations are shown from 1950 to 2012 as the annual mean anomaly relative to 1961–1990 (squares) and smoothed (solid lines). For smoothing, first, the trend of each of the observational data sets was calculated by locally weighted scatterplot smoothing (Cleveland, 1979; $f = 1/3$). Then, the 11-year running means of the residuals were determined with reflected ends for the last 5 years. Finally, the trend was added back to the 11-year running means of the residuals.

2

Observations: Atmosphere and Surface

Coordinating Lead Authors:

Dennis L. Hartmann (USA), Albert M.G. Klein Tank (Netherlands), Matilde Rusticucci (Argentina)

Lead Authors:

Lisa V. Alexander (Australia), Stefan Brönnimann (Switzerland), Yassine Abdul-Rahman Charabi (Oman), Frank J. Dentener (EU/Netherlands), Edward J. Dlugokencky (USA), David R. Easterling (USA), Alexey Kaplan (USA), Brian J. Soden (USA), Peter W. Thorne (USA/Norway/UK), Martin Wild (Switzerland), Panmao Zhai (China)

Contributing Authors:

Robert Adler (USA), Richard Allan (UK), Robert Allan (UK), Donald Blake (USA), Owen Cooper (USA), Aiguo Dai (USA), Robert Davis (USA), Sean Davis (USA), Markus Donat (Australia), Vitali Fioletov (Canada), Erich Fischer (Switzerland), Leopold Haimberger (Austria), Ben Ho (USA), John Kennedy (UK), Elizabeth Kent (UK), Stefan Kinne (Germany), James Kossin (USA), Norman Loeb (USA), Carl Mears (USA), Christopher Merchant (UK), Steve Montzka (USA), Colin Morice (UK), Cathrine Lund Myhre (Norway), Joel Norris (USA), David Parker (UK), Bill Randel (USA), Andreas Richter (Germany), Matthew Rigby (UK), Ben Santer (USA), Dian Seidel (USA), Tom Smith (USA), David Stephenson (UK), Ryan Teuling (Netherlands), Junhong Wang (USA), Xiaolan Wang (Canada), Ray Weiss (USA), Kate Willett (UK), Simon Wood (UK)

Review Editors:

Jim Hurrell (USA), Jose Marengo (Brazil), Fredolin Tangang (Malaysia), Pedro Viterbo (Portugal)

This chapter should be cited as:

Hartmann, D.L., A.M.G. Klein Tank, M. Rusticucci, L.V. Alexander, S. Brönnimann, Y. Charabi, F.J. Dentener, E.J. Dlugokencky, D.R. Easterling, A. Kaplan, B.J. Soden, P.W. Thorne, M. Wild and P.M. Zhai, 2013: Observations: Atmosphere and Surface. In: *Climate Change 2013: The Physical Science Basis. Contribution of Working Group I to the Fifth Assessment Report of the Intergovernmental Panel on Climate Change* [Stocker, T.F., D. Qin, G.-K. Plattner, M. Tignor, S.K. Allen, J. Boschung, A. Nauels, Y. Xia, V. Bex and P.M. Midgley (eds.)]. Cambridge University Press, Cambridge, United Kingdom and New York, NY, USA.

Table of Contents

Executive Summary	161	2.7 Changes in Atmospheric Circulation and Patterns of Variability	223
2.1 Introduction	164	2.7.1 Sea Level Pressure.....	223
2.2 Changes in Atmospheric Composition	165	2.7.2 Surface Wind Speed.....	224
2.2.1 Well-Mixed Greenhouse Gases.....	165	2.7.3 Upper-Air Winds.....	226
Box 2.1: Uncertainty in Observational Records	165	2.7.4 Tropospheric Geopotential Height and Tropopause.....	226
2.2.2 Near-Term Climate Forcers.....	170	2.7.5 Tropical Circulation.....	226
2.2.3 Aerosols.....	174	2.7.6 Jets, Storm Tracks and Weather Types.....	229
Box 2.2: Quantifying Changes in the Mean: Trend Models and Estimation	179	2.7.7 Stratospheric Circulation.....	230
2.3 Changes in Radiation Budgets	180	2.7.8 Changes in Indices of Climate Variability.....	230
2.3.1 Global Mean Radiation Budget.....	181	Box 2.5: Patterns and Indices of Climate Variability	232
2.3.2 Changes in Top of the Atmosphere Radiation Budget.....	182	References	237
2.3.3 Changes in Surface Radiation Budget.....	183	Frequently Asked Questions	
Box 2.3: Global Atmospheric Reanalyses	185	FAQ 2.1 How Do We Know the World Has Warmed?	198
2.4 Changes in Temperature	187	FAQ 2.2 Have There Been Any Changes in Climate Extremes?	218
2.4.1 Land Surface Air Temperature.....	187	Supplementary Material	
2.4.2 Sea Surface Temperature and Marine Air Temperature.....	190	<i>Supplementary Material is available in online versions of the report.</i>	
2.4.3 Global Combined Land and Sea Surface Temperature.....	192		
2.4.4 Upper Air Temperature.....	194		
2.5 Changes in Hydrological Cycle	201		
2.5.1 Large-Scale Changes in Precipitation.....	201		
2.5.2 Streamflow and Runoff.....	204		
2.5.3 Evapotranspiration Including Pan Evaporation.....	205		
2.5.4 Surface Humidity.....	205		
2.5.5 Tropospheric Humidity.....	206		
2.5.6 Clouds.....	208		
2.6 Changes in Extreme Events	208		
2.6.1 Temperature Extremes.....	209		
2.6.2 Extremes of the Hydrological Cycle.....	213		
2.6.3 Tropical Storms.....	216		
2.6.4 Extratropical Storms.....	217		
Box 2.4: Extremes Indices	221		

Executive Summary

The evidence of climate change from observations of the atmosphere and surface has grown significantly during recent years. At the same time new improved ways of characterizing and quantifying uncertainty have highlighted the challenges that remain for developing long-term global and regional climate quality data records. Currently, the observations of the atmosphere and surface indicate the following changes:

Atmospheric Composition

It is certain that atmospheric burdens of the well-mixed greenhouse gases (GHGs) targeted by the Kyoto Protocol increased from 2005 to 2011. The atmospheric abundance of carbon dioxide (CO₂) was 390.5 ppm (390.3 to 390.7)¹ in 2011; this is 40% greater than in 1750. Atmospheric nitrous oxide (N₂O) was 324.2 ppb (324.0 to 324.4) in 2011 and has increased by 20% since 1750. Average annual increases in CO₂ and N₂O from 2005 to 2011 are comparable to those observed from 1996 to 2005. Atmospheric methane (CH₄) was 1803.2 ppb (1801.2 to 1805.2) in 2011; this is 150% greater than before 1750. CH₄ began increasing in 2007 after remaining nearly constant from 1999 to 2006. Hydrofluorocarbons (HFCs), perfluorocarbons (PFCs), and sulphur hexafluoride (SF₆) all continue to increase relatively rapidly, but their contributions to radiative forcing are less than 1% of the total by well-mixed GHGs. {2.2.1.1}

For ozone-depleting substances (Montreal Protocol gases), it is certain that the global mean abundances of major chlorofluorocarbons (CFCs) are decreasing and HCFCs are increasing. Atmospheric burdens of major CFCs and some halons have decreased since 2005. HCFCs, which are transitional substitutes for CFCs, continue to increase, but the spatial distribution of their emissions is changing. {2.2.1.2}

Because of large variability and relatively short data records, confidence² in stratospheric H₂O vapour trends is low. Near-global satellite measurements of stratospheric water vapour show substantial variability but small net changes for 1992–2011. {2.2.2.1}

It is certain that global stratospheric ozone has declined from pre-1980 values. Most of the decline occurred prior to the mid 1990s; since then ozone has remained nearly constant at about 3.5% below the 1964–1980 level. {2.2.2.2}

Confidence is medium in large-scale increases of tropospheric ozone across the Northern Hemisphere (NH) since the 1970s.

Confidence is low in ozone changes across the Southern Hemisphere (SH) owing to limited measurements. It is *likely*³ that surface ozone trends in eastern North America and Western Europe since 2000 have levelled off or decreased and that surface ozone strongly increased in East Asia since the 1990s. Satellite and surface observations of ozone precursor gases NO_x, CO, and non-methane volatile organic carbons indicate strong regional differences in trends. Most notably NO₂ has *likely* decreased by 30 to 50% in Europe and North America and increased by more than a factor of 2 in Asia since the mid-1990s. {2.2.2.3, 2.2.2.4}

It is very likely that aerosol column amounts have declined over Europe and the eastern USA since the mid 1990s and increased over eastern and southern Asia since 2000. These shifting aerosol regional patterns have been observed by remote sensing of aerosol optical depth (AOD), a measure of total atmospheric aerosol load. Declining aerosol loads over Europe and North America are consistent with ground-based *in situ* monitoring of particulate mass. *Confidence* in satellite based global average AOD trends is *low*. {2.2.3}

Radiation Budgets

Satellite records of top of the atmosphere radiation fluxes have been substantially extended since AR4, and it is unlikely that significant trends exist in global and tropical radiation budgets since 2000. Interannual variability in the Earth's energy imbalance related to El Niño-Southern Oscillation is consistent with ocean heat content records within observational uncertainty. {2.3.2}

Surface solar radiation likely underwent widespread decadal changes after 1950, with decreases ('dimming') until the 1980s and subsequent increases ('brightening') observed at many land-based sites. There is *medium confidence* for increasing downward thermal and net radiation at land-based observation sites since the early 1990s. {2.3.3}

Temperature

It is certain that Global Mean Surface Temperature has increased since the late 19th century. Each of the past three decades has been successively warmer at the Earth's surface than all the previous decades in the instrumental record, and the first decade of the 21st century has been the warmest. The globally averaged combined land and ocean surface temperature data as calculated by a linear trend, show a warming of 0.85 [0.65 to 1.06] °C, over the period 1880–2012, when multiple independently produced datasets exist, and

¹ Values in parentheses are 90% confidence intervals. Elsewhere in this chapter usually the half-widths of the 90% confidence intervals are provided for the estimated change from the trend method.

² In this Report, the following summary terms are used to describe the available evidence: limited, medium, or robust; and for the degree of agreement: low, medium, or high. A level of confidence is expressed using five qualifiers: very low, low, medium, high, and very high, and typeset in italics, e.g., *medium confidence*. For a given evidence and agreement statement, different confidence levels can be assigned, but increasing levels of evidence and degrees of agreement are correlated with increasing confidence (see Section 1.4 and Box TS.1 for more details).

³ In this Report, the following terms have been used to indicate the assessed likelihood of an outcome or a result: Virtually certain 99–100% probability, Very likely 90–100%, Likely 66–100%, About as likely as not 33–66%, Unlikely 0–33%, Very unlikely 0–10%, Exceptionally unlikely 0–1%. Additional terms (Extremely likely: 95–100%, More likely than not >50–100%, and Extremely unlikely 0–5%) may also be used when appropriate. Assessed likelihood is typeset in italics, e.g., *very likely* (see Section 1.4 and Box TS.1 for more details).

about 0.72°C [0.49°C to 0.89°C] over the period 1951–2012. The total increase between the average of the 1850–1900 period and the 2003–2012 period is 0.78 [0.72 to 0.85] °C and the total increase between the average of the 1850–1900 period and the reference period for projections, 1986–2005, is 0.61 [0.55 to 0.67] °C, based on the single longest dataset available. For the longest period when calculation of regional trends is sufficiently complete (1901–2012), almost the entire globe has experienced surface warming. In addition to robust multi-decadal warming, global mean surface temperature exhibits substantial decadal and interannual variability. Owing to natural variability, trends based on short records are very sensitive to the beginning and end dates and do not in general reflect long-term climate trends. As one example, the rate of warming over the past 15 years (1998–2012; 0.05 [–0.05 to +0.15] °C per decade), which begins with a strong El Niño, is smaller than the rate calculated since 1951 (1951–2012; 0.12 [0.08 to 0.14] °C per decade). Trends for 15-year periods starting in 1995, 1996, and 1997 are 0.13 [0.02 to 0.24], 0.14 [0.03 to 0.24] and 0.07 [–0.02 to 0.18], respectively. Several independently analyzed data records of global and regional land-surface air temperature (LSAT) obtained from station observations are in broad agreement that LSAT has increased. Sea surface temperatures (SSTs) have also increased. Intercomparisons of new SST data records obtained by different measurement methods, including satellite data, have resulted in better understanding of uncertainties and biases in the records. {2.4.1, 2.4.2, 2.4.3; Box 9.2}

It is unlikely that any uncorrected urban heat-island effects and land use change effects have raised the estimated centennial globally averaged LSAT trends by more than 10% of the reported trend. This is an average value; in some regions with rapid development, urban heat island and land use change impacts on regional trends may be substantially larger. {2.4.1.3}

Confidence is medium in reported decreases in observed global diurnal temperature range (DTR), noted as a key uncertainty in the AR4. Several recent analyses of the raw data on which many previous analyses were based point to the potential for biases that differently affect maximum and minimum average temperatures. However, apparent changes in DTR are much smaller than reported changes in average temperatures and therefore it is *virtually certain* that maximum and minimum temperatures have increased since 1950. {2.4.1.2}

Based on multiple independent analyses of measurements from radiosondes and satellite sensors it is virtually certain that globally the troposphere has warmed and the stratosphere has cooled since the mid-20th century. Despite unanimous agreement on the sign of the trends, substantial disagreement exists among available estimates as to the rate of temperature changes, particularly outside the NH extratropical troposphere, which has been well sampled by radiosondes. Hence there is only *medium confidence* in the rate of change and its vertical structure in the NH extratropical troposphere and *low confidence* elsewhere. {2.4.4}

Hydrological Cycle

Confidence in precipitation change averaged over global land areas since 1901 is low for years prior to 1951 and medium afterwards. Averaged over the mid-latitude land areas of the

Northern Hemisphere, precipitation has likely increased since 1901 (medium confidence before and high confidence after 1951). For other latitudinal zones area-averaged long-term positive or negative trends have *low confidence* due to data quality, data completeness or disagreement amongst available estimates. {2.5.1.1, 2.5.1.2}

It is very likely that global near surface and tropospheric air specific humidity have increased since the 1970s. However, during recent years the near surface moistening over land has abated (*medium confidence*). As a result, fairly widespread decreases in relative humidity near the surface are observed over the land in recent years. {2.4.4, 2.5.4, 2.5.5}

While trends of cloud cover are consistent between independent data sets in certain regions, substantial ambiguity and therefore low confidence remains in the observations of global-scale cloud variability and trends. {2.5.6}

Extreme Events

It is very likely that the numbers of cold days and nights have decreased and the numbers of warm days and nights have increased globally since about 1950. There is only *medium confidence* that the length and frequency of warm spells, including heat waves, has increased since the middle of the 20th century mostly owing to lack of data or of studies in Africa and South America. However, it is *likely* that heatwave frequency has increased during this period in large parts of Europe, Asia and Australia. {2.6.1}

It is likely that since about 1950 the number of heavy precipitation events over land has increased in more regions than it has decreased. *Confidence is highest* for North America and Europe where there have been *likely* increases in either the frequency or intensity of heavy precipitation with some seasonal and/or regional variation. It is *very likely* that there have been trends towards heavier precipitation events in central North America. {2.6.2.1}

Confidence is low for a global-scale observed trend in drought or dryness (lack of rainfall) since the middle of the 20th century, owing to lack of direct observations, methodological uncertainties and geographical inconsistencies in the trends. Based on updated studies, AR4 conclusions regarding global increasing trends in drought since the 1970s were probably overstated. However, this masks important regional changes: the frequency and intensity of drought have *likely* increased in the Mediterranean and West Africa and *likely* decreased in central North America and north-west Australia since 1950. {2.6.2.2}

Confidence remains low for long-term (centennial) changes in tropical cyclone activity, after accounting for past changes in observing capabilities. However, it is *virtually certain* that the frequency and intensity of the strongest tropical cyclones in the North Atlantic has increased since the 1970s. {2.6.3}

Confidence in large-scale trends in storminess or storminess proxies over the last century is low owing to inconsistencies

between studies or lack of long-term data in some parts of the world (particularly in the SH). {2.6.4}

Because of insufficient studies and data quality issues *confidence* is also *low* for trends in small-scale severe weather events such as hail or thunderstorms. {2.6.2.4}

Atmospheric Circulation and Indices of Variability

It is *likely* that circulation features have moved poleward since the 1970s, involving a widening of the tropical belt, a poleward shift of storm tracks and jet streams, and a contraction of the northern polar vortex. Evidence is more robust for the NH. It is *likely* that the Southern Annular Mode has become more positive since the 1950s. {2.7.5, 2.7.6, 2.7.8; Box 2.5}

Large variability on interannual to decadal time scales hampers robust conclusions on long-term changes in atmospheric circulation in many instances. *Confidence* is *high* that the increase in the northern mid-latitude westerly winds and the North Atlantic Oscillation (NAO) index from the 1950s to the 1990s and the weakening of the Pacific Walker circulation from the late 19th century to the 1990s have been largely offset by recent changes. {2.7.5, 2.7.8, Box 2.5}

Confidence in the existence of long-term changes in remaining aspects of the global circulation is *low* owing to observational limitations or limited understanding. These include surface winds over land, the East Asian summer monsoon circulation, the tropical cold-point tropopause temperature and the strength of the Brewer Dobson circulation. {2.7.2, 2.7.4, 2.7.5, 2.7.7}

2.1 Introduction

This chapter assesses the scientific literature on atmospheric and surface observations since AR4 (IPCC, 2007). The most likely changes in physical climate variables or climate forcing agents are identified based on current knowledge, following the IPCC AR5 uncertainty guidance (Mastrandrea et al., 2011).

As described in AR4 (Trenberth et al., 2007), the climate comprises a variety of space- and timescales: from the diurnal cycle, to interannual variability such as the El Niño-Southern Oscillation (ENSO), to multi-decadal variations. ‘Climate change’ refers to a change in the state of the climate that can be identified by changes in the mean and/or the variability of its properties and that persists for an extended period of time (Annex III: Glossary). In this chapter, climate change is examined for the period with instrumental observations, since about 1850. Change prior to this date is assessed in Chapter 5. The word ‘trend’ is used to designate a long-term movement in a time series that may be regarded, together with the oscillation and random component, as composing the observed values (Annex III: Glossary). Where numerical values are given, they are equivalent linear changes (Box 2.2), though more complex nonlinear changes in the variable will often be clear from the description and plots of the time series.

In recent decades, advances in the global climate observing system have contributed to improved monitoring capabilities. In particular, satellites provide additional observations of climate change, which have been assessed in this and subsequent chapters together with more traditional ground-based and radiosonde observations. Since AR4, substantial developments have occurred including the production of revised data sets, more digital data records, and new data set efforts. New dynamical reanalysis data sets of the global atmosphere have been published (Box 2.3). These various innovations have improved understanding of data issues and uncertainties (Box 2.1).

Developing homogeneous long-term records from these different sources remains a challenge. The longest observational series are land surface air temperatures (LSATs) and sea surface temperatures (SSTs). Like all physical climate system measurements, they suffer from non-climatic artefacts that must be taken into account (Box 2.1). The global combined LSAT and SST remains an important climate change measure for several reasons. Climate sensitivity is typically assessed in the context of global mean surface temperature (GMST) responses to a doubling of CO₂ (Chapter 8) and GMST is thus a key metric in the climate change policy framework. Also, because it extends back in time farther than any other global instrumental series, GMST is key to understanding both the causes of change and the patterns, role and magnitude of natural variability (Chapter 10). Starting at various points in the 20th century, additional observations, including balloon-borne measurements and satellite measurements, and reanalysis products allow analyses of indicators such as atmospheric composition, radiation budgets, hydrological cycle changes, extreme event characterizations and circulation indices. A full understanding of the climate system characteristics and changes requires analyses of all such variables as well as ocean (Chapter 3) and cryosphere (Chapter 4) indicators. Through such a holistic analysis, a clearer and more robust assessment of the changing climate system emerges (FAQ 2.1).

This chapter starts with an assessment of the observations of the abundances of greenhouse gases (GHGs) and of aerosols, the main drivers of climate change (Section 2.2). Global trends in GHGs are indicative of the imbalance between sources and sinks in GHG budgets, and play an important role in emissions verification on a global scale. The radiative forcing (RF) effects of GHGs and aerosols are assessed in Chapter 8. The observed changes in radiation budgets are discussed in Section 2.3. Aerosol–cloud interactions are assessed in Chapter 7. Section 2.4 provides an assessment of observed changes in surface and atmospheric temperature. Observed change in the hydrological cycle, including precipitation and clouds, is assessed in Section 2.5. Changes in variability and extremes (such as cold spells, heat waves, droughts and tropical cyclones) are assessed in Section 2.6. Section 2.7 assesses observed changes in the circulation of the atmosphere and its modes of variability, which help determine seasonal and longer-term anomalies at regional scales (Chapter 14).

Trends have been assessed where possible for multi-decadal periods starting in 1880, 1901 (referred to as long-term trends) and in 1951, 1979 (referred to as short-term trends). The time elapsed since AR4 extends the period for trend calculation from 2005 to 2012 for many variables. The GMST trend since 1998 has also been considered (see also Box 9.2) as well as the trends for sequential 30-year segments of the time series. For many variables derived from satellite data, information is available for 1979–2012 only. In general, trend estimates are more reliable for longer time intervals, and trends computed on short intervals have a large uncertainty. Trends for short intervals are very sensitive to the start and end years. An exception to this is trends in GHGs, whose accurate measurement and long lifetimes make them well-mixed and less susceptible to year-to-year variability, so that trends computed on relatively short intervals are very meaningful for these variables. Where possible, the time interval 1961–1990 has been chosen as the climatological reference period (or normal period) for averaging. This choice enables direct comparisons with AR4, but is different from the present-day climate period (1986–2005) used as a reference in the modelling chapters of AR5 and Annex I: Atlas of Global and Regional Climate Projections.

It is important to note that the question of whether the observed changes are outside the possible range of natural internal climate variability and consistent with the climate effects from changes in atmospheric composition is not addressed in this chapter, but rather in Chapter 10. No attempt has been undertaken to further describe and interpret the observed changes in terms of multi-decadal oscillatory (or low-frequency) variations, (long-term) persistence and/or secular trends (e.g., as in Cohn and Lins, 2005; Koutsoyiannis and Montanari, 2007; Zorita et al., 2008; Lennartz and Bunde, 2009; Mills, 2010; Mann, 2011; Wu et al., 2011; Zhou and Tung, 2012; Tung and Zhou, 2013). In this chapter, the robustness of the observed changes is assessed in relation to various sources of observational uncertainty (Box 2.1). In addition, the reported trend significance and statistical confidence intervals provide an indication of how large the observed trend is compared to the range of observed variability in a given aspect of the climate system (see Box 2.2 for a description of the statistical trend model applied). Unless otherwise stated, 90% confidence intervals are given. The chapter also examines the physical consistency across

different observations, which helps to provide additional confidence in the reported changes. Additional information about data sources and methods is described in the Supplementary Material to Chapter 2.

2.2 Changes in Atmospheric Composition

2.2.1 Well-Mixed Greenhouse Gases

AR4 (Forster et al., 2007; IPCC, 2007) concluded that increasing atmospheric burdens of well-mixed GHGs resulted in a 9% increase in their RF from 1998 to 2005. Since 2005, the atmospheric abundances of many well-mixed GHG increased further, but the burdens of some ozone-depleting substances (ODS) whose production and use were controlled by the Montreal Protocol on Substances that Deplete the Ozone Layer (1987; hereinafter, 'Montreal Protocol') decreased.

Based on updated *in situ* observations, this assessment concludes that these trends resulted in a 7.5% increase in RF from GHGs from 2005 to 2011, with carbon dioxide (CO₂) contributing 80%. Of note

is an increase in the average growth rate of atmospheric methane (CH₄) from ~0.5 ppb yr⁻¹ during 1999–2006 to ~6 ppb yr⁻¹ from 2007 through 2011. Current observation networks are sufficient to quantify global annual mean burdens used to calculate RF and to constrain global emission rates (with knowledge of loss rates), but they are not sufficient for accurately estimating regional scale emissions and how they are changing with time.

The globally, annually averaged well-mixed GHG mole fractions reported here are used in Chapter 8 to calculate RF. A direct, inseparable connection exists between observed changes in atmospheric composition and well-mixed GHG emissions and losses (discussed in Chapter 6 for CO₂, CH₄, and N₂O). A global GHG budget consists of the total atmospheric burden, total global rate of production or emission (i.e., sources), and the total global rate of destruction or removal (i.e., sinks). Precise, accurate systematic observations from independent globally distributed measurement networks are used to estimate global annual mean well-mixed GHG mole fractions at the Earth's surface, and these allow estimates of global burdens. Emissions are predominantly from surface sources, which are described in Chapter 6 for CO₂, CH₄, and N₂O. Direct

Box 2.1 | Uncertainty in Observational Records

The vast majority of historical (and modern) weather observations were not made explicitly for climate monitoring purposes. Measurements have changed in nature as demands on the data, observing practices and technologies have evolved. These changes almost always alter the characteristics of observational records, changing their mean, their variability or both, such that it is necessary to process the raw measurements before they can be considered useful for assessing the true climate evolution. This is true of all observing techniques that measure physical atmospheric quantities. The uncertainty in observational records encompasses instrumental/recording errors, effects of representation (e.g., exposure, observing frequency or timing), as well as effects due to physical changes in the instrumentation (such as station relocations or new satellites). All further processing steps (transmission, storage, gridding, interpolating, averaging) also have their own particular uncertainties. Because there is no unique, unambiguous, way to identify and account for non-climatic artefacts in the vast majority of records, there must be a degree of uncertainty as to how the climate system has changed. The only exceptions are certain atmospheric composition and flux measurements whose measurements and uncertainties are rigorously tied through an unbroken chain to internationally recognized absolute measurement standards (e.g., the CO₂ record at Mauna Loa; Keeling et al., 1976a).

Uncertainty in data set production can result either from the choice of parameters within a particular analytical framework—parametric uncertainty, or from the choice of overall analytical framework—structural uncertainty. Structural uncertainty is best estimated by having multiple independent groups assess the same data using distinct approaches. More analyses assessed now than in AR4 include published estimates of parametric or structural uncertainty. It is important to note that the literature includes a very broad range of approaches. Great care has been taken in comparing the published uncertainty ranges as they almost always do not constitute a like-for-like comparison. In general, studies that account for multiple potential error sources in a rigorous manner yield larger uncertainty ranges. This yields an apparent paradox in interpretation as one might think that smaller uncertainty ranges should indicate a better product. However, in many cases this would be an incorrect inference as the smaller uncertainty range may instead reflect that the published estimate considered only a subset of the plausible sources of uncertainty. Within the timeseries figures, where this issue would be most acute, such parametric uncertainty estimates are therefore not generally included. Consistent with AR4 HadCRUT4 uncertainties in GMST are included in Figure 2.19, which in addition includes structural uncertainties in GMST.

To conclude, the vast majority of the raw observations used to monitor the state of the climate contain residual non-climatic influences. Removal of these influences cannot be done definitively and neither can the uncertainties be unambiguously assessed. Therefore, care is required in interpreting both data products and their stated uncertainty estimates. Confidence can be built from: redundancy in efforts to create products; data set heritage; and cross-comparisons of variables that would be expected to co-vary for physical reasons, such as LSATs and SSTs around coastlines. Finally, trends are often quoted as a way to synthesize the data into a single number. Uncertainties that arise from such a process and the choice of technique used within this chapter are described in more detail in Box 2.2.

use of observations of well-mixed GHG to model their regional budgets can also play an important role in verifying inventory estimates of emissions (Nisbet and Weiss, 2010).

Systematic measurements of well-mixed GHG in ambient air began at various times during the last six decades, with earlier atmospheric histories being reconstructed from measurements of air stored in air archives and trapped in polar ice cores or in firn. In contrast to the physical meteorological parameters discussed elsewhere in this chapter, measurements of well-mixed GHG are reported relative to standards developed from fundamental SI base units (SI = International System of Units) as dry-air mole fractions, a unit that is conserved with changes in temperature and pressure (Box 2.1). This eliminates dilution by H₂O vapour, which can reach 4% of total atmospheric composition. Here, the following abbreviations are used: ppm = $\mu\text{mol mol}^{-1}$; ppb = nmol mol^{-1} ; and ppt = pmol mol^{-1} . Unless noted otherwise, averages of National Oceanic and Atmospheric Administration (NOAA) and Advanced Global Atmospheric Gases Experiment (AGAGE) annually averaged surface global mean mole fractions is described in Section 2.2.1 (see Supplementary Material 2.SM.2 for further species not listed here).

Table 2.1 summarizes globally, annually averaged well-mixed GHG mole fractions from four independent measurement programs. Sampling strategies and techniques for estimating global means and their uncertainties vary among programs. Differences among measurement programs are relatively small and will not add significantly to uncertainty in RF. Time series of the well-mixed GHG are plotted in Figures 2.1 (CO₂), 2.2 (CH₄), 2.3 (N₂O), and 2.4 (halogen-containing compounds).

2.2.1.1 Kyoto Protocol Gases (Carbon Dioxide, Methane, Nitrous Oxide, Hydrofluorocarbons, Perfluorocarbons and Sulphur Hexafluoride)

2.2.1.1.1 Carbon Dioxide

Precise, accurate systematic measurements of atmospheric CO₂ at Mauna Loa, Hawaii and South Pole were started by C. D. Keeling from Scripps Institution of Oceanography in the late 1950s (Keeling et al., 1976a; Keeling et al., 1976b). The 1750 globally averaged abundance of atmospheric CO₂ based on measurements of air extracted from ice cores and from firn is 278 ± 2 ppm (Etheridge et al., 1996). Globally averaged CO₂ mole fractions since the start of the instrumental record

Table 2.1 | Global annual mean surface dry-air mole fractions and their change since 2005 for well-mixed greenhouse gases (GHGs) from four measurement networks. Units are ppt except where noted. Uncertainties are 90% confidence intervals^a. REs (radiative efficiency) and lifetimes (except CH₄ and N₂O, which are from Prather et al., 2012) are from Chapter 8.

Species	Lifetime (yr)	RE (W m ⁻² ppb ⁻¹)	2011 Global Annual Mean			Global Increase from 2005 to 2011		
			UCI	SIO ^b /AGAGE	NOAA	UCI	SIO ^b /AGAGE	NOAA
CO ₂ (ppm)		1.37×10^{-5}		390.48 ± 0.28	390.44 ± 0.16		11.67 ± 0.37	11.66 ± 0.13
CH ₄ (ppb)	9.1	3.63×10^{-4}	1798.1 ± 0.6	1803.1 ± 4.8	1803.2 ± 1.2	26.6 ± 0.9	28.9 ± 6.8	28.6 ± 0.9
N ₂ O (ppb)	131	3.03×10^{-3}		324.0 ± 0.1	324.3 ± 0.1		4.7 ± 0.2	5.24 ± 0.14
SF ₆	3200	0.575		7.26 ± 0.02	7.31 ± 0.02		1.65 ± 0.03	1.64 ± 0.01
CF ₄	50,000	0.1		79.0 ± 0.1			4.0 ± 0.2	
C ₂ F ₆	10,000	0.26		4.16 ± 0.02			0.50 ± 0.03	
HFC-125	28.2	0.219		9.58 ± 0.04			5.89 ± 0.07	
HFC-134a	13.4	0.159	63.4 ± 0.9	62.4 ± 0.3	63.0 ± 0.6	27.7 ± 1.4	28.2 ± 0.4	28.2 ± 0.1
HFC-143a	47.1	0.159		12.04 ± 0.07			6.39 ± 0.10	
HFC-152a	1.5	0.094		6.4 ± 0.1			3.0 ± 0.2	
HFC-23	222	0.176		24.0 ± 0.3			5.2 ± 0.6	
CFC-11	45	0.263	237.9 ± 0.8	236.9 ± 0.1	238.5 ± 0.2	-13.2 ± 0.8	-12.7 ± 0.2	-13.0 ± 0.1
CFC-12	100	0.32	525.3 ± 0.8	529.5 ± 0.2	527.4 ± 0.4	-12.8 ± 0.8	-13.4 ± 0.3	-14.1 ± 0.1
CFC-113	85	0.3	74.9 ± 0.6	74.29 ± 0.06	74.40 ± 0.04	-4.6 ± 0.8	-4.25 ± 0.08	-4.35 ± 0.02
HCFC-22	11.9	0.2	209.0 ± 1.2	213.4 ± 0.8	213.2 ± 1.2	41.5 ± 1.4	44.6 ± 1.1	44.3 ± 0.2
HCFC-141b	9.2	0.152	20.8 ± 0.5	21.38 ± 0.09	21.4 ± 0.2	3.7 ± 0.5	3.70 ± 0.1	3.76 ± 0.03
HCFC-142b	17.2	0.186	21.0 ± 0.5	21.35 ± 0.06	21.0 ± 0.1	4.9 ± 0.5	5.72 ± 0.09	5.73 ± 0.04
CCl ₄	26	0.175	87.8 ± 0.6	85.0 ± 0.1	86.5 ± 0.3	-6.4 ± 0.5	-6.9 ± 0.2	-7.8 ± 0.1
CH ₂ Cl ₂	5	0.069	6.8 ± 0.6	6.3 ± 0.1	6.35 ± 0.07	-14.8 ± 0.5	-11.9 ± 0.2	-12.1 ± 0.1

Notes:

AGAGE = Advanced Global Atmospheric Gases Experiment; NOAA = National Oceanic and Atmospheric Administration, Earth System Research Laboratory, Global Monitoring Division; SIO = Scripps Institution of Oceanography, University of California, San Diego; UCI = University of California, Irvine, Department of Chemistry. HFC-125 = CHF₂CF₃; HFC-134a = CH₂FCF₃; HFC-143a = CH₃CF₃; HFC-152a = CH₃CHF₂; HFC-23 = CHF₃; CFC-11 = CCl₃F; CFC-12 = CCl₂F₂; CFC-113 = CClF₂CCl₂F; HCFC-22 = CHClF₂; HCFC-141b = CH₃CCl₂F; HCFC-142b = CH₃CClF₂.

^a Each program uses different methods to estimate uncertainties.

^b SIO reports only CO₂; all other values reported in these columns are from AGAGE. SIO CO₂ program and AGAGE are not affiliated with each other.

Budget lifetimes are shown; for CH₄ and N₂O, perturbation lifetimes (12.4 years for CH₄ and 121 years for N₂O) are used to estimate global warming potentials (Chapter 8).

Year 1750 values determined from air extracted from ice cores are below detection limits for all species except CO₂ (278 ± 2 ppm), CH₄ (722 ± 25 ppb), N₂O (270 ± 7 ppb) and CF₄ (34.7 ± 0.2 ppt). Centennial variations up to 10 ppm CO₂, 40 ppb CH₄, and 10 ppb occur throughout the late-Holocene (Chapter 6).

are plotted in Figure 2.1. The main features in the contemporary CO_2 record are the long-term increase and the seasonal cycle resulting from photosynthesis and respiration by the terrestrial biosphere, mostly in the Northern Hemisphere (NH). The main contributors to increasing atmospheric CO_2 abundance are fossil fuel combustion and land use change (Section 6.3). Multiple lines of observational evidence indicate that during the past few decades, most of the increasing atmospheric burden of CO_2 is from fossil fuel combustion (Tans, 2009). Since the last year for which the AR4 reported (2005), CO_2 has increased by 11.7 ppm to 390.5 ppm in 2011 (Table 2.1). From 1980 to 2011, the average annual increase in globally averaged CO_2 (from 1 January in one year to 1 January in the next year) was 1.7 ppm yr^{-1} (1 standard deviation = 0.5 ppm yr^{-1} ; 1 ppm globally corresponds to 2.1 PgC increase in the atmospheric burden). Since 2001, CO_2 has increased at 2.0 ppm yr^{-1} (1 standard deviation = 0.3 ppm yr^{-1}). The CO_2 growth rate varies from year to year; since 1980 the range in annual increase is $0.7 \pm 0.1 \text{ ppm}$ in 1992 to $2.9 \pm 0.1 \text{ ppm}$ in 1998. Most of this interannual variability in growth rate is driven by small changes in the balance between photosynthesis and respiration on land, each having global fluxes of $\sim 120 \text{ PgC yr}^{-1}$ (Chapter 6).

2.2.1.1.2 Methane

Globally averaged CH_4 in 1750 was $722 \pm 25 \text{ ppb}$ (after correction to the NOAA-2004 CH_4 standard scale) (Etheridge et al., 1998; Dlugokencky et al., 2005), although human influences on the global CH_4 budget may have begun thousands of years earlier than this time that is normally considered 'pre-industrial' (Ruddiman, 2003; Ferretti et al., 2005; Ruddiman, 2007). In 2011, the global annual mean was $1803 \pm 2 \text{ ppb}$. Direct atmospheric measurements of CH_4 of sufficient spatial coverage to calculate global annual means began in 1978 and are plotted through 2011 in Figure 2.2a. This time period is characterized by a decreasing growth rate (Figure 2.2b) from the early 1980s until 1998, stabilization from 1999 to 2006, and an increasing atmospheric burden from 2007 to 2011 (Rigby et al., 2008; Dlugokencky et al.,

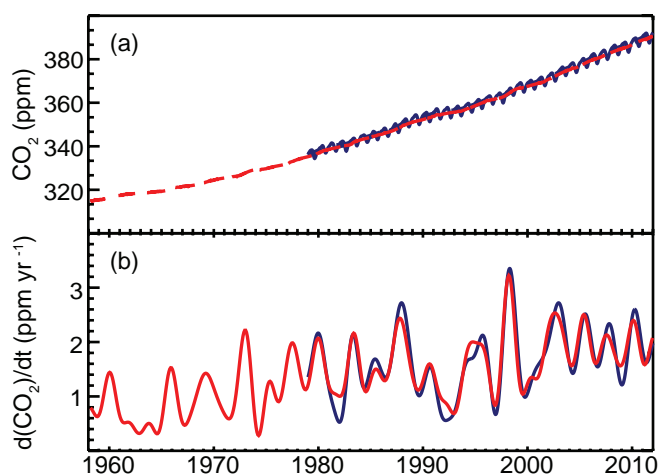


Figure 2.1 | (a) Globally averaged CO_2 dry-air mole fractions from Scripps Institution of Oceanography (SIO) at monthly time resolution based on measurements from Mauna Loa, Hawaii and South Pole (red) and NOAA/ESRL/GMD at quasi-weekly time resolution (blue). SIO values are deseasonalized. (b) Instantaneous growth rates for globally averaged atmospheric CO_2 using the same colour code as in (a). Growth rates are calculated as the time derivative of the deseasonalized global averages (Dlugokencky et al., 1994).

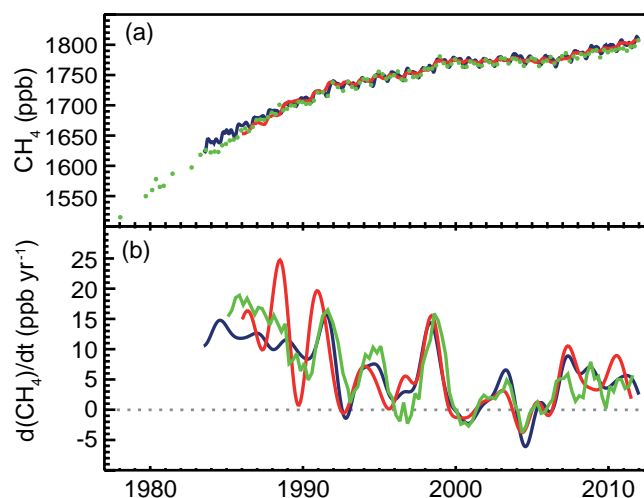


Figure 2.2 | (a) Globally averaged CH_4 dry-air mole fractions from UCI (green; four values per year, except prior to 1984, when they are of lower and varying frequency), AGAGE (red; monthly), and NOAA/ESRL/GMD (blue; quasi-weekly). (b) Instantaneous growth rate for globally averaged atmospheric CH_4 using the same colour code as in (a). Growth rates were calculated as in Figure 2.1.

2009). Assuming no long-term trend in hydroxyl radical (OH) concentration, the observed decrease in CH_4 growth rate from the early 1980s through 2006 indicates an approach to steady state where total global emissions have been approximately constant at $\sim 550 \text{ Tg} (\text{CH}_4) \text{ yr}^{-1}$. Superimposed on the long-term pattern is significant interannual variability; studies of this variability are used to improve understanding of the global CH_4 budget (Chapter 6). The most likely drivers of increased atmospheric CH_4 were anomalously high temperatures in the Arctic in 2007 and greater than average precipitation in the tropics during 2007 and 2008 (Dlugokencky et al., 2009; Bousquet, 2011). Observations of the difference in CH_4 between zonal averages for northern and southern polar regions (53° to 90°) (Dlugokencky et al., 2009, 2011) suggest that, so far, it is unlikely that there has been a permanent measurable increase in Arctic CH_4 emissions from wetlands and shallow sub-sea CH_4 clathrates.

Reaction with the hydroxyl radical (OH) is the main loss process for CH_4 (and for hydrofluorocarbons (HFCs) and hydrochlorofluorocarbons (HCFCs)), and it is the largest term in the global CH_4 budget. Therefore, trends and interannual variability in OH concentration significantly impact our understanding of changes in CH_4 emissions. Methyl chloroform (CH_3CCl_3 ; Section 2.2.1.2) has been used extensively to estimate globally averaged OH concentrations (e.g., Prinn et al., 2005). AR4 reported no trend in OH from 1979 to 2004, and there is no evidence from this assessment to change that conclusion for 2005 to 2011. Montzka et al. (2011a) exploited the exponential decrease and small emissions in CH_3CCl_3 to show that interannual variations in OH concentration from 1998 to 2007 are $2.3 \pm 1.5\%$, which is consistent with estimates based on CH_4 , tetrachloroethene (C_2Cl_4), dichloromethane (CH_2Cl_2), chloromethane (CH_3Cl) and bromomethane (CH_3Br).

2.2.1.1.3 Nitrous Oxide

Globally averaged N_2O in 2011 was 324.2 ppb, an increase of 5.0 ppb over the value reported for 2005 in AR4 (Table 2.1). This is an increase

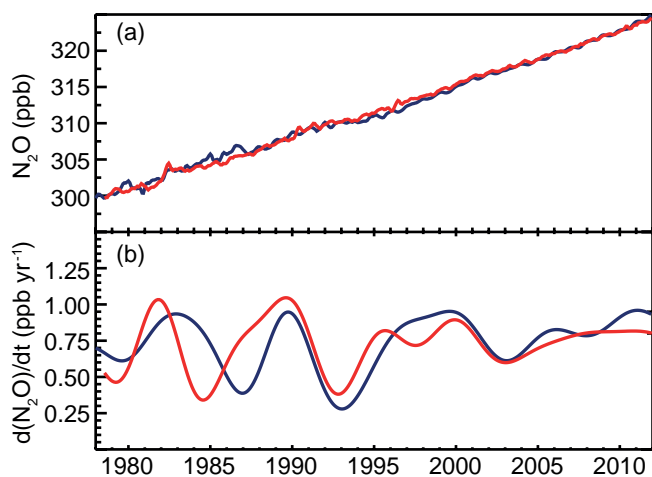


Figure 2.3 | (a) Globally averaged N₂O dry-air mole fractions from AGAGE (red) and NOAA/ESRL/GMD (blue) at monthly resolution. (b) Instantaneous growth rates for globally averaged atmospheric N₂O. Growth rates were calculated as in Figure 2.1.

of 20% over the estimate for 1750 from ice cores, 270 ± 7 ppb (Prather et al., 2012). Measurements of N₂O and its isotopic composition in firn air suggest the increase, at least since the early 1950s, is dominated by emissions from soils treated with synthetic and organic (manure) nitrogen fertilizer (Rockmann and Levin, 2005; Ishijima et al., 2007; Davidson, 2009; Syakila and Kroeze, 2011). Since systematic measurements began in the late 1970s, N₂O has increased at an average rate of ~ 0.75 ppb yr⁻¹ (Figure 2.3). Because the atmospheric burden of CFC-12 is decreasing, N₂O has replaced CFC-12 as the third most important well-mixed GHG contributing to RF (Elkins and Dutton, 2011).

Persistent latitudinal gradients in annually averaged N₂O are observed at background surface sites, with maxima in the northern subtropics, values about 1.7 ppb lower in the Antarctic, and values about 0.4 ppb lower in the Arctic (Huang et al., 2008). These persistent gradients contain information about anthropogenic emissions from fertilizer use at northern tropical to mid-latitudes and natural emissions from soils and ocean upwelling regions of the tropics. N₂O time series also contain seasonal variations with peak-to-peak amplitudes of about 1 ppb in high latitudes of the NH and about 0.4 ppb at high southern and tropical latitudes. In the NH, exchange of air between the stratosphere (where N₂O is destroyed by photochemical processes) and troposphere is the dominant contributor to observed seasonal cycles, not seasonality in emissions (Jiang et al., 2007). Nevison et al. (2011) found correlations between the magnitude of detrended N₂O seasonal minima and lower stratospheric temperature, providing evidence for a stratospheric influence on the timing and amplitude of the seasonal cycle at surface monitoring sites. In the Southern Hemisphere (SH), observed seasonal cycles are also affected by stratospheric influx, and by ventilation and thermal out-gassing of N₂O from the oceans.

2.2.1.1.4 Hydrofluorocarbons, Perfluorocarbons, Sulphur Hexafluoride and Nitrogen Trifluoride

The budgets of HFCs, PFCs and SF₆ were recently reviewed in Chapter 1 of the Scientific Assessment of Ozone Depletion: 2010 (Montzka et al., 2011b), so only a brief description is given here. The current atmos-

pheric abundances of these species are summarized in Table 2.1 and plotted in Figure 2.4.

Atmospheric HFC abundances are low and their contribution to RF is small relative to that of the CFCs and HCFCs they replace (less than 1% of the total by well-mixed GHGs; Chapter 8). As they replace CFCs and HCFCs phased out by the Montreal Protocol, however, their contribution to future climate forcing is projected to grow considerably in the absence of controls on global production (Velders et al., 2009).

HFC-134a is a replacement for CFC-12 in automobile air conditioners and is also used in foam blowing applications. In 2011, it reached 62.7 ppt, an increase of 28.2 ppt since 2005. Based on analysis of high-frequency measurements, the largest emissions occur in North America, Europe and East Asia (Stohl et al., 2009).

HFC-23 is a by-product of HCFC-22 production. Direct measurements of HFC-23 in ambient air at five sites began in 2007. The 2005 global annual mean used to calculate the increase since AR4 in Table 2.1, 5.2 ppt, is based on an archive of air collected at Cape Grim, Tasmania (Miller et al., 2010). In 2011, atmospheric HFC-23 was at 24.0 ppt. Its growth rate peaked in 2006 as emissions from developing countries

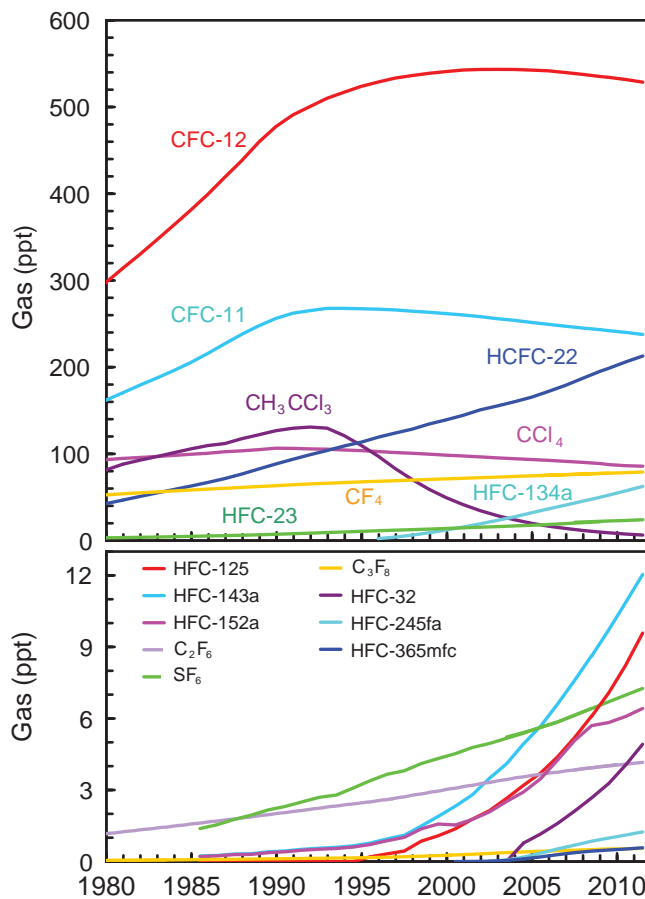


Figure 2.4 | Globally averaged dry-air mole fractions at the Earth's surface of the major halogen-containing well-mixed GHG. These are derived mainly using monthly mean measurements from the AGAGE and NOAA/ESRL/GMD networks. For clarity, only the most abundant chemicals are shown in different compound classes and results from different networks have been combined when both are available.

increased, then declined as emissions were reduced through abatement efforts under the Clean Development Mechanism (CDM) of the UNFCCC. Estimates of total global emissions based on atmospheric observations and bottom-up inventories agree within uncertainties (Miller et al., 2010; Montzka et al., 2010). Currently, the largest emissions of HFC-23 are from East Asia (Yokouchi et al., 2006; Kim et al., 2010; Stohl et al., 2010); developed countries emit less than 20% of the global total. Keller et al. (2011) found that emissions from developed countries may be larger than those reported to the UNFCCC, but their contribution is small. The lifetime of HFC-23 was revised from 270 to 222 years since AR4.

After HFC-134a and HFC-23, the next most abundant HFCs are HFC-143a at 12.04 ppt in 2011, 6.39 ppt greater than in 2005; HFC-125 (O'Doherty et al., 2009) at 9.58 ppt, increasing by 5.89 ppt since 2005; HFC-152a (Greally et al., 2007) at 6.4 ppt with a 3.0 ppt increase since 2005; and HFC-32 at 4.92 ppt in 2011, 3.77 ppt greater than in 2005. Since 2005, all of these were increasing exponentially except for HFC-152a, whose growth rate slowed considerably in about 2007 (Figure 2.4). HFC-152a has a relatively short atmospheric lifetime of 1.5 years, so its growth rate will respond quickly to changes in emissions. Its major uses are as a foam blowing agent and aerosol spray propellant while HFC-143a, HFC-125, and HFC-32 are mainly used in refrigerant blends. The reasons for slower growth in HFC-152a since about 2007 are unclear. Total global emissions of HFC-125 estimated from the observations are within about 20% of emissions reported to the UNFCCC, after accounting for estimates of unreported emissions from East Asia (O'Doherty et al., 2009).

CF_4 and C_2F_6 (PFCs) have lifetimes of 50 kyr and 10 kyr, respectively, and they are emitted as by-products of aluminium production and used in plasma etching of electronics. CF_4 has a natural lithospheric source (Deeds et al., 2008) with a 1750 level determined from Greenland and Antarctic firn air of 34.7 ± 0.2 ppt (Worton et al., 2007; Muhle et al., 2010). In 2011, atmospheric abundances were 79.0 ppt for CF_4 , increasing by 4.0 ppt since 2005, and 4.16 ppt for C_2F_6 , increasing by 0.50 ppt. The sum of emissions of CF_4 reported by aluminium producers and for non-aluminium production in EDGAR (Emission Database for Global Atmospheric Research) v4.0 accounts for only about half of global emissions inferred from atmospheric observations (Muhle et al., 2010). For C_2F_6 , emissions reported to the UNFCCC are also substantially lower than those estimated from atmospheric observations (Muhle et al., 2010).

The main sources of atmospheric SF_6 emissions are electricity distribution systems, magnesium production, and semi-conductor manufacturing. Global annual mean SF_6 in 2011 was 7.29 ppt, increasing by 1.65 ppt since 2005. SF_6 has a lifetime of 3200 years, so its emissions accumulate in the atmosphere and can be estimated directly from its observed rate of increase. Levin et al. (2010) and Rigby et al. (2010) showed that SF_6 emissions decreased after 1995, most likely because of emissions reductions in developed countries, but then increased after 1998. During the past decade, they found that actual SF_6 emissions from developed countries are at least twice the reported values.

NF_3 was added to the list of GHG in the Kyoto Protocol with the Doha Amendment, December, 2012. Arnold et al. (2013) determined 0.59 ppt

for its global annual mean mole fraction in 2008, growing from almost zero in 1978. In 2011, NF_3 was 0.86 ppt, increasing by 0.49 ppt since 2005. These abundances were updated from the first work to quantify NF_3 by Weiss et al. (2008). Initial bottom-up inventories underestimated its emissions; based on the atmospheric observations, NF_3 emissions were 1.18 ± 0.21 Gg in 2011 (Arnold et al., 2013).

In summary, it is certain that atmospheric burdens of well-mixed GHGs targeted by the Kyoto Protocol increased from 2005 to 2011. The atmospheric abundance of CO_2 was 390.5 ± 0.2 ppm in 2011; this is 40% greater than before 1750. Atmospheric N_2O was 324.2 ± 0.2 ppb in 2011 and has increased by 20% since 1750. Average annual increases in CO_2 and N_2O from 2005 to 2011 are comparable to those observed from 1996 to 2005. Atmospheric CH_4 was 1803.2 ± 2.0 ppb in 2011; this is 150% greater than before 1750. CH_4 began increasing in 2007 after remaining nearly constant from 1999 to 2006. HFCs, PFCs, and SF_6 all continue to increase relatively rapidly, but their contributions to RF are less than 1% of the total by well-mixed GHGs (Chapter 8).

2.2.1.2 Ozone-Depleting Substances (Chlorofluorocarbons, Chlorinated Solvents, and Hydrochlorofluorocarbons)

CFC atmospheric abundances are decreasing (Figure 2.4) because of the successful reduction in emissions resulting from the Montreal Protocol. By 2010, emissions from ODSs had been reduced by ~ 11 Pg CO_2 -eq yr^{-1} , which is five to six times the reduction target of the first commitment period (2008–2012) of the Kyoto Protocol (2 Pg CO_2 -eq yr^{-1}) (Velders et al., 2007). These avoided equivalent- CO_2 emissions account for the offsets to RF by stratospheric O_3 depletion caused by ODSs and the use of HFCs as substitutes for them. Recent observations in Arctic and Antarctic firn air further confirm that emissions of CFCs are entirely anthropogenic (Martinerie et al., 2009; Montzka et al., 2011b). CFC-12 has the largest atmospheric abundance and GWP-weighted emissions (which are based on a 100-year time horizon) of the CFCs. Its tropospheric abundance peaked during 2000–2004. Since AR4, its global annual mean mole fraction declined by 13.8 ppt to 528.5 ppt in 2011. CFC-11 continued the decrease that started in the mid-1990s, by 12.9 ppt since 2005. In 2011, CFC-11 was 237.7 ppt. CFC-113 decreased by 4.3 ppt since 2005 to 74.3 ppt in 2011. A discrepancy exists between top-down and bottom-up methods for calculating CFC-11 emissions (Montzka et al., 2011b). Emissions calculated using top-down methods come into agreement with bottom-up estimates when a lifetime of 64 years is used for CFC-11 in place of the accepted value of 45 years; this longer lifetime (64 years) is at the upper end of the range estimated by Douglass et al. (2008) with models that more accurately simulate stratospheric circulation. Future emissions of CFCs will largely come from 'banks' (i.e., material residing in existing equipment or stores) rather than current production.

The mean decrease in globally, annually averaged carbon tetrachloride (CCl_4) based on NOAA and AGAGE measurements since 2005 was 7.4 ppt, with an atmospheric abundance of 85.8 ppt in 2011 (Table 2.1). The observed rate of decrease and inter-hemispheric difference of CCl_4 suggest that emissions determined from the observations are on average greater and less variable than bottom-up emission estimates, although large uncertainties in the CCl_4 lifetime result in large uncertainties in the top-down estimates of emissions (Xiao et al., 2010;

Montzka et al., 2011b). CH_3CCl_3 has declined exponentially for about a decade, decreasing by 12.0 ppt since 2005 to 6.3 ppt in 2011.

HCFCs are classified as 'transitional substitutes' by the Montreal Protocol. Their global production and use will ultimately be phased out, but their global production is not currently capped and, based on changes in observed spatial gradients, there has likely been a shift in emissions within the NH from regions north of about 30°N to regions south of 30°N (Montzka et al., 2009). Global levels of the three most abundant HCFCs in the atmosphere continue to increase. HCFC-22 increased by 44.5 ppt since 2005 to 213.3 ppt in 2011. Developed country emissions of HCFC-22 are decreasing, and the trend in total global emissions is driven by large increases from south and Southeast Asia (Saikawa et al., 2012). HCFC-141b increased by 3.7 ppt since 2005 to 21.4 ppt in 2011, and for HCFC-142b, the increase was 5.73 ppt to 21.1 ppt in 2011. The rates of increase in these three HCFCs increased since 2004, but the change in HCFC-141b growth rate was smaller and less persistent than for the other two, which approximately doubled from 2004 to 2007 (Montzka et al., 2009).

In summary, for ODS, whose production and consumption are controlled by the Montreal Protocol, it is certain that the global mean abundances of major CFCs are decreasing and HCFCs are increasing. Atmospheric burdens of CFC-11, CFC-12, CFC-113, CCl_4 , CH_3CCl_3 and some halons have decreased since 2005. HCFCs, which are transitional substitutes for CFCs, continue to increase, but the spatial distribution of their emissions is changing.

2.2.2 Near-Term Climate Forcers

This section covers observed trends in stratospheric water vapour; stratospheric and tropospheric ozone (O_3); the O_3 precursor gases, nitrogen dioxide (NO_2) and carbon monoxide (CO); and column and surface aerosol. Since trend estimates from the cited literature are used here, issues such as data records of different length, potential lack of comparability among measurement methods and different trend calculation methods, add to the uncertainty in assessing trends.

2.2.2.1 Stratospheric Water Vapour

Stratospheric H_2O vapour has an important role in the Earth's radiative balance and in stratospheric chemistry. Increased stratospheric H_2O vapour causes the troposphere to warm and the stratosphere to cool (Manabe and Strickler, 1964; Solomon et al., 2010), and also causes increased rates of stratospheric O_3 loss (Stenke and Grewe, 2005). Water vapour enters the stratosphere through the cold tropical tropopause. As moisture-rich air masses are transported through this region, most water vapour condenses resulting in extremely dry lower stratospheric air. Because tropopause temperature varies seasonally, so does H_2O abundance there. Other contributions include oxidation of methane within the stratosphere, and possibly direct injection of H_2O vapour in overshooting deep convection (Schiller et al., 2009). AR4 reported that stratospheric H_2O vapour showed significant long-term variability and an upward trend over the last half of the 20th century, but no net increase since 1996. This updated assessment finds large interannual variations that have been observed by independent measurement techniques, but no significant net changes since 1996.

The longest continuous time series of stratospheric water vapour abundance is from *in situ* measurements made with frost point hygrometers starting in 1980 over Boulder, USA (40°N, 105°W) (Scherer et al., 2008), with values ranging from 3.5 to 5.5 ppm, depending on altitude. These observations have been complemented by long-term global satellite observations from SAGE II (1984–2005; Stratospheric Aerosol and Gas Experiment II (Chu et al., 1989)), HALOE (1991–2005; Halogen Occultation Experiment (Russell et al., 1993)), Aura MLS (2004–present; Microwave Limb Sounder (Read et al., 2007)) and Envisat MIPAS (2002–2012; Michelson Interferometer for Passive Atmospheric Sounding (Milz et al., 2005; von Clarmann et al., 2009)). Discrepancies in water vapour mixing ratios from these different instruments can be attributed to differences in the vertical resolution of measurements, along with other factors. For example, offsets of up to 0.5 ppm in lower stratospheric water vapour mixing ratios exist between the most current versions of HALOE (v19) and Aura MLS (v3.3) retrievals during their 16-month period of overlap (2004 to 2005), although such biases can be removed to generate long-term records. Since AR4, new studies characterize the uncertainties in measurements from individual types of *in situ* H_2O sensors (Vömel et al., 2007b; Vömel et al., 2007a; Weinstock et al., 2009), but discrepancies between different instruments (50 to 100% at H_2O mixing ratios less than 10 ppm), particularly for high-altitude measurements from aircraft, remain largely unexplained.

Observed anomalies in stratospheric H_2O from the near-global combined HALOE+MLS record (1992–2011) (Figure 2.5) include effects linked to the stratospheric quasi-biennial oscillation (QBO) influence on tropopause temperatures, plus a step-like drop after 2001 (noted in AR4), and an increasing trend since 2005. Variability during 2001–2011 was large yet there was only a small net change from 1992 through 2011. These interannual water vapour variations for the satellite record are closely linked to observed changes in tropical tropopause temperatures (Fueglistaler and Haynes, 2005; Randel et al., 2006; Rosenlof and Reid, 2008; Randel, 2010), providing reasonable understanding of observed changes. The longer record of Boulder balloon measurements (since 1980) has been updated and reanalyzed (Scherer et al., 2008; Hurst et al., 2011), showing decadal-scale variability and a long-term stratospheric (16 to 26 km) increase of 1.0 ± 0.2 ppm for 1980–2010. Agreement between interannual changes inferred from the Boulder and HALOE+MLS data is good for the period since 1998 but was poor during 1992–1996. About 30% of the positive trend during 1980–2010 determined from frost point hygrometer data (Fujiwara et al., 2010; Hurst et al., 2011) can be explained by increased production of H_2O from CH_4 oxidation (Rohs et al., 2006), but the remainder cannot be explained by changes in tropical tropopause temperatures (Fueglistaler and Haynes, 2005) or other known factors.

In summary, near-global satellite measurements of stratospheric H_2O show substantial variability for 1992–2011, with a step-like decrease after 2000 and increases since 2005. Because of this large variability and relatively short time series, *confidence* in long-term stratospheric H_2O trends is *low*. There is good understanding of the relationship between the satellite-derived H_2O variations and tropical tropopause temperature changes. Stratospheric H_2O changes from temporally sparse balloon-borne observations at one location (Boulder, Colorado) are in good agreement with satellite observations from 1998 to the present, but discrepancies exist for changes during 1992–1996. Long-

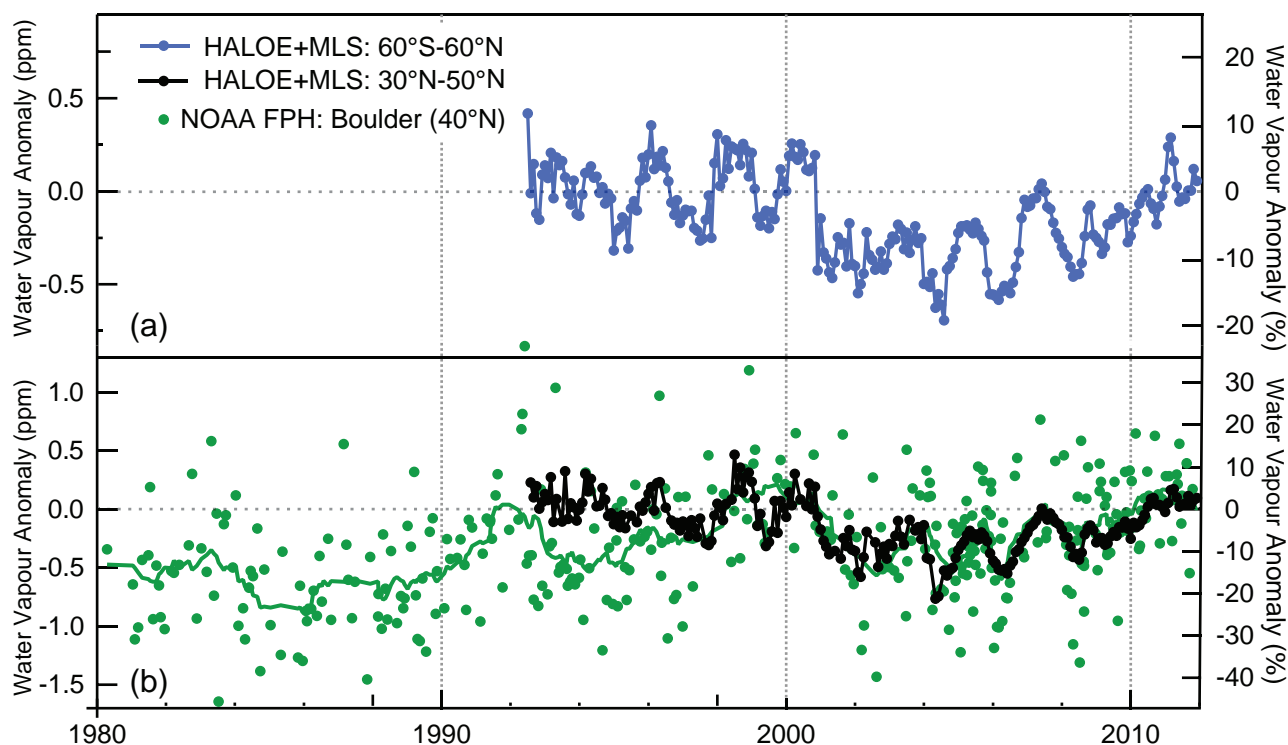


Figure 2.5 | Water vapour anomalies in the lower stratosphere (~16 to 19 km) from satellite sensors and *in situ* measurements normalized to 2000–2011. (a) Monthly mean water vapour anomalies at 83 hPa for 60°S to 60°N (blue) determined from HALOE and MLS satellite sensors. (b) Approximately monthly balloon-borne measurements of stratospheric water vapour from Boulder, Colorado at 40°N (green dots; green curve is 15-point running mean) averaged over 16 to 18 km and monthly means as in (a), but averaged over 30°N to 50°N (black)

term balloon measurements from Boulder indicate a net increase of 1.0 ± 0.2 ppm over 16 to 26 km for 1980–2010, but these long-term increases cannot be fully explained by changes in tropical tropopause temperatures, methane oxidation or other known factors.

2.2.2.2 Stratospheric Ozone

AR4 did not explicitly discuss measured stratospheric ozone trends. For the current assessment report such trends are relevant because they are the basis for revising the RF from -0.05 ± 0.10 W m⁻² in 1750 to -0.10 ± 0.15 W m⁻² in 2005 (Section 8.3.3.2). These values strongly depend on the vertical distribution of the stratospheric ozone changes.

Total ozone is a good proxy for stratospheric ozone because tropospheric ozone accounts for only about 10% of the total ozone column. Long-term total ozone changes over various latitudinal belts, derived from Weber et al. (2012), are illustrated in Figure 2.6 (a–d). Annually averaged total column ozone declined during the 1980s and early 1990s and has remained constant for the past decade, about 3.5 and 2.5% below the 1964–1980 average for the entire globe (not shown) and 60°S to 60°N, respectively, with changes occurring mostly outside the tropics, particularly the SH, where the current extratropical (30°S to 60°S) mean values are 6% below the 1964–1980 average, compared to 3.5% for the NH extratropics (Douglass et al., 2011). In the NH, the 1993 minimum of about –6% was caused primarily by ozone loss through heterogeneous reactions on volcanic aerosols from Mt. Pinatubo.

Two altitude regions are mainly responsible for long-term changes in total column ozone (Douglass et al., 2011). In the upper stratosphere (35 to 45 km), there was a strong and statistically significant decline (about 10%) up to the mid-1990s and little change or a slight increase since. The lower stratosphere, between 20 and 25 km over mid-latitudes, also experienced a statistically significant decline (7 to 8%) between 1979 and the mid-1990s, followed by stabilization or a slight (2 to 3%) ozone increase.

Springtime averages of total ozone poleward of 60° latitude in the Arctic and Antarctic are shown in Figure 2.6e. By far the strongest ozone loss in the stratosphere occurs in austral spring over Antarctica (ozone hole) and its impact on SH climate is discussed in Chapters 11, 12 and 14. Interannual variability in polar stratospheric ozone abundance and chemistry is driven by variability in temperature and transport due to year-to-year differences in dynamics. This variability is particularly large in the Arctic, where the most recent large depletion occurred in 2011, when chemical ozone destruction was, for the first time in the observational record, comparable to that in the Antarctic (Manney et al., 2011).

In summary, it is certain that global stratospheric ozone has declined from pre-1980 values. Most of the decline occurred prior to the mid-1990s; since then there has been little net change and ozone has remained nearly constant at about 3.5% below the 1964–1980 level.

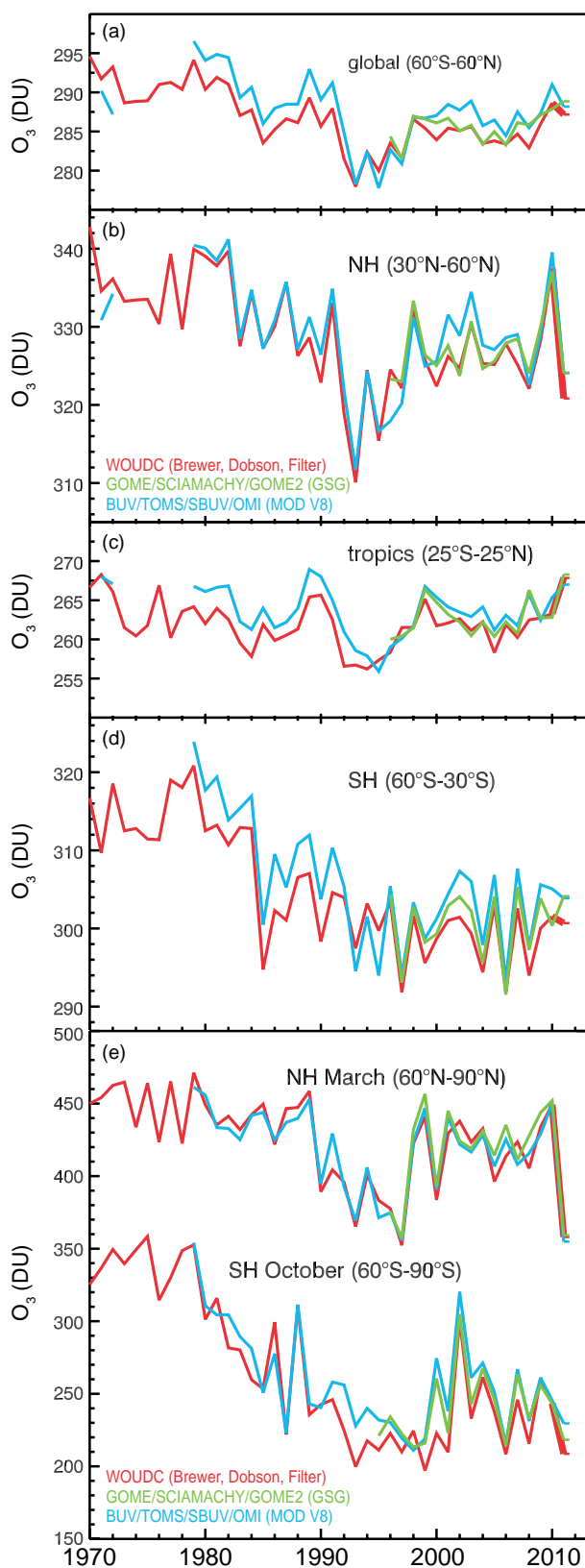


Figure 2.6 | Zonally averaged, annual mean total column ozone in Dobson Units (DU; $1 \text{ DU} = 2.69 \times 10^{16} \text{ O}_3/\text{cm}^2$) from ground-based measurements combining Brewer, Dobson, and filter spectrometer data WOUDC (red), GOME/SCIAMACHY/GOME-2 GSG (green) and merged satellite BUV/TOMS/SBUV/OMI MOD V8 (blue) for (a) Non-Polar Global (60°S to 60°N), (b) NH (30°N to 60°N), (c) Tropics (25°S to 25°N), (d) SH (30°S to 60°S) and (e) March NH Polar (60°N to 90°N) and October SH Polar. (Adapted from Weber et al., 2012; see also for abbreviations.)

2.2.2.3 Tropospheric Ozone

Tropospheric ozone is a short-lived trace gas that either originates in the stratosphere or is produced *in situ* by precursor gases and sunlight (e.g., Monks et al., 2009). An important GHG with an estimated RF of $0.40 \pm 0.20 \text{ W m}^{-2}$ (Chapter 8), tropospheric ozone also impacts human health and vegetation at the surface. Its average atmospheric lifetime of a few weeks produces a global distribution highly variable by season, altitude and location. These characteristics and the paucity of long-term measurements make the assessment of long-term global ozone trends challenging. However, new studies since AR4 provide greater understanding of surface and free tropospheric ozone trends from the 1950s through 2010. An extensive compilation of measured ozone trends is presented in the Supplementary Material, Figure 2.SM.1 and Table 2.SM.2.

The earliest (1876–1910) quantitative ozone observations are limited to Montsouris near Paris where ozone averaged 11 ppb (Volz and Kley, 1988). Semiquantitative ozone measurements from more than 40 locations around the world in the late 1800s and early 1900s range from 5 to 32 ppb with large uncertainty (Pavelin et al., 1999). The low 19th century ozone values cannot be reproduced by most models (Section 8.2.3.1), and this discrepancy is an important factor contributing to uncertainty in RF calculations (Section 8.3.3.1). Limited quantitative measurements from the 1870s to 1950s indicate that surface ozone in Europe increased by more than a factor of 2 compared to observations made at the end of the 20th century (Marengo et al., 1994; Parrish et al., 2012).

Satellite-based tropospheric column ozone retrievals across the tropics and mid-latitudes reveal a greater burden in the NH than in the SH (Ziemke et al., 2011). Tropospheric column ozone trend analyses are few. An analysis by Ziemke et al. (2005) found no trend over the tropical Pacific Ocean but significant positive trends (5 to 9% per decade) in the mid-latitude Pacific of both hemispheres during 1979–2003. Significant positive trends (2 to 9% per decade) were found across broad regions of the tropical South Atlantic, India, southern China, southeast Asia, Indonesia and the tropical regions downwind of China (Beig and Singh, 2007).

Long-term ozone trends at the surface and in the free troposphere (of importance for calculating RF, Chapter 8) can be assessed only from *in situ* measurements at a limited number of sites, leaving large areas such as the tropics and SH sparsely sampled (Table 2.SM.2, Figure 2.7). Nineteen predominantly rural surface sites or regions around the globe have long-term records that stretch back to the 1970s, and in two cases the 1950s (Lelieveld et al., 2004; Parrish et al., 2012; Oltmans et al., 2013). Thirteen of these sites are in the NH, and 11 sites have statistically significant positive trends of 1 to 5 ppb per decade, corresponding to >100% ozone increases since the 1950s and 9 to 55% ozone increases since the 1970s. In the SH, three of six sites have significant trends of approximately 2 ppb per decade and three have insignificant trends. Free tropospheric monitoring since the 1970s is more limited. Significant positive trends since 1971 have been observed using ozone sondes above Western Europe, Japan and coastal Antarctica (rates of increase range from 1 to 3 ppb per decade), but not at all levels (Oltmans et al., 2013). In addition, aircraft have measured

significant upper tropospheric trends in one or more seasons above the north-eastern USA, the North Atlantic Ocean, Europe, the Middle East, northern India, southern China and Japan (Schnadt Poberaj et al., 2009). Insignificant free tropospheric trends were found above the Mid-Atlantic USA (1971–2010) (Oltmans et al., 2013) and in the upper troposphere above the western USA (1975–2001) (Schnadt Poberaj et al., 2009). No site or region showed a significant negative trend.

In recent decades ozone precursor emissions have decreased in Europe and North America and increased in Asia (Granier et al., 2011), impacting ozone production on regional and hemispheric scales (Skeie et al., 2011). Accordingly, 1990–2010 surface ozone trends vary regionally. In Europe ozone generally increased through much of the 1990s but since 2000 ozone has either levelled off or decreased at rural and mountain-top sites, as well as for baseline ozone coming ashore at Mace Head, Ireland (Tarasova et al., 2009; Logan et al., 2012; Parrish et al., 2012; Oltmans et al., 2013). In North America surface ozone has increased in eastern and Arctic Canada, but is unchanged in central and western Canada (Oltmans et al., 2013). Surface ozone has increased in baseline air masses coming ashore along the west coast of the USA (Parrish et al., 2012) and at half of the rural sites in the western USA during spring (Cooper et al., 2012). In the eastern USA surface ozone has decreased strongly in summer, is largely unchanged in spring and has increased in winter (Lefohn et al., 2010; Cooper et al., 2012). East Asian surface ozone is generally increasing (Table 2.SM.2) and at downwind sites ozone is increasing at Mauna Loa, Hawaii but decreasing at Minami Tori Shima in the subtropical western North Pacific (Oltmans et al., 2013). In the SH ozone has increased at the eight available sites, although trends are insignificant at four sites (Helmig et al., 2007; Oltmans et al., 2013).

Owing to methodological changes, free tropospheric ozone observations are most reliable since the mid-1990s. Ozone has decreased above Europe since 1998 (Logan et al., 2012) and is largely unchanged above Japan (Oltmans et al., 2013). Otherwise the remaining regions with measurements (North America, North Pacific Ocean, SH) show a range of positive trends (both significant and insignificant) depending on altitude, with no site having a negative trend at any altitude (Table 2.SM.2).

In summary, there is *medium confidence* from limited measurements in the late 19th through mid-20th century that European surface ozone more than doubled by the end of the 20th century. There is *medium confidence* from more widespread measurements beginning in the 1970s that surface ozone has increased at most (non-urban) sites in the NH (1 to 5 ppb per decade), while there is *low confidence* for ozone increases (2 ppb per decade) in the SH. Since 1990 surface ozone has *likely* increased in East Asia, while surface ozone in the eastern USA and Western Europe has levelled off or is decreasing. Ozone monitoring in the free troposphere since the 1970s is very limited and indicates a weaker rate of increase than at the surface. Satellite instruments can now quantify the present-day tropospheric ozone burden on a near-global basis; significant tropospheric ozone column increases were observed over extended tropical regions of southern Asia, as well as mid-latitude regions of the South and North Pacific Ocean since 1979.

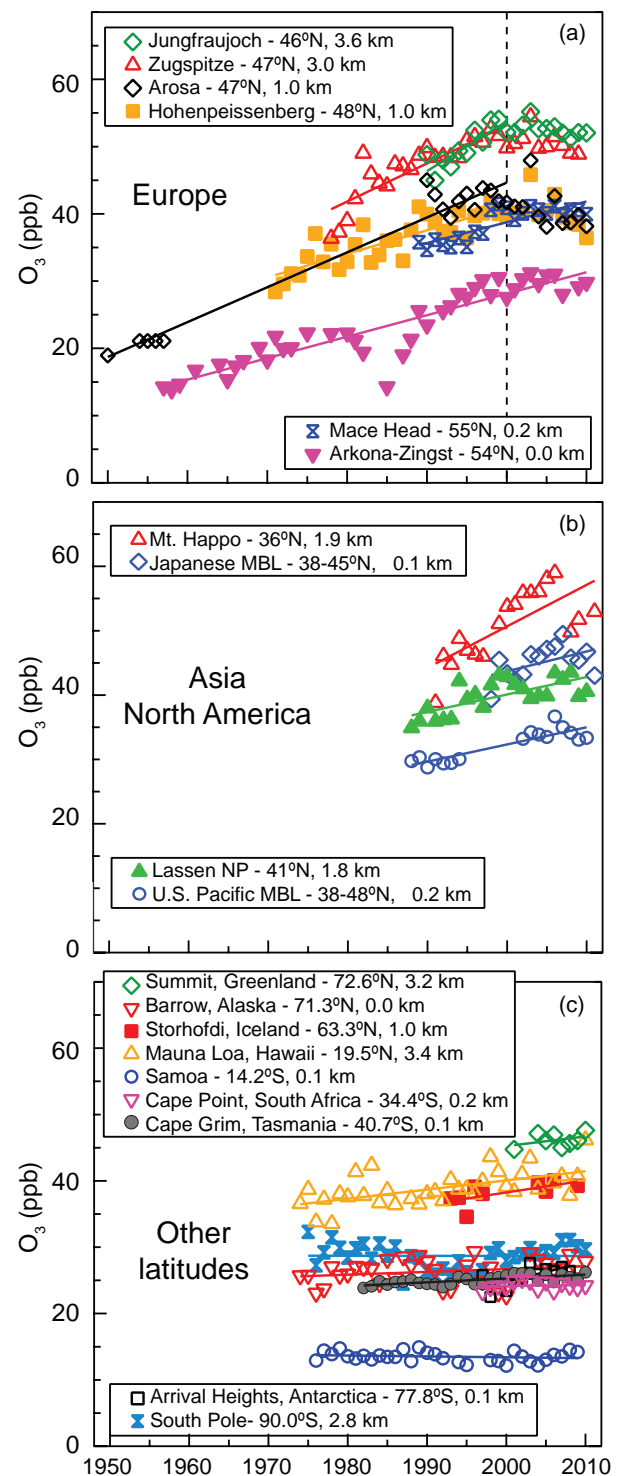


Figure 2.7 | Annual average surface ozone concentrations from regionally representative ozone monitoring sites around the world. (a) Europe. (b) Asia and North America. (c) Remote sites in the Northern and Southern Hemispheres. The station name in the legend is followed by its latitude and elevation. Time series include data from all times of day and trend lines are linear regressions following the method of Parrish et al. (2012). Trend lines are fit through the full time series at each location, except for Jungfrauoch, Zugspitze, Arosa and Hohenpeissenberg where the linear trends end in 2000 (indicated by the dashed vertical line in (a)). Twelve of these 19 sites have significant positive ozone trends (i.e., a trend of zero lies outside the 95% confidence interval); the seven sites with non-significant trends are: Japanese MBL (marine boundary layer), Summit (Greenland), Barrow (Alaska), Storhofdi (Iceland), Samoa (tropical South Pacific Ocean), Cape Point (South Africa) and South Pole (Antarctica).

2.2.2.4 Carbon Monoxide, Non-Methane Volatile Organic Compounds and Nitrogen Dioxide

Emissions of carbon monoxide (CO), non-methane volatile organic compounds (NMVOCs) and NO_x (NO + NO₂) do not have a direct effect on RF, but affect climate indirectly as precursors to tropospheric O₃ and aerosol formation, and their impacts on OH concentrations and CH₄ lifetime. NMVOCs include aliphatic, aromatic and oxygenated hydrocarbons (e.g., aldehydes, alcohols and organic acids), and have atmospheric lifetimes ranging from hours to months. Global coverage of NMVOC measurements is poor, except for a few compounds. Reports on trends generally indicate declines in a range of NMVOCs in urban and rural regions of North America and Europe on the order of a few percent to more than 10% yr⁻¹. Global ethane levels reported by Simpson et al. (2012) declined by about 21% from 1986 to 2010. Measurements of air extracted from firn suggest that NMVOC concentrations were growing until 1980 and declined afterwards (Aydin et al., 2011; Worton et al., 2012). Satellite retrievals of formaldehyde column abundances from 1997 to 2007 show significant positive trends over northeastern China (4% yr⁻¹) and India (1.6% yr⁻¹), possibly related to strong increases in anthropogenic NMVOC emissions, whereas negative trends of about -3% yr⁻¹ are observed over Tokyo, Japan and the northeast USA urban corridor as a result of pollution regulation (De Smedt et al., 2010).

The major sources of atmospheric CO are *in situ* production by oxidation of hydrocarbons (mostly CH₄ and isoprene) and direct emission resulting from incomplete combustion of biomass and fossil fuels. An analysis of MOPITT (Measurements of Pollutants in the Troposphere) and AIRS (Atmospheric Infrared Sounder) satellite data suggest a clear and consistent decline of CO columns for 2002–2010 over a number of polluted regions in Europe, North America and Asia with a global trend of about -1% yr⁻¹ (Yurganov et al., 2010; Fortems-Cheiney et al., 2011; Worden et al., 2013). Analysis of satellite data using two more instruments for recent overlapping years shows qualitatively similar decreasing trends (Worden et al., 2013), but the magnitude of trends remains uncertain owing to the presence of instrument biases. Small CO decreases observed in the NOAA and AGAGE networks are consistent with slight declines in global anthropogenic CO emissions over the same time (Supplementary Material 2.SM.2).

Due to its short atmospheric lifetime (approximately hours), NO_x concentrations are highly variable in time and space. AR4 described the potential of satellite observations of NO₂ to verify and improve NO_x emission inventories and their trends and reported strong NO₂ increases by 50% over the industrial areas of China from 1996 to 2004. An extension of this analysis reveals increases between a factor of 1.7 and 3.2 over parts of China, while over Europe and the USA NO₂ has decreased by 30 to 50% between 1996 and 2010 (Hilboll et al., 2013).

Figure 2.8 shows the changes relative to 1996 in satellite-derived tropospheric NO₂ columns, with a strong upward trend over central eastern China and an overall downward trend in Japan, Europe and the USA. NO₂ reductions in the USA are very pronounced after 2004, related to differences in effectiveness of NO_x emission abatements in the USA and also to changes in atmospheric chemistry of NO_x (Russell et al., 2010). Increasingly, satellite data are used to derive trends in anthropogenic

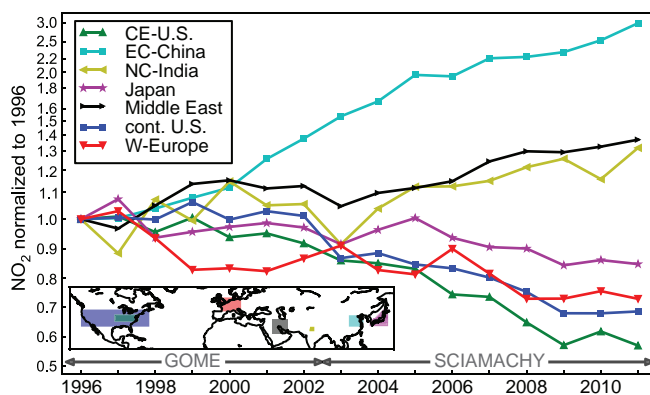


Figure 2.8 | Relative changes in tropospheric NO₂ column amounts (logarithmic scale) in seven selected world regions dominated by high NO_x emissions. Values are normalized for 1996 and derived from the GOME (Global Ozone Monitoring Experiment) instrument from 1996 to 2002 and SCIAMACHY (Scanning Imaging Spectrometer for Atmospheric Cartography) from 2003 to 2011 (Hilboll et al., 2013). The regions are indicated in the map inset.

NO_x emissions, with Castellanos and Boersma (2012) reporting overall increases in global emissions, driven by Asian emission increases of up to 29% yr⁻¹ (1996–2006), while moderate decreases up to 7% yr⁻¹ (1996–2006) are reported for North America and Europe.

In summary, satellite and surface observations of ozone precursor gases NO_x, CO, and non-methane volatile organic carbons indicate strong regional differences in trends. Most notably, NO₂ has *likely* decreased by 30 to 50% in Europe and North America and increased by more than a factor of 2 in Asia since the mid-1990s.

2.2.3 Aerosols

This section assesses trends in aerosol resulting from both anthropogenic and natural sources. The significance of aerosol changes for global dimming and brightening is discussed in Section 2.3. Chapter 7 provides additional discussion of aerosol properties, while Chapter 8 discusses future RF and the ice-core records that contain information on aerosol changes prior to the 1980s. Chapter 11 assesses air quality–climate change interactions. Because of the short lifetime (days to weeks) of tropospheric aerosol, trends have a strong regional signature. Aerosol from anthropogenic sources (i.e., fossil and biofuel burning) are confined mainly to populated regions in the NH, whereas aerosol from natural sources, such as desert dust, sea salt, volcanoes and the biosphere, are important in both hemispheres and likely dependent on climate and land use change (Carslaw et al., 2010). Owing to inter-annual variability, long-term trends in aerosols from natural sources are more difficult to identify (Mahowald et al., 2010).

2.2.3.1 Aerosol Optical Depth from Remote Sensing

AOD is a measure of the integrated columnar aerosols load and is an important parameter for evaluating aerosol–radiation interactions. AR4 described early attempts to retrieve AOD from satellites but did not provide estimates of temporal changes in tropospheric aerosol. Little high-accuracy information on AOD changes exists prior to 1995. Better satellite sensors and ground-based sun-photometer networks,

along with improved retrieval methods and methodological intercomparisons, allow assessment of regional AOD trends since about 1995.

AOD sun photometer measurements at two stations in northern Germany, with limited regional representativity, suggest a long-term decline of AOD in Europe since 1986 (Ruckstuhl et al., 2008). Ground-based, cloud-screened solar broadband radiometer measurements provide longer time-records than spectrally selective sun-photometer data, but are less specific for aerosol retrieval. Multi-decadal records over Japan (Kudo et al., 2011) indicate an AOD increase until the mid-1980s, followed by an AOD decrease until the late 1990s and almost constant AOD in the 2000s. Similar broad-band solar radiative flux multi-decadal trends have been observed for urban–industrial regions of Europe and North America (Wild et al., 2005), and were linked to successful measures to reduce sulphate (precursor) emissions since the mid-1980s (Section 2.3). An indirect method to estimate AOD is offered by ground-based visibility observations. These data are more ambiguous to interpret, but records go further back in time than broadband, sun photometer and satellite data. A multi-regional analysis for 1973–2007 (Wang et al., 2009a) shows that prior to the 1990s visibility-derived AOD was relatively constant in most regions analysed (except for positive trends in southern Asia), but after 1990 positive AOD trends were observed over Asia, and parts of South America, Australia and Africa, and mostly negative AOD trends were found over Europe. In North America, a small stepwise decrease of visibility after 1993 was likely related to methodological changes (Wang et al., 2012f).

AOD can be determined most accurately with sun photometers that measure direct solar intensity in the absence of cloud interferences with an absolute uncertainty of single measurements of $\pm 0.01\%$ (Holben et al., 1998). AERONET (AERosol RObotic NETwork) is a global sun photometer network (Holben et al., 1998), with densest coverage over Europe and North America. AERONET AOD temporal trends were examined in independent studies (de Meij et al., 2012; Hsu et al., 2012; Yoon et al., 2012), using different data selection and statistical methods. Hsu et al. (2012) investigated AOD trends at 12 AERONET sites with data coverage of at least 10 years between 1997 and 2010. Yoon et al. (2012) investigated AOD and size trends at 14 AERONET sites with data coverage varying between 4 and 12 years between 1997 and 2009. DeMeij et al. (2012) investigated AOD trends between 2000 and 2009 (550 nm; monthly data) at 62 AERONET sites mostly located in USA and Europe. Each of these studies noted an increase in AOD over East Asia and reductions in North America and Europe. The only dense sun photometer network over southern Asia, ARFINET (Aerosol Radiative Forcing over India NETwork), shows an increase in AOD of about $2\% \text{ yr}^{-1}$ during the last one to two decades (Krishna Moorthy et al., 2013), with an absolute uncertainty of ± 0.02 at 500 nm (Krishna Moorthy et al., 2007). In contrast, negative AOD trends are identified at more than 80% of examined European and North American AERONET sites (de Meij et al., 2012). Decreasing AOD is also observed near the west coast of northern Africa, where aerosol loads are dominated by Saharan dust outflow. Positive AOD trends are found over the Arabian Peninsula, where aerosol is dominated by dust. Inconsistent AOD trends reported for stations in central Africa result from the use of relatively short time series with respect to the large interannual variability caused by wildfires and dust emissions.

Aerosol products from dedicated satellite sensors complement surface-based AOD with better spatial coverage. The quality of the satellite-derived AOD strongly depends on the retrieval's ability to remove scenes contaminated by clouds and to accurately account for reflectivity at the Earth's surface. Due to relatively weak reflectance of incoming sunlight by the sea surface, the typical accuracy of retrieved AOD over oceans (uncertainty of $0.03 + 0.05 \cdot \text{AOD}$; Kahn et al. (2007)) is usually better than over continents (uncertainty of $0.05 + 0.15 \cdot \text{AOD}$, Levy et al. (2010)).

Satellite-based AOD trends at 550 nm over oceans from conservatively cloud-screened MODIS data (Zhang and Reid, 2010) for 2000–2009 are presented in Figure 2.9. Strongly positive AOD trends were observed over the oceans adjacent to southern and eastern Asia. Positive AOD trends are also observed over most tropical oceans. The negative MODIS AOD trends observed over coastal regions of Europe and near the east coast of the USA are in agreement with sun photometer observations and *in situ* measurements (Section 2.2.3.2) of aerosol mass in these regions. These regional changes over oceans are consistent with analyses of AVHRR (Advanced Very High Resolution Radiometer) trends for 1981–2005 (Mishchenko et al., 2007; Cermak et al., 2010; Zhao et al., 2011), except over the Southern Ocean (45°S to 60°S), where negative AOD trends of AVHRR retrievals are neither confirmed by MODIS after 2001 (Zhang and Reid, 2010) nor by ATSR-2 (Along Track Scanning Radiometer) for 1995–2001 (Thomas et al., 2010).

Satellite-based AOD changes for both land and oceans (Figure 2.9b) were examined with re-processed SeaWiFS (Sea-viewing Wide Field-of-view Sensor) AOD data for 1998–2010 (Hsu et al., 2012). A small positive global average AOD trend is reported, which is likely influenced by interannual natural aerosol emissions variability (e.g., related to ENSO or North Atlantic Oscillation (NAO); Box 2.5), and compensating larger positive and negative regional AOD trends. In addition, temporal changes in aerosol composition are ignored in the retrieval algorithms, giving more uncertain trends than suggested by statistical analysis alone (Mishchenko et al., 2012). Thus, *confidence is low* for global satellite derived AOD trends over these relatively short time periods.

The sign and magnitude of SeaWiFS regional AOD trends over continents are in agreement with most AOD trends by ground-based sun photometer data (see above) and with MODIS trends (Figure 2.9). The strong positive AOD trend over the Arabian Peninsula occurs mainly during spring (MAM) and summer (JJA), during times of dust transport, and is also visible in MODIS data (Figure 2.9). The positive AOD trend over southern and eastern Asia is strongest during the dry seasons (DJF, MAM), when reduced wet deposition allows anthropogenic aerosol to accumulate in the troposphere. AOD over the Saharan outflow region off western Africa displays the strongest seasonal AOD trend differences, with AOD increases only in spring, but strong AOD decreases during the other seasons. SeaWiFS AOD decreases over Europe and the USA and increases over southern and eastern Asia (especially during the dry season) are in agreement with reported temporal trends in anthropogenic emissions, and surface observations (Section 2.2.3.2).

In summary, based on satellite- and surface-based remote sensing it is *very likely* that AOD has decreased over Europe and the eastern

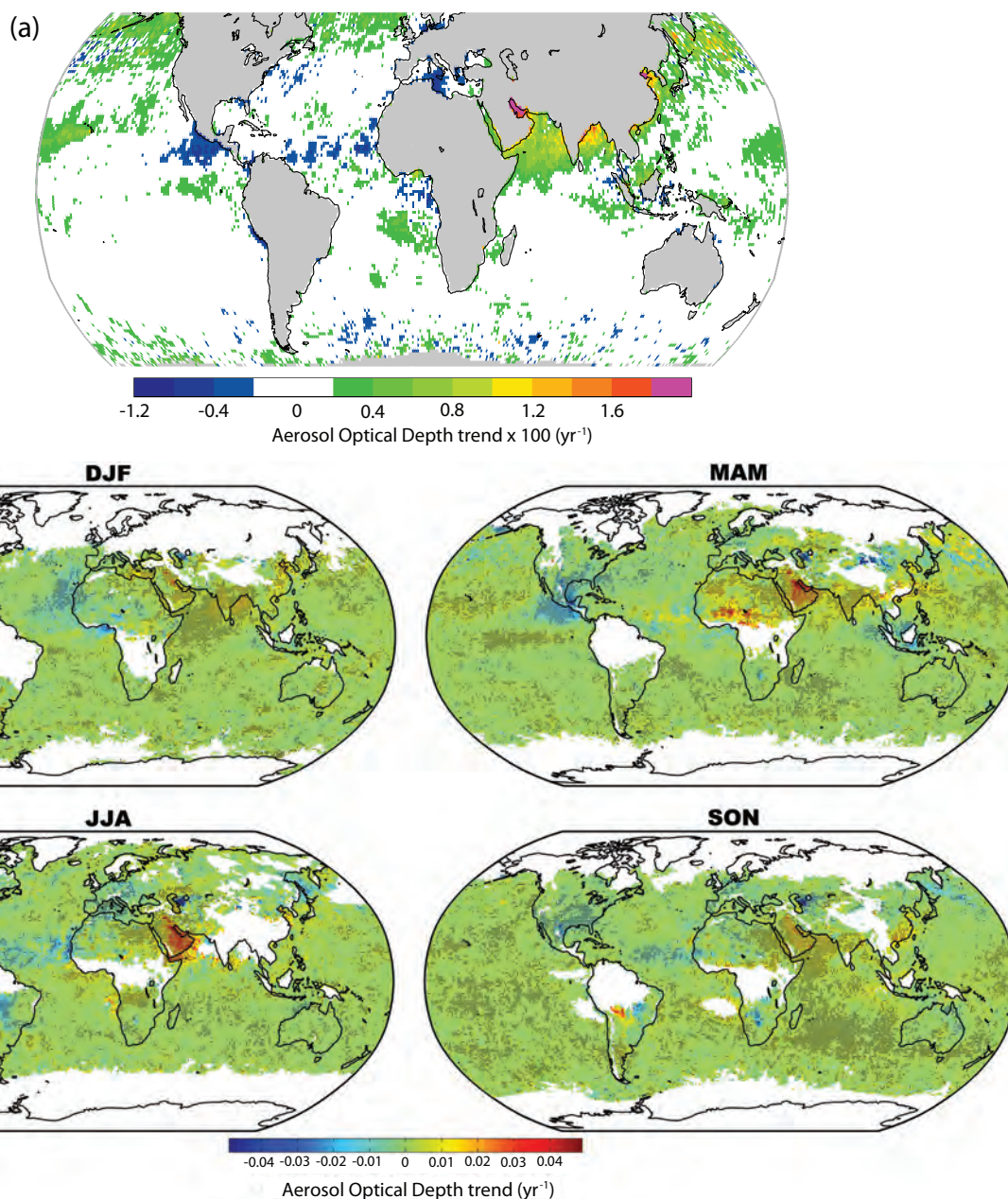


Figure 2.9 | (a) Annual average aerosol optical depth (AOD) trends at 0.55 μm for 2000–2009, based on de-seasonalized, conservatively cloud-screened MODIS aerosol data over oceans (Zhang and Reid, 2010). Negative AOD trends off Mexico are due to enhanced volcanic activity at the beginning of the record. Most non-zero trends are significant (i.e., a trend of zero lies outside the 95% confidence interval). (b) Seasonal average AOD trends at 0.55 μm for 1998–2010 using SeaWiFS data (Hsu et al., 2012). White areas indicate incomplete or missing data. Black dots indicate significant trends (i.e., a trend of zero lies outside the 95% confidence interval).

USA since the mid 1990s and increased over eastern and southern Asia since 2000. In the 2000s dust-related AOD has been increasing over the Arabian Peninsula and decreasing over the North Atlantic Ocean. Aerosol trends over other regions are less strong or not significant during this period owing to relative strong interannual variability. Overall, *confidence* in satellite-based global average AOD trends is *low*.

2.2.3.2 *In Situ* Surface Aerosol Measurements

AR4 did not report trends in long-term surface-based *in situ* measurements of particulate matter, its components or its properties. This section summarizes reported trends of PM_{10} , $\text{PM}_{2.5}$ (particulate matter

with aerodynamic diameters <10 and <2.5 μm , respectively), sulphate and equivalent black carbon/elemental carbon, from regionally representative measurement networks. An overview of current networks and definitions pertinent to aerosol measurements is given in Supplementary Material 2.SM.2.3. Studies reporting trends representative of regional changes are presented in Table 2.2. Long-term data are almost entirely from North America and Europe, whereas a few individual studies on aerosol trends in India and China are reported in Supplementary Material 2.SM.2.3. Figure 2.10 gives an overview of observed PM_{10} , $\text{PM}_{2.5}$, and sulphate trends in North America and Europe for 1990–2009 and 2000–2009.

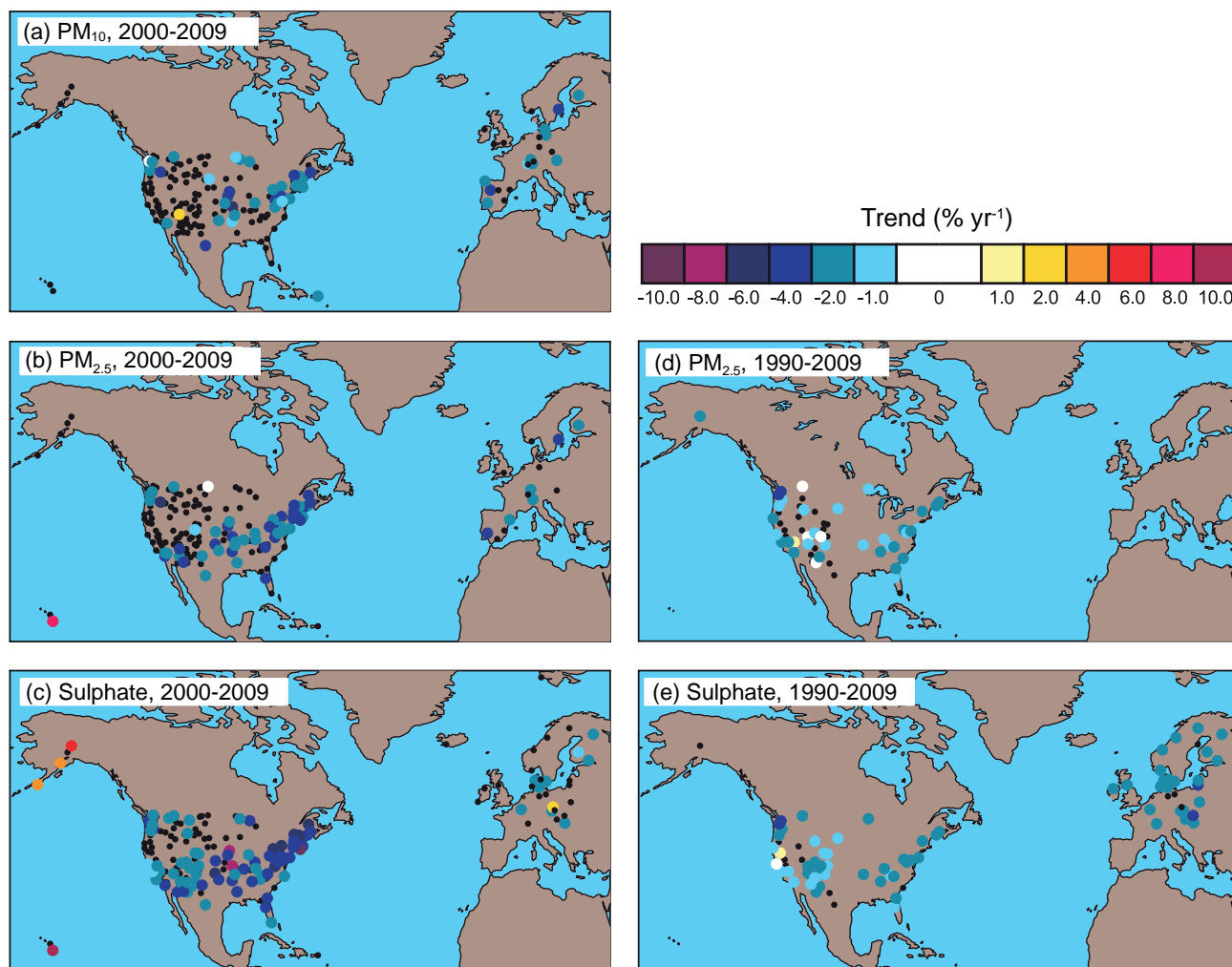


Figure 2.10 | Trends in particulate matter (PM_{10} and $PM_{2.5}$ with aerodynamic diameters <10 and <2.5 μm , respectively) and sulphate in Europe and USA for two overlapping periods 2000–2009 (a, b, c) and 1990–2009 (d, e). The trends are based on measurements from the EMEP (Torseth et al., 2012) and IMPROVE (Hand et al., 2011) networks in Europe and USA, respectively. Sites with significant trends (i.e., a trend of zero lies outside the 95% confidence interval) are shown in colour; black dots indicate sites with non-significant trends.

In Europe, strong downward trends are observed for PM_{10} , $PM_{2.5}$ and sulphate from the rural stations in the EMEP (European Monitoring and Evaluation Programme) network. For 2000–2009, $PM_{2.5}$ shows an average reduction of $3.9\% \text{ yr}^{-1}$ for the six stations with significant trends, while trends are not significant at seven other stations. Over 2000–2009, PM_{10} at 12 (out of 24) sites shows significant downward trend of on average $2.6\% \text{ yr}^{-1}$. Similarly sulphate strongly decreased at $3.1\% \text{ yr}^{-1}$ from 1990 to 2009 with 26 of 30 sites having significant reductions. The largest decrease occurred before 2000, while for 2000–2009, the trends were weaker and less robust. This is consistent with reported emission reductions of 65% from 1990 to 2000 and 28% from 2001 to 2009 (Yttri et al., 2011; Torseth et al., 2012). Model analysis (Pozzoli et al., 2011) attributed the trends in large part to emission changes.

In the USA, the largest reductions in PM and sulphate are observed in the 2000s, rather than the 1990s as in Europe. IMPROVE (U.S. Interagency Monitoring of Protected Visual Environments Network) $PM_{2.5}$ measurements (Hand et al., 2011) show significant downward trends averaging $4.0\% \text{ yr}^{-1}$ for 2000–2009 at sites with significant trends,

and $2.1\% \text{ yr}^{-1}$ at all sites, and PM_{10} decreases of $3.1\% \text{ yr}^{-1}$ for 2000–2009. Declines of $PM_{2.5}$ and SO_4^{2-} in Canada are very similar (Hidy and Pennell, 2010), with annual mean $PM_{2.5}$ at urban measurement sites decreasing by $3.6\% \text{ yr}^{-1}$ during 1985–2006 (Canada, 2012).

In the eastern and southwestern USA, IMPROVE data show strong sulphate declines, which range from 2 to $6\% \text{ yr}^{-1}$, with an average of $2.3\% \text{ yr}^{-1}$ for the sites with significant negative trends for 1990–2009. However, four IMPROVE sites show strong SO_4^{2-} increases from 2000 to 2009, amounting to $11.9\% \text{ yr}^{-1}$, at Hawaii (1225 m above sea level), and 4 to $7\% \text{ yr}^{-1}$ at three sites in southwest Alaska.

A recent study on long-term trends in aerosol optical properties from 24 globally distributed background sites (Collaud Coen et al., 2013) reported statistically significant trends at 16 locations, but the sign and magnitude of the trends varied largely with the aerosol property considered and geographical region (Table 2.3). Among the sites, this study reported strong increases in absorption and scattering coefficients in the free troposphere at Mauna Loa, Hawaii (3400 m above sea level), which is a regional feature also evident in the satellite-based AOD

Table 2.2 | Trend estimates for various aerosol variables reported in the literature, using data sets with at least 10 years of measurements. Unless otherwise noted, trends of individual stations were reported in % yr⁻¹, and 95% confidence intervals. The standard deviation (in parentheses) is determined from the individual trends of a set of regional stations.

Aerosol variable	Trend, % yr ⁻¹ (1σ, standard deviation)	Period	Reference	Comments
Europe				
PM _{2.5}	-2.9 (1.31) -3.9 (0.87) ^b	2000–2009	(Adapted from Torseth et al., 2012) Regional background sites	13 sites available, 6 sites show statistically significant results. Average change was -0.37 and -0.52 ^b mg m ⁻³ yr ⁻¹ .
PM ₁₀	-1.9 (1.43) -2.6 (1.19) ^b	2000–2009		24 sites available, 12 sites show statistically significant results. Average change was -0.29 and -0.40 ^b mg m ⁻³ yr ⁻¹ .
SO ₄ ²⁻	-3.0 (0.82) -3.1 (0.72) ^b	1990–2009		30 sites available, 26 sites show statistically significant results. Average change was -0.04 and -0.04 ^b mg m ⁻³ yr ⁻¹ .
SO ₄ ²⁻	-1.5 (1.41) -2.0 (1.8) ^b	2000–2009		30 sites available, 10 sites show statistically significant results. Average change was -0.01 and -0.01 ^b mg m ⁻³ yr ⁻¹ .
PM ₁₀	-1.9	1991–2008	(Barnpadimos et al., 2012) Rural and urban sites	10 sites in Switzerland. The trend is adjusted for change in meteorology—unadjusted data did not differ strongly. The average change was -0.51 mg m ⁻³ yr ⁻¹ .
USA				
PM _{2.5}	-2.1 (2.08) -4.0 (1.01) ^b	2000–2009	Adapted from (Hand et al., 2011) Regional background sites	153 sites available, 52 sites show statistically significant negative results. Only 1 site shows statistically positive trend.
PM _{2.5}	-1.5 (1.25) -2.1 (0.97) ^b	1990–2009		153 sites available, 39 sites show statistically significant results.
PM ₁₀	-1.7 (2.00) -3.1 (1.65) ^b	2000–2009		154 sites available, 37 sites show statistically significant results.
SO ₄ ²⁻	-3.0 (2.86) -3.0 (0.62) ^b	2000–2009		154 sites available, 83 sites show statistically significant negative results. 4 sites showed statistical positive trend.
SO ₄ ²⁻	-2.0 (1.07) -2.3 (0.85) ^b	1990–2009		103 sites available, 41 sites show statistically significant results.
Total Carbon	-2.5 to -7.5	1989–2008	(Hand et al., 2011) Regional background sites	The trend interval includes about 50 sites mainly located along the East and West Coasts of the USA; fewer sites were situated in the central part of the continent.
Arctic				
EBC ^a	-3.8 (0.7) ^c	1989–2008	(Hirdman et al., 2010)	Alert, Canada 62.3°W 82.5°N
SO ₄ ²⁻	-3.0 (0.6) ^c	1985–2006		
EBC ^a	Not sig. ^c	1998–2008		Barrow, Alaska, 156.6°W 71.3° N
SO ₄ ²⁻	Not sig. ^c	1997–2008		
EBC ^a	-9.0 (5.0) ^c	2002–2009		Zeppelin, Svalbard, 11.9°E 78.9° N
SO ₄ ²⁻	-1.9 (1.7) ^c	1990–2008		

Notes:

^a Equivalent black carbon.

^b Trend numbers indicated refer to the subset of stations with significant changes over time—generally in regions strongly influenced by anthropogenic emissions (Figure 2.10).

^c Trend values significant at 1% level.

trends (illustrated in Figure 2.9). Possible explanations for these changes include the influence of increasing Asian emissions and changes in clouds and removal processes. More and longer Asian time series, coupled with transport analyses, are needed to corroborate these findings. Aerosol number concentrations (Asmi et al., 2013) are declining significantly at most sites in Europe, North America, the Pacific and the Caribbean, but increasing at South Pole based on a study of 17 globally distributed remote sites.

Total carbon (= light absorbing carbon + organic carbon) measurements indicate highly significant downward trends between 2.5 and 7.5% yr⁻¹ along the east and west coasts of the USA, and smaller and less significant trends in other regions of the USA from 1989 to 2008 (Hand et al., 2011; Murphy et al., 2011).

In Europe, Torseth et al. (2012) suggest a slight reduction in elemental carbon concentrations at two stations from 2001 to 2009, subject to

large interannual variability. Collaud Coen et al. (2013) reported consistent negative trends in the aerosol absorption coefficient at stations in the continental USA, Arctic and Antarctica, but mostly insignificant trends in Europe over the last decade.

In the Arctic, changes in aerosol impact the atmosphere's radiative balance as well as snow and ice albedo. Similar to Europe and the USA, Hirdman et al. (2010) reported downward trends in equivalent black carbon and SO₄²⁻ for two out of total three Arctic stations and attributed them to emission changes.

In summary, declining AOD in Europe and North America is corroborated by *very likely* downward trends in ground-based *in situ* particulate matter measurements since the mid-1980s. Robust evidence from around 200 regional background sites with *in situ* ground based aerosol measurements indicate downward trends in the last two decades of PM_{2.5} in parts of Europe (2 to 6% yr⁻¹) and the USA (1 to 2.5% yr⁻¹),

Table 2.3 | Summary table of aerosol optical property trends reported in the literature, using data sets with at least 10 years of measurements. Otherwise as in Table 2.2.

Region	Trend, % yr ⁻¹ (1σ, standard deviation)	Period	Reference	Comments
Scattering coefficient				
Europe (4/1)	+0.6 (1.9) +2.7 ^a	2001–2010	Adapted from (Collaud Coen et al., 2013) Regional background sites	Trend study including 24 regional background sites with more than 10 years of observations. Regional averages for last 10 years are included here. Values in parenthesis show total number of sites/number of sites with significant trend.
USA (14/10)	–2.0 (2.5) –2.9 (2.4) ^a			
Mauna Loa (1/1)	+2.7			
Arctic (1/0)	+2.4			
Antarctica (1/0)	+2.5			
Absorption coefficient				
Europe (3/0)	+0.3 (0.4)	2001–2010	Adapted from (Collaud Coen et al., 2013) Regional background sites	Trend study of aerosol optical properties including 24 regional background sites with more than 10 years of observations. Regional averages for last 10 years are included here. Values in parenthesis show total number of sites and number of sites with significant trend.
USA (1/1)	–2.0			
Mauna Loa (1/1)	+9.0			
Arctic (1/1)	–6.5			
Antarctica (1/1)	–0.1			
Particle number concentration				
Europe (4/2)	–0.9 (1.8) –2.3 (1.0) ^a	2001–2010	Adapted from (Asmi et al., 2013) Regional background sites	Trend study of particle number concentration (N) and size distribution including 17 regional background sites. Regional averages of particle number concentration for last 10 years are included here. Values in parentheses show total number of sites and number of sites with significant trend.
North America and Caribbean (3/3)	–5.3 (2.8) –6.6 (1.1) ^a			
Mauna Loa (1/1)	–3.5			
Arctic (1/0)	–1.3			
Antarctica (2/2)	+2.7 (1.4)			

Notes:

^a Trend numbers indicated refer to the subset of stations with significant changes over time—generally in regions strongly influenced by anthropogenic emissions (Figure 2.10).

Box 2.2 | Quantifying Changes in the Mean: Trend Models and Estimation

Many statistical methods exist for estimating trends in environmental time series (see Chandler and Scott, 2011 for a review). The assessment of long-term changes in historical climate data requires trend models that are transparent and robust, and that can provide credible uncertainty estimates.

Linear Trends

Historical climate trends are frequently described and quantified by estimating the linear component of the change over time (e.g., AR4). Such linear trend modelling has broad acceptance and understanding based on its frequent and widespread use in the published research assessed in this report, and its strengths and weaknesses are well known (von Storch and Zwiers, 1999; Wilks, 2006). Challenges exist in assessing the uncertainty in the trend and its dependence on the assumptions about the sampling distribution (Gaussian or otherwise), uncertainty in the data, dependency models for the residuals about the trend line, and treating their serial correlation (Von Storch, 1999; Santer et al., 2008).

The quantification and visualization of temporal changes are assessed in this chapter using a linear trend model that allows for first-order autocorrelation in the residuals (Santer et al., 2008; Supplementary Material 2.SM.3). Trend slopes in such a model are the same as ordinary least squares trends; uncertainties are computed using an approximate method. The 90% confidence interval quoted is solely that arising from sampling uncertainty in estimating the trend. Structural uncertainties, to the extent sampled, are apparent from the range of estimates from different data sets. Parametric and other remaining uncertainties (Box 2.1), for which estimates are provided with some data sets, are not included in the trend estimates shown here, so that the same method can be applied to all data sets considered.

Nonlinear Trends

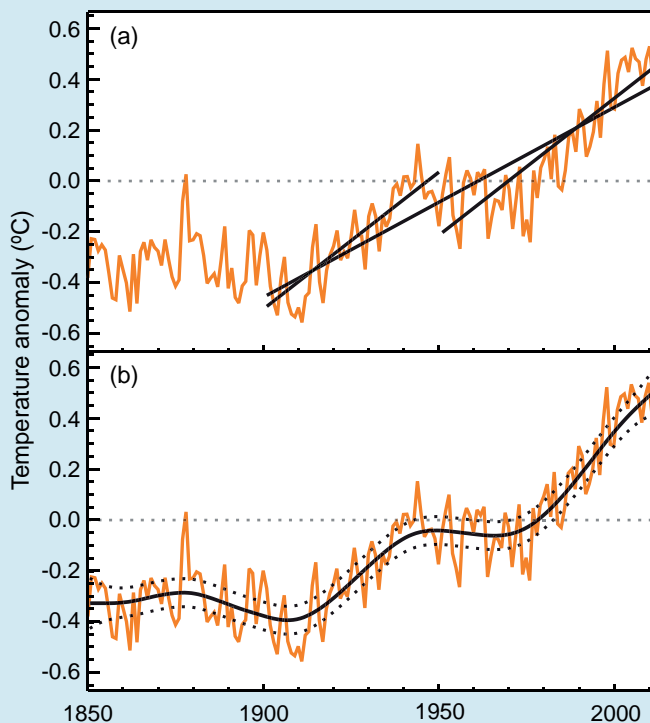
There is no *a priori* physical reason why the long-term trend in climate variables should be linear in time. Climatic time series often have trends for which a straight line is not a good approximation (e.g., Seidel and Lanzante, 2004). The residuals from a linear fit in time often do not follow a simple autoregressive or moving average process, and linear trend estimates can easily change when recalculated (continued on next page)

Box 2.2 (continued)

for shorter or longer time periods or when new data are added. When linear trends for two parts of a longer time series are calculated separately, the trends calculated for two shorter periods may be very different (even in sign) from the trend in the full period, if the time series exhibits significant nonlinear behavior in time (Box 2.2, Table 1).

Many methods have been developed for estimating the long-term change in a time series without assuming that the change is linear in time (e.g., Wu et al., 2007; Craigmile and Guttorp, 2011). Box 2.2, Figure 1 shows the linear least squares and a nonlinear trend fit to the GMST values from the HadCRUT4 data set (Section 2.4.3). The nonlinear trend is obtained by fitting a smoothing spline trend (Wood, 2006; Scinocca et al., 2010) while allowing for first-order autocorrelation in the residuals (Supplementary Material 2.SM.3). The results indicate that there are significant departures from linearity in the trend estimated this way.

Box 2.2, Table 1 shows estimates of the change in the GMST from the two methods. The methods give similar estimates with 90% confidence intervals that overlap one another. Smoothing methods that do not assume the trend is linear can provide useful information on the structure of change that is not as well treated with linear fits. The linear trend fit is used in this chapter because it can be applied consistently to all the data sets, is relatively simple, transparent and easily comprehended, and is frequently used in the published research assessed here.



Box 2.2, Figure 1 | (a) Global mean surface temperature (GMST) anomalies relative to a 1961–1990 climatology based on HadCRUT4 annual data. The straight black lines are least squares trends for 1901–2012, 1901–1950 and 1951–2012. (b) Same data as in (a), with smoothing spline (solid curve) and the 90% confidence interval on the smooth curve (dashed lines). Note that the (strongly overlapping) 90% confidence intervals for the least square lines in (a) are omitted for clarity. See Figure 2.20 for the other two GMST data products.

Box 2.2, Table 1 | Estimates of the mean change in global mean surface temperature (GMST) between 1901 and 2012, 1901 and 1950, and 1951 and 2012, obtained from the linear (least squares) and nonlinear (smoothing spline) trend models. Half-widths of the 90% confidence intervals are also provided for the estimated changes from the two trend methods.

Method	Trends in °C per decade		
	1901–2012	1901–1950	1951–2012
Least squares	0.075 ± 0.013	0.107 ± 0.026	0.106 ± 0.027
Smoothing spline	0.081 ± 0.010	0.070 ± 0.016	0.090 ± 0.018

and also for SO_4^{2-} (2 to 5% yr^{-1}). The strongest decreases were in the 1990s in Europe and in the 2000s in the USA. There is robust evidence for downward trends of light absorbing aerosol in the USA and the Arctic, while elsewhere in the world *in situ* time series are lacking or not long enough to reach statistical significance.

2.3 Changes in Radiation Budgets

The radiation budget of the Earth is a central element of the climate system. On average, radiative processes warm the surface and cool the atmosphere, which is balanced by the hydrological cycle and sensible

heating. Spatial and temporal energy imbalances due to radiation and latent heating produce the general circulation of the atmosphere and oceans. Anthropogenic influence on climate occurs primarily through perturbations of the components of the Earth radiation budget.

The radiation budget at the top of the atmosphere (TOA) includes the absorption of solar radiation by the Earth, determined as the difference between the incident and reflected solar radiation at the TOA, as well as the thermal outgoing radiation emitted to space. The surface radiation budget takes into account the solar fluxes absorbed at the Earth's surface, as well as the upward and downward thermal radiative fluxes emitted by the surface and atmosphere, respectively. In view of new

observational evidence since AR4, the mean state as well as multi-decadal changes of the surface and TOA radiation budgets are assessed in the following.

2.3.1 Global Mean Radiation Budget

Since AR4, knowledge on the magnitude of the radiative energy fluxes in the climate system has improved, requiring an update of the global annual mean energy balance diagram (Figure 2.11). Energy exchanges between Sun, Earth and Space are observed from space-borne platforms such as the Clouds and the Earth's Radiant Energy System (CERES, Wielicki et al., 1996) and the Solar Radiation and Climate Experiment (SORCE, Kopp and Lawrence, 2005) which began data collection in 2000 and 2003, respectively. The total solar irradiance (TSI) incident at the TOA is now much better known, with the SORCE Total Irradiance Monitor (TIM) instrument reporting uncertainties as low as 0.035%, compared to 0.1% for other TSI instruments (Kopp et al., 2005). During the 2008 solar minimum, SORCE/TIM observed a solar irradiance of $1360.8 \pm 0.5 \text{ W m}^{-2}$ compared to $1365.5 \pm 1.3 \text{ W m}^{-2}$ for instruments launched prior to SORCE and still operating in 2008 (Section 8.4.1.1). Kopp and Lean (2011) conclude that the SORCE/TIM value of TSI is the most credible value because it is validated by a National Institute of Standards and Technology calibrated cryogenic radiometer. This revised TSI estimate corresponds to a solar irradiance close to 340 W m^{-2} globally averaged over the Earth's sphere (Figure 2.11).

The estimate for the reflected solar radiation at the TOA in Figure 2.11, 100 W m^{-2} , is a rounded value based on the CERES Energy Balanced and Filled (EBAF) satellite data product (Loeb et al., 2009, 2012b) for the period 2001–2010. This data set adjusts the solar and thermal TOA fluxes within their range of uncertainty to be consistent with independent estimates of the global heating rate based on *in situ* ocean observations (Loeb et al., 2012b). This leaves 240 W m^{-2} of solar radiation absorbed by the Earth, which is nearly balanced by thermal emission to space of about 239 W m^{-2} (based on CERES EBAF), considering a global heat storage of 0.6 W m^{-2} (imbalance term in Figure 2.11) based on Argo data from 2005 to 2010 (Hansen et al., 2011; Loeb et al., 2012b; Box 3.1). The stated uncertainty in the solar reflected TOA fluxes from CERES due to uncertainty in absolute calibration alone is about 2% (2-sigma), or equivalently 2 W m^{-2} (Loeb et al., 2009). The uncertainty of the outgoing thermal flux at the TOA as measured by CERES due to calibration is $\sim 3.7 \text{ W m}^{-2}$ (2σ). In addition to this, there is uncertainty in removing the influence of instrument spectral response on measured radiance, in radiance-to-flux conversion, and in time-space averaging, which adds up to another 1 W m^{-2} (Loeb et al., 2009).

The components of the radiation budget at the surface are generally more uncertain than their counterparts at the TOA because they cannot be directly measured by passive satellite sensors and surface measurements are not always regionally or globally representative. Since AR4, new estimates for the downward thermal infrared (IR) radiation at

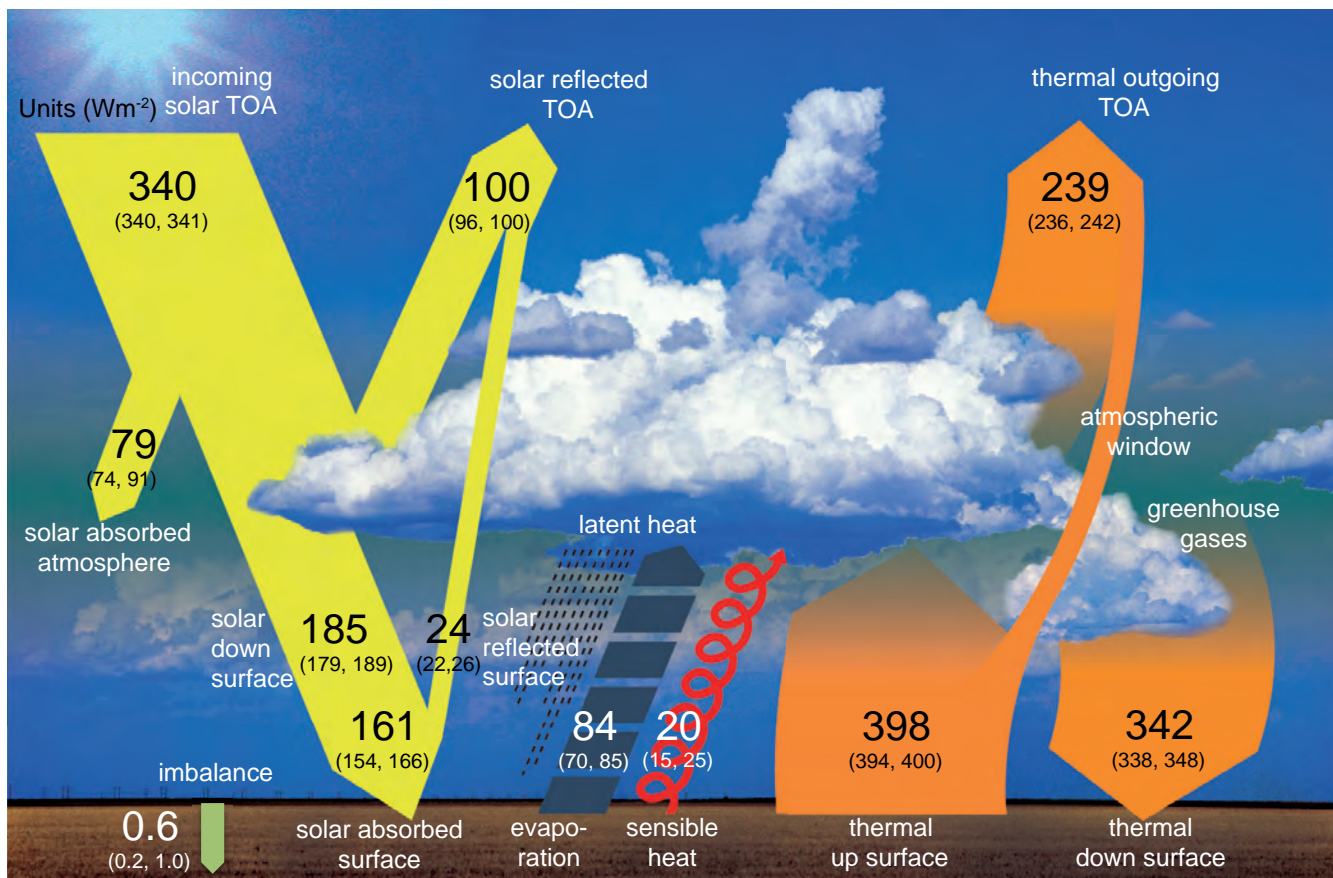


Figure 2.11: | Global mean energy budget under present-day climate conditions. Numbers state magnitudes of the individual energy fluxes in W m^{-2} , adjusted within their uncertainty ranges to close the energy budgets. Numbers in parentheses attached to the energy fluxes cover the range of values in line with observational constraints. (Adapted from Wild et al., 2013.)

the surface have been established that incorporate critical information on cloud base heights from space-borne radar and lidar instruments (L'Ecuyer et al., 2008; Stephens et al., 2012a; Kato et al., 2013). In line with studies based on direct surface radiation measurements (Wild et al., 1998, 2013) these studies propose higher values of global mean downward thermal radiation than presented in previous IPCC assessments and typically found in climate models, exceeding 340 W m^{-2} (Figure 2.11). This aligns with the downward thermal radiation in the ERA-Interim and ERA-40 reanalyses (Box 2.3), of 341 and 344 W m^{-2} , respectively (Berrisford et al., 2011). Estimates of global mean downward thermal radiation computed as a residual of the other terms of the surface energy budget (Kiehl and Trenberth, 1997; Trenberth et al., 2009) are lower (324 to 333 W m^{-2}), highlighting remaining uncertainties in estimates of both radiative and non-radiative components of the surface energy budget.

Estimates of absorbed solar radiation at the Earth's surface include considerable uncertainty. Published global mean values inferred from satellite retrievals, reanalyses and climate models range from below 160 W m^{-2} to above 170 W m^{-2} . Recent studies taking into account surface observations as well as updated spectroscopic parameters and continuum absorption for water vapor favour values towards the lower bound of this range, near 160 W m^{-2} , and an atmospheric solar absorption around 80 W m^{-2} (Figure 2.11) (Kim and Ramanathan, 2008; Trenberth et al., 2009; Kim and Ramanathan, 2012; Trenberth and Fasullo, 2012b; Wild et al., 2013). The ERA-Interim and ERA-40 reanalyses further support an atmospheric solar absorption of this magnitude (Berrisford et al., 2011). Latest satellite-derived estimates constrained by CERES now also come close to these values (Kato et al., in press). Recent independently derived surface radiation estimates favour therefore a global mean surface absorbed solar flux near 160 W m^{-2} and a downward thermal flux slightly above 340 W m^{-2} , respectively (Figure 2.11).

The global mean latent heat flux is required to exceed 80 W m^{-2} to close the surface energy balance in Figure 2.11, and comes close to the 85 W m^{-2} considered as upper limit by Trenberth and Fasullo (2012b) in view of current uncertainties in precipitation retrieval in the Global Precipitation Climatology Project (GPCP, Adler et al., 2012) (the latent heat flux corresponds to the energy equivalent of evaporation, which globally equals precipitation; thus its magnitude may be constrained by global precipitation estimates). This upper limit has recently been challenged by Stephens et al. (2012b). The emerging debate reflects potential remaining deficiencies in the quantification of the radiative and non-radiative energy balance components and associated uncertainty ranges, as well as in the consistent representation of the global mean energy and water budgets (Stephens et al., 2012b; Trenberth and Fasullo, 2012b; Wild et al., 2013). Relative uncertainty in the globally averaged sensible heat flux estimate remains high owing to the very limited direct observational constraints (Trenberth et al., 2009; Stephens et al., 2012b).

In summary, newly available observations from both space-borne and surface-based platforms allow a better quantification of the Global Energy Budget, even though notable uncertainties remain, particularly in the estimation of the non-radiative surface energy balance components.

2.3.2 Changes in Top of the Atmosphere Radiation Budget

While the previous section emphasized the temporally-averaged state of the radiation budget, the focus in the following is on the temporal (multi-decadal) changes of its components. Variations in TSI are discussed in Section 8.4.1. AR4 reported large changes in tropical TOA radiation between the 1980s and 1990s based on observations from the Earth Radiation Budget Satellite (ERBS) (Wielicki et al., 2002; Wong et al., 2006). Although the robust nature of the large decadal changes in tropical radiation remains to be established, several studies have suggested links to changes in atmospheric circulation (Allan and Slingo, 2002; Chen et al., 2002; Clement and Soden, 2005; Merrifield, 2011) (Section 2.7).

Since AR4, CERES enabled the extension of satellite records of TOA fluxes into the 2000s (Loeb et al., 2012b). The extended records from CERES suggest no noticeable trends in either the tropical or global radiation budget during the first decade of the 21st century (e.g., Andronova et al., 2009; Harries and Belotti, 2010; Loeb et al., 2012a, 2012b). Comparisons between ERBS/CERES thermal radiation and that derived from the NOAA High Resolution Infrared Radiation Sounder (HIRS) (Lee et al., 2007) show good agreement until approximately 1998, corroborating the rise of 0.7 W m^{-2} between the 1980s and 1990s reported in AR4. Thereafter the HIRS thermal fluxes show much higher values, likely due to changes in the channels used for HIRS/3 instruments launched after October 1998 compared to earlier HIRS instruments (Lee et al., 2007).

On a global scale, interannual variations in net TOA radiation and ocean heating rate (OHR) should correspond, as oceans have a much larger effective heat capacity than land and atmosphere, and therefore serve as the main reservoir for heat added to the Earth-atmosphere system (Box 3.1). Wong et al. (2006) showed that interannual variations in these two data sources are in good agreement for 1992–2003. In the ensuing 5 years, however, Trenberth and Fasullo (2010) note that the two diverge with ocean *in situ* measurements (Levitus et al., 2009), indicating a decline in OHR, in contrast to expectations from the observed net TOA radiation. The divergence after 2004 is referred to as “missing energy” by Trenberth and Fasullo (2012b), who further argue that the main sink of the missing energy likely occurs at ocean depths below 275 m. Loeb et al. (2012b) compared interannual variations in CERES net radiation with OHRs derived from three independent ocean heat content anomaly analyses and included an error analysis of both CERES and the OHRs. They conclude that the apparent decline in OHR is not statistically robust and that differences between interannual variations in OHR and satellite net TOA flux are within the uncertainty of the measurements (Figure 2.12). They further note that between January 2001 and December 2012, the Earth has been steadily accumulating energy at a rate of $0.50 \pm 0.43 \text{ W m}^{-2}$ (90% CI). Hansen et al. (2011) obtained a similar value for 2005–2010 using an independent analysis of the ocean heat content anomaly data (von Schuckmann and Le Traon, 2011). The variability in the Earth's energy imbalance is strongly influenced by ocean circulation changes relating to the ENSO (Box 2.5); during cooler La Niña years (e.g., 2009) less thermal radiation is emitted and the climate system gains heat while the reverse is true for warmer El Niño years (e.g., 2010) (Figure 2.12).

In summary, satellite records of TOA radiation fluxes have been substantially extended since AR4. It is *unlikely* that significant trends exist in global and tropical radiation budgets since 2000. Interannual variability in the Earth's energy imbalance related to ENSO is consistent with ocean heat content records within observational uncertainty.

2.3.3 Changes in Surface Radiation Budget

2.3.3.1 Surface Solar Radiation

Changes in radiative fluxes at the surface can be traced further back in time than the satellite-based TOA fluxes, although only at selected terrestrial locations where long-term records exist. Monitoring of radiative fluxes from land-based stations began on a widespread basis in the mid-20th century, predominantly measuring the downward solar component, also known as global radiation or surface solar radiation (SSR).

AR4 reported on the first indications for substantial decadal changes in observational records of SSR. Specifically, a decline of SSR from the beginning of widespread measurements in the 1950s until the mid-1980s has been observed at many land-based sites (popularly known as 'global dimming'; Stanhill and Cohen, 2001; Liepert, 2002), as well as a partial recovery from the 1980s onward ('brightening'; Wild et al., 2005) (see the longest available SSR series of Stockholm, Sweden, in Figure 2.13 as an illustrative example).

Since AR4, numerous studies have substantiated the findings of significant decadal SSR changes observed both at worldwide distributed terrestrial sites (Dutton et al., 2006; Wild et al., 2008; Gilgen et al., 2009; Ohmura, 2009; Wild, 2009 and references therein) as well as in specific regions. In Europe, Norris and Wild (2007) noted a dimming between 1971 and 1986 of 2.0 to 3.1 $W m^{-2}$ per decade and subsequent brightening of 1.1 to 1.4 $W m^{-2}$ per decade from 1987 to 2002 in a pan-European time series comprising 75 sites. Similar tendencies were found at sites in northern Europe (Stjern et al., 2009), Estonia (Russak, 2009) and Moscow (Abakumova et al., 2008). Chiacchio and Wild (2010) pointed out that dimming and subsequent brightening in Europe is seen mainly in spring and summer. Brightening in Europe from the 1980s onward was further documented at sites in Switzerland, Germany, France, the Benelux, Greece, Eastern Europe and the Iberian Peninsula (Ruckstuhl et al., 2008; Wild et al., 2009; Zerefos et al., 2009; Sanchez-Lorenzo et al., 2013). Concurrent brightening of 2 to 8 $W m^{-2}$ per decade was also noted at continental sites in the USA (Long et al., 2009; Riihimaki et al., 2009; Augustine and Dutton, 2013). The general pattern of dimming and consecutive brightening was further found at numerous sites in Japan (Norris and Wild, 2009; Ohmura, 2009; Kudo et al., 2011) and in the SH in New Zealand (Liley, 2009). Analyses of observations from sites in China confirmed strong declines in SSR from the 1960s to 1980s on the order of 2 to 8 $W m^{-2}$ per decade, which also did not persist in the 1990s (Che et al., 2005; Liang and Xia, 2005; Qian et al., 2006; Shi et al., 2008; Norris and Wild, 2009; Xia, 2010a). On the other hand, persistent dimming since the mid-20th

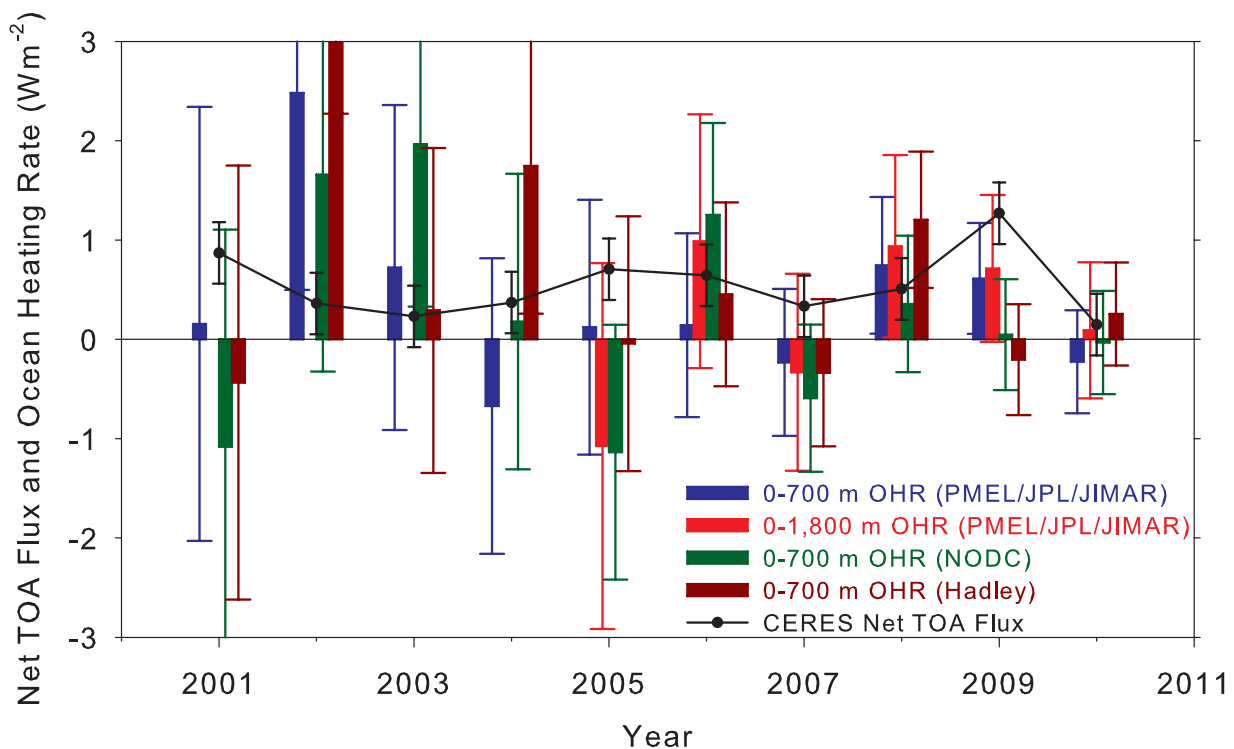


Figure 2.12 | Comparison of net top of the atmosphere (TOA) flux and upper ocean heating rates (OHRs). Global annual average (July to June) net TOA flux from CERES observations (based on the EBAF-TOA_Ed2.6r product) (black line) and 0–700 (blue) and 0–1800 m (red) OHR from the Pacific Marine Environmental Laboratory/Jet Propulsion Laboratory/Joint Institute for Marine and Atmospheric Research (PMEL/JPL/JIMAR), 0–700 m OHR from the National Oceanic Data Center (NODC) (green; Levitus et al., 2009), and 0–700 m OHR from the Hadley Center (brown; Palmer et al., 2007). The length of the coloured bars corresponds to the magnitude of OHR. Thin vertical lines are error bars, corresponding to the magnitude of uncertainties. Uncertainties for all annual OHR are given at one standard error derived from ocean heat content anomaly uncertainties (Lyman et al., 2010). CERES net TOA flux uncertainties are given at the 90% confidence level determined following Loeb et al. (2012b). (Adapted from Loeb et al., 2012b.)

century with no evidence for a trend reversal was noted at sites in India (Wild et al., 2005; Kumari et al., 2007; Kumari and Goswami, 2010; Soni et al., 2012) and in the Canadian Prairie (Cutforth and Judiesch, 2007). Updates on latest SSR changes observed since 2000 provide a less coherent picture (Wild, 2012). They suggest a continuation of brightening at sites in Europe, USA, and parts of Asia, a levelling off at sites in Japan and Antarctica, and indications for a renewed dimming in parts of China (Wild et al., 2009; Xia, 2010a).

The longest observational SSR records, extending back to the 1920s and 1930s at a few sites in Europe, further indicate some brightening during the first half of the 20th century, known as 'early brightening' (cf. Figure 2.13) (Ohmura, 2009; Wild, 2009). This suggests that the decline in SSR, at least in Europe, was confined to a period between the 1950s and 1980s.

A number of issues remain, such as the quality and representativeness of some of the SSR data as well as the large-scale significance of the phenomenon (Wild, 2012). The historic radiation records are of variable quality and rigorous quality control is necessary to avoid spurious trends (Dutton et al., 2006; Shi et al., 2008; Gilgen et al., 2009; Tang et al., 2011; Wang et al., 2012e; Sanchez-Lorenzo et al., 2013). Since the mid-1990s, high-quality data are becoming increasingly available from new sites of the Baseline Surface Radiation Network (BSRN) and Atmospheric Radiation Measurement (ARM) Program, which allow the determination of SSR variations with unprecedented accuracy (Ohmura et al., 1998). Alpert et al. (2005) and Alpert and Kishcha (2008) argued that the observed SSR decline between 1960 and 1990 was larger in densely populated than in rural areas. The magnitude of this 'urbanization effect' in the radiation data is not yet well quantified. Dimming and brightening is, however, also notable at remote and rural sites (Dutton et al., 2006; Karnieli et al., 2009; Liley, 2009; Russak, 2009; Wild, 2009; Wang et al., 2012d).

Globally complete satellite estimates have been available since the early 1980s (Hatzianastassiou et al., 2005; Pinker et al., 2005; Hinkelman et al., 2009). Because satellites do not directly measure the surface fluxes, they have to be inferred from measurable TOA signals using empirical or physical models to remove atmospheric perturbations. Available satellite-derived products qualitatively agree on a brightening from the mid-1980s to 2000 averaged globally as well as over oceans, on the order of 2 to 3 W m⁻² per decade (Hatzianastassiou et al., 2005; Pinker et al., 2005; Hinkelman et al., 2009). Averaged over land, however, trends are positive or negative depending on the respective satellite product (Wild, 2009). Knowledge of the decadal variation of aerosol burdens and optical properties, required in satellite retrievals of SSR and considered relevant for dimming/brightening particularly over land, is very limited (Section 2.2.3). Extensions of satellite-derived SSR beyond 2000 indicate tendencies towards a renewed dimming at the beginning of the new millennium (Hinkelman et al., 2009; Hatzianastassiou et al., 2012).

Reconstructions of SSR changes from more widely measured meteorological variables can help to increase their spatial and temporal coverage. Multi-decadal SSR changes have been related to observed changes in sunshine duration, atmospheric visibility, diurnal temperature range (DTR; Section 2.4.1.2) and pan evaporation (Section 2.5.3).

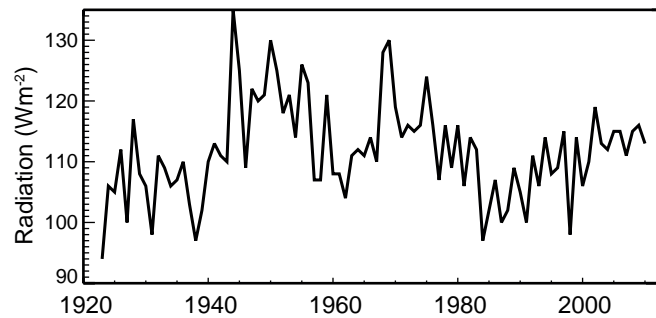


Figure 2.13 | Annual mean Surface Solar Radiation (SSR) as observed at Stockholm, Sweden, from 1923 to 2010. Stockholm has the longest SSR record available worldwide. (Updated from Wild (2009) and Ohmura (2009).)

Overall, these proxies provide independent evidence for the existence of large-scale multi-decadal variations in SSR. Specifically, widespread observations of declines in pan evaporation from the 1950s to the 1980s were related to SSR dimming amongst other factors (Roderick and Farquhar, 2002). The observed decline in DTR over global land surfaces from the 1950s to the 1980s (Section 2.4.1.2), and its stabilisation thereafter fits to a large-scale dimming and subsequent brightening, respectively (Wild et al., 2007). Widespread brightening after 1980 is further supported by reconstructions from sunshine duration records (Wang et al., 2012e). Over Europe, SSR dimming and subsequent brightening is consistent with concurrent declines and increases in sunshine duration (Sanchez-Lorenzo et al., 2008), evaporation in energy limited environments (Teuling et al., 2009), visibility records (Vautard et al., 2009; Wang et al., 2009b) and DTR (Makowski et al., 2009). The early brightening in the 1930s and 1940s seen in a few European SSR records is in line with corresponding changes in sunshine duration and DTR (Sanchez-Lorenzo et al., 2008; Wild, 2009; Sanchez-Lorenzo and Wild, 2012). In China, the levelling off in SSR in the 1990s after decades of decline coincides with similar tendencies in the pan evaporation records, sunshine duration and DTR (Liu et al., 2004a; Liu et al., 2004b; Qian et al., 2006; Ding et al., 2007; Wang et al., 2012d). Dimming up to the 1980s and subsequent brightening is also indicated in a set of 237 sunshine duration records in South America (Raichijk, 2011).

2.3.3.2 Surface Thermal and Net Radiation

Thermal radiation, also known as longwave, terrestrial or far-IR radiation is sensitive to changes in atmospheric GHGs, temperature and humidity. Long-term measurements of the thermal surface components as well as surface net radiation are available at far fewer sites than SSR. Downward thermal radiation observations started to become available during the early 1990s at a limited number of globally distributed terrestrial sites. From these records, Wild et al. (2008) determined an overall increase of 2.6 W m⁻² per decade over the 1990s, in line with model projections and the expectations of an increasing greenhouse effect. Wang and Liang (2009) inferred an increase in downward thermal radiation of 2.2 W m⁻² per decade over the period 1973–2008 from globally available terrestrial observations of temperature, humidity and cloud fraction. Prata (2008) estimated a slightly lower increase of 1.7 W m⁻² per decade for clear sky conditions over the earlier period 1964–1990, based on observed temperature and

humidity profiles from globally distributed land-based radiosonde stations and radiative transfer calculations. Philipona et al. (2004; 2005) and Wacker et al. (2011) noted increasing downward thermal fluxes recorded in the Swiss Alpine Surface Radiation Budget (ASRB) network since the mid-1990s, corroborating an increasing greenhouse effect. For mainland Europe, Philipona et al. (2009) estimated an increase of downward thermal radiation of 2.4 to 2.7 W m⁻² per decade for the period 1981–2005.

There is limited observational information on changes in surface net radiation, in large part because measurements of upward fluxes at the surface are made at only a few sites and are not spatially representative. Wild et al. (2004, 2008) inferred a decline in land surface net radiation on the order of 2 W m⁻² per decade from the 1960s to the 1980s, and an increase at a similar rate from the 1980s to 2000, based on estimated changes of the individual radiative components that constitute the surface net radiation. Philipona et al. (2009) estimated an increase in surface net radiation of 1.3 to 2 W m⁻² per decade for central Europe and the Alps between 1981 and 2005.

2.3.3.3 Implications from Observed Changes in Related Climate Elements

The observed multi-decadal SSR variations cannot be explained by changes in TSI, which are an order of magnitude smaller (Willson and Mordvinov, 2003). They therefore have to originate from alterations in the transparency of the atmosphere, which depends on the presence of clouds, aerosols and radiatively active gases (Kvlevag and Myhre, 2007; Kim and Ramanathan, 2008). Cloud cover changes (Section 2.5.7) effectively modulate SSR on an interannual basis, but their contribution to the longer-term SSR trends is ambiguous. Although cloud cover changes were found to explain the trends in some areas (e.g., Liley, 2009), this is not always the case, particularly in relatively polluted regions (Qian et al., 2006; Norris and Wild, 2007, 2009; Wild, 2009; Kudo et al., 2012). SSR dimming and brightening has also been observed under cloudless atmospheres at various locations, pointing to a prominent role of atmospheric aerosols (Wild et al., 2005; Qian et al., 2007; Ruckstuhl et al., 2008; Sanchez-Lorenzo et al., 2009; Wang et al., 2009b; Zerefos et al., 2009).

Box 2.3 | Global Atmospheric Reanalyses

Dynamical reanalyses are increasingly used for assessing weather and climate phenomena. Given their more frequent use in this assessment compared to AR4, their characteristics are described in more detail here.

Reanalyses are distinct from, but complement, more ‘traditional’ statistical approaches to assessing the raw observations. They aim to produce continuous reconstructions of past atmospheric states that are consistent with all observations as well as with atmospheric physics as represented in a numerical weather prediction model, a process termed data assimilation. Unlike real-world observations, reanalyses are uniform in space and time and provide non-observable variables (e.g., potential vorticity).

Several groups are actively pursuing reanalysis development at the global scale, and many of these have produced several generations of reanalyses products (Box 2.3, Table 1). Since the first generation of reanalyses produced in the 1990s, substantial development has taken place. The NASA Modern-Era Retrospective Analysis for Research and Applications (MERRA) and ERA-Interim reanalyses show improved tropical precipitation and hence better represent the global hydrological cycle (Dee et al., 2011b). The NCEP/CFSR reanalysis *(continued on next page)*

Box 2.3, Table 1 | Overview of global dynamical reanalysis data sets (ranked by start year; the period extends to present if no end year is provided). A further description of reanalyses and their technical derivation is given in pp. S33–35 of Blunden et al. (2011). Approximate resolution is calculated as 1000 km * 20/N (with N denoting the spectral truncation, Laprise, 1992).

Institution	Reanalysis	Period	Approximate Resolution at Equator	Reference
Cooperative Institute for Research in Environmental Sciences (CIRES), National Oceanic and Atmospheric Administration (NOAA), USA	20th Century Reanalysis, Vers. 2 (20CR)	1871–2010	320 km	Compo et al. (2011)
National Centers for Environmental Prediction (NCEP) and National Center for Atmospheric Research (NCAR), USA	NCEP/NCAR R1 (NNR)	1948–	320 km	Kistler et al. (2001)
European Centre for Medium-Range Weather Forecasts (ECMWF)	ERA-40	1957–2002	125 km	Uppala et al. (2005)
Japan Meteorological Agency (JMA)	JRA-55	1958–	60 km	Ebita et al. (2011)
National Centers for Environmental Prediction (NCEP), US Department of Energy, USA	NCEP/DOE R2	1979–	320 km	Kanamitsu et al. (2002)
Japan Meteorological Agency (JMA)	JRA-25	1979–	190 km	Onogi et al. (2007)
National Aeronautics and Space Administration (NASA), USA	MERRA	1979–	75 km	Rienecker et al. (2011)
European Centre for Medium-Range Weather Forecasts (ECMWF)	ERA-Interim	1979–	80 km	Dee et al. (2011b)
National Centers for Environmental Prediction (NCEP), USA	CFSR	1979–	50 km	Saha et al. (2010)

Box 2.3 (continued)

uses a coupled ocean–atmosphere–land–sea–ice model (Saha et al., 2010). The 20th Century Reanalyses (20CR, Compo et al., 2011) is a 56-member ensemble and covers 140 years by assimilating only surface and sea level pressure (SLP) information. This variety of groups and approaches provides some indication of the robustness of reanalyses when compared. In addition to the global reanalyses, several regional reanalyses exist or are currently being produced.

Reanalyses products provide invaluable information on time scales ranging from daily to interannual variability. However, they may often be unable to characterize long-term trends (Trenberth et al., 2011). Although reanalyses projects by definition use a ‘frozen’ assimilation system, there are many other sources of potential errors. In addition to model biases, changes in the observational systems (e.g., coverage, introduction of satellite data) and time-dependent errors in the underlying observations or in the boundary conditions lead to step changes in time, even in latest generation reanalyses (Bosilovich et al., 2011).

Errors of this sort were ubiquitous in early generation reanalyses and rendered them of limited value for trend characterization (Thorne and Vose, 2010). Subsequent products have improved and uncertainties are better understood (Dee et al., 2011a), but artefacts are still present. As a consequence, trend adequacy depends on the variable under consideration, the time period and the region of interest. For example, surface air temperature and humidity trends over land in the ERA-Interim reanalysis compare well with observations (Simmons et al., 2010), but polar tropospheric temperature trends in ERA-40 disagree with trends derived from radiosonde and satellite observations (Bitz and Fu, 2008; Grant et al., 2008; Graversen et al., 2008; Thorne, 2008; Screen and Simmonds, 2011) owing to problems that were resolved in ERA-Interim (Dee et al., 2011a).

Studies based on reanalyses are used cautiously in AR5 and known inadequacies are pointed out and referenced. Later generation reanalyses are preferred where possible; however, literature based on these new products is still sparse.

Aerosols can directly attenuate SSR by scattering and absorbing solar radiation, or indirectly, through their ability to act as cloud condensation nuclei, thereby changing cloud reflectivity and lifetime (Chapter 7). SSR dimming and brightening is often reconcilable with trends in anthropogenic emission histories and atmospheric aerosol loadings (Stern, 2006; Streets et al., 2006; Mishchenko et al., 2007; Ruckstuhl et al., 2008; Ohvri et al., 2009; Russak, 2009; Streets et al., 2009; Cermak et al., 2010; Wild, 2012). Recent trends in aerosol optical depth derived from satellites indicate a decline in Europe since 2000 (Section 2.2.3), in line with evidence from SSR observations. However, direct aerosol effects alone may not be able to account for the full extent of the observed SSR changes in remote regions with low pollution levels (Dutton and Bodhaine, 2001; Schwartz, 2005). Aerosol indirect effects have not yet been well quantified, but have the potential to amplify aerosol-induced SSR trends, particularly in relatively pristine environments, such as over oceans (Wild, 2012).

SSR trends are also qualitatively in line with observed multi-decadal surface warming trends (Chapter 10), with generally smaller warming rates during phases of declining SSR, and larger warming rates in phases of increasing SSR (Wild et al., 2007). This is seen more pronounced for the relatively polluted NH than the more pristine SH (Wild, 2012). For Europe, Vautard et al. (2009) found that a decline in the frequency of low-visibility conditions such as fog, mist and haze over the past 30 years and associated SSR increase may be responsible for 10 to 20% of Europe’s recent daytime warming, and 50% of Eastern European warming. Philipona (2012) noted that both warming and brightening are weaker in the European Alps compared to the surrounding lowlands with stronger aerosol declines since 1981.

Reanalyses and observationally based methods have been used to show that increased atmospheric moisture with warming (Willett et al., 2008; Section 2.5) enhances thermal radiative emission of the atmosphere to the surface, leading to reduced net thermal cooling of the surface (Prata, 2008; Allan, 2009; Philipona et al., 2009; Wang and Liang, 2009).

In summary, the evidence for widespread multi-decadal variations in solar radiation incident on land surfaces has been substantiated since AR4, with many of the observational records showing a decline from the 1950s to the 1980s (‘dimming’), and a partial recovery thereafter (‘brightening’). *Confidence* in these changes is *high* in regions with high station densities such as over Europe and parts of Asia. These *likely* changes are generally supported by observed changes in related, but more widely measured variables, such as sunshine duration, DTR and hydrological quantities, and are often in line with aerosol emission patterns. Over some remote land areas and over the oceans, *confidence* is *low* owing to the lack of direct observations, which hamper a truly global assessment. Satellite-derived SSR fluxes support the existence of brightening also over oceans, but are less consistent over land surface where direct aerosol effects become more important. There are also indications for increasing downward thermal and net radiation at terrestrial stations since the early 1990s with *medium confidence*.

2.4 Changes in Temperature

2.4.1 Land Surface Air Temperature

2.4.1.1 Large-Scale Records and Their Uncertainties

AR4 concluded global land-surface air temperature (LSAT) had increased over the instrumental period of record, with the warming rate approximately double that reported over the oceans since 1979. Since AR4, substantial developments have occurred including the production of revised data sets, more digital data records, and new data set efforts. These innovations have improved understanding of data issues and uncertainties, allowing better quantification of regional changes. This reinforces confidence in the reported globally averaged LSAT time series behaviour.

Global Historical Climatology Network Version 3 (GHCNv3) incorporates many improvements (Lawrimore et al., 2011) but was found to be virtually indistinguishable at the global mean from version 2 (used in AR4). Goddard Institute of Space Studies (GISS) continues to provide an estimate based upon primarily GHCN, accounting for urban impacts through nightlights adjustments (Hansen et al., 2010). CRUTEM4 (Jones et al., 2012) incorporates additional station series and also newly homogenized versions of many individual station records. A new data product from a group based predominantly at Berkeley (Rohde et al., 2013a) uses a method that is substantially distinct from earlier efforts (further details on all the data sets and data availability are given in Supplementary Material 2.SM.4). Despite the range of approaches, the long-term variations and trends broadly agree among these various LSAT estimates, particularly after 1900. Global LSAT has increased (Figure 2.14, Table 2.4).

Since AR4, various theoretical challenges have been raised over the verity of global LSAT records (Pielke et al., 2007). Globally, sampling and methodological independence has been assessed through sub-sampling (Parker et al., 2009; Jones et al., 2012), creation of an entirely new and structurally distinct product (Rohde et al., 2013b) and a complete reprocessing of GHCN (Lawrimore et al., 2011). None of these yielded more than minor perturbations to the global LSAT records since 1900. Willett et al. (2008) and Peterson et al. (2011) explicitly showed that changes in specific and relative humidity (Section 2.5.5) were physically consistent with reported temperature trends, a result replicated in the ERA reanalyses (Simmons et al., 2010). Various investigators (Onogi et al., 2007; Simmons et al., 2010; Parker, 2011; Vose et al., 2012a) showed that LSAT estimates from modern reanalyses were in quantitative agreement with observed products.

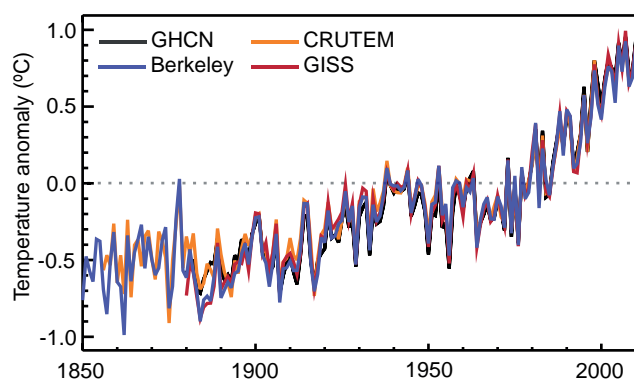


Figure 2.14 | Global annual average land-surface air temperature (LSAT) anomalies relative to a 1961–1990 climatology from the latest versions of four different data sets (Berkeley, CRUTEM, GHCN and GISS).

Particular controversy since AR4 has surrounded the LSAT record over the United States, focussed on siting quality of stations in the US Historical Climatology Network (USHCN) and implications for long-term trends. Most sites exhibit poor current siting as assessed against official WMO siting guidance, and may be expected to suffer potentially large siting-induced absolute biases (Fall et al., 2011). However, overall biases for the network since the 1980s are *likely* dominated by instrument type (owing to replacement of Stevenson screens with maximum minimum temperature systems (MMTS) in the 1980s at the majority of sites), rather than siting biases (Menne et al., 2010; Williams et al., 2012). A new automated homogeneity assessment approach (also used in GHCNv3, Menne and Williams, 2009) was developed that has been shown to perform as well or better than other contemporary approaches (Venema et al., 2012). This homogenization procedure *likely* removes much of the bias related to the network-wide changes in the 1980s (Menne et al., 2010; Fall et al., 2011; Williams et al., 2012). Williams et al. (2012) produced an ensemble of data set realizations using perturbed settings of this procedure and concluded through assessment against plausible test cases that there existed a propensity to under-estimate adjustments. This propensity is critically dependent upon the (unknown) nature of the inhomogeneities in the raw data records. Their homogenization increases both minimum temperature and maximum temperature centennial-time-scale USA average LSAT trends. Since 1979 these adjusted data agree with a range of reanalysis products whereas the raw records do not (Fall et al., 2010; Vose et al., 2012a).

Regional analyses of LSAT have not been limited to the United States. Various national and regional studies have undertaken assessments for Europe (Winkler, 2009; Bohm et al., 2010; Tietavainen et al., 2010; van

Table 2.4: | Trend estimates and 90% confidence intervals (Box 2.2) for LSAT global average values over five common periods.

Data Set	Trends in °C per decade				
	1880–2012	1901–2012	1901–1950	1951–2012	1979–2012
CRUTEM4.1.1.0 (Jones et al., 2012)	0.086 ± 0.015	0.095 ± 0.020	0.097 ± 0.029	0.175 ± 0.037	0.254 ± 0.050
GHCNv3.2.0 (Lawrimore et al., 2011)	0.094 ± 0.016	0.107 ± 0.020	0.100 ± 0.033	0.197 ± 0.031	0.273 ± 0.047
GISS (Hansen et al., 2010)	0.095 ± 0.015	0.099 ± 0.020	0.098 ± 0.032	0.188 ± 0.032	0.267 ± 0.054
Berkeley (Rohde et al., 2013)	0.094 ± 0.013	0.101 ± 0.017	0.111 ± 0.034	0.175 ± 0.029	0.254 ± 0.049

der Schrier et al., 2011), China (Li et al., 2009; Zhen and Zhong-Wei, 2009; Li et al., 2010a; Tang et al., 2010), India (Jain and Kumar, 2012), Australia (Trewin, 2012), Canada (Vincent et al., 2012), South America, (Falvey and Garreaud, 2009) and East Africa (Christy et al., 2009). These analyses have used a range of methodologies and, in many cases, more data and metadata than available to the global analyses. Despite the range of analysis techniques they are generally in broad agreement with the global products in characterizing the long-term changes in mean temperatures. This includes some regions, such as the Pacific coast of South America, that have exhibited recent cooling (Falvey and Garreaud, 2009). Of specific importance for the early global records, large (>1°C) summer time warm bias adjustments for many European 19th century and early 20th century records were revisited and broadly confirmed by a range of approaches (Bohm et al., 2010; Brunet et al., 2011).

Since AR4 efforts have also been made to interpolate Antarctic records from the sparse, predominantly coastal ground-based network (Chapman and Walsh, 2007; Monaghan et al., 2008; Steig et al., 2009; O'Donnell et al., 2011). Although these agree that Antarctica as a whole has warmed since the late 1950s, substantial multi-annual to multi-decadal variability and uncertainties in reconstructed magnitude and spatial trend structure yield only *low confidence* in the details of pan-Antarctic regional LSAT changes.

In summary, it is certain that globally averaged LSAT has risen since the late 19th century and that this warming has been particularly marked since the 1970s. Several independently analyzed global and regional LSAT data products support this conclusion. There is *low confidence* in changes prior to 1880 owing to the reduced number of estimates, non-standardized measurement techniques, the greater spread among the estimates and particularly the greatly reduced observational sampling. *Confidence* is also *low* in the spatial detail and magnitude of LSAT trends in sparsely sampled regions such as Antarctica. Since AR4 significant efforts have been undertaken to identify and adjust for data issues and new estimates have been produced. These innovations have further strengthened overall understanding of the global LSAT records.

2.4.1.2 Diurnal Temperature Range

In AR4 diurnal temperature range (DTR) was found, globally, to have narrowed since 1950, with minimum daily temperatures increasing faster than maximum daily temperatures. However, significant multi-decadal variability was highlighted including a recent period from 1997 to 2004 of no change, as both maximum and minimum temperatures rose at similar rates. The Technical Summary of AR4 highlighted changes in DTR and their causes as a key uncertainty. Since AR4, uncertainties in DTR and its physical interpretation have become even more apparent.

No dedicated global analysis of DTR has been undertaken subsequent to Vose et al. (2005a), although global behaviour has been discussed in two broader ranging analyses. Rohde et al. (2012) and Wild et al. (2007) note an apparent reversal since the mid-1980s; with DTR subsequently increasing. This decline and subsequent increase in DTR over global land surfaces is qualitatively consistent with the dimming and subsequent brightening noted in Section 2.3.3.1. Donat et al. (2013c)

using HadEX2 (Section 2.6) find significant decreasing DTR trends in more than half of the land areas assessed but less than 10% of land with significant increases since 1951. Available trend estimates ($-0.04 \pm 0.01^\circ\text{C}$ per decade over 1950–2011 (Rohde et al., 2013b) and -0.066°C per decade over 1950–2004 (Vose et al., 2005a)) are much smaller than global mean LSAT average temperature trends over 1951–2012 (Table 2.4). It therefore logically follows that globally averaged maximum and minimum temperatures over land have both increased by in excess of 0.1°C per decade since 1950.

Regionally, Makowski et al. (2008) found that DTR behaviour in Europe over 1950 to 2005 changed from a decrease to an increase in the 1970s in Western Europe and in the 1980s in Eastern Europe. Sen Roy and Balling (2005) found significant increases in both maximum and minimum temperatures for India, but little change in DTR over 1931–2002. Christy et al. (2009) reported that for East Africa there has been no pause in the narrowing of DTR in recent decades. Zhou and Ren (2011) reported a significant decrease in DTR over mainland China of -0.15°C per decade during 1961–2008.

Various investigators (e.g., Christy et al. (2009), Pielke and Matsui (2005), Zhou and Ren (2011)) have raised doubts about the physical interpretation of minimum temperature trends, hypothesizing that microclimate and local atmospheric composition impacts are more apparent because the dynamical mixing at night is much reduced. Parker (2006) investigated this issue arguing that if data were affected in this way, then a trend difference would be expected between calm and windy nights. However, he found no such minimum temperature differences on a global average basis. Using more complex boundary layer modelling techniques, Steeneveld et al. (2011) and McNider et al. (2012) showed much lower sensitivity to windspeed variations than posited by Pielke and Matsui but both concluded that boundary layer understanding was key to understanding the minimum temperature changes. Data analysis and long-term side-by-side instrumentation field studies show that real non-climatic data artefacts certainly affect maximum and minimum differently in the raw records for both recent (Fall et al., 2011; Williams et al., 2012) and older (Bohm et al., 2010; Brunet et al., 2011) records. Hence there could be issues over interpretation of apparent DTR trends and variability in many regions (Christy et al., 2006, 2009; Fall et al., 2011; Zhou and Ren, 2011; Williams et al., 2012), particularly when accompanied by regional-scale land-use/land-cover (LULC) changes (Christy et al., 2006).

In summary, *confidence* is *medium* in reported decreases in observed global DTR, noted as a key uncertainty in AR4. Several recent analyses of the raw data on which many previous analyses were based point to the potential for biases that differently affect maximum and minimum average temperatures. However, apparent changes in DTR are much smaller than reported changes in average temperatures and therefore it is *virtually certain* that maximum and minimum temperatures have increased since 1950.

2.4.1.3 Land Use Change and Urban Heat Island Effects

In AR4 Urban Heat Island (UHI) effects were concluded to be real local phenomena with negligible impact on large-scale trends. UHI and land-use land-cover change (LULC) effects arise mainly because the

modified surface affects the storage and transfer of heat, water and airflow. For single discrete locations these impacts may dominate all other factors.

Regionally, most attention has focused on China. A variety of investigations have used methods as diverse as SST comparisons (e.g., Jones et al., 2008), urban minus rural (e.g., Ren et al., 2008; Yang et al., 2011), satellite observations (Ren and Ren, 2011) and observations minus reanalysis (e.g., Hu et al., 2010; Yang et al., 2011). Interpretation is complicated because often studies have used distinct versions of station series. For example, the effect in Beijing is estimated at 80% (Ren et al., 2007) or 40% (Yan et al., 2010) of the observed trend depending on data corrections applied. A representative sample of these studies suggest the effect of UHI and LULC is approximately 20% of the trend in Eastern China as a whole and of the order 0.1°C per decade nationally (Table 1 in Yang et al., 2011) over the last 30 years, but with very substantial uncertainties. These effects have *likely* been partially or completely accounted for in many homogenized series (e.g., Li et al., 2010b; Yan et al., 2010). Fujibe (2009) ascribes about 25% of Japanese warming trends in 1979–2006 to UHI effects. Das et al. (2011) confirmed that many Japanese sites have experienced UHI warming but that rural stations show unaffected behaviour when compared to nearby SSTs.

There is an important distinction to be made between UHI trend effects in regions underseeing rapid development and those that have been developed for a long time. Jones and Lister (2009) and Wilby et al. (2011) using data from London (UK) concluded that some sites that have always been urban and where the UHI has not grown in magnitude will exhibit regionally indicative trends that agree with nearby rural locations and that in such cases the time series may exhibit multi-decadal trends driven primarily by synoptic variations. A lack of obvious time-varying UHI influences was also noted for Sydney, Melbourne and Hobart in Australia by Trewin (2012). The impacts of urbanization also will be dependent on the natural LULC characteristics that they replace. Zhang et al. (2010) found no evidence for urban influences in the desert North West region of China despite rapid urbanization.

Global adjusted data sets *likely* account for much of the UHI effect present in the raw data. For the US network, Hausfather et al. (2013) showed that the adjustments method used in GHCNv3 removed much of an apparent systematic difference between urban and rural locations, concluding that this arose from adjustment of biased urban location data. Globally, Hansen et al. (2010) used satellite-based nightlight radiances to estimate the worldwide influence on LSAT of local urban development. Adjustments reduced the global 1900–2009 temperature change (averaged over land and ocean) only from 0.71°C to 0.70°C. Wickham et al. (2013) also used satellite data and found that urban locations in the Berkeley data set exhibited even less warming than rural stations, although not statistically significantly so, over 1950 to 2010.

Studies of the broader effects of LULC since AR4 have tended to focus on the effects of irrigation on temperatures, with a large number of studies in the Californian central belt (Christy et al., 2006; Kueppers et al., 2007; Bonfils et al., 2008; Lo and Famiglietti, 2013). They find cooler average temperatures and a marked reduction in DTR in areas of active irrigation and ascribe this to increased humidity; effectively a repar-

titution of moist and dry energy terms. Reanalyses have also been used to estimate the LULC signature in LSAT trends. Fall et al. (2010) found that the North American Regional Reanalysis generated overall surface air temperature trends for 1979–2003 similar to observed records. Observations-minus-reanalysis trends were most positive for barren and urban areas, in accord with the results of Lim et al. (2008) using the NCEP/NCAR and ERA-40 reanalyses, and negative in agricultural areas.

McKittrick and Michaels (2004) and de Laat and Maurellis (2006) assessed regression of trends with national socioeconomic and geographical indicators, concluding that UHI and related LULC have caused much of the observed LSAT warming. AR4 concluded that this correlation ceases to be statistically significant if one takes into account the fact that the locations of greatest socioeconomic development are also those that have been most warmed by atmospheric circulation changes but provided no explicit evidence for this overall assessment result. Subsequently McKittrick and Michaels (2007) concluded that about half the reported warming trend in global-average land surface air temperature in 1980–2002 resulted from local land surface changes and faults in the observations. Schmidt (2009) undertook a quantitative analysis that supported AR4 conclusions that much of the reported correlation largely arose due to naturally occurring climate variability and model over-fitting and was not robust. Taking these factors into account, modified analyses by McKittrick (2010) and McKittrick and Nierenberg (2010) still yielded significant evidence for such contamination of the record.

In marked contrast to regression based studies, several studies have shown the methodologically diverse set of modern reanalysis products and the various LSAT records at global and regional levels to be similar since at least the mid-20th century (Simmons et al., 2010; Parker, 2011; Ferguson and Villarini, 2012; Jones et al., 2012; Vose et al., 2012a). These reanalyses do not directly assimilate the LSAT measurements but rather infer LSAT estimates from an observational constraint provided by much of the rest of the global observing system, thus representing an independent estimate. A hypothesized residual significant warming artefact argued for by regression-based analyses is therefore physically inconsistent with many other components of the global observing system according to a broad range of state-of-the-art data assimilation models (Box 2.3). Further, Efthymiadis and Jones (2010) estimated an absolute upper limit on urban influence globally of 0.02°C per decade, or about 15% of the total LSAT trends, in 1951–2009 from trends of coastal land and SST.

In summary, it is indisputable that UHI and LULC are real influences on raw temperature measurements. At question is the extent to which they remain in the global products (as residual biases in broader regionally representative change estimates). Based primarily on the range of urban minus rural adjusted data set comparisons and the degree of agreement of these products with a broad range of reanalysis products, it is *unlikely* that any uncorrected urban heat-island effects and LULC change effects have raised the estimated centennial globally averaged LSAT trends by more than 10% of the reported trend (*high confidence*, based on robust evidence and high agreement). This is an average value; in some regions with rapid development, UHI and LULC change impacts on regional trends may be substantially larger.

2.4.2 Sea Surface Temperature and Marine Air Temperature

AR4 concluded that ‘recent’ warming (since the 1950s) is strongly evident at all latitudes in SST over each ocean. Prominent spatio-temporal structures including the ENSO and decadal variability patterns in the Pacific Ocean (Box 2.5) and a hemispheric asymmetry in the Atlantic Ocean were highlighted as contributors to the regional differences in surface warming rates, which in turn affect atmospheric circulation. Since AR4 the availability of metadata has increased, data completeness has improved and a number of new SST products have been produced. Intercomparisons of data obtained by different measurement methods, including satellite data, have resulted in better understanding of errors and biases in the record.

2.4.2.1 Advances in Assembling Data Sets and in Understanding Data Errors

2.4.2.1.1 *In situ* data records

Historically, most SST observations were obtained from moving ships. Buoy measurements comprise a significant and increasing fraction of *in situ* SST measurements from the 1980s onward (Figure 2.15). Improvements in the understanding of uncertainty have been expedited by the use of metadata (Kent et al., 2007) and the recovery of

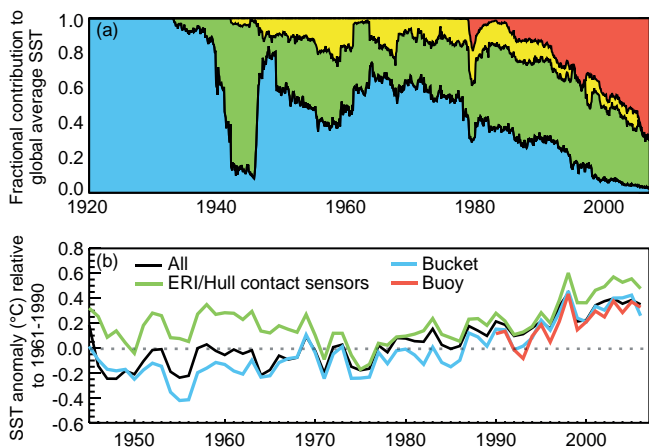


Figure 2.15 | Temporal changes in the prevalence of different measurement methods in the International Comprehensive Ocean-Atmosphere Data Set (ICOADS). (a) Fractional contributions of observations made by different measurement methods: bucket observations (blue), engine room intake (ERI) and hull contact sensor observations (green), moored and drifting buoys (red), and unknown (yellow). (b) Global annual average sea surface temperature (SST) anomalies based on different kinds of data: ERI and hull contact sensor (green), bucket (blue), buoy (red), and all (black). Averages are computed over all $5^\circ \times 5^\circ$ grid boxes where both ERI/hull and bucket measurements, but not necessarily buoy data, were available. (Adapted from Kennedy et al., 2011a.)

Table 2.5 | Trend estimates and 90% confidence intervals (Box 2.2) for two subsequent versions of the HadSST data set over five common periods. HadSST2 has been used in AR4; HadSST3 is used in this chapter.

Data Set	Trends in $^\circ\text{C}$ per decade				
	1880–2012	1901–2012	1901–1950	1951–2012	1979–2012
HadSST3 (Kennedy et al., 2011a)	0.054 ± 0.012	0.067 ± 0.013	0.117 ± 0.028	0.074 ± 0.027	0.124 ± 0.030
HadSST2 (Rayner et al., 2006)	0.051 ± 0.015	0.069 ± 0.012	0.084 ± 0.055	0.098 ± 0.017	0.121 ± 0.033

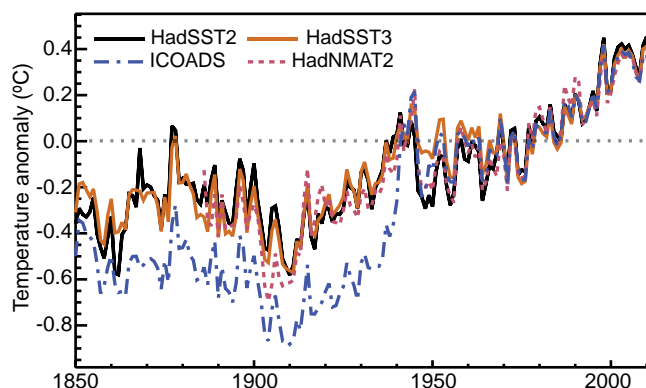


Figure 2.16 | Global annual average sea surface temperature (SST) and Night Marine Air Temperature (NMAT) relative to a 1961–1990 climatology from gridded data sets of SST observations (HadSST2 and its successor HadSST3), the raw SST measurement archive (ICOADS, v2.5) and night marine air temperatures data set HadNMAT2 (Kent et al., 2013). HadSST2 and HadSST3 both are based on SST observations from versions of the ICOADS data set, but differ in degree of measurement bias correction.

observer instructions and other related documents. Early data were systematically cold biased because they were made using canvas or wooden buckets that, on average, lost heat to the air before the measurements were taken. This effect has long been recognized (Brooks, 1926), and prior to AR4 represented the only artefact adjusted in gridded SST products, such as HadSST2 (Rayner et al., 2006) and ERSST (Smith et al., 2005, 2008), which were based on ‘bucket correction’ methods by Folland and Parker (1995) and Smith and Reynolds (2002), respectively. The adjustments, made using ship observations of Night Marine Air Temperature (NMAT) and other sources, had a striking effect on the SST global mean estimates: note the difference in 1850–1941 between HadSST2 and International Comprehensive Ocean-Atmosphere Data Set (ICOADS) curves in Figure 2.16 (a brief description of SST and NMAT data sets and their methods is given in Supplementary Material 2.SM.4.3).

Buckets of improved design and measurement methods with smaller, on average, biases came into use after 1941 (Figure 2.15, top); average biases were reduced further in recent decades, but not eliminated (Figure 2.15, bottom). Increasing density of SST observations made possible the identification (Reynolds et al., 2002, 2010; Kennedy et al., 2012) and partial correction of more recent period biases (Kennedy et al., 2011a). In particular, it is hypothesized that the proximity of the hot engine often biases engine room intake (ERI) measurements warm (Kent et al., 2010). Because of the prevalence of the ERI measurements among SST data from ships, the ship SSTs are biased warm by 0.12°C to 0.18°C on average compared to the buoy data (Reynolds et al., 2010; Kennedy et al., 2011a, 2012). An assessment of the potential impact of modern biases can be ascertained by considering the difference

between HadSST3 (bias corrections applied throughout) and HadSST2 (bucket corrections only) global means (Figure 2.16): it is particularly prominent in 1945–1970 period, when rapid changes in prevalence of ERI and bucket measurements during and after the World War II affect HadSST2 owing to the uncorrected measurement biases (Thompson et al., 2008), while these are corrected in HadSST3. Nevertheless, for periods longer than a century the effect of HadSST3–HadSST2 differences on linear trend slopes is small relative to the trend uncertainty (Table 2.5). Some degree of independent check on the validity of HadSST3 adjustments comes from a comparison to sub-surface temperature data (Gouretski et al., 2012) (see Section 3.2).

The traditional approach to modeling random error of *in situ* SST data assumed the independence of individual measurements. Kent and Berry (2008) identified the need to account for error correlation for measurements from the same “platform” (i.e., an individual ship or buoy), while measurement errors from different platforms remain independent. Kennedy et al. (2011b) achieved that by introducing platform-dependent biases, which are constant within the same platform, but change randomly from one platform to another. Accounting for such correlated errors in HadSST3 resulted in estimated error for global and hemispheric monthly means that are more than twice the estimates given by HadSST2. The uncertainty in many, but not all, components of the HadSST3 product is represented by the ensemble of its realizations (Figure 2.17).

Data sets of marine air temperatures (MATs) have traditionally been restricted to nighttime series only (NMAT data sets) due to the direct solar heating effect on the daytime measurements, although corrected daytime MAT records for 1973–present are already available (Berry and Kent, 2009). Other major biases, affecting both nighttime and daytime MAT are due to increasing deck height with the general increase in the size of ships over time and non-standard measurement practices. Recently these biases were re-examined and explicit uncertainty calculation undertaken for NMAT by Kent et al. (2013), resulting in the HadNMAT2 data set.

2.4.2.1.2 Satellite SST data records

Satellite SST data sets are based on measuring electromagnetic radiation that left the ocean surface and got transmitted through the atmosphere. Because of the complexity of processes involved, the majority of such data has to be calibrated on the basis of *in situ* observations. The resulting data sets, however, provide a description of global SST fields with a level of spatial detail unachievable by *in situ* data only. The principal IR sensor is the Advanced Very High Resolution Radiometer (AVHRR). Since AR4, the AVHRR time series has been reprocessed consistently back to March 1981 (Casey et al., 2010) to create the AVHRR Pathfinder v5.2 data set. Passive microwave data sets of SST are available since 1997 equatorward of 40° and near-globally since 2002 (Wentz et al., 2000; Gentemann et al., 2004). They are generally less accurate than IR-based SST data sets, but their superior coverage in areas of persistent cloudiness provides SST estimates where the IR record has none (Reynolds et al., 2010).

The (Advanced) Along Track Scanning Radiometer (A)ATSR series of three sensors was designed for climate monitoring of SST; their com-

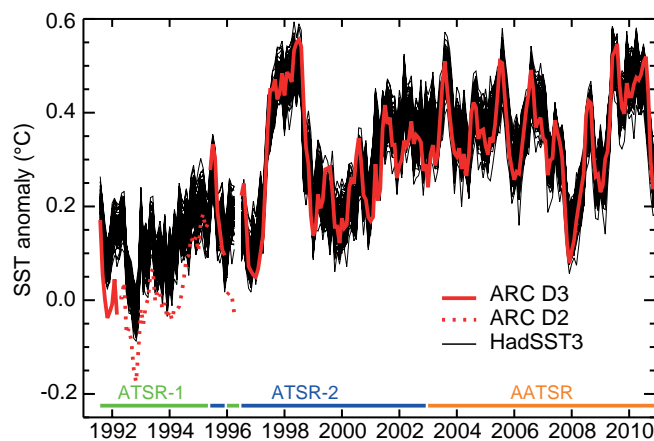


Figure 2.17 | Global monthly mean sea surface temperature (SST) anomalies relative to a 1961–1990 climatology from satellites (ATSRs) and *in situ* records (HadSST3). Black lines: the 100-member HadSST3 ensemble. Red lines: ATSR-based nighttime subsurface temperature at 0.2 m depth ($SST_{0.2m}$) estimates from the ATSR Reprocessing for Climate (ARC) project. Retrievals based on three spectral channels (D3, solid line) are more accurate than retrievals based on only two (D2, dotted line). Contributions of the three different ATSR missions to the curve shown are indicated at the bottom. The *in situ* and satellite records were co-located within $5^\circ \times 5^\circ$ monthly grid boxes: only those where both data sets had data for the same month were used in the comparison. (Adapted from Merchant et al. 2012.)

bined record starts in August 1991 and exceeds two decades (it stopped with the demise of the ENVISAT platform in 2012). The (A) ATSRs are ‘dual-view’ IR radiometers intended to allow atmospheric effects removal without the use of *in situ* observations. Since AR4, (A)ATSR observations have been reprocessed with new estimation techniques (Embury and Merchant, 2011). The resulting SST products seem to be more accurate than many *in situ* observations (Embury et al., 2011). In terms of monthly global means, the agreement is illustrated in Figure 2.17. By analyzing (A)ATSR and *in situ* data together, Kennedy et al. (2012) verified and extended existing models for biases and random errors of *in situ* data.

2.4.2.2 Interpolated SST Products and Trends

SST data sets form a major part of global surface temperature analyses considered in this assessment report. To use an SST data set as a boundary condition for atmospheric reanalyses products (Box 2.3) or in atmosphere-only climate simulations (considered in Chapter 9 onwards), gridded data sets with complete coverage over the global ocean are typically needed. These are usually based on a special form of kriging (optimal interpolation) procedure that retains large-scale correlation structures and can accommodate very sparse data coverage. For the pre-satellite era (generally, before October 1981) only *in situ* data are used; for the latter period some products also use AVHRR data. Figure 2.18 compares interpolated SST data sets that extend back to the 19th century with the uninterpolated HadSST3 and HadNMAT2 products. Linear trend estimates for global mean SSTs from those products updated through 2012 are presented in Table 2.6. Differences between the trends from different data sets are larger when the calculation period is shorter (1979–2012) or has lower quality data (1901–1950); these are due mainly to different data coverage of underlying observational data sets and bias correction methods used in these products.

Table 2.6 | Trend estimates and 90% confidence intervals (Box 2.2) for interpolated SST data sets (uninterpolated state-of-the-art HadSST3 data set is included for comparison). Dash indicates not enough data available for trend calculation.

Data Set	Trends in °C per decade				
	1880–2012	1901–2012	1901–1950	1951–2012	1979–2012
HadISST (Rayner et al., 2003)	0.042 ± 0.007	0.052 ± 0.007	0.067 ± 0.024	0.064 ± 0.015	0.072 ± 0.024
COBE-SST (Ishii et al., 2005)	–	0.058 ± 0.007	0.066 ± 0.032	0.071 ± 0.014	0.073 ± 0.020
ERSSTv3b (Smith et al., 2008)	0.054 ± 0.015	0.071 ± 0.011	0.097 ± 0.050	0.088 ± 0.017	0.105 ± 0.031
HadSST3 (Kennedy et al., 2011a)	0.054 ± 0.012	0.067 ± 0.013	0.117 ± 0.028	0.074 ± 0.027	0.124 ± 0.030

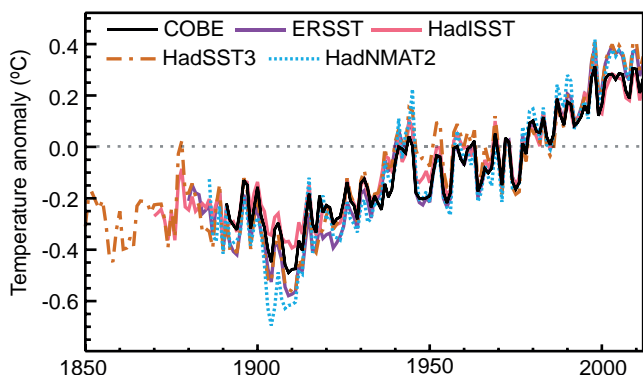


Figure 2.18 | Global annual average sea surface temperature (SST) and Night Marine Air Temperature (NMAT) relative to a 1961–1990 climatology from state of the art data sets. Spatially interpolated products are shown by solid lines; non-interpolated products by dashed lines.

In summary, it is certain that global average sea surface temperatures (SSTs) have increased since the beginning of the 20th century. Since AR4, major improvements in availability of metadata and data completeness have been made, and a number of new global SST records have been produced. Intercomparisons of new SST data records obtained by different measurement methods, including satellite data, have resulted in better understanding of uncertainties and biases in the records. Although these innovations have helped highlight and quantify uncertainties and affect our understanding of the character of changes since the mid-20th century, they do not alter the conclusion that global SSTs have increased both since the 1950s and since the late 19th century.

2.4.3 Global Combined Land and Sea Surface Temperature

AR4 concluded that the GMST had increased, with the last 50 years increasing at almost double the rate of the last 100 years. Subsequent developments in LSAT and SST have led to better understanding of the data and their uncertainties as discussed in preceding sections. This improved understanding has led to revised global products.

Changes have been made to all three GMST data sets that were used in AR4 (Hansen et al., 2010; Morice et al., 2012; Vose et al., 2012b). These are now in somewhat better agreement with each other over recent years, in large part because HadCRUT4 now better samples the NH high latitude land regions (Jones et al., 2012; Morice et al., 2012) which comparisons to reanalyses had shown led to a propensity for HadCRUT3 to underestimate recent warming (Simmons et al., 2010).

Starting in the 1980s each decade has been significantly warmer at the Earth’s surface than any preceding decade since the 1850s in HadCRUT4, a data set that explicitly quantifies a large number of sources of uncertainty (Figure 2.19). Each of the last three decades is also the warmest in the other two GMST data sets, but these have substantially less mature and complete uncertainty estimates, precluding such an assessment of significance of their decadal differences. The GISS and MLOST data sets fall outside the 90% CI of HadCRUT4 for several decades in the 20th century (Figure 2.19). These decadal differences could reflect residual biases in one or more data set, an incomplete treatment of uncertainties in HadCRUT4.1 or a combination of these effects (Box 2.1). The data sets utilize different LSAT (Section 2.4.1) and SST (Section 2.4.2) component records (Supplementary Material 2.SM.4.3.4) that in the case of SST differ somewhat in their multi-decadal trend behaviour (Table 2.6 compare HadSST3 and ERSSTv3b).

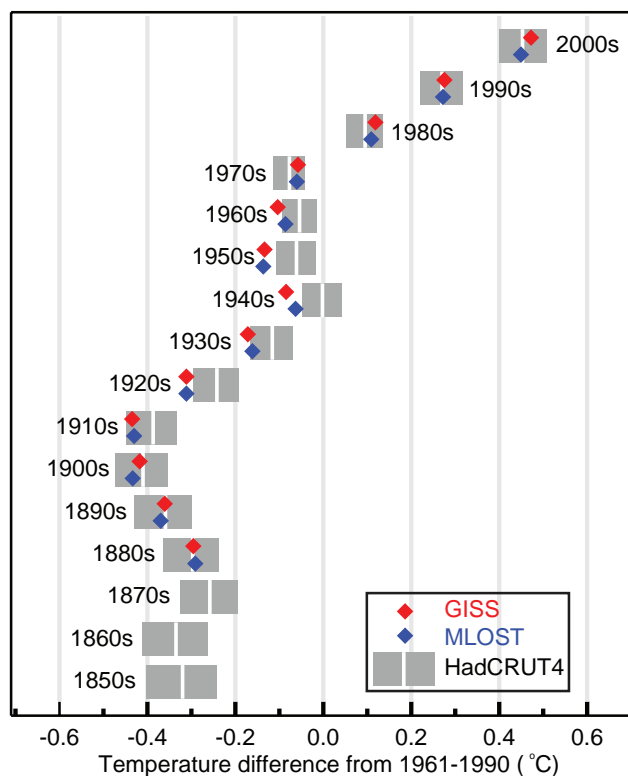


Figure 2.19 | Decadal global mean surface temperature (GMST) anomalies (white vertical lines in grey blocks) and their uncertainties (90% confidence intervals as grey blocks) based upon the land-surface air temperature (LSAT) and sea surface temperature (SST) combined HadCRUT4 (v4.1.1.0) ensemble (Morice et al., 2012). Anomalies are relative to a 1961–1990 climatology. 1850s indicates the period 1850–1859, and so on. NCDC MLOST and GISS data set best-estimates are also shown.

All ten of the warmest years have occurred since 1997, with 2010 and 2005 effectively tied for the warmest year on record in all three products. However, uncertainties on individual annual values are sufficiently large that the ten warmest years are statistically indistinguishable from one another. The global-mean trends are significant for all data sets and multi-decadal periods considered in Table 2.7. Using HadCRUT4 and its uncertainty estimates, the warming from 1850–1900 to 1986–2005 (reference period for the modelling chapters and Annex I) is 0.61 [0.55 to 0.67] °C (90% confidence interval), and the warming from 1850–1900 to 2003–2012 (the most recent decade) is 0.78 [0.72 to 0.85] °C (Supplementary Material 2.SM.4.3.3).

Differences between data sets are much smaller than both interannual variability and the long-term trend (Figure 2.20). Since 1901 almost the whole globe has experienced surface warming (Figure 2.21). Warming has not been linear; most warming occurred in two periods: around 1900 to around 1940 and around 1970 onwards (Figure 2.22). Shorter periods are noisier and so proportionately less of the sampled globe exhibits statistically significant trends at the grid box level (Figure 2.22). The two periods of global mean warming exhibit very distinct spatial signatures. The early 20th century warming was largely a NH mid- to high-latitude phenomenon, whereas the more recent warming is more global in nature. These distinctions may yield important information as to causes (Chapter 10). Differences between data sets are larger in earlier periods (Figures 2.19, 2.20), particularly prior to the 1950s when observational sampling is much more geographically incomplete (and many of the well sampled areas may have been globally unrepresentative (Brönnimann, 2009)), data errors and subsequent methodological impacts are larger (Thompson et al., 2008), and different ways of accounting for data void regions are more important (Vose et al., 2005b).

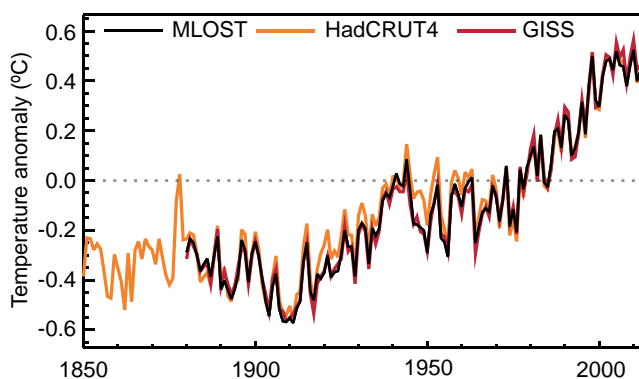


Figure 2.20 | Annual global mean surface temperature (GMST) anomalies relative to a 1961–1990 climatology from the latest version of the three combined land-surface air temperature (LSAT) and sea surface temperature (SST) data sets (HadCRUT4, GISS and NCDC MLOST). Published data set uncertainties are not included for reasons discussed in Box 2.1.

Much interest has focussed on the period since 1998 and an observed reduction in warming trend, most marked in NH winter (Cohen et al., 2012). Various investigators have pointed out the limitations of such short-term trend analysis in the presence of auto-correlated series variability and that several other similar length phases of no warming exist in all the observational records and in climate model simulations

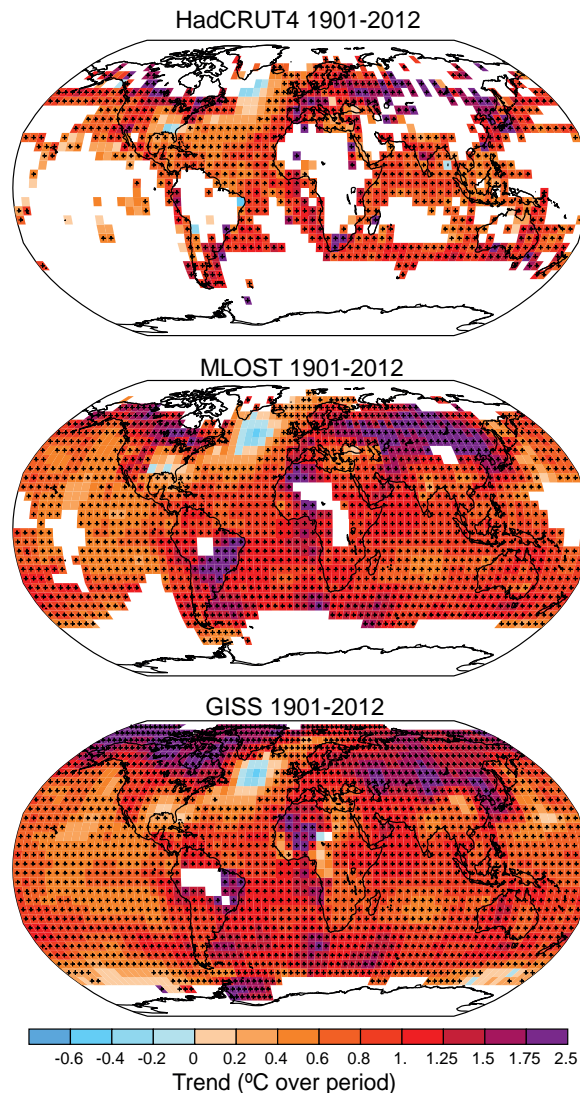


Figure 2.21 | Trends in surface temperature from the three data sets of Figure 2.20 for 1901–2012. White areas indicate incomplete or missing data. Trends have been calculated only for those grid boxes with greater than 70% complete records and more than 20% data availability in first and last decile of the period. Black plus signs (+) indicate grid boxes where trends are significant (i.e., a trend of zero lies outside the 90% confidence interval). Differences in coverage primarily reflect the degree of interpolation to account for data void regions undertaken by the data set providers ranging from none beyond grid box averaging (HadCRUT4) to substantial (GISS).

Table 2.7 | Same as Table 2.4, but for global mean surface temperature (GMST) over five common periods.

Data Set	Trends in °C per decade				
	1880–2012	1901–2012	1901–1950	1951–2012	1979–2012
HadCRUT4 (Morice et al., 2012)	0.062 ± 0.012	0.075 ± 0.013	0.107 ± 0.026	0.106 ± 0.027	0.155 ± 0.033
NCDC MLOST (Vose et al., 2012b)	0.064 ± 0.015	0.081 ± 0.013	0.097 ± 0.040	0.118 ± 0.021	0.151 ± 0.037
GISS (Hansen et al., 2010)	0.065 ± 0.015	0.083 ± 0.013	0.090 ± 0.034	0.124 ± 0.020	0.161 ± 0.033

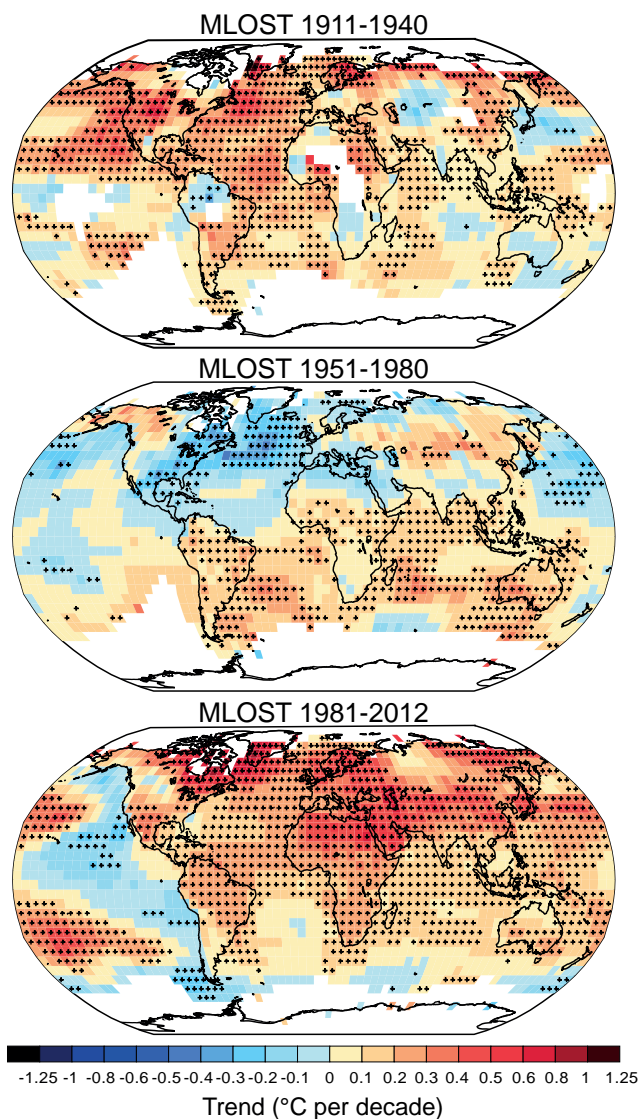


Figure 2.22 | Trends in surface temperature from NCDC MLOST for three non-consecutive shorter periods (1911–1940; 1951–1980; 1981–2012). White areas indicate incomplete or missing data. Trends and significance have been calculated as in Figure 2.21.

(Easterling and Wehner, 2009; Peterson et al., 2009; Liebmann et al., 2010; Foster and Rahmstorf, 2011; Santer et al., 2011). This issue is discussed in the context of model behaviour, forcings and natural variability in Box 9.2 and Section 10.3.1. Regardless, all global combined LSAT and SST data sets exhibit a statistically non-significant warming trend over 1998–2012 ($0.042^{\circ}\text{C} \pm 0.093^{\circ}\text{C}$ per decade (HadCRUT4); $0.037^{\circ}\text{C} \pm 0.085^{\circ}\text{C}$ per decade (NCDC MLOST); $0.069^{\circ}\text{C} \pm 0.082^{\circ}\text{C}$ per decade (GISS)). An average of the trends from these three data sets yields an estimated change for the 1998–2012 period of 0.05 [–0.05 to +0.15] $^{\circ}\text{C}$ per decade. Trends of this short length are very sensitive to the precise period selection with trends calculated in the same manner for the 15-year periods starting in 1995, 1996, and 1997 being 0.13 [0.02 to 0.24], 0.14 [0.03 to 0.24] and 0.07 [–0.02 to 0.18] (all $^{\circ}\text{C}$ per decade), respectively.

In summary, it is certain that globally averaged near surface temperatures have increased since the late 19th century. Each of the past

three decades has been warmer than all the previous decades in the instrumental record, and the decade of the 2000s has been the warmest. The globally averaged combined land and ocean surface temperature data as calculated by a linear trend, show a warming of 0.85 [0.65 to 1.06] $^{\circ}\text{C}$, over the period 1880–2012, when multiple independently produced datasets exist, about 0.89°C [0.69 to 1.08] $^{\circ}\text{C}$ over the period 1901–2012, and about 0.72 [0.49 to 0.89] $^{\circ}\text{C}$ over the period 1951–2012. The total increase between the average of the 1850–1900 period and the 2003–2012 period is 0.78 [0.72 to 0.85] $^{\circ}\text{C}$ and the total increase between the average of the 1850–1900 period and the reference period for projections 1986–2005 is 0.61 [0.55 to 0.67] $^{\circ}\text{C}$, based on the single longest dataset available. For the longest period when calculation of regional trends is sufficiently complete (1901–2012), almost the entire globe has experienced surface warming. In addition to robust multi-decadal warming, global mean surface temperature exhibits substantial decadal and interannual variability. Owing to natural variability, trends based on short records are very sensitive to the beginning and end dates and do not in general reflect long-term climate trends. As one example, the rate of warming over the past 15 years (1998–2012; 0.05 [–0.05 to +0.15] $^{\circ}\text{C}$ per decade), which begins with a strong El Niño, is smaller than the rate calculated since 1951 (1951–2012; 0.12 [0.08 to 0.14] $^{\circ}\text{C}$ per decade). Trends for 15-year periods starting in 1995, 1996, and 1997 are 0.13 [0.02 to 0.24], 0.14 [0.03 to 0.24] and 0.07 [–0.02 to 0.18], respectively..

2.4.4 Upper Air Temperature

AR4 summarized that globally the troposphere had warmed at a rate greater than the GMST over the radiosonde record, while over the shorter satellite era the GMST and tropospheric warming rates were indistinguishable. Trends in the tropics were more uncertain than global trends although even this region was concluded to be warming. Globally, the stratosphere was reported to be cooling over the satellite era starting in 1979. New advances since AR4 have highlighted the substantial degree of uncertainty in both satellite and balloon-borne radiosonde records and led to some revisions and improvements in existing products and the creation of a number of new data products.

2.4.4.1 Advances in Multi-Decadal Observational Records

The major global radiosonde records extend back to 1958, with temperatures, measured as the balloon ascends, reported at mandatory pressure levels. Satellites have monitored tropospheric and lower stratospheric temperature trends since late 1978 through the Microwave Sounding Unit (MSU) and its follow-on Advanced Microwave Sounding Unit (AMSU) since 1998. These measures of upwelling radiation represent bulk (volume averaged) atmospheric temperature (Figure 2.23). The ‘Mid-Tropospheric’ (MT) MSU channel that most directly corresponds to the troposphere has 10 to 15% of its signal from both the skin temperature of the Earth’s surface and the stratosphere. Two alternative approaches have been suggested for removing the stratospheric component based on differencing of view angles (LT) and statistical recombination (*G) with the ‘Lower Stratosphere’ (LS) channel (Spencer and Christy, 1992; Fu et al., 2004). The MSU satellite series also included a Stratospheric Sounding Unit (SSU) that measured at higher altitudes (Seidel et al., 2011).

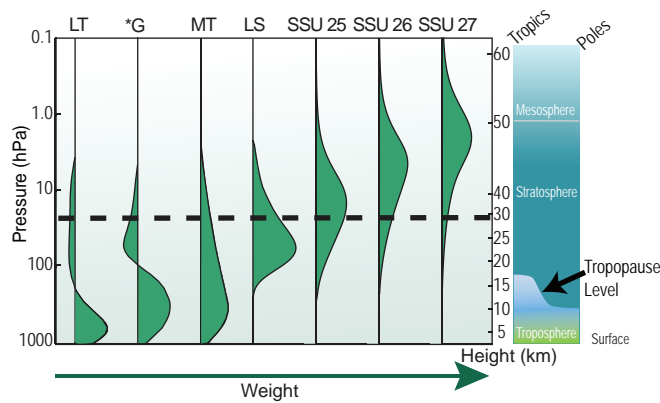


Figure 2.23 | Vertical weighting functions for those satellite temperature retrievals discussed in this chapter (modified from Seidel et al. (2011)). The dashed line indicates the typical maximum altitude achieved in the historical radiosonde record. The three SSU channels are denoted by the designated names 25, 26 and 27. LS (Lower Stratosphere) and MT (Mid Troposphere) are two direct MSU measures and LT (Lower Troposphere) and *G (Global Troposphere) are derived quantities from one or more of these that attempt to remove the stratospheric component from MT.

At the time of AR4 there were only two ‘global’ radiosonde data sets that included treatment of homogeneity issues: RATPAC (Free et al., 2005) and HadAT (Thorne et al., 2005). Three additional estimates have appeared since AR4 based on novel and distinct approaches. A group at the University of Vienna have produced RAOBCORE and RICH (Haimberger, 2007; Haimberger et al., 2008, 2012) using ERA reanalysis products (Box 2.3). Sherwood and colleagues developed an iterative universal kriging approach for radiosonde data to create IUK (Sherwood et al., 2008) and concluded that non-climatic data issues leading to spurious cooling remained in the deep tropics even after homogenization. The HadAT group created an automated version, undertook systematic experimentation and concluded that the parametric uncertainty (Box 2.1) was of the same order of magnitude as the apparent climate signal (McCarthy et al., 2008; Titchner et al., 2009; Thorne et al., 2011). A similar ensemble approach has also been applied to the RICH product (Haimberger et al., 2012). These various ensembles and new products exhibit more tropospheric warming / less stratospheric cooling than pre-existing products at all levels. Globally the radiosonde records all imply the troposphere has warmed and the stratosphere cooled since 1958 but with uncertainty that grows with height and is much greater outside the better-sampled NH extra-tropics (Thorne et al., 2011; Haimberger et al., 2012), where it is of the order 0.1°C per decade.

For MSU, AR4 considered estimates produced from three groups: UAH (University of Alabama in Huntsville); RSS (Remote Sensing Systems) and VG2 (now no longer updated). A new product has been created by NOAA labelled STAR, using a fundamentally distinct approach for the critical inter-satellite warm target calibration step (Zou et al., 2006a). STAR exhibits more warming/less cooling at all levels than UAH and RSS. For MT and LS, Zou and Wang (2010) concluded that this does not relate primarily to use of their inter-satellite calibration technique but rather differences in other processing steps. RSS also produced a parametric uncertainty ensemble (Box 2.1) employing a Monte Carlo approach allowing methodological inter-dependencies to be fully expressed (Mears et al., 2011). For large-scale trends dominant

effects were inter-satellite offset determinations and, for tropospheric channels, diurnal drift. Uncertainties were concluded to be of the order 0.1°C per decade at the global mean for both tropospheric channels (where it is of comparable magnitude to the long-term trends) and the stratospheric channel.

SSU provides the only long-term near-global temperature data above the lower stratosphere, with the series terminating in 2006. Some AMSU-A channels have replaced this capability and efforts to understand the effect of changed measurement properties have been undertaken (Kobayashi et al., 2009). Until recently only one SSU data set existed (Nash and Edge, 1989), updated by Randel et al. (2009). Liu and Weng (2009) have produced an intermediate analysis for Channels 25 and 26 (but not Channel 27). Wang et al. (2012g), building on insights from several of these recent studies, have produced a more complete analysis. Differences between the independent estimates are much larger than differences between MSU records or radiosonde records at lower levels, with substantial inter-decadal time series behaviour departures, zonal trend structure, and global trend differences of the order 0.5°C per decade (Seidel et al., 2011; Thompson et al., 2012; Wang et al., 2012g). Although all SSU data sets agree that the stratosphere is cooling, there is therefore *low confidence* in the details above the lower stratosphere.

In summary, many new data sets have been produced since AR4 from radiosondes and satellites with renewed interest in satellite measurements above the lower stratosphere. Several studies have attempted to quantify the parametric uncertainty (Box 2.1) more rigorously. These various data sets and analyses have served to highlight the degree of uncertainty in the data and derived products.

2.4.4.2 Intercomparisons of Various Long-Term Radiosonde and MSU Products

Since AR4 there have been a large number of intercomparisons between radiosonde and MSU data sets. Interpretation is complicated, as most studies considered data set versions that have since been superseded. Several studies compared UAH and RSS products to local, regional or global raw/homogenized radiosonde data (Christy and Norris, 2006, 2009; Christy et al., 2007, 2010, 2011; Randall and Herman, 2008; Mears et al., 2012; Po-Chedley and Fu, 2012). Early studies focussed on the time of transition from NOAA-11 to NOAA-12 (early 1990s) which indicated an apparent issue in RSS. Christy et al. (2007) noted that this coincided with the Mt Pinatubo eruption and that RSS was the only product, either surface or tropospheric, that exhibited tropical warming immediately after the eruption when cooling would be expected. Using reanalysis data Bengtsson and Hodges (2011) also found evidence of a potential jump in RSS in 1993 over the tropical oceans. Mears et al. (2012) cautioned that an El Niño event quasi-simultaneous with Pinatubo complicates interpretation. They also highlighted several other periods of disagreement between radiosonde records and MSU records. All MSU records were most uncertain when satellite orbits are drifting rapidly (Christy and Norris, 2006, 2009). Mears et al. (2011) found that trend differences between RSS and other data sets could not be explained in many cases by parametric uncertainties in RSS alone. It was repeatedly cautioned that there were potential common biases (of varying magnitude) between the different MSU

records or between the different radiosonde records which complicate intercomparisons (Christy and Norris, 2006, 2009; Mears et al., 2012).

In summary, assessment of the large body of studies comparing various long-term radiosonde and MSU products since AR4 is hampered by data set version changes, and inherent data uncertainties. These factors substantially limit the ability to draw robust and consistent inferences from such studies about the true long-term trends or the value of different data products.

2.4.4.3 Additional Evidence from Other Technologies and Approaches

Global Positioning System (GPS) radio occultation (RO) currently represents the only self-calibrated SI traceable raw satellite measurements (Anthes et al., 2008; Anthes, 2011). The fundamental observation is time delay of the occulted signal's phase traversing the atmosphere. The time delay is a function of several atmospheric physical state variables. Subsequent analysis converts the time delay to temperature and other parameters, which inevitably adds some degree of uncertainty to the derived temperature data. Intercomparisons of GPS-RO products show that differences are largest for derived geophysical parameters (including temperature), but are still small relative to other observing technologies (Ho et al., 2012). Comparisons to MSU and radiosondes (Kuo et al., 2005; Ho et al., 2007, 2009a, 2009b; He et al., 2009; Baringer et al., 2010; Sun et al., 2010; Ladstadter et al., 2011) show substantive agreement in interannual behaviour, but also some multi-year drifts that require further examination before this additional data source can usefully arbitrate between different MSU and radiosonde trend estimates.

Atmospheric winds are driven by thermal gradients. Radiosonde winds are far less affected by time-varying biases than their temperatures (Gruber and Haimberger, 2008; Sherwood et al., 2008; Section 2.7.3). Allen and Sherwood (2007) initially used radiosonde wind to infer temperatures within the Tropical West Pacific warm pool region, then extended this to a global analysis (Allen and Sherwood, 2008) yielding a distinct tropical upper tropospheric warming trend maximum within the vertical profile, but with large uncertainty. Winds can only quantify relative changes and require an initialization (location and trend at that location) (Allen and Sherwood, 2008). The large uncertainty range was predominantly driven by this initialization choice, a finding later confirmed by Christy et al. (2010), who in addition questioned the stability given the sparse geographical sampling, particularly in the tropics, and possible systematic sampling effects amongst other potential issues. Initializing closer to the tropics tended to reduce or remove the appearance of a tropical upper tropospheric warming trend maximum (Allen and Sherwood, 2008; Christy et al., 2010). There is only *low confidence* in trends inferred from 'thermal winds' given the relative immaturity of the analyses and their large uncertainties.

In summary, new technologies and approaches have emerged since AR4. However, these new technologies and approaches either constitute too short a record or are too immature to inform assessments of long-term trends at the present time.

2.4.4.4 Synthesis of Free Atmosphere Temperature Estimates

Global-mean lower tropospheric temperatures have increased since the mid-20th century (Figure 2.24, bottom). Structural uncertainties (Box 2.1) are larger than at the surface but it can still be concluded that globally the troposphere has warmed (Table 2.8). On top of this long-term trend are superimposed short-term variations that are highly correlated with those at the surface but of somewhat greater amplitude. Global mean lower stratospheric temperatures have decreased since the mid-20th century punctuated by short-lived warming events associated with explosive volcanic activity (Figure 2.24a). However, since the mid-1990s little net change has occurred. Cooling rates are on average greater from radiosonde data sets than MSU data sets. This *very likely* relates to widely recognized cooling biases in radiosondes (Mears et al., 2006) which all data set producers explicitly caution are *likely* to remain to some extent in their final products (Free and Seidel, 2007; Haimberger et al., 2008; Sherwood et al., 2008; Thorne et al., 2011).

In comparison to the surface (Figure 2.22), tropospheric layers exhibit smoother geographic trends (Figure 2.25) with warming dominating cooling north of approximately 45°S and greatest warming in high northern latitudes. The lower stratosphere cooled almost everywhere but this cooling exhibits substantial large-scale structure. Cooling is greatest in the highest southern latitudes and smallest in high northern latitudes. There are also secondary stratospheric cooling maxima in the mid-latitude regions of each hemisphere.

Available global and regional trends from radiosondes since 1958 (Figure 2.26) show agreement that the troposphere has warmed and the stratosphere cooled. While there is little ambiguity in the sign of the changes, the rate and vertical structure of change are distinctly data set dependent, particularly in the stratosphere. Differences are greatest in the tropics and SH extra-tropics where the historical radiosonde data coverage is poorest. Not shown in the figure for clarity are estimates of parametric data set uncertainties or trend-fit uncertainties—both of which are of the order of at least 0.1°C per decade (Section 2.4.4.1).

Differences in trends between available radiosonde data sets are greater during the satellite era than for the full radiosonde period of record in all regions and at most levels (Figure 2.27; cf. Figure 2.26). The RAOBCORE product exhibits greater vertical trend gradients than other data sets and it has been posited that this relates to its dependency on reanalysis fields (Sakamoto and Christy, 2009; Christy et al., 2010). MSU trend estimates in the troposphere are generally bracketed by the radiosonde range. In the stratosphere MSU deep layer estimates tend to show slightly less cooling. Over both 1958–2011 and 1979–2011 there is some evidence in the radiosonde products taken as a whole that the tropical tropospheric trends increase with height. But the magnitude and the structure is highly data set dependent.

In summary, based on multiple independent analyses of measurements from radiosondes and satellite sensors it is *virtually certain* that globally the troposphere has warmed and the stratosphere has cooled since the mid-20th century. Despite unanimous agreement on the sign of the trends, substantial disagreement exists among available estimates as to the rate of temperature changes, particularly outside the NH extra-tropical troposphere, which has been well sampled by radiosondes.

Table 2.8 | Trend estimates and 90% confidence intervals (Box 2.2) for radiosonde and MSU data set global average values over the radiosonde (1958–2012) and satellite periods (1979–2012). LT indicates Lower Troposphere, MT indicates Mid Troposphere and LS indicates Lower Stratosphere (Figure 2.23). Satellite records start only in 1979 and STAR do not produce an LT product.

Data Set	Trends in °C per decade					
	1958–2012			1979–2012		
	LT	MT	LS	LT	MT	LS
HadAT2 (Thorne et al., 2005)	0.159 ± 0.038	0.095 ± 0.034	-0.339 ± 0.086	0.162 ± 0.047	0.079 ± 0.057	-0.436 ± 0.204
RAOBCORE 1.5 (Haimberger et al., 2012)	0.156 ± 0.031	0.109 ± 0.029	-0.186 ± 0.087	0.139 ± 0.049	0.079 ± 0.054	-0.266 ± 0.227
RICH-obs (Haimberger et al., 2012)	0.162 ± 0.031	0.102 ± 0.029	-0.285 ± 0.087	0.158 ± 0.046	0.081 ± 0.052	-0.331 ± 0.241
RICH-tau (Haimberger et al., 2012)	0.168 ± 0.032	0.111 ± 0.030	-0.280 ± 0.085	0.160 ± 0.046	0.083 ± 0.052	-0.345 ± 0.238
RATPAC (Free et al., 2005)	0.136 ± 0.028	0.076 ± 0.028	-0.338 ± 0.092	0.128 ± 0.044	0.039 ± 0.051	-0.468 ± 0.225
UAH (Christy et al., 2003)				0.138 ± 0.043	0.043 ± 0.042	-0.372 ± 0.201
RSS (Mears and Wentz, 2009a, 2009b)				0.131 ± 0.045	0.079 ± 0.043	-0.268 ± 0.177
STAR (Zou and Wang, 2011)					0.123 ± 0.047	-0.320 ± 0.175

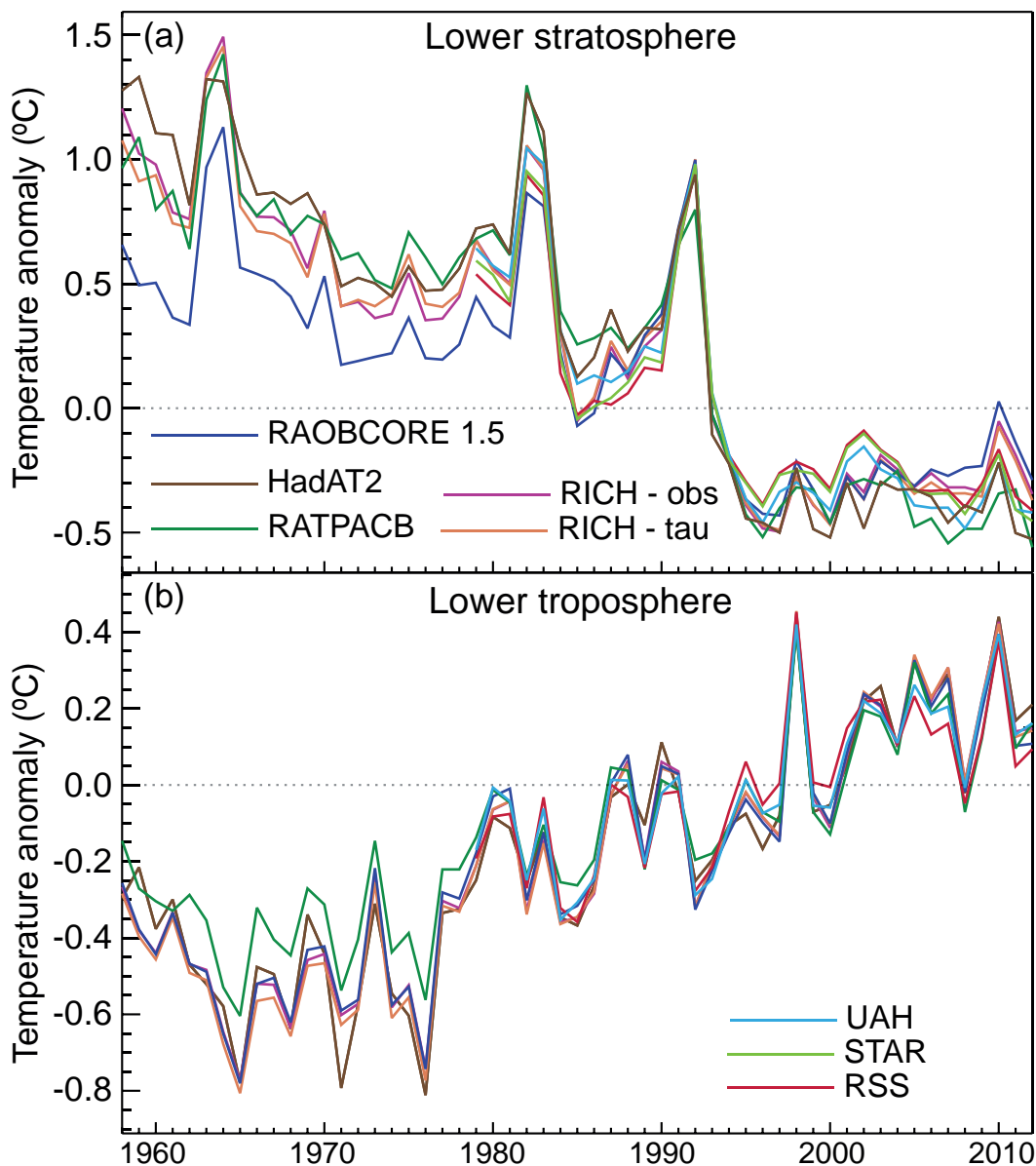


Figure 2.24 | Global annual average lower stratospheric (top) and lower tropospheric (bottom) temperature anomalies relative to a 1981–2010 climatology from different data sets. STAR does not produce a lower tropospheric temperature product. Note that the y-axis resolution differs between the two panels.

Frequently Asked Questions

FAQ 2.1 | How Do We Know the World Has Warmed?

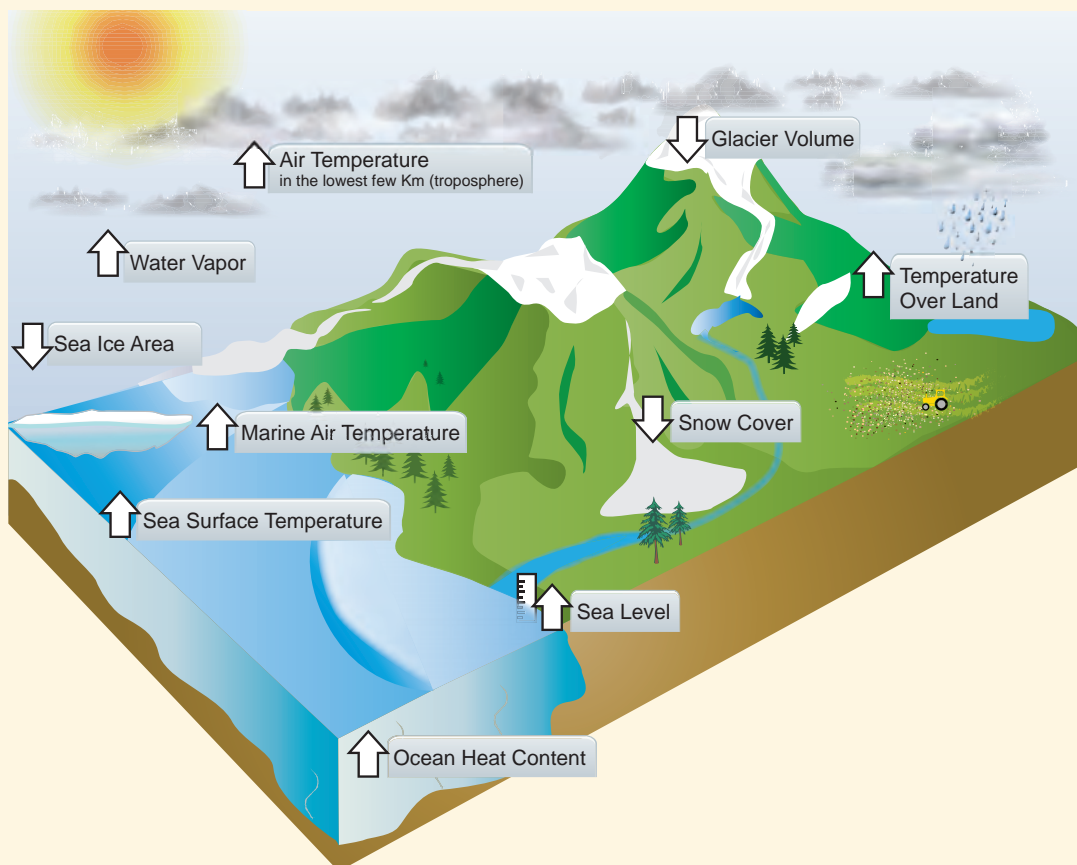
Evidence for a warming world comes from multiple independent climate indicators, from high up in the atmosphere to the depths of the oceans. They include changes in surface, atmospheric and oceanic temperatures; glaciers; snow cover; sea ice; sea level and atmospheric water vapour. Scientists from all over the world have independently verified this evidence many times. That the world has warmed since the 19th century is unequivocal.

Discussion about climate warming often centres on potential residual biases in temperature records from land-based weather stations. These records are very important, but they only represent one indicator of changes in the climate system. Broader evidence for a warming world comes from a wide range of independent physically consistent measurements of many other, strongly interlinked, elements of the climate system (FAQ 2.1, Figure 1).

A rise in global average surface temperatures is the best-known indicator of climate change. Although each year and even decade is not always warmer than the last, global surface temperatures have warmed substantially since 1900.

Warming land temperatures correspond closely with the observed warming trend over the oceans. Warming oceanic air temperatures, measured from aboard ships, and temperatures of the sea surface itself also coincide, as borne out by many independent analyses.

The atmosphere and ocean are both fluid bodies, so warming at the surface should also be seen in the lower atmosphere, and deeper down into the upper oceans, and observations confirm that this is indeed the case. Analyses of measurements made by weather balloon radiosondes and satellites consistently show warming of the troposphere, the active weather layer of the atmosphere. More than 90% of the excess energy absorbed by the climate system since at least the 1970s has been stored in the oceans as can be seen from global records of ocean heat content going back to the 1950s. (continued on next page)



FAQ 2.1, Figure 1 | Independent analyses of many components of the climate system that would be expected to change in a warming world exhibit trends consistent with warming (arrow direction denotes the sign of the change), as shown in FAQ 2.1, Figure 2.

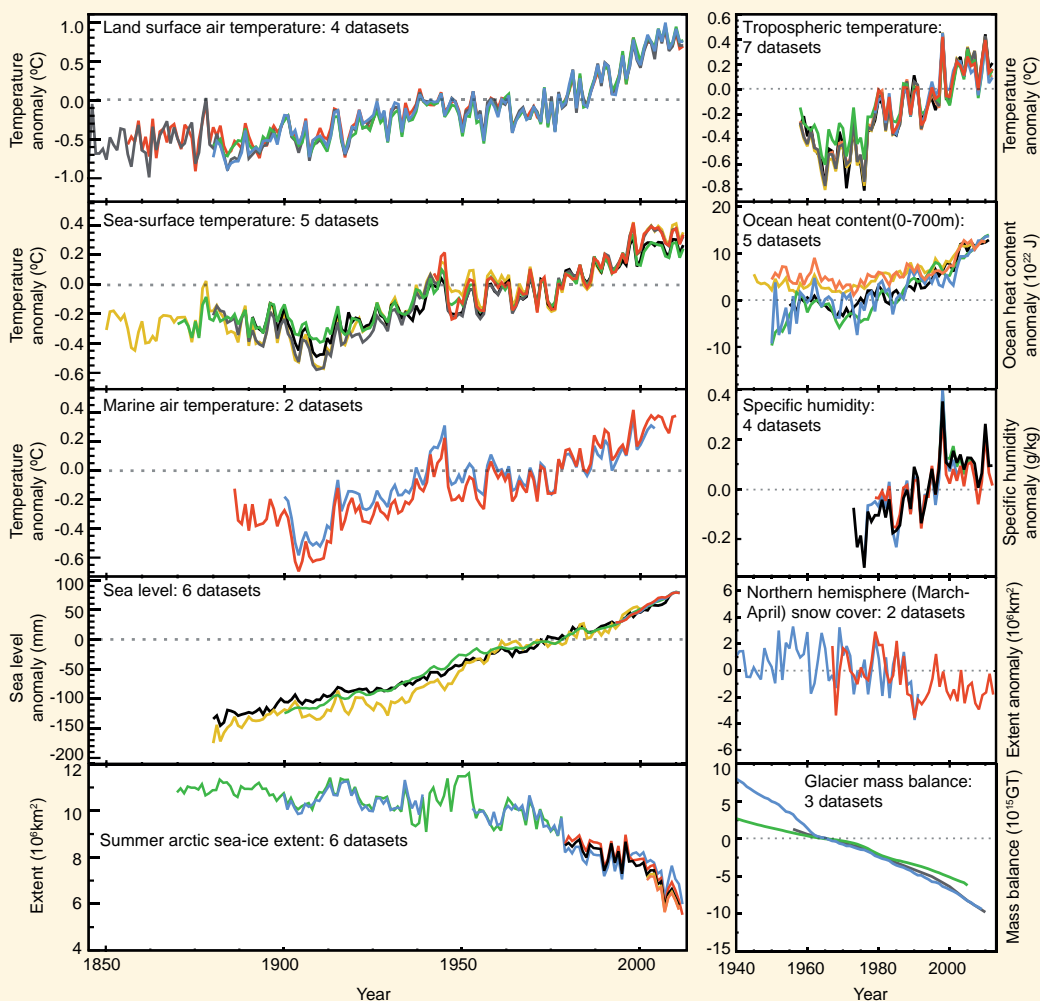
FAQ 2.1 (continued)

As the oceans warm, the water itself expands. This expansion is one of the main drivers of the independently observed rise in sea levels over the past century. Melting of glaciers and ice sheets also contribute, as do changes in storage and usage of water on land.

A warmer world is also a moister one, because warmer air can hold more water vapour. Global analyses show that specific humidity, which measures the amount of water vapour in the atmosphere, has increased over both the land and the oceans.

The frozen parts of the planet—known collectively as the cryosphere—affect, and are affected by, local changes in temperature. The amount of ice contained in glaciers globally has been declining every year for more than 20 years, and the lost mass contributes, in part, to the observed rise in sea level. Snow cover is sensitive to changes in temperature, particularly during the spring, when snow starts to melt. Spring snow cover has shrunk across the NH since the 1950s. Substantial losses in Arctic sea ice have been observed since satellite records began, particularly at the time of the minimum extent, which occurs in September at the end of the annual melt season. By contrast, the increase in Antarctic sea ice has been smaller.

Individually, any single analysis might be unconvincing, but analysis of these different indicators and independent data sets has led many independent research groups to *all* reach the same conclusion. From the deep oceans to the top of the troposphere, the evidence of warmer air and oceans, of melting ice and rising seas all points unequivocally to one thing: the world has warmed since the late 19th century (FAQ 2.1, Figure 2).



FAQ 2.1, Figure 2 | Multiple independent indicators of a changing global climate. Each line represents an independently derived estimate of change in the climate element. In each panel all data sets have been normalized to a common period of record. A full detailing of which source data sets go into which panel is given in the Supplementary Material 2.SM.5.

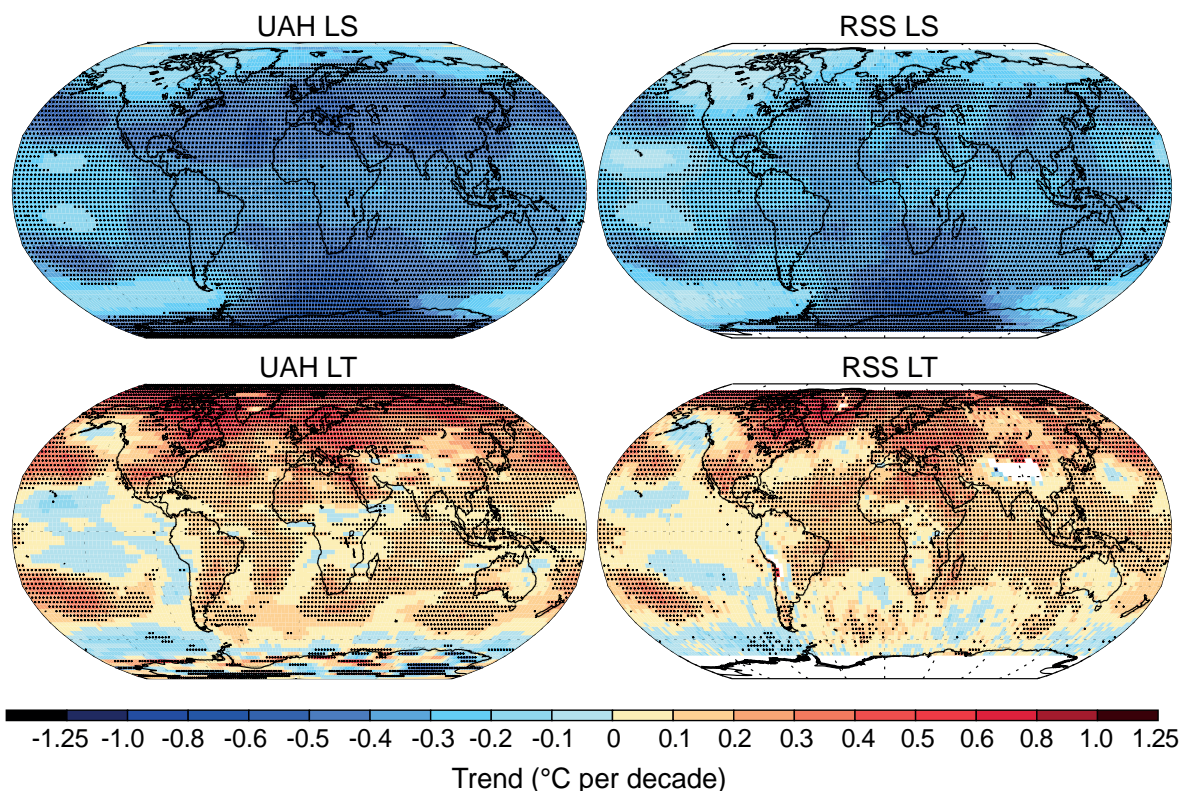


Figure 2.25 | Trends in MSU upper air temperature over 1979–2012 from UAH (left-hand panels) and RSS (right-hand panels) and for LS (top row) and LT (bottom row). Data are temporally complete within the sampled domains for each data set. White areas indicate incomplete or missing data. Black plus signs (+) indicate grid boxes where trends are significant (i.e., a trend of zero lies outside the 90% confidence interval).

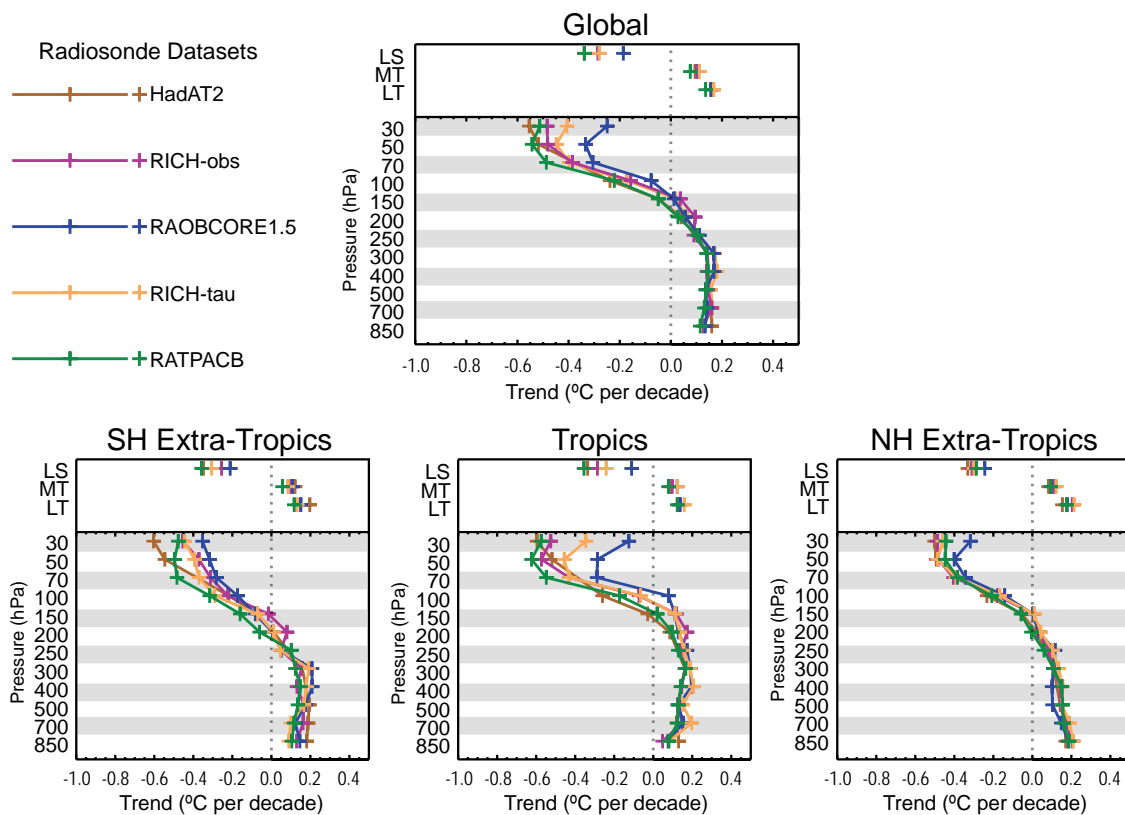


Figure 2.26 | Trends in upper air temperature for all available radiosonde data products that contain records for 1958–2012 for the globe (top) and tropics (20°N to 20°S) and extra-tropics (bottom). The bottom panel trace in each case is for trends on distinct pressure levels. Note that the pressure axis is not linear. The top panel points show MSU layer measure trends. MSU layer equivalents have been processed using the method of Thorne et al. (2005). No attempts have been made to sub-sample to a common data mask.

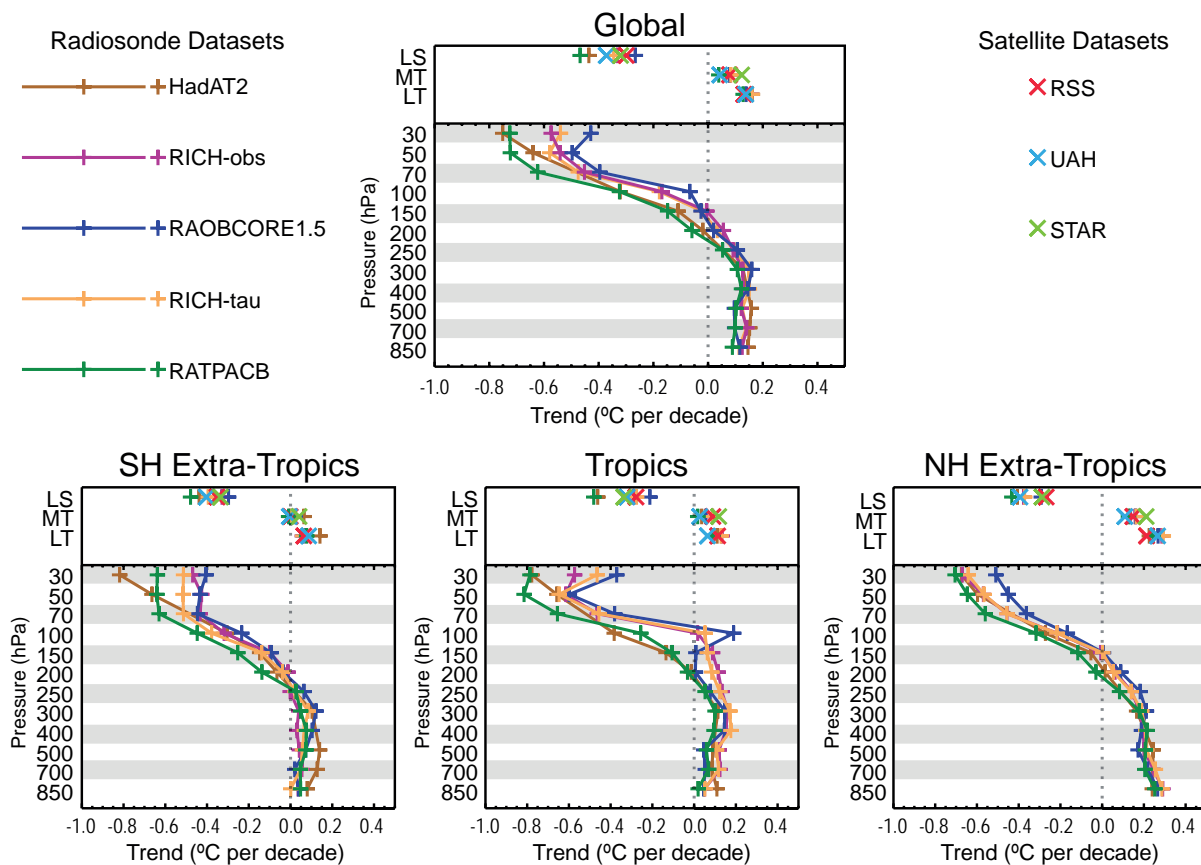


Figure 2.27 | As Figure 2.26 except for the satellite era 1979–2012 period and including MSU products (RSS, STAR and UAH).

Hence there is only *medium confidence* in the rate of change and its vertical structure in the NH extratropical troposphere and *low confidence* elsewhere.

2.5 Changes in Hydrological Cycle

This section covers the main aspects of the hydrological cycle, including large-scale average precipitation, stream flow and runoff, soil moisture, atmospheric water vapour, and clouds. Meteorological drought is assessed in Section 2.6. Ocean precipitation changes are assessed in Section 3.4.3 and changes in the area covered by snow in Section 4.5.

2.5.1 Large-Scale Changes in Precipitation

2.5.1.1 Global Land Areas

AR4 concluded that precipitation has generally increased over land north of 30°N over the period 1900–2005 but downward trends dominate the tropics since the 1970s. AR4 included analysis of both the GHCN (Vose et al., 1992) and CRU (Mitchell and Jones, 2005) gauge-based precipitation data sets for the globally averaged annual precipitation over land. For both data sets the overall linear trend from 1900 to 2005 (1901–2002 for CRU) was positive but not statistically significant (Table 3.4 from AR4). Other periods covered in AR4 (1951–2005 and 1979–2005) showed a mix of negative and positive trends depending on the data set.

Since AR4, existing data sets have been updated and a new data set developed. Figure 2.28 shows the century-scale variations and trends on globally and zonally averaged annual precipitation using five data sets: GHCN V2 (updated through 2011; Vose et al., 1992), Global Precipitation Climatology Project V2.2 (GPCP) combined raingauge–satellite product (Adler et al., 2003), CRU TS 3.10.01 (updated from Mitchell and Jones, 2005), Global Precipitation Climatology Centre V6 (GPCC) data set (Becker et al., 2013) and a reconstructed data set by Smith et al. (2012). Each data product incorporates a different number of station series for each region. The Smith et al. product is a statistical reconstruction using Empirical Orthogonal Functions, similar to the NCDC MLOST global temperature product (Section 2.4.3) that does provide coverage for most of the global surface area although only land is included here. The data sets based on *in situ* observations only start in 1901, but the Smith et al. data set ends in 2008, while the other three data sets contain data until at least 2010.

For the longest common period of record (1901–2008) all datasets exhibit increases in globally averaged precipitation, with three of the four showing statistically significant changes (Table 2.9). However, there is a factor of almost three spread in the magnitude of the change which serves to create *low confidence*. Global trends for the shorter period (1951–2008) show a mix of statistically non-significant positive and negative trends amongst the four data sets with the infilled Smith et al. (2012) analysis showing increases and the remainder decreases. These differences among data sets indicate that long-term increases

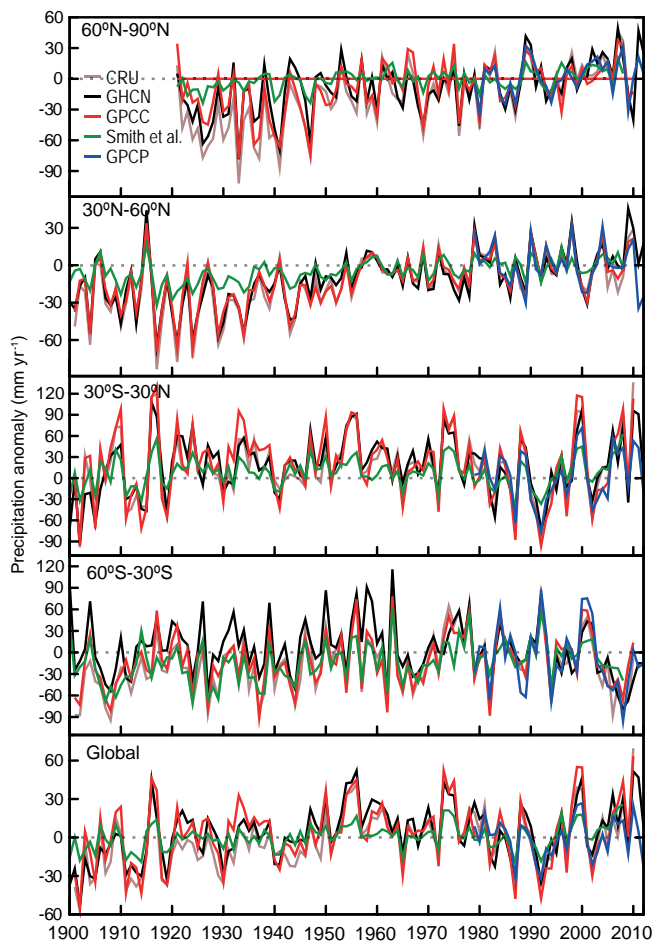


Figure 2.28 | Annual precipitation anomalies averaged over land areas for four latitudinal bands and the globe from five global precipitation data sets relative to a 1981–2000 climatology.

in global precipitation discussed in AR4 are uncertain, owing in part to issues in data coverage in the early part of the 20th century (Wan et al., 2013).

In summary, *confidence* in precipitation change averaged over global land areas is *low* for the years prior to 1950 and *medium* afterwards because of insufficient data, particularly in the earlier part of the record. Available globally incomplete records show mixed and non-significant long-term trends in reported global mean changes. Further, when virtually all the land area is filled in using a reconstruction method, the resulting time series shows less change in land-based precipitation since 1900.

Table 2.9 | Trend estimates and 90% confidence intervals (Box 2.2) for annual precipitation for each time series in Figure 2.28 over two common periods of record.

Data Set	Area	Trends in mm yr ⁻¹ per decade	
		1901–2008	1951–2008
CRU TS 3.10.01 (updated from Mitchell and Jones, 2005)	Global	2.77 ± 1.46	-2.12 ± 3.52
GHCN V2 (updated through 2011; Vose et al., 1992)	Global	2.08 ± 1.66	-2.77 ± 3.92
GPCC V6 (Becker et al., 2013)	Global	1.48 ± 1.65	-1.54 ± 4.50
Smith et al. (2012)	Global	1.01 ± 0.64	0.68 ± 2.07

2.5.1.2 Spatial Variability of Observed Trends

The latitude band plots in Figure 2.28 suggest that precipitation over tropical land areas (30°S to 30°N) has increased over the last decade reversing the drying trend that occurred from the mid-1970s to mid-1990s. As a result the period 1951–2008 shows no significant overall trend in tropical land precipitation in any of the datasets (Table 2.10). Longer term trends (1901–2008) in the tropics, shown in Table 2.10, are also non-significant for each of the four data sets. The mid-latitudes of the NH (30°N to 60°N) show an overall increase in precipitation from 1901 to 2008 with statistically significant trends for each data set. For the shorter period (1951–2008) the trends are also positive but non-significant for three of the four data sets. For the high latitudes of the NH (60°N to 90°N) where data completeness permits trend calculations solely for the 1951–2008 period, all datasets show increases but there is a wide range of magnitudes and the infilled Smith et al. series shows small and insignificant trends (Table 2.10). Fewer data from high latitude stations make these trends less certain and yield *low confidence* in resulting zonal band average estimates. In the mid-latitudes of the SH (60°S to 30°S) there is limited evidence of long-term increases with three data sets showing significant trends for the 1901–2008 period but GHCN having negative trends that are not significant. For the 1951–2008 period changes in SH mid-latitude precipitation are less certain, with one data set showing a significant trend towards drying, two showing non-significant drying trends and the final dataset suggesting increases in precipitation. All data sets show an abrupt decline in SH mid-latitude precipitation in the early 2000s (Figure 2.28) consistent with enhanced drying that has very recently recovered. These results for latitudinal changes are broadly consistent with the global satellite observations for the 1979–2008 period (Allan et al., 2010) and land-based gauge measurements for the 1950–1999 period (Zhang et al., 2007a).

In AR4, maps of observed trends of annual precipitation for 1901–2005 were calculated using GHCN interpolated to a 5° × 5° latitude/longitude grid. Trends (in percent per decade) were calculated for each grid box and showed statistically significant changes, particularly increases in eastern and northwestern North America, parts of Europe and Russia, southern South America and Australia, declines in the Sahel region of Africa, and a few scattered declines elsewhere.

Figure 2.29 shows the spatial variability of long-term trends (1901–2010) and more recent trends (1951–2010) over land in annual precipitation using the CRU, GHCN and GPC data sets. The trends are computed from land-only grid box time series using each native data set grid resolution. The patterns of these absolute trends (in mm yr⁻¹ per decade) are broadly similar to the trends (in percent per decade) relative

Table 2.10 | Trend estimates and 90% confidence intervals (Box 2.2) for annual precipitation for each time series in Figure 2.28 over two periods. Dashes indicate not enough data available for trend calculation. For the latitudinal band 90°S to 60°S not enough data exist for each product in either period.

Data Set	Area	Trends in mm yr ⁻¹ per decade	
		1901–2008	1951–2008
CRU TS 3.10.01 (updated from Mitchell and Jones, 2005)	60°N–90°N	–	5.82 ± 2.72
	30°N–60°N	3.82 ± 1.14	1.13 ± 2.01
	30°S–30°N	0.89 ± 2.89	–4.22 ± 8.27
	60°S–30°S	3.88 ± 2.28	–3.73 ± 5.94
GHCN V2 (updated through 2011; Vose et al., 1992)	60°N–90°N	–	4.52 ± 2.64
	30°N–60°N	3.23 ± 1.10	1.39 ± 1.98
	30°S–30°N	1.01 ± 3.00	–5.15 ± 7.28
	60°S–30°S	–0.57 ± 2.27	–8.01 ± 5.63
GPCC V6 (Becker et al., 2013)	60°N–90°N	–	2.69 ± 2.54
	30°N–60°N	3.14 ± 1.05	1.50 ± 1.93
	30°S–30°N	–0.48 ± 3.35	–4.16 ± 9.65
	60°S–30°S	2.40 ± 2.01	–0.51 ± 5.45
Smith et al. (2012)	60°N–90°N	–	0.63 ± 1.27
	30°N–60°N	1.44 ± 0.50	0.97 ± 0.88
	30°S–30°N	0.43 ± 1.48	0.67 ± 4.75
	60°S–30°S	2.94 ± 1.40	0.78 ± 3.31

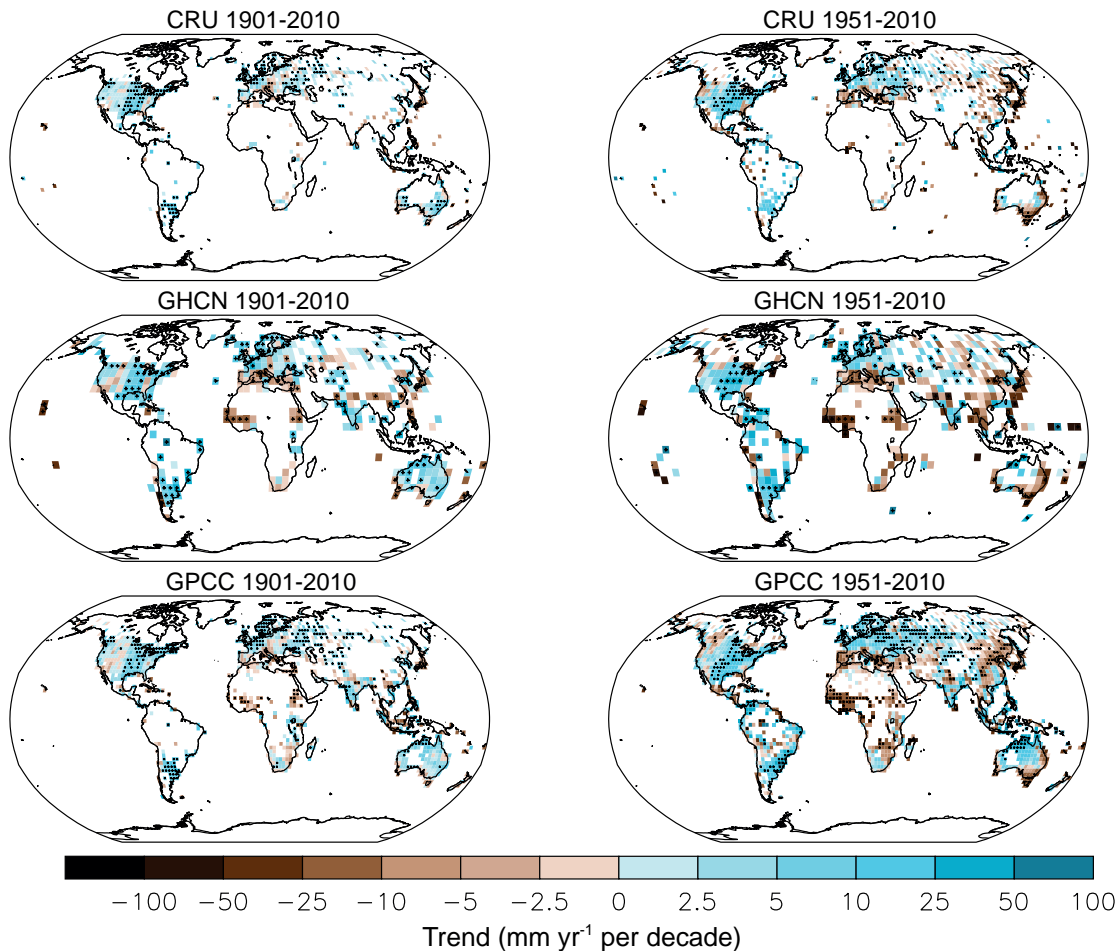


Figure 2.29 | Trends in annual precipitation over land from the CRU, GHCN and GPCC data sets for 1901–2010 (left-hand panels) and 1951–2010 (right-hand panels). Trends have been calculated only for those grid boxes with greater than 70% complete records and more than 20% data availability in first and last decile of the period. White areas indicate incomplete or missing data. Black plus signs (+) indicate grid boxes where trends are significant (i.e., a trend of zero lies outside the 90% confidence interval).

to local climatology (Supplementary Material 2.SM.6.1). Increases for the period 1901–2010 are seen in the mid- and higher-latitudes of both the NH and SH consistent with the reported changes for latitudinal bands. At the grid box scale, statistically significant trends occur in most of the same areas, in each data set but are far more limited than for temperature over a similar length period (cf. Figure 2.21). The GPCP map shows the most areas with significant trends. Comparing the maps in Figure 2.29, most areas for which trends can be calculated for both periods show similar trends between the 1901–2010 period and the 1951–2010 period with few exceptions (e.g., South Eastern Australia,). Trends over shorter periods can differ from those implied for the longest periods. For example, since the late 1980s trends in the Sahel region have been significantly positive (not shown).

In summary, when averaged over the land areas of the mid-latitudes of the NH, all datasets show a *likely* overall increase in precipitation (*medium confidence* since 1901, but *high confidence* after 1951). For all other zones one or more of data sparsity, quality, or a lack of quantitative agreement amongst available estimates yields *low confidence* in characterisation of such long-term trends in zonally averaged precipitation. Nevertheless, changes in some more regional or shorter-term recent changes can be quantified. It is *likely* there was an abrupt decline in SH mid-latitude precipitation in the early 2000s consistent with enhanced drying that has very recently recovered. Precipitation in the tropical land areas has increased (*medium confidence*) over the last decade, reversing the drying trend that occurred from the mid-1970s to mid-1990s reported in AR4.

2.5.1.3 Changes in Snowfall

AR4 draws no conclusion on global changes in snowfall. Changes in snowfall are discussed on a region-by-region basis, but focussed mainly on North America and Eurasia. Statistically significant increases were found in most of Canada, parts of northern Europe and Russia. A number of areas showed a decline in the number of snowfall events, especially those where climatological averaged temperatures were close to 0°C and where warming led to earlier onset of spring. Also, an increase in lake-effect snowfall was found for areas near the North American Great Lakes.

Since AR4, most published literature has considered again changes in snowfall in North America. These studies have confirmed that more winter-time precipitation is falling as rain rather than snow in the western USA (Knowles et al., 2006), the Pacific Northwest and Central USA (Feng and Hu, 2007). Kunkel et al. (2009) analyzed trends using a specially quality-controlled data set of snowfall observations over the contiguous USA and found that snowfall has been declining in the western USA, northeastern USA and southern margins of the seasonal snow region, but increasing in the western Great Plains and Great Lakes regions. Snowfall in Canada has increased mainly in the north while a significant decrease was observed in the southwestern part of the country for 1950–2009 (Mekis and Vincent, 2011).

Other regions that have been analyzed include Japan (Takeuchi et al., 2008), where warmer winters in the heavy snowfall areas on Honshu are associated with decreases in snowfall and precipitation in general. Shekar et al. (2010) found declines in total seasonal snowfall along

with increases in maximum and minimum temperatures in the western Himalaya. Serquet et al. (2011) analyzed snowfall and rainfall days since 1961 and found the proportion of snowfall days to rainfall days in Switzerland was declining in association with increasing temperatures. Scherrer and Appenzeller (2006) found a trend in a pattern of variability of snowfall in the Swiss Alps that indicated decreasing snow at low altitudes relative to high altitudes, but with large decadal variability in key snow indicators (Scherrer et al., 2013). Van Ommen and Morgan (2010) draw a link between increased snowfall in coastal East Antarctica and increased southwest Western Australia drought. However, Monaghan and Bromwich (2008) found an increase in snow accumulation over all Antarctica from the late 1950s to 1990, then a decline to 2004. Thus snowfall changes in Antarctica remain uncertain.

In summary, in most regions analyzed, it is *likely* that decreasing numbers of snowfall events are occurring where increased winter temperatures have been observed (North America, Europe, Southern and East Asia). *Confidence* is *low* for the changes in snowfall over Antarctica.

2.5.2 Streamflow and Runoff

AR4 concluded that runoff and river discharge generally increased at high latitudes, with some exceptions. No consistent long-term trend in discharge was reported for the world's major rivers on a global scale.

River discharge is unique among water cycle components in that it both spatially and temporally integrates surplus waters upstream within a catchment (Shiklomanov et al., 2010) which makes it well suited for *in situ* monitoring (Arndt et al., 2010). The most recent comprehensive analyses (Milliman et al., 2008; Dai et al., 2009) do not support earlier work (Labat et al., 2004) that reported an increasing trend in global river discharge associated with global warming during the 20th century. It must be noted that many if not most large rivers, especially those for which a long-term streamflow record exists, have been impacted by human influences such as dam construction or land use, so results must be interpreted with caution. Dai et al. (2009) assembled a data set of 925 most downstream stations on the largest rivers monitoring 80% of the global ocean draining land areas and capturing 73% of the continental runoff. They found that discharges in about one-third of the 200 largest rivers (including the Congo, Mississippi, Yenisey, Paraná, Ganges, Colombia, Uruguay and Niger) show statistically significant trends during 1948–2004, with the rivers having downward trends (45) outnumbering those with upward trends (19). Decreases in streamflow were found over many low and mid-latitude river basins such as the Yellow River in northern China since 1960s (Piao et al., 2010) where precipitation has decreased. Increases in streamflow during the latter half of the 20th century also have been reported over regions with increased precipitation, such as parts of the USA (Groisman et al., 2004), and in the Yangtze River in southern China (Piao et al., 2010). In the Amazon basin an increase of discharge extremes is observed over recent decades (Espinoza Villar et al., 2009). For France, Giuntoli et al. (2013) found that the sign of the temporal trends in natural streamflows varies with period studied. In that case study, significant correlations between median to low flows and the Atlantic Multidecadal Oscillation (AMO; Section 2.7.8) result in long quasi-periodic oscillations.

At high latitudes, increasing winter base flow and mean annual stream flow resulting from possible permafrost thawing were reported in northwest Canada (St. Jacques and Sauchyn, 2009). Rising minimum daily flows also have been observed in northern Eurasian rivers (Smith et al., 2007). For ocean basins other than the Arctic, and for the global ocean as a whole, the data for continental discharge show small or downward trends, which are statistically significant for the Pacific ($-9.4 \text{ km}^3 \text{ yr}^{-1}$). Precipitation is a major driver for the discharge trends and for the large interannual-to-decadal variations (Dai et al., 2009). However, for the Arctic drainage areas, Adam and Lettenmaier (2008) found that upward trends in streamflow are not accompanied by increasing precipitation, especially over Siberia, based on available observations. Zhang et al. (2012a) argued that precipitation measurements are sparse and exhibit large cold-season biases in the Arctic drainage areas and hence there would be large uncertainties using these data to investigate their influence on streamflow.

Recently, Stahl et al. (2010) and Stahl and Tallaksen (2012) investigated streamflow trends based on a data set of near-natural streamflow records from more than 400 small catchments in 15 countries across Europe for 1962–2004. A regional coherent pattern of annual streamflow trends was revealed with negative trends in southern and eastern regions, and generally positive trends elsewhere. Subtle regional differences in the subannual changes in various streamflow metrics also can be captured in regional studies such as by Monk et al. (2011) for Canadian rivers.

In summary, the most recent comprehensive analyses lead to the conclusion that *confidence* is *low* for an increasing trend in global river discharge during the 20th century.

2.5.3 Evapotranspiration Including Pan Evaporation

AR4 concluded that decreasing trends were found in records of pan evaporation over recent decades over the USA, India, Australia, New Zealand, China and Thailand and speculated on the causes including decreased surface solar radiation, sunshine duration, increased specific humidity and increased clouds. However, AR4 also reported that direct measurements of evapotranspiration over global land areas are scarce, and concluded that reanalysis evaporation fields are not reliable because they are not well constrained by precipitation and radiation.

Since AR4 gridded data sets have been developed that estimate actual evapotranspiration from either atmospheric forcing and thermal remote sensing, sometimes in combination with direct measurements (e.g., from FLUXNET, a global network of flux towers), or interpolation of FLUXNET data using regression techniques, providing an unprecedented look at global evapotranspiration (Mueller et al., 2011). On a global scale, evapotranspiration over land increased from the early 1980s up to the late 1990s (Wild et al., 2008; Jung et al., 2010; Wang et al., 2010) and Wang et al. (2010) found that global evapotranspiration increased at a rate of 0.6 W m^{-2} per decade for the period 1982–2002. After 1998, a lack of moisture availability in SH land areas, particularly decreasing soil moisture, has acted as a constraint to further increase of global evapotranspiration (Jung et al., 2010).

Zhang et al. (2007b) found decreasing pan evaporation at stations across the Tibetan Plateau, even with increasing air temperature. Similarly, decreases in pan evaporation were also found for northeastern India (Jhajharia et al., 2009) and the Canadian Prairies (Burn and Hesch, 2007). A continuous decrease in reference and pan evaporation for the period 1960–2000 was reported by Xu et al. (2006a) for a humid region in China, consistent with reported continuous increase in aerosol levels over China (Qian et al., 2006; Section 2.2.4). Roderick et al. (2007) examined the relationship between pan evaporation changes and many of the possible causes listed above using a physical model and conclude that many of the decreases (USA, China, Tibetan Plateau, Australia) cited previously are related to declining wind speeds and to a lesser extent decreasing solar radiation. Fu et al. (2009) provided an overview of pan evaporation trends and concluded the major possible causes, changes in wind speed, humidity and solar radiation, have been occurring, but that the importance of each is regionally dependent.

The recent increase in incoming shortwave radiation in regions with decreasing aerosol concentrations (Section 2.2.3) can explain positive evapotranspiration trends only in the humid part of Europe. In semiarid and arid regions, trends in evapotranspiration largely follow trends in precipitation (Jung et al., 2010). Trends in surface winds (Section 2.7.2) and CO_2 (Section 2.2.1.1.1) also alter the partitioning of available energy into evapotranspiration and sensible heat. While surface wind trends may explain pan evaporation trends over Australia (Rayner, 2007; Roderick et al., 2007), their impact on actual evapotranspiration is limited due to the compensating effect of boundary-layer feedbacks (van Heerwaarden et al., 2010). In vegetated regions, where a large part of evapotranspiration comes from transpiration through plants' stomata, rising CO_2 concentrations can lead to reduced stomatal opening and evapotranspiration (Idso and Brazel, 1984; Leakey et al., 2006). Additional regional effects that impact evapotranspiration trends are lengthening of the growing season and land use change.

In summary, there is *medium confidence* that pan evaporation continued to decline in most regions studied since AR4 related to changes in wind speed, solar radiation and humidity. On a global scale, evapotranspiration over land increased (*medium confidence*) from the early 1980s up to the late 1990s. After 1998, a lack of moisture availability in SH land areas, particularly decreasing soil moisture, has acted as a constraint to further increase of global evapotranspiration.

2.5.4 Surface Humidity

AR4 reported widespread increases in surface air moisture content since 1976, along with near-constant relative humidity over large scales though with some significant changes specific to region, time of day or season.

In good agreement with previous analysis from Dai (2006), Willett et al. (2008) show widespread increasing specific humidity across the globe from the homogenized gridded monthly mean anomaly product HadCRUH (1973–2003). Both Dai and HadCRUH products that are blended land and ocean data products end in 2003 but HadISDH (1973–2012) (Willett et al., 2013) and the NOCS product (Berry and Kent, 2009) are available over the land and ocean respectively through 2012. There

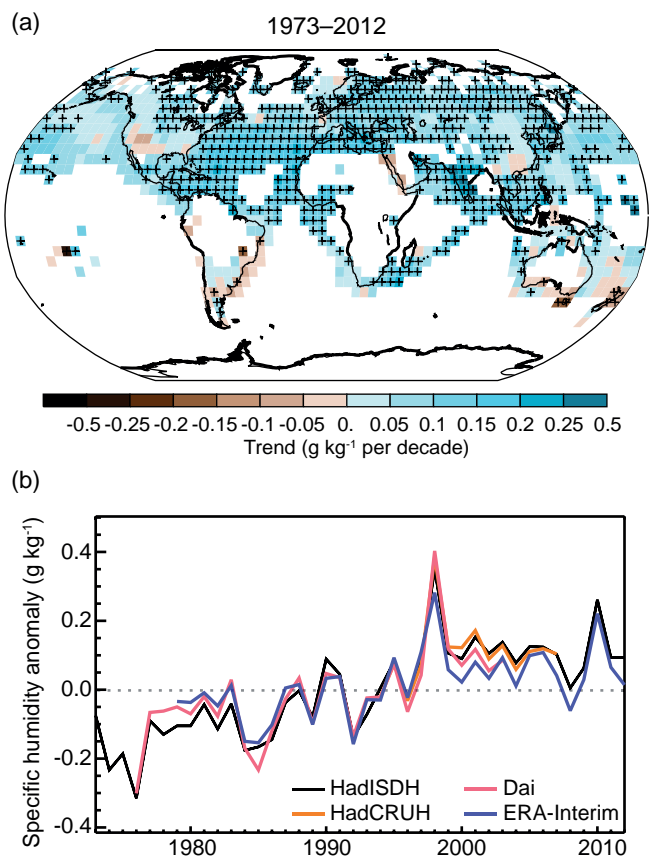


Figure 2.30 | (a) Trends in surface specific humidity from HadISDH and NOCS over 1973–2012. Trends have been calculated only for those grid boxes with greater than 70% complete records and more than 20% data availability in first and last decile of the period. White areas indicate incomplete or missing data. Black plus signs (+) indicate grid boxes where trends are significant (i.e., a trend of zero lies outside the 90% confidence interval). (b) Global annual average anomalies in land surface specific humidity from Dai (2006; red), HadCRUH (Willett et al., 2013; orange), HadISDH (Willett et al., 2013; black), and ERA-Interim (Simmons et al., 2010; blue). Anomalies are relative to the 1979–2003 climatology.

are some small isolated but coherent areas of drying over some of the more arid land regions (Figure 2.30a). Moistening is largest in the tropics and in the extratropics during summer over both land and ocean. Large uncertainty remains over the SH where data are sparse. Global specific humidity is sensitive to large-scale phenomena such as ENSO (Figure 2.30b; Box 2.5). It is strongly correlated with land surface temperature averages over the 23 Giorgi and Francisco (2000) regions for the period 1973–1999 and exhibits increases mostly at or above the

increase expected from the Clausius–Clapeyron relation (about 7% °C⁻¹; Annex III: Glossary) with *high confidence* (Willett et al., 2010). Land surface humidity trends are similar in ERA-Interim to observed estimates of homogeneity-adjusted data sets (Simmons et al., 2010; Figure 2.30b).

Since 2000 surface specific humidity over land has remained largely unchanged (Figure 2.30) whereas land areas have on average warmed slightly (Figure 2.14), implying a reduction in land region relative humidity. This may be linked to the greater warming of the land surface relative to the ocean surface (Joshi et al., 2008). The marine specific humidity (Berry and Kent, 2009), like that over land, shows widespread increases that correlate strongly with SST. However, there is a marked decline in marine relative humidity around 1982. This is reported in Willett et al. (2008) where its origin is concluded to be a non-climatic data issue owing to a change in reporting practice for dewpoint temperature.

In summary, it is *very likely* that global near surface air specific humidity has increased since the 1970s. However, during recent years the near surface moistening over land has abated (*medium confidence*). As a result, fairly widespread decreases in relative humidity near the surface are observed over the land in recent years.

2.5.5 Tropospheric Humidity

As reported in AR4, observations from radiosonde and GPS measurements over land, and satellite measurements over ocean indicate increases in tropospheric water vapour at near-global spatial scales which are consistent with the observed increase in atmospheric temperature over the last several decades. Tropospheric water vapour plays an important role in regulating the energy balance of the surface and TOA, provides a key feedback mechanism and is essential to the formation of clouds and precipitation.

2.5.5.1 Radiosonde

Radiosonde humidity data for the troposphere were used sparingly in AR4, noting a renewed appreciation for biases with the operational radiosonde data that had been highlighted by several major field campaigns and intercomparisons. Since AR4 there have been three distinct efforts to homogenize the tropospheric humidity records from operational radiosonde measurements (Durre et al., 2009; McCarthy et al., 2009; Dai et al., 2011) (Supplementary Material 2.SM.6.1, Table 2.SM.9). Over the common period of record from 1973 onwards, the resulting estimates are in substantive agreement regarding specific

Table 2.11 | Trend estimates and 90% confidence intervals (Box 2.2) for surface humidity over two periods.

	Data Set	Trends in % per decade	
		1976–2003	1973–2012
Land	HadISDH (Willett et al., 2008)	0.127 ± 0.037	0.091 ± 0.023
	HadCRUH_land (Willett et al., 2008)	0.128 ± 0.043	
	Dai_land (Dai, 2006)	0.099 ± 0.046	
Ocean	NOCS (Berry and Kent, 2009)	0.114 ± 0.064	0.090 ± 0.033
	HadCRUH_marine (Willett et al., 2008)	0.065 ± 0.049	
	Dai_marine (Dai, 2006)	0.058 ± 0.044	

humidity trends at the largest geographical scales. On average, the impact of the correction procedures is to remove an artificial temporal trend towards drying in the raw data and indicate a positive trend in free tropospheric specific humidity over the period of record. In each analysis, the rate of increase in the free troposphere is concluded to be largely consistent with that expected from the Clausius–Clapeyron relation (about 7% per degree Celsius). There is no evidence for a significant change in free tropospheric relative humidity, although a decrease in relative humidity at lower levels is observed (Section 2.5.5). Indeed, McCarthy et al. (2009) show close agreement between their radiosonde product at the lowest levels and HadCRUH (Willett et al., 2008).

2.5.5.2 Global Positioning System

Since the early 1990s, estimates of column integrated water vapour have been obtained from ground-based Global Positioning System (GPS) receivers. An international network started with about 100 stations in 1997 and has currently been expanded to more than 500 (primarily land-based) stations. Several studies have compiled GPS water vapour data sets for climate studies (Jin et al., 2007; Wang et al., 2007; Wang and Zhang, 2008, 2009). Using such data, Mears et al. (2010) demonstrated general agreement of the interannual anomalies between ocean-based satellite and land-based GPS column integrated water vapour data. The interannual water vapour anomalies are closely tied to the atmospheric temperature changes in a manner consistent with that expected from the Clausius–Clapeyron relation. Jin et al. (2007) found an average column integrated water vapour trend of about 2 kg m^{-2} per decade during 1994–2006 for 150 (primarily land-based) stations over the globe, with positive trends at most NH stations and negative trends in the SH. However, given the short length (about 10 years) of the GPS records, the estimated trends are very sensitive to the start and end years and the analyzed time period (Box 2.2).

2.5.5.3 Satellite

AR4 reported positive decadal trends in lower and upper tropospheric water vapour based on satellite observations for the period 1988–2004. Since AR4, there has been continued evidence for increases in lower tropospheric water vapour from microwave satellite measurements of column integrated water vapour over oceans (Santer et al., 2007; Wentz et al., 2007) and globally from satellite measurements of spectrally resolved reflected solar radiation (Mieruch et al., 2008). The interannual variability and longer-term trends in column-integrated water vapour over oceans are closely tied to changes in SST at the global scale and interannual anomalies show remarkable agreement with low-level specific humidity anomalies from HadCRUH (O’Gorman et al., 2012). The rate of moistening at large spatial scales over oceans is close to that expected from the Clausius–Clapeyron relation (about 7% per degree Celsius) with invariant relative humidity (Figure 2.31). Satellite measurements also indicate that the globally averaged upper tropospheric relative humidity has changed little over the period 1979–2010 while the troposphere has warmed, implying an increase in the mean water vapour mass in the upper troposphere (Shi and Bates, 2011).

Interannual variations in temperature and upper tropospheric water vapour from IR satellite data are consistent with a constant RH

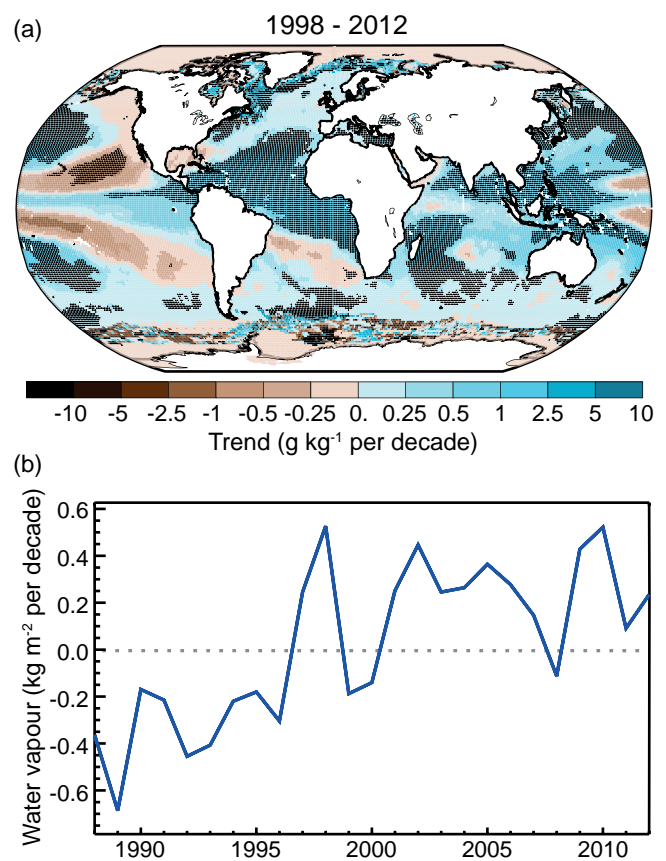


Figure 2.31 | (a) Trends in column integrated water vapour over ocean surfaces from Special Sensor Microwave Imager (Wentz et al., 2007) for the period 1988–2010. Trends have been calculated only for those grid boxes with greater than 70% complete records and more than 20% data availability in first and last decile of the period. Black plus signs (+) indicate grid boxes where trends are significant (i.e., a trend of zero lies outside the 90% confidence interval). (b) Global annual average anomalies in column integrated water vapour averaged over ocean surfaces. Anomalies are relative to the 1988–2007 average.

behavior at large spatial scales (Dessler et al., 2008; Gettelman and Fu, 2008; Chung et al., 2010). On decadal time-scales, increased GHG concentrations reduce clear-sky outgoing long-wave radiation (Allan, 2009; Chung and Soden, 2010), thereby influencing inferred relationships between moisture and temperature. Using Meteosat IR radiances, Brogniez et al. (2009) demonstrated that interannual variations in free tropospheric humidity over subtropical dry regions are heavily influenced by meridional mixing between the deep tropics and the extra tropics. Regionally, upper tropospheric humidity changes in the tropics were shown to relate strongly to the movement of the ITCZ based upon microwave satellite data (Xavier et al., 2010). Shi and Bates (2011) found an increase in upper tropospheric humidity over the equatorial tropics from 1979 to 2008. However there was no significant trend found in tropical-mean or global-mean averages, indicating that on these time and space scales the upper troposphere has seen little change in relative humidity over the past 30 years. While microwave satellite measurements have become increasingly relied upon for studies of upper tropospheric humidity, the absence of a homogenized data set across multiple satellite platforms presents some difficulty in documenting coherent trends from these records (John et al., 2011).

2.5.5.4 Reanalyses

Using NCEP reanalyses for the period 1973–2007, Paltridge et al. (2009) found negative trends in specific humidity above 850 hPa over both the tropics and southern mid-latitudes, and above 600 hPa in the NH mid-latitudes. However, as noted in AR4, reanalysis products suffer from time dependent biases and have been shown to simulate unrealistic trends and variability over the ocean (Mears et al., 2007; John et al., 2009) (Box 2.3). Some reanalysis products do reproduce observed variability in low level humidity over land (Simmons et al., 2010), more complete assessments of multiple reanalysis products yield substantially different and even opposing trends in free tropospheric specific humidity (Chen et al., 2008; Dessler and Davis, 2010). Consequently, reanalysis products are still considered to be unsuitable for the analysis of tropospheric water vapour trends (Sherwood et al., 2010).

In summary, radiosonde, GPS and satellite observations of tropospheric water vapour indicate *very likely* increases at near global scales since the 1970s occurring at a rate that is generally consistent with the Clausius-Clapeyron relation (about 7% per degree Celsius) and the observed increase in atmospheric temperature. Significant trends in tropospheric relative humidity at large spatial scales have not been observed, with the exception of near-surface air over land where relative humidity has decreased in recent years (Section 2.5.5).

2.5.6 Clouds

2.5.6.1 Surface Observations

AR4 reported that surface-observed total cloud cover may have increased over many land areas since the middle of the 20th century, including the USA, the former USSR, Western Europe, mid-latitude Canada and Australia. A few regions exhibited decreases, including China and central Europe. Trends were less globally consistent since the early 1970s, with regional reductions in cloud cover reported for western Asia and Europe but increases over the USA.

Analyses since AR4 have indicated decreases in cloud occurrence/cover in recent decades over Poland (Wibig, 2008), China and the Tibetan Plateau (Duan and Wu, 2006; Endo and Yasunari, 2006; Xia, 2010b), in particular for upper level clouds (Warren et al., 2007) and also over Africa, Eurasia and in particular South America (Warren et al., 2007). Increased frequency of overcast conditions has been reported for some regions, such as Canada, from 1953 to 2002 (Milewska, 2004), with no statistically significant trends evident over Australia (Jovanovic et al., 2011) and North America (Warren et al., 2007). A global analysis of surface observations spanning the period 1971–2009 (Eastman and Warren, 2012) indicates a small decline in total cloud cover of about 0.4% per decade which is largely attributed to declining mid- and high-level cloud cover and is most prominent in the middle latitudes.

Regional variability in surface-observed cloudiness over the ocean appeared more credible than zonal and global mean variations in AR4. Multidecadal changes in upper-level cloud cover and total cloud cover over particular areas of the tropical Indo-Pacific Ocean were consistent with island precipitation records and SST variability. This has been extended more recently by Deser et al. (2010a), who found that an

eastward shift in tropical convection and total cloud cover from the western to central equatorial Pacific occurred over the 20th century and attributed it to a long-term weakening of the Walker circulation (Section 2.7.5). Eastman et al. (2011) report that, after the removal of apparently spurious globally coherent variability, cloud cover decreased in all subtropical stratocumulus regions from 1954 to 2008.

2.5.6.2 Satellite Observations

Satellite cloud observations offer the advantage of much better spatial and temporal coverage compared to surface observations. However they require careful efforts to identify and correct for temporal discontinuities in the data sets associated with orbital drift, sensor degradation, and inter-satellite calibration differences. AR4 noted that there were substantial uncertainties in decadal trends of cloud cover in all satellite data sets available at the time and concluded that there was no clear consensus regarding the decadal changes in total cloud cover. Since AR4 there has been continued effort to assess the quality of and develop improvements to multi-decadal cloud products from operational satellite platforms (Evan et al., 2007; O'Dell et al., 2008; Heidinger and Pavolonis, 2009).

Several satellite data sets offer multi-decadal records of cloud cover (Stubenrauch et al., 2013). AR4 noted that there were discrepancies in global cloud cover trends between ISCCP and other satellite data products, notably a large downward trend of global cloudiness in ISCCP since the late 1980s which is inconsistent with PATMOS-x and surface observations (Baringer et al., 2010). Recent work has confirmed the conclusion of AR4, that much of the downward trend in ISCCP is spurious and an artefact of changes in satellite viewing geometry (Evan et al., 2007). An assessment of long-term variations in global-mean cloud amount from nine different satellite data sets by Stubenrauch et al. (2013) found differences between data sets were comparable in magnitude to the interannual variability (2.5 to 3.5%). Such inconsistencies result from differences in sampling as well as changes in instrument calibration and inhibit an accurate assessment of global-scale cloud cover trends.

Satellite observations of low-level marine clouds suggest no long-term trends in cloud liquid water path or optical properties (O'Dell et al., 2008; Rausch et al., 2010). On regional scales, trends in cloud properties over China have been linked to changes in aerosol concentrations (Qian et al., 2009; Bennartz et al., 2011) (Section 2.2.3).

In summary, surface-based observations show region- and height-specific variations and trends in cloudiness but there remains substantial ambiguity regarding global-scale cloud variations and trends, especially from satellite observations. Although trends of cloud cover are consistent between independent data sets in certain regions, substantial ambiguity and therefore *low confidence* remains in the observations of global-scale cloud variability and trends.

2.6 Changes in Extreme Events

AR4 highlighted the importance of understanding changes in extreme climate events (Annex III: Glossary) because of their disproportionate

impact on society and ecosystems compared to changes in mean climate (see also IPCC Working Group II). More recently a comprehensive assessment of observed changes in extreme events was undertaken by the IPCC Special Report on Managing the Risks of Extreme Events and Disasters to Advance Climate Change Adaptation (SREX) (Seneviratne et al., 2012; Section 1.3.3).

Data availability, quality and consistency especially affect the statistics of extremes and some variables are particularly sensitive to changing measurement practices over time. For example, historical tropical cyclone records are known to be heterogeneous owing to changing observing technology and reporting protocols (Section 14.6.1) and when records from multiple ocean basins are combined to explore global trends, because data quality and reporting protocols vary substantially between regions (Knapp and Kruk, 2010). Similar problems have been discovered when analysing wind extremes, because of the sensitivity of measurements to changing instrumentation and observing practice (e.g., Smits et al., 2005; Wan et al., 2010).

Numerous regional studies indicate that changes observed in the frequency of extremes can be explained or inferred by shifts in the overall probability distribution of the climate variable (Griffiths et al., 2005; Ballester et al., 2010; Simolo et al., 2011). However, it should be noted that these studies refer to counts of threshold exceedance—frequency, duration—which closely follow mean changes. Departures from high percentiles/return periods (intensity, severity, magnitude) are highly sensitive to changes in the shape and scale parameters of the distribution (Schär et al., 2004; Clark et al., 2006; Della-Marta et al., 2007a, 2007b; Fischer and Schär, 2010) and geographical location. Debate continues over whether variance as well as mean changes are affecting global temperature extremes (Hansen et al., 2012; Rhines and Huybers, 2013) as illustrated in Figure 1.8 and FAQ 2.2, Figure 1. In the following sections the conclusions from both AR4 and SREX are reviewed along with studies subsequent to those assessments.

2.6.1 Temperature Extremes

AR4 concluded that it was *very likely* that a large majority of global land areas had experienced decreases in indices of cold extremes and increases in indices of warm extremes, since the middle of the 20th century, consistent with warming of the climate. In addition, globally averaged multi-day heat events had *likely* exhibited increases over a similar period. SREX updated AR4 but came to similar conclusions while using the revised AR5 uncertainty guidance (Seneviratne et al., 2012). Further evidence since then indicates that the level of *confidence* that the majority of warm and cool extremes show warming remains *high*.

A large amount of evidence continues to support the conclusion that most global land areas analysed have experienced significant warming of both maximum and minimum temperature extremes since about 1950 (Donat et al., 2013c). Changes in the occurrence of cold and warm days (based on daily maximum temperatures) are generally less marked (Figure 2.32). ENSO (Box 2.5) influences both maximum and minimum temperature variability especially around the Pacific Rim (e.g., Kenyon and Hegerl, 2008; Alexander et al., 2009) but often affecting cold and warm extremes differently. Different data sets using different gridding methods and/or input data (Supplementary Material 2.SM.7) indicate large coherent trends in temperature extremes globally, associated with warming (Figure 2.32). The level of quality control varies between these data sets. For example, HadEX2 (Donat et al., 2013c) uses more rigorous quality control which leads to a reduced station sample compared to GHCNDEX (Donat et al., 2013a) or HadGHCND (Caesar et al., 2006). However, despite these issues data sets compare remarkably consistently even though the station networks vary through time (Figure 2.32; Table 2.12). Other data sets that have assessed these indices, but cover a shorter period, also agree very well over the period of overlapping data, e.g., HadEX (Alexander et al., 2006) and Duke (Morak et al., 2011, 2013).

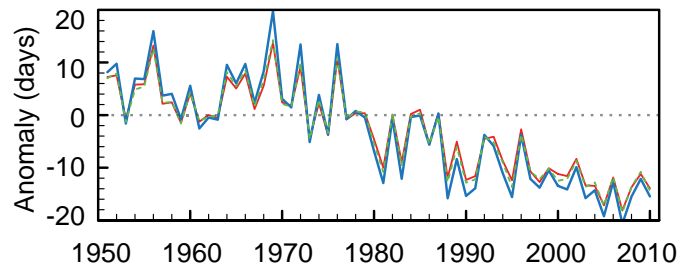
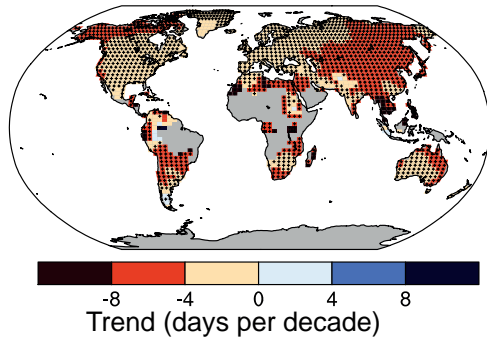
The shift in the distribution of nighttime temperatures appears greater than daytime temperatures although whether distribution changes are simply linked to increases in the mean or other moments is an active area of research (Ballester et al., 2010; Simolo et al., 2011; Donat and Alexander, 2012; Hansen et al., 2012). Indeed, all data sets examined (Duke, GHCNDEX, HadEX, HadEX2 and HadGHCND), indicate a faster increase in minimum temperature extremes than maximum temperature extremes. While DTR declines have only been assessed with *medium confidence* (Section 2.4.1.2), *confidence* of accelerated increases in minimum temperature extremes compared to maximum temperature extremes is *high* due to the more consistent patterns of warming in minimum temperature extremes globally.

Regional changes in a range of climate indices are assessed in Table 2.13. These indicate *likely* increases across most continents in unusually warm days and nights and/or reductions in unusually cold days and nights including frosts. Some regions have experienced close to a doubling of the occurrence of warm and a halving of the occurrence of cold nights, for example, parts of the Asia-Pacific region (Choi et al., 2009) and parts of Eurasia (Klein Tank et al., 2006; Donat et al., 2013a, 2013c) since the mid-20th century. Changes in both local and global SST patterns (Section 2.4.2) and large scale circulation patterns (Section 2.7) have been shown to be associated with regional changes in temperature extremes (Barrucand et al., 2008; Scaife et al., 2008;

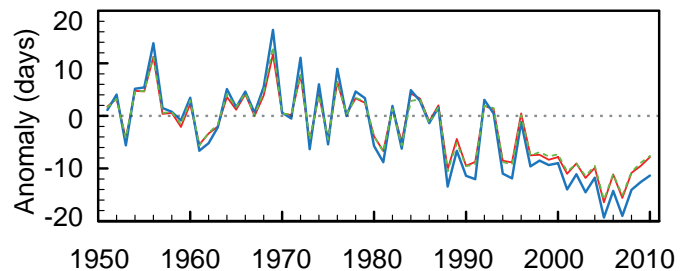
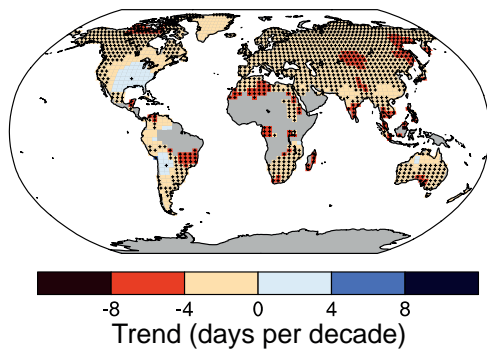
Table 2.12 | Trend estimates and 90% confidence intervals (Box 2.2) for global values of cold nights (TN10p), cold days (TX10p), warm nights (TN90p) and warm days (TX90p) over the periods 1951–2010 and 1979–2010 (see Box 2.4, Table 1 for more information on indices).

Data Set	Trends in % per decade							
	TN10p		TX10p		TN90p		TX90p	
	1951–2010	1979–2010	1951–2010	1979–2010	1951–2010	1979–2010	1951–2010	1979–2010
HadEX2 (Donat et al., 2013c)	-3.9 ± 0.6	-4.2 ± 1.2	-2.5 ± 0.7	-4.1 ± 1.4	4.5 ± 0.9	6.8 ± 1.8	2.9 ± 1.2	6.3 ± 2.2
HadGHCND (Caesar et al., 2006)	-4.5 ± 0.7	-4.0 ± 1.5	-3.3 ± 0.8	-5.0 ± 1.6	5.8 ± 1.3	8.6 ± 2.3	4.2 ± 1.8	9.4 ± 2.7
GHCNDEX (Donat et al., 2013a)	-3.9 ± 0.6	-3.9 ± 1.3	-2.6 ± 0.7	-3.9 ± 1.4	4.3 ± 0.9	6.3 ± 1.8	2.9 ± 1.2	6.1 ± 2.2

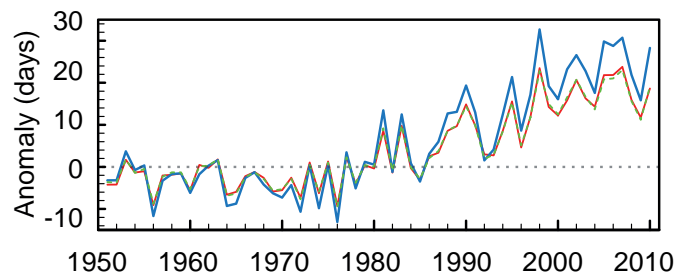
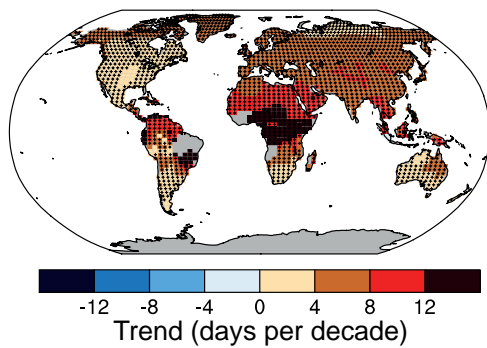
(a) Cold Nights



(b) Cold Days



(c) Warm Nights



(d) Warm Days

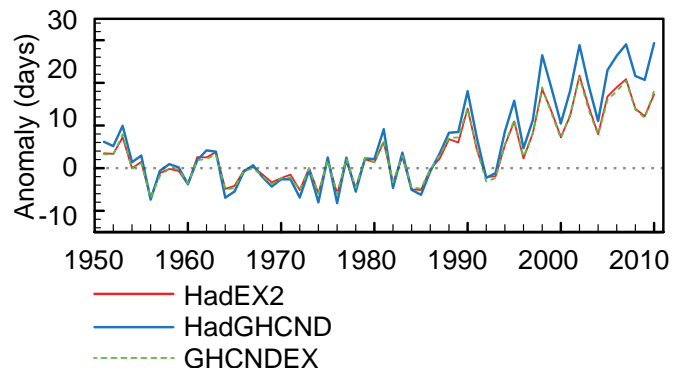
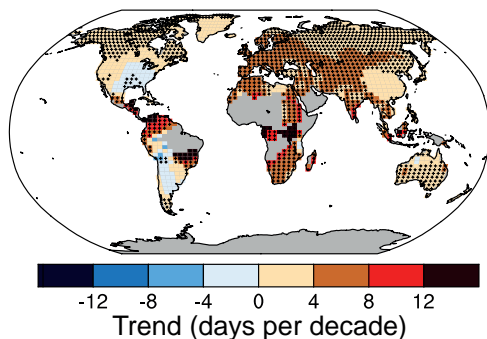


Figure 2.32 | Trends in annual frequency of extreme temperatures over the period 1951–2010, for (a) cold nights (TN10p), (b) cold days (TX10p), (c) warm nights (TN90p) and (d) warm days (TX90p) (Box 2.4, Table 1). Trends were calculated only for grid boxes that had at least 40 years of data during this period and where data ended no earlier than 2003. Grey areas indicate incomplete or missing data. Black plus signs (+) indicate grid boxes where trends are significant (i.e., a trend of zero lies outside the 90% confidence interval). The data source for trend maps is HadEX2 (Donat et al., 2013c) updated to include the latest version of the European Climate Assessment data set (Klok and Tank, 2009). Beside each map are the near-global time series of annual anomalies of these indices with respect to 1961–1990 for three global indices data sets: HadEX2 (red); HadGHCND (Caesar et al., 2006; blue) and updated to 2010 and GHCNDEX (Donat et al., 2013a; green). Global averages are only calculated using grid boxes where all three data sets have at least 90% of data over the time period. Trends are significant (i.e., a trend of zero lies outside the 90% confidence interval) for all the global indices shown.

Table 2.13 | Regional observed changes in a range of climate indices since the middle of the 20th century. Assessments are based on a range of ‘global’ studies and assessments (Groisman et al., 2005; Alexander et al., 2006; Caesar et al., 2006; Sheffield and Wood, 2008; Dai, 2011a, 2011b, 2013; Seneviratne et al., 2012; Sheffield et al., 2012; Donat et al., 2013a, 2013c; van der Schrier et al., 2013) and selected regional studies as indicated. Bold text indicates where the assessment is somewhat different to SREX Table 3-2. In each such case a footnote explains why the assessment is different. See also Figures 2.32 and 2.33.

Region	Warm Days (e.g., TX90p ^a)	Cold Days (e.g., TX10p ^a)	Warm Nights (e.g., TN90p ^a , TR ^a)	Cold Nights/Frosts (e.g., TN10p ^a , FD ^a)	Heat Waves / Warm Spells ^a	Extreme Precipitation (e.g., RX1day ^a , R95p ^a , R99p ^a)	Dryness (e.g., CDD ^a) / Drought ^b
North America and Central America	<i>High confidence: Likely overall increase but spatially varying trends^{1,2}</i>	<i>High confidence: Likely overall decrease but with spatially varying trends^{1,2}</i>	<i>High confidence: Likely overall increase^{1,2}</i>	<i>High confidence: Likely overall decrease^{1,2}</i>	<i>Medium confidence: increases in more regions than decreases^{1,3} but 1930s dominates longer term trends in the USA⁴</i>	<i>High confidence: Likely overall increase^{1,2,5} but some spatial variation</i> <i>High confidence: Very likely increase central North America^{6,7}</i>	<i>Medium confidence: decrease¹ but spatially varying trends</i> <i>High confidence^b: Likely decrease central North America⁴</i>
South America	<i>Medium confidence^b: Overall increase⁸</i>	<i>Medium confidence^b: Overall decrease⁸</i>	<i>Medium confidence^b: Overall increase⁸</i>	<i>Medium confidence^b: Overall decrease⁸</i>	<i>Low confidence: insufficient evidence (lack of literature) and spatially varying trends but some evidence of increases in more areas than decreases⁸</i>	<i>Medium confidence^b: Increases in more regions than decreases^{8,9} but spatially varying trends</i>	<i>Low confidence: limited literature and spatially varying trends⁸</i>
Europe and Mediterranean	<i>High confidence: Likely overall increase^{10,11,12}</i>	<i>High confidence: Likely overall decrease^{11,12}</i>	<i>High confidence: Likely overall increase^{11,12}</i>	<i>High confidence: Likely overall decrease^{10,11,12}</i>	<i>High confidence^b: Likely increases in most regions^{3,13}</i>	<i>High confidence^{b,c}: Likely increases in more regions than decreases^{5,15,16} but regional and seasonal variation</i>	<i>Medium confidence: spatially varying trends</i> <i>High confidence^b: Likely increase in Mediterranean^{17,18}</i>
Africa and Middle East	<i>Low to medium confidence^{b,d}: limited data in many regions but increases in most regions assessed</i> <i>Medium confidence^b: increase North Africa and Middle East^{19,20}</i> <i>High confidence^b: Likely increase southern Africa^{21,22,23}</i>	<i>Low to medium confidence^{b,d}: limited data in many regions but decreases in most regions assessed</i> <i>Medium confidence^b: decrease North Africa and Middle East^{19,20}</i> <i>High confidence^b: Likely decrease southern Africa^{21,22,23}</i>	<i>Medium confidence^{b,d}: limited data in many regions but increases in most regions assessed</i> <i>Medium confidence^b: increase North Africa and Middle East^{19,20}</i> <i>High confidence^b: Likely increase southern Africa^{21,22,23}</i>	<i>Medium confidence^{b,d}: limited data in many regions but decreases in most regions assessed</i> <i>Medium confidence^b: decrease North Africa and Middle East^{19,20}</i> <i>High confidence^b: Likely decrease southern Africa^{21,22,23}</i>	<i>Low confidence^d: insufficient evidence (lack of literature)</i> <i>Medium confidence: increase in North Africa and Middle East and southern Africa^{3,19,21,22}</i>	<i>Low confidence^d: insufficient evidence and spatially varying trends</i> <i>Medium confidence^b: increases in more regions than decreases in southern Africa but spatially varying trends depending on index^{5,21,22}</i>	<i>Medium confidence^d: increase^{19,22,24}</i> <i>High confidence^b: Likely increase in West Africa^{25,26} although 1970s Sahel drought dominates the trend</i>
Asia (excluding South-east Asia)	<i>High confidence^{b,e}: Likely overall increase^{27,28,29,30,31,32}</i>	<i>High confidence^{b,e}: Likely overall decrease^{27,28,29,30,31,32}</i>	<i>High confidence^{b,e}: Likely overall increase^{27,28,29,30,31,32}</i>	<i>High confidence^{b,e}: Likely overall increase^{27,28,29,30,31,32}</i>	<i>Medium confidence^{b,e}: Spatially varying trends and insufficient data in some regions</i> <i>High confidence^{b,c}: Likely more areas of increases than decreases^{3,28,33}</i>	<i>Low to medium confidence^{b,e}:</i> <i>Low confidence due to insufficient evidence or spatially varying trends.</i> <i>Medium confidence: increases in more regions than decreases^{5,34,35,36}</i>	<i>Low to medium confidence^{b,e}</i> <i>Medium confidence: Increase in eastern Asia^{36,37}</i>
South-east Asia and Oceania	<i>High confidence^{b,f}: Likely overall increase^{27,38,39,40}</i>	<i>High confidence^{b,f}: Likely overall decrease^{27,38,39}</i>	<i>High confidence^{b,f}: Likely overall increase^{27,38,39,40}</i>	<i>High confidence^{b,f}: Likely overall decrease^{27,38,39}</i>	<i>Low confidence (due lack of literature) to high confidence^{b,f} depending on region</i> <i>High confidence²: Likely overall increase in Australia^{3,14,41}</i>	<i>Low confidence (lack of literature) to high confidence^{b,f}</i> <i>High confidence: Likely decrease in southern Australia^{42,43} but index and season dependent</i>	<i>Low to medium confidence^{b,f}: inconsistent trends between studies in SE Asia. Overall increase in dryness in southern and eastern Australia</i> <i>High confidence^b: Likely decrease northwest Australia^{25,26,44}</i>

(continued on next page)



(Table 2.13 continued)

Notes:

- ^a See Table 1 in Box 2.4, for definitions.
- ^b More recent literature updates the assessment from SREX Table 3-2 (including 'global' studies).
- ^c This represents a measure of the area affected which is different from what was assessed in SREX Table 3-2.
- ^d This represents a slightly different region than that assessed in SREX Table 3-2 as it includes the Middle East.
- ^e This represents a slightly different region than that assessed in SREX Table 3-2 as it excludes Southeast Asia.
- ^f This represents a slightly different region than that assessed in SREX Table 3-2 as it combines SE Asia and Oceania.
- ^g Definitions for warm spells and heat waves vary (Perkins and Alexander, 2012) but here we are commonly assessing the Warm Spell Duration Index (WSDI; Zhang et al., 2011) or other heat wave indices (e.g., HWF, HWM; (Fischer and Schär, 2010; Perkins et al., 2012) that have defined multi-day heat extremes relative to either daily maximum or minimum temperatures (or both) above a high (commonly 90th) percentile relative to a late-20th century reference period.
- ^h See Box 2.4 and Section 2.6.1 for definitions.
- ¹ Kunkel et al. (2008), ² Peterson et al. (2008), ³ Perkins et al. (2012), ⁴ Peterson et al. (2013), ⁵ Westra et al. (2013), ⁶ Groisman et al. (2012), ⁷ Villarini et al. (2013), ⁸ Skansi et al. (2013), ⁹ Haylock et al. (2006), ¹⁰ Andrade et al. (2012), ¹¹ Efthymiadis et al. (2011), ¹² Moberg et al. (2006), ¹³ Della-Marta et al. (2007a), ¹⁴ Perkins and Alexander (2012), ¹⁵ Van den Besselaar et al. (2012), ¹⁶ Zolina et al. (2009), ¹⁷ Sousa et al. (2011), ¹⁸ Hoerling et al. (2012), ¹⁹ Donat et al. (2013b), ²⁰ Zhang et al. (2005), ²¹ Kruger and Sekele (2013), ²² New et al. (2006), ²³ Vincent et al. (2011), ²⁴ Aguilar et al. (2009), ²⁵ Dai (2013), ²⁶ Sheffield et al. (2012), ²⁷ Choi et al. (2009), ²⁸ Rahimzadeh et al. (2009), ²⁹ Revadekar et al. (2012), ³⁰ Tank et al. (2006), ³¹ You et al. (2010), ³² Zhou and Ren (2011), ³³ Ding et al. (2010), ³⁴ Krishna Moorthy et al. (2009), ³⁵ Pattanaik and Rajeevan (2010), ³⁶ Wang et al. (2012b), ³⁷ Fischer et al. (2011), ³⁸ Caesar et al. (2011), ³⁹ Chambers and Griffiths (2008), ⁴⁰ Wang et al. (2013), ⁴¹ Tryhorn and Risbey (2006), ⁴² Gallant et al. (2007), ⁴³ King et al. (2013), ⁴⁴ Jones et al. (2009).

Alexander et al., 2009; Li et al., 2012), particularly in regions around the Pacific Rim (Kenyon and Hegerl, 2008). Globally, there is evidence of large-scale warming trends in the extremes of temperature, especially minimum temperature, since the beginning of the 20th century (Donat et al., 2013c).

There are some exceptions to this large-scale warming of temperature extremes including central North America, eastern USA (Alexander et al., 2006; Kunkel et al., 2008; Peterson et al., 2008) and some parts of South America (Alexander et al., 2006; Rusticucci and Renom, 2008; Skansi et al., 2013) which indicate changes consistent with cooling in these locations. However, these exceptions appear to be mostly associated with changes in maximum temperatures (Donat et al., 2013c). The so-called 'warming hole' in central North America and eastern USA, where temperatures have cooled relative to the significant warming elsewhere in the region, is associated with observed changes in the hydrological cycle and land-atmosphere interaction (Pan et al., 2004; Portmann et al., 2009a; Portmann et al., 2009b; Misra et al., 2012) and decadal and multi-decadal variability linked with the Atlantic and Pacific Oceans (Meehl et al., 2012; Weaver, 2012).

Since AR4 many studies have analysed local to regional changes in multi-day temperature extremes in more detail, specifically addressing different heat wave aspects such as frequency, intensity, duration and spatial extent (Box 2.4, FAQ 2.2). Several high-profile heat waves have occurred in recent years (e.g., in Europe in 2003 (Beniston, 2004), Australia in 2009 (Pezza et al., 2012), Russia in 2010 (Barriopedro et al., 2011; Dole et al., 2011; Trenberth and Fasullo, 2012a) and USA in 2010/2011 (Hoerling et al., 2012) (Section 10.6.2) which have had severe impacts (see WGII). Heat waves are often associated with quasi-stationary anticyclonic circulation anomalies that produce prolonged hot conditions at the surface (Black and Sutton, 2007; Garcia-Herrera et al., 2010), but long-term changes in the persistence of these anomalies are still relatively poorly understood (Section 2.7). Heat waves can also be amplified by pre-existing dry soil conditions in transitional climate zones (Ferranti and Viterbo, 2006; Fischer et al., 2007; Seneviratne et al., 2010; Mueller and Seneviratne, 2012) and the persistence of those soil-moisture anomalies (Lorenz et al., 2010). Dry soil-moisture conditions are either induced by precipitation deficits (Della-Mar-

ta et al., 2007b; Vautard et al., 2007), or evapotranspiration excesses (Black and Sutton, 2007; Fischer et al., 2007), or a combination of both (Seneviratne et al., 2010). This amplification of soil moisture-temperature feedbacks is suggested to have partly enhanced the duration of extreme summer heat waves in southeastern Europe during the latter part of the 20th century (Hirschi et al., 2011), with evidence emerging of a signature in other moisture-limited regions (Mueller and Seneviratne, 2012).

Table 2.13 shows that there has been a *likely* increasing trend in the frequency of heatwaves since the middle of the 20th century in Europe and Australia and across much of Asia where there are sufficient data. However, *confidence* on a global scale is *medium* owing to lack of studies over Africa and South America but also in part owing to differences in trends depending on how heatwaves are defined (Perkins et al., 2012). Using monthly means as a proxy for heatwaves Coumou et al. (2013) and Hansen et al. (2012) indicate that record-breaking temperatures in recent decades substantially exceed what would be expected by chance but caution is required when making inferences between these studies and those that deal with multi-day events and/or use more complex definitions for heatwave events. There is also evidence in some regions that periods prior to the 1950s had more heatwaves (e.g., over the USA, the decade of the 1930s stands out and is also associated with extreme drought conditions (Peterson et al., 2013) whereas conversely in other regions heatwave trends may have been underestimated owing to poor quality and/or consistency of data (e.g., Della-Marta et al. (2007a) over Western Europe; Kuglitsch et al. (2009, 2010) over the Mediterranean). Recent available studies also suggest that the number of cold spells has reduced significantly since the 1950s (Donat et al., 2013a, 2013c).

In summary, new analyses continue to support the AR4 and SREX conclusions that since about 1950 it is *very likely* that the numbers of cold days and nights have decreased and the numbers of warm days and nights have increased overall on the global scale, that is, for land areas with sufficient data. It is *likely* that such changes have also occurred across most of North America, Europe, Asia and Australia. There is *low to medium confidence* in historical trends in daily temperature extremes in Africa and South America as there is either

insufficient data or trends vary across these regions. This, combined with issues with defining events, leads to the assessment that there is *medium confidence* that globally the length and frequency of warm spells, including heat waves, has increased since the middle of the 20th century although it is *likely* that heatwave frequency has increased during this period in large parts of Europe, Asia and Australia.

2.6.2 Extremes of the Hydrological Cycle

In Section 2.5 mean state changes in different aspects of the hydrological cycle are discussed. In this section we focus on the more extreme aspects of the cycle including extreme rainfall, severe local weather events like hail, flooding and droughts. Extreme events associated with tropical and extratropical storms are discussed in Sections 2.6.3 and 2.6.4 respectively.

2.6.2.1 Precipitation Extremes

AR4 concluded that substantial increases are found in heavy precipitation events. It was *likely* that annual heavy precipitation events had disproportionately increased compared to mean changes between 1951 and 2003 over many mid-latitude regions, even where there had been a reduction in annual total precipitation. Rare precipitation (such as the highest annual daily precipitation total) events were *likely* to have increased over regions with sufficient data since the late 19th century. SREX supported this view, as have subsequent analyses, but noted large spatial variability within and between regions (Table 3.2 of Seneviratne et al., 2012).

Given the diverse climates across the globe, it has been difficult to provide a universally valid definition of 'extreme precipitation'. However, Box 2.4 Table 1 indicates some of the common definitions that are used in the scientific literature. In general, statistical tests indicate changes in precipitation extremes are consistent with a wetter climate (Section 7.6.5), although with a less spatially coherent pattern of change than temperature, in that there are large areas that show increasing trends and large areas that show decreasing trends and a lower level of statistical significance than for temperature change (Alexander et al., 2006; Donat et al., 2013a, 2013c). Using R95p and SDII indices (Box 2.4), Figures 2.33a and 2.33b show these areas for heavy precipitation amounts and precipitation intensity where sufficient data are available in the HadEX2 data set (Donat et al., 2013c) although there are more areas showing significant increases than decreases. Although changes in large-scale circulation patterns have a substantial influence on precipitation extremes globally (Alexander et al., 2009; Kenyon and Hegerl, 2010), Westra et al. (2013) showed, using *in situ* data over land, that trends in the wettest day of the year indicate more increases than would be expected by chance. Over the tropical oceans satellite measurements show an increase in the frequency of the heaviest rainfall during warmer (El Niño) years (Allan and Soden, 2008).

Regional trends in precipitation extremes since the middle of the 20th century are varied (Table 2.13). In most continents *confidence* in trends is not higher than *medium* except in North America and Europe where there have been *likely* increases in either the frequency or intensity of heavy precipitation. This assessment increases to *very likely* for central North America. For North America it is also *likely* that increases

have occurred during the whole of the 20th century (Pryor et al., 2009; Donat et al., 2013c; Villarini et al., 2013). For South America the most recent integrative studies indicate heavy rain events are increasing in frequency and intensity over the continent as a whole (Donat et al., 2013c; Skansi et al., 2013). For Europe and the Mediterranean, the assessment masks some regional and seasonal variation. For example, much of the increase reported in Table 2.13 is found in winter although with decreasing trends in some other regions such as northern Italy, Poland and some Mediterranean coastal sites (Pavan et al., 2008; Lupikasza, 2010; Toreti et al., 2010). There are mixed regional trends across Asia and Oceania but with some indication that increases are being observed in more regions than decreases while recent studies focused on Africa, in general, have not found significant trends in extreme precipitation (see Chapter 14 for more on regional variations and trends).

The above studies generally use indices which reflect 'moderate' extremes, for example, events occurring as often as 5% or 10% of the time (Box 2.4). Only a few regions have sufficient data to assess trends in rarer precipitation events reliably, for example, events occurring on average once in several decades. Using Extreme Value Theory, DeGaetano (2009) showed a 20% reduction in the return period for extreme precipitation events over large parts of the contiguous USA from 1950 to 2007. For Europe from 1951 to 2010, Van den Besselaar et al. (2012) reported a median reduction in 5- to 20-year return periods of 21%, with a range between 2% and 58% depending on the subregion and season. This decrease in return times for rare extremes is qualitatively similar to the increase in moderate extremes for these regions reported above, and also consistent with earlier local results for the extreme tail of the distribution reported in AR4.

The aforementioned studies refer to daily precipitation extremes, although rainfall will often be limited to part of the day only. The literature on sub-daily scales is too limited for a global assessment although it is clear that analysis and framing of questions regarding sub-daily precipitation extremes is becoming more critical (Trenberth, 2011). Available regional studies have shown results that are even more complex than for daily precipitation and with variations in the spatial patterns of trends depending on event formulation and duration. However, regional studies show indications of more increasing than decreasing trends (Sen Roy, 2009; for India) (Sen Roy and Rouault, 2013; for South Africa) (Westra and Sisson, 2011; for Australia). Some studies present evidence of scaling of sub-daily precipitation with temperature that is outside that expected from the Clausius–Clapeyron relation (about 7% per degree Celsius) (Lenderink and Van Meijgaard, 2008; Haerter et al., 2010; Jones et al., 2010; Lenderink et al., 2011; Utsumi et al., 2011), but scaling beyond that expected from thermodynamic theories is controversial (Section 7.6.5).

In summary, further analyses continue to support the AR4 and SREX conclusions that it is *likely* that since 1951 there have been statistically significant increases in the number of heavy precipitation events (e.g., above the 95th percentile) in more regions than there have been statistically significant decreases, but there are strong regional and sub-regional variations in the trends. In particular, many regions present statistically non-significant or negative trends, and, where seasonal changes have been assessed, there are also variations between seasons (e.g., more consistent trends in winter than in summer in Europe). The

overall most consistent trends towards heavier precipitation events are found in central North America (*very likely* increase) but assessment for Europe shows *likely* increases in more regions than decreases.

2.6.2.2 Floods

AR4 WGI Chapter 3 (Trenberth et al., 2007) did not assess changes in floods but AR4 WGII concluded that there was not a general global trend in the incidence of floods (Kundzewicz et al., 2007). SREX went further to suggest that there was low agreement and thus *low confidence* at the global scale regarding changes in the magnitude or frequency of floods or even the sign of changes.

AR5 WGII assesses floods in regional detail accounting for the fact that trends in floods are strongly influenced by changes in river management (see also Section 2.5.2). Although the most evident flood trends appear to be in northern high latitudes, where observed warming trends have been largest, in some regions no evidence of a trend in extreme flooding has been found, for example, over Russia based on daily river discharge (Shiklomanov et al., 2007). Other studies for Europe (Hannaford and Marsh, 2008; Renard et al., 2008; Petrow and Merz, 2009; Stahl et al., 2010) and Asia (Jiang et al., 2008; Delgado et al., 2010) show evidence for upward, downward or no trend in the magnitude and frequency of floods, so that there is currently no clear and widespread evidence for observed changes in flooding except for the earlier spring flow in snow-dominated regions (Seneviratne et al., 2012).

In summary, there continues to be a lack of evidence and thus *low confidence* regarding the sign of trend in the magnitude and/or frequency of floods on a global scale.

2.6.2.3 Droughts

AR4 concluded that droughts had become more common, especially in the tropics and sub-tropics since about 1970. SREX provided a comprehensive assessment of changes in observed droughts (Section 3.5.1 and Box 3.3 of SREX), updated the conclusions provided by AR4 and stated that the type of drought considered and the complexities in defining drought (Annex III: Glossary) can substantially affect the conclusions regarding trends on a global scale (Chapter 10). Based on evidence since AR4, SREX concluded that there were not enough direct observations of dryness to suggest *high confidence* in observed trends globally, although there was *medium confidence* that since the 1950s some regions of the world have experienced more intense and longer droughts. The differences between AR4 and SREX are due primarily to analyses post-AR4, differences in how both assessments considered drought and updated IPCC uncertainty guidance.

There are very few direct measurements of drought related variables, such as soil moisture (Robock et al., 2000), so drought proxies (e.g., PDSI, SPI, SPEI; Box 2.4) and hydrological drought proxies (e.g., Vidal et al., 2010; Dai, 2011b) are often used to assess drought. The chosen proxy (e.g., precipitation, evapotranspiration, soil moisture or streamflow) and time scale can strongly affect the ranking of drought events (Sheffield et al., 2009; Vidal et al., 2010). Analyses of these indirect indices come with substantial uncertainties. For example, PDSI may not

be comparable across climate zones. A self-calibrating (sc-) PDSI can replace the fixed empirical constants in PDSI with values representative of the local climate (Wells et al., 2004). Furthermore, for studies using simulated soil moisture, the type of potential evapotranspiration model used can lead to significant differences in the estimation of the regions affected and the areal extent of drought (Sheffield et al., 2012), but the overall effect of a more physically realistic parameterisation is debated (van der Schrier et al., 2013).

Because drought is a complex variable and can at best be incompletely represented by commonly used drought indices, discrepancies in the interpretation of changes can result. For example, Sheffield and Wood (2008) found decreasing trends in the duration, intensity and severity of drought globally. Conversely, Dai (2011a,b) found a general global increase in drought, although with substantial regional variation and individual events dominating trend signatures in some regions (e.g., the 1970s prolonged Sahel drought and the 1930s drought in the USA and Canadian Prairies). Studies subsequent to these continue to provide somewhat different conclusions on trends in global droughts and/or dryness since the middle of the 20th century (Sheffield et al., 2012; Dai, 2013; Donat et al., 2013c; van der Schrier et al., 2013).

Van der Schrier et al. (2013), using monthly sc-PDSI, found no strong case either for notable drying or moisture increase on a global scale over the periods 1901–2009 or 1950–2009, and this largely agrees with the results of Sheffield et al. (2012) over the latter period. A comparison between the sc-PDSI calculated by van der Schrier et al. (2013) and that of Dai (2011a) shows that the dominant mode of variability is very similar, with a temporal evolution suggesting a trend toward drying. However, the same analysis for the 1950–2009 period shows an initial increase in drying in the Van der Schrier et al. data set, followed by a decrease from the mid-1980s onwards, while the Dai data show a continuing increase until 2000. The difference in trends between the sc-PDSI data set of Van der Schrier et al. and Dai appears to be due to the different calibration periods used, the shorter 1950–1979 period in the latter study resulting in higher index values from 1980 onwards, although the associated spatial patterns are similar. In addition, the observed precipitation forcing data set differs between studies, with van der Schrier et al. (2013) and Sheffield et al. (2012) using CRU TS 3.10.01 (updated from Mitchell and Jones, 2005). This data set uses fewer stations and has been wetter than some other precipitation products in the last couple of decades (Figure 2.29, Table 2.9), although the best data set to use is still an open question. Despite this, a measure of sc-PDSI with potential evapotranspiration estimated using the Penman–Montieth equation shows an increase in the percentage of land area in drought since 1950 (Sheffield et al., 2012; Dai, 2013), while van der Schrier et al. (2013) also finds a slight increase in the percentage of land area in severe drought using the same measure. This is qualitatively consistent with the trends in surface soil moisture found for the shorter period 1988–2010 by Dorigo et al. (2012) using a new multi-satellite data set and changes in observed streamflow (Dai, 2011b). However all these studies draw somewhat different conclusions and the compelling arguments both for (Dai, 2011b, 2013) and against (Sheffield et al., 2012; van der Schrier et al., 2013) a significant increase in the land area experiencing drought has hampered global assessment.

Studies that support an increasing trend towards the land area affected by drought seem to be at odds with studies that look at trends in dryness (i.e., lack of rainfall). For example, Donat et al. (2013c) found that the annual maximum number of consecutive dry days has declined since the 1950s in more regions than it has increased (Figure 2.33c). However, only regions in Russia and the USA indicate significant changes and there is a lack of information for this index over large regions, especially Africa. Most other studies focussing on global dryness find similar results, with decadal variability dominating longer-term trends (Frich et al., 2002; Alexander et al., 2006; Donat et al., 2013a). However, Giorgi et al. (2011) indicate that ‘hydroclimatic intensity’ (Box 2.4, Chapter 7), a measure which combines both dry spell length and precipitation intensity, has increased over the latter part of the 20th century in response to a warming climate. They show that positive trends (reflecting an increase in the length of drought and/or extreme precipitation events) are most marked in Europe, India, parts of South America and East Asia although trends appear to have decreased (reflecting a decrease in the length of drought and/or extreme precipitation events) in Australia and northern South America (Figure 2.33c). Data availability, quality and length of record remain issues in drawing conclusions on a global scale, however.

Despite differences between the conclusions drawn by global studies, there are some areas in which they agree. Table 2.13 indicates that there is *medium confidence* of an increase in dryness or drought in East Asia with *high confidence* that this is the case in the Mediterranean and West Africa. There is also *high confidence* of decreases in dryness or drought in central North America and north-west Australia.

In summary, the current assessment concludes that there is not enough evidence at present to suggest more than *low confidence* in a global-scale observed trend in drought or dryness (lack of rainfall) since the middle of the 20th century, owing to lack of direct observations, geographical inconsistencies in the trends, and dependencies of inferred trends on the index choice. Based on updated studies, AR4 conclusions regarding global increasing trends in drought since the 1970s were probably overstated. However, it is *likely* that the frequency and intensity of drought has increased in the Mediterranean and West Africa and decreased in central North America and north-west Australia since 1950.

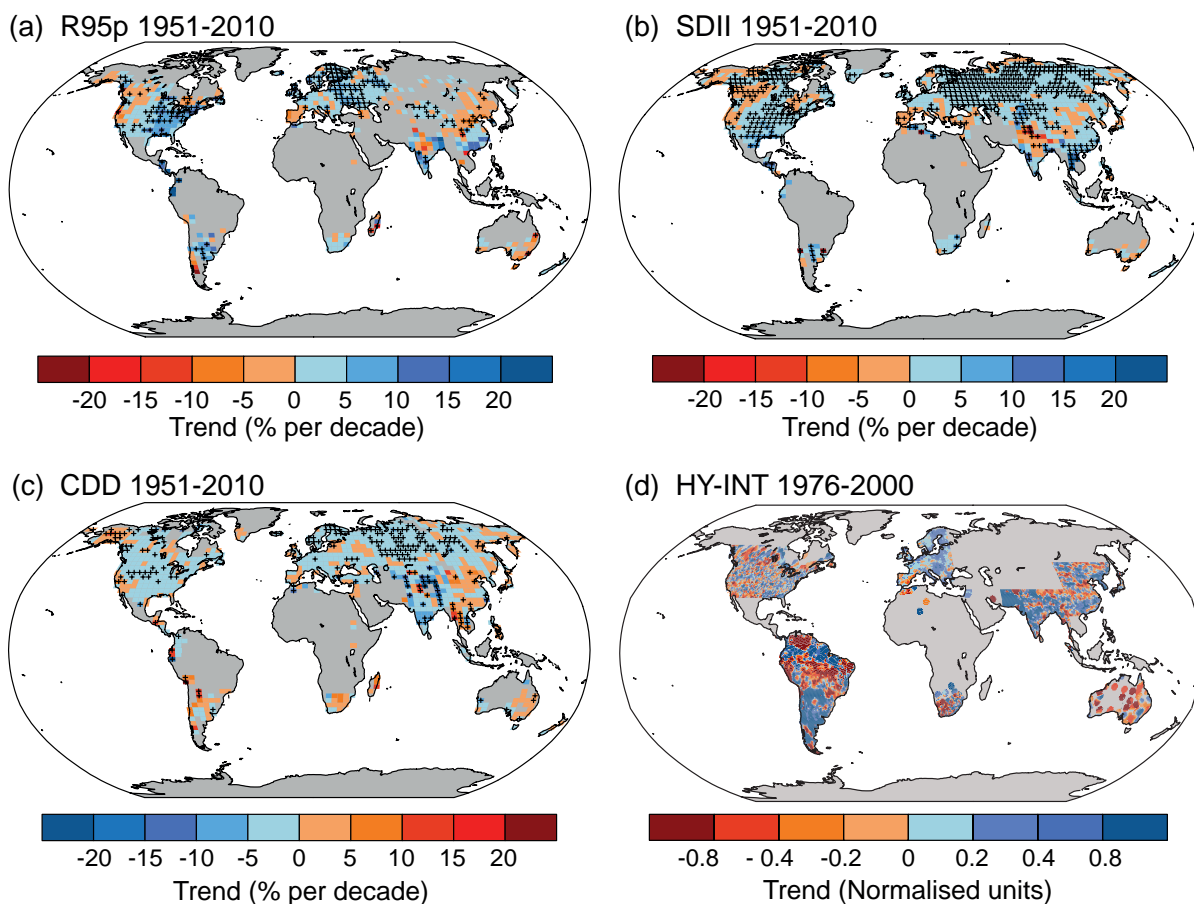


Figure 2.33 | Trends in (a) annual amount of precipitation from days >95th percentile (R95p), (b) daily precipitation intensity (SDII) and (c) frequency of the annual maximum number of consecutive dry days (CDD) (Box 2.4, Table 1). Trends are shown as relative values for better comparison across different climatic regions. Trends were calculated only for grid boxes that had at least 40 years of data during this period and where data ended no earlier than 2003. Grey areas indicate incomplete or missing data. Black plus signs (+) indicate grid boxes where trends are significant (i.e., a trend of zero lies outside the 90% confidence interval). The data source for trend maps is HadEX2 (Donat et al., 2013a) updated to include the latest version of the European Climate Assessment data set (Klok and Tank, 2009). (d) Trends (normalized units) in hydroclimatic intensity (HY-INT: a multiplicative measure of length of dry spell and precipitation intensity) over the period 1976–2000 (adapted from Giorgi et al., 2011). An increase (decrease) in HY-INT reflects an increase (decrease) in the length of drought and /or extreme precipitation events.

2.6.2.4 Severe Local Weather Events

Another extreme aspect of the hydrological cycle is severe local weather phenomena such as hail or thunder storms. These are not well observed in many parts of the world because the density of surface meteorological observing stations is too coarse to measure all such events. Moreover, homogeneity of existing reporting is questionable (Verbout et al., 2006; Doswell et al., 2009). Alternatively, measures of severe thunderstorms or hailstorms can be derived by assessing the environmental conditions that are favourable for their formation but this method is very uncertain (Seneviratne et al., 2012). SREX highlighted studies such as those of Brooks and Dotzek (2008), who found significant variability but no clear trend in the past 50 years in severe thunderstorms in a region east of the Rocky Mountains in the USA, Cao (2008), who found an increasing frequency of severe hail events in Ontario, Canada during the period 1979–2002 and Kunz et al. (2009), who found that hail days significantly increased during the period 1974–2003 in southwest Germany. Hailpad studies from Italy (Eccel et al., 2012) and France (Berthet et al., 2011) suggest slight increases in larger hail sizes and a correlation between the fraction of precipitation falling as hail with average summer temperature while in Argentina between 1960 and 2008 the annual number of hail events was found to be increasing in some regions and decreasing in others (Mezher et al., 2012). In China between 1961 and 2005, the number of hail days has been found to generally decrease, with the highest occurrence between 1960 and 1980 but with a sharp drop since the mid-1980s (CMA, 2007; Xie et al., 2008). However, there is little consistency in hail size changes in different regions of China since 1980 (Xie et al., 2010). Remote sensing offers a potential alternative to surface-based meteorological networks for detecting changes in small scale severe weather phenomenon such as proxy measurements of lightning from satellites (Zipser et al., 2006) but there remains little convincing evidence that changes in severe thunderstorms or hail have occurred since the middle of the 20th century (Brooks, 2012).

In summary, there is *low confidence* in observed trends in small-scale severe weather phenomena such as hail and thunderstorms because of historical data inhomogeneities and inadequacies in monitoring systems.

2.6.3 Tropical Storms

AR4 concluded that it was *likely* that an increasing trend had occurred in intense tropical cyclone activity since 1970 in some regions but that there was no clear trend in the annual numbers of tropical cyclones. Subsequent assessments, including SREX and more recent literature indicate that it is difficult to draw firm conclusions with respect to the confidence levels associated with observed trends prior to the satellite era and in ocean basins outside of the North Atlantic.

Section 14.6.1 discusses changes in tropical storms in detail. Current data sets indicate no significant observed trends in global tropical cyclone frequency over the past century and it remains uncertain whether any reported long-term increases in tropical cyclone frequency are robust, after accounting for past changes in observing capabilities (Knutson et al., 2010). Regional trends in tropical cyclone frequency and the frequency of very intense tropical cyclones have been identified in the

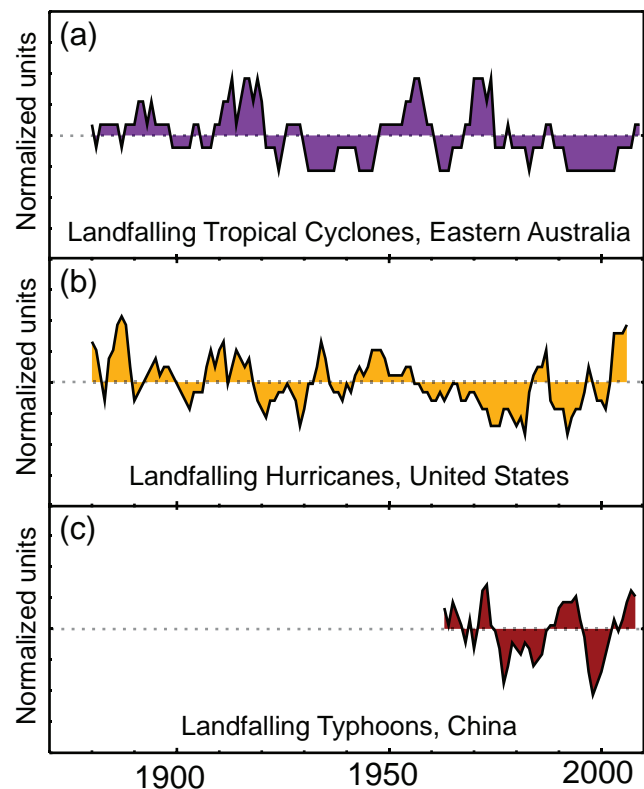


Figure 2.34 | Normalized 5-year running means of the number of (a) adjusted land falling eastern Australian tropical cyclones (adapted from Callaghan and Power (2011) and updated to include 2010/2011 season) and (b) unadjusted land falling U.S. hurricanes (adapted from Vecchi and Knutson (2011)) and (c) land-falling typhoons in China (adapted from CMA, 2011). Vertical axis ticks represent one standard deviation, with all series normalized to unit standard deviation after a 5-year running mean was applied.

North Atlantic and these appear robust since the 1970s (Kossin et al. 2007) (*very high confidence*). However, argument reigns over the cause of the increase and on longer time scales the fidelity of these trends is debated (Landsea et al., 2006; Holland and Webster, 2007; Landsea, 2007; Mann et al., 2007b) with different methods for estimating undercounts in the earlier part of the record providing mixed conclusions (Chang and Guo, 2007; Mann et al., 2007a; Kunkel et al., 2008; Vecchi and Knutson, 2008, 2011). No robust trends in annual numbers of tropical storms, hurricanes and major hurricanes counts have been identified over the past 100 years in the North Atlantic basin. Measures of land-falling tropical cyclone frequency (Figure 2.34) are generally considered to be more reliable than counts of all storms which tend to be strongly influenced by those that are weak and/or short lived. Callaghan and Power (2011) find a statistically significant decrease in Eastern Australia land-falling tropical cyclones since the late 19th century although including 2010/2011 season data this trend becomes non-significant (i.e., a trend of zero lies just inside the 90% confidence interval). Significant trends are not found in other oceans on shorter time scales (Chan and Xu, 2009; Kubota and Chan, 2009; Mohapatra et al., 2011; Weinkle et al., 2012), although Grinsted et al. (2012) find a significant positive trend in eastern USA using tide-gauge data from 1923–2008 as a proxy for storm surges associated with land-falling hurricanes. Differences between tropical cyclone studies highlight the challenges that still lie ahead in assessing long-term trends.

Arguably, storm frequency is of limited usefulness if not considered in tandem with intensity and duration measures. Intensity measures in historical records are especially sensitive to changing technology and improving methodology. However, over the satellite era, increases in the intensity of the strongest storms in the Atlantic appear robust (Kossin et al., 2007; Elsner et al., 2008) but there is limited evidence for other regions and the globe. Time series of cyclone indices such as power dissipation, an aggregate compound of tropical cyclone frequency, duration and intensity that measures total wind energy by tropical cyclones, show upward trends in the North Atlantic and weaker upward trends in the western North Pacific since the late 1970s (Emanuel, 2007), but interpretation of longer-term trends is again constrained by data quality concerns (Landsea et al., 2011).

In summary, this assessment does not revise the SREX conclusion of *low confidence* that any reported long-term (centennial) increases in tropical cyclone activity are robust, after accounting for past changes in observing capabilities. More recent assessments indicate that it is *unlikely* that annual numbers of tropical storms, hurricanes and major hurricanes counts have increased over the past 100 years in the North Atlantic basin. Evidence, however, is for a *virtually certain* increase in the frequency and intensity of the strongest tropical cyclones since the 1970s in that region.

2.6.4 Extratropical Storms

AR4 noted a *likely* net increase in frequency/intensity of NH extreme extratropical cyclones and a poleward shift in storm tracks since the 1950s. SREX further consolidated the AR4 assessment of poleward shifting storm tracks, but revised the assessment of the confidence levels associated with regional trends in the intensity of extreme extratropical cyclones.

Studies using reanalyses continue to support a northward and eastward shift in the Atlantic cyclone activity during the last 60 years with both more frequent and more intense wintertime cyclones in the high-latitude Atlantic (Schneider et al., 2007; Raible et al., 2008; Vilibic and Sepic, 2010) and fewer in the mid-latitude Atlantic (Wang et al., 2006b; Raible et al., 2008). Some studies show an increase in intensity and number of extreme Atlantic cyclones (Paciorek et al., 2002; Lehmann et al., 2011) while others show opposite trends in eastern Pacific and North America (Gulev et al., 2001). Comparisons between studies are hampered because of the sensitivities in identification schemes and/or different definitions for extreme cyclones (Ulbrich et al., 2009; Neu et al., 2012). The fidelity of research findings also rests largely with the underlying reanalyses products that are used (Box 2.3). See also Section 14.6.2.

Over longer periods studies of severe storms or storminess have been performed for Europe where long running *in situ* pressure and wind observations exist. Direct wind speed measurements, however, either have short records or are hampered by inconsistencies due to changing instrumentation and observing practice over time (Smits et al., 2005; Wan et al., 2010). In most cases, therefore wind speed or storminess proxies are derived from *in situ* pressure measurements or reanalyses data, the quality and consistency of which vary. *In situ* observations indicate no clear trends over the past century or longer (Hanna et al., 2008; Matulla et al., 2008; Allan et al., 2009; Barring and Fortuniak,

2009), with substantial decadal and longer fluctuations but with some regional and seasonal trends (Wang et al., 2009c, 2011). Figure 2.35 shows some of these changes for boreal winter using geostrophic wind speeds indicating that decreasing trends outnumber increasing trends (Wang et al., 2011), although with few that are statistically significant. Although Donat et al. (2011) and Wang et al. (2012h) find significant increases in both the strength and frequency of wintertime storms for large parts of Europe using the 20CR (Compo et al., 2011), there is debate over whether this is an artefact of the changing number of assimilated observations over time (Cornes and Jones, 2011; Krueger et al., 2013) even though Wang et al. (2012h) find good agreement between the 20CR trends and those derived from geostrophic wind extremes in the North Sea region.

SREX noted that available studies using reanalyses indicate a decrease in extratropical cyclone activity (Zhang et al., 2004) and intensity (Zhang et al., 2004; Wang et al., 2009d) over the last 50 years has been reported for northern Eurasia (60°N to 40°N) linked to a possible northward shift with increased cyclone frequency in the higher latitudes and decrease in the lower latitudes. The decrease at lower latitudes was also found in East Asia (Wang et al., 2012h) and is also supported by a study of severe storms by Zou et al. (2006b) who used sub-daily *in situ* pressure data from a number of stations across China.

SREX also notes that, based on reanalyses, North American cyclone numbers have increased over the last 50 years, with no statistically significant change in cyclone intensity (Zhang et al., 2004). Hourly SLP data from Canadian stations showed that winter cyclones have become significantly more frequent, longer lasting, and stronger in the lower Canadian Arctic over the last 50 years (1953–2002), but less frequent and weaker in the south, especially along the southeast and southwest Canadian coasts (Wang et al., 2006a). Further south, a tendency toward weaker low-pressure systems over the past few decades was found for U.S. east coast winter cyclones using reanalyses, but no statistically significant trends in the frequency of occurrence of systems (Hirsch et al., 2001).

Using the 20CR (Compo et al., 2011), Wang et al. (2012h) found substantial increases in extratropical cyclone activity in the SH (20°S to 90°S). However, for southeast Australia, a decrease in activity is found and this agrees well with geostrophic wind extremes derived from *in situ* surface pressure observations (Alexander et al., 2011). This strengthens the evidence of a southward shift in storm tracks previously noted using older reanalyses products (Fyfe, 2003; Hope et al., 2006). Frederiksen and Frederiksen (2007) linked the reduction in cyclogenesis at 30°S and southward shift to a decrease in the vertical mean meridional temperature gradient. There is some inconsistency among reanalysis products for the SH regarding trends in the frequency of intense extratropical cyclones (Lim and Simmonds, 2007; Pezza et al., 2007; Lim and Simmonds, 2009) although studies tend to agree on a trend towards more intense systems, even when inhomogeneities associated with changing numbers of observations have been taken into account (Wang et al., 2012h). However, further undetected contamination of these trends owing to issues with the reanalyses products cannot be ruled out (Box 2.3) and this lowers our confidence in long-term trends. Links between extratropical cyclone activity and large-scale variability are discussed in Sections 2.7 and 14.6.2.

Frequently Asked Questions

FAQ 2.2 | Have There Been Any Changes in Climate Extremes?

There is strong evidence that warming has led to changes in temperature extremes—including heat waves—since the mid-20th century. Increases in heavy precipitation have probably also occurred over this time, but vary by region. However, for other extremes, such as tropical cyclone frequency, we are less certain, except in some limited regions, that there have been discernable changes over the observed record.

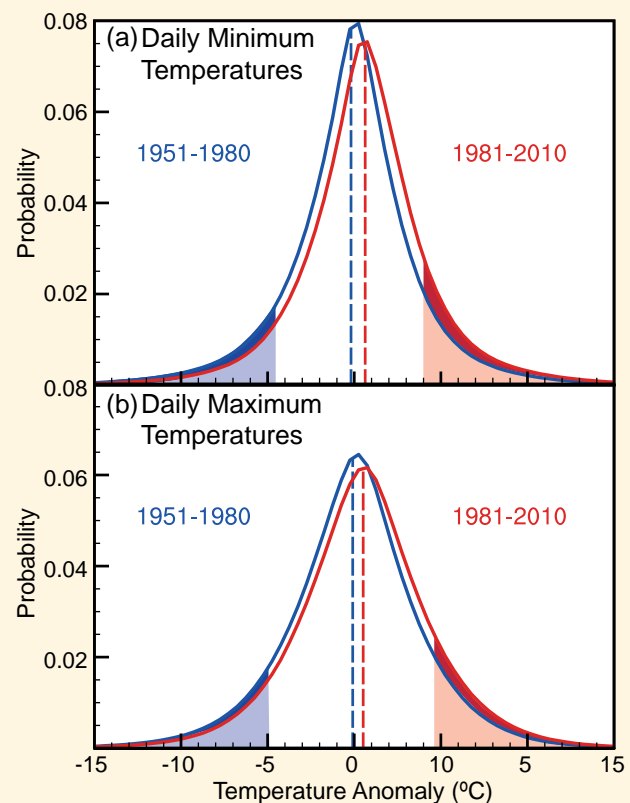
From heat waves to cold snaps or droughts to flooding rains, recording and analysing climate extremes poses unique challenges, not just because these events are rare, but also because they invariably happen in conjunction with disruptive conditions. Furthermore, there is no consistent definition in the scientific literature of what constitutes an extreme climatic event, and this complicates comparative global assessments.

Although, in an absolute sense, an extreme climate event will vary from place to place—a hot day in the tropics, for instance, may be a different temperature to a hot day in the mid-latitudes—international efforts to monitor extremes have highlighted some significant global changes.

For example, using consistent definitions for cold (<10th percentile) and warm (>90th percentile) days and nights it is found that warm days and nights have increased and cold days and nights have decreased for most regions of the globe; a few exceptions being central and eastern North America, and southern South America but mostly only related to daytime temperatures. Those changes are generally most apparent in minimum temperature extremes, for example, warm nights. Data limitations make it difficult to establish a causal link to increases in average temperatures, but FAQ 2.2, Figure 1 indicates that daily global temperature extremes have indeed changed. Whether these changes are simply associated with the average of daily temperatures increasing (the dashed lines in FAQ 2.2, Figure 1) or whether other changes in the distribution of daytime and nighttime temperatures have occurred is still under debate.

Warm spells or heat waves, that is, periods containing consecutive extremely hot days or nights, have also been assessed, but there are fewer studies of heat wave characteristics than those that compare changes in merely warm days or nights. Most global land areas with available data have experienced more heat waves since the middle of the 20th century. One exception is the south-eastern USA, where heat wave frequency and duration measures generally show decreases. This has been associated with a so-called ‘warming hole’ in this region, where precipitation has also increased and may be related to interactions between the land and the atmosphere and long-term variations in the Atlantic and Pacific Oceans. However, for large regions, particularly in Africa and South America, information on changes in heatwaves is limited.

For regions such as Europe, where historical temperature reconstructions exist going back several hundreds of years, indications are that some areas have experienced a disproportionate number of extreme heat waves in recent decades. *(continued on next page)*



FAQ 2.2, Figure 1 | Distribution of (a) daily minimum and (b) daily maximum temperature anomalies relative to a 1961–1990 climatology for two periods: 1951–1980 (blue) and 1981–2010 (red) using the HadGHCND data set. The shaded blue and red areas represent the coldest 10% and warmest 10% respectively of (a) nights and (b) days during the 1951–1980 period. The darker shading indicates by how much the number of the coldest days and nights has reduced (dark blue) and by how much the number of the warmest days and nights has increased (dark red) during the 1981–2010 period compared to the 1951–1980 period.

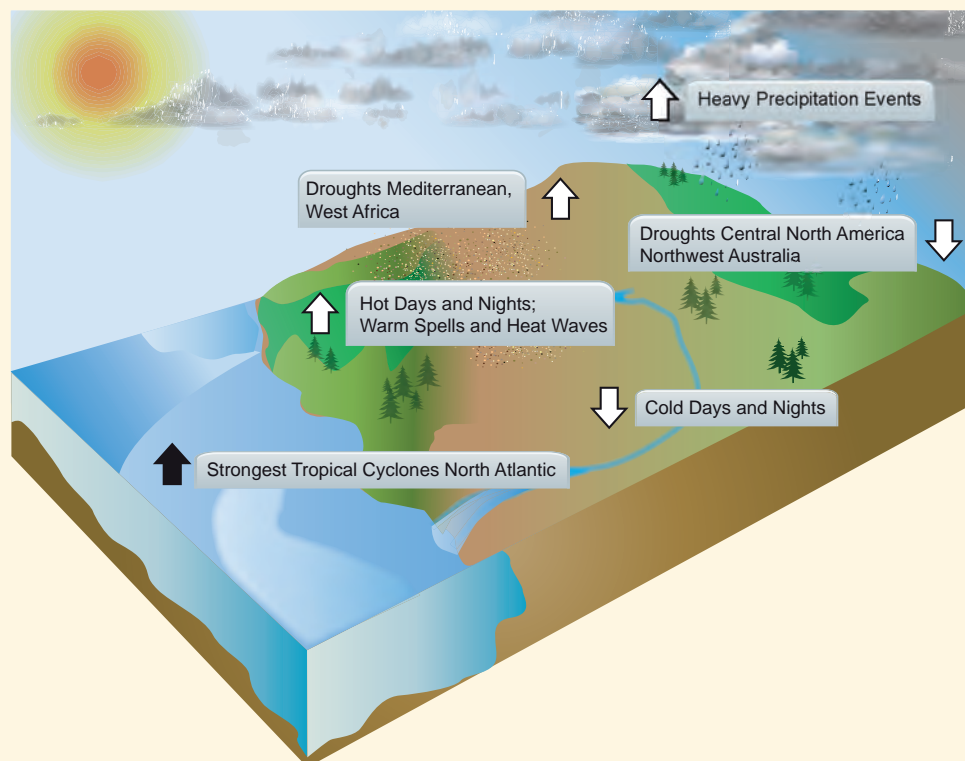
FAQ 2.2 (continued)

Changes in extremes for other climate variables are generally less coherent than those observed for temperature, owing to data limitations and inconsistencies between studies, regions and/or seasons. However, increases in precipitation extremes, for example, are consistent with a warmer climate. Analyses of land areas with sufficient data indicate increases in the frequency and intensity of extreme precipitation events in recent decades, but results vary strongly between regions and seasons. For instance, evidence is most compelling for increases in heavy precipitation in North America, Central America and Europe, but in some other regions—such as southern Australia and western Asia—there is evidence of decreases. Likewise, drought studies do not agree on the sign of the global trend, with regional inconsistencies in trends also dependent on how droughts are defined. However, indications exist that droughts have increased in some regions (e.g., the Mediterranean) and decreased in others (e.g., central North America) since the middle of the 20th century.

Considering other extremes, such as tropical cyclones, the latest assessments show that due to problems with past observing capabilities, it is difficult to make conclusive statements about long-term trends. There is very strong evidence, however, that storm activity has increased in the North Atlantic since the 1970s.

Over periods of a century or more, evidence suggests slight decreases in the frequency of tropical cyclones making landfall in the North Atlantic and the South Pacific, once uncertainties in observing methods have been considered. Little evidence exists of any longer-term trend in other ocean basins. For extratropical cyclones, a poleward shift is evident in both hemispheres over the past 50 years, with further but limited evidence of a decrease in wind storm frequency at mid-latitudes. Several studies suggest an increase in intensity, but data sampling issues hamper these assessments.

FAQ 2.2, Figure 2 summarizes some of the observed changes in climate extremes. Overall, the most robust global changes in climate extremes are seen in measures of daily temperature, including to some extent, heat waves. Precipitation extremes also appear to be increasing, but there is large spatial variability, and observed trends in droughts are still uncertain except in a few regions. While robust increases have been seen in tropical cyclone frequency and activity in the North Atlantic since the 1970s, the reasons for this are still being debated. There is limited evidence of changes in extremes associated with other climate variables since the mid-20th century.



FAQ 2.2, Figure 2 | Trends in the frequency (or intensity) of various climate extremes (arrow direction denotes the sign of the change) since the middle of the 20th century (except for North Atlantic storms where the period covered is from the 1970s).

Studies that have examined trends in wind extremes from observations or regional reanalysis products tend to point to declining trends in extremes in mid-latitudes (Pirazzoli and Tomasin, 2003; Smits et al., 2005; Pryor et al., 2007; Zhang et al., 2007b) and increasing trends in high latitudes (Lynch et al., 2004; Turner et al., 2005; Hundecha et al., 2008; Stegall and Zhang, 2012). Other studies have compared the trends from observations with reanalysis data and reported differing or even opposite trends in the reanalysis products (Smits et al., 2005; McVicar et al., 2008). On the other hand, declining trends reported by Xu et al. (2006b) over China between 1969 and 2000 were generally consistent with trends in NCEP reanalysis. Trends extracted from

reanalysis products must be treated with caution however, although usually with later generation products providing improvements over older products (Box 2.3).

In summary, *confidence* in large scale changes in the intensity of extreme extratropical cyclones since 1900 is *low*. There is also *low confidence* for a clear trend in storminess proxies over the last century due to inconsistencies between studies or lack of long-term data in some parts of the world (particularly in the SH). Likewise, *confidence* in trends in extreme winds is *low*, owing to quality and consistency issues with analysed data.

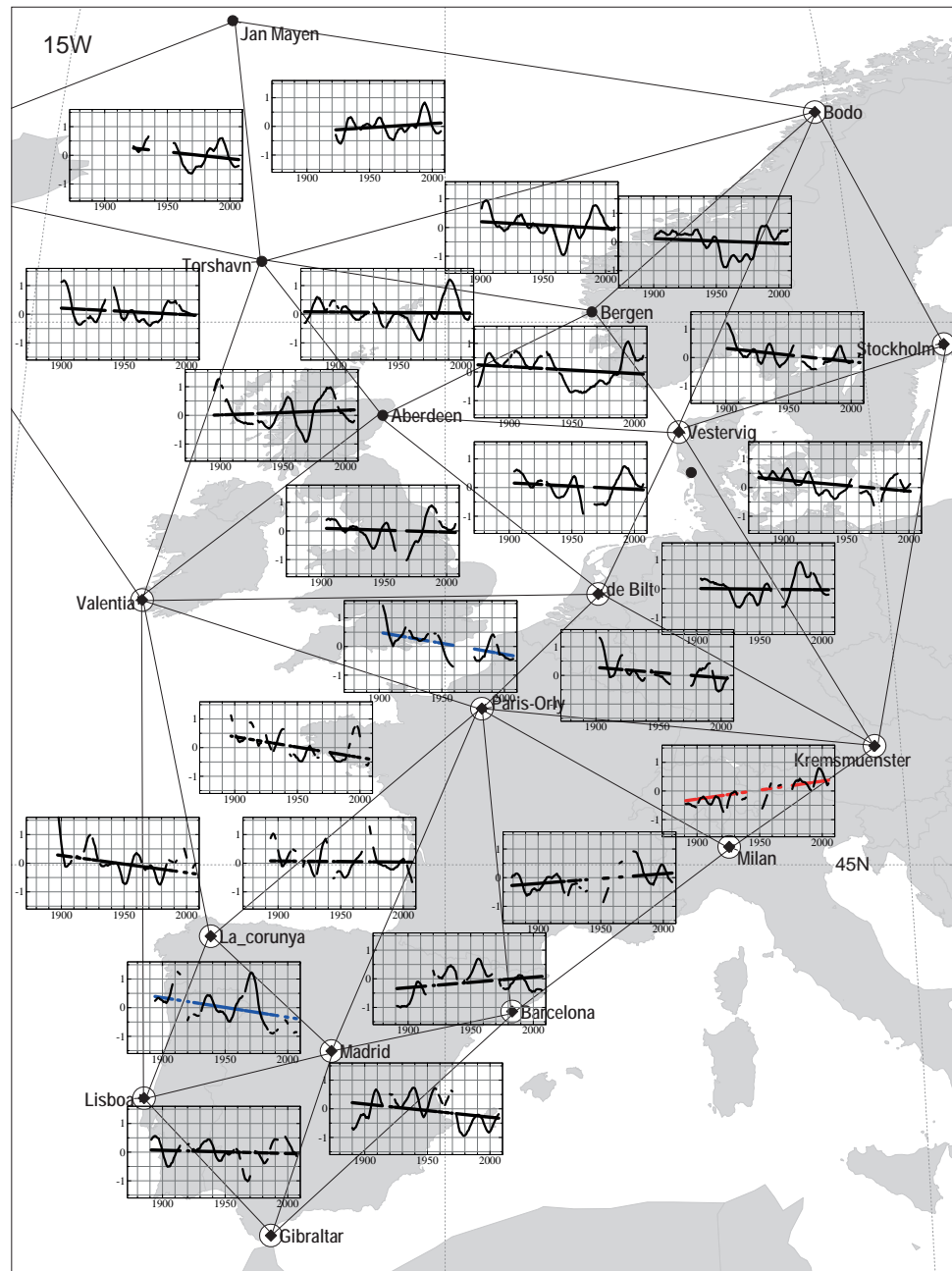


Figure 2.35 | 99th percentiles of geostrophic wind speeds for winter (DJF). Triangles show regions where geostrophic wind speeds have been calculated from *in situ* surface pressure observations. Within each pressure triangle, Gaussian low-pass filtered curves and estimated linear trends of the 99th percentile of these geostrophic wind speeds for winter are shown. The ticks of the time (horizontal) axis range from 1875 to 2005, with an interval of 10 years. Disconnections in lines show periods of missing data. Red (blue) trend lines indicate upward (downward) significant trends (i.e., a trend of zero lies outside the 95% confidence interval). (From Wang et al., 2011.)

Box 2.4 | Extremes Indices

As SREX highlighted, there is no unique definition of what constitutes a climate extreme in the scientific literature given variations in regions and sectors affected (Stephenson et al., 2008). Much of the available research is based on the use of so-called ‘extremes indices’ (Zhang et al., 2011). These indices can either be based on the probability of occurrence of given quantities or on absolute or percentage threshold exceedances (relative to a fixed climatological period) but also include more complex definitions related to duration, intensity and persistence of extreme events. For example, the term ‘heat wave’ can mean very different things depending on the index formulation for the application for which it is required (Perkins and Alexander, 2012).

Box 2.4, Table 1 lists a number of specific indices that appear widely in the literature and have been chosen to provide some consistency across multiple chapters in AR5 (along with the location of associated figures and text). These indices have been generally chosen for their robust statistical properties and their applicability across a wide range of climates. Another important criterion is that data for these indices are broadly available over both space and time. The existing near-global land-based data sets cover at least the post-1950 period but for regions such as Europe, North America, parts of Asia and Australia much longer analyses are available. The same indices used in observational studies (this chapter) are also used to diagnose climate model output (Chapters 9, 10, 11 and 12).

The types of indices discussed here do not include indices such as NIÑO3 representing positive and negative phases of ENSO (Box 2.5), nor do they include extremes such as 1 in 100 year events. Typically extreme indices assessed here reflect more ‘moderate’ extremes, for example, events occurring as often as 5% or 10% of the time (Box 2.4, Table 1). Predefined extreme indices are usually easier to obtain than the underlying daily climate data, which are not always freely exchanged by meteorological services. However, some of these indices do represent rarer events, for example, annual maxima or minima. Analyses of these and rarer extremes (e.g., with longer

(continued on next page)

Box 2.4, Table 1 | Definitions of extreme temperature and precipitation indices used in IPCC (after Zhang et al., 2011). The most common units are shown but these may be shown as normalized or relative depending on application in different chapters.

Index	Descriptive name	Definition	Units	Figures/Tables	Section
TXx	Warmest daily Tmax	Seasonal/annual maximum value of daily maximum temperature	°C	Box 2.4, Figure 1, Figures 9.37, 10.17, 12.13	Box 2.4, 9.5.4.1, 10.6.1.1, 12.4.3.3
TNx	Warmest daily Tmin	Seasonal/annual maximum value of daily minimum temperature	°C	Figures 9.37, 10.17	9.5.4.1, 10.6.1.1
TXn	Coldest daily Tmax	Seasonal/annual minimum value of daily maximum temperature	°C	Figures 9.37, 10.17, 12.13	9.5.4.1, 10.6.1.1, 12.4.3.3
TNn	Coldest daily Tmin	Seasonal/annual minimum value of daily minimum temperature	°C	Figures 9.37, 10.17, 12.13	9.5.4.1, 10.6.1.1
TN10p	Cold nights	Days (or fraction of time) when daily minimum temperature <10th percentile	Days (%)	Figures 2.32, 9.37, 10.17 Tables 2.11, 2.12	2.6.1, 9.5.4.1, 10.6.1.1, 11.3.2.5.1
TX10p	Cold days	Days (or fraction of time) when daily maximum temperature <10th percentile	Days (%)	Figures 2.32, 9.37, 10.17, 11.17	2.6.1, 9.5.4.1, 10.6.1.1, 11.3.2.5.1,
TN90p	Warm nights	Days (or fraction of time) when daily minimum temperature >90th percentile	Days (%)	Figures 2.32, 9.37, 10.17 Tables 2.11, 2.12	2.6.1, 9.5.4.1, 10.6.1.1, 11.3.2.5.1
TX90p	Warm days	Days (or fraction of time) when daily maximum temperature >90th percentile	Days (%)	Figures 2.32, 9.37, 10.17, 11.17 Tables 2.11, 2.12	2.6.1, 9.5.4.1, 10.6.1.1, 11.3.2.5.1,
FD	Frost days	Frequency of daily minimum temperature <0°C	Days	Figures 9.37, 12.13 Table 2.12	2.6.1, 9.5.4.1, 10.6.1.1, 12.4.3.3
TR	Tropical nights	Frequency of daily minimum temperature >20°C	Days	Figures 9.37, 12.13	9.5.4.1, 12.4.3.3
RX1day	Wettest day	Maximum 1-day precipitation	mm	Figures 9.37, 10.10 Table 2.12, 12.27	2.6.2.1, 9.5.4.1, 10.6.1.2, 12.4.5.5
RX5day	Wettest consecutive five days	Maximum of consecutive 5-day precipitation	mm	Figures 9.37, 12.26, 14.1	9.5.4.1, 10.6.1.2, 12.4.5.5, 14.2.1
SDII	Simple daily intensity index	Ratio of annual total precipitation to the number of wet days (≥1 mm)	mm day ⁻¹	Figures 2.33, 9.37, 14.1	2.6.2.1, 9.5.4.1, 14.2.1
R95p	Precipitation from very wet days	Amount of precipitation from days >95th percentile	mm	Figures 2.33, 9.37, 11.17 Table 2.12	2.6.2.1, 9.5.4.1, 11.3.2.5.1
CDD	Consecutive dry days	Maximum number of consecutive days when precipitation <1 mm	Days	Figures 2.33, 9.37, 12.26, 14.1	2.6.2.3, 9.5.4.1, 12.4.5.5, 14.2.1

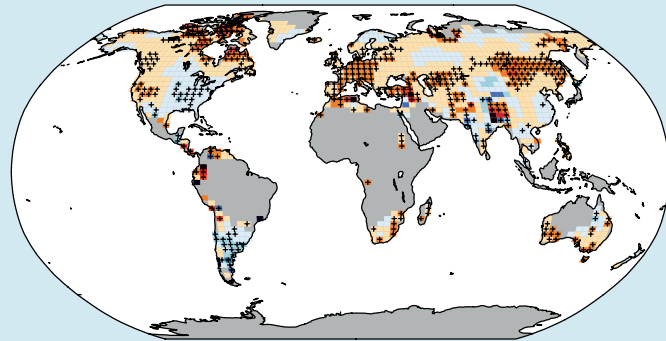
Box 2.4 (continued)

return period thresholds) are making their way into a growing body of literature which, for example, are using Extreme Value Theory (Coles, 2001) to study climate extremes (Zwiers and Kharin, 1998; Brown et al., 2008; Sillmann et al., 2011; Zhang et al., 2011; Kharin et al., 2013).

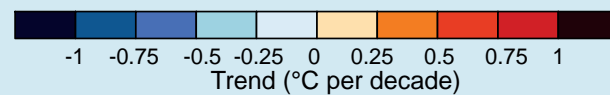
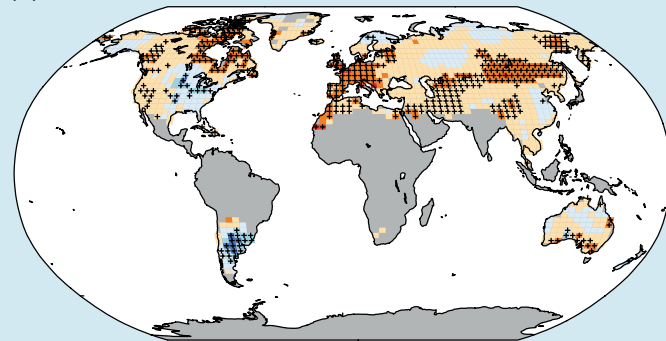
Extreme indices are more generally defined for daily temperature and precipitation characteristics (Zhang et al., 2011) although research is developing on the analysis of sub-daily events but mostly only on regional scales (Sen Roy, 2009; Shiu et al., 2009; Jones et al., 2010; Jakob et al., 2011; Lenderink et al., 2011; Shaw et al., 2011). Temperature and precipitation indices are sometimes combined to investigate 'extremeness' (e.g., hydroclimatic intensity, HY-INT; Giorgi et al., 2011) and/or the areal extent of extremes (e.g., the Climate Extremes Index (CEI) and its variants (Gleason et al., 2008; Gallant and Karoly, 2010; Ren et al., 2011). Indices rarely include other weather and climate variables, such as wind speed, humidity or physical impacts (e.g., streamflow) and phenomena. Some examples are available in the literature for wind-based (Della-Marta et al., 2009) and pressure-based (Beniston, 2009) indices, for health-relevant indices combining temperature and relative humidity characteristics (Diffenbaugh et al., 2007; Fischer and Schär, 2010) and for a range of dryness or drought indices (e.g., Palmer Drought Severity Index (PDSI) Palmer, 1965; Standardised Precipitation Index (SPI), Standardised Precipitation Evapotranspiration Index (SPEI) Vicente-Serrano et al., 2010) and wetness indices (e.g., Standardized Soil Wetness Index (SSWI); Vidal et al., 2010). (continued on next page)

In addition to the complication of defining an index, the results depend also on the way in which indices are calculated (to create global averages, for example). This is due to the fact that different algorithms may be employed to create grid box averages from station data, or that extremes indices may be calculated from gridded daily data or at station locations and then gridded. All of these factors add uncertainty to the calculation of an extreme. For example, the spatial patterns of trends in the hottest day of the year differ slightly between data sets, although when globally averaged, trends are similar over the second half of the 20th century (Box 2.4, Figure 1). Further discussion of the parametric and structural uncertainties in data sets is given in Box 2.1.

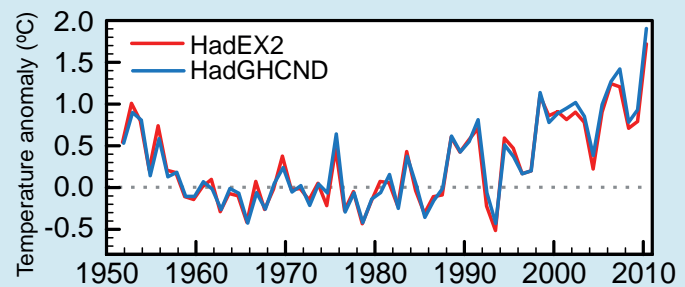
(a) HadEX2 1951-2010



(b) HadGHCND 1951-2010



(c) Global land average



Box 2.4, Figure 1 | Trends in the warmest day of the year using different data sets for the period 1951–2010. The data sets are (a) HadEX2 (Donat et al., 2013c) updated to include the latest version of the European Climate Assessment data set (Klok and Tank, 2009), (b) HadGHCND (Caesar et al., 2006) using data updated to 2010 (Donat et al., 2013a) and (c) Globally averaged annual warmest day anomalies for each data set. Trends were calculated only for grid boxes that had at least 40 years of data during this period and where data ended no earlier than 2003. Grey areas indicate incomplete or missing data. Black plus signs (+) indicate grid boxes where trends are significant (i.e., a trend of zero lies outside the 90% confidence interval). Anomalies are calculated using grid boxes only where both data sets have data and where 90% of data are available.

2.7 Changes in Atmospheric Circulation and Patterns of Variability

Changes in atmospheric circulation and indices of climate variability, as expressed in sea level pressure (SLP), wind, geopotential height (GPH), and other variables were assessed in AR4. Substantial multi-decadal variability was reported in the large-scale atmospheric circulation over the Atlantic and the Pacific. With respect to trends, a decrease was found in tropospheric GPH over high latitudes of both hemispheres and an increase over the mid-latitudes in boreal winter for the period 1979–2001. These changes were found to be associated with an intensification and poleward displacement of Atlantic and southern mid-latitude jet streams and enhanced storm track activity in the NH from the 1960s to at least the 1990s. Changes in the North Atlantic Oscillation (NAO) and the Southern Annular Mode (SAM) towards their positive phases were observed, but it was noted that the NAO returned to its long-term mean state from the mid-1990s to the early 2000s.

Since AR4, more and improved observational data sets and reanalysis data sets (Box 2.3) have been published. Uncertainties and inaccuracies in all data sets are better understood (Box 2.1). The studies since AR4 assessed in this section support the poleward movement of circulation features since the 1970s and the change in the SAM. At the same time, large decadal-to-multidecadal variability in atmospheric circulation is found that partially offsets previous trends in other circulation features such as the NAO or the Pacific Walker circulation.

This section assesses observational evidence for changes in atmospheric circulation in fields of SLP, GPH, and wind, in circulation features (such as the Hadley and Walker circulation, monsoons, or jet streams; Annex III: Glossary), as well as in circulation variability modes. Regional climate effects of the circulation changes are discussed in Chapter 14.

2.7.1 Sea Level Pressure

AR4 concluded that SLP in December to February decreased between 1948 and 2005 in the Arctic, Antarctic and North Pacific. More recent studies using updated data for the period 1949–2009 (Gillett and Stott, 2009) also find decreases in SLP in the high latitudes of both hemispheres in all seasons and increasing SLP in the tropics and subtropics most of the year. However, due to decadal variability SLP trends are sensitive to the choice of the time period (Box 2.2), and they depend on the data set.

The spatial distribution of SLP represents the distribution of atmospheric mass, which is the surface imprint of the atmospheric circulation. Barometric measurements are made in weather stations or on board ships. Fields are produced from the observations by interpolation or using data assimilation into weather models. One of the most widely used observational data sets is HadSLP2 (Allan and Ansell, 2006), which integrates 2228 historical global terrestrial stations with marine observations from the ICOADS on a $5^\circ \times 5^\circ$ grid. Other observation products (e.g., Trenberth and Paolino, 1980; for the extratropical NH) or reanalyses are also widely used to address changes in SLP. Although the quality of SLP data is considered good, there are discrepancies between gridded SLP data sets in regions with sparse observations, e.g., over Antarctica (Jones and Lister, 2007).

Van Haren et al. (2012) found a strong SLP decrease over the Mediterranean in January to March from 1961 to 2000. For the more recent period (1979–2012) trends in SLP, consistent across different data sets (shown in Figure 2.36 for ERA-Interim), are negative in the tropical and northern subtropical Atlantic during most of the year as well as, in May to October, in northern Siberia. Positive trends are found year-round over the North and South Pacific and South Atlantic. Trends in

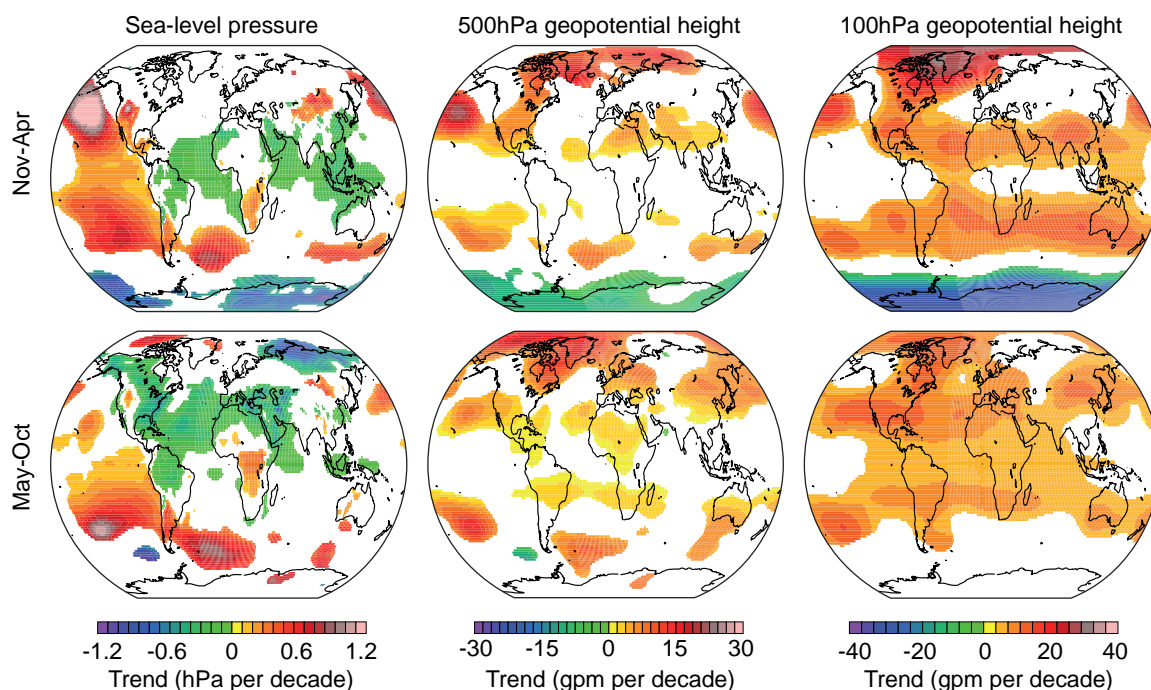


Figure 2.36 | Trends in (left) sea level pressure (SLP), (middle) 500 hPa geopotential height (GPH) and (right) 100 hPa GPH in (top) November to April 1979/1980 to 2011/2012 and (bottom) May to October 1979 to 2011 from ERA-Interim data. Trends are shown only if significant (i.e., a trend of zero lies outside the 90% confidence interval).

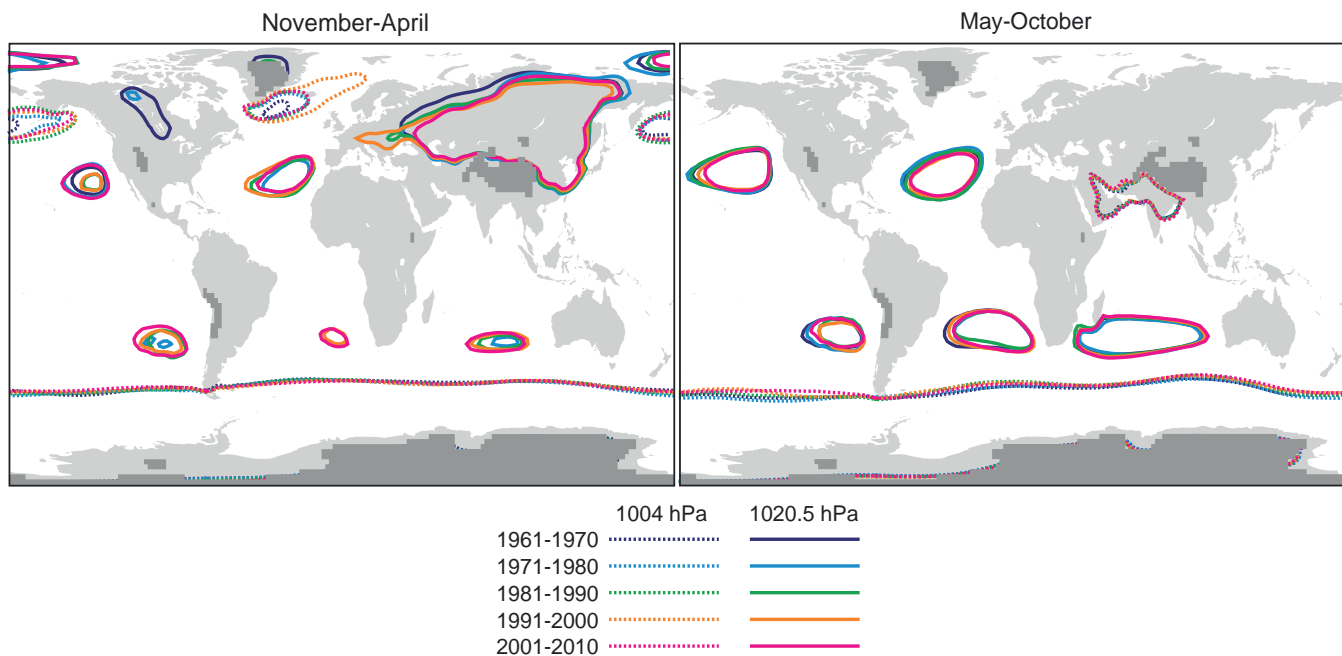


Figure 2.37 | Decadal averages of sea level pressure (SLP) from the 20th Century Reanalysis (20CR) for (left) November of previous year to April and (right) May to October shown by two selected contours: 1004 hPa (dashed lines) and 1020.5 hPa (solid lines). Topography above 2 km above mean sea level in 20CR is shaded in dark grey.

the equatorial Pacific zonal SLP gradient during the 20th century (e.g., Vecchi et al., 2006; Power and Kociuba, 2011a, 2011b) are discussed in Section 2.7.5.

The position and strength of semi-permanent pressure centres show no clear evidence for trends since 1951. However, prominent variability is found on decadal time scales (Figure 2.37). Consistent across different data sets, the Azores high and the Icelandic low in boreal winter, as captured by the high and low SLP contours, were both small in the 1960s and 1970s, large in the 1980s and 1990s, and again smaller in the 2000s. Favre and Gershunov (2006) find an eastward shift of the Aleutian low from the mid-1970s to 2001, which persisted during the 2000s (Figure 2.37). The Siberian High exhibits pronounced decadal-to-multidecadal variability (Panagiotopoulos et al., 2005; Huang et al., 2010), with a recent (1998 to 2012) strengthening and northward expansion (Zhang et al., 2012b). In boreal summer, the Atlantic and Pacific high-pressure systems extended more westward in the 1960s and 1970s than later. On interannual time scales, variations in pressure centres are related to modes of climate variability. Trends in the indices that capture the strength of these modes are reported in Section 2.7.8, their characteristics and impacts are discussed in Chapter 14.

In summary, sea level pressure has *likely* decreased from 1979 to 2012 over the tropical Atlantic and increased over large regions of the Pacific and South Atlantic, but trends are sensitive to the time period analysed owing to large decadal variability.

2.7.2 Surface Wind Speed

AR4 concluded that mid-latitude westerly winds have generally increased in both hemispheres. Because of shortcomings in the observations, SREX stated that *confidence* in surface wind trends is *low*. Further studies assessed here confirm this assessment.

Surface wind measurements over land and ocean are based on largely separate observing systems. Early marine observations were based on ship speed through the water or sails carried or on visual estimates of sea state converted to the wind speed using the Beaufort scale. Anemometer measurements were introduced starting in the 1950s. The transition from Beaufort to measured winds introduced a spurious trend, compounded by an increase in mean anemometer height over time (Kent et al., 2007; Thomas et al., 2008). ICOADS release 2.5 (Woodruff et al., 2011) contains information on measurement methods and wind measurement heights, permitting adjustment for these effects. The ICOADS-based data set WASWind (1950–2010; Tokinaga and Xie, 2011a) and the interpolated product NOCS v.2.0 (1973–present; Berry and Kent, 2011) include such corrections, among other improvements.

Marine surface winds are also measured from space using various microwave range instruments: scatterometers and synthetic aperture radars retrieve wind vectors, while altimeters and passive radiometers measure wind speed only (Bourassa et al., 2010). The latter type provides the longest continuous record, starting in July 1987. Satellite-based interpolated marine surface wind data sets use objective analysis methods to blend together data from different satellites and atmospheric reanalyses. The latter provide wind directions as in Blended Sea Winds (BSW; Zhang et al., 2006), or background fields as in Cross-Calibrated Multi-Platform winds (CCMP; Atlas et al., 2011) and OAFflux (Yu and Weller, 2007). CCMP uses additional dynamical constraints, *in situ* data and a recently homogenized data set of SSM/I observations (Wentz et al., 2007), among other satellite sources.

Figure 2.38 compares 1988–2010 linear trends in surface wind speeds from interpolated data sets based on satellite data, from interpolated and non-interpolated data sets based on *in situ* data, and from atmospheric reanalyses. Note that these trends over a 23-year-long period primarily reflect decadal variability in winds, rather than long-

term climate change (Box 2.2). Kent et al. (2012) recently intercompared several of these data sets and found large differences. The differences in trend patterns in Figure 2.38 are large as well. Nevertheless, some statistically significant features are present in most data sets, including a pattern of positive and negative trend bands across the North Atlantic Ocean (Section 2.7.6.2.) and positive trends along the west coast of North America. Strengthening of the Southern Ocean winds, consistent with the increasing trend in the SAM (Section 2.7.8) and with the observed changes in wind stress fields described in Section 3.4.4, can be seen in satellite-based analyses and atmospheric reanalyses in Figure 2.38. Alternating Southern Ocean trend signs in the NOCS v.2.0 panel are due to interpolation of very sparse *in situ* data (cf. the panel for the uninterpolated WASWind product).

Surface winds over land have been measured with anemometers on a global scale for decades, but until recently the data have been rarely

used for trend analysis. Global data sets lack important meta information on instrumentation and siting (McVicar et al., 2012). Long, homogenized instrumental records are rare (e.g., Usbeck et al., 2010; Wan et al., 2010). Moreover, wind speed trends are sensitive to the anemometer height (Troccoli et al., 2012). Winds near the surface can be derived from reanalysis products (Box 2.3), but discrepancies are found when comparing trends therein with trends for land stations (Smits et al., 2005; McVicar et al., 2008).

Over land, a weakening of seasonal and annual mean as well as maximum winds is reported for many regions from around the 1960s or 1970s to the early 2000s (a detailed review is given in McVicar et al. (2012)), including China and the Tibetan Plateau (Xu et al., 2006b; Guo et al., 2010) (but levelling off since 2000; Lin et al., 2012), Western and southern Europe (e.g., Earl et al., 2013), much of the USA (Pryor et al., 2007), Australia (McVicar et al., 2008) and southern and western

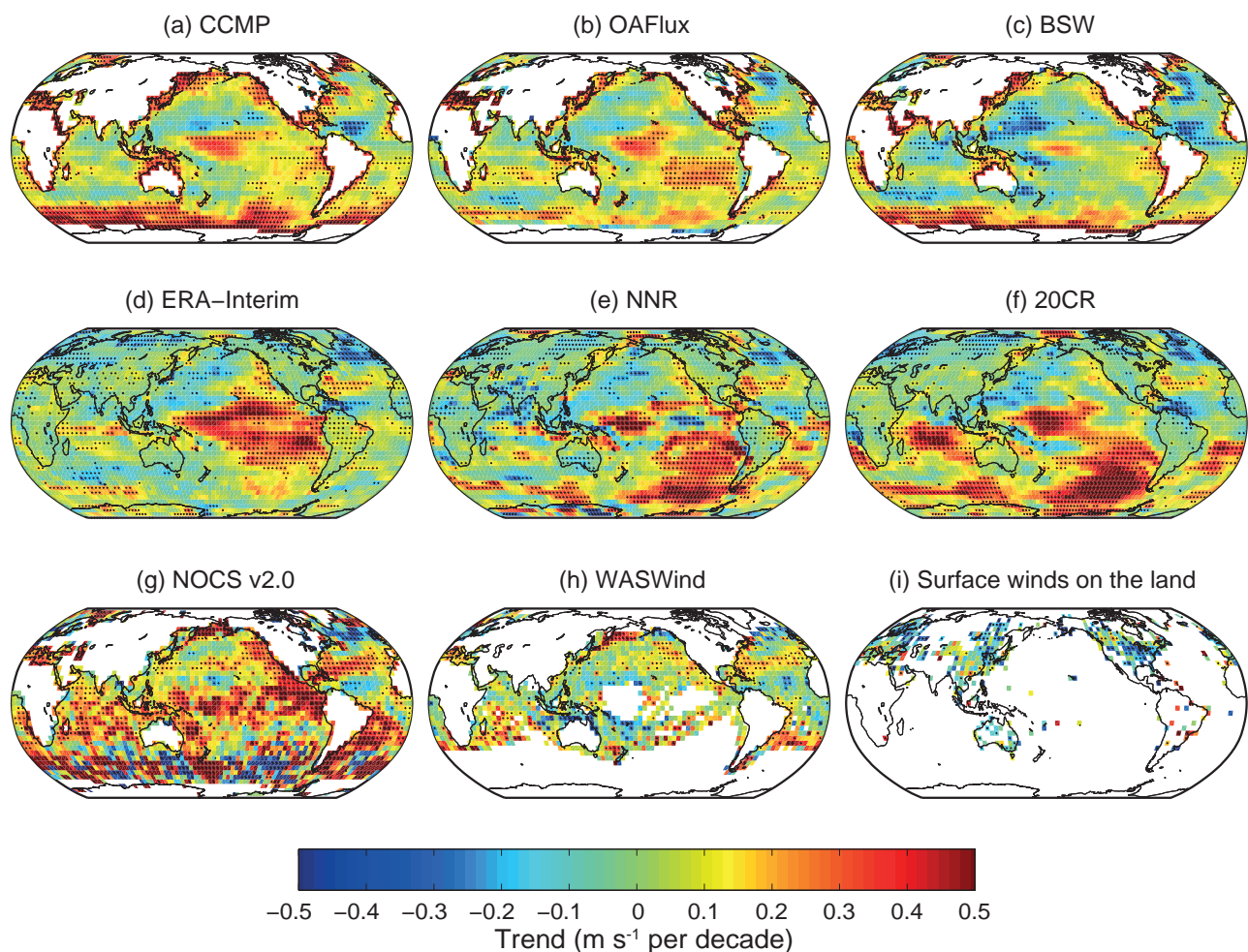


Figure 2.38 | Trends in surface wind speed for 1988–2010. Shown in the top row are data sets based on the satellite wind observations: (a) Cross-Calibrated Multi-Platform wind product (CCMP; Atlas et al., 2011); (b) wind speed from the Objectively Analyzed Air-Sea Heat Fluxes data set, release 3 (OAFlex); (c) Blended Sea Winds (BSW; Zhang et al., 2006); in the middle row are data sets based on surface observations: (d) ERA-Interim; (e) NCEP-NCAR, v.1 (NNR); (f) 20th Century Reanalysis (20CR, Compo et al., 2011), and in the bottom row are surface wind speeds from atmospheric reanalyses: (g) wind speed from the Surface Flux Data set, v.2, from NOC, Southampton, UK (Berry and Kent, 2009); (h) Wave- and Anemometer-based Sea Surface Wind (WASWind; Tokinaga and Xie, 2011a); and (i) Surface Winds on the Land (Vautard et al., 2010). Wind speeds correspond to 10 m heights in all products. Land station winds (panel f) are also for 10 m (but anemometer height is not always reported) except for the Australian data where they correspond to 2 m height. To improve readability of plots, all data sets (including land station data) were averaged to the $4^\circ \times 4^\circ$ uniform longitude-latitude grid. Trends were computed for the annually averaged timeseries of $4^\circ \times 4^\circ$ cells. For all data sets except land station data, an annual mean was considered available only if monthly means for no less than eight months were available in that calendar year. Trend values were computed only if no less than 17 years had values and at least 1 year was available among the first and last 3 years of the period. White areas indicate incomplete or missing data. Black plus signs (+) indicate grid boxes where trends are significant (i.e., a trend of zero lies outside the 90% confidence interval).

Canada (Wan et al., 2010). Increasing wind speeds were found at high latitudes in both hemispheres, namely in Alaska from 1921 to 2001 (Lynch et al., 2004), in the central Canadian Arctic and Yukon from the 1950 to the 2000s (Wan et al., 2010) and in coastal Antarctica over the second half of the 20th century (Turner et al., 2005). A global review of 148 studies showed that near-surface terrestrial wind speeds are declining in the Tropics and the mid-latitudes of both hemispheres at a rate of -0.14 m s^{-1} per decade (McVicar et al., 2012). Vautard et al. (2010), analysing a global land surface wind data set from 1979 to 2008, found negative trends on the order of -0.1 m s^{-1} per decade over large portions of NH land areas. The wind speed trend pattern over land inferred from their data (1988–2010, Figure 2.38) has many points with magnitudes much larger than those in the reanalysis products, which appear to underestimate systematically the wind speed over land, as well as in coastal regions (Kent et al., 2012).

In summary, *confidence* is *low* in changes in surface wind speed over the land and over the oceans owing to remaining uncertainties in data sets and measures used.

2.7.3 Upper-Air Winds

In contrast to surface winds, winds above the planetary boundary layer have received little attention in AR4. Radiosondes and pilot balloon observations are available from around the 1930s (Stickler et al., 2010). Temporal inhomogeneities in radiosonde wind records are less common, but also less studied, than those in radiosonde temperature records (Gruber and Haimberger, 2008; Section 2.4.4.3). Upper air winds can also be derived from tracking clouds or water vapour in satellite imagery (Menzel, 2001) or from measurements using wind profilers, aircraft or thermal observations, all of which serve as an input to reanalyses (Box 2.3).

In the past few years, interest in an accurate depiction of upper air winds has grown, as they are essential for estimating the state and changes of the general atmospheric circulation and for explaining changes in the surface winds (Vautard et al., 2010). Allen and Sherwood (2008), analysing wind shear from radiosonde data, found significant positive zonal mean zonal wind trends in the northern extratropics in the upper troposphere and stratosphere and negative trends in the tropical upper troposphere for the period 1979–2005. Vautard et al. (2010) find increasing wind speed in radiosonde observations in the lower and middle troposphere from 1979 to 2008 over Europe and North America and decreasing wind speeds over Central and East Asia. However, systematic global trend analyses of radiosonde winds are rare, prohibiting an assessment of upper-air wind trends (specific features such as monsoons, jet streams and storms are discussed in Sections 2.7.5, 2.7.6 and 2.6, respectively).

In summary, upper-air winds are less studied than other aspects of the circulation, and less is known about the quality of data products, hence *confidence* in upper-air wind trends is *low*.

2.7.4 Tropospheric Geopotential Height and Tropopause

AR4 concluded that over the NH between 1960 and 2000, boreal winter and annual means of tropospheric GPH decreased over high latitudes and increased over the mid-latitudes. AR4 also reported an increase in tropical tropopause height and a slight cooling of the tropical cold-point tropopause.

Changes in GPH, which can be addressed using radiosonde data or reanalysis data (Box 2.3), reflect SLP and temperature changes in the atmospheric levels below. The spatial gradients of the trend indicate changes in the upper-level circulation. As for SLP, tropospheric GPH trends strongly depend on the period analysed due to pronounced decadal variability. For the 1979–2012 period, trends for 500 hPa GPH from the ERA-Interim reanalysis (Figure 2.36) as well as for other reanalyses show a significant decrease only at southern high latitudes in November to April, but significant positive GPH trends in the subtropics and northern high latitudes. Hence the change in the time period leads to a different trend pattern as compared to AR4. The seasonality and spatial dependence of 500 hPa GPH trends over Antarctica was highlighted by Neff et al. (2008), based upon radiosonde data over the period 1957–2007.

Minimum temperatures near the tropical tropopause (and therefore tropical tropopause height) are important as they affect the water vapour input into the stratosphere (Section 2.2.2.1). Studies since AR4 confirm the increase in tropopause height (Wang et al., 2012c). For tropical tropopause temperatures, studies based on radiosonde data and reanalyses partly support a cooling between the 1990s and the early 2000s (Randel et al., 2006; Randel and Jensen, 2013), but uncertainties in long-term trends of the tropical cold-point tropopause temperature from radiosondes (Wang et al., 2012c; Randel and Jensen, 2013) and reanalyses (Gettelman et al., 2010) are large and *confidence* is therefore *low*.

In summary, tropospheric geopotential height *likely* decreased from 1979 to 2012 at SH high latitudes in austral summer and increased in the subtropics and NH high latitudes. *Confidence* in trends of the tropical cold-point tropopause is *low* owing to remaining uncertainties in the data.

2.7.5 Tropical Circulation

In AR4, large interannual variability of the Hadley and Walker circulation was highlighted, as well as the difficulty in addressing changes in these features in the light of discrepancies between data sets. AR4 also found that rainfall in many monsoon systems exhibits decadal changes, but that data uncertainties restrict confidence in trends. SREX also attributed *low confidence* to observed trends in monsoons.

Observational evidence for trends and variability in the strength of the Hadley and Walker circulations (Annex III: Glossary), the monsoons, and the width of the tropical belt is based on radiosonde and reanalyses data (Box 2.3). In addition, changes in the tropical circulation imprint on other fields that are observed from space (e.g., total ozone, outgoing longwave radiation). Changes in the average state of the tropical circulation are constrained to some extent by changes in the water

cycle (Held and Soden, 2006; Schneider et al., 2010). Changes in the monsoon systems are expressed through altered circulation, moisture transport and convergence, and precipitation. Only a few monsoon studies address circulation changes, while most work focuses on precipitation.

Several studies report a weakening of the global monsoon circulations as well as a decrease of global land monsoon rainfall or of the number of precipitation days over the past 40 to 50 years (Zhou et al., 2008, see also SREX; Liu et al., 2011). Concerning the East Asian Monsoon, a year-round decrease is reported for wind speeds over China at the surface and in the lower troposphere based on surface observations and radiosonde data (Guo et al., 2010; Jiang et al., 2010; Vautard et al., 2010; Xu et al., 2010). The changes in wind speed are concomitant with changes in pressure centres such as a westward extension of the Western Pacific Subtropical High (Gong and Ho, 2002; Zhou et al., 2009b). A weakening of the East Asian summer monsoon since the

1920s is also found in SLP gradients (Zhou et al., 2009a). However, trends derived from wind observations and circulation trends from reanalysis data carry large uncertainties (Figure 2.38), and monsoon rainfall trends depend, for example, on the definition of the monsoon area (Hsu et al., 2011). For instance, using a new definition of monsoon area, an increase in northern hemispheric and global summer monsoon (land and ocean) precipitation is reported from 1979 to 2008 (Hsu et al., 2011; Wang et al., 2012a).

The additional data sets that became available since AR4 confirm the large interannual variability of the Hadley and Walker circulation. The strength of the northern Hadley circulation (Figure 2.39) in boreal winter and of the Pacific Walker circulation in boreal fall and winter is largely related to the ENSO (Box 2.5). This association dominates interannual variability and affects trends. Data sets do not agree well with respect to trends in the Hadley circulation (Figure 2.39). Two widely used reanalysis data sets, NNR and ERA-40, both have demonstrated

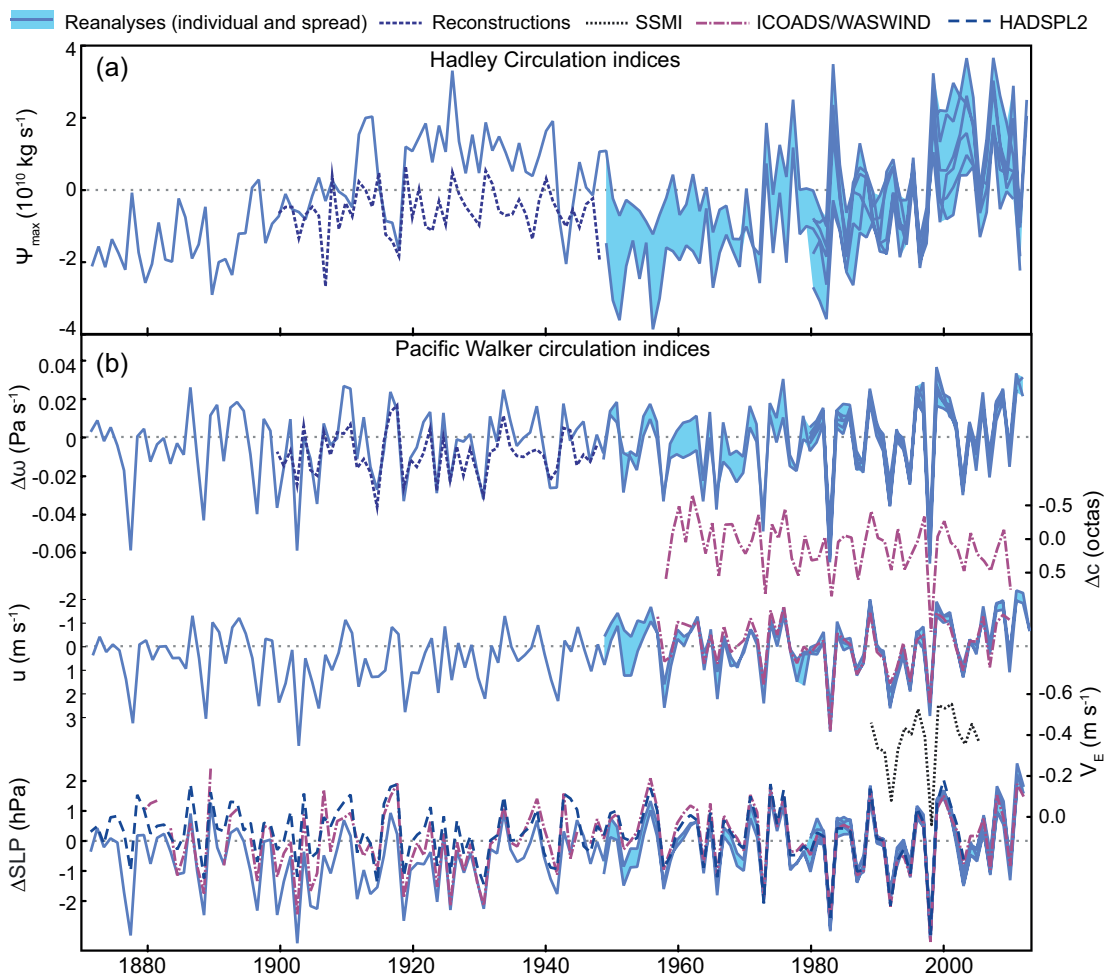


Figure 2.39 | (a) Indices of the strength of the northern Hadley circulation in December to March (Ψ_{\max} is the maximum of the meridional mass stream function at 500 hPa between the equator and 40°N). (b) Indices of the strength of the Pacific Walker circulation in September to January ($\Delta\omega$ is the difference in the vertical velocity between [10°S to 10°N, 180°W to 100°W] and [10°S to 10°N, 100°E to 150°E] as in Oort and Yienger (1996), Δc is the difference in cloud cover between [6°N to 12°S, 165°E to 149°W] and [18°N to 6°N, 165°E to 149°W] as in Deser et al. (2010a), v_E is the effective wind index from SSM/I satellite data, updated from Sohn and Park (2010), u is the zonal wind at 10 m averaged in the region [10°S to 10°N, 160°E to 160°W], ΔSLP is the SLP difference between [5°S to 5°N, 160°W to 80°W] and [5°S to 5°N, 80°E to 160°E] as in Vecchi et al. (2006)). Reanalysis data sets include 20CR, NCEP/NCAR, ERA-Interim, JRA-25, MERRA, and CFSR, except for the zonal wind at 10 m (20CR, NCEP/NCAR, ERA-Interim), where available until January 2013. ERA-40 and NCEP2 are not shown as they are outliers with respect to the strength trend of the northern Hadley circulation (Mitas and Clement, 2005; Song and Zhang, 2007; Hu et al., 2011; Stachnik and Schumacher, 2011). Observation data sets include HadSLP2 (Section 2.7.1), ICOADS (Section 2.7.2; only 1957–2009 data are shown) and WASWIND (Section 2.7.2), reconstructions are from Brönnimann et al. (2009). Where more than one time series was available, anomalies from the 1980/1981 to 2009/2010 mean values of each series are shown.

shortcomings with respect to tropical circulation; hence their increases in the Hadley circulation strength since the 1970s might be artificial (Mitas and Clement, 2005; Song and Zhang, 2007; Hu et al., 2011; Stachnik and Schumacher, 2011). Later generation reanalysis data sets including ERA-Interim (Brönnimann et al., 2009; Nguyen et al., 2013) as well as satellite humidity data (Sohn and Park, 2010) also suggest a strengthening from the mid 1970s to present, but the magnitude is strongly data set dependent.

Consistent changes in different observed variables suggest a weakening of the Pacific Walker circulation during much of the 20th century that has been largely offset by a recent strengthening. A weakening is indicated by trends in the zonal SLP gradient across the equatorial Pacific (Section 2.7.1, Table 2.14) from 1861 to 1992 (Vecchi et al., 2006), or from 1901 to 2004 (Power and Kociuba, 2011b). Boreal spring and summer contribute most strongly to the centennial trend (Nicholls, 2008; Karnauskas et al., 2009), as well as to the trend in the second half of the 20th century (Tokinaga et al., 2012). For boreal fall and winter, when the circulation is strongest, no trend is found in the Pacific Walker circulation based on the vertical velocity at 500 hPa from reanalyses (Compo et al., 2011), equatorial Pacific 10 m zonal winds, or SLP in Darwin (Nicholls, 2008; Figure 2.39). However, there are inconsistencies between ERA-40 and NNR (Chen et al., 2008). Deser et al. (2010a) find changes in marine air temperature and cloud cover over the Pacific that are consistent with a weakening of the Walker circulation during most of the 20th century (Section 2.5.7.1 and Yu and Zwiers, 2010). Tokinaga et al. (2012) find robust evidence for a weakening of the Walker circulation (most notably over the Indian Ocean) from 1950 to 2008 based on observations of cloud cover, surface wind, and SLP. Since the 1980s or 1990s, however, trends in the Pacific Walker

circulation have reversed (Figure 2.39; Luo et al., 2012). This is evident from changes in SLP (see equatorial Southern Oscillation Index (SOI) trends in Table 2.14 and Box 2.5, Figure 1), vertical velocity (Compo et al., 2011), water vapour flux from satellite and reanalysis data (Sohn and Park, 2010), or sea level height (Merrifield, 2011). It is also consistent with the SST trend pattern since 1979 (Meng et al., 2012; see also Figure 2.22).

Observed changes in several atmospheric parameters suggest that the width of the tropical belt has increased at least since 1979 (Seidel et al., 2008; Forster et al., 2011; Hu et al., 2011). Since AR4, wind, temperature, radiation, and ozone information from radiosondes, satellites, and reanalyses had been used to diagnose the tropical belt width and estimate their trends. Annual mean time series of the tropical belt width from various sources are shown in Figure 2.40.

Since 1979 the region of low column ozone values typical of the tropics has expanded in the NH (Hudson et al., 2006; Hudson, 2012). Based on radiosonde observations and reanalyses, the region of the high tropical tropopause has expanded since 1979, and possibly since 1960 (Seidel and Randel, 2007; Birner, 2010; Lucas et al., 2012), although widening estimates from different reanalyses and using different methodologies show a range of magnitudes (Seidel and Randel, 2007; Birner, 2010).

Several lines of evidence indicate that climate features at the edges of the Hadley cell have also moved poleward since 1979. Subtropical jet metrics from reanalysis zonal winds (Strong and Davis, 2007, 2008; Archer and Caldeira, 2008b, 2008a) and layer-average satellite temperatures (Fu et al., 2006; Fu and Lin, 2011) also indicate widening, although 1979–2009 wind-based trends (Davis and Rosenlof, 2011)

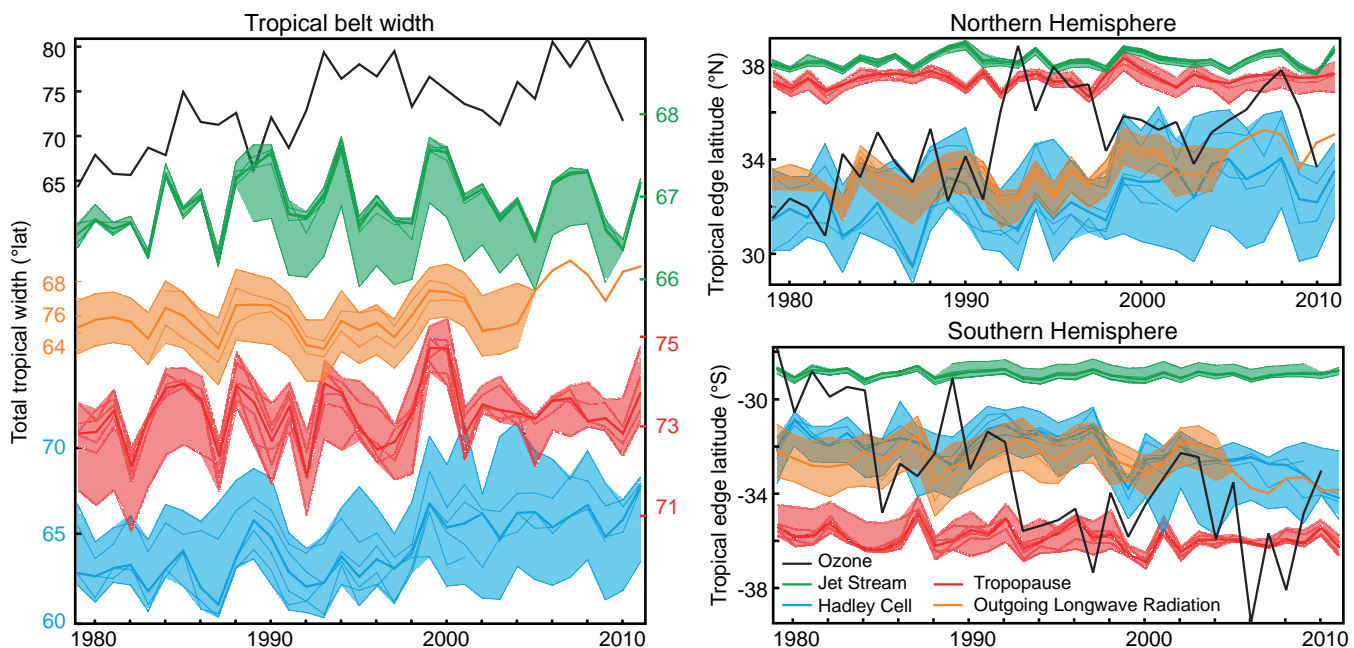


Figure 2.40 | Annual average tropical belt width (left) and tropical edge latitudes in each hemisphere (right). The tropopause (red), Hadley cell (blue), and jet stream (green) metrics are based on reanalyses (NCEP/NCAR, ERA-40, JRA25, ERA-Interim, CFSR, and MERRA, see Box 2.3); outgoing longwave radiation (orange) and ozone (black) metrics are based on satellite measurements. The ozone metric refers to equivalent latitude (Hudson et al., 2006; Hudson, 2012). Adapted and updated from Seidel et al. (2008) using data presented in Davis and Rosenlof (2011) and Hudson (2012). Where multiple data sets are available for a particular metric, all are shown as light solid lines, with shading showing their range and a heavy solid line showing their median.

are not statistically significant. Changes in subtropical outgoing long-wave radiation, a surrogate for high cloud, also suggest widening (Hu and Fu, 2007), but the methodology and results are disputed (Davis and Rosenlof, 2011). Widening of the tropical belt is also found in precipitation patterns (Hu and Fu, 2007; Davis and Rosenlof, 2011; Hu et al., 2011; Kang et al., 2011; Zhou et al., 2011), including in SH regions (Cai et al., 2012).

The qualitative consistency of these observed changes in independent data sets suggests a widening of the tropical belt between at least 1979 and 2005 (Seidel et al., 2008), and possibly longer. Widening estimates range between around 0° and 3° latitude per decade, but their uncertainties have been only partially explored (Birner, 2010; Davis and Rosenlof, 2011).

In summary, large interannual-to-decadal variability is found in the strength of the Hadley and Walker circulation. The *confidence* in trends in the strength of the Hadley circulation is *low* due to uncertainties in reanalysis data sets. Recent strengthening of the Pacific Walker circulation has largely offset the weakening trend from the 19th century to the 1990s (*high confidence*). Several lines of independent evidence indicate a widening of the tropical belt since the 1970s. The suggested weakening of the East Asian monsoon has *low confidence*, given the nature and quality of the evidence.

2.7.6 Jets, Storm Tracks and Weather Types

2.7.6.1 Mid-latitude and Subtropical Jets and Storm Track Position

AR4 reported a poleward displacement of Atlantic and southern polar front jet streams from the 1960s to at least the mid-1990s and a poleward shift of the northern hemispheric storm tracks. However, it was also noted that uncertainties are large and that NNR and ERA-40 disagree in important aspects. SREX also reported a poleward shift of NH and SH storm tracks. Studies since AR4 confirm that in the NH, the jet core has been migrating towards the pole since the 1970s, but trends in the jet speed are uncertain. Additional studies assessed here further support the poleward shift of the North Atlantic storm track from the 1950s to the early 2000s.

Subtropical and mid-latitude jet streams are three-dimensional entities that vary meridionally, zonally, and vertically. The position of the mid-latitude jet streams is related to the position of the mid-latitude storm tracks; regions of enhanced synoptic activity due to the passage of cyclones (Section 2.6). Jet stream winds can be determined from radiosonde measurements of GPH using quasi-geostrophic flow assumptions. Using reanalysis data sets (Box 2.3), it is possible to track three-dimensional jet variations by identifying a surface of maximum wind (SMW), although a high vertical resolution is required for identification of jets.

Various new analyses based on NCEP/NCAR and ERA-40 reanalyses as well as MSU/AMSU lower stratospheric temperatures (Section 2.4.4) confirm that the jet streams (mid-latitude and subtropical) have been moving poleward in most regions in the NH over the last three decades (Fu et al., 2006; Hu and Fu, 2007; Strong and Davis, 2007; Archer and

Caldeira, 2008a; Fu and Lin, 2011) but no clear trend is found in the SH (Swart and Fyfe, 2012). There is inconsistency with respect to jet speed trends based upon whether one uses an SMW-based or isobaric-based approach (Strong and Davis, 2007, 2008; Archer and Caldeira, 2008b, 2008a) and the choice of analysis periods due to inhomogeneities in reanalyses (Archer and Caldeira, 2008a). In general, jets have become more common (and jet speeds have increased) over the western and central Pacific, eastern Canada, the North Atlantic and Europe (Strong and Davis, 2007; Barton and Ellis, 2009), trends that are concomitant with regional increases in GPH gradients and circumpolar vortex contraction (Frauenfeld and Davis, 2003; Angell, 2006). From a climate dynamics perspective, these trends are driven by regional patterns of tropospheric and lower stratospheric warming or cooling and thus are coupled to large-scale circulation variability.

The North Atlantic storm track is closely associated with the NAO (Schneider et al., 2007). Studies based on ERA-40 reanalysis (Schneider et al., 2007), SLP measurements from ships (Chang, 2007), sea level time series (Vilibic and Sepic, 2010), and cloud analyses (Bender et al., 2012) support a poleward shift and intensification of the North Atlantic cyclone tracks from the 1950s to the early 2000s (Sorteberg and Walsh, 2008; Cornes and Jones, 2011).

2.7.6.2 Weather Types and Blocking

In AR4, weather types were not assessed as such, but an increase in blocking frequency in the Western Pacific and a decrease in North Atlantic were noted.

Changes in the frequency of weather types are of interest since weather extremes are often associated with specific weather types. For instance, persistent blocking of the westerly flow was essential in the development of the 2010 heat wave in Russia (Dole et al., 2011) (Section 9.5.2.2 and Box 14.2). Synoptic classifications or statistical clustering (Philipp et al., 2007) are commonly used to classify the weather on a given day. Feature-based methods are also used (Crocini-Maspoli et al., 2007a). All these methods require daily SLP or upper-level fields.

Trends in synoptic weather types have been best analysed for central Europe since the mid-20th century, where several studies describe an increase in westerly or cyclonic weather types in winter but an increase of anticyclonic, dry weather types in summer (Philipp et al., 2007; Werner et al., 2008; Trnka et al., 2009). An eastward shift of blocking events over the North Atlantic (fewer cases of blocking over Greenland and more frequent blocking over the eastern North Atlantic) and the North Pacific was found by Davini et al. (2012) using NCEP/NCAR reanalysis since 1951 and by Crocini-Maspoli et al. (2007a) in ERA-40 reanalysis during the period 1957–2001. Mokhov et al. (2013) find an increase in blocking duration over the NH year-round since about 1990 in a study based on NCEP/NCAR reanalysis data from 1969–2011. For the SH, Dong et al. (2008) found a decrease in number of blocking days but increase in intensity of blocking over the period 1948–1999. Differences in blocking index definitions, the sensitivity of some indices to changes in the mean field, and strong interannual variability in all seasons (Kreienkamp et al., 2010), partly related to circulation variability modes (Crocini-Maspoli et al., 2007b), complicate a global assessment of blocking trends.

In summary, there is evidence for a poleward shift of storm tracks and jet streams since the 1970s. Based on the consistency of these trends with the widening of the tropical belt (Section 2.7.5), trends that are based on many different data sets, variables, and approaches, it is *likely* that circulation features have moved poleward since the 1970s. Methodological differences between studies mean there is *low confidence* in characterizing the global nature of any change in blocking.

2.7.7 Stratospheric Circulation

Changes in the polar vortices were assessed in AR4. A significant decrease in lower-stratospheric GPH in summer over Antarctica since 1969 was found, whereas trends in the Northern Polar Vortex were considered uncertain owing to its large variability.

The most important characteristics of the stratospheric circulation for climate and for trace gas distribution are the winter and spring polar vortices and Sudden Stratospheric Warmings (rapid warmings of the middle stratosphere that may lead to a collapse of the Polar Vortex), the Quasi-Biennial Oscillation (an oscillation of equatorial zonal winds with a downward phase propagation) and the Brewer-Dobson circulation (BDC, the meridional overturning circulation transporting air upward in the tropics, poleward to the winter hemisphere, and downward at polar and subpolar latitudes; Annex III: Glossary). Radiosonde observations, reanalysis data sets and space-borne temperature or trace gas observations are used to address changes in the stratospheric circulation, but all of these sources of information carry large trend uncertainties.

The AR4 assessment was corroborated further in Forster et al. (2011) and in updated 100 hPa GPH trends from ERA-Interim reanalysis (Box 2.3, Figure 2.36). There is *high confidence* that lower stratospheric GPH over Antarctica has decreased in spring and summer at least since 1979. Cohen et al. (2009) reported an increase in the number of Arctic sudden stratospheric warmings during the last two decades. However, interannual variability in the Arctic Polar Vortex is large, uncertainties in reanalysis products are high (Tegtmeier et al., 2008), and trends depend strongly on the time period analysed (Langematz and Kunze, 2008).

The BDC is only indirectly observable via wave activity diagnostics (which represent the main driving mechanism of the BDC), via temperatures or via the distribution of trace gases which may allow the determination of the ‘age of air’ (i.e., the time an air parcel has resided in the stratosphere after its entry from the troposphere). Randel et al. (2006), found a sudden decrease in global lower stratospheric water vapour and ozone around 2001 that is consistent with an increase in the mean tropical upwelling, that is, the tropical branch of the BDC (Rosenlof and Reid, 2008; Section 2.2.2.1; Lanzante, 2009; Randel and Jensen, 2013). On the other hand, Engel et al. (2009) found no statistically significant change in the age of air in the 24–35 km layer over the NH mid-latitudes from measurements of chemically inert trace gases from 1975 to 2005. However, this does not rule out trends in the lower stratospheric branch of the BDC or trends in mid to low latitude mixing (Bonisch et al., 2009; Ray et al., 2010). All of these methods are subject to considerable uncertainties, and they might shed light only on some aspects of the BDC. *Confidence* in trends in the BDC is therefore *low*.

In summary, it is *likely* that lower-stratospheric geopotential height over Antarctica has decreased in spring and summer at least since 1979. Owing to uncertainties in the data and approaches used, *confidence* in trends in the Brewer–Dobson circulation is *low*.

2.7.8 Changes in Indices of Climate Variability

AR4 assessed changes in indices of climate variability. The NAO and SAM were found to exhibit positive trends (strengthened mid-latitude westerlies) from the 1960s to 1990s, but the NAO has returned to its long-term mean state since then.

Indices of climate variability describe the state of the climate system with regards to individual modes of climate variability. Together with corresponding spatial patterns, they summarize large fractions of spatio-temporal climate variability. Inferences about significant trends in indices are generally hampered by relative shortness of climate records, their uncertainties and the presence of large variability on decadal and multidecadal time scales.

Table 2.14 summarizes observed changes in well-known indices of climate variability (see Box 2.5, Table 1 for precise definitions). Even the indices that explicitly include detrending of the entire record (e.g., Deser et al., 2010b), can exhibit statistically significant trends over shorter sub-periods. Confidence intervals in Table 2.14 that do not contain zero indicate trend significance at 10% level; however, the trends significant at 5% and 1% levels are emphasized in the discussion that follows. Chapter 14 discusses the main features and physical meaning of individual climate modes.

The NAO index reached very low values in the winter of 2010 (Osborn, 2011). As a result, with the exception of the principal component (PC)-based NAO index, which still shows a 5% significant positive trend from 1951 to present, other NAO or North Annular Mode (NAM) indices do not show significant trends of either sign for the periods presented in Table 2.14. In contrast, the SAM maintained the upward trend (Table 2.14). Fogt et al. (2009) found a positive trend in the SAM index from 1957 to 2005. Visbeck (2009), in a station-based index, found an increase in recent decades (1970s to 2000s).

The observed detrended multidecadal SST anomaly averaged over the North Atlantic Ocean area is often called Atlantic Multi-decadal Oscillation Index (AMO; see Box 2.5, Table 1, Figure 1). The warming trend in the “revised” AMO index since 1979 is significant at 1% level (Table 2.14) but cannot be readily interpreted because of the difficulty with reliable removal of the SST warming trend from it (Deser et al., 2010b).

On decadal and inter-decadal time scales the Pacific climate shows an irregular oscillation with long periods of persistence in individual stages and prominent shifts between them. Pacific Decadal Oscillation (PDO), Inter-decadal Pacific Oscillation (IPO) and North Pacific Index (NPI) indices characterize this variability for both hemispheres and agree well with each other (Box 2.5, Figure 1). While AR4 noted climate impacts of the 1976–1977 PDO phase transition, the shift in the opposite direction, both in PDO and IPO, may have occurred at the end of 1990s (Cai and van Rensch, 2012; Dai, 2012). Significance of 1979–2012 trends in PDO and NPI then would be an artefact of this

Table 2.14 | Trends for selected indices listed in Box 2.5, Table 1. Each index was standardized for its longest available period contained within the 1870–2012 interval. Standardization was done on the December-to-March (DJFM) means for the NAO, NAM and Pacific-North American pattern (PNA), on seasonal anomalies for Pacific-South American patterns (PSA1, PSA2) and on monthly anomalies for all other indices. Standardized monthly and seasonal anomalies were further averaged to annual means. Trend values computed for annual or DJFM means are given in standard deviation per decade with their 90% confidence intervals. Index records where the source is not explicitly indicated were computed from either HadISST1 (for SST-based indices), or HadSLP2r (for SLP-based indices) or NNR fields of 500 hPa or 850 hPa geopotential height. CoA stands for 'Centers of Action' index definitions. Linear trends for 1870–2012 were removed from ATL3, BMI and DMI.

Index Name	Trends in standard deviation units per decade		
	1901–2012	1951–2012	1979–2012
(–1)*SOI from CPC		0.004 ± 0.103	–0.243 ± 0.233
(–1)*SOI Troup from BOM records	0.012 ± 0.039	0.018 ± 0.104	–0.247 ± 0.236
SOI Darwin from BOM records	0.028 ± 0.036	0.082 ± 0.085	–0.116 ± 0.195
(–1)*EQSOI	0.001 ± 0.051	–0.076 ± 0.143	–0.558 ^b ± 0.297
NIÑO3.4	–0.003 ± 0.042	0.012 ± 0.105	–0.156 ± 0.274
NIÑO3.4 (ERSST v.3b)	0.067 ^a ± 0.045	0.054 ± 0.103	–0.085 ± 0.259
NIÑO3.4 (COBE SST)	0.024 ± 0.041	0.008 ± 0.107	–0.154 ± 0.289
NIÑO3	0.007 ± 0.039	0.043 ± 0.095	–0.143 ± 0.256
NIÑO3 (ERSST v.3b)	0.069 ± 0.039	0.098 ± 0.092	–0.073 ± 0.236
NIÑO3 (COBE SST)	0.034 ± 0.036	0.054 ± 0.096	–0.113 ± 0.258
NIÑO4	0.026 ± 0.054	0.068 ± 0.145	–0.102 ± 0.380
EMI	–0.059 ± 0.061	–0.119 ± 0.189	–0.131 ± 0.580
(–1)*TNI	0.019 ± 0.052	0.066 ± 0.167	0.030 ± 0.550
PDO from Mantua et al. (1997)	–0.017 ± 0.071	0.112 ± 0.189	–0.460 ^a ± 0.284
(–1)*NPI	–0.026 ^a ± 0.022	0.010 ± 0.046	–0.169 ^a ± 0.105
AMO revised	–0.001 ± 0.111	–0.012 ± 0.341	0.779 ^b ± 0.291
NAO stations from Jones et al. (1997)	–0.044 ± 0.056	0.095 ± 0.149	–0.136 ± 0.394
NAO stations from Hurrell (1995)	–0.001 ± 0.066	0.171 ± 0.179	–0.214 ± 0.400
NAO PC from Hurrell (1995)	0.012 ± 0.059	0.198 ^a ± 0.148	–0.037 ± 0.401
NAM PC	0.003 ± 0.048	0.141 ± 0.123	0.029 ± 0.360
SAM Z850 PC		0.268 ^b ± 0.063	0.100 ± 0.109
SAM SLP grid 40°S to 70°S	0.139 ^b ± 0.026	0.198 ^b ± 0.052	0.294 ^a ± 0.131
SAM SLP stations from Marshall (2003)			0.128 ^a ± 0.097
PNA CoA		0.113 ± 0.114	–0.103 ± 0.298
PNA RPC from CPC		0.202 ^b ± 0.111	0.019 ± 0.271
PSA Karoly (1989) CoA definition		–0.267 ^b ± 0.079	–0.233 ^a ± 0.174
(–1)*PSA Yuan and Li (2008) CoA definition		–0.211 ^b ± 0.069	–0.208 ± 0.189
PSA1 PC		–0.163 ^a ± 0.103	–0.368 ^a ± 0.245
PSA2 PC		0.200 ^b ± 0.066	0.036 ± 0.156
ATL3	0.035 ± 0.043	0.125 ^a ± 0.088	0.186 ± 0.193
AONM PC	0.064 ^a ± 0.051	0.138 ^a ± 0.109	0.327 ^a ± 0.230
AMM PC	0.019 ± 0.058	–0.015 ± 0.155	0.309 ± 0.324
IOBM PC	0.075 ^a ± 0.051	0.314 ^b ± 0.082	0.201 ± 0.206
BMI	0.072 ^a ± 0.050	0.294 ^b ± 0.083	0.189 ± 0.206
IODM PC	–0.016 ± 0.034	–0.031 ± 0.093	–0.052 ± 0.203
DMI	0.030 ± 0.033	0.080 ± 0.090	0.211 ± 0.210

Notes:

^a Trend values significant at the 5% level.

^b Trend values significant at the 1% level.

change; incidentally, no significant trends in these indices were seen for longer periods (Table 2.14). Nevertheless, Pacific changes since the 1980s (positive for NPI and negative for PDO and IPO) are consistent with the observed SLP changes (Section 2.7.1) and with reversing trends in the Walker Circulation (Section 2.7.5), which was reported to be slowing down during much of the 20th century but sped up again since the 1990s. Equatorial SOI shows an increasing trend since 1979 at 1% significance; more traditionally defined SOI indices do not show significant trends (Table 2.14).

NIÑO3.4 and NIÑO3 show a century-scale warming trend significant at 5% level, if computed from the ERSSTv3b data set (Section 2.4.2) but not if calculated from other data sets (Table 2.14). Furthermore, the sign (and significance) of the trend in east–west SST gradient across the Pacific remains ambiguous (Vecchi and Soden, 2007; Bunge and Clarke, 2009; Karnauskas et al., 2009; Deser et al., 2010a) (Section 14.4.1).

In addition to changes in the mean values of climate indices, changes in the associated spatial patterns are also possible. In particular, the diversity of detail of different ENSO events and possible distinction between their “flavors” have received significant attention (Section 14.4.2). These efforts also intensified the discussion of useful ENSO indices in the literature. Starting from the work of Trenberth and Stepaniak (2001), who proposed to characterize the evolution of ENSO events with the Trans-Niño Index (TNI), which is virtually uncorrelated with the standard ENSO index NIÑO3.4, other alternative ENSO indices have been introduced and proposals were made for classifying ENSO events according to the indices they primarily maximize. While a traditional, ‘canonical’ El Niño event type (Rasmusson and Carpenter, 1982) is viewed as the ‘eastern Pacific’ type, some of the alternative indices purport to identify events that have central Pacific maxima and are called dateline El Niño (Larkin and Harrison, 2005), Modoki (Ashok et al., 2007), or Central Pacific El Niño (Kao and Yu, 2009). However, no consensus has been reached regarding the appropriate classification

of ENSO events. Takahashi et al. (2011) and Ren and Jin (2011) have presented many of the popular ENSO indices as elements in a two-dimensional linear space spanned by a pair of such indices. ENSO indices that involve central and western Pacific SST (NIÑO4, EMI, TNI) show no significant trends.

Significant positive PNA trends and negative and positive trends in the first and second PSA modes respectively are observed over the last 60 years (Table 2.14). However, the level of significance of these trends depends on the index definition and on the data set used. The positive trend in the Atlantic Ocean ‘Niño’ mode (AONM) index and in ATL3 are due to the intensified warming in the eastern Tropical Atlantic that causes the the weakening of the Atlantic equatorial cold tongue: these changes were noticed by Tokinaga and Xie (2011b) with regards to the last 60-year period. The Indian Ocean Basin Mode (IOBM) has a strong warming trend (significant at 1% since the middle of the 20th century). This phenomenon is well-known (Du and Xie, 2008) and its consequences for the regional climate is a subject of active research (Du et al., 2009; Xie et al., 2009).

In summary, large variability on interannual to decadal time scales and remaining differences between data sets precludes robust conclusions on long-term changes in indices of climate variability. *Confidence is high* that the increase in the NAO index from the 1950s to the 1990s has been largely offset by recent changes. It is *likely* that the SAM index has become more positive since the 1950s.

Box 2.5 | Patterns and Indices of Climate Variability

Much of the spatial structure of climate variability can be described as a combination of ‘preferred’ patterns. The most prominent of these are known as modes of climate variability and they impact weather and climate on many spatial and temporal scales (Chapter 14). Individual climate modes historically have been identified through spatial teleconnections: correlations between regional climate variations at widely separated, geographically fixed spatial locations. An index describing temporal variations of the climate mode in question can be formed, for example, by adding climate anomalies calculated from meteorological records at stations exhibiting the strongest correlation with the mode and subtracting anomalies at stations exhibiting anticorrelation. By regressing climate records from other places on this index, one derives a spatial climate pattern characterizing this mode. Patterns of climate variability have also been derived using a variety of mathematical techniques such as principal component analysis (PCA). These patterns and their indices are useful both because they efficiently describe climate variability in terms of a few preferred modes and also because they can provide clues about how the variability is sustained (Box 14.1 provides formal definitions of these terms).

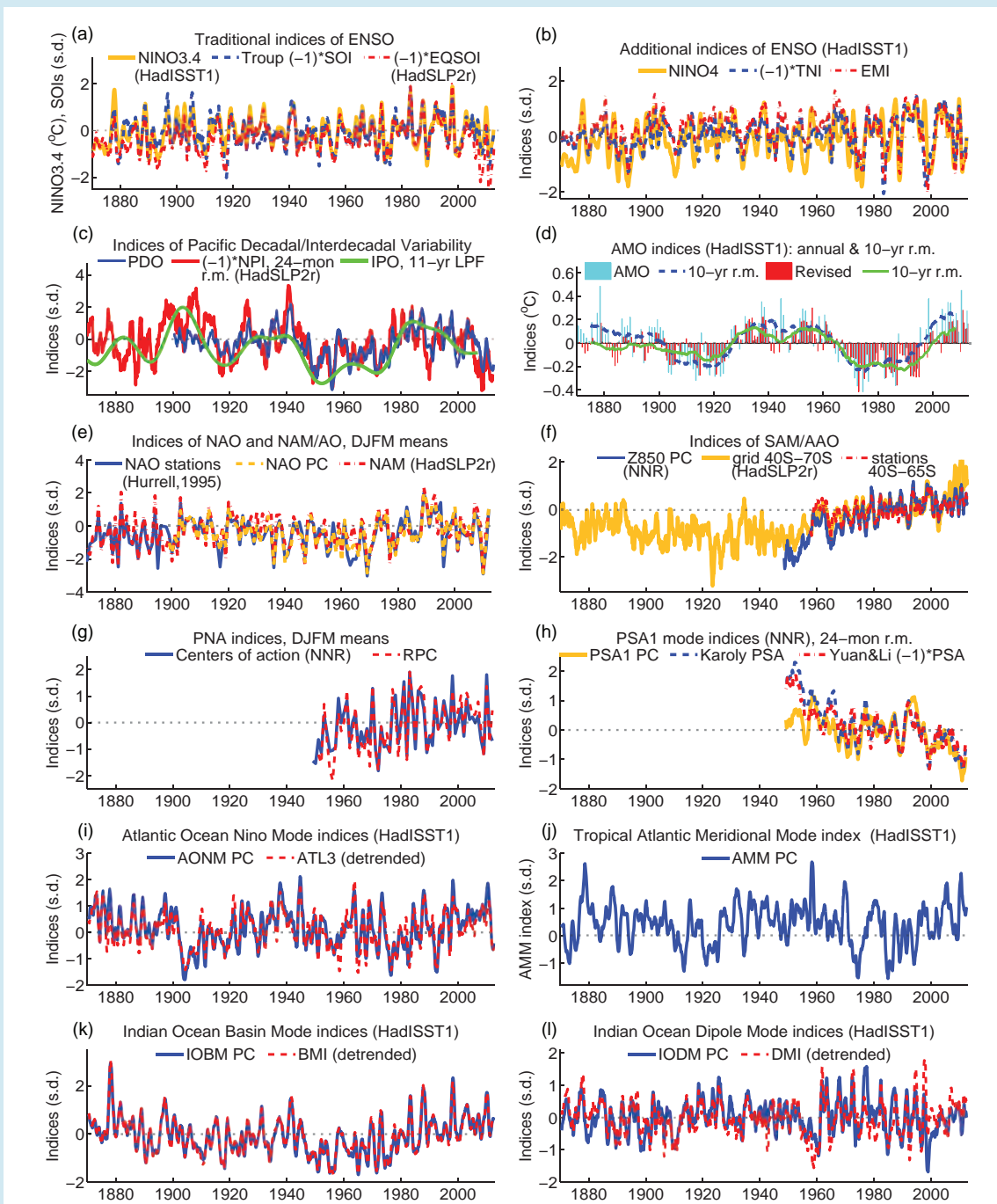
Box 2.5, Table 1 lists some prominent modes of large-scale climate variability and indices used for defining them. Changes in these indices are associated with large-scale climate variations on interannual and longer time scales. With some exceptions, indices shown have been used by a variety of authors. They are defined relatively simply from raw or statistically analyzed observations of a single climate variable, which has a history of surface observations. For most of these indices at least a century-long record is available for climate research. *(continued on next page)*

Box 2.5, Table 1 | Established indices of climate variability with global or regional influence. Z500, Z700 and Z850 denote geopotential height at the 500, 700 and 850 hPa levels, respectively. The subscripts s and a denote “standardized” and “anomalies”, respectively. Further information is given in Supplementary Material 2.SM.8. Climate impacts of these modes are listed in Box 14.1. (continued on next page)

Climate Phenomenon		Index Name	Index Definition	Primary Reference(s)
El Niño – Southern Oscillation (ENSO)	Traditional indices of ENSO-related Tropical Pacific variability	NIÑO1+2	SST _a averaged over [10°S–0°, 90°W–80°W]	Rasmusson and Wallace (1983), Cane (1986)
		NIÑO3	Same as above but for [5°S–5°N, 150°W–90°W]	
		NIÑO4	Same as above but for [5°S–5°N, 160°E–150°W]	
		NIÑO3.4	Same as above but for [5°S–5°N, 170°W–120°W]	Trenberth (1997)
		Troup Southern Oscillation Index (SOI)	Standardized for each calendar month SLP _s difference: Tahiti minus Darwin, ×10	Troup (1965)
		SOI	Standardized difference of SLP _{sa} : Tahiti minus Darwin	Trenberth (1984); Ropelewski and Jones (1987)
		Darwin SOI	Darwin SLP _{sa}	Trenberth and Hoar (1996)
	Equatorial SOI (EQSOI)	Standardized difference of standardized averages of SLP _s over equatorial [5°S–5°N] Pacific Ocean areas: [130°W–80°W] minus [90°E–140°E]	Bell and Halpert (1998)	
	Indices of ENSO events evolution and type	Trans-Niño Index (TNI)	NIÑO1+2 _s minus NIÑO4 _s	Trenberth and Stepaniak (2001)
El Niño Modoki Index (EMI)		SST _s [165°E–140°W, 10°S–10°N] minus ½*[110°W–70°W, 15°S–5°N] minus ½*[125°E–145°E, 10°S–20°N]	Ashok et al. (2007)	
Pacific Decadal and Interdecadal Variability		Pacific Decadal Oscillation (PDO)	1st PC of monthly N. Pacific SST _s field [20°N–70°N] with subtracted global mean	Mantua et al. (1997); Zhang et al. (1997)
		Inter-decadal Pacific Oscillation (IPO)	Projection of a global SST _s onto the IPO pattern, which is found as one of the leading Empirical Orthogonal Functions of a low-pass filtered global SST _s field	Folland et al. (1999); Power et al. (1999); Parker et al. (2007)
		North Pacific Index (NPI)	SLP _s averaged over [30°N–65°N; 160°E–140°W]	Trenberth and Hurrell (1994)
North Atlantic Oscillation (NAO)		Azores-Iceland NAO Index	SLP _{sa} difference: Lisbon/Ponta Delgada minus Stykkisholmur/ Reykjavik	Hurrell (1995)
		PC-based NAO Index	Leading PC of SLP _s over the Atlantic sector	Hurrell (1995)
		Gibraltar – South-west Iceland NAO Index	Standardized for each calendar month SLP _s difference: Gibraltar minus SW Iceland / Reykjavik	Jones et al. (1997)
Annular modes	Northern Annular Mode (NAM)	PC-based NAM or Arctic Oscillation (AO) index	1st PC of the monthly mean SLP _s poleward of 20°N	Thompson and Wallace (1998, 2000)
	Southern Annular Mode (SAM)	PC-based SAM or Antarctic Oscillation (AAO) index	1st PC of Z850 _s or Z700 _s south of 20°S	Thompson and Wallace (2000)
		Grid-based SAM index: 40°S–70°S difference	Difference between standardized zonally averaged SLP _s at 40°S and 70°S, using gridded SLP fields	Nan and Li (2003)
		Station-based SAM index: 40°S–65°S	Difference in standardized zonal mean SLP _s at 40°S and 65°S, using station data	Marshall (2003)
Pacific/North America (PNA) atmospheric teleconnection		PNA index based on centers of action	¼[(20°N, 160°W) – (45°N, 165°W) + (55°N, 115°W) – (30°N, 85°W)] in the Z500 _{sa} field	Wallace and Gutzler (1981)
		PNA from rotated PCA	Rotated PC (RPC) from the analysis of the NH Z500 _s field	Barnston and Livezey (1987)
Pacific/South America (PSA) atmospheric teleconnection		PSA1 and PSA2 mode indices (PC-based)	2nd and 3rd PCs respectively of SH seasonal Z500 _s	Mo and Paegle (2001)
		PSA index (centers of action)	[–(35°S, 150°W) + (60°S, 120°W) – (45°S, 60°W)] in the Z500 _s field [(45°S, 170°W) – (67.5°S, 120°W) + (50°S, 45°W)]/3 in the Z500 _s field	Karoly (1989) Yuan and Li (2008)
Atlantic Ocean Multidecadal Variability		Atlantic Multi-decadal Oscillation (AMO) index	10-year running mean of linearly detrended Atlantic mean SST _s [0°–70°N]	Enfield et al. (2001)
		Revised AMO index	As above, but detrended by subtracting SST _s [60°S–60°N] mean	Trenberth and Shea (2006)
Tropical Atlantic Ocean Variability	Atlantic Ocean Niño Mode (AONM)	ATL3	SST _s averaged over [3°S–3°N, 20°W–0°]	Zebiak (1993)
		PC-based AONM	1st PC of the detrended tropical Atlantic monthly SST _s (20°S–20°N)	Deser et al. (2010b)
	Tropical Atlantic Meridional Mode (AMM)	PC-based AMM Index	2nd PC of the detrended tropical Atlantic monthly SST _s (20°S–20°N)	
Tropical Indian Ocean Variability	Indian Ocean Basin Mode (IOBM)	Basin mean index (BMI)	SST _s averaged over [40°–110°E, 20°S–20°N]	Yang et al. (2007)
		IOBM, PC-based Index	The first PC of the IO detrended SST _s (40°E–110° E, 20°S–20°N)	Deser et al. (2010b)
	Indian Ocean Dipole Mode (IODM)	PC-based IODM index	The second PC of the IO detrended SST _s (40°E–110° E, 20°S–20°N)	
		Dipole Mode Index (DMI)	SST _s difference: [50°E–70°E, 10°S–10°N] minus [90°E–110°E, 10°S–0°]	Saji et al. (1999)

Box 2.5 (continued)

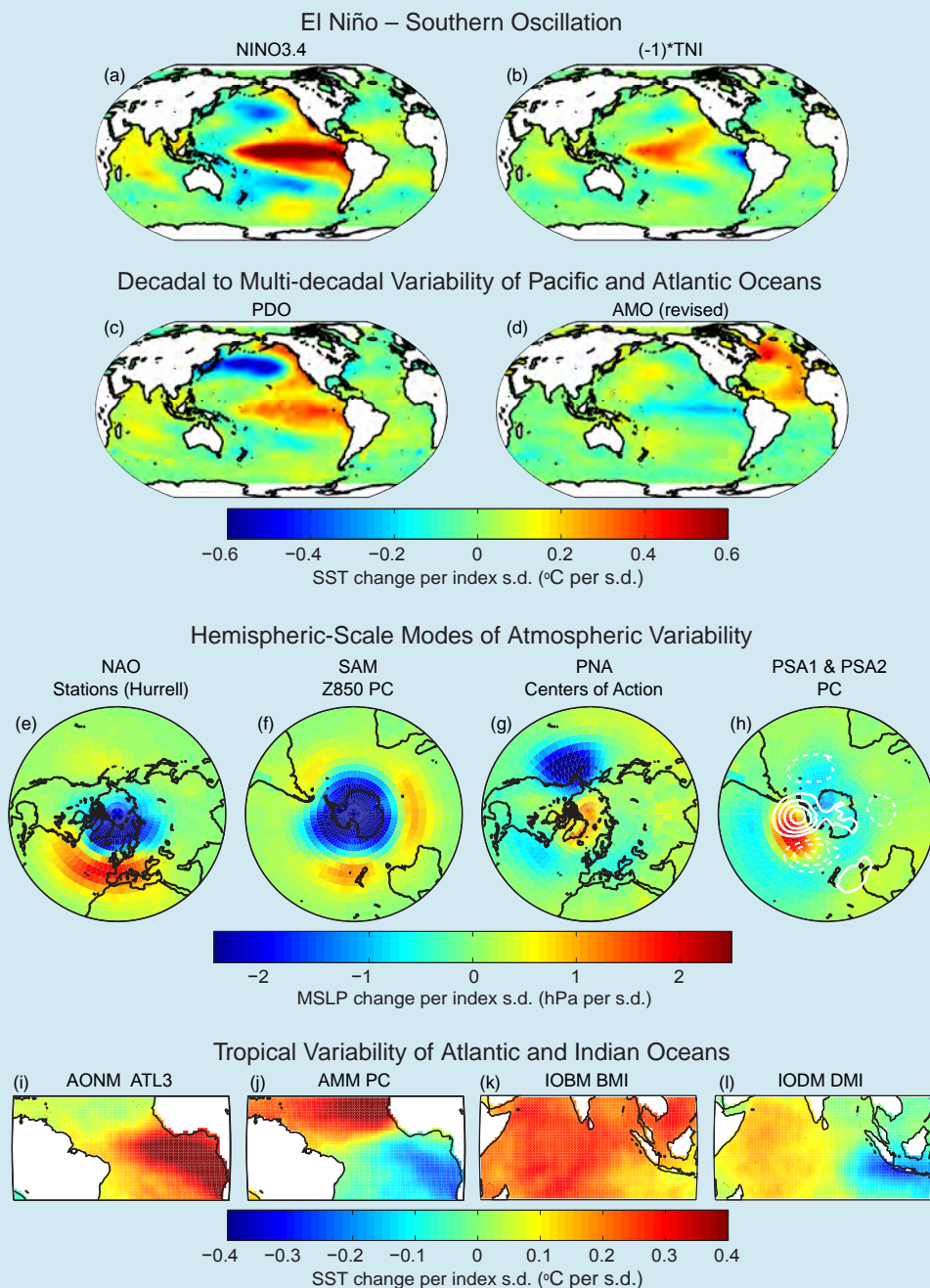
Most climate modes are illustrated by several indices (Box 2.5, Figure 1), which often behave similarly to each other. Spatial patterns of SST or SLP associated with these climate modes are illustrated in Box 2.5, Figure 2. They can be interpreted as a change in the SST or SLP field associated with one standard deviation change in the index. (continued on next page)



Box 2.5, Figure 1 | Some indices of climate variability, as defined in Box 2.5, Table 1, plotted in the 1870–2012 interval. Where ‘HadISST1’, ‘HadSLP2r’, or ‘NNR’ are indicated, the indices were computed from the sea surface temperature (SST) or sea level pressure (SLP) values of the former two data sets or from 500 or 850 hPa geopotential height fields from the NNR. Data set references given in the panel titles apply to all indices shown in that panel. Where no data set is specified, a publicly available version of an index from the authors of a primary reference given in Box 2.5, Table 1 was used. All indices were standardized with regard to 1971–2000 period except for Niño3.4 (centralized for 1971–2000) and AMO indices (centralized for 1901–1970). Indices marked as “detrended” had their linear trend for 1870–2012 removed. All indices are shown as 12-month running means except when the temporal resolution is explicitly indicated (e.g., ‘DJFM’ for December-to-March averages) or smoothing level (e.g., 11-year LPF for a low-pass filter with half-power at 11 years).

Box 2.5 (continued)

The difficulty of identifying a universally 'best' index for any particular climate mode is due to the fact that no simply defined indicator can achieve a perfect separation of the target phenomenon from all other effects occurring in the climate system. As a result, each index is affected by many climate phenomena whose relative contributions may change with the time period and the data set used. Limited length and quality of the observational record further compound this problem. Thus the choice of index is always application specific.



Box 2.5, Figure 2 | Spatial patterns of climate modes listed in Box 2.5, Table 1. All patterns shown here are obtained by regression of either sea surface temperature (SST) or sea level pressure (SLP) fields on the standardized index of the climate mode. For each climate mode one of the specific indices shown in Box 2.5, Figure 1 was used, as identified in the panel subtitles. SST and SLP fields are from HadSST1 and HadSLP2r data sets (interpolated gridded products based on data sets of historical observations). Regressions were done on monthly means for all patterns except for NAO and PNA, which were done with the DJFM means, and for PSA1 and PSA2, where seasonal means were used. Each regression was done for the longest period within the 1870-2012 interval when the index was available. For each pattern the time series was linearly de-trended over the entire regression interval. All patterns are shown by color plots, except for PSA2, which is shown by white contours over the PSA1 color plot (contour steps are 0.5 hPa, zero contour is skipped, negative values are indicated by dash).

Acknowledgements

The authors of Chapter 2 wish to thank Wenche Aas (NILU, Kjeller), Erika Coppola (ICTP, Trieste), Ritesh Gautam (NASA GSFC, Greenbelt), Jenny Hand (CIARA, Fort Collins), Andreas Hilboll (U. Bremen, Bremen), Glenn Hyatt (NOAA NCDC, Asheville), David Parrish (NOAA ESRL-CSD, Boulder), Deborah Misch (LMI, Inc, Asheville), Jared Rennie (CICS-NC, Asheville), Deborah Riddle (NOAA NCDC, Asheville), Sara Veasey (NOAA NCDC, Asheville), Mark Weber (U. Bremen, Bremen), Yin Xungang (STG Inc., Asheville), Teresa Young (STG, Asheville) and Jianglong Zhang (U. North Dakota, Grand Forks) for their critical contributions to the production of figures in this work.

References

- Abakumova, G. M., E. V. Gorbarenko, E. I. Nezval, and O. A. Shilovtseva, 2008: Fifty years of actinometrical measurements in Moscow. *Int. J. Remote Sens.*, **29**, 2629–2665.
- Adam, J. C., and D. P. Lettenmaier, 2008: Application of new precipitation and reconstructed streamflow products to streamflow trend attribution in northern Eurasia. *J. Clim.*, **21**, 1807–1828.
- Adler, R. F., G. J. Gu, and G. J. Huffman, 2012: Estimating climatological bias errors for the global Precipitation Climatology Project (GPCP). *J. Appl. Meteor. Climatol.*, **51**, 84–99.
- Adler, R. F., et al., 2003: The version-2 global precipitation climatology project (GPCP) monthly precipitation analysis (1979–present). *J. Hydrometeorol.*, **4**, 1147–1167.
- Aguilar, E., et al., 2009: Changes in temperature and precipitation extremes in western central Africa, Guinea Conakry, and Zimbabwe, 1955–2006. *J. Geophys. Res. Atmos.*, **114**, D02115.
- Alexander, L. V., P. Uotila, and N. Nicholls, 2009: Influence of sea surface temperature variability on global temperature and precipitation extremes. *J. Geophys. Res. Atmos.*, **114**, D18116.
- Alexander, L. V., X. L. Wang, H. Wan, and B. Trewin, 2011: Significant decline in storminess over southeast Australia since the late 19th century. *Aust. Meteor. Ocean. J.*, **61**, 23–30.
- Alexander, L. V., et al., 2006: Global observed changes in daily climate extremes of temperature and precipitation. *J. Geophys. Res. Atmos.*, **111**, D05109.
- Allan, R., and T. Ansell, 2006: A new globally complete monthly historical gridded mean sea level pressure dataset (HadSLP2): 1850–2004. *J. Clim.*, **19**, 5816–5842.
- Allan, R., S. Tett, and L. Alexander, 2009: Fluctuations in autumn-winter severe storms over the British Isles: 1920 to present. *Int. J. Climatol.*, **29**, 357–371.
- Allan, R. P., 2009: Examination of relationships between clear-sky longwave radiation and aspects of the atmospheric hydrological cycle in climate models, reanalyses, and observations. *J. Clim.*, **22**, 3127–3145.
- Allan, R. P., and A. Slingo, 2002: Can current climate model forcings explain the spatial and temporal signatures of decadal OLR variations? *Geophys. Res. Lett.*, **29**, 1141.
- Allan, R. P., and B. J. Soden, 2008: Atmospheric warming and the amplification of precipitation extremes. *Science*, **321**, 1481–1484.
- Allan, R. P., B. J. Soden, V. O. John, W. Ingram, and P. Good, 2010: Current changes in tropical precipitation. *Environ. Res. Lett.*, **5**, 025205.
- Allen, R. J., and S. C. Sherwood, 2007: Utility of radiosonde wind data in representing climatological variations of tropospheric temperature and baroclinicity in the western tropical Pacific. *J. Clim.*, **20**, 5229–5243.
- Allen, R. J., and S. C. Sherwood, 2008: Warming maximum in the tropical upper troposphere deduced from thermal winds. *Nature Geosci.*, **1**, 399–403.
- Alpert, P., and P. Kishcha, 2008: Quantification of the effect of urbanization on solar dimming. *Geophys. Res. Lett.*, **35**, L08801.
- Alpert, P., P. Kishcha, Y. J. Kaufman, and R. Schwarzbard, 2005: Global dimming or local dimming? Effect of urbanization on sunlight availability. *Geophys. Res. Lett.*, **32**, L17802.
- Andrade, C., S. Leite, and J. Santos, 2012: Temperature extremes in Europe: Overview of their driving atmospheric patterns. *Nat. Hazards Earth Syst. Sci.*, **12**, 1671–1691.
- Andronova, N., J. E. Penner, and T. Wong, 2009: Observed and modeled evolution of the tropical mean radiation budget at the top of the atmosphere since 1985. *J. Geophys. Res. Atmos.*, **114**, D14106.
- Angell, J. K., 2006: Changes in the 300-mb North Circumpolar Vortex, 1963–2001. *J. Clim.*, **19**, 2984–2994.
- Anthes, R. A., 2011: Exploring Earth's atmosphere with radio occultation: contributions to weather, climate and space weather. *Atmos. Meas. Tech.*, **4**, 1077–1103.
- Anthes, R. A., et al., 2008: The COSMOC/FORMOSAT-3 Mission—Early results. *Bull. Am. Meteor. Soc.*, **89**, 313.
- Archer, C. L., and K. Caldeira, 2008a: Reply to comment by Courtenay Strong and Robert E. Davis on “Historical trends in the jet streams”. *Geophys. Res. Lett.*, **35**, L24807.
- Archer, C. L., and K. Caldeira, 2008b: Historical trends in the jet streams. *Geophys. Res. Lett.*, **35**, L08803.
- Arndt, D. S., M. O. Baringer, and M. R. Johnson, 2010: State of the Climate in 2009. *Bull. Am. Meteor. Soc.*, **91**, S1–.
- Arnold, T., et al., 2013: Nitrogen trifluoride global emissions estimated from updated atmospheric measurements. *Proc. Natl. Acad. Sci. U.S.A.*, **110**, 2029–2034.
- Ashok, K., S. K. Behera, S. A. Rao, H. Y. Weng, and T. Yamagata, 2007: El Niño Modoki and its possible teleconnection. *J. Geophys. Res. Oceans*, **112**, C11007.
- Asmi, A., et al., 2013: Aerosol decadal trends – Part 2: In-situ aerosol particle number concentrations at GAW and ACTRIS stations. *Atmos. Chem. Phys.*, **13**, 895–916.
- Atlas, R., R. Hoffman, J. Ardizzone, S. Leidner, J. Jusem, D. Smith, and D. Gombos, 2011: A cross-calibrated multiplatform ocean wind velocity product for meteorological and oceanographic applications. *Bull. Am. Meteor. Soc.*, **92**, 157–.
- Augustine, J. A., and E. G. Dutton, 2013: Variability of the surface radiation budget over United States from 1996 through 2011 from high-quality measurements. *J. Geophys. Res.*, **118**, 43–53.
- Aydin, M., et al., 2011: Recent decreases in fossil-fuel emissions of ethane and methane derived from firm air. *Nature*, **476**, 198–201.
- Ballester, J., F. Giorgi, and X. Rodo, 2010: Changes in European temperature extremes can be predicted from changes in PDF central statistics. *Clim. Change*, **98**, 277–284.
- Baringer, M. O., D. S. Arndt, and M. R. Johnson, 2010: State of the Climate in 2009. *Bull. Am. Meteor. Soc.*, **91**, S1–.
- Barnpadimos, I., J. Keller, D. Oderbolz, C. Hueglin, and A. S. H. Prévôt, 2012: One decade of parallel fine (PM_{2.5}) and coarse (PM₁₀–PM_{2.5}) particulate matter measurements in Europe: trends and variability. *Atmos. Chem. Phys.*, **12**, 3189–3203.
- Barnston, A. G., and R. E. Livezey, 1987: Classification, seasonality and persistence of low-frequency atmospheric circulation patterns. *Mon. Weather Rev.*, **115**, 1083–1126.
- Barring, L., and K. Fortuniak, 2009: Multi-indices analysis of southern Scandinavian storminess 1780–2005 and links to interdecadal variations in the NW Europe–North Sea region. *Int. J. Climatol.*, **29**, 373–384.
- Barriopedro, D., E. M. Fischer, J. Luterbacher, R. Trigo, and R. Garcia-Herrera, 2011: The hot summer of 2010: Redrawing the temperature record map of Europe. *Science*, **332**, 220–224.
- Barrucand, M., M. Rusticucci, and W. Vargas, 2008: Temperature extremes in the south of South America in relation to Atlantic Ocean surface temperature and Southern Hemisphere circulation. *J. Geophys. Res. Atmos.*, **113**, D20111.
- Barton, N. P., and A. W. Ellis, 2009: Variability in wintertime position and strength of the North Pacific jet stream as represented by re-analysis data. *Int. J. Climatol.*, **29**, 851–862.
- Becker, A., et al., 2013: A description of the global land-surface precipitation data products of the Global Precipitation Climatology Centre with sample applications including centennial (trend) analysis from 1901–present. *Earth Syst. Sci. Data*, **5**, 71–99.
- Beig, G., and V. Singh, 2007: Trends in tropical tropospheric column ozone from satellite data and MOZART model. *Geophys. Res. Lett.*, **34**, L17801.
- Bell, G. D., and M. S. Halpert, 1998: Climate assessment for 1997. *Bull. Am. Meteor. Soc.*, **79**, S1–S50.
- Bender, F. A. M., V. Ramanathan, and G. Tselioudis, 2012: Changes in extratropical storm track cloudiness 1983–2008: Observational support for a poleward shift. *Clim. Dyn.*, **38**, 2037–2053.
- Bengtsson, L., and K. I. Hodges, 2011: On the evaluation of temperature trends in the tropical troposphere. *Clim. Dyn.*, **36**, 419–430.
- Beniston, M., 2004: The 2003 heat wave in Europe: A shape of things to come? An analysis based on Swiss climatological data and model simulations. *Geophys. Res. Lett.*, **31**, L02202.
- Beniston, M., 2009: Decadal-scale changes in the tails of probability distribution functions of climate variables in Switzerland. *Int. J. Climatol.*, **29**, 1362–1368.
- Bennartz, R., J. Fan, J. Rausch, L. Leung, and A. Heidinger, 2011: Pollution from China increases cloud droplet number, suppresses rain over the East China Sea. *Geophys. Res. Lett.*, **38**, L09704.
- Berrisford, P., et al., 2011: Atmospheric conservation properties in ERA-Interim. *Q. J. R. Meteor. Soc.*, **137**, 1381–1399.
- Berry, D., and E. Kent, 2011: Air-Sea fluxes from ICOADS: The construction of a new gridded dataset with uncertainty estimates. *Int. J. Climatol.*, **31**, 987–1001.
- Berry, D. I., and E. C. Kent, 2009: A new air-sea interaction gridded dataset from ICOADS with uncertainty estimates. *Bull. Am. Meteor. Soc.*, **90**, 645–656.

- Berthet, C., J. Dessens, and J. Sanchez, 2011: Regional and yearly variations of hail frequency and intensity in France. *Atmos. Res.*, **100**, 391–400.
- Birner, T., 2010: Recent widening of the tropical belt from global tropopause statistics: Sensitivities. *J. Geophys. Res. Atmos.*, **115**, D23109.
- Bitz, C. M., and Q. Fu, 2008: Arctic warming aloft is data set dependent. *Nature*, **455**, E3–E4.
- Black, E., and R. Sutton, 2007: The influence of oceanic conditions on the hot European summer of 2003. *Clim. Dyn.*, **28**, 53–66.
- Blunden, J., D. S. Arndt, and M. O. Baringer, 2011: State of the Climate in 2010. *Bull. Am. Meteor. Soc.*, **92**, S17–.
- Bohm, R., P. D. Jones, J. Hiebl, D. Frank, M. Brunetti, and M. Maugeri, 2010: The early instrumental warm-bias: A solution for long central European temperature series 1760–2007. *Clim. Change*, **101**, 41–67.
- Bonfils, C., P. B. Duffy, B. D. Santer, T. M. L. Wigley, D. B. Lobell, T. J. Phillips, and C. Deser, 2008: Identification of external influences on temperatures in California. *Clim. Change*, **87**, S43–S55.
- Bonisch, H., A. Engel, J. Curtius, T. Birner, and P. Hoor, 2009: Quantifying transport into the lowermost stratosphere using simultaneous in-situ measurements of SF₆ and CO₂. *Atmos. Chem. Phys.*, **9**, 5905–5919.
- Bosilovich, M. G., F. R. Robertson, and J. Chen, 2011: Global energy and water budgets in MERRA. *J. Clim.*, **24**, 5721–5739.
- Bourassa, M. A., S. T. Gille, D. L. Jackson, J. B. Roberts, and G. A. Wick, 2010: Ocean winds and turbulent air-sea fluxes inferred from remote sensing. *Oceanography*, **23**, 36–51.
- Bousquet, P., 2011: Source attribution of the changes in atmospheric methane from 2006–2008. *Atmos. Chem. Phys. Discuss.*, **10**, 27603–27630.
- Brogneiz, H., R. Roca, and L. Picon, 2009: Study of the free tropospheric humidity interannual variability using meteosat data and an advection-condensation transport model. *J. Clim.*, **22**, 6773–6787.
- Brönnimann, S., 2009: Early twentieth-century warming. *Nature Geosci.*, **2**, 735–736.
- Brönnimann, S., et al., 2009: Variability of large-scale atmospheric circulation indices for the Northern Hemisphere during the past 100 years. *Meteorol. Z.*, **18**, 379–396.
- Brooks, C. F., 1926: Observing water-surface temperatures at sea. *Mon. Wea. Rev.*, **54**, 241–253.
- Brooks, H., 2012: Severe thunderstorms and climate change. *Atmos. Res.*, **123**, S1, 129–138.
- Brooks, H. E., and N. Dotzek, 2008: The spatial distribution of severe convective storms and an analysis of their secular changes. In: *Climate Extremes and Society* [H. F. Diaz and R. J. Murnane (eds.) Cambridge University Press, pp. 35–53.
- Brown, S. J., J. Caesar, and C. A. T. Ferro, 2008: Global changes in extreme daily temperature since 1950. *J. Geophys. Res. Atmos.*, **113**, D05115.
- Brunet, M., et al., 2011: The minimization of the screen bias from ancient Western Mediterranean air temperature records: an exploratory statistical analysis. *Int. J. Climatol.*, **31**, 1879–1895.
- Bunge, L., and A. J. Clarke, 2009: A verified estimation of the El Niño Index Niño-3.4 since 1877. *J. Clim.*, **22**, 3979–3992.
- Burn, D. H., and N. M. Hesch, 2007: Trends in evaporation for the Canadian prairies. *J. Hydrol.*, **336**, 61–73.
- Caesar, J., L. Alexander, and R. Vose, 2006: Large-scale changes in observed daily maximum and minimum temperatures: Creation and analysis of a new gridded data set. *J. Geophys. Res. Atmos.*, **111**, D05101.
- Caesar, J., et al., 2011: Changes in temperature and precipitation extremes over the Indo-Pacific region from 1971 to 2005. *Int. J. Climatol.*, **31**, 791–801.
- Cai, W., and P. van Rensch, 2012: The 2011 southeast Queensland extreme summer rainfall: A confirmation of a negative Pacific Decadal Oscillation phase? *Geophys. Res. Lett.*, **39**, L08702.
- Cai, W., T. Cowan, and M. Thatcher, 2012: Rainfall reductions over Southern Hemisphere semi-arid regions: The role of subtropical dry zone expansion. *Sci. Rep.*, **2**, 702.
- Callaghan, J., and S. B. Power, 2011: Variability and decline in the number of severe tropical cyclones making land-fall over eastern Australia since the late nineteenth century. *Clim. Dyn.*, **37**, 647–662.
- Canada, 2012: Canadian Smog Science Assessment – Highlights and Key Messages. Environment Canada and Health Canada, 64 pp.
- Cane, M. A., 1986: El-Niño. *Annu. Rev. Earth Planet. Sci.*, **14**, 43–70.
- Cao, Z. H., 2008: Severe hail frequency over Ontario, Canada: Recent trend and variability. *Geophys. Res. Lett.*, **35**, L14803.
- Carslaw, K. S., O. Boucher, D. Spracklen, G. Mann, J. G. Rae, S. Woodward, and M. Kumala, 2010: A review of natural aerosol interactions and feedbacks within the Earth system. *Atmos. Chem. Phys.*, **10**, 1701–1737.
- Casey, K. S., T. B. Brandon, P. Cornillon, and R. Evans, 2010: The past, present and future of the AVHRR Pathfinder SST Program. In: *Oceanography from Space: Revisited* [V. Barale, J. F. R. Gower, and L. Alberotanza (eds.)]. Springer Science+Business Media, New York, 323–341.
- Castellanos, P., and K. F. Boersma, 2012: Reductions in nitrogen oxides over Europe driven by environmental policy and economic recession. *Sci. Rep.*, **2**, 265.
- Cermak, J., M. Wild, R. Knutti, M. I. Mishchenko, and A. K. Heidinger, 2010: Consistency of global satellite-derived aerosol and cloud data sets with recent brightening observations. *Geophys. Res. Lett.*, **37**, L21704.
- Chambers, L., and G. Griffiths, 2008: The changing nature of temperature extremes in Australia and New Zealand. *Aust. Meteorol. Mag.*, **57**, 13–35.
- Chan, J. C. L., and M. Xu, 2009: Inter-annual and inter-decadal variations of landfalling tropical cyclones in East Asia. Part I: time series analysis. *Int. J. Climatol.*, **29**, 1285–1293.
- Chandler, R. E., and E. M. Scott, 2011: *Statistical Methods for Trend Detection and Analysis in the Environmental Sciences*. John Wiley & Sons, Hoboken, NJ.
- Chang, E. K. M., 2007: Assessing the increasing trend in Northern Hemisphere winter storm track activity using surface ship observations and a statistical storm track model. *J. Clim.*, **20**, 5607–5628.
- Chang, E. K. M., and Y. J. Guo, 2007: Is the number of North Atlantic tropical cyclones significantly underestimated prior to the availability of satellite observations? *Geophys. Res. Lett.*, **34**, L14801.
- Chapman, W. L., and J. E. Walsh, 2007: A synthesis of Antarctic temperatures. *J. Clim.*, **20**, 4096–4117.
- Che, H. Z., et al., 2005: Analysis of 40 years of solar radiation data from China, 1961–2000. *Geophys. Res. Lett.*, **32**, L06803.
- Chen, J. Y., B. E. Carlson, and A. D. Del Genio, 2002: Evidence for strengthening of the tropical general circulation in the 1990s. *Science*, **295**, 838–841.
- Chen, J. Y., A. D. Del Genio, B. E. Carlson, and M. G. Bosilovich, 2008: The spatio-temporal structure of twentieth-century climate variations in observations and reanalyses. Part I: Long-term trend. *J. Clim.*, **21**, 2611–2633.
- Chiacchio, M., and M. Wild, 2010: Influence of NAO and clouds on long-term seasonal variations of surface solar radiation in Europe. *J. Geophys. Res. Atmos.*, **115**, D00d22.
- Choi, G., et al., 2009: Changes in means and extreme events of temperature and precipitation in the Asia Pacific Network region, 1955–2007. *Int. J. Climatol.*, **29**, 1906–1925.
- Christy, J. R., and W. B. Norris, 2006: Satellite and VIZ-radiosonde intercomparisons for diagnosis of nonclimatic influences. *J. Atmos. Ocean. Technol.*, **23**, 1181–1194.
- Christy, J. R., and W. B. Norris, 2009: Discontinuity issues with radiosonde and satellite temperatures in the Australian Region 1979–2006. *J. Atmos. Ocean Technol.*, **26**, 508–522.
- Christy, J. R., W. B. Norris, and R. T. McNider, 2009: Surface temperature variations in East Africa and possible causes. *J. Clim.*, **22**, 3342–3356.
- Christy, J. R., R. W. Spencer, and W. B. Norris, 2011: The role of remote sensing in monitoring global bulk tropospheric temperatures. *Int. J. Remote Sens.*, **32**, 671–685.
- Christy, J. R., W. B. Norris, K. Redmond, and K. P. Gallo, 2006: Methodology and results of calculating central California surface temperature trends: Evidence of human-induced climate change? *J. Clim.*, **19**, 548–563.
- Christy, J. R., W. B. Norris, R. W. Spencer, and J. J. Hnilo, 2007: Tropospheric temperature change since 1979 from tropical radiosonde and satellite measurements. *J. Geophys. Res. Atmos.*, **112**, D06102.
- Christy, J. R., R. W. Spencer, W. B. Norris, W. D. Braswell, and D. E. Parker, 2003: Error estimates of version 5.0 of MSU-AMSU bulk atmospheric temperatures. *J. Atmos. Ocean Technol.*, **20**, 613–629.
- Christy, J. R., et al., 2010: What do observational datasets say about modeled tropospheric temperature trends since 1979? , 2148–2169.
- Chu, W. P., M. P. McCormick, J. Lenoble, C. Brogniez, and P. Pruvost, 1989: SAGE II inversion algorithm. *J. Geophys. Res. Atmos.*, **94**, 8339–8351.
- Chung, E. S., and B. J. Soden, 2010: Investigating the influence of carbon dioxide and the stratosphere on the long-term tropospheric temperature monitoring from HIRS. *J. Appl. Meteor. Climatol.*, **49**, 1927–1937.

- Chung, E. S., D. Yeomans, and B. J. Soden, 2010: An assessment of climate feedback processes using satellite observations of clear-sky OLR. *Geophys. Res. Lett.*, **37**, L02702.
- Clark, R. T., S. J. Brown, and J. M. Murphy, 2006: Modeling Northern Hemisphere summer heat extreme changes and their uncertainties using a physics ensemble of climate sensitivity experiments. *J. Clim.*, **19**, 4418–4435.
- Clement, A. C., and B. Soden, 2005: The sensitivity of the tropical-mean radiation budget. *J. Clim.*, **18**, 3189–3203.
- CMA, 2007: *Atlas of China Disastrous Weather and Climate*. Chinese Meteorological Administration. Beijing, China.
- CMA, 2011: China Climate Change Bulletin. Chinese Meteorological Administration. Beijing, China.
- Cohen, J., M. Barlow, and K. Saito, 2009: Decadal fluctuations in planetary wave forcing modulate global warming in late boreal winter. *J. Clim.*, **22**, 4418–4426.
- Cohen, J. L., J. C. Furtado, M. Barlow, V. A. Alexeev, and J. E. Cherry, 2012: Asymmetric seasonal temperature trends. *Geophys. Res. Lett.*, **39**, L04705.
- Cohn, T. A., and H. F. Lins, 2005: Nature's style: Naturally trendy. *Geophys. Res. Lett.*, **32**, L23402.
- Coles, S., 2001: *An Introduction to Statistical Modeling of Extreme Values*. Springer Science+Business Media, New York, 208 pp.
- Collaud Coen, M., et al., 2013: Aerosol decadal trends – Part 1: In-situ optical measurements at GAW and IMPROVE stations. *Atmos. Chem. Phys.*, **13**, 869–894.
- Compo, G. P., et al., 2011: The twentieth century reanalysis project. *Q. J. Roy. Meteorol. Soc.*, **137**, 1–28.
- Cooper, O. R., R. S. Gao, D. Tarasick, T. Leblanc, and C. Sweeney, 2012: Long-term ozone trends at rural ozone monitoring sites across the United States, 1990–2010. *J. Geophys. Res.*, **117**, D22307.
- Cornes, R. C., and P. D. Jones, 2011: An examination of storm activity in the northeast Atlantic region over the 1851–2003 period using the EMULATE gridded MSLP data series. *J. Geophys. Res. Atmos.*, **116**, D16110.
- Coumou, D., A. Robinson, and S. Rahmstorf, 2013: Global increase in record-breaking monthly-mean temperatures. *Clim. Change*, **118**, 771–782.
- Craigmile, P. F., and P. Guttorp, 2011: Space-time modelling of trends in temperature series. *J. Time Ser. Anal.*, **32**, 378–395.
- Croci-Maspoli, M., C. Schwierz, and H. C. Davies, 2007a: A multifaceted climatology of atmospheric blocking and its recent linear trend. *J. Clim.*, **20**, 633–649.
- Croci-Maspoli, M., C. Schwierz, and H. C. Davies, 2007b: Atmospheric blocking: Space-time links to the NAO and PNA. *Clim. Dyn.*, **29**, 713–725.
- Cutforth, H. W., and D. Judiesch, 2007: Long-term changes to incoming solar energy on the Canadian Prairie. *Agr. Forest Meteorol.*, **145**, 167–175.
- Dai, A., 2006: Recent climatology, variability, and trends in global surface humidity. *J. Clim.*, **19**, 3589–3606.
- Dai, A., 2011a: Characteristics and trends in various forms of the Palmer Drought Severity Index during 1900–2008. *J. Geophys. Res. Atmos.*, **116**, D12115.
- Dai, A., 2012: The influence of the inter-decadal Pacific oscillation on US precipitation during 1923–2010. *Clim. Dyn.*, **41**, 633–646.
- Dai, A., 2013: Increasing drought under global warming in observations and models. *Nature Clim. Change*, **3**, 52–58.
- Dai, A., T. T. Qian, K. E. Trenberth, and J. D. Milliman, 2009: Changes in continental freshwater discharge from 1948 to 2004. *J. Clim.*, **22**, 2773–2792.
- Dai, A. G., 2011b: Drought under global warming: A review. *Clim. Change*, **2**, 45–65.
- Dai, A. G., J. H. Wang, P. W. Thorne, D. E. Parker, L. Haimberger, and X. L. Wang, 2011: A new approach to homogenize daily radiosonde humidity data. *J. Clim.*, **24**, 965–991.
- Das, L., J. D. Annan, J. C. Hargreaves, and S. Emori, 2011: Centennial scale warming over Japan: Are the rural stations really rural? *Atmos. Sci. Lett.*, **12**, 362–367.
- Davidson, E., 2009: The contribution of manure and fertilizer nitrogen to atmospheric nitrous oxide since 1860. *Nature Geosci.*, **2**, 659–662.
- Davini, P., C. Cagnazzo, S. Gualdi, and A. Navarra, 2012: Bidimensional diagnostics, variability, and trends of Northern Hemisphere blocking. *J. Clim.*, **25**, 6496–6509.
- Davis, S. M., and K. H. Rosenlof, 2011: A multidagnostic intercomparison of tropical width time series using reanalyses and satellite observations. *J. Clim.*, **25**, 1061–1078.
- De Laat, A. T. J., and A. N. Maurellis, 2006: Evidence for influence of anthropogenic surface processes on lower tropospheric and surface temperature trends. *Int. J. Climatol.*, **26**, 897–913.
- de Meij, A., A. Pozzer, and J. Lelieveld, 2012: Trend analysis in aerosol optical depths and pollutant emission estimates between 2000 and 2009. *Atmos. Environ.*, **51**, 75–85.
- De Smedt, I., T. Stavrakou, J. F. Müller, R. J. van der A, and M. Van Roozendael, 2010: Trend detection in satellite observations of formaldehyde tropospheric columns. *Geophys. Res. Lett.*, **37**, L18808.
- Dee, D. P., E. Kallen, A. J. Simmons, and L. Haimberger, 2011a: Comments on “Reanalyses suitable for characterizing long-term trends”. *Bull. Am. Meteor. Soc.*, **92**, 65–70.
- Dee, D. P., et al., 2011b: The ERA-Interim reanalysis: Configuration and performance of the data assimilation system. *Q. J. R. Meteor. Soc.*, **137**, 553–597.
- Deeds, D., et al., 2008: Evidence for crustal degassing of CF₄ and SF₆ in Mojave Desert groundwaters. *Geochim. Cosmochim. Acta*, **72**, 999–1013.
- DeGaetano, A. T., 2009: Time-dependent changes in extreme-precipitation return-period amounts in the continental United States. *J. Appl. Meteor. Climatol.*, **48**, 2086–2099.
- Delgado, J. M., H. Apel, and B. Merz, 2010: Flood trends and variability in the Mekong River. *Hydrol. Earth Syst. Sci.*, **14**, 407–418.
- Della-Marta, P. M., M. R. Haylock, J. Luterbacher, and H. Wanner, 2007a: Doubled length of western European summer heat waves since 1880. *J. Geophys. Res. Atmos.*, **112**, D15103.
- Della-Marta, P. M., J. Luterbacher, H. von Weissenfluh, E. Xoplaki, M. Brunet, and H. Wanner, 2007b: Summer heat waves over western Europe 1880–2003, their relationship to large-scale forcings and predictability. *Clim. Dyn.*, **29**, 251–275.
- Della-Marta, P. M., H. Mathis, C. Frei, M. A. Liniger, J. Kleinn, and C. Appenzeller, 2009: The return period of wind storms over Europe. *Int. J. Climatol.*, **29**, 437–459.
- Deser, C., A. S. Phillips, and M. A. Alexander, 2010a: Twentieth century tropical sea surface temperature trends revisited. *Geophys. Res. Lett.*, **37**, L10701.
- Deser, C., M. A. Alexander, S. P. Xie, and A. S. Phillips, 2010b: Sea surface temperature variability: Patterns and mechanisms. *Annu. Rev. Mar. Sci.*, **2**, 115–143.
- Dessler, A. E., and S. M. Davis, 2010: Trends in tropospheric humidity from reanalysis systems. *J. Geophys. Res. Atmos.*, **115**, D19127.
- Dessler, A. E., Z. Zhang, and P. Yang, 2008: Water-vapor climate feedback inferred from climate fluctuations, 2003–2008. *Geophys. Res. Lett.*, **35**, L20704.
- Diffenbaugh, N. S., J. S. Pal, F. Giorgi, and X. J. Gao, 2007: Heat stress intensification in the Mediterranean climate change hotspot. *Geophys. Res. Lett.*, **34**, L11706.
- Ding, T., W. H. Qian, and Z. W. Yan, 2010: Changes in hot days and heat waves in China during 1961–2007. *Int. J. Climatol.*, **30**, 1452–1462.
- Ding, Y. H., G. Y. Ren, Z. C. Zhao, Y. Xu, Y. Luo, Q. P. Li, and J. Zhang, 2007: Detection, causes and projection of climate change over China: An overview of recent progress. *Adv. Atmos. Sci.*, **24**, 954–971.
- Dlugokencky, E., E. Nisbet, R. Fisher, and D. Lowry, 2011: Global atmospheric methane: Budget, changes and dangers. *Philos. Trans. R. Soc. London Ser. A*, **369**, 2058–2072.
- Dlugokencky, E., et al., 2005: Conversion of NOAA atmospheric dry air CH₄ mole fractions to a gravimetrically prepared standard scale. *J. Geophys. Res. Atmos.*, **110**, D18306.
- Dlugokencky, E., et al., 2009: Observational constraints on recent increases in the atmospheric CH₄ burden. *Geophys. Res. Lett.*, L18803.
- Dlugokencky, E. J., K. A. Masaire, P. M. Lang, P. P. Steele, and E. G. Nisbet, 1994: A dramatic decrease in the growth rate of atmospheric methane in the Northern Hemisphere during 1992. *Geophys. Res. Lett.*, **21**, 45–48.
- Dole, R., et al., 2011: Was there a basis for anticipating the 2010 Russian heat wave? *Geophys. Res. Lett.*, **38**, L06702.
- Donat, M. G., and L. V. Alexander, 2012: The shifting probability distribution of global daytime and night-time temperatures. *Geophys. Res. Lett.*, **39**, L14707.
- Donat, M. G., D. Renggli, S. Wild, L. V. Alexander, G. C. Leckebusch, and U. Ulbrich, 2011: Reanalysis suggests long-term upward trends in European storminess since 1871. *Geophys. Res. Lett.*, **38**, L14703.
- Donat, M. G., L. V. Alexander, H. Yang, I. Durre, R. Vose, and J. Caesar, 2013a: Global land-based datasets for monitoring climatic extremes. *Bull. Am. Meteor. Soc.*, **94**, 997–1006.
- Donat, M. G., et al., 2013b: Changes in extreme temperature and precipitation in the Arab region: Long-term trends and variability related to ENSO and NAO. *Int. J. Climatol.*, doi:10.1002/joc.3707.
- Donat, M. G., et al., 2013c: Updated analyses of temperature and precipitation extreme indices since the beginning of the twentieth century: The HadEX2 dataset. *J. Geophys. Res. Atmos.*, **118**, 2098–2118.
- Dong, L., T. J. Vogelsang, and S. J. Colucci, 2008: Interdecadal trend and ENSO-related interannual variability in Southern Hemisphere blocking. *J. Clim.*, **21**, 3068–3077.

- Dorigo, W., R. de Jeu, D. Chung, R. Parinussa, Y. Liu, W. Wagner, and D. Fernández-Prieto, 2012: Evaluating global trends (1988–2010) in harmonized multi-satellite surface soil moisture. *Geophys. Res. Lett.*, **39**, L18405.
- Doswell, C., H. Brooks, and N. Dotzek, 2009: On the implementation of the enhanced Fujita scale in the USA. *Atmos. Res.*, **93**, 554–563.
- Douglas, A., et al., 2008: Relationship of loss, mean age of air and the distribution of CFCs to stratospheric circulation and implications for atmospheric lifetimes. *J. Geophys. Res. Atmos.*, **113**, D14309.
- Douglas, A., et al., 2011: WMO/UNEP scientific assessment of ozone depletion: 2010. In: *Stratospheric Ozone and Surface Ultraviolet Radiation*. World Meteorological Organisation, Geneva, Switzerland.
- Du, Y., and S. Xie, 2008: Role of atmospheric adjustments in the tropical Indian Ocean warming during the 20th century in climate models. *Geophys. Res. Lett.*, **35**, L08712.
- Du, Y., S. Xie, G. Huang, and K. Hu, 2009: Role of air-sea interaction in the long persistence of El Niño-induced North Indian Ocean warming. *J. Clim.*, **22**, 2023–2038.
- Duan, A. M., and G. X. Wu, 2006: Change of cloud amount and the climate warming on the Tibetan Plateau. *Geophys. Res. Lett.*, **33**, L22704.
- Durre, I., C. N. Williams, X. G. Yin, and R. S. Vose, 2009: Radiosonde-based trends in precipitable water over the Northern Hemisphere: An update. *J. Geophys. Res. Atmos.*, **114**, D05112.
- Dutton, E. G., and B. A. Bodhaine, 2001: Solar irradiance anomalies caused by clear-sky transmission variations above Mauna Loa: 1958–99. *J. Clim.*, **14**, 3255–3262.
- Dutton, E. G., D. W. Nelson, R. S. Stone, D. Longenecker, G. Carbaugh, J. M. Harris, and J. Wendell, 2006: Decadal variations in surface solar irradiance as observed in a globally remote network. *J. Geophys. Res. Atmos.*, **111**, D19101.
- Earl, N., S. Dorling, R. Hewston, and R. von Glasow, 2013: 1980–2010 Variability in U.K. surface wind climate. *J. Climate*, **26**, 1172–1191.
- Easterling, D., and M. Wehner, 2009: Is the climate warming or cooling? *Geophys. Res. Lett.*, **36**, L08706.
- Eastman, R., and S. G. Warren, 2012: A 39-yr survey of cloud changes from land stations worldwide 1971–2009: Long-term trends, relation to aerosols, and expansion of the Tropical Belt. *J. Clim.*, **26**, 1286–1303.
- Eastman, R., S. G. Warren, and C. J. Hahn, 2011: Variations in cloud cover and cloud types over the ocean from surface observations, 1954–2008. *J. Clim.*, **24**, 5914–5934.
- Ebita, A., et al., 2011: The Japanese 55-year reanalysis “JRA-55”: An interim report. *Sola*, **7**, 149–152.
- Eccel, E., P. Cau, K. Riemann-Campe, and F. Biasoli, 2012: Quantitative hail monitoring in an alpine area: 35-year climatology and links with atmospheric variables. *Int. J. Climatol.*, **32**, 503–517.
- Efthymiadis, D., C. M. Goodess, and P. D. Jones, 2011: Trends in Mediterranean gridded temperature extremes and large-scale circulation influences. *Nat. Hazards Earth Syst. Sci.*, **11**, 2199–2214.
- Efthymiadis, D. A., and P. D. Jones, 2010: Assessment of maximum possible urbanization influences on land temperature data by comparison of land and marine data around coasts. *Atmosphere*, **1**, 51–61.
- Elkins, J. W., and G. S. Dutton, 2011: Nitrous oxide and sulfur hexafluoride. *Bull. Am. Meteor. Soc.*, **92**, 2.
- Elsner, J. B., J. P. Kossin, and T. H. Jagger, 2008: The increasing intensity of the strongest tropical cyclones. *Nature*, **455**, 92–95.
- Emanuel, K., 2007: Environmental factors affecting tropical cyclone power dissipation. *J. Clim.*, **20**, 5497–5509.
- Embury, O., and C. J. Merchant, 2011: Reprocessing for climate of sea surface temperature from the along-track scanning radiometers: A new retrieval scheme. *Remote Sens. Environ.*, **116**, 47–61.
- Embury, O., C. J. Merchant, and G. K. Corlett, 2011: A reprocessing for climate of sea surface temperature from the along-track scanning radiometers: Preliminary validation, accounting for skin and diurnal variability. *Remote Sens. Environ.*, **116**, 62–78.
- Endo, N., and T. Yasunari, 2006: Changes in low cloudiness over China between 1971 and 1996. *J. Clim.*, **19**, 1204–1213.
- Enfield, D. B., A. M. Mestas-Nunez, and P. J. Trimble, 2001: The Atlantic multidecadal oscillation and its relation to rainfall and river flows in the continental US. *Geophys. Res. Lett.*, **28**, 2077–2080.
- Engel, A., et al., 2009: Age of stratospheric air unchanged within uncertainties over the past 30 years. *Nature Geosci.*, **2**, 28–31.
- Espinoza Villar, J. C., et al., 2009: Contrasting regional diSchärge evolutions in the Amazon basin (1974–2004). *J. Hydrol.*, **375**, 297–311.
- Etheridge, D., L. Steele, R. Francey, and R. Langenfelds, 1998: Atmospheric methane between 1000 AD and present: Evidence of anthropogenic emissions and climatic variability. *J. Geophys. Res. Atmos.*, 15979–15993.
- Etheridge, D. M., L. P. Steele, R. L. Langenfelds, R. J. Francey, J. M. Barnola, and V. I. Morgan, 1996: Natural and anthropogenic changes in atmospheric CO₂ over the last 1000 years from air in Antarctic ice and firn. *J. Geophys. Res. Atmos.*, 4115–4128.
- Evan, A. T., A. K. Heidinger, and D. J. Vimont, 2007: Arguments against a physical long-term trend in global ISCCP cloud amounts. *Geophys. Res. Lett.*, **34**, L04701.
- Fall, S., D. Niyogi, A. Gluhovsky, R. A. Pielke, E. Kalnay, and G. Rochon, 2010: Impacts of land use land cover on temperature trends over the continental United States: Assessment using the North American regional reanalysis. *Int. J. Climatol.*, **30**, 1980–1993.
- Fall, S., A. Watts, J. Nielsen-Gammon, E. Jones, D. Niyogi, J. R. Christy, and R. A. Pielke, 2011: Analysis of the impacts of station exposure on the US Historical Climatology Network temperatures and temperature trends. *J. Geophys. Res. Atmos.*, **116**, D14120.
- Falvey, M., and R. D. Garreaud, 2009: Regional cooling in a warming world: Recent temperature trends in the southeast Pacific and along the west coast of subtropical South America (1979–2006). *J. Geophys. Res. Atmos.*, **114**, D04102.
- Favre, A., and A. Gershunov, 2006: Extra-tropical cyclonic/anticyclonic activity in north-eastern Pacific and air temperature extremes in western North America. *Clim. Dyn.*, **26**, 617–629.
- Feng, S., and Q. Hu, 2007: Changes in winter snowfall/precipitation ratio in the contiguous United States. *J. Geophys. Res. Atmos.*, **112**, D15109.
- Ferguson, C. R., and G. Villarini, 2012: Detecting inhomogeneities in the twentieth century reanalysis over the central United States. *J. Geophys. Res. Atmos.*, **117**, D05123.
- Ferranti, L., and P. Viterbo, 2006: The European summer of 2003: Sensitivity to soil water initial conditions. *J. Clim.*, **19**, 3659–3680.
- Ferretti, D., et al., 2005: Unexpected changes to the global methane budget over the past 2000 years. *Science*, **309**, 1714–1717.
- Fischer, E. M., and C. Schär, 2010: Consistent geographical patterns of changes in high-impact European heatwaves. *Nature Geosci.*, **3**, 398–403.
- Fischer, E. M., S. I. Seneviratne, P. L. Vidale, D. Luthi, and C. Schär, 2007: Soil moisture–atmosphere interactions during the 2003 European summer heat wave. *J. Clim.*, **20**, 5081–5099.
- Fischer, T., M. Gemmer, L. Liu, and B. Su, 2011: Temperature and precipitation trends and dryness/wetness pattern in the Zhujiang River Basin, South China, 1961–2007. *Quatern. Int.*, **244**, 138–148.
- Fogt, R. L., J. Perlwitz, A. J. Monaghan, D. H. Bromwich, J. M. Jones, and G. J. Marshall, 2009: Historical SAM variability. Part II: Twentieth-century variability and trends from reconstructions, observations, and the IPCC AR4 models. *J. Clim.*, **22**, 5346–5365.
- Folland, C. K., and D. E. Parker, 1995: Correction of instrumental biases in historical sea-surface temperature data. *Q. J. R. Meteor. Soc.*, **121**, 319–367.
- Folland, C. K., D. E. Parker, A. Colman, and W. R., 1999: Large scale modes of ocean surface temperature since the late nineteenth century. In: *Beyond El Niño: Decadal and Interdecadal Climate Variability* [A. Navarra (ed.)] Springer-Verlag, New York, pp. 73–102.
- Forster, P., et al., 2007: Changes in atmospheric constituents and in radiative forcing. In: *Climate Change 2007: The Physical Science Basis. Contribution of Working Group I to the Fourth Assessment Report of the Intergovernmental Panel on Climate Change* [Solomon, S., D. Qin, M. Manning, Z. Chen, M. Marquis, K. B. Averyt, M. Tignor and H. L. Miller (eds.)] Cambridge University Press, Cambridge, United Kingdom and New York, NY, USA, 129–234.
- Forster, P. M., et al., 2011: Stratospheric changes and climate. Scientific Assessment of Ozone Depletion: 2010. Global Ozone Research and Monitoring Project–Report No. 52. World Meteorological Organization, Geneva, Switzerland, 1–60.
- Fortems-Cheiney, A., F. Chevallier, I. Pison, P. Bousquet, S. Szopa, M. N. Deeter, and C. Clerbaux, 2011: Ten years of CO emissions as seen from Measurements of Pollution in the Troposphere (MOPITT). *J. Geophys. Res.*, **116**, D05304.
- Foster, G., and S. Rahmstorf, 2011: Global temperature evolution 1979–2010. *Environ. Res. Lett.*, **6**, 044022.
- Frauenfeld, O. W., and R. E. Davis, 2003: Northern Hemisphere circumpolar vortex trends and climate change implications. *J. Geophys. Res. Atmos.*, **108**, 4423.
- Frederiksen, J. S., and C. S. Frederiksen, 2007: Interdecadal changes in Southern Hemisphere winter storm track modes. *Tellus A*, **59**, 599–617.

- Free, M., and D. J. Seidel, 2007: Comments on “biases in stratospheric and tropospheric temperature trends derived from historical radiosonde data”. *J. Clim.*, **20**, 3704–3709.
- Free, M., D. J. Seidel, J. K. Angell, J. Lanzante, I. Durre, and T. C. Peterson, 2005: Radiosonde Atmospheric Temperature Products for Assessing Climate (RATPAC): A new data set of large-area anomaly time series. *J. Geophys. Res. Atmos.*, **110**, D22101.
- Frich, P., L. V. Alexander, P. Della-Marta, B. Gleason, M. Haylock, A. Tank, and T. Peterson, 2002: Observed coherent changes in climatic extremes during the second half of the twentieth century. *Clim. Res.*, **19**, 193–212.
- Fu, G. B., S. P. Charles, and J. J. Yu, 2009: A critical overview of pan evaporation trends over the last 50 years. *Clim. Change*, **97**, 193–214.
- Fu, Q., and P. Lin, 2011: Poleward shift of subtropical jets inferred from satellite-observed lower stratospheric temperatures. *J. Clim.*, **24**, 5597–5603.
- Fu, Q., C. M. Johanson, S. G. Warren, and D. J. Seidel, 2004: Contribution of stratospheric cooling to satellite-inferred tropospheric temperature trends. *Nature*, **429**, 55–58.
- Fu, Q., C. M. Johanson, J. M. Wallace, and T. Reichler, 2006: Enhanced mid-latitude tropospheric warming in satellite measurements. *Science*, **312**, 1179–1179.
- Fueglistaler, S., and P. H. Haynes, 2005: Control of interannual and longer-term variability of stratospheric water vapor. *J. Geophys. Res. Atmos.*, **110**, D24108.
- Fujiabe, F., 2009: Detection of urban warming in recent temperature trends in Japan. *Int. J. Climatol.*, **29**, 1811–1822.
- Fujiwara, M., et al., 2010: Seasonal to decadal variations of water vapor in the tropical lower stratosphere observed with balloon-borne cryogenic frost point hygrometers. *J. Geophys. Res. Atmos.*, **115**, D18304.
- Fyfe, J. C., 2003: Extratropical southern hemisphere cyclones: Harbingers of climate change? *J. Clim.*, **16**, 2802–2805.
- Gallant, A., K. Hennessy, and J. Risbey, 2007: Trends in rainfall indices for six Australian regions: 1910–2005. *Aust. Meteor. Mag.*, **56**, 223–239.
- Gallant, A. J. E., and D. J. Karoly, 2010: A Combined Climate Extremes Index for the Australian Region. *J. Clim.*, **23**, 6153–6165.
- Garcia-Herrera, R., J. Diaz, R. M. Trigo, J. Luterbacher, and E. M. Fischer, 2010: A review of the European summer heat wave of 2003. *Crit. Rev. Environ. Sci. Technol.*, **40**, 267–306.
- Gentemann, C., F. Wentz, C. Mears, and D. Smith, 2004: In situ validation of Tropical Rainfall Measuring Mission microwave sea surface temperatures. *J. Geophys. Res. Oceans*, **109**, C04021.
- Gottelman, A., and Q. Fu, 2008: Observed and simulated upper-tropospheric water vapor feedback. *J. Clim.*, **21**, 3282–3289.
- Gottelman, A., et al., 2010: Multimodel assessment of the upper troposphere and lower stratosphere: Tropics and global trends. *J. Geophys. Res. Atmos.*, **115**, D00M08.
- Gilgen, H., A. Roesch, M. Wild, and A. Ohmura, 2009: Decadal changes in shortwave irradiance at the surface in the period from 1960 to 2000 estimated from Global Energy Balance Archive Data. *J. Geophys. Res. Atmos.*, **114**, D00d08.
- Gillett, N. P., and P. A. Stott, 2009: Attribution of anthropogenic influence on seasonal sea level pressure. *Geophys. Res. Lett.*, **36**, L23709.
- Giorgi, F., and R. Francisco, 2000: Evaluating uncertainties in the prediction of regional climate change. *Geophys. Res. Lett.*, **27**, 1295–1298.
- Giorgi, F., E. S. Im, E. Coppola, N. S. Diffenbaugh, X. J. Gao, L. Mariotti, and Y. Shi, 2011: Higher hydroclimatic intensity with global warming. *J. Clim.*, **24**, 5309–5324.
- Giuntoli, I., B. Renard, J. P. Vidal, and A. Bard, 2013: Low flows in France and their relationship to large-scale climate indices. *J. Hydrol.*, **482**, 105–118.
- Gleason, K. L., J. H. Lawrimore, D. H. Levinson, T. R. Karl, and D. J. Karoly, 2008: A revised US Climate Extremes Index. *J. Clim.*, **21**, 2124–2137.
- Gong, D. Y., and C. H. Ho, 2002: The Siberian High and climate change over middle to high latitude Asia. *Theor. Appl. Climatol.*, **72**, 1–9.
- Gouretski, V., J. Kennedy, T. Boyer, and A. Kohl, 2012: Consistent near-surface ocean warming since 1900 in two largely independent observing networks. *Geophys. Res. Lett.*, **39**, L19606.
- Granier, C., et al., 2011: Evolution of anthropogenic and biomass burning emissions of air pollutants at global and regional scales during the 1980–2010 period. *Clim. Change*, **109**, 163–190.
- Grant, A. N., S. Brönnimann, and L. Haimberger, 2008: Recent Arctic warming vertical structure contested. *Nature*, **455**, E2–E3.
- Graversen, R. G., T. Mauritsen, M. Tjernstrom, E. Kallen, and G. Svensson, 2008: Vertical structure of recent Arctic warming. *Nature*, **451**, 53–U54.
- Greally, B., et al., 2007: Observations of 1,1-difluoroethane (HFC-152a) at AGAGE and SOGE monitoring stations in 1994–2004 and derived global and regional emission estimates. *J. Geophys. Res. Atmos.*, **112**, D06308.
- Griffiths, G. M., et al., 2005: Change in mean temperature as a predictor of extreme temperature change in the Asia-Pacific region. *Int. J. Climatol.*, **25**, 1301–1330.
- Grinsted, A., J. C. Moore, and S. Jevrejeva, 2012: Homogeneous record of Atlantic hurricane surge threat since 1923. *Proc. Natl. Acad. Sci. U.S.A.*, **109**, 19601–19605.
- Groisman, P., R. Knight, and T. Karl, 2012: Changes in intense precipitation over the central United States. *J. Hydrometeorol.*, **13**, 47–66.
- Groisman, P., R. Knight, T. R. Karl, D. Easterling, B. M. Sun, and J. Lawrimore, 2004: Contemporary changes of the hydrological cycle over the contiguous United States: Trends derived from in situ observations. *J. Hydrometeorol.*, **5**, 64–85.
- Groisman, P. Y., R. W. Knight, D. R. Easterling, T. R. Karl, G. C. Hegerl, and V. A. N. Razuvayev, 2005: Trends in intense precipitation in the climate record. *J. Clim.*, **18**, 1326–1350.
- Gruber, C., and L. Haimberger, 2008: On the homogeneity of radiosonde wind time series. *Meteorol. Z.*, **17**, 631–643.
- Gulev, S. K., O. Zolina, and S. Grigoriev, 2001: Extratropical cyclone variability in the Northern Hemisphere winter from the NCEP/NCAR reanalysis data. *Clim. Dyn.*, **17**, 795–809.
- Guo, H., M. Xu, and Q. Hub, 2010: Changes in near-surface wind speed in China: 1969–2005. *Int. J. Climatol.*, **31**, 349–358.
- Haerter, J., P. Berg, and S. Hagemann, 2010: Heavy rain intensity distributions on varying time scales and at different temperatures. *J. Geophys. Res. Atmos.*, **115**, D17102.
- Haimberger, L., 2007: Homogenization of radiosonde temperature time series using innovation statistics. *J. Clim.*, **20**, 1377–1403.
- Haimberger, L., C. Tavalato, and S. Sperka, 2008: Toward elimination of the warm bias in historic radiosonde temperature records—Some new results from a comprehensive intercomparison of upper-air data. *J. Clim.*, **21**, 4587–4606.
- Haimberger, L., C. Tavalato, and S. Sperka, 2012: Homogenization of the global radiosonde temperature dataset through combined comparison with reanalysis background series and neighboring stations. *J. Clim.*, **25**, 8108–8131.
- Hand, J. L., et al., 2011: IMPROVE, spatial and seasonal patterns and temporal variability of haze and its constituents in the United States. Cooperative Institute for Research in the Atmosphere and Colorado University.
- Hanna, E., J. Cappelen, R. Allan, T. Jonsson, F. Le Blancq, T. Lillington, and K. Hickey, 2008: New insights into North European and North Atlantic surface pressure variability, storminess, and related climatic change since 1830. *J. Clim.*, **21**, 6739–6766.
- Hannaford, J., and T. Marsh, 2008: High-flow and flood trends in a network of undisturbed catchments in the UK. *Int. J. Climatol.*, **28**, 1325–1338.
- Hansen, J., M. Sato, and R. Ruedy, 2012: Perception of climate change. *Proc. Natl. Acad. Sci. U.S.A.*, **109**, E2415–E2423.
- Hansen, J., R. Ruedy, M. Sato, and K. Lo, 2010: Global surface temperature change. *Rev. Geophys.*, **48**, RG4004.
- Hansen, J., M. Sato, P. Kharecha, and K. von Schuckmann, 2011: Earth’s energy imbalance and implications. *Atmos. Chem. Phys.*, **11**, 13421–13449.
- Harries, J. E., and C. Belotti, 2010: On the variability of the global net radiative energy balance of the nonequilibrium Earth. *J. Clim.*, **23**, 1277–1290.
- Hatzianastassiou, N., C. Matsoukas, A. Fotiadis, K. G. Pavlakis, E. Drakakis, D. Hatzidimitriou, and I. Vardavas, 2005: Global distribution of Earth’s surface shortwave radiation budget. *Atmos. Chem. Phys.*, **5**, 2847–2867.
- Hatzianastassiou, N., C. D. Papadimas, C. Matsoukas, K. Pavlakis, A. Fotiadis, M. Wild, and I. Vardavas, 2012: Recent regional surface solar radiation dimming and brightening patterns: inter-hemispherical asymmetry and a dimming in the Southern Hemisphere. *Atmos. Sci. Lett.*, **13**, 43–48.
- Hausfather, Z., M. J. Menne, C. N. Williams, T. Masters, R. Broberg, and D. Jones, 2013: Quantifying the effect of urbanization on U.S. Historical Climatology Network temperature records. *J. Geophys. Res. Atmos.*, **118**, 481–494.
- Haylock, M. R., et al., 2006: Trends in total and extreme South American rainfall in 1960–2000 and links with sea surface temperature. *J. Clim.*, **19**, 1490–1512.
- He, W. Y., S. P. Ho, H. B. Chen, X. J. Zhou, D. Hunt, and Y. H. Kuo, 2009: Assessment of radiosonde temperature measurements in the upper troposphere and lower stratosphere using COSMIC radio occultation data. *Geophys. Res. Lett.*, **36**, L17807.
- Heidinger, A. K., and M. J. Pavolonis, 2009: Gazing at cirrus clouds for 25 years through a split window. Part I: Methodology. *J. Appl. Meteor. Climatol.*, **48**, 1100–1116.

- Held, I. M., and B. J. Soden, 2006: Robust responses of the hydrological cycle to global warming. *J. Clim.*, **19**, 5686–5699.
- Helmig, D., et al., 2007: A review of surface ozone in the polar regions. *Atmos. Environ.*, **41**, 5138–5161.
- Hidy, G. M., and G. T. Pennell, 2010: Multipollutant air quality management: 2010 critical review. *J. Air Waste Manage. Assoc.*, **60**, 645–674.
- Hilboll, A., A. Richter, and J. P. Burrows, 2013: Long-term changes of tropospheric NO₂ over megacities derived from multiple satellite instruments. *Atmos. Chem. Phys.*, **13**, 4145–4169.
- Hinkelman, L. M., P. W. Stackhouse, B. A. Wielicki, T. P. Zhang, and S. R. Wilson, 2009: Surface insolation trends from satellite and ground measurements: Comparisons and challenges. *J. Geophys. Res. Atmos.*, **114**, D00d20.
- Hirdman, D., et al., 2010: Long-term trends of black carbon and sulphate aerosol in the Arctic: Changes in atmospheric transport and source region emissions. *Atmos. Chem. Phys.*, **10**, 9351–9368.
- Hirsch, M. E., A. T. DeGaetano, and S. J. Colucci, 2001: An East Coast winter storm climatology. *J. Clim.*, **14**, 882–899.
- Hirschi, M., et al., 2011: Observational evidence for soil-moisture impact on hot extremes in southeastern Europe. *Nature Geosci.*, **4**, 17–21.
- Ho, S. P., W. He, and Y. H. Kuo, 2009a: Construction of consistent temperature records in the lower stratosphere using Global Positioning System Radio Occultation Data and Microwave Sounding measurements. New Horizons in Occultation Research, Springer-Verlag Berlin, 207–217.
- Ho, S. P., Y. H. Kuo, Z. Zeng, and T. C. Peterson, 2007: A comparison of lower stratosphere temperature from microwave measurements with CHAMP GPS RO data. *Geophys. Res. Lett.*, **34**, L15701.
- Ho, S. P., M. Goldberg, Y. H. Kuo, C. Z. Zou, and W. Schreiner, 2009b: Calibration of temperature in the lower stratosphere from microwave measurements using COSMIC radio occultation data: Preliminary results. *Terr. Atmos. Ocean. Sci.*, **20**, 87–100.
- Ho, S. P., et al., 2012: Reproducibility of GPS radio occultation data for climate monitoring: Profile-to-profile inter-comparison of CHAMP climate records 2002 to 2008 from six data centers. *J. Geophys. Res. Atmos.*, **117**, D18111.
- Hoerling, M., et al., 2012: Anatomy of an extreme event. *J. Clim.*, **26**, 2811–2832.
- Holben, B. N., et al., 1998: AERONET—A federated instrument network and data archive for aerosol characterization. *Remote Sens. Environ.*, **66**, 1–16.
- Holland, G. J., and P. J. Webster, 2007: Heightened tropical cyclone activity in the North Atlantic: Natural variability or climate trend? *Philos. Trans. R. Soc. London Ser. A*, **365**, 2695–2716.
- Hope, P. K., W. Drosowsky, and N. Nicholls, 2006: Shifts in the synoptic systems influencing southwest Western Australia. *Clim. Dyn.*, **26**, 751–764.
- Hsu, N. C., et al., 2012: Global and regional trends of aerosol optical depth over land and ocean using SeaWiFS measurements from 1997 to 2010. *Atmos. Chem. Phys. Discuss.*, **12**, 8465–8501.
- Hsu, P. C., T. Li, and B. Wang, 2011: Trends in global monsoon area and precipitation over the past 30 years. *Geophys. Res. Lett.*, **38**, L08701.
- Hu, Y., and Q. Fu, 2007: Observed poleward expansion of the Hadley circulation since 1979. *Atmos. Chem. Phys.*, **7**, 5229–5236.
- Hu, Y. C., W. J. Dong, and Y. He, 2010: Impact of land surface forcings on mean and extreme temperature in eastern China. *J. Geophys. Res. Atmos.*, **115**, 11.
- Hu, Y. Y., C. Zhou, and J. P. Liu, 2011: Observational evidence for the poleward expansion of the Hadley circulation. *Adv. Atmos. Sci.*, **28**, 33–44.
- Huang, J., et al., 2008: Estimation of regional emissions of nitrous oxide from 1997 to 2005 using multinetwork measurements, a chemical transport model, and an inverse method. *J. Geophys. Res. Atmos.*, **113**, D17313.
- Huang, W.-R., S.-Y. Wang, and J. C. L. Chan, 2010: Discrepancies between global reanalyses and observations in the interdecadal variations of Southeast Asian cold surge. *Int. J. Climatol.*, **31**, 2272–2280.
- Hudson, R. D., 2012: Measurements of the movement of the jet streams at mid-latitudes, in the Northern and Southern Hemispheres, 1979 to 2010. *Atmos. Chem. Phys.*, **12**, 7797–7808.
- Hudson, R. D., M. F. Andrade, M. B. Follette, and A. D. Frolov, 2006: The total ozone field separated into meteorological regimes—Part II: Northern Hemisphere mid-latitude total ozone trends. *Atmos. Chem. Phys.*, **6**, 5183–5191.
- Hundecha, Y., A. St-Hilaire, T. Ouarda, S. El Adlouni, and P. Gachon, 2008: A nonstationary extreme value analysis for the assessment of changes in extreme annual wind speed over the Gulf of St. Lawrence, Canada. *J. Appl. Meteor. Climatol.*, **47**, 2745–2759.
- Hurrell, J. W., 1995: Decadal trends in the North Atlantic Oscillation: Regional temperatures and precipitation. *Science*, **269**, 676–679.
- Hurst, D., 2011: Stratospheric water vapor trends over Boulder, Colorado: Analysis of the 30 year Boulder record. *J. Geophys. Res.*, **116**, D02306.
- Idso, S. B., and A. J. Brazel, 1984: Rising atmospheric carbon-dioxide concentrations may increase streamflow. *Nature*, **312**, 51–53.
- IPCC, 2007: *Clim. Change 2007: The Physical Science Basis. Contribution of Working Group I to the Fourth Assessment Report of the Intergovernmental Panel on Climate Change (IPCC)* [Solomon, S., D. Qin, M. Manning, Z. Chen, M. Marquis, K. B. Averyt, M. Tignor and H. L. Miller (eds.)]. Cambridge University Press, Cambridge, United Kingdom and New York, NY, USA, 996 pp.
- Ishii, M., A. Shouji, S. Sugimoto, and T. Matsumoto, 2005: Objective analyses of sea-surface temperature and marine meteorological variables for the 20th century using i-coads and the Kobe collection. *Int. J. Climatol.*, **25**, 865–879.
- Ishijima, K., et al., 2007: Temporal variations of the atmospheric nitrous oxide concentration and its delta N-15 and delta O-18 for the latter half of the 20th century reconstructed from firn air analyses. *J. Geophys. Res. Atmos.*, **112**, D03305.
- Jain, S. K., and V. Kumar, 2012: Trend analysis of rainfall and temperature data for India. *Curr. Sci.*, **102**, 37–49.
- Jakob, D., D. Karoly, and A. Seed, 2011: Non-stationarity in daily and sub-daily intense rainfall—Part 2: Regional assessment for sites in south-east Australia. *Nat. Hazards Earth Syst. Sci.*, **11**, 2273–2284.
- Jhajharia, D., S. Shrivastava, D. Sarkar, and S. Sarkar, 2009: Temporal characteristics of pan evaporation trends under humid conditions of northeast India. *Agr. Forest Meteorol.*, **336**, 61–73.
- Jiang, T., Z. W. Kundzewicz, and B. Su, 2008: Changes in monthly precipitation and flood hazard in the Yangtze River Basin, China. *Int. J. Climatol.*, **28**, 1471–1481.
- Jiang, X., W. Ku, R. Shia, Q. Li, J. Elkins, R. Prinn, and Y. Yung, 2007: Seasonal cycle of N₂O: Analysis of data. *Global Biogeochem. Cycles*, **21**, GB1006.
- Jiang, Y., Y. Luo, Z. C. Zhao, and S. W. Tao, 2010: Changes in wind speed over China during 1956–2004. *Theor. Appl. Climatol.*, **99**, 421–430.
- Jin, S. G., J. U. Park, J. H. Cho, and P. H. Park, 2007: Seasonal variability of GPS-derived zenith tropospheric delay (1994–2006) and climate implications. *J. Geophys. Res. Atmos.*, **112**, D09110.
- John, V. O., R. P. Allan, and B. J. Soden, 2009: How robust are observed and simulated precipitation responses to tropical ocean warming? *Geophys. Res. Lett.*, **36**, L14702.
- John, V. O., G. Holl, R. P. Allan, S. A. Buehler, D. E. Parker, and B. J. Soden, 2011: Clear-sky biases in satellite infrared estimates of upper tropospheric humidity and its trends. *J. Geophys. Res. Atmos.*, **116**, D14108.
- Jones, D. A., W. Wang, and R. Fawcett, 2009: High-quality spatial climate data-sets for Australia. *Australian Meteor. Ocean. J.*, **58**, 233–248.
- Jones, P. D., and D. H. Lister, 2007: Intercomparison of four different Southern Hemisphere sea level pressure datasets. *Geophys. Res. Lett.*, **34**, L10704.
- Jones, P. D., and D. H. Lister, 2009: The urban heat island in Central London and urban-related warming trends in Central London since 1900. *Weather*, **64**, 323–327.
- Jones, P. D., T. Jonsson, and D. Wheeler, 1997: Extension to the North Atlantic Oscillation using early instrumental pressure observations from Gibraltar and south-west Iceland. *Int. J. Climatol.*, **17**, 1433–1450.
- Jones, P. D., D. H. Lister, and Q. Li, 2008: Urbanization effects in large-scale temperature records, with an emphasis on China. *J. Geophys. Res. Atmos.*, **113**, D16122.
- Jones, P. D., D. H. Lister, T. J. Osborn, C. Harpham, M. Salmon, and C. P. Morice, 2012: Hemispheric and large-scale land-surface air temperature variations: An extensive revision and an update to 2010. *J. Geophys. Res. Atmos.*, **117**, D05127.
- Jones, R., S. Westra, and A. Sharma, 2010: Observed relationships between extreme sub-daily precipitation, surface temperature, and relative humidity. *Geophys. Res. Lett.*, **37**, L22805.
- Joshi, M. M., J. M. Gregory, M. J. Webb, D. M. H. Sexton, and T. C. Johns, 2008: Mechanisms for the land/sea warming contrast exhibited by simulations of climate change. *Clim. Dyn.*, **30**, 455–465.
- Jovanovic, B., D. Collins, K. Braganza, D. Jakob, and D. A. Jones, 2011: A high-quality monthly total cloud amount dataset for Australia. *Clim. Change*, **108**, 485–517.
- Jung, M., et al., 2010: Recent decline in the global land evapotranspiration trend due to limited moisture supply. *Nature*, **467**, 951–954.
- Kahn, R. A., et al., 2007: Satellite-derived aerosol optical depth over dark water from MISR and MODIS: Comparisons with AERONET and implications for climatological studies. *J. Geophys. Res. Atmos.*, **112**, D18205.

- Kanamitsu, M., W. Ebisuzaki, J. Woollen, S. K. Yang, J. J. Hnilo, M. Fiorino, and G. L. Potter, 2002: NCEP-DOE AMIP-II reanalysis (R-2). *Bull. Am. Meteor. Soc.*, **83**, 1631–1643.
- Kang, S. M., L. M. Polvani, J. C. Fyfe, and M. Sigmond, 2011: Impact of polar ozone depletion on subtropical Precipitation. *Science*, **332**, 951–954.
- Kao, H. Y., and J. Y. Yu, 2009: Contrasting Eastern-Pacific and Central-Pacific types of ENSO. *J. Clim.*, **22**, 615–632.
- Karnauskas, K. B., R. Seager, A. Kaplan, Y. Kushnir, and M. A. Cane, 2009: Observed strengthening of the zonal sea surface temperature gradient across the equatorial Pacific Ocean. *J. Clim.*, **22**, 4316–4321.
- Karnieli, A., et al., 2009: Temporal trend in anthropogenic sulfur aerosol transport from central and eastern Europe to Israel. *J. Geophys. Res. Atmos.*, **114**, D00d19.
- Karoly, D., 1989: Southern-Hemisphere circulation features associated with El Niño–Southern Oscillation. *J. Clim.*, **2**, 1239–1252.
- Kato, S., et al.: Surface irradiances consistent with CERES-derived top-of-atmosphere shortwave and longwave irradiances. *J. Clim.*, **26**, 2719–2740.
- Keeling, C., R. Bacastow, A. Bainbridge, C. Ekdahl, P. Guenther, L. Waterman, and J. Chin, 1976a: Atmospheric Carbon-Dioxide Variations at Mauna-Loa Observatory, Hawaii. *Tellus*, **28**, 538–551.
- Keeling, C. D., J. A. Adams, and C. A. Ekdahl, 1976b: Atmospheric carbo-dioxide variations at South Pole. *Tellus*, **28**, 553–564.
- Keller, C., D. Brunner, S. Henne, M. Vollmer, S. O’Doherty, and S. Reimann, 2011: Evidence for under-reported western European emissions of the potent greenhouse gas HFC-23. *Geophys. Res. Lett.*, **38**, L15808.
- Kennedy, J. J., N. A. Rayner, and R. O. Smith, 2012: Using AATSR data to assess the quality of in situ sea surface temperature observations for climate studies. *Remote Sens. Environ.*, **116**, 79–92.
- Kennedy, J. J., N. A. Rayner, R. O. Smith, D. E. Parker, and M. Saunby, 2011a: Reassessing biases and other uncertainties in sea surface temperature observations measured in situ since 1850: 2. Biases and homogenization. *J. Geophys. Res. Atmos.*, **116**, D14104.
- Kennedy, J. J., N. A. Rayner, R. O. Smith, M. Saunby, and D. E. Parker, 2011b: Reassessing biases and other uncertainties in sea surface temperature observations since 1850, part 1: Measurement and sampling uncertainties. *J. Geophys. Res.*, **116**, D14103.
- Kent, E. C., and D. I. Berry, 2008: Assessment of the Marine Observing System (ASMOS): Final report. *National Oceanography Centre Southampton Research and Consultancy Report*, 55 pp.
- Kent, E. C., S. D. Woodruff, and D. I. Berry, 2007: Metadata from WMO publication no. 47 and an assessment of voluntary observing ship observation heights in ICOADS. *J. Atmos. Ocean Technol.*, **24**, 214–234.
- Kent, E. C., S. Fangohr, and D. I. Berry, 2012: A comparative assessment of monthly mean wind speed products over the global ocean. *Int. J. Climatol.*, **33**, 2530–2541.
- Kent, E. C., J. J. Kennedy, D. I. Berry, and R. O. Smith, 2010: Effects of instrumentation changes on sea surface temperature measured in situ. *Clim. Change*, **1**, 718–728.
- Kent, E. C., N. A. Rayner, D. I. Berry, M. Saunby, B. I. Moat, J. J. Kennedy, and D. E. Parker, 2013: Global analysis of night marine air temperature and its uncertainty since 1880, the HadNMT2 Dataset. *J. Geophys. Res.*, **118**, 1281–1298.
- Kenyon, J., and G. C. Hegerl, 2008: Influence of modes of climate variability on global temperature extremes. *J. Clim.*, **21**, 3872–3889.
- Kenyon, J., and G. C. Hegerl, 2010: Influence of modes of climate variability on global precipitation extremes. *J. Clim.*, **23**, 6248–6262.
- Khari, V., F. Zwiers, X. Zhang, and M. Wehner, 2013: Changes in temperature and precipitation extremes in the CMIP5 ensemble. *Climatic Change*, **119**, 345–357.
- Kiehl, J. T., and K. E. Trenberth, 1997: Earth’s annual global mean energy budget. *Bull. Am. Meteor. Soc.*, **78**, 197–208.
- Kim, D., and V. Ramanathan, 2012: Improved estimates and understanding of global albedo and atmospheric solar absorption. *Geophys. Res. Lett.*, **39**, L24704.
- Kim, D. Y., and V. Ramanathan, 2008: Solar radiation budget and radiative forcing due to aerosols and clouds. *J. Geophys. Res. Atmos.*, **113**, D02203.
- Kim, J., et al., 2010: Regional atmospheric emissions determined from measurements at Jeju Island, Korea: Halogenated compounds from China. *Geophys. Res. Lett.*, **37**, L12801.
- King, A., L. Alexander, and M. Donat, 2013: The efficacy of using gridded data to examine extreme rainfall characteristics: A case study for Australia. *Inter. J. Climatol.*, **33**, 2376–2387.
- Kistler, R., et al., 2001: The NCEP-NCAR 50-year reanalysis: Monthly means CD-ROM and documentation. *Bull. Am. Meteor. Soc.*, **82**, 247–267.
- Klein Tank, A. M. G., et al., 2006: Changes in daily temperature and precipitation extremes in central and south Asia. *J. Geophys. Res. Atmos.*, **111**, D16105.
- Klok, E. J., and A. Tank, 2009: Updated and extended European dataset of daily climate observations. *Int. J. Climatol.*, **29**, 1182–1191.
- Knapp, K. R., and M. C. Kruk, 2010: Quantifying interagency differences in tropical cyclone best-track wind speed estimates. *Mon. Weather Rev.*, **138**, 1459–1473.
- Knowles, N., M. D. Dettinger, and D. R. Cayan, 2006: Trends in snowfall versus rainfall in the western United States. *J. Clim.*, **19**, 4545–4559.
- Knutson, T. R., et al., 2010: Tropical cyclones and climate change. *Nature Geosci.*, **3**, 157–163.
- Kobayashi, S., M. Matricardi, D. Dee, and S. Uppala, 2009: Toward a consistent reanalysis of the upper stratosphere based on radiance measurements from SSU and AMSU-A. *Q. J. R. Meteorol. Soc.*, **135**, 2086–2099.
- Kopp, G., and G. Lawrence, 2005: The Total Irradiance Monitor (TIM): Instrument design. *Solar Phys.*, **230**, 91–109.
- Kopp, G., and J. L. Lean, 2011: A new, lower value of total solar irradiance: Evidence and climate significance. *Geophys. Res. Lett.*, **38**, L01706.
- Kopp, G., G. Lawrence, and G. Rottman, 2005: The Total Irradiance Monitor (TIM): Science results. *Solar Phys.*, **230**, 129–139.
- Kossin, J. P., K. R. Knapp, D. J. Vimont, R. J. Murnane, and B. A. Harper, 2007: A globally consistent reanalysis of hurricane variability and trends. *Geophys. Res. Lett.*, **34**, L04815.
- Koutsoyiannis, D., and A. Montanari, 2007: Statistical analysis of hydroclimatic time series: Uncertainty and insights. *Water Resour. Res.*, **43**, W05429.
- Kreienkamp, F., A. Spekat, and W. Enke, 2010: Stationarity of atmospheric waves and blocking over Europe based on a reanalysis dataset and two climate scenarios. *Theor. Appl. Climatol.*, **102**, 205–212.
- Krishna Moorthy, K., S. Suresh Babu, and S. K. Satheesh, 2007: Temporal heterogeneity in aerosol characteristics and the resulting radiative impact at a tropical coastal station—Part 1: Microphysical and optical properties. *Ann. Geophys.*, **25**, 2293–2308.
- Krishna Moorthy, K., S. Suresh Babu, M. R. Manoj, and S. K. Satheesh, 2013: Buildup of Aerosols over the Indian Region. *Geophys. Res. Lett.*, **40**, 1011–1014.
- Krishna Moorthy, K., S. S. Babu, S. K. Satheesh, S. Lal, M. M. Sarin, and S. Ramachandran, 2009: Climate implications of atmospheric aerosols and trace gases: Indian Scenario, Climate Sense. World Meteorological Organisation, Geneva, Switzerland, pp. 157–160.
- Krueger, O., F. Schenk, F. Feser, and R. Weisse, 2013: Inconsistencies between long-term trends in storminess derived from the 20CR reanalysis and observations. *J. Clim.*, **26**, 868–874.
- Kruger, A., and S. Sekele, 2013: Trends in extreme temperature indices in South Africa: 1962–2009. *Int. J. Climatol.*, **33**, 661–676.
- Kubota, H., and J. C. L. Chan, 2009: Interdecadal variability of tropical cyclone landfall in the Philippines from 1902 to 2005. *Geophys. Res. Lett.*, **36**, L12802.
- Kudo, R., A. Uchiyama, A. Yamazaki, T. Sakami, and O. Ijima, 2011: Decadal changes in aerosol optical thickness and single scattering albedo estimated from ground-based broadband radiometers: A case study in Japan. *J. Geophys. Res.*, **116**, D03207.
- Kudo, R., A. Uchiyama, O. Ijima, N. Ohkawara, and S. Ohta, 2012: Aerosol impact on the brightening in Japan. *J. Geophys. Res. Atmos.*, **117**, 11.
- Kueppers, L. M., M. A. Snyder, and L. C. Sloan, 2007: Irrigation cooling effect: Regional climate forcing by land-use change. *Geophys. Res. Lett.*, **34**, L03703.
- Kuglitsch, F. G., A. Toreti, E. Xoplaki, P. M. Della-Marta, J. Luterbacher, and H. Wanner, 2009: Homogenization of daily maximum temperature series in the Mediterranean. *J. Geophys. Res. Atmos.*, **114**, D15108.
- Kuglitsch, F. G., A. Toreti, E. Xoplaki, P. M. Della-Marta, C. S. Zerefos, M. Turkes, and J. Luterbacher, 2010: Heat wave changes in the eastern Mediterranean since 1960. *Geophys. Res. Lett.*, **37**, L04802.
- Kumari, B. P., and B. N. Goswami, 2010: Seminal role of clouds on solar dimming over the Indian monsoon region. *Geophys. Res. Lett.*, **37**, L06703.
- Kumari, B. P., A. L. Londhe, S. Daniel, and D. B. Jadhav, 2007: Observational evidence of solar dimming: Offsetting surface warming over India. *Geophys. Res. Lett.*, **34**, L21810.

- Kundzewicz, Z. W., et al., 2007: Freshwater resources and their management. *Climate Change 2007: Impacts, Adaptation and Vulnerability. Contribution of Working Group II to the Fourth Assessment Report of the Intergovernmental Panel on Climate Change* [Solomon, S., D. Qin, M. Manning, Z. Chen, M. Marquis, K. B. Averyt, M. Tignor and H. L. Miller (eds.)]. Cambridge University Press, Cambridge, United Kingdom and New York, NY, USA, 172–210.
- Kunkel, K. E., M. A. Palecki, L. Ensor, D. Easterling, K. G. Hubbard, D. Robinson, and K. Redmond, 2009: Trends in twentieth-century US extreme snowfall seasons. *J. Clim.*, **22**, 6204–6216.
- Kunkel, K. E., et al., 2008: Observed changes in weather and climate extremes. In: *Weather and Climate Extremes in a Changing Climate. Regions of Focus: North America, Hawaii, Caribbean, and U.S. Pacific Islands* [T. R. Karl, G. A. Meehl, D. M. Christopher, S. J. Hassol, A. M. Waple, and W. L. Murray (eds.)]. A Report by the U.S. Climate Change Science Program and the Subcommittee on Global Change Research.
- Kunz, M., J. Sander, and C. Kottmeier, 2009: Recent trends of thunderstorm and hailstorm frequency and their relation to atmospheric characteristics in southwest Germany. *Int. J. Climatol.*, **29**, 2283–2297.
- Kuo, Y. H., W. S. Schreiner, J. Wang, D. L. Rossiter, and Y. Zhang, 2005: Comparison of GPS radio occultation soundings with radiosondes. *Geophys. Res. Lett.*, **32**, L05817.
- Kvalevag, M. M., and G. Myhre, 2007: Human impact on direct and diffuse solar radiation during the industrial era. *J. Clim.*, **20**, 4874–4883.
- L'Ecuyer, T. S., N. B. Wood, T. Haladay, G. L. Stephens, and P. W. Stackhouse, 2008: Impact of clouds on atmospheric heating based on the R04 CloudSat fluxes and heating rates data set. *J. Geophys. Res. Atmos.*, **113**, 15.
- Labat, D., Y. Godderis, J. L. Probst, and J. L. Guyot, 2004: Evidence for global runoff increase related to climate warming. *Adv. Water Resour.*, **27**, 631–642.
- Ladstadter, F., A. K. Steiner, U. Foelsche, L. Haimberger, C. Tavolato, and G. Kirchner, 2011: An assessment of differences in lower stratospheric temperature records from (A)MSU, radiosondes and GPS radio occultation. *Atmos. Meas. Tech.*, **4**, 1965–1977.
- Landsea, C. W., 2007: Counting Atlantic tropical cyclones back to 1900. *EOS Trans. (AGU)*, **88**, 197–202.
- Landsea, C. W., B. A. Harper, K. Hoarau, and J. A. Knaff, 2006: Can we detect trends in extreme tropical cyclones? *Science*, **313**, 452–454.
- Landsea, C. W., et al., 2011: A reanalysis of the 1921–30 Atlantic Hurricane Database. *J. Clim.*, **25**, 865–885.
- Langematz, U., and M. Kunze, 2008: Dynamical changes in the Arctic and Antarctic stratosphere during spring. In: *Climate Variability and Extremes during the Past 100 Years. Advances in Global Change Research* [S. Brönnimann, J. Luterbacher, T. Ewen, H. F. Diaz, R. S. Stolarski, and U. Neu (eds.)], Springer, pp. 293–301.
- Lanzante, J. R., 2009: Comment on “Trends in the temperature and water vapor content of the tropical lower stratosphere: Sea surface connection” by Karen H. Rosenlof and George C. Reid. *J. Geophys. Res. Atmos.*, **114**, D12104.
- Laprise, R., 1992: The resolution of global spectral models. *Bull. Am. Meteor. Soc.*, **73**, 1453–1454.
- Larkin, N. K., and D. E. Harrison, 2005: On the definition of El Niño and associated seasonal average US weather anomalies. *Geophys. Res. Lett.*, **32**, L13705.
- Lawrimore, J. H., M. J. Menne, B. E. Gleason, C. N. Williams, D. B. Wueertz, R. S. Vose, and J. Rennie, 2011: An overview of the Global Historical Climatology Network monthly mean temperature data set, version 3. *J. Geophys. Res. Atmos.*, **116**, D19121.
- Leakey, A. D. B., M. Uribelarra, E. A. Ainsworth, S. L. Naidu, A. Rogers, D. R. Ort, and S. P. Long, 2006: Photosynthesis, productivity, and yield of maize are not affected by open-air elevation of CO₂ concentration in the absence of drought. *Plant Physiol.*, **140**, 779–790.
- Lee, H. T., A. Gruber, R. G. Ellingson, and I. Laszlo, 2007: Development of the HIRS outgoing longwave radiation climate dataset. *J. Atmos. Ocean Technol.*, **24**, 2029–2047.
- Lefohn, A. S., D. Shadwick, and S. J. Oltmans, 2010: Characterizing changes in surface ozone levels in metropolitan and rural areas in the United States for 1980–2008 and 1994–2008. *Atmos. Environ.*, **44**, 5199–5210.
- Lehmann, A., K. Getzlaff, and J. Harlass, 2011: Detailed assessment of climate variability in the Baltic Sea area for the period 1958 to 2009. *Clim. Res.*, **46**, 185–196.
- Lelieveld, J., J. van Aardenne, H. Fischer, M. de Reus, J. Williams, and P. Winkler, 2004: Increasing ozone over the Atlantic Ocean. *Science*, **304**, 1483–1487.
- Lenderink, G., and E. Van Meijgaard, 2008: Increase in hourly precipitation extremes beyond expectations from temperature changes. *Nature Geosci.*, **1**, 511–514.
- Lenderink, G., H. Y. Mok, T. C. Lee, and G. J. van Oldenborgh, 2011: Scaling and trends of hourly precipitation extremes in two different climate zones – Hong Kong and the Netherlands. *Hydrol. Earth Syst. Sci. Discuss.*, **8**, 4701–4719.
- Lennartz, S., and A. Bunde, 2009: Trend evaluation in records with long-term memory: Application to global warming. *Geophys. Res. Lett.*, **36**, L16706.
- Levin, I., et al., 2010: The global SF₆ source inferred from long-term high precision atmospheric measurements and its comparison with emission inventories. *Atmos. Chem. Phys.*, **10**, 2655–2662.
- Levitus, S., J. I. Antonov, T. P. Boyer, R. A. Locarnini, H. E. Garcia, and A. V. Mishonov, 2009: Global ocean heat content 1955–2008 in light of recently revealed instrumentation problems. *Geophys. Res. Lett.*, **36**, 5.
- Levy, R. C., L. A. Remer, R. G. Kleidman, S. Mattoo, C. Ichoku, R. Kahn, and T. F. Eck, 2010: Global evaluation of the Collection 5 MODIS dark-target aerosol products over land. *Atmos. Chem. Phys.*, **10**, 10399–10420.
- Li, Q., H. Zhang, X. Liu, J. Chen, W. Li, and P. Jones, 2009: A mainland China homogenized historical temperature dataset of 1951–2004. *Bull. Am. Meteor. Soc.*, **90**, 1062–1065.
- Li, Q., W. Dong, W. Li, X. Gao, P. Jones, J. Kennedy, and D. Parker, 2010a: Assessment of the uncertainties in temperature change in China during the last century. *Chin. Sci. Bull.*, **55**, 1974–1982.
- Li, Q. X., et al., 2010b: Assessment of surface air warming in northeast China, with emphasis on the impacts of urbanization. *Theor. Appl. Climatol.*, **99**, 469–478.
- Li, Z., et al., 2012: Changes of daily climate extremes in southwestern China during 1961–2008. *Global Planet. Change*, **80–81**, 255–272.
- Liang, F., and X. A. Xia, 2005: Long-term trends in solar radiation and the associated climatic factors over China for 1961–2000. *Ann. Geophys.*, **23**, 2425–2432.
- Liebmann, B., R. M. Dole, C. Jones, I. Blade, and D. Allured, 2010: Influence of choice of time period on global surface temperature trend estimates. *Bull. Am. Meteor. Soc.*, **91**, 1485–1471.
- Liepert, B. G., 2002: Observed reductions of surface solar radiation at sites in the United States and worldwide from 1961 to 1990. *Geophys. Res. Lett.*, **29**, 1421.
- Liley, J. B., 2009: New Zealand dimming and brightening. *J. Geophys. Res. Atmos.*, **114**, D00d10.
- Lim, E. P., and I. Simmonds, 2007: Southern Hemisphere winter extratropical cyclone characteristics and vertical organization observed with the ERA-40 data in 1979–2001. *J. Clim.*, **20**, 2675–2690.
- Lim, E. P., and I. Simmonds, 2009: Effect of tropospheric temperature change on the zonal mean circulation and SH winter extratropical cyclones. *Clim. Dyn.*, **33**, 19–32.
- Lim, Y. K., M. Cai, E. Kalnay, and L. Zhou, 2008: Impact of vegetation types on surface temperature change. *J. Appl. Meteor. Climatol.*, **47**, 411–424.
- Lin, C., K. Yang, J. Qin, and R. Fu, 2012: Observed coherent trends of surface and upper-air wind speed over China since 1960. *J. Clim.*, **26**, 2891–2903.
- Liu, B., M. Xu, and M. Henderson, 2011: Where have all the showers gone? Regional declines in light precipitation events in China, 1960–2000. *Int. J. Climatol.*, **31**, 1177–1191.
- Liu, B. H., M. Xu, M. Henderson, and W. G. Gong, 2004a: A spatial analysis of pan evaporation trends in China, 1955–2000. *J. Geophys. Res. Atmos.*, **109**, D15102.
- Liu, B. H., M. Xu, M. Henderson, Y. Qi, and Y. Q. Li, 2004b: Taking China's temperature: Daily range, warming trends, and regional variations, 1955–2000. *J. Clim.*, **17**, 4453–4462.
- Liu, Q. H., and F. Z. Weng, 2009: Recent stratospheric temperature observed from satellite measurements. *Sola*, **5**, 53–56.
- Lo, M.-H., and J. S. Famiglietti, 2013: Irrigation in California's Central Valley strengthens the southwestern U.S. water cycle. *Geophys. Res. Lett.*, **40**, 301–306.
- Loeb, N. G., et al., 2009: Toward optimal closure of the Earth's top-of-atmosphere radiation budget. *J. Clim.*, **22**, 748–766.
- Loeb, N. G., et al., 2012a: Advances in understanding top-of-atmosphere radiation variability from satellite observations. *Surv. Geophys.*, **33**, 359–385.
- Loeb, N. G., et al., 2012b: Observed changes in top-of-the-atmosphere radiation and upper-ocean heating consistent within uncertainty. *Nature Geosci.*, **5**, 110–113.
- Logan, J. A., et al., 2012: Changes in ozone over Europe since 1990: Analysis of ozone measurements from sondes, regular aircraft (MOZAIC), and alpine surface sites. *J. Geophys. Res.*, **117**, D09301.
- Long, C. N., E. G. Dutton, J. A. Augustine, W. Wiscombe, M. Wild, S. A. McFarlane, and C. J. Flynn, 2009: Significant decadal brightening of downwelling shortwave in the continental United States. *J. Geophys. Res. Atmos.*, **114**, D00d06.

- Lorenz, R., E. B. Jaeger, and S. I. Seneviratne, 2010: Persistence of heat waves and its link to soil moisture memory. *Geophys. Res. Lett.*, **37**, L09703.
- Lucas, C., H. Nguyen, and B. Timbal, 2012: An observational analysis of Southern Hemisphere tropical expansion. *J. Geophys. Res.*, **117**, D17112.
- Luo, J. J., W. Sasaki, and Y. Masumoto, 2012: Indian Ocean warming modulates Pacific climate change. *Proc. Natl. Acad. Sci. U.S.A.*, **109**, 18701–18706.
- Lupikasza, E., 2010: Spatial and temporal variability of extreme precipitation in Poland in the period 1951–2006. *Int. J. Climatol.*, **30**, 991–1007.
- Lyman, J. M., et al., 2010: Robust warming of the global upper ocean. *Nature*, **465**, 334–337.
- Lynch, A. H., J. A. Curry, R. D. Brunner, and J. A. Maslanik, 2004: Toward an integrated assessment of the impacts of extreme wind events on Barrow, Alaska. *Bull. Am. Meteor. Soc.*, **85**, 209–.
- Mahowald, N., et al., 2010: Observed 20th century desert dust variability: Impact on climate and biogeochemistry. *Atmos. Chem. Phys.*, **10**, 10875–10893.
- Makowski, K., M. Wild, and A. Ohmura, 2008: Diurnal temperature range over Europe between 1950 and 2005. *Atmos. Chem. Phys.*, **8**, 6483–6498.
- Makowski, K., E. B. Jaeger, M. Chiacchio, M. Wild, T. Ewen, and A. Ohmura, 2009: On the relationship between diurnal temperature range and surface solar radiation in Europe. *J. Geophys. Res. Atmos.*, **114**, D00d07.
- Manabe, S., and R. F. Strickler, 1964: Thermal equilibrium of the atmosphere with a convective adjustment. *Journal of the Atmospheric Sciences*, **21**, 361–385.
- Mann, M. E., 2011: On long range dependence in global surface temperature series. *Clim. Change*, **107**, 267–276.
- Mann, M. E., T. A. Sabbatelli, and U. Neu, 2007a: Evidence for a modest undercount bias in early historical Atlantic tropical cyclone counts. *Geophys. Res. Lett.*, **34**, L22707.
- Mann, M. E., K. A. Emanuel, G. J. Holland, and P. J. Webster, 2007b: Atlantic tropical cyclones revisited. *EOS Transactions (AGU)*, **88**, 349–350.
- Manney, G. L., et al., 2011: Unprecedented Arctic ozone loss in 2011. *Nature*, **478**, 469–475.
- Mantua, N. J., S. R. Hare, Y. Zhang, J. M. Wallace, and R. C. Francis, 1997: A Pacific interdecadal climate oscillation with impacts on salmon production. *Bull. Am. Meteor. Soc.*, **78**, 1069–1079.
- Marenco, A., H. Gouget, P. Nédélec, and J. P. Pagés, 1994: Evidence of a long-term increase in tropospheric ozone from Pic du Midi series: Consequences: positive radiative forcing. *J. Geophys. Res.*, **99**, 16,617–616, 632.
- Marshall, G. J., 2003: Trends in the southern annular mode from observations and reanalyses. *J. Clim.*, **16**, 4134–4143.
- Martinerie, P., et al., 2009: Long-lived halocarbon trends and budgets from atmospheric chemistry modelling constrained with measurements in polar firn. *Atmos. Chem. Phys.*, 3911–3934.
- Mastrandrea, M., et al., 2011: The IPCC AR5 guidance note on consistent treatment of uncertainties: A common approach across the working groups. *Clim. Change*, **108**, 675–691.
- Matulla, C., W. Schoner, H. Alexandersson, H. von Storch, and X. L. Wang, 2008: European storminess: Late nineteenth century to present. *Clim. Dyn.*, **31**, 125–130.
- McCarthy, M. P., P. W. Thorne, and H. A. Titchner, 2009: An analysis of tropospheric humidity trends from radiosondes. *J. Clim.*, **22**, 5820–5838.
- McCarthy, M. P., H. A. Titchner, P. W. Thorne, S. F. B. Tett, L. Haimberger, and D. E. Parker, 2008: Assessing bias and uncertainty in the HadAT-adjusted radiosonde climate record. *J. Clim.*, **21**, 817–832.
- McKittrick, R., 2010: Atmospheric circulations do not explain the temperature-industrialization correlation. *Stat. Politics Policy*, **1**, issue 1.
- McKittrick, R., and P. J. Michaels, 2004: A test of corrections for extraneous signals in gridded surface temperature data. *Clim. Res.*, **26**, 159–173.
- McKittrick, R., and N. Nierenberg, 2010: Socioeconomic patterns in climate data. *J. Econ. Soc. Meas.*, **35**, 149–175.
- McKittrick, R. R., and P. J. Michaels, 2007: Quantifying the influence of anthropogenic surface processes and inhomogeneities on gridded global climate data. *J. Geophys. Res. Atmos.*, **112**, D24S09.
- McNider, R. T., et al., 2012: Response and sensitivity of the nocturnal boundary layer over land to added longwave radiative forcing. *J. Geophys. Res.*, **117**, D14106.
- McVicar, T. R., T. G. Van Niel, L. T. Li, M. L. Roderick, D. P. Rayner, L. Ricciardulli, and R. J. Donohue, 2008: Wind speed climatology and trends for Australia, 1975–2006: Capturing the stilling phenomenon and comparison with near-surface reanalysis output. *Geophys. Res. Lett.*, **35**, L20403.
- McVicar, T. R., et al., 2012: Global review and synthesis of trends in observed terrestrial near-surface wind speeds: Implications for evaporation. *J. Hydrol.*, **416**, 182–205.
- Mears, C., J. Wang, S. Ho, L. Zhang, and X. Zhou, 2010: Total column water vapor, in State of the Climate in 2009. *Bull. Am. Meteor. Soc.* [D. S. Arndt, M. O. Baringer, and M. R. Johnson (eds.)].
- Mears, C. A., and F. J. Wentz, 2009a: Construction of the remote sensing systems V3.2 atmospheric temperature records from the MSU and AMSU microwave sounders. *J. Atmos. Ocean Technol.*, **26**, 1040–1056.
- Mears, C. A., and F. J. Wentz, 2009b: Construction of the RSS V3.2 lower-tropospheric temperature dataset from the MSU and AMSU microwave sounders. *J. Atmos. Ocean Technol.*, **26**, 1493–1509.
- Mears, C. A., F. J. Wentz, and P. W. Thorne, 2012: Assessing the value of Microwave Sounding Unit-radiosonde comparisons in ascertaining errors in climate data records of tropospheric temperatures. *J. Geophys. Res. Atmos.*, **117**, D19103.
- Mears, C. A., F. J. Wentz, P. Thorne, and D. Bernie, 2011: Assessing uncertainty in estimates of atmospheric temperature changes from MSU and AMSU using a Monte-Carlo estimation technique. *J. Geophys. Res. Atmos.*, **116**.
- Mears, C. A., C. E. Forest, R. W. Spencer, R. S. Vose, and R. W. Reynolds, 2006: What is our understanding of the contribution made by observational or methodological uncertainties to the previously reported vertical differences in temperature trends? In: *Temperature Trends in the Lower Tmosphere: Steps for Understanding and Reconciling Differences* [T. R. Karl, S. J. Hassol, C. D. Miller, and W. L. Murray (eds.)], 71–88.
- Mears, C. A., B. D. Santer, F. J. Wentz, K. E. Taylor, and M. F. Wehner, 2007: Relationship between temperature and precipitable water changes over tropical oceans. *Geophys. Res. Lett.*, **34**, L24709.
- Meehl, G. A., J. M. Arblaster, and G. Branstator, 2012: Mechanisms contributing to the warming hole and the consequent U.S. East–West differential of heat extremes. *J. Clim.*, **25**, 6394–6408.
- Mekis, É., and L. A. Vincent, 2011: An overview of the second generation adjusted daily precipitation dataset for trend analysis in Canada. *Atmosphere-Ocean*, **49**, 163–177.
- Meng, Q. J., M. Latif, W. Park, N. S. Keenlyside, V. A. Semenov, and T. Martin, 2012: Twentieth century Walker Circulation change: Data analysis and model experiments. *Clim. Dyn.*, **38**, 1757–1773.
- Menne, M. J., and C. N. Williams, 2009: Homogenization of temperature series via pairwise comparisons. *J. Clim.*, **22**, 1700–1717.
- Menne, M. J., C. N. Williams, and M. A. Palecki, 2010: On the reliability of the US surface temperature record. *J. Geophys. Res. Atmos.*, **115**, D11108.
- Menzel, W. P., 2001: Cloud tracking with satellite imagery: From the pioneering work of Ted Fujita to the present. *Bull. Am. Meteor. Soc.*, **82**, 33–47.
- Merchant, C. J., et al., 2012: A 20 year independent record of sea surface temperature for climate from Along Track Scanning Radiometer. *J. Geophys. Res.*, **117**, C12013.
- Merrifield, M. A., 2011: A shift in western tropical Pacific sea level trends during the 1990s. *J. Clim.*, **24**, 4126–4138.
- Mezher, R. N., M. Doyle, and V. Barros, 2012: Climatology of hail in Argentina. *Atmos. Res.*, **114–115**, 70–82.
- Mieruch, S., S. Noel, H. Bovensmann, and J. P. Burrows, 2008: Analysis of global water vapour trends from satellite measurements in the visible spectral range. *Atmos. Chem. Phys.*, **8**, 491–504.
- Milewska, E. J., 2004: Baseline cloudiness trends in Canada 1953–2002. *Atmos. Ocean*, **42**, 267–280.
- Miller, B., et al., 2010: HFC-23 (CHF3) emission trend response to HCFC-22 (CHClF2) production and recent HFC-23 emission abatement measures. *Atmos. Chem. Phys.*, **10**, 7875–7890.
- Milliman, J. D., K. L. Farnsworth, P. D. Jones, K. H. Xu, and L. C. Smith, 2008: Climatic and anthropogenic factors affecting river discharge to the global ocean, 1951–2000. *Global Planet. Change*, **62**, 187–194.
- Mills, T. C., 2010: ‘Skinning a cat’: Alternative models of representing temperature trends. *Clim. Change*, **101**, 415–426.
- Milz, M., et al., 2005: Water vapor distributions measured with the Michelson Interferometer for passive atmospheric sounding on board Envisat (MIPAS/Envisat). *J. Geophys. Res.*, **110**, D24307.
- Mishchenko, M. I., et al., 2007: Long-term satellite record reveals likely recent aerosol trend. *Science*, **315**, 1543–1543.

- Mishchenko, M. I., et al., 2012: Aerosol retrievals from channel-1 and -2 AVHRR radiances: Long-term trends updated and revisited. *J. Quant. Spectr. Radiat. Trans.*, **113**, 1974–1980.
- Misra, V., J. P. Michael, R. Boyles, E. P. Chassignet, M. Griffin, and J. J. O'Brien, 2012: Reconciling the spatial distribution of the surface temperature trends in the southeastern United States. *J. Clim.*, **25**, 3610–3618.
- Mitas, C. M., and A. Clement, 2005: Has the Hadley cell been strengthening in recent decades? *Geophys. Res. Lett.*, **32**, L030809.
- Mitchell, T. D., and P. D. Jones, 2005: An improved method of constructing a database of monthly climate observations and associated high-resolution grids. *Int. J. Climatol.*, **25**, 693–712.
- Mo, K., and J. Paegle, 2001: The Pacific-South American modes and their downstream effects. *Int. J. Climatol.*, **21**, 1211–1229.
- Moberg, A., et al., 2006: Indices for daily temperature and precipitation extremes in Europe analyzed for the period 1901–2000. *J. Geophys. Res. Atmos.*, **111**, D22106.
- Mohapatra, M., B. K. Mandyopadhyay, and A. Tyagi, 2011: Best track parameters of tropical cyclones over the North Indian Ocean: A review. *Natural Hazards*, **63**, 1285–1317.
- Mokhov, I. I., M. G. Akperov, M. A. Prokofyeva, A. V. Timazhev, A. R. Lupo, and H. Le Treut, 2013: Blockings in the Northern Hemisphere and Euro-Atlantic region: Estimates of changes from reanalyses data and model simulations. *Doklady, Earth Sci.*, **449**, 430–433.
- Monaghan, A. J., and D. H. Bromwich, 2008: Advances describing recent Antarctic climate variability. *Bull. Am. Meteorol. Soc.*, **89**, 1295–1306.
- Monaghan, A. J., D. H. Bromwich, W. Chapman, and J. C. Comiso, 2008: Recent variability and trends of Antarctic near-surface temperature. *J. Geophys. Res. Atmos.*, **113**, D04105.
- Monk, W., D. L. Peters, D. J. Baird, and R. A. Curry, 2011: Trends in indicator hydrological variables for Canadian rivers. *Hydrol. Proc.*, **25**, 3086–3100.
- Monks, P. S., et al., 2009: Atmospheric composition change – global and regional air quality. *Atmos. Environ.*, **43**, 5268–5350.
- Montzka, S., B. Hall, and J. Elkins, 2009: Accelerated increases observed for hydrochlorofluorocarbons since 2004 in the global atmosphere. *Geophys. Res. Lett.*, **36**, L03804.
- Montzka, S., M. Krol, E. Dlugokencky, B. Hall, P. Jockel, and J. Lelieveld, 2011: Small interannual variability of global atmospheric hydroxyl. *Science*, **331**, 67–69.
- Montzka, S., L. Kuijpers, M. Battle, M. Aydin, K. Verhulst, E. Saltzman, and D. Fahey, 2010: Recent increases in global HFC-23 emissions. *Geophys. Res. Lett.*, **37**, L02808.
- Montzka, S. A., et al., 2011b: Ozone-depleting substances (ODSs) and related chemicals. In Scientific Assessment of Ozone Depletion: 2010, Global Ozone Research and Monitoring Project—Report No. 52. World Meteorological Organization, Geneva, Switzerland, 516 pp.
- Morak, S., G. C. Hegerl, and J. Kenyon, 2011: Detectable regional changes in the number of warm nights. *Geophys. Res. Lett.*, **38**, 5.
- Morak, S., G. C. Hegerl, and N. Christidis, 2013: Detectable changes in the frequency of temperature extremes. *J. Clim.*, **26**, 1561–1574.
- Morice, C. P., J. J. Kennedy, N. A. Rayner, and P. D. Jones, 2012: Quantifying uncertainties in global and regional temperature change using an ensemble of observational estimates: The HadCRUT4 data set. *J. Geophys. Res. Atmos.*, **117**, 22.
- Mueller, B., and S. Seneviratne, 2012: Hot days induced by precipitation deficits at the global scale. *Proc. Natl. Acad. Sci. U.S.A.*, **109**, 12398–12403.
- Mueller, B., et al., 2011: Evaluation of global observations-based evapotranspiration datasets and IPCC AR4 simulations. *Geophys. Res. Lett.*, **38**, L06402.
- Muhle, J., et al., 2010: Perfluorocarbons in the global atmosphere: tetrafluoromethane, hexafluoroethane, and octafluoropropane. *Atmos. Chem. Phys.*, **10**, 5145–5164.
- Murphy, D. M., et al., 2011: Decreases in elemental carbon and fine particle mass in the United States. *Atmos. Chem. Phys.*, **11**, 4679–4686.
- Nan, S., and J. P. Li, 2003: The relationship between the summer precipitation in the Yangtze River Valley and the boreal spring Southern Hemisphere annular mode. *Geophys. Res. Lett.*, **30**, 2266.
- Nash, J., and P. R. Edge, 1989: Temperature changes in the stratosphere and lower mesosphere 197–1988 inferred from TOVS radiance observations. *Adv. Space Res.*, **9**, 333–341.
- Neff, W., J. Perlwitz, and M. Hoerling, 2008: Observational evidence for asymmetric changes in tropospheric heights over Antarctica on decadal time scales. *Geophys. Res. Lett.*, **35**, L18703.
- Neu, U., et al., 2012: IMILAST: A community effort to intercompare extratropical cyclone detection and tracking algorithms. *Bull. Am. Meteor. Soc.*, **94**, 529–547.
- Nevison, C., et al., 2011: Exploring causes of interannual variability in the seasonal cycles of tropospheric nitrous oxide. *Atmos. Chem. Phys.*, **11**, 3713–3730.
- New, M., et al., 2006: Evidence of trends in daily climate extremes over southern and west Africa. *J. Geophys. Res. Atmos.*, **111**, D14102.
- Nguyen, H., B. Timbal, I. Smith, A. Evans, and C. Lucas, 2013: The Hadley circulation in reanalyses: Climatology, variability and change. *J. Clim.*, **26**, 3357–3376.
- Nicholls, N., 2008: Recent trends in the seasonal and temporal behaviour of the El Niño-Southern Oscillation. *Geophys. Res. Lett.*, **35**, L19703.
- Nisbet, E., and R. Weiss, 2010: Top-down versus bottom-up. *Science*, **328**, 1241–1243.
- Norris, J. R., and M. Wild, 2007: Trends in aerosol radiative effects over Europe inferred from observed cloud cover, solar “dimming” and solar “brightening”. *J. Geophys. Res. Atmos.*, **112**, D08214.
- Norris, J. R., and M. Wild, 2009: Trends in aerosol radiative effects over China and Japan inferred from observed cloud cover, solar dimming, and solar brightening. *J. Geophys. Res. Atmos.*, **114**, D00d15.
- O'Dell, C. W., F. J. Wentz, and R. Bennartz, 2008: Cloud liquid water path from satellite-based passive microwave observations: A new climatology over the global oceans. *J. Clim.*, **21**, 1721–1739.
- O'Doherty, S., et al., 2009: Global and regional emissions of HFC-125 (CHF₂CF₃) from in situ and air archive atmospheric observations at AGAGE and SOGE observatories. *J. Geophys. Res. Atmos.*, **109**, D06310.
- O'Donnell, R., N. Lewis, S. McIntyre, and J. Condon, 2011: Improved methods for PCA-based reconstructions: Case study using the Steig et al. (2009) Antarctic Temperature Reconstruction. *J. Clim.*, **24**, 2099–2115.
- O'Gorman, P., R. P. Allan, M. P. Byrne, and M. Previdi, 2012: Energetic constraints on precipitation under climate change. *Surv. Geophys.*, **33**, 585–608.
- Ohmura, A., 2009: Observed decadal variations in surface solar radiation and their causes. *J. Geophys. Res. Atmos.*, **114**, D00d05.
- Ohmura, A., et al., 1998: Baseline Surface Radiation Network (BSRN/WCRP): New precision radiometry for climate research. *Bull. Am. Meteor. Soc.*, **79**, 2115–2136.
- Ohvri, H., et al., 2009: Global dimming and brightening versus atmospheric column transparency, Europe, 1906–2007. *J. Geophys. Res. Atmos.*, **114**, D00d12.
- Oltmans, S. J., et al., 2013: Recent tropospheric ozone changes – A pattern dominated by slow or no growth. *Atmos. Environ.*, **67**, 331–351.
- Onogi, K., et al., 2007: The JRA-25 reanalysis. *J. Meteorol. Soc. Jpn.*, **85**, 369–432.
- Oort, A. H., and J. J. Yienger, 1996: Observed interannual variability in the Hadley circulation and its connection to ENSO. *J. Clim.*, **9**, 2751–2767.
- Osborn, T. J., 2011: Winter 2009/2010 temperatures and a record breaking North Atlantic Oscillation index. *Weather*, **66**, 19–21.
- Paciorek, C. J., J. S. Risbey, V. Ventura, and R. D. Rosen, 2002: Multiple indices of Northern Hemisphere cyclone activity, winters 1949–99. *J. Clim.*, **15**, 1573–1590.
- Palmer, M. D., K. Haines, S. F. B. Tett, and T. J. Ansell, 2007: Isolating the signal of ocean global warming. *Geophys. Res. Lett.*, **34**, 6.
- Palmer, W. C., 1965: Meteorological drought. *US Weather Bureau Research Paper*, **45**, 58 pages.
- Paltridge, G., A. Arking, and M. Pook, 2009: Trends in middle- and upper-level tropospheric humidity from NCEP reanalysis data. *Theor. Appl. Climatol.*, **98**, 351–359.
- Pan, Z. T., R. W. Arritt, E. S. Takle, W. J. Gutowski, C. J. Anderson, and M. Segal, 2004: Altered hydrologic feedback in a warming climate introduces a “warming hole”. *Geophys. Res. Lett.*, **31**, L17109.
- Panagiotopoulos, F., M. Shahgedanova, A. Hannachi, and D. B. Stephenson, 2005: Observed trends and teleconnections of the Siberian high: A recently declining center of action. *J. Clim.*, **18**, 1411–1422.
- Parker, D., C. Folland, A. Scaife, J. Knight, A. Colman, P. Baines, and B. Dong, 2007: Decadal to multidecadal variability and the climate change background. *J. Geophys. Res. Atmos.*, **112**, D18115.
- Parker, D. E., 2006: A demonstration that large-scale warming is not urban. *J. Clim.*, **19**, 2882–2895.
- Parker, D. E., 2011: Recent land surface air temperature trends assessed using the 20th century reanalysis. *J. Geophys. Res. Atmos.*, **116**, D20125.
- Parker, D. E., P. Jones, T. C. Peterson, and J. Kennedy, 2009: Comment on “Unresolved issues with the assessment of multidecadal global land surface temperature trends” by Roger A. Pielke Sr. et al. *J. Geophys. Res. Atmos.*, **114**, D05104.
- Parrish, D. D., et al., 2012: Long-term changes in lower tropospheric baseline ozone concentrations at northern mid-latitudes. *Atmos. Chem. Phys.*, **12**, 11485–11504.

- Pattanaik, D. R., and M. Rajeevan, 2010: Variability of extreme rainfall events over India during southwest monsoon season. *Meteorol. Appl.*, **17**, 88–104.
- Pavan, V., R. Tomozeiu, C. Cacciamani, and M. Di Lorenzo, 2008: Daily precipitation observations over Emilia-Romagna: Mean values and extremes. *Int. J. Climatol.*, **28**, 2065–2079.
- Pavelin, E. G., C. E. Johnson, S. Rughooputh, and R. Toumi, 1999: Evaluation of pre-industrial surface ozone measurements made using Schlonbein's method. *Atmos. Environ.*, **33**, 919–929.
- Perkins, S. E., and L. V. Alexander, 2012: On the measurement of heat waves. *J. Clim.*, **26**, 4500–4517.
- Perkins, S. E., L. V. Alexander, and J. R. Nairn, 2012: Increasing frequency, intensity and duration of observed global heatwaves and warm spells. *Geophys. Res. Lett.*, **39**, L20714.
- Peterson, T. C., K. M. Willett, and P. W. Thorne, 2011: Observed changes in surface atmospheric energy over land. *Geophys. Res. Lett.*, **38**, L16707.
- Peterson, T. C., X. B. Zhang, M. Brunet-India, and J. L. Vazquez-Aguirre, 2008: Changes in North American extremes derived from daily weather data. *J. Geophys. Res. Atmos.*, **113**, D07113.
- Peterson, T. C., et al., 2009: State of the Climate in 2008. *Bull. Am. Meteor. Soc.*, **90**, S13–.
- Peterson, T. C., et al., 2013: Monitoring and understanding changes in heat waves, cold waves, floods and droughts in the United States: State of knowledge. *Bull. Am. Meteor. Soc.*, **94**, 821–834.
- Petrov, T., and B. Merz, 2009: Trends in flood magnitude, frequency and seasonality in Germany in the period 1951–2002. *J. Hydrol.*, **371**, 129–141.
- Pezza, A., P. van Rensch, and W. Cai, 2012: Severe heat waves in Southern Australia: Synoptic climatology and large scale connections. *Clim. Dyn.*, **38**, 209–224.
- Pezza, A. B., I. Simmonds, and J. A. Renwick, 2007: Southern Hemisphere cyclones and anticyclones: Recent trends and links with decadal variability in the Pacific Ocean. *Int. J. Climatol.*, **27**, 1403–1419.
- Philipona, R., 2012: Greenhouse warming and solar brightening in and around the Alps. *Int. J. Climatol.*, **33**, 1530–1537.
- Philipona, R., K. Behrens, and C. Ruckstuhl, 2009: How declining aerosols and rising greenhouse gases forced rapid warming in Europe since the 1980s. *Geophys. Res. Lett.*, **36**, L02806.
- Philipona, R., B. Dürr, A. Ohmura, and C. Ruckstuhl, 2005: Anthropogenic greenhouse forcing and strong water vapor feedback increase temperature in Europe. *Geophys. Res. Lett.*, **32**, L19809.
- Philipona, R., B. Dürr, C. Marty, A. Ohmura, and M. Wild, 2004: Radiative forcing-measured at Earth's surface—corroborate the increasing greenhouse effect. *Geophys. Res. Lett.*, **31**, L03202.
- Philipp, A., P. M. Della-Marta, J. Jacobeit, D. R. Fereday, P. D. Jones, A. Moberg, and H. Wanner, 2007: Long-term variability of daily North Atlantic-European pressure patterns since 1850 classified by simulated annealing clustering. *J. Clim.*, **20**, 4065–4095.
- Piao, S., et al., 2010: The impacts of climate change on water resources and agriculture in China. *Nature*, **467**, 43–51.
- Pielke, R. A., and T. Matsui, 2005: Should light wind and windy nights have the same temperature trends at individual levels even if the boundary layer averaged heat content change is the same? *Geophys. Res. Lett.*, **32**, L21813.
- Pielke, R. A., Sr., et al., 2007: Unresolved issues with the assessment of multidecadal global land surface temperature trends. *J. Geophys. Res. Atmos.*, **112**, D24S08.
- Pinker, R. T., B. Zhang, and E. G. Dutton, 2005: Do satellites detect trends in surface solar radiation? *Science*, **308**, 850–854.
- Pirazzoli, P. A., and A. Tomasin, 2003: Recent near-surface wind changes in the central Mediterranean and Adriatic areas. *Int. J. Climatol.*, **23**, 963–973.
- Po-Chedley, S., and Q. Fu, 2012: A bias in the Midtropospheric Channel Warm Target Factor on the NOAA-9 Microwave Sounding Unit. *J. Atmos. Ocean Technol.*, **29**, 646–652.
- Portmann, R., S. Solomon, and G. Hegerl, 2009a: Spatial and seasonal patterns in climate change, temperatures, and precipitation across the United States. *Proc. Natl. Acad. Sci. U.S.A.*, **106**, 7324–7329.
- Portmann, R. W., S. Solomon, and G. C. Hegerl, 2009b: Linkages between climate change, extreme temperature and precipitation across the United States. *Proc. Natl. Acad. Sci. U.S.A.*, **106**, 7324–7329.
- Power, S., T. Casey, C. Folland, A. Colman, and V. Mehta, 1999: Inter-decadal modulation of the impact of ENSO on Australia. *Clim. Dyn.*, **15**, 319–324.
- Power, S. B., and G. Kociuba, 2011a: The impact of global warming on the Southern Oscillation Index. *Clim. Dynamics*, **37**, 1745–1754.
- Power, S. B., and G. Kociuba, 2011b: What caused the observed twentieth-century weakening of the Walker Circulation? *J. Clim.*, **24**, 6501–6514.
- Pozzoli, L., et al., 2011: Reanalysis of tropospheric sulfate aerosol and ozone for the period 1980–2005 using the aerosol-chemistry-climate model ECHAM5–HAMMOZ. *Atmos. Chem. Phys.*, **11**, 9563–9594.
- Prata, F., 2008: The climatological record of clear-sky longwave radiation at the Earth's surface: Evidence for water vapour feedback? *Int. J. Remote Sens.*, **29**, 5247–5263.
- Prather, M., C. Holmes, and J. Hsu, 2012: Reactive greenhouse gas scenarios: Systematic exploration of uncertainties and the role of atmospheric chemistry. *Geophys. Res. Lett.*, **39**, L09803.
- Prinn, R., et al., 2005: Evidence for variability of atmospheric hydroxyl radicals over the past quarter century. *Geophys. Res. Lett.*, **L07809**.
- Pryor, S. C., R. J. Barthelmie, and E. S. Riley, 2007: Historical evolution of wind climates in the USA - art. no. 012065. In: *Science of Making Torque from Wind* [M. O. L. Hansen and K. S. Hansen (eds.)], **75**, 12065–12065.
- Pryor, S. C., J. A. Howe, and K. E. Kunkel, 2009: How spatially coherent and statistically robust are temporal changes in extreme precipitation in the contiguous USA? *Int. J. Climatol.*, **29**, 31–45.
- Qian, Y., D. P. Kaiser, L. R. Leung, and M. Xu, 2006: More frequent cloud-free sky and less surface solar radiation in China from 1955 to 2000. *Geophys. Res. Lett.*, **33**, L01812.
- Qian, Y., W. G. Wang, L. R. Leung, and D. P. Kaiser, 2007: Variability of solar radiation under cloud-free skies in China: The role of aerosols. *Geophys. Res. Lett.*, **34**, L12804.
- Qian, Y., D. Gong, J. Fan, L. Leung, R. Bennartz, D. Chen, and W. Wang, 2009: Heavy pollution suppresses light rain in China: Observations and modeling. *J. Geophys. Res. Atmos.*, **114**, D00K02.
- Rahimzadeh, F., A. Asgari, and E. Fattahi, 2009: Variability of extreme temperature and precipitation in Iran during recent decades. *Int. J. Climatol.*, **29**, 329–343.
- Raible, C. C., P. M. Della-Marta, C. Schwierz, H. Wernli, and R. Blender, 2008: Northern hemisphere extratropical cyclones: A comparison of detection and tracking methods and different reanalyses. *Mon. Weather Rev.*, **136**, 880–897.
- Raichijk, C., 2011: Observed trends in sunshine duration over South America. *Int. J. Climatol.*, **32**, 669–680.
- Randall, R. M., and B. M. Herman, 2008: Using limited time period trends as a means to determine attribution of discrepancies in microwave sounding unit-derived tropospheric temperature time series. *J. Geophys. Res. Atmos.*, **113**, D05105.
- Randel, W. J., 2010: Variability and trends in stratospheric temperature and water vapor. *The Stratosphere: Dynamics, Transport and Chemistry*, S. Polvani, and Waugh, Ed., American Geophysical Union, 123–135.
- Randel, W. J., and E. J. Jensen, 2013: Physical processes in the tropical tropopause layer and their roles in a changing climate. *Nature Geosci.*, **169**–176.
- Randel, W. J., F. Wu, H. Vömel, G. E. Nedoluha, and P. Forster, 2006: Decreases in stratospheric water vapor after 2001: Links to changes in the tropical tropopause and the Brewer-Dobson circulation. *J. Geophys. Res. Atmos.*, **111**, D12312.
- Randel, W. J., et al., 2009: An update of observed stratospheric temperature trends. *J. Geophys. Res. Atmos.*, **114**, D02107.
- Rasmusson, E. M., and T. H. Carpenter, 1982: Variations in tropical sea surface temperature and surface wind fields associated with the Southern Oscillation/El Niño. *Mon. Weather Rev.*, **110**, 354–384.
- Rasmusson, E. M., and J. M. Wallace, 1983: Meteorological aspects of the El Niño–Southern Oscillation. *Science*, **222**, 1195–1202.
- Rausch, J., A. Heidinger, and R. Bennartz, 2010: Regional assessment of microphysical properties of marine boundary layer cloud using the PATMOS-x dataset. *J. Geophys. Res. Atmos.*, **115**, D23212.
- Ray, E. A., et al., 2010: Evidence for changes in stratospheric transport and mixing over the past three decades based on multiple data sets and tropical leaky pipe analysis. *J. Geophys. Res. Atmos.*, **115**, D21304.
- Rayner, D. P., 2007: Wind run changes: The dominant factor affecting pan evaporation trends in Australia. *J. Clim.*, **20**, 3379–3394.
- Rayner, N. A., et al., 2003: Global analyses of sea surface temperature, sea ice, and night marine air temperature since the late nineteenth century. *J. Geophys. Res. Atmos.*, **108**, 37.
- Rayner, N. A., et al., 2006: Improved analyses of changes and uncertainties in sea surface temperature measured in situ since the mid-nineteenth century: The HadSST2 dataset. *J. Clim.*, **19**, 446–469.

- Read, W. G., et al., 2007: Aura Microwave Limb Sounder upper tropospheric and lower stratospheric H₂O and relative humidity with respect to ice validation. *J. Geophys. Res. Atmos.*, **112**, D24535.
- Ren, G., et al., 2011: Change in climatic extremes over mainland China based on an integrated extreme climate index. *Clim. Res.*, **50**, 113–124.
- Ren, G. Y., Z. Y. Chu, Z. H. Chen, and Y. Y. Ren, 2007: Implications of temporal change in urban heat island intensity observed at Beijing and Wuhan stations. *Geophys. Res. Lett.*, **34**, L05711.
- Ren, G. Y., Y. Q. Zhou, Z. Y. Chu, J. X. Zhou, A. Y. Zhang, J. Guo, and X. F. Liu, 2008: Urbanization effects on observed surface air temperature trends in north China. *J. Clim.*, **21**, 1333–1348.
- Ren, H.-L., and F.-F. Jin, 2011: Niño indices for two types of ENSO. *Geophys. Res. Lett.*, **38**, L04704.
- Ren, Y. Y., and G. Y. Ren, 2011: A remote-sensing method of selecting reference stations for evaluating urbanization effect on surface air temperature trends. *J. Clim.*, **24**, 3179–3189.
- Renard, B., et al., 2008: Regional methods for trend detection: Assessing field significance and regional consistency. *Water Resour. Res.*, **44**, W08419.
- Revadekar, J., D. Kothawale, S. Patwardhan, G. Pant, and K. Kumar, 2012: About the observed and future changes in temperature extremes over India. *Nat. Hazards*, **60**, 1133–1155.
- Reynolds, R., N. Rayner, T. Smith, D. Stokes, and W. Wang, 2002: An improved in situ and satellite SST analysis for climate. *J. Clim.*, **15**, 1609–1625.
- Reynolds, R. W., C. L. Gentemann, and G. K. Corlett, 2010: Evaluation of AATSR and TMI Satellite SST Data. *J. Clim.*, **23**, 152–165.
- Rhines, A., and P. Huybers, 2013: Frequent summer temperature extremes reflect changes in the mean, not the variance. *Proc. Natl. Acad. Sci. U.S.A.*, **110**, E546–E546.
- Rienecker, M. M., Suarez, M. J., Gelaro, R., Todling, R., Bacmeister, J., Liu, E., Bosilovich, M. G., Schubert, S. D., Takacs, L., Kim, G.-K., Bloom, S., Chen, J., Collins, D., Conaty, A., da Silva, A., Gu, W., Joiner, J., Koster, R. D., Lucchesi, R., Molod, A., Owens, T., Pawson, S., Pegion, P., Redder, C. R., Reichle, R., Robertson, F. R., Ruddick, A. G., Sienkiewicz, M., and Woollen, J., 2011: MERRA: NASA's modern-era retrospective analysis for research and applications. *J. Clim.*, **24**, 3624–3648.
- Rigby, M., et al., 2008: Renewed growth of atmospheric methane. *Geophys. Res. Lett.*, **35**, L22805.
- Rigby, M., et al., 2010: History of atmospheric SF₆ from 1973 to 2008. *Atmos. Chem. Phys.*, **10**, 10305–10320.
- Riihimäki, L. D., F. E. Vignola, and C. N. Long, 2009: Analyzing the contribution of aerosols to an observed increase in direct normal irradiance in Oregon. *J. Geophys. Res. Atmos.*, **114**, D00d02.
- Robock, A., et al., 2000: The Global Soil Moisture Data Bank. *Bull. Am. Meteor. Soc.*, **81**, 1281–1299.
- Rockmann, T., and I. Levin, 2005: High-precision determination of the changing isotopic composition of atmospheric N₂O from 1990 to 2002. *J. Geophys. Res. Atmos.*, **110**, D21304.
- Roderick, M. L., and G. D. Farquhar, 2002: The cause of decreased pan evaporation over the past 50 years. *Science*, **298**, 1410–1411.
- Roderick, M. L., L. D. Rotstayn, G. D. Farquhar, and M. T. Hobbs, 2007: On the attribution of changing pan evaporation. *Geophys. Res. Lett.*, **34**, L17403.
- Rohde, R., et al., 2013a: A new estimate of the average Earth surface land temperature spanning 1753 to 2011. *Geoinfor. Geostat.: An Overview*, **1**, doi:10.4172/gigs.1000101.
- Rohde, R., et al., 2013b: Berkeley Earth temperature averaging process. *Geoinfor Geostat.: An Overview*, **1**, doi:10.4172/gigs.1000103.
- Rohs, S., et al., 2006: Long-term changes of methane and hydrogen in the stratosphere in the period 1978–2003 and their impact on the abundance of stratospheric water vapor. *J. Geophys. Res. Atmos.*, **111**, D14315.
- Ropelewski, C. F., and P. D. Jones, 1987: An extension of the Tahiti–Darwin Southern Oscillation Index. *Mon. Weather Rev.*, **115**, 2161–2165.
- Rosenlof, K. H., and G. C. Reid, 2008: Trends in the temperature and water vapor content of the tropical lower stratosphere: Sea surface connection. *J. Geophys. Res. Atmos.*, **113**, D06107.
- Ruckstuhl, C., et al., 2008: Aerosol and cloud effects on solar brightening and the recent rapid warming. *Geophys. Res. Lett.*, **35**, L12708.
- Ruddiman, W., 2003: The anthropogenic greenhouse era began thousands of years ago. *Clim. Change*, 261–293.
- Ruddiman, W., 2007: The early anthropogenic hypothesis: Challenges and responses. *Rev. Geophys.*, **45**, RG4001.
- Russak, V., 2009: Changes in solar radiation and their influence on temperature trend in Estonia (1955–2007). *J. Geophys. Res. Atmos.*, **114**, D00d01.
- Russell, A. R., L. C. Valin, E. J. Bucsela, M. O. Wenig, and R. C. Cohen, 2010: Space-based constraints on spatial and temporal patterns of NO_x emissions in California, 2005–2008. *Environ. Sci. Technol.*, **44**, 3608–3615.
- Russell, J., et al., 1993: The halogen occultation experiment. *J. Geophys. Res. Atmos.*, **98**, 10777–10797.
- Rusticucci, M., and M. Renom, 2008: Variability and trends in indices of quality-controlled daily temperature extremes in Uruguay. *Int. J. Climatol.*, **28**, 1083–1095.
- Saha, S., et al., 2010: The NCEP climate forecast system reanalysis. *Bull. Am. Meteor. Soc.*, **91**, 1015–1057.
- Saikawa, E., et al., 2012: Global and regional emissions estimates for HCFC-22. *Atmos. Chem. Phys. Discuss.*, **12**, 18423–18285.
- Saji, N. H., B. N. Goswami, P. N. Vinayachandran, and T. Yamagata, 1999: A dipole mode in the tropical Indian Ocean. *Nature*, **401**, 360–363.
- Sakamoto, M., and J. R. Christy, 2009: The influences of TOVS radiance assimilation on temperature and moisture tendencies in JRA-25 and ERA-40. *J. Atmos. Ocean Technol.*, **26**, 1435–1455.
- Sanchez-Lorenzo, A., and M. Wild, 2012: Decadal variations in estimated surface solar radiation over Switzerland since the late 19th century. *Atmos. Chem. Phys. Discussion*, **12**, 10815–10843.
- Sanchez-Lorenzo, A., J. Calbo, and J. Martin-Vide, 2008: Spatial and temporal trends in sunshine duration over Western Europe (1938–2004). *J. Clim.*, **21**, 6089–6098.
- Sanchez-Lorenzo, A., J. Calbo, and M. Wild, 2013: Global and diffuse solar radiation in Spain: Building a homogeneous dataset and assessing their trends. *Global Planet. Change*, **100**, 343–352.
- Sanchez-Lorenzo, A., J. Calbo, M. Brunetti, and C. Deser, 2009: Dimming/brightening over the Iberian Peninsula: Trends in sunshine duration and cloud cover and their relations with atmospheric circulation. *J. Geophys. Res. Atmos.*, **114**, D00d09.
- Santer, B., et al., 2008: Consistency of modelled and observed temperature trends in the tropical troposphere. *Int. J. Climatol.*, **28**, 1703–1722.
- Santer, B. D., et al., 2007: Identification of human-induced changes in atmospheric moisture content. *Proc. Natl. Acad. Sci. U.S.A.*, **104**, 15248–15253.
- Santer, B. D., et al., 2011: Separating signal and noise in atmospheric temperature changes: The importance of timescale. *J. Geophys. Res. Atmos.*, **116**, D22105.
- Scaife, A., C. Folland, L. Alexander, A. Moberg, and J. Knight, 2008: European climate extremes and the North Atlantic Oscillation. *J. Clim.*, **21**, 72–83.
- Schär, C., P. L. Vidale, D. Luthi, C. Frei, C. Haberli, M. A. Liniger, and C. Appenzeller, 2004: The role of increasing temperature variability in European summer heatwaves. *Nature*, **427**, 332–336.
- Scherer, M., H. Vömel, S. Fueglistaler, S. J. Oltmans, and J. Staehelin, 2008: Trends and variability of midlatitude stratospheric water vapour deduced from the re-evaluated Boulder balloon series and HALOE. *Atmos. Chem. Phys.*, **8**, 1391–1402.
- Scherrer, S. C., and C. Appenzeller, 2006: Swiss Alpine snow pack variability: Major patterns and links to local climate and large-scale flow. *Clim. Res.*, **32**, 187–199.
- Scherrer, S. C., C. Wüthrich, M. Croci-Maspoli, R. Weingartner, and C. Appenzeller, 2013: Snow variability in the Swiss Alps 1864–2009. *Int. J. Climatol.*, doi: 10.1002/joc.3653.
- Schiller, C., J. U. Grooss, P. Konopka, F. Plager, F. H. Silva dos Santos, and N. Spelten, 2009: Hydration and dehydration at the tropical tropopause. *Atmos. Chem. Phys.*, **9**, 9647–9660.
- Schmidt, G. A., 2009: Spurious correlations between recent warming and indices of local economic activity. *Int. J. Climatol.*, **29**, 2041–2048.
- Schnadt Poberaj, C., J. Staehelin, D. Brunner, V. Thouret, H. De Backer, and R. Stübi, 2009: Long-term changes in UT/LS ozone between the late 1970s and the 1990s deduced from the GASP and MOZAIK aircraft programs and from ozonesondes. *Atmos. Chem. Phys.*, **9**, 5343–5369.
- Schneider, T., P. A. O’Gorman, and X. J. Levine, 2010: Water vapour and the dynamics of climate changes. *Rev. Geophys.*, RG3001.
- Schneidereit, A., R. Blender, K. Fraedrich, and F. Lunkeit, 2007: Icelandic climate and north Atlantic cyclones in ERA-40 reanalyses. *Meteorol. Z.*, **16**, 17–23.
- Schwartz, R. D., 2005: Global dimming: Clear-sky atmospheric transmission from astronomical extinction measurements. *J. Geophys. Res. Atmos.*, **110**.
- Scinocca, J. F., D. B. Stephenson, T. C. Bailey, and J. Austin, 2010: Estimates of past and future ozone trends from multimodel simulations using a flexible smoothing spline methodology. *J. Geophys. Res. Atmos.*, **115**.
- Screen, J. A., and I. Simmonds, 2011: Erroneous Arctic temperature trends in the ERA-40 reanalysis: A closer look. *J. Clim.*, **24**, 2620–2627.

- Seidel, D. J., and J. R. Lanzante, 2004: An assessment of three alternatives to linear trends for characterizing global atmospheric temperature changes. *J. Geophys. Res. Atmos.*, **109**, D14108.
- Seidel, D. J., and W. J. Randel, 2007: Recent widening of the tropical belt: Evidence from tropopause observations. *J. Geophys. Res. Atmos.*, **112**, D20113.
- Seidel, D. J., Q. Fu, W. J. Randel, and T. J. Reichler, 2008: Widening of the tropical belt in a changing climate. *Nature Geosci.*, **1**, 21–24.
- Seidel, D. J., N. P. Gillett, J. R. Lanzante, K. P. Shine, and P. W. Thorne, 2011: Stratospheric temperature trends: Our evolving understanding. *Clim. Change*, **2**, 592–616.
- Sen Roy, S., 2009: A spatial analysis of extreme hourly precipitation patterns in India. *Int. J. Climatol.*, **29**, 345–355.
- Sen Roy, S., and R. C. Balling, 2005: Analysis of trends in maximum and minimum temperature, diurnal temperature range, and cloud cover over India. *Geophys. Res. Lett.*, **32**, L12702.
- Sen Roy, S., and M. Rouault, 2013: Spatial patterns of seasonal scale trends in extreme hourly precipitation in South Africa. *Appl. Geogr.*, **39**, 151–157.
- Seneviratne, S. I., et al., 2010: Investigating soil moisture-climate interactions in a changing climate: A review. *Earth Sci. Rev.*, **99**, 125–161.
- Seneviratne, S. I., et al., 2012: Changes in climate extremes and their impacts on the natural physical environment. In: *IPCC Special Report on Extremes*, 109–230.
- Serquet, G., C. Marty, J. P. Dulex, and M. Rebetez, 2011: Seasonal trends and temperature dependence of the snowfall/precipitation-day ratio in Switzerland. *Geophys. Res. Lett.*, **38**, L07703.
- Shaw, S. B., A. A. Royem, and S. J. Riha, 2011: The relationship between extreme hourly precipitation and surface temperature in different hydroclimatic regions of the United States. *J. Hydrometeorol.*, **12**, 319–325.
- Sheffield, J., and E. F. Wood, 2008: Global trends and variability in soil moisture and drought characteristics, 1950–2000, from observation-driven simulations of the terrestrial hydrologic cycle. *J. Clim.*, **21**, 432–458.
- Sheffield, J., E. Wood, and M. Roderick, 2012: Little change in global drought over the past 60 years. *Nature*, **491**, 435–.
- Sheffield, J., K. Andreadis, E. Wood, and D. Lettenmaier, 2009: Global and continental drought in the second half of the twentieth century: Severity-area-duration analysis and temporal variability of large-scale events. *J. Clim.*, **22**, 1962–1981.
- Shekar, M., H. Chand, S. Kumar, K. Srinivasan, and A. Ganju, 2010: Climate change studies in the western Himalaya. *Ann. Glaciol.*, **51**, 105–112.
- Sherwood, S. C., R. Roca, and T. M. Weckwerth, 2010: Tropospheric water vapor, convection, and climate. *Rev. Geophys.*, **48**, RG2001.
- Sherwood, S. C., C. L. Meyer, R. J. Allen, and H. A. Titchner, 2008: Robust tropospheric warming revealed by iteratively homogenized radiosonde data. *J. Clim.*, **21**, 5336–5350.
- Shi, G. Y., et al., 2008: Data quality assessment and the long-term trend of ground solar radiation in China. *J. Appl. Meteor. Climatol.*, **47**, 1006–1016.
- Shi, L., and J. J. Bates, 2011: Three decades of intersatellite-calibrated High-Resolution Infrared Radiation Sounder upper tropospheric water vapor. *J. Geophys. Res. Atmos.*, **116**, D04108.
- Shiklomanov, A. I., R. B. Lammers, M. A. Rawlins, L. C. Smith, and T. M. Pavelsky, 2007: Temporal and spatial variations in maximum river discharge from a new Russian data set. *J. Geophys. Res. Biogeosci.*, **112**.
- Shiklomanov, I. A., V. Y. Georgievskii, V. I. Babkin, and Z. A. Balonishnikova, 2010: Research problems of formation and estimation of water resources and water availability changes of the Russian Federation. *Russ. Meteorol. Hydrol.*, **35**, 13–19.
- Shiu, C. J., S. C. Liu, and J. P. Chen, 2009: Diurnally asymmetric trends of temperature, humidity, and precipitation in Taiwan. *J. Clim.*, **22**, 5635–5649.
- Sillmann, J., M. Croci-Maspoli, M. Kallache, and R. W. Katz, 2011: Extreme cold winter temperatures in Europe under the influence of North Atlantic atmospheric blocking. *J. Clim.*, **24**, 5899–5913.
- Simmons, A. J., K. M. Willett, P. D. Jones, P. W. Thorne, and D. P. Dee, 2010: Low-frequency variations in surface atmospheric humidity, temperature, and precipitation: Inferences from reanalyses and monthly gridded observational data sets. *J. Geophys. Res. Atmos.*, **115**, D01110.
- Simolo, C., M. Brunetti, M. Maugeri, and T. Nanni, 2011: Evolution of extreme temperatures in a warming climate. *Geophys. Res. Lett.*, **38**, 6.
- Simpson, I. J., et al., 2012: Long-term decline of global atmospheric ethane concentrations and implications for methane. *Nature*, **488**, 490–494.
- Skansi, M., et al., 2013: Warming and wetting signals emerging from analysis of changes in climate extreme indices over South America. *Global Planet. Change*, **100**, 295–307.
- Skeie, R. B., T. K. Berntsen, G. Myhre, K. Tanaka, M. M. Kvalevåg, and C. R. Hoyle, 2011: Anthropogenic radiative forcing time series from pre-industrial times until 2010. *Atmos. Chem. Phys.*, **11**, 11827–11857.
- Smith, L. C., T. Pavelsky, G. MacDonald, I. A. Shiklomanov, and R. Lammers, 2007: Rising minimum daily flows in northern Eurasian rivers suggest a growing influence of groundwater in the high-latitude water cycle. *J. Geophys. Res.*, **112**, G04S47.
- Smith, T. M., and R. W. Reynolds, 2002: Bias corrections for historical sea surface temperatures based on marine air temperatures. *J. Clim.*, **15**, 73–87.
- Smith, T. M., T. C. Peterson, J. H. Lawrimore, and R. W. Reynolds, 2005: New surface temperature analyses for climate monitoring. *Geophys. Res. Lett.*, **32**, L14712.
- Smith, T. M., R. W. Reynolds, T. C. Peterson, and J. Lawrimore, 2008: Improvements to NOAA's historical merged land-ocean surface temperature analysis (1880–2006). *J. Clim.*, **21**, 2283–2296.
- Smith, T. M., P. A. Arkin, L. Ren, and S. S. P. Shen, 2012: Improved reconstruction of global precipitation since 1900. *J. Atmos. Ocean. Technol.*, **29**, 1505–1517.
- Smits, A., A. Tank, and G. P. Konnen, 2005: Trends in storminess over the Netherlands, 1962–2002. *Int. J. Climatol.*, **25**, 1331–1344.
- Sohn, B. J., and S. C. Park, 2010: Strengthened tropical circulations in past three decades inferred from water vapor transport. *J. Geophys. Res. Atmos.*, **115**, D15112.
- Solomon, S., K. Rosenlof, R. Portmann, J. Daniel, S. Davis, T. Sanford, and G. Plattner, 2010: Contributions of stratospheric water vapor to decadal changes in the rate of global warming. *Science*, **327**, 1219–1223.
- Song, H., and M. H. Zhang, 2007: Changes of the boreal winter Hadley circulation in the NCEP-NCAR and ECMWF reanalyses: A comparative study. *J. Clim.*, **20**, 5191–5200.
- Soni, V. K., G. Pandithurai, and D. S. Pai, 2012: Evaluation of long-term changes of solar radiation in India. *Int. J. Climatol.*, **32**, 540–551.
- Sorteberg, A., and J. E. Walsh, 2008: Seasonal cyclone variability at 70 degrees N and its impact on moisture transport into the Arctic. *Tellus A*, **60**, 570–586.
- Sousa, P., R. Trigo, P. Aizpuru, R. Nieto, L. Gimeno, and R. Garcia-Herrera, 2011: Trends and extremes of drought indices throughout the 20th century in the Mediterranean. *Nat. Hazards Earth Syst. Sci.*, **11**, 33–51.
- Spencer, R. W., and J. R. Christy, 1992: Precision and radiosonde validation of satellite gridpoint temperature anomalies. 2. A tropospheric retrieval and trends during 1979–90. *J. Clim.*, **5**, 858–866.
- St. Jacques, J.-M., and D. Sauchyn, 2009: Increasing winter baseflow and mean annual streamflow from possible permafrost thawing in the Northwest Territories, Canada. *Geophys. Res. Lett.*, **36**, L01401.
- Stachnik, J. P., and C. Schumacher, 2011: A comparison of the Hadley circulation in modern reanalyses. *J. Geophys. Res. Atmos.*, **116**, D22102.
- Stahl, K., and L. M. Tallaksen, 2012: Filling the white space on maps of European runoff trends: Estimates from a multi-model ensemble. *Hydrol. Earth Syst. Sci. Discuss.*, **9**, 2005–2032.
- Stahl, K., et al., 2010: Streamflow trends in Europe: Evidence from a dataset of near-natural catchments. *Hydrol. Earth Syst. Sci.*, **14**, 2367–2382.
- Stanhill, G., and S. Cohen, 2001: Global dimming: A review of the evidence for a widespread and significant reduction in global radiation with discussion of its probable causes and possible agricultural consequences. *Agr. Forest Meteorol.*, **107**, 255–278.
- Steenefeld, G. J., A. A. M. Holtslag, R. T. McNider, and R. A. Pielke, 2011: Screen level temperature increase due to higher atmospheric carbon dioxide in calm and windy nights revisited. *J. Geophys. Res. Atmos.*, **116**.
- Stegall, S., and J. Zhang, 2012: Wind field climatology, changes, and extremes in the Chukchi-Beaufort Seas and Alaska North Slope during 1979–2009. *J. Clim.*, **25**, 8075–8089.
- Steig, E. J., D. P. Schneider, S. D. Rutherford, M. E. Mann, J. C. Comiso, and D. T. Shindell, 2009: Warming of the Antarctic ice-sheet surface since the 1957 International Geophysical Year. *Nature*, **460**, 766–766.
- Stenke, A., and V. Grewe, 2005: Simulation of stratospheric water vapor trends: Impact on stratospheric ozone chemistry. *Atmos. Chem. Phys.*, **5**, 1257–1272.
- Stephens, G. L., M. Wild, P. W. Stackhouse, T. L'Ecuyer, S. Kato, and D. S. Henderson, 2012a: The global character of the flux of downward longwave radiation. *J. Clim.*, **25**, 2329–2340.

- Stephens, G. L., et al., 2012b: An update on Earth's energy balance in light of the latest global observations. *Nature Geosci.*, **5**, 691–696.
- Stephenson, D. B., H. F. Diaz, and R. J. Murnane, 2008: Definition, diagnosis and origin of extreme weather and climate events. In: *Climate Extremes and Society* [R. J. Murnane, and H. F. Diaz (eds.)] Cambridge University Press, Cambridge, United Kingdom and New York, NY, USA, pp. 11–23.
- Stern, D. I., 2006: Reversal of the trend in global anthropogenic sulfur emissions. *Global Environ. Change Hum. Policy Dimens.*, **16**, 207–220.
- Stickler, A., et al., 2010: The Comprehensive Historical Upper-Air Network. *Bull. Am. Meteor. Soc.*, **91**, 741–751.
- Stjern, C. W., J. E. Kristjansson, and A. W. Hansen, 2009: Global dimming and global brightening - an analysis of surface radiation and cloud cover data in northern Europe. *Int. J. Climatol.*, **29**, 643–653.
- Stohl, A., et al., 2009: An analytical inversion method for determining regional and global emissions of greenhouse gases: Sensitivity studies and application to halocarbons. *Atmos. Chem. Phys.*, 1597–1620.
- Stohl, A., et al., 2010: Hydrochlorofluorocarbon and hydrofluorocarbon emissions in East Asia determined by inverse modeling. *Atmos. Chem. Phys.*, 3545–3560.
- Streets, D. G., Y. Wu, and M. Chin, 2006: Two-decadal aerosol trends as a likely explanation of the global dimming/brightening transition. *Geophys. Res. Lett.*, **33**, L15806.
- Streets, D. G., et al., 2009: Anthropogenic and natural contributions to regional trends in aerosol optical depth, 1980–2006. *J. Geophys. Res. Atmos.*, **114**, D00D18.
- Strong, C., and R. E. Davis, 2007: Winter jet stream trends over the Northern Hemisphere. *Q. J. R. Meteorol. Soc.*, **133**, 2109–2115.
- Strong, C., and R. E. Davis, 2008: Comment on “Historical trends in the jet streams” by Cristina L. Archer and Ken Caldeira. *Geophys. Res. Lett.*, L24806.
- Stubenrauch, C. J., et al., 2013: Assessment of global cloud datasets from satellite: Project and database initiated by the GEWEX radiation panel. *Bull. Am. Meteorol. Soc.*, **94**, 1031–1049.
- Sun, B. M., A. Reale, D. J. Seidel, and D. C. Hunt, 2010: Comparing radiosonde and COSMIC atmospheric profile data to quantify differences among radiosonde types and the effects of imperfect collocation on comparison statistics. *J. Geophys. Res. Atmos.*, **115**, D23104.
- Swart, N. C., and J. C. Fyfe, 2012: Observed and simulated changes in the Southern Hemisphere surface westerly wind-stress. *Geophys. Res. Lett.*, **39**, L16711.
- Syakila, A., and C. Kroeze, 2011: The global nitrous oxide budget revisited. *Greenhouse Gas Meas. Management*, **1**, 17–26.
- Takahashi, K., A. Montecinos, K. Goubanova, and B. Dewitte, 2011: ENSO regimes: Reinterpreting the canonical and Modoki El Niño. *Geophys. Res. Lett.*, **38**, L10704.
- Takeuchi, Y., Y. Endo, and S. Murakami, 2008: High correlation between winter precipitation and air temperature in heavy-snowfall areas in Japan. *Ann. Glaciol.*, **49**, 7–10.
- Tang, G., Y. Ding, S. Wang, G. Ren, H. Liu, and L. Zhang, 2010: Comparative analysis of China surface air temperature series for the past 100 years. *Adv. Climate Change Res.*, **1**, 11–19.
- Tang, W. J., K. Yang, J. Qin, C. C. K. Cheng, and J. He, 2011: Solar radiation trend across China in recent decades: a revisit with quality-controlled data. *Atmos. Chem. Phys.*, **11**, 393–406.
- Tank, A., et al., 2006: Changes in daily temperature and precipitation extremes in central and south Asia. *J. Geophys. Res. Atmos.*, **111**, D16105.
- Tans, P., 2009: An accounting of the observed increase in oceanic and atmospheric CO₂ and an outlook for the future. *Oceanography*, 26–35.
- Tarasova, O. A., I. A. Senik, M. G. Sosonkin, J. Cui, J. Staehelin, and A. S. H. PrÄvÄř, 2009: Surface ozone at the Caucasian site Kislovodsk High Mountain Station and the Swiss Alpine site Jungfraujoch: Data analysis and trends (1990–2006). *Atmos. Chem. Phys.*, **9**, 4157–4175.
- Tegtmeier, S., K. Kruger, I. Wohltmann, K. Schoellhammer, and M. Rex, 2008: Variations of the residual circulation in the Northern Hemispheric winter. *J. Geophys. Res. Atmos.*, **113**, D16109.
- Teuling, A. J., et al., 2009: A regional perspective on trends in continental evaporation. *Geophys. Res. Lett.*, **36**, L02404.
- Thomas, B., E. Kent, V. Swail, and D. Berry, 2008: Trends in ship wind speeds adjusted for observation method and height. *Int. J. Climatol.*, **28**, 747–763.
- Thomas, G. E., et al., 2010: Validation of the GRAPE single view aerosol retrieval for ATSR-2 and insights into the long term global AOD trend over the ocean. *Atmos. Chem. Phys.*, **10**, 4849–4866.
- Thompson, D. W. J., and J. M. Wallace, 1998: The Arctic Oscillation signature in the wintertime geopotential height and temperature fields. *Geophys. Res. Lett.*, **25**, 1297–1300.
- Thompson, D. W. J., and J. M. Wallace, 2000: Annular modes in the extratropical circulation. Part I: Month-to-month variability. *J. Clim.*, **13**, 1000–1016.
- Thompson, D. W. J., J. J. Kennedy, J. M. Wallace, and P. D. Jones, 2008: A large discontinuity in the mid-twentieth century in observed global-mean surface temperature. *Nature*, **453**, 646–649.
- Thompson, D. W. J., et al., 2012: The mystery of recent stratospheric temperature trends. *Nature*, **491**, 692–697.
- Thorne, P. W., 2008: Arctic tropospheric warming amplification? *Nature*, **455**, E1–E2.
- Thorne, P. W., and R. S. Vose, 2010: Reanalyses suitable for characterizing long-term trends: Are They Really Achievable? *Bull. Am. Meteor. Soc.*, **91**, 353–.
- Thorne, P. W., D. E. Parker, S. F. B. Tett, P. D. Jones, M. McCarthy, H. Coleman, and P. Brohan, 2005: Revisiting radiosonde upper air temperatures from 1958 to 2002. *J. Geophys. Res. Atmos.*, **110**.
- Thorne, P. W., et al., 2011: A quantification of uncertainties in historical tropical tropospheric temperature trends from radiosondes. *J. Geophys. Res. Atmos.*, **116**, D12116.
- Tietavainen, H., H. Tuomenvirta, and A. Venalainen, 2010: Annual and seasonal mean temperatures in Finland during the last 160 years based on gridded temperature data. *Int. J. Climatol.*, **30**, 2247–2256.
- Titchner, H. A., P. W. Thorne, M. P. McCarthy, S. F. B. Tett, L. Haimberger, and D. E. Parker, 2009: Critically reassessing tropospheric temperature trends from radiosondes using realistic validation experiments. *J. Clim.*, **22**, 465–485.
- Tokinaga, H., and S.-P. Xie, 2011a: Wave and anemometer-based sea surface wind (WASWind) for climate change analysis. *J. Clim.*, 267–285.
- Tokinaga, H., and S. P. Xie, 2011b: Weakening of the equatorial Atlantic cold tongue over the past six decades. *Nature Geosci.*, **4**, 222–226.
- Tokinaga, H., S. P. Xie, A. Timmermann, S. McGregor, T. Ogata, H. Kubota, and Y. M. Okumura, 2012: Regional patterns of tropical Indo-Pacific climate change: Evidence of the Walker circulation weakening. *J. Clim.*, **25**, 1689–1710.
- Toreti, A., E. Xoplaki, D. Maraun, F. G. Kuglitsch, H. Wanner, and J. Luterbacher, 2010: Characterisation of extreme winter precipitation in Mediterranean coastal sites and associated anomalous atmospheric circulation patterns. *Nat. Hazards Earth Syst. Sci.*, **10**, 1037–1050.
- Torseth, K., et al., 2012: Introduction to the European Monitoring and Evaluation Programme (EMEP) and observed atmospheric composition change during 1972–2009. *Atmos. Chem. Phys. Discuss.*, **12**, 1733–1820.
- Trenberth, K., 2011: Changes in precipitation with climate change. *Clim. Res.*, **47**, 123–138.
- Trenberth, K., and J. Fasullo, 2012a: Climate extremes and climate change: The Russian heat wave and other climate extremes of 2010. *J. Geophys. Res. Atmos.*, **117**, D17103.
- Trenberth, K. E., 1984: Signal versus noise in the Southern Oscillation. *Mon. Weather Rev.*, **112**, 326–332.
- Trenberth, K. E., 1997: The definition of El Niño. *Bull. Am. Meteor. Soc.*, **78**, 2771–2777.
- Trenberth, K. E., and D. A. Paolino, 1980: The Northern Hemisphere Sea-Level Pressure Data Set – Trends, errors, and discontinuities. *Mon. Weather Rev.*, **108**, 855–872.
- Trenberth, K. E., and J. W. Hurrell, 1994: Decadal atmosphere-ocean variations in the Pacific. *Clim. Dyn.*, **9**, 303–319.
- Trenberth, K. E., and T. J. Hoar, 1996: The 1990–1995 El Niño Southern Oscillation event: Longest on record. *Geophys. Res. Lett.*, **23**, 57–60.
- Trenberth, K. E., and D. P. Stepaniak, 2001: Indices of El Niño evolution. *J. Clim.*, **14**, 1697–1701.
- Trenberth, K. E., and D. J. Shea, 2006: Atlantic hurricanes and natural variability in 2005. *Geophys. Res. Lett.*, **33**, L12704.
- Trenberth, K. E., and J. T. Fasullo, 2010: Climate change tracking Earth's energy. *Science*, **328**, 316–317.
- Trenberth, K. E., and J. T. Fasullo, 2012b: Tracking Earth's energy: From El Niño to global warming. *Surv. Geophys.*, **33**, 413–426.
- Trenberth, K. E., J. T. Fasullo, and J. Kiehl, 2009: Earth's Global energy budget. *Bull. Am. Meteor. Soc.*, **90**, 311.
- Trenberth, K. E., J. T. Fasullo, and J. Mackaro, 2011: Atmospheric moisture transports from ocean to land and global energy flows in reanalyses. *J. Clim.*, **24**, 4907–4924.

- Trenberth, K. E., et al., 2007: Observations: Surface and atmospheric climate change. In: *Climate Change 2007: The Physical Science Basis. Contribution of Working Group I to the Fourth Assessment Report of the Intergovernmental Panel on Climate Change* [Solomon, S., D. Qin, M. Manning, Z. Chen, M. Marquis, K. B. Averyt, M. Tignor and H. L. Miller (eds.)]. Cambridge University Press, Cambridge, United Kingdom and New York, NY, USA.
- Trewin, B., 2012: A daily homogenized temperature data set for Australia. *Int. J. Climatol.*, **33**, 1510–1529.
- Trnka, M., J. Kyselý, M. Možny, and M. Dubrovský, 2009: Changes in Central-European soil-moisture availability and circulation patterns in 1881–2005. *Int. J. Climatol.*, **29**, 655–672.
- Trocchioli, A., K. Müller, P. Coppin, R. Davy, C. Russell, and A. L. Hirsch, 2012: Long-term wind speed trends over Australia. *J. Climate*, **25**, 170–183.
- Troup, A. J., 1965: Southern Oscillation. *Q. J. R. Meteorol. Soc.*, **91**, 490–.
- Tryhorn, L., and J. Risbey, 2006: On the distribution of heat waves over the Australian region. *Aust. Meteorol. Mag.*, **55**, 169–182.
- Tung, K.-K., and J. Zhou, 2013: Using data to attribute episodes of warming and cooling in instrumental records. *Proc. Natl. Acad. Sci. U.S.A.*, **110**, 2058–2063.
- Turner, J., et al., 2005: Antarctic climate change during the last 50 years. *Int. J. Climatol.*, **25**, 279–294.
- Ulbrich, U., G. C. Leckebusch, and J. G. Pinto, 2009: Extra-tropical cyclones in the present and future climate: A review. *Theor. Appl. Climatol.*, **96**, 117–131.
- Uppala, S. M., et al., 2005: The ERA-40 re-analysis. *Q. J. R. Meteorol. Soc.*, **131**, 2961–3012.
- Usbeck, T., T. Wohlgemuth, C. Pfister, R. Volz, M. Beniston, and M. Dobbertin, 2010: Wind speed measurements and forest damage in Canton Zurich (Central Europe) from 1891 to winter 2007. *Int. J. Climatol.*, **30**, 347–358.
- Utsumi, N., S. Seto, S. Kanae, E. Maeda, and T. Oki, 2011: Does higher surface temperature intensify extreme precipitation? *Geophys. Res. Lett.*, **38**, L16708.
- van den Besselaar, E. J. M., A. M. G. Klein Tank, and T. A. Buishand, 2012: Trends in European precipitation extremes over 1951–2010. *Int. J. Climatol.*, **33**, 2682–2689.
- van der Schrier, G., A. van Ulden, and G. J. van Oldenborgh, 2011: The construction of a Central Netherlands temperature. *Clim. Past*, **7**, 527–542.
- van der Schrier, G., J. Barichivich, K. R. Briffa, and P. D. Jones, 2013: A scPDSI-based global dataset of dry and wet spells for 1901–2009. *J. Geophys. Res. Atmos.*, **118**, 4025–4048.
- van Haren, R., G. J. van Oldenborgh, G. Lenderink, M. Collins, and W. Hazeleger, 2012: SST and circulation trend biases cause an underestimation of European precipitation trends. *Clim. Dyn.*, **40**, 1–20.
- van Heerwaarden, C. C., J. V. G. de Arellano, and A. J. Teuling, 2010: Land-atmosphere coupling explains the link between pan evaporation and actual evapotranspiration trends in a changing climate. *Geophys. Res. Lett.*, **37**, L21401.
- van Ommen, T. D., and V. Morgan, 2010: Snowfall increase in coastal East Antarctica linked with southwest Western Australian drought. *Nature Geosci.*, **3**, 267–272.
- Vautard, R., P. Yiou, and G. J. van Oldenborgh, 2009: Decline of fog, mist and haze in Europe over the past 30 years. *Nature Geosci.*, **2**, 115–119.
- Vautard, R., J. Cattiaux, P. Yiou, J. N. Thepaut, and P. Ciais, 2010: Northern Hemisphere atmospheric stilling partly attributed to an increase in surface roughness. *Nature Geosci.*, **3**, 756–761.
- Vautard, R., et al., 2007: Summertime European heat and drought waves induced by wintertime Mediterranean rainfall deficit. *Geophys. Res. Lett.*, **34**, L07711
- Vecchi, G. A., and B. J. Soden, 2007: Global warming and the weakening of the tropical circulation. *J. Clim.*, **20**, 4316–4340.
- Vecchi, G. A., and T. R. Knutson, 2008: On estimates of historical north Atlantic tropical cyclone activity. *J. Clim.*, **21**, 3580–3600.
- Vecchi, G. A., and T. R. Knutson, 2011: Estimating annual numbers of Atlantic hurricanes missing from the HURDAT database (1878–1965) using ship track density. *J. Clim.*, **24**, 1736–1746.
- Vecchi, G. A., B. J. Soden, A. T. Wittenberg, I. M. Held, A. Leetmaa, and M. J. Harrison, 2006: Weakening of tropical Pacific atmospheric circulation due to anthropogenic forcing. *Nature*, **441**, 73–76.
- Velders, G., S. Andersen, J. Daniel, D. Fahey, and M. McFarland, 2007: The importance of the Montreal Protocol in protecting climate. *Proc. Natl. Acad. Sci. U.S.A.*, **104**, 4814–4819.
- Velders, G., D. Fahey, J. Daniel, M. McFarland, and S. Andersen, 2009: The large contribution of projected HFC emissions to future climate forcing. *Proc. Natl. Acad. Sci. U.S.A.*, **106**, 10949–10954.
- Venema, V. K. C., et al., 2012: Benchmarking homogenization algorithms for monthly data. *Clim. Past*, **8**, 89–115.
- Verbout, S., H. Brooks, L. Leslie, and D. Schultz, 2006: Evolution of the US tornado database: 1954–2003. *Weather Forecast.*, **21**, 86–93.
- Vicente-Serrano, S. M., S. Begueria, and J. I. Lopez-Moreno, 2010: A multiscale drought index sensitive to global warming: The Standardized Precipitation Evapotranspiration Index. *J. Clim.*, **23**, 1696–1718.
- Vidal, J., E. Martin, L. Franchisteguy, F. Habets, J. Soubeyroux, M. Blanchard, and M. Baillon, 2010: Multilevel and multiscale drought reanalysis over France with the Safran-Isba-Modcou hydrometeorological suite. *Hydrol. Earth Syst. Sci.*, **14**, 459–478.
- Vilibic, I., and J. Sepic, 2010: Long-term variability and trends of sea level storminess and extremes in European Seas. *Global Planet. Change*, **71**, 1–12.
- Villarini, G., J. Smith, and G. Vecchi, 2013: Changing frequency of heavy rainfall over the central United States. *J. Clim.*, **26**, 351–357.
- Vincent, L., et al., 2011: Observed trends in indices of daily and extreme temperature and precipitation for the countries of the western Indian Ocean, 1961–2008. *J. Geophys. Res. Atmos.*, **116**, D10108.
- Vincent, L. A., X. L. L. Wang, E. J. Milewska, H. Wan, F. Yang, and V. Swail, 2012: A second generation of homogenized Canadian monthly surface air temperature for climate trend analysis. *J. Geophys. Res. Atmos.*, **117**, D18110.
- Visbeck, M., 2009: A station-based Southern Annular Mode Index from 1884 to 2005. *J. Clim.*, **22**, 940–950.
- Volz, A., and D. Kley, 1988: Evaluation of the Montsouris series of ozone measurements made in the 19th century. *Nature*, **332**, 240–242.
- Vömel, H., D. E. David, and K. Smith, 2007a: Accuracy of tropospheric and stratospheric water vapor measurements by the cryogenic frost point hygrometer: Instrumental details and observations. *J. Geophys. Res. Atmos.*, **112**, D08305.
- Vömel, H., et al., 2007b: Validation of Aura Microwave Limb Sounder water vapor by balloon-borne cryogenic frost point hygrometer measurements. *J. Geophys. Res. Atmos.*, **112**, D24537.
- von Clarmann, T., et al., 2009: Retrieval of temperature, H₂O, O₃, HNO₃, CH₄, N₂O, ClONO₂ and ClO from MIPAS reduced resolution nominal mode limb emission measurements. *Atmos. Meas. Tech.*, **2**, 159–175.
- von Schuckmann, K., and P.-Y. Le Traou, 2011: How well can we derive global ocean indicators from Argo data? *Ocean Sci.*, **7**, 783–791.
- Von Storch, H., 1999: Misuses of statistical analysis in climate research. *Analysis of Climate Variability: Applications of Statistical Techniques*, 2nd edition [H. Von Storch and A. Navarra (eds.)]. Springer-Verlag, New York, and Heidelberg, Germany, pp. 11–26.
- von Storch, H., and F. W. Zwiers, 1999: *Statistical Analysis in Climate Research*. Cambridge University Press, Cambridge, United Kingdom and New York, NY, USA, 484 pp.
- Vose, R. S., D. R. Easterling, and B. Gleason, 2005a: Maximum and minimum temperature trends for the globe: An update through 2004. *Geophys. Res. Lett.*, **32**, L23822.
- Vose, R. S., D. Wuertz, T. C. Peterson, and P. D. Jones, 2005b: An intercomparison of trends in surface air temperature analyses at the global, hemispheric, and grid-box scale. *Geophys. Res. Lett.*, **32**, L18718.
- Vose, R. S., S. Applequist, M. J. Menne, C. N. Williams, Jr., and P. Thorne, 2012a: An intercomparison of temperature trends in the US Historical Climatology Network and recent atmospheric reanalyses. *Geophys. Res. Lett.*, **39**, L10703.
- Vose, R. S., Oak Ridge National Laboratory. Environmental Sciences Division., U.S. Global Change Research Program, United States. Dept. of Energy. Office of Health and Environmental Research., Carbon Dioxide Information Analysis Center (U.S.), and Martin Marietta Energy Systems Inc., 1992: *The Global Historical Climatology Network: Long-Term Monthly Temperature, Precipitation, Sea Level Pressure, and Station Pressure Data*. Carbon Dioxide Information Analysis Center. Available to the public from N.T.I.S., 1 v. (various pagings)
- Vose, R. S., et al., 2012b: NOAA's Merged Land-Ocean Surface Temperature Analysis. *Bull. Am. Meteor. Soc.*, **93**, 1677–1685.
- Wacker, S., J. Grobner, K. Hocke, N. Kampfer, and L. Vuilleumier, 2011: Trend analysis of surface cloud-free downwelling long-wave radiation from four Swiss sites. *J. Geophys. Res. Atmos.*, **116**, 13.
- Wallace, J. M., and D. S. Gutzler, 1981: Teleconnections in the geopotential height field during the Northern Hemisphere winter. *Mon. Weather Rev.*, **109**, 784–812.
- Wan, H., X. L. Wang, and V. R. Swail, 2010: Homogenization and trend analysis of Canadian near-surface wind speeds. *J. Clim.*, **23**, 1209–1225.

- Wan, H., X. Zhang, F. Zwiers, S. Emori, and H. Shiogama, 2013: Effect of data coverage on the estimation of mean and variability of precipitation at global and regional scales. *J. Geophys. Res.*, **118**, 534–546.
- Wang, B., J. Liu, H. J. Kim, P. J. Webster, and S. Y. Yim, 2012a: Recent change of the global monsoon precipitation (1979–2008). *Clim. Dyn.*, **39**, 1123–1135.
- Wang, H., et al., 2012b: Extreme climate in China: Facts, simulation and projection. *Meteorol. Z.*, **21**, 279–304.
- Wang, J. H., and L. Y. Zhang, 2008: Systematic errors in global radiosonde precipitable water data from comparisons with ground-based GPS measurements. *J. Clim.*, **21**, 2218–2238.
- Wang, J. H., and L. Y. Zhang, 2009: Climate applications of a global, 2-hourly atmospheric precipitable water dataset derived from IGS tropospheric products. *J. Geodes.*, **83**, 209–217.
- Wang, J. H., L. Y. Zhang, A. Dai, T. Van Hove, and J. Van Baelen, 2007: A near-global, 2-hourly data set of atmospheric precipitable water from ground-based GPS measurements. *J. Geophys. Res. Atmos.*, **112**, D11107.
- Wang, J. S., D. J. Seidel, and M. Free, 2012c: How well do we know recent climate trends at the tropical tropopause? *J. Geophys. Res. Atmos.*, **117**, D09118.
- Wang, K., R. E. Dickinson, and S. Liang, 2009a: Clear sky visibility has decreased over land globally from 1973 to 2007. *Science*, **323**, 1468–1470.
- Wang, K., H. Ye, F. Chen, Y. Z. Xiong, and C. P. Wang, 2012d: Urbanization effect on the diurnal temperature range: Different roles under solar dimming and brightening. *J. Clim.*, **25**, 1022–1027.
- Wang, K. C., and S. L. Liang, 2009: Global atmospheric downward longwave radiation over land surface under all-sky conditions from 1973 to 2008. *J. Geophys. Res. Atmos.*, **114**, D19101.
- Wang, K. C., R. E. Dickinson, and S. L. Liang, 2009b: Clear sky visibility has decreased over land globally from 1973 to 2007. *Science*, **323**, 1468–1470.
- Wang, K. C., R. E. Dickinson, M. Wild, and S. L. Liang, 2010: Evidence for decadal variation in global terrestrial evapotranspiration between 1982 and 2002: 2. Results. *J. Geophys. Res. Atmos.*, **115**, D20113.
- Wang, K. C., R. E. Dickinson, M. Wild, and S. Liang, 2012e: Atmospheric impacts on climatic variability of surface incident solar radiation. *Atmos. Chem. Phys.*, **12**, 9581–9592.
- Wang, K. C., R. E. Dickinson, L. Su, and K. E. Trenberth, 2012f: Contrasting trends of mass and optical properties of aerosols over the Northern Hemisphere from 1992 to 2011. *Atmos. Chem. Phys.*, **12**, 9387–9398.
- Wang, L. K., C. Z. Zou, and H. F. Qian, 2012g: Construction of stratospheric temperature data records from Stratospheric Sounding Units. *J. Clim.*, **25**, 2931–2946.
- Wang, X., H. Wan, and V. Swail, 2006a: Observed changes in cyclone activity in Canada and their relationships to major circulation regimes. *J. Clim.*, **19**, 896–915.
- Wang, X., B. Trewin, Y. Feng, and D. Jones, 2013: Historical changes in Australian temperature extremes as inferred from extreme value distribution analysis. *Geophys. Res. Lett.*, **40**, 573–578.
- Wang, X., Y. Feng, G. P. Compo, V. R. Swail, F. W. Zwiers, R. J. Allan, and P. D. Sardeshmukh, 2012: Trends and low frequency variability of extra-tropical cyclone activity in the ensemble of twentieth century reanalysis. *Clim. Dyn.*, **40**, 2775–2800.
- Wang, X., et al., 2011: Trends and low-frequency variability of storminess over western Europe, 1878–2007. *Clim. Dyn.*, **37**, 2355–2371.
- Wang, X. L. L., V. R. Swail, and F. W. Zwiers, 2006b: Climatology and changes of extra-tropical cyclone activity: Comparison of ERA-40 with NCEP-NCAR reanalysis for 1958–2001. *J. Clim.*, **19**, 3145–3166.
- Wang, X. L. L., F. W. Zwiers, V. R. Swail, and Y. Feng, 2009c: Trends and variability of storminess in the Northeast Atlantic region, 1874–2007. *Clim. Dyn.*, **33**, 1179–1195.
- Wang, X. M., P. M. Zhai, and C. C. Wang, 2009d: Variations in extratropical cyclone activity in northern East Asia. *Adv. Atmos. Sci.*, **26**, 471–479.
- Warren, S. G., R. M. Eastman, and C. J. Hahn, 2007: A survey of changes in cloud cover and cloud types over land from surface observations, 1971–96. *J. Clim.*, **20**, 717–738.
- Weaver, S. J., 2012: Factors associated with decadal variability in Great Plains summertime surface temperatures. *J. Clim.*, **26**, 343–350.
- Weber, M., W. Steinbrecht, C. Long, V. E. Fioletov, S. H. Frith, R. Stolarski, and P. A. Newman, 2012: Stratospheric ozone [in “State of the Climate in 2011”]. *Bull. Am. Met. Soc.*, **93**, S46–S44.
- Weinkle, J., R. Maue, and R. Pielke, 2012: Historical global tropical cyclone landfalls. *J. Clim.*, **25**, 4729–4735.
- Weinstock, E. M., et al., 2009: Validation of the Harvard Lyman-alpha in situ water vapor instrument: Implications for the mechanisms that control stratospheric water vapor. *J. Geophys. Res. Atmos.*, **114**.
- Weiss, R., J. Muhle, P. Salameh, and C. Harth, 2008: Nitrogen trifluoride in the global atmosphere. *Geophys. Res. Lett.*, **35**, L20821.
- Wells, N., S. Goddard, and M. J. Hayes, 2004: A self-calibrating Palmer Drought Severity Index. *J. Clim.*, **17**, 2335–2351.
- Wentz, F., C. Gentemann, D. Smith, and D. Chelton, 2000: Satellite measurements of sea surface temperature through clouds. *Science*, **288**, 847–850.
- Wentz, F. J., L. Ricciardulli, K. Hilburn, and C. Mears, 2007: How much more rain will global warming bring? *Science*, **317**, 233–235.
- Werner, P. C., F. W. Gerstengarbe, and F. Wechsung, 2008: Grosswetterlagen and precipitation trends in the Elbe River catchment. *Meteorol. Z.*, **17**, 61–66.
- Westra, S., and S. Sisson, 2011: Detection of non-stationarity in precipitation extremes using a max-stable process model. *J. Hydrol.*, **406**, 119–128.
- Westra, S., L. Alexander, and F. Zwiers, 2013: Global increasing trends in annual maximum daily precipitation. *J. Clim.*, **26**, 3904–3918.
- Wibig, J., 2008: Cloudiness variations in Lodz in the second half of the 20th century. *Int. J. Climatol.*, **28**, 479–491.
- Wickham, C., et al., 2013: Influence of urban heating on the global temperature land average using rural sites identified from MODIS classifications. *Geoinfor Geostat: An Overview*, **1**, 1:2. doi:10.4172/gigs.1000104.
- Wielicki, B. A., B. R. Barkstrom, E. F. Harrison, R. B. Lee, G. L. Smith, and J. E. Cooper, 1996: Clouds and the Earth’s radiant energy system (CERES): An Earth observing system experiment. *Bull. Am. Meteor. Soc.*, **77**, 853–868.
- Wielicki, B. A., et al., 2002: Evidence for large decadal variability in the tropical mean radiative energy budget. *Science*, **295**, 841–844.
- Wilby, R. L., P. D. Jones, and D. H. Lister, 2011: Decadal variations in the nocturnal heat island of London. *Weather*, **66**, 59–64.
- Wild, M., 2009: Global dimming and brightening: A review. *J. Geophys. Res. Atmos.*, **114**, D00D16.
- Wild, M., 2012: Enlightening global dimming and brightening. *Bull. Am. Meteor. Soc.*, **93**, 27–37.
- Wild, M., A. Ohmura, and K. Makowski, 2007: Impact of global dimming and brightening on global warming. *Geophys. Res. Lett.*, **34**, L04702.
- Wild, M., J. Grieser, and C. Schaer, 2008: Combined surface solar brightening and increasing greenhouse effect support recent intensification of the global land-based hydrological cycle. *Geophys. Res. Lett.*, **35**, L17706.
- Wild, M., A. Ohmura, H. Gilgen, and D. Rosenfeld, 2004: On the consistency of trends in radiation and temperature records and implications for the global hydrological cycle. *Geophys. Res. Lett.*, **31**, L11201.
- Wild, M., A. Ohmura, H. Gilgen, E. Roeckner, M. Giorgetta, and J. J. Morcrette, 1998: The disposition of radiative energy in the global climate system: GCM-calculated versus observational estimates. *Clim. Dyn.*, **14**, 853–869.
- Wild, M., D. Folini, C. Schär, N. Loeb, E. G. Dutton, and G. König-Langlo, 2013: The global energy balance from a surface perspective. *Clim. Dyn.*, **40**, 3107–3134.
- Wild, M., B. Truesell, A. Ohmura, C. N. Long, G. König-Langlo, E. G. Dutton, and A. Tsvetkov, 2009: Global dimming and brightening: An update beyond 2000. *J. Geophys. Res. Atmos.*, **114**, D00d13.
- Wild, M., et al., 2005: From dimming to brightening: Decadal changes in solar radiation at Earth’s surface. *Science*, **308**, 847–850.
- Wilks, D. S., 2006: *Statistical Methods in the Atmospheric Sciences*, 2nd edition. Elsevier, Philadelphia, 627 pp.
- Willett, K. M., P. D. Jones, N. P. Gillett, and P. W. Thorne, 2008: Recent Changes in Surface Humidity: Development of the HadCRUH dataset. *J. Clim.*, **21**, 5364–5383.
- Willett, K. M., P. D. Jones, P. W. Thorne, and N. P. Gillett, 2010: A comparison of large scale changes in surface humidity over land in observations and CMIP3 general circulation models. *Environ. Res. Lett.*, **5**.
- Willett, K. M., et al., 2013: HadISDH: an updateable land surface specific humidity product for climate monitoring. *Clim. Past*, **9**, 657–677.
- Williams, C. N., M. J. Menne, and P. W. Thorne, 2012: Benchmarking the performance of pairwise homogenization of surface temperatures in the United States. *J. Geophys. Res. Atmos.*, **117**.
- Willson, R. C., and A. V. Mordvinov, 2003: Secular total solar irradiance trend during solar cycles 21–23. *Geophys. Res. Lett.*, **30**, 1199.
- Winkler, P., 2009: Revision and necessary correction of the long-term temperature series of Hohenpeissenberg, 1781–2006. *Theor. Appl. Climatol.*, **98**, 259–268.

- Wong, T., B. A. Wielicki, R. B. Lee, G. L. Smith, K. A. Bush, and J. K. Willis, 2006: Re-examination of the observed decadal variability of the earth radiation budget using altitude-corrected ERBE/ERBS nonscanner WFOV data. *J. Clim.*, **19**, 4028–4040.
- Wood, S. N., 2006: *Generalized Additive Models: An Introduction with R*. CRC/Chapman & Hall, Boca Raton, FL, USA.
- Woodruff, S. D., et al., 2011: ICOADS Release 2.5: Extensions and enhancements to the Surface Marine Meteorological Archive. *Int. J. Climatol.*, **31**, 951–967.
- Worden, H. M., et al., 2013: Decadal record of satellite carbon monoxide observations. *Atmos. Chem. Phys.*, **13**, 837–850.
- Worton, D., et al., 2007: Atmospheric trends and radiative forcings of CF4 and C2F6 inferred from firn air. *Environ. Sci. Technol.*, **41**, 2184–2189.
- Worton, D. R., et al., 2012: Evidence from firn air for recent decreases in non-methane hydrocarbons and a 20th century increase in nitrogen oxides in the northern hemisphere. *Atmos. Environ.*, **54**, 592–602.
- Wu, Z., N. E. Huang, S. R. Long, and C.-K. Peng, 2007: On the trend, detrending, and variability of nonlinear and nonstationary time series. *Proc. Natl. Acad. Sci. U.S.A.*, **104**, 14889–14894.
- Wu, Z., N. E. Huang, J. M. Wallace, B. V. Smoliak, and X. Chen, 2011: On the time-varying trend in global-mean surface temperature. *Clim. Dyn.*, **37**, 759–773.
- Xavier, P. K., V. O. John, S. A. Buehler, R. S. Ajayamohan, and S. Sijkumar, 2010: Variability of Indian summer monsoon in a new upper tropospheric humidity data set. *Geophys. Res. Lett.*, **37**, L05705.
- Xia, X., 2010a: A closer looking at dimming and brightening in China during 1961–2005. *Ann. Geophys.*, **28**, 1121–1132.
- Xia, X. G., 2010b: Spatiotemporal changes in sunshine duration and cloud amount as well as their relationship in China during 1954–2005. *J. Geophys. Res. Atmos.*, **115**, D00K06.
- Xiao, X., et al., 2010: Atmospheric three-dimensional inverse modeling of regional industrial emissions and global oceanic uptake of carbon tetrachloride. *Atmos. Chem. Phys.*, **10**, 10421–10434.
- Xie, B., Q. Zhang, and Y. Wang, 2010: Observed characteristics of hail size in four regions in China during 1980–2005. *J. Clim.*, **23**, 4973–4982.
- Xie, B. G., Q. H. Zhang, and Y. Q. Wang, 2008: Trends in hail in China during 1960–2005. *Geophys. Res. Lett.*, **35**, L13801.
- Xie, S., K. Hu, J. Hafner, H. Tokinaga, Y. Du, G. Huang, and T. Sampe, 2009: Indian Ocean capacitor effect on Indo-Western Pacific climate during the summer following El Niño. *J. Clim.*, **22**, 730–747.
- Xu, C. Y., L. B. Gong, J. Tong, and D. L. Chen, 2006a: Decreasing reference evapotranspiration in a warming climate – A case of Changjiang (Yangtze) River catchment during 1970–2000. *Adv. Atmos. Sci.*, **23**, 513–520.
- Xu, K. H., J. D. Milliman, and H. Xu, 2010: Temporal trend of precipitation and runoff in major Chinese Rivers since 1951. *Global Planet. Change*, **73**, 219–232.
- Xu, M., C. P. Chang, C. B. Fu, Y. Qi, A. Robock, D. Robinson, and H. M. Zhang, 2006b: Steady decline of east Asian monsoon winds, 1969–2000: Evidence from direct ground measurements of wind speed. *J. Geophys. Res. Atmos.*, **111**.
- Yan, Z. W., Z. Li, Q. X. Li, and P. Jones, 2010: Effects of site change and urbanisation in the Beijing temperature series 1977–2006. *Int. J. Climatol.*, **30**, 1226–1234.
- Yang, J., Q. Liu, S.-P. Xie, Z. Liu, and L. Wu, 2007: Impact of the Indian Ocean SST basin mode on the Asian summer monsoon. *Geophys. Res. Lett.*, **34**, L02708.
- Yang, X. C., Y. L. Hou, and B. D. Chen, 2011: Observed surface warming induced by urbanization in east China. *J. Geophys. Res. Atmos.*, **116**, 12.
- Yokouchi, Y., S. Taguchi, T. Saito, Y. Tohjima, H. Tanimoto, and H. Mukai, 2006: High frequency measurements of HFCs at a remote site in east Asia and their implications for Chinese emissions. *Geophys. Res. Lett.*, **33**, L21814.
- Yoon, J., W. von Hoyningen-Huene, A. A. Kokhanovsky, M. Vountas, and J. P. Burrows, 2012: Trend analysis of aerosol optical thickness and Angstrom exponent derived from the global AERONET spectral observations. *Atmos. Meas. Tech.*, **5**, 1271–1299.
- You, Q., et al., 2010: Changes in daily climate extremes in China and their connection to the large scale atmospheric circulation during 1961–2003. *Clim. Dyn.*, **36**, 2399–2417.
- Yttri, K. E., et al., 2011: Transboundary particulate matter in Europe, Status Report 2011. In: *Co-operative Programme for Monitoring and Evaluation of the Long Range Transmission of Air Pollutants (Joint CCC, MSC-W, CEIP and CIAM report 2011)*. NILU - Chemical Coordinating Centre - CCC. http://emep.int/publ/common_publications.html
- Yu, B., and F. W. Zwiers, 2010: Changes in equatorial atmospheric zonal circulations in recent decades. *Geophys. Res. Lett.*, **37**, L05701.
- Yu, L., and R. Weller, 2007: Objectively analyzed air-sea heat fluxes for the global ice-free oceans (1981–2005). *Bull. Am. Meteor. Soc.*, **88**, 527–539.
- Yuan, X., and C. Li, 2008: Climate modes in southern high latitudes and their impacts on Antarctic sea ice. *J. Geophys. Res. Oceans*, **113**, C06S91.
- Yurganov, L., W. McMillan, E. Grechko, and A. Dzhola, 2010: Analysis of global and regional CO burdens measured from space between 2000 and 2009 and validated by ground-based solar tracking spectrometers. *Atmos. Chem. Phys.*, **10**, 3479–3494.
- Zebiak, S. E., 1993: Air-sea interaction in the equatorial Atlantic region. *J. Clim.*, **6**, 1567–1568.
- Zerefos, C. S., et al., 2009: Solar dimming and brightening over Thessaloniki, Greece, and Beijing, China. *Tellus B*, **61**, 657–665.
- Zhang, A. Y., G. Y. Ren, J. X. Zhou, Z. Y. Chu, Y. Y. Ren, and G. L. Tang, 2010: On the urbanization effect on surface air temperature trends over China. *Acta Meteorol. Sin.*, **68**, 957–966.
- Zhang, H., J. Bates, and R. Reynolds, 2006: Assessment of composite global sampling: Sea surface wind speed. *Geophys. Res. Lett.*, **33**, L17714.
- Zhang, J., and J. S. Reid, 2010: A decadal regional and global trend analysis of the aerosol optical depth using a data-assimilation grade over-water MODIS and Level 2 MISR aerosol products. *Atmos. Chem. Phys.*, **10**, 10949–10963.
- Zhang, X., J. He, J. Zhang, I. Polaykov, R. Gerdes, J. Inoue, and P. Wu, 2012a: Enhanced poleward moisture transport and amplified northern high-latitude wetting trend. *Nature Clim. Change*, **3**, 47–51.
- Zhang, X., et al., 2007a: Detection of human influence on twentieth-century precipitation trends. *Nature*, **448**, 461–U464.
- Zhang, X., et al., 2011: Indices for monitoring changes in extremes based on daily temperature and precipitation data. *Wiley Interdis. Rev. Clim. Change*, **2**, 851–870.
- Zhang, X. B., et al., 2005: Trends in Middle East climate extreme indices from 1950 to 2003. *J. Geophys. Res. Atmos.*, **110**, D22104.
- Zhang, X. D., C. H. Lu, and Z. Y. Guan, 2012b: Weakened cyclones, intensified anticyclones and recent extreme cold winter weather events in Eurasia. *Environ. Res. Lett.*, **7**, 044044.
- Zhang, X. D., J. E. Walsh, J. Zhang, U. S. Bhatt, and M. Ikeda, 2004: Climatology and interannual variability of Arctic cyclone activity: 1948–2002. *J. Clim.*, **17**, 2300–2317.
- Zhang, Y., J. M. Wallace, and D. S. Battisti, 1997: ENSO-like interdecadal variability: 1900–93. *J. Clim.*, **10**, 1004–1020.
- Zhang, Y. Q., C. M. Liu, Y. H. Tang, and Y. H. Yang, 2007b: Trends in pan evaporation and reference and actual evapotranspiration across the Tibetan Plateau. *J. Geophys. Res. Atmos.*, **112**, D12110.
- Zhao, X. P. T., A. K. Heidinger, and K. R. Knapp, 2011: Long-term trends of zonally averaged aerosol optical thickness observed from operational satellite AVHRR instrument. *Meteorol. Appl.*, **18**, 440–445.
- Zhen, L., and Y. Zhong-Wei, 2009: Homogenized daily mean maximum/minimum temperature series for China from 1960–2008. 237–243.
- Zhou, J., and K.-K. Tung, 2012: Deducing multidecadal anthropogenic global warming trends using multiple regression Analysis. *J. Atmos. Sci.*, **70**, 3–8.
- Zhou, T., L. Zhang, and H. Li, 2008: Changes in global land monsoon area and total rainfall accumulation over the last half century. *Geophys. Res. Lett.*, **35**, L16707.
- Zhou, T. J., D. Y. Gong, J. Li, and B. Li, 2009a: Detecting and understanding the multi-decadal variability of the East Asian summer monsoon – Recent progress and state of affairs. *Meteorol. Z.*, **18**, 455–467.
- Zhou, T. J., et al., 2009b: Why the Western Pacific subtropical high has extended westward since the late 1970s. *J. Clim.*, **22**, 2199–2215.
- Zhou, Y. P., K. M. Xu, Y. C. Sud, and A. K. Betts, 2011: Recent trends of the tropical hydrological cycle inferred from Global Precipitation Climatology Project and International Satellite Cloud Climatology Project data. *J. Geophys. Res. Atmos.*, **116**, D09101.
- Zhou, Y. Q., and G. Y. Ren, 2011: Change in extreme temperature event frequency over mainland China, 1961–2008. *Clim. Res.*, **50**, 125–139.
- Ziemke, J. R., S. Chandra, and P. K. Bhartia, 2005: A 25-year data record of atmospheric ozone in the Pacific from Total Ozone Mapping Spectrometer (TOMS) cloud slicing: Implications for ozone trends in the stratosphere and troposphere. *J. Geophys. Res.*, **110**, D15105.
- Ziemke, J. R., S. Chandra, G. J. Labow, P. K. Bhartia, L. Froidevaux, and J. C. Witte, 2011: A global climatology of tropospheric and stratospheric ozone derived from Aura OMI and MLS measurements. *Atmos. Chem. Phys.*, **11**, 9237–9251.

- Zipser, E. J., C. Liu, D. J. Cecil, S. W. Nesbitt, and D. P. Yorty, 2006: Where are the most intense thunderstorms on Earth? *Bull. Am. Meteor. Soc.*, **87**, 1057–1071.
- Zolina, O., C. Simmer, K. Belyaev, A. Kapala, and S. Gulev, 2009: Improving estimates of heavy and extreme precipitation using daily records from European rain gauges. *J. Hydrometeor.*, **10**, 701–716.
- Zorita, E., T. F. Stocker, and H. von Storch, 2008: How unusual is the recent series of warm years? *Geophys. Res. Lett.*, **35**, L24706.
- Zou, C. Z., and W. H. Wang, 2010: Stability of the MSU-derived atmospheric temperature trend. *J. Atmos. Ocean Technol.*, **27**, 1960–1971.
- Zou, C. Z., and W. H. Wang, 2011: Intersatellite calibration of AMSU-A observations for weather and climate applications. *J. Geophys. Res. Atmos.*, **116**, D23113.
- Zou, C. Z., M. D. Goldberg, Z. H. Cheng, N. C. Grody, J. T. Sullivan, C. Y. Cao, and D. Topley, 2006a: Recalibration of microwave sounding unit for climate studies using simultaneous nadir overpasses. *J. Geophys. Res. Atmos.*, **111**, L17701.
- Zou, X., L. V. Alexander, D. Parker, and J. Caesar, 2006b: Variations in severe storms over China. *Geophys. Res. Lett.*, **33**.
- Zwiers, F. W., and V. V. Kharin, 1998: Changes in the extremes of the climate simulated by CCC GCM2 under CO₂ doubling. *J. Clim.*, **11**, 2200–2222.